Experimental study of the formation of pollutants during the combustion of bio-oil surrogate molecules

Sylvain Namysl

▶ **To cite this version:**

Sylvain Namysl. Experimental study of the formation of pollutants during the combustion of bio-oil surrogate molecules. Chemical and Process Engineering. Université de Lorraine, 2019. English. NNT : 2019LORR0279 . tel-02559037

HAL Id: tel-02559037
https://hal.univ-lorraine.fr/tel-02559037

Submitted on 30 Apr 2020

HAL is a multi-disciplinary open access archive for the deposit and dissemination of scientific research documents, whether they are published or not. The documents may come from teaching and research institutions in France or abroad, or from public or private research centers.

L'archive ouverte pluridisciplinaire **HAL**, est destinée au dépôt et à la diffusion de documents scientifiques de niveau recherche, publiés ou non, émanant des établissements d'enseignement et de recherche français ou étrangers, des laboratoires publics ou privés.

AVERTISSEMENT

Ce document est le fruit d'un long travail approuvé par le jury de soutenance et mis à disposition de l'ensemble de la communauté universitaire élargie.

Il est soumis à la propriété intellectuelle de l'auteur. Ceci implique une obligation de citation et de référencement lors de l'utilisation de ce document.

D'autre part, toute contrefaçon, plagiat, reproduction illicite encourt une poursuite pénale.

Contact : ddoc-theses-contact@univ-lorraine.fr

LIENS

Code de la Propriété Intellectuelle. articles L 122. 4
Code de la Propriété Intellectuelle. articles L 335.2- L 335.10
http://www.cfcopies.com/V2/leg/leg_droi.php
http://www.culture.gouv.fr/culture/infos-pratiques/droits/protection.htm

UNIVERSITE DE LORRAINE-LRGP-ENSIC-NANCY

THESE

Presented at the Université de Lorraine

Ecole Doctorale SIMPPé : Sciences et Ingénierie des Molécules, des Produits, des Procédés et de l'énergie
Laboratoire Réactions et Génie des Procédés (UMR 7274 CNRS)
For the acquisition of the grade of

DOCTEUR DE L'UNIVERSITE DE LORRAINE

Speciality: « Génie des Procédés, des Produits et des Molécules »

By

Sylvain NAMYSL

Experimental study of the formation of pollutants during the combustion of bio-oil surrogate molecules

Defended in public on November 26, 2019

Members of the jury

President:	
Prof. P. Glarborg	**Technical University of Denmark, Denmark**
Reviewers:	
Prof. M.U. Alzueta	**I3A, University of Zaragoza, Zaragoza, Spain**
Prof. K. Van Geem	**LCT, University of Ghent, Ghent, Belgium**
Examiner:	
Dr. A. Roubaud	**CEA, Grenoble**
PhD supervisor:	
Dr. F. Battin-Leclerc	**LRGP, CNRS-Université de Lorraine, Nancy**
PhD co-supervisor :	
Dr. O. Herbinet	**LRGP, CNRS-Université de Lorraine, Nancy**

Laboratoire Réactions et Génie des procédés (LRGP) UMR 7274, 1 Rue Grandville, 54001 Nancy

UNIVERSITE DE LORRAINE-LRGP-ENSIC-NANCY

THESE

Présentée à l'Université de Lorraine

Ecole Doctorale SIMPPé : Sciences et Ingénierie des Molécules, des Produits, des Procédés et de l'énergie
Laboratoire Réactions et Génie des Procédés (UMR 7274 CNRS)
Pour l'obtention du grade de

DOCTEUR DE L'UNIVERSITE DE LORRAINE

Spécialité: « Génie des Procédés, des Produits et des Molécules »

Par

Sylvain NAMYSL

Etude expérimentale de la formation de polluants lors de la combustion de molécules modèles de bio-huiles

Soutenue publiquement le 26 Novembre 2019 devant la Commission d'Examen

Membres du jury

Président:	
Prof. P. Glarborg	**Technical University of Denmark, Danemark**
Rapporteurs:	
Prof. M.U. Alzueta	**I3A, University of Zaragoza, Zaragoza, Espagne**
Prof. K. Van Geem	**LCT, University of Ghent, Ghent, Belgique**
Examinateurs:	
Dr. A. Roubaud	**CEA, Grenoble**
Directrice de thèse:	
Dr. F. Battin-Leclerc	**LRGP, CNRS-Université de Lorraine, Nancy**
Co-directeur de thèse:	
Dr. O. Herbinet	**LRGP, CNRS-Université de Lorraine, Nancy**

Laboratoire Réactions et Génie des procédés (LRGP) UMR 7274, 1 Rue Grandville, 54001 Nancy

REMERCIEMENTS

Voilà le moment délicat et redouté des remerciements. Entre les oublis et les phrases potentiellement mal interprétées, il y a plus d'un obstacle qui surgissent à ce moment précis. Pourtant après avoir rédigé environ 300 pages sur un sujet comme la combustion, on ne pense pas que se sera cette étape le problème. Bon… Allez ! On se lance.

Comment ne pas remercier tout d'abord Frédérique et Olivier, qui m'ont recruté pour travailler avec eux et avec qui se fut un plaisir de partager ces trois années. Entre les congrès, les réunions et les nombreux skypes on a eu de quoi s'occuper et c'est avec des souvenirs agréables et positifs que je repars du LRGP. Grosse pensée à Yu et Nicolas, qui ont été là depuis le début et avec qui j'ai passé de très bons moments que ce soit à Lille ou à Dublin. Désolé Amal, je n'ai pas vraiment pris le temps de venir discuter avec toi à mes grands regrets, mais ce congrès à Lisbonne restera un souvenir impérissable. Bonne chance pour la suite à vous trois.

Merci à Matteo, Alessandro et Tiziano, nos collègues de Milan qui m'ont accueilli pendant un mois. Ce fut un réel plaisir et je vous souhaite bonne chance pour la suite.

Merci à tous les collègues de GCR et à tous les personnels du LRPG avec qui j'ai passé 3 ans. Ces pauses café animées avec toute l'équipe me manquent déjà (PS : Rendez la cafetière !!). Certains sont partis du laboratoire avant moi et d'autres y sont encore et à tous je vous souhaite tout plein de réussite dans vos projets professionnels et personnels. Il y a eu aussi tous les membres du BJC avec qui il y a eu tant de réunions improductives mais aussi de beaux évènements.

Bonne chance à tous ceux qui sont toujours en thèse : Susu, Lulu, Jojo et Maty ! Bon courage à nos chers post-docs adorés Zak, Juan Carlos, Amina et Albert. Bon courage Louise dans tes études de bibliothèquage (je n'écrirai pas ici la citation de Camaille mais l'idée y est). Bonne chance Lucia, petit ange parti trop vite à Paris.

Mention spéciale à Yohann, Lubin et Laetitia qui ont aussi supporté toutes les plaintes et les histoires malgré eux à l'insu de leur plein gré autour souvent des quelques bières. Et dire que tout ça a commencé avec un PRD…

Et enfin grosse pensée à mon petit poussin qui a été avec moi tout au long de cette thèse et qui j'espère voudra bien me supporter pour encore quelques années. Viva Las Charmas.

Gros bisous à ma famille !!! Ils pensaient que j'allais rester étudiant toute ma vie !!!

Merci à tous ceux qui sont venus à la soutenance et au pot. Big up à Laetitia et Lulu pour les cadeaux : vous gérez !!

Ouais là on commence à plus avoir d'inspiration (et plus trop de place). En même temps, je n'avais pas vraiment prévu cette section. Faut avouer que ce n'est pas très marrant à faire. Là j'ai bien envie d'aller sur YouTube faut bien se l'avouer. D'ailleurs quand on est petit, on se dit « Quand je serai grand, je ferai ce que je veux » ; donc mise en application !!!

Pavé César, ceux qui ont lu te saluent !

RÉSUMÉ EN FRANCAIS

L'énergie est l'un des piliers fondamentaux du progrès de l'humanité. Depuis la découverte du feu jusqu'à l'invention des centrales nucléaires, le développement de l'humanité a été guidé par sa capacité à produire de l'énergie à partir de différentes sources, principalement d'origine fossiles. Mais de nos jours, produire de l'énergie en quantité suffisante sans aucun impact sur l'environnement est devenu une question prédominante comparé à la production d'énergie brute. Les préoccupations ne se limitent plus à la quantité mais plutôt à la notion de qualité. L'épuisement programmé des stocks de combustibles fossiles ainsi que la détérioration de l'écosystème planétaire doivent conduire à une nouvelle ère de développement et de recherche de solutions alternatives respectueuses de l'environnement et responsables.

En 2019, les Nations Unies estiment la population mondiale à environ 7,715 milliards d'habitants, soit une augmentation d'un milliard par rapport aux 6,145 milliards d'habitants en 2000 (United Nation et al., 2019). Cette croissance importante de la population entraîne une demande énergétique de plus en plus importante dans le monde et en particulier dans les pays en développement, tels que la Chine ou l'Inde. L'Agence Internationale de l'Energie (IEA) estime que la demande mondiale devrait passer d'environ 9 000 MTep en 2017 à environ 13 000 MTep en 2040, avec une augmentation dans toutes les régions du monde (IEA, 2018a). Afin de répondre à la demande mondiale future, deux solutions sont possibles: augmenter la consommation de combustibles fossiles ou développer de nouvelles sources d'énergie, telles que les biocarburants. En 2016, les combustibles fossiles représentaient environ 80% de l'approvisionnement mondial total en énergie primaire, comme le montre la Figure 1. Toutefois, cette ressource est limitée et a un impact considérable sur la pollution de l'environnement en raison de la production de gaz à effet de serre. Le développement de nouvelles sources d'énergie est donc essentiel pour soutenir la croissance de la population et de la demande en énergie.

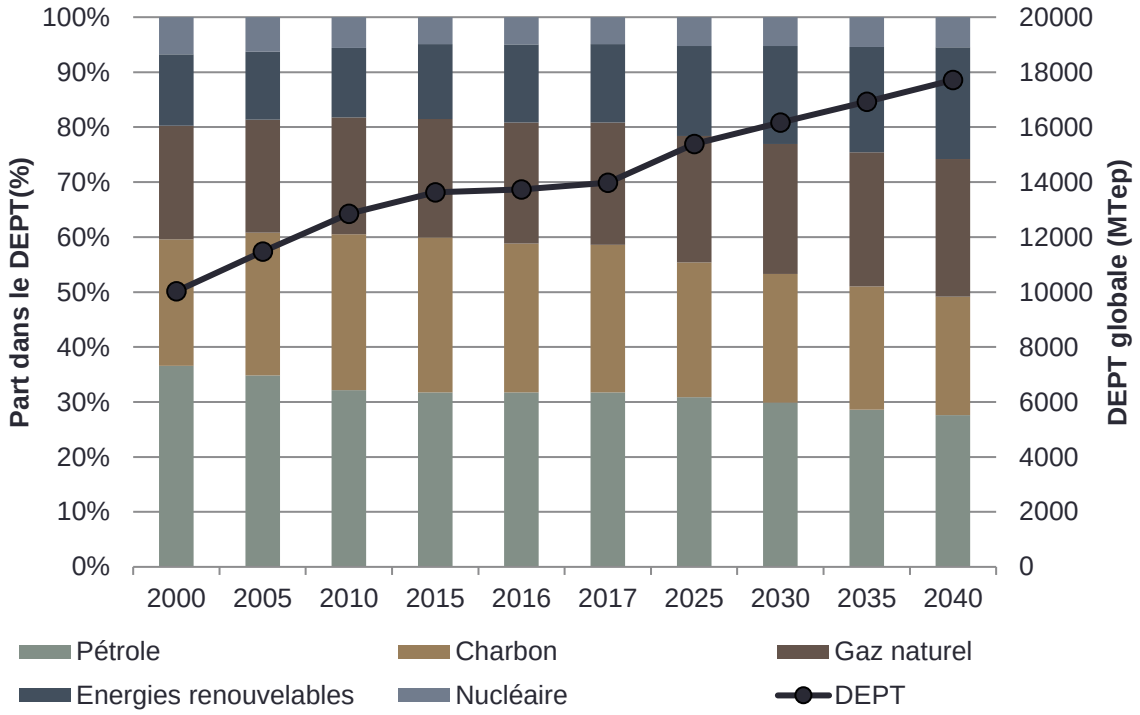

Figure : 1. Demande d'énergie primaire totale (DEPT) par source au fil des ans en MTep (mégatonnes d'équivalent pétrole)(IEA, 2018a)

La Figure 2 présente un aperçu plus détaillé des différentes sources d'énergies renouvelables. La source principale est la bioénergie qui correspond à l'énergie générée par la conversion de produits solides, liquides et gazeux dérivés de la biomasse. Sa part dans le bouquet énergétique devrait continuer à augmenter dans les années à venir en raison de sa disponibilité immédiate et des préoccupations environnementales. La catégorie «Autres» correspond à la contribution de l'énergie éolienne, des panneaux solaires, de l'énergie solaire thermique et de l'énergie géothermique. La part des énergies renouvelables va augmenter dans les prochaines années selon l'IEA (IEA, 2019) et notamment celle liée à la biomasse. Les autres sources d'énergies renouvelables sont également supposées augmenter, mais dans une moindre mesure que la biomasse.

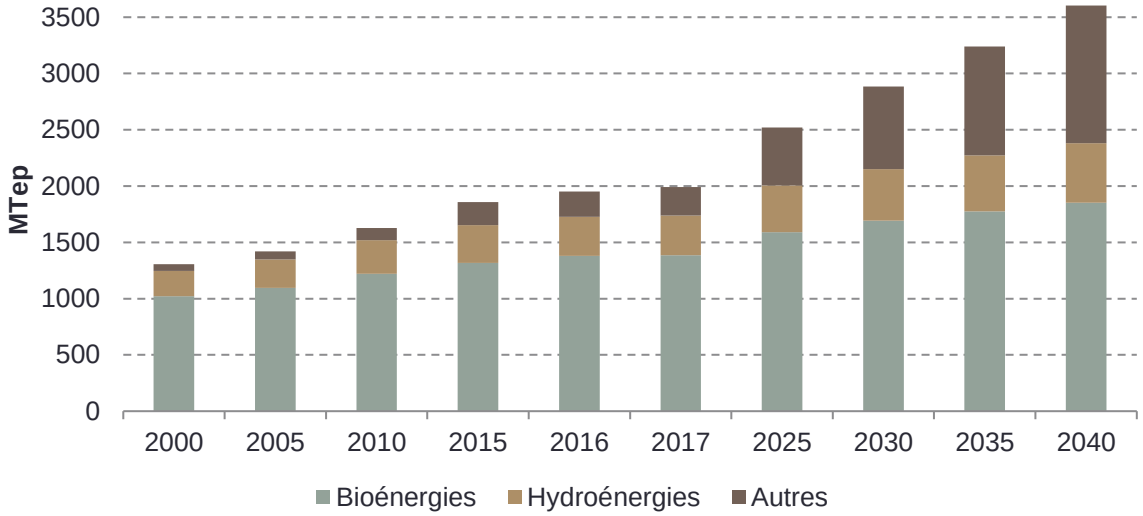

Figure : 2. Source d'énergie renouvelable en MTep au fil des ans (IEA, 2019)

La biomasse peut être définie comme toute matière organique, c'est-à-dire un matériau biologique, disponible sur une base renouvelable. Cela inclut les matières premières dérivées d'animaux ou de plantes, tels que le bois et les cultures, ainsi que les déchets organiques de sources municipales et industrielles (IEA and FAO, 2017).

La plupart des types finaux de biomasse proviennent de sources végétales, qui sont composées principalement de matière lignocellulosique (Chirat, 2017). Ce type de biomasse est composé de trois polymères:

- Cellulose (environ 50%)
- Hémicelluloses (30-20%)
- Lignine (20-30%)

La cellulose est composée d'un polymère linéaire de glucose, comme le montre la Figure 3. Il s'agit du polysaccharide le plus abondant sur Terre, avec un stock mondial disponible de 100 milliards de tonnes. Il est utilisé dans l'industrie du papier et également dans le domaine pharmaceutique pour la synthèse additive.

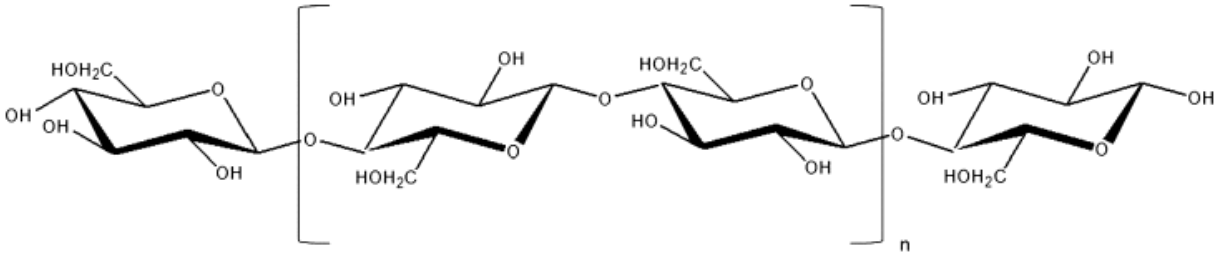

Figure : 3. Structure du polymère de cellulose (Chirat, 2017).

Contrairement à la cellulose, les hémicelluloses sont composées de différents monosaccharides: les hexoses et les pentoses. La composition en hémicelluloses est très variable selon les sources de biomasse. Les principaux sucres présents dans le bois et formant des hémicelluloses sont représentés sur la Figure 4.

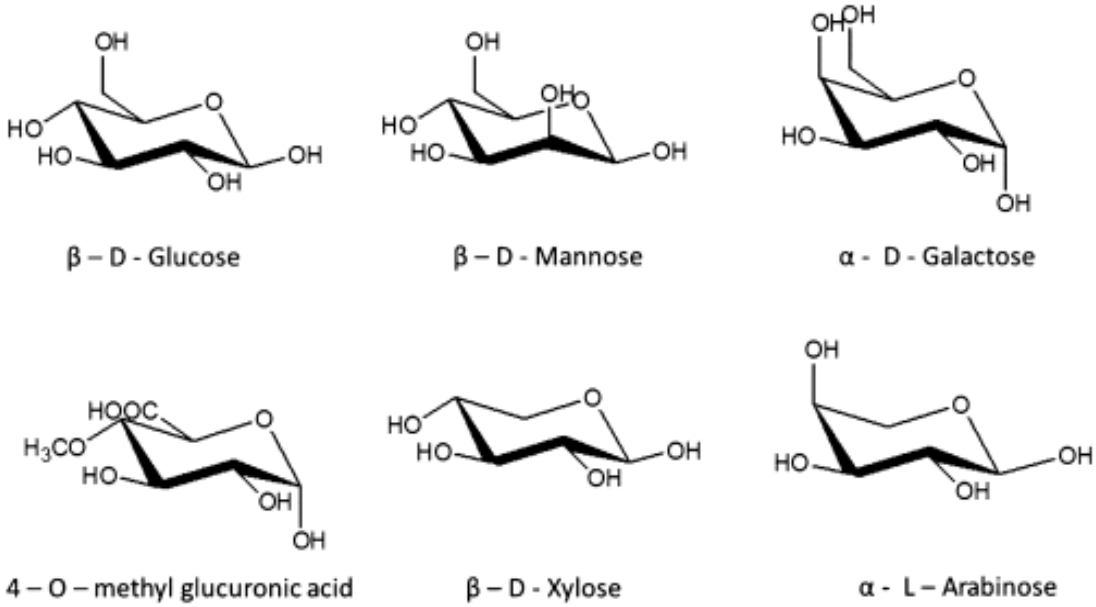

Figure : 4. Molécules de monosaccharides composant les hémicelluloses (Chirat, 2017).

Le dernier élément composant la biomasse végétale est la lignine. La lignine est le deuxième composé principal du bois et assure la rigidité de toute structure végétale. La lignine est composée d'unités phénylpropane liées entre elles par des ponts éther pour former un polymère complexe. C'est le seul composant capable de produire des composés aromatiques similaires à ceux produits par la pétrochimie. La Figure 5 présente un exemple de structure de la lignine, montrant la présence d'unités phényle.

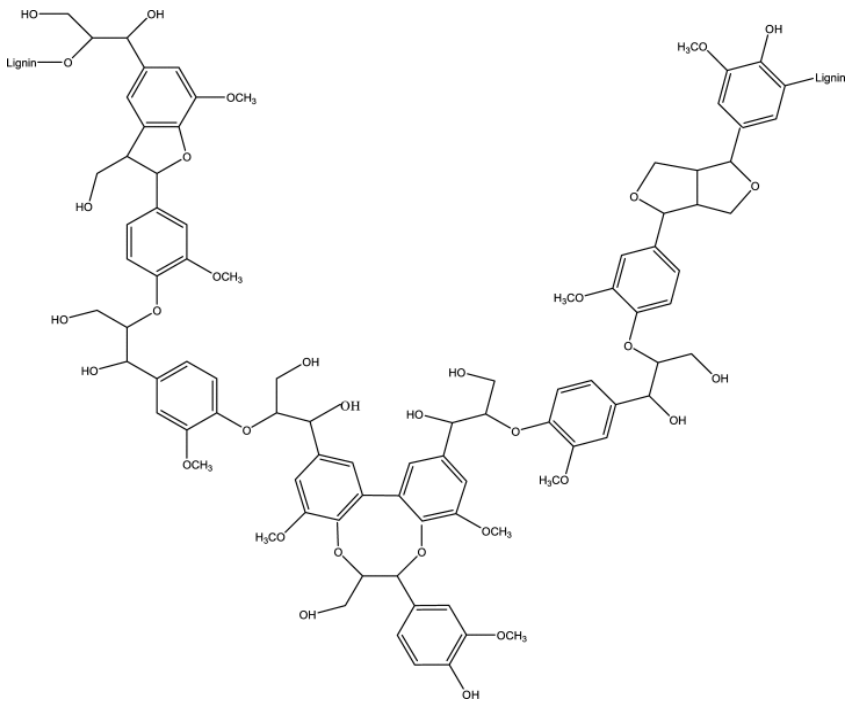

Figure : 5. Exemple de structure représentant un polymère de lignine (Chirat, 2017)

Il existe de nombreuses manières de transformer la biomasse pour produire de l'énergie (IEA and FAO, 2017). Certaines conduisent à la production de biocarburants pour le transport et d'autres à la production directe d'électricité ou de chaleur par combustion, comme illustré par la Figure 6. Cette figure présente également des exemples de processus et de produits pour différentes matières premières de biomasse.

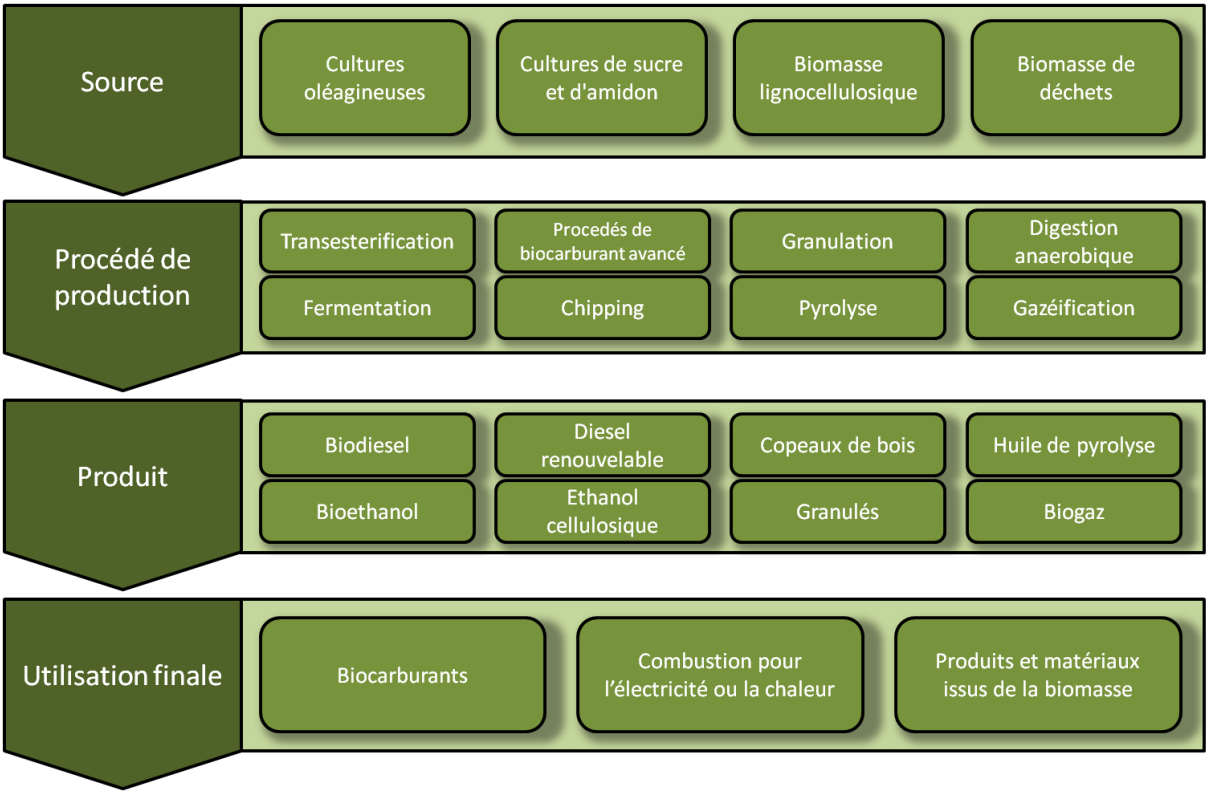

Figure : 6. De la biomasse à l'énergie: les voies de la bioénergie (IEA and FAO, 2017)

Les biocarburants ainsi produits peuvent être utilisés pour remplacer en partie ou complètement les carburants d'origine fossiles. Cette possibilité peut en effet être envisagée dans le milieu des transports (avec l'ajout d'éthanol dans les essences par exemple) ou dans le milieu industriel.

Le projet IMPROOF est un projet financé par l'Union européenne dans le cadre du programme SPIRE (Djokic et al., 2017). Son objectif est d'améliorer de 20% l'efficacité énergétique des fours de vapocraquage et, parallèlement, de réduire de 25% par tonne d'éthylène produite les émissions de polluants tels que les NO_x ou les gaz à effet de serre. Ce consortium regroupe 11 partenaires de 6 pays différents, dont 7 industriels, qui donnent à ce projet une orientation industrielle spécifique.

Pour atteindre les objectifs, le projet s'est concentré sur trois améliorations:

- Le développement de nouveau design et de nouveaux matériaux pour les tubes utilisés dans le four: l'utilisation d'un nouveau design 3D pour les tubes avec de nouveaux matériaux empêchera la formation de coke à la surface du réacteur. La minimisation de cette couche aidera à réduire la formation de CO_2 lors du craquage. Le nouveau design contribuera également à optimiser le transfert de chaleur à la paroi.
- La mise en œuvre de revêtements à haute émissivité sur la paroi du four: afin de réduire la consommation de combustible dans le four, de nouveaux revêtements à haute émissivité ont été étudiés. Ils contribueront à récupérer une partie de la chaleur et ainsi à réduire la consommation de carburant pour atteindre la même température.
- L'utilisation de carburants alternatifs et renouvelables: afin de réduire l'impact des fours de vapocraquage sur les émissions de CO_2, l'utilisation de combustibles renouvelables issus de la biomasse a été envisagée. Ces carburants peuvent être du biogaz ou de la bio-huile et réduiront la production nette de CO_2 de l'installation.

Une combinaison d'études de laboratoire, de simulations et de mises au point de pilotes industriels a été mise en place pour tester et valider les résultats de chaque axe d'amélioration.

Cette thèse porte sur la partie concernant les carburants alternatifs et en particulier les bio-huiles. La première tâche consistait à définir un substitut pour les bio-huiles à l'aide des données présentées dans la littérature. En utilisant la classification proposée par Negahdar (2016), six familles chimiques ont été sélectionnées. Une base de données expérimentale pour la combustion de ces produits de substitution, obtenue grâce à un réacteur agité par jets gazeux, a été établie. Cette base de données a ensuite été utilisée pour développer et valider des modèles cinétiques détaillés afin de reproduire la combustion de ces substituants de bio-huiles. Les simulations des résultats obtenus ont été réalisées en collaboration avec l'équipe du Professeur Faravelli de Politechnico di Milano.

La Figure 7 présente comment cette thèse s'inscrit dans le cadre du projet IMPROOF.

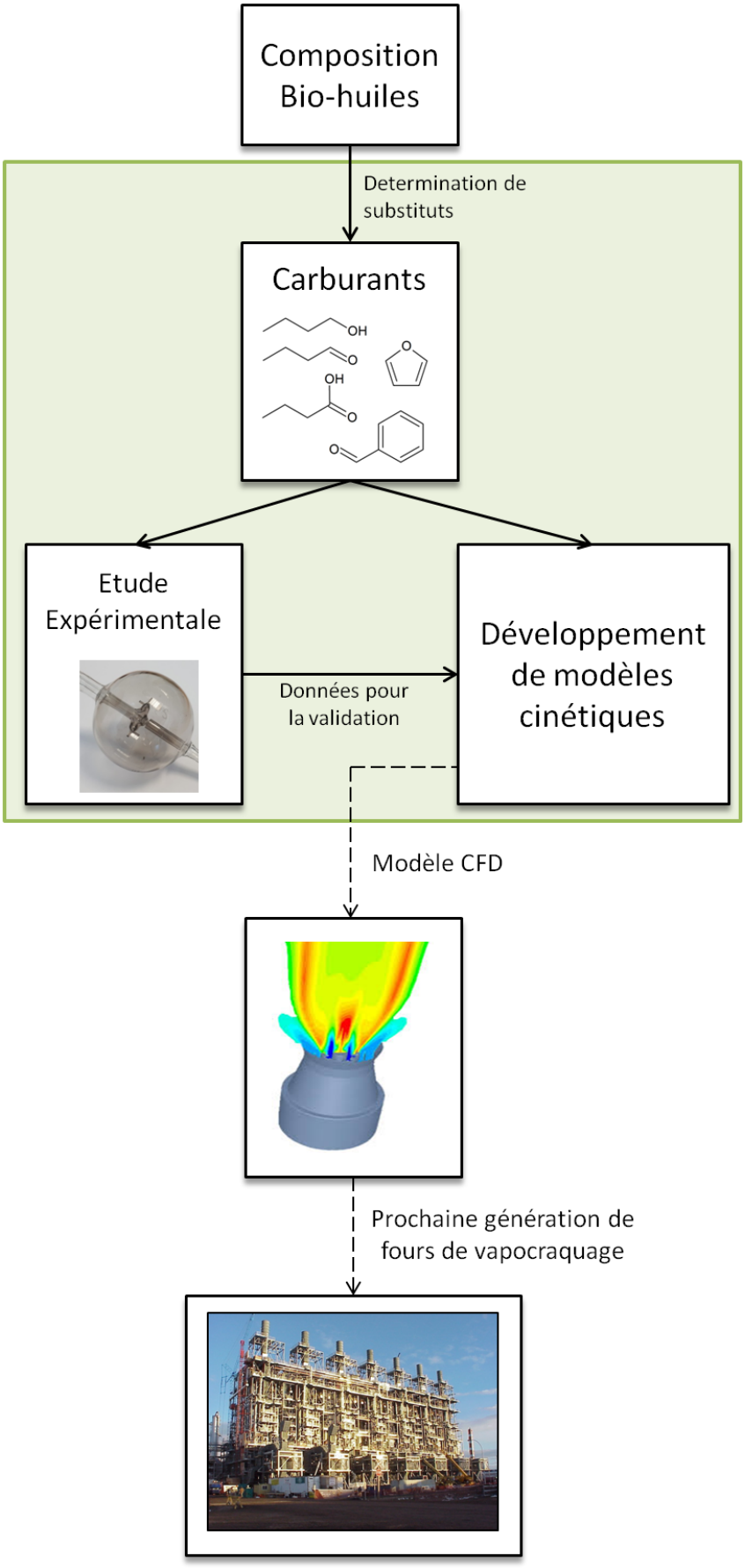

Figure : 7. Schéma de présentation du projet IMPROOF et du cadre de cette thèse

Il existe principalement deux façons de produire de la bio-huile à partir de la biomasse. La première est la liquéfaction sous pression de la biomasse afin d'obtenir de l'huile. Cette huile nécessite quelques étapes de purification supplémentaires pour isoler une fraction pouvant servir de combustible. L'autre façon est la pyrolyse de la biomasse. Avec ce second processus, trois produits principaux sont obtenus, comme le montre la Figure 8:

- Le coke ou charbon, qui est le résidu solide.
- Un gaz principalement composés de CO, CO_2, CH_4…
- Un liquide correspondant à la bio-huile.

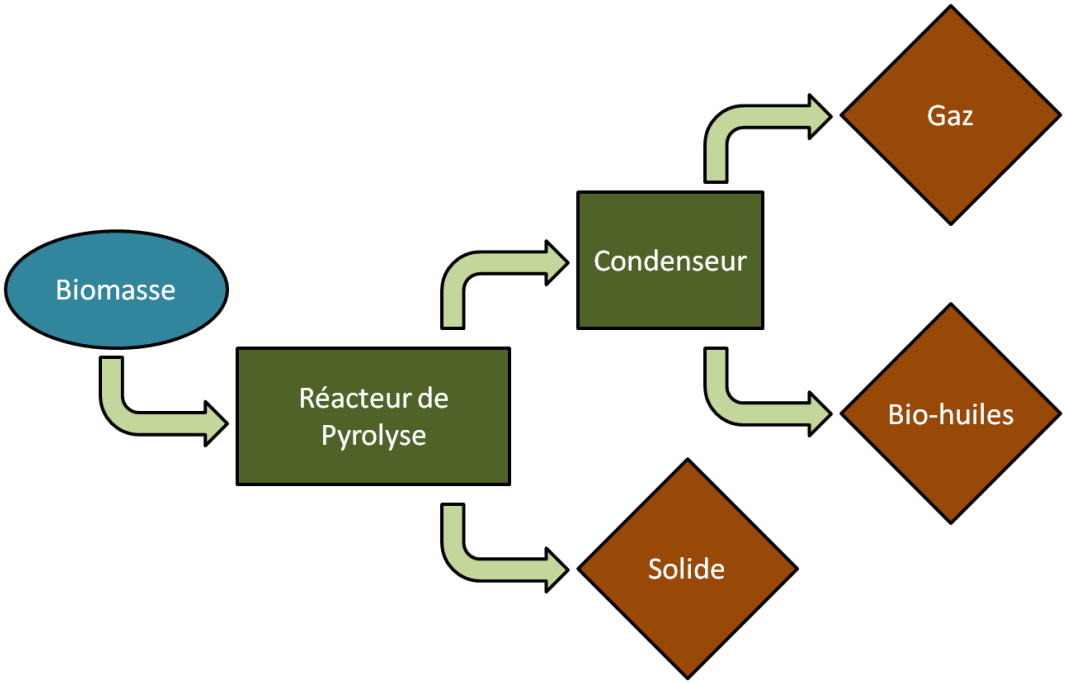

Figure : 8. Schéma de principe du procédé de pyrolyse de la biomasse (Guedes et al., 2018)

De nombreux auteurs ont tenté de caractériser les produits présents dans les bio-huiles, mais aucun n'a réussi à identifier leur composition complète. Leurs compositions complexes ne nous permettent pas encore de définir un substitut clair. La détermination de la composition de la bio-huile est toujours limitée par les outils analytiques, même si de nouvelles techniques sont maintenant disponibles (par exemple, la chromatographie en phase gazeuse bidimensionnelle). La composition de la biomasse d'origine est déterminante dans la composition finale autant que les conditions du procédé. Ainsi, dans le but de comparer les bio-huiles, chaque composant est classé parmi des familles chimiques. Cependant, il n'y a pas de classification unifiée, il a donc fallu en sélectionner une dans le cadre de cette thèse. La classification utilisée dans ce travail est la même que celle utilisée par Negahdar (2016). Elle contient trois principales familles de composés: les composés non aromatiques, les composés hétérocycliques et les composés aromatiques. Chacune peut être divisée en sous-familles chimiques. Cette méthode permet de comparer différentes huiles biologiques.

En utilisant la classification de Negahdar (2016) et les compositions de certaines bio-huiles de référence, la composition d'un mélange de substitution pour la bio-huile a pu être formulée. Ce substitut n'est pas composé d'espèces chimiques mais comprend des familles chimiques telles que les alcools ou les acides. Cette approche permet une meilleure flexibilité et permet de représenter chaque type de bio-huile existante. Pour

avoir la meilleure prédiction possible de la réactivité d'une bio-huile, notre substitut est composé de six familles chimiques différentes:

- Alcools et diols
- Aldéhydes et Cétones
- Acides carboxyliques
- Furane et dérivés
- Composés aromatiques oxygénés
- Composés azotés

En comprenant le comportement et la formation des produits de combustion de chaque famille, nous serons en mesure de mieux évaluer et de prédire la réactivité des bio-huiles. Notre composition de substitution est résumée graphiquement à la Figure 9.

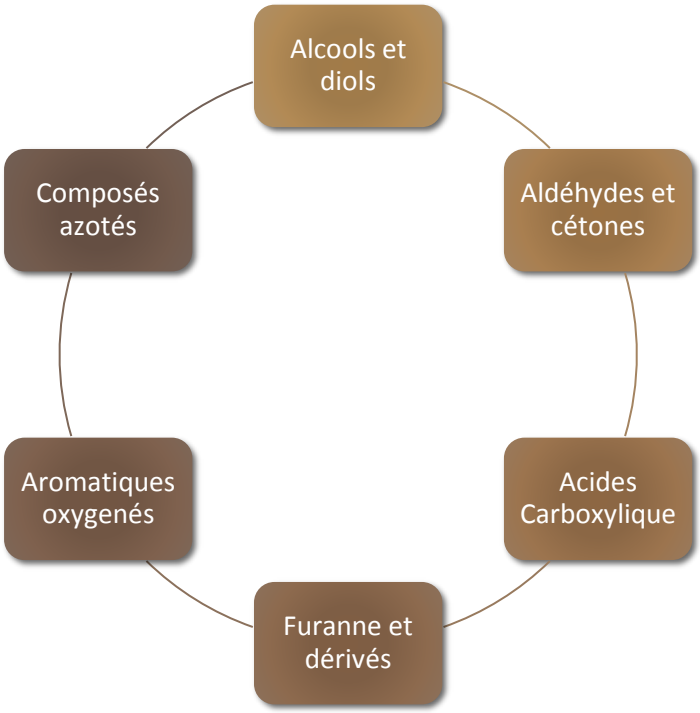

Figure : 9. Composition du substitut des bio-huiles.

Durant cette thèse, une revue de la littérature a été réalisée pour chaque famille. L'objectif était d'identifier les résultats expérimentaux et les modèles cinétiques déjà publiés et de détecter ce qui pouvait faire défaut pour une évaluation complète de la réactivité de ces composés. Cet état de l'art nous a aidés à sélectionner les composés pertinents à étudier par la suite.

De nombreuses études ont été trouvées dans la littérature au sujet de la combustion des alcools légers (à savoir l'éthanol ou le propanol) ou de petits aldéhydes (principalement l'acétaldéhyde), mais la combustion des composés les plus lourds, tels que le pentanol ou le pentanal, a beaucoup moins été étudiée. La décomposition de composés poly-oxygénés, tels que les acides carboxyliques ou les aromatiques, comme les aldéhydes aromatiques, a également été moins étudiées. Presque uniquement la pyrolyse de composés aromatiques oxygénés a été étudiée, avec un manque de données dans des conditions d'oxydation. Les connaissances sur les polluants formés et leurs voies de formation font notamment encore défaut.

Notre approche consistait donc à étudier chacune de ces familles en choisissant avec soin des composés représentatifs et à déterminer leurs comportements en combustion. Le présent manuscrit présente une étude approfondie dans un réacteur agité par jets gazeux avec des analyses par chromatographie en phase gazeuse de l'oxydation des alcools, des aldéhydes et des acides carboxyliques linéaires en C_4 à C_5, ainsi que celle du furanne et du benzaldéhyde. À notre connaissance, les études sur l'oxydation des acides carboxyliques et du benzaldéhyde ont été les toutes premières publiées.

Au cours de ce travail, huit combustibles ont été étudiés expérimentalement. Le Tableau 1 résume la liste des carburants étudiés et les conditions expérimentales associées.

Tableau 1. Liste des combustibles étudiés et des conditions expérimentales associées.

Nom	Structure	Formule	Conditions expérimentales
n-Butanol	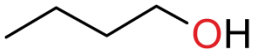	$C_4H_{10}O$	T=500-1100K, P=1 atm, φ=0,5-1-2
n-Pentanol	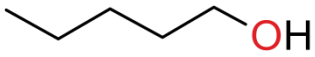	$C_5H_{12}O$	T=500-1100K, P=1 atm, φ=0,5-1-2
n-Butanal	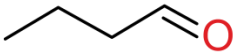	C_4H_8O	T=500-1100K, P=1 atm, φ=0,5-1-2
n-Pentanal	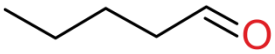	$C_5H_{10}O$	T=500-1100K, P=1 atm, φ=0,5-1-2
Acide butanoïque	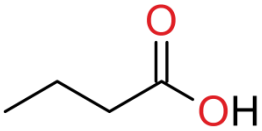	$C_4H_8O_2$	T=800-1100K, P=1 atm, φ=0,5-1-2
Acide pentanoïque	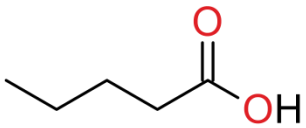	$C_5H_{10}O_2$	T=800-1100K, P=1 atm, φ=∞-0,5-1-2
Furanne	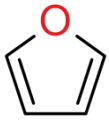	C_4H_4O	T=700-1100K, P=1 atm, φ=0,5-1-2
Benzaldéhyde	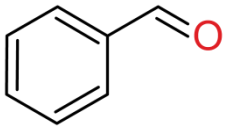	C_7H_6O	T=700-1100K, P=1 atm, φ=0,5-1-2

L'appareil expérimental utilisé et décrit à la Figure 10, est composé de 4 zones:

I: stockage du carburant liquide et contrôle du débit liquide

II: Contrôle des débits de gaz et chambre d'évaporation

III: préchauffage et réacteur

IV: Contrôle de la pression et chromatographes en phase gazeuse pour les analyses

La Figure 10 montre aussi les outils analytiques utilisés pour cette étude, quatre chromatographes en phase gazeuse.

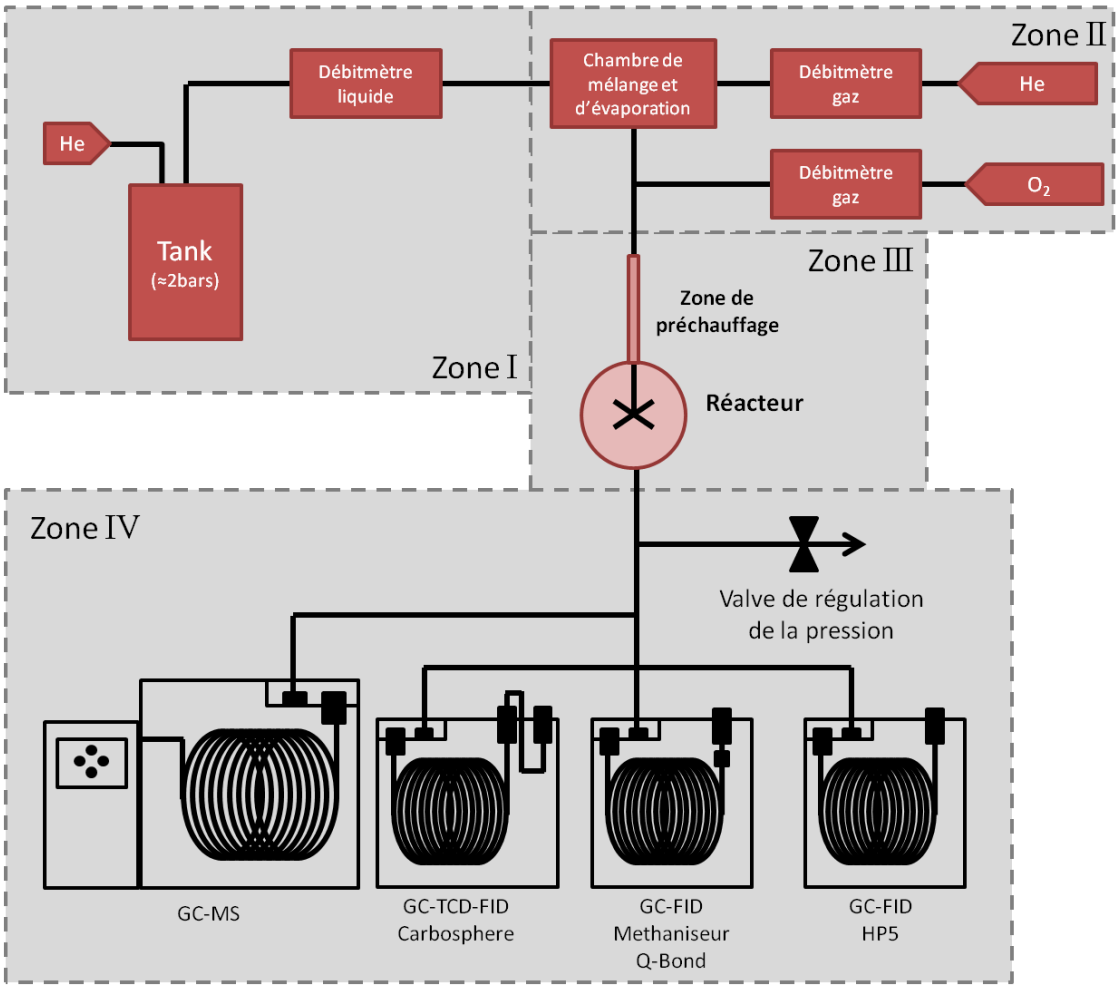

Figure : 10. Schéma de l'installation JSR utilisée dans cette étude

Le réacteur consiste en une sphère de silice fondue (volume 92 cm^3) équipée de quatre buses d'injection placées dans une croix située au centre de la sphère. La Figure 11 montre une image d'un réacteur agité par jets gazeux. Le gaz entre dans le réacteur par le tube de gauche et sort du réacteur par le tube de droite. Au centre, on distingue les quatre buses en forme de croix.

Figure : 11. Photo d'un réacteur à agité par jets gazeux. La buse d'injection en forme de croix est visible au centre du réacteur.

Le diamètre intérieur de chaque buse d'injection est d'environ 0,3 mm, ce qui entraîne la création de jets turbulents à l'intérieur de la sphère. Ce procédé d'injection assure une turbulence élevée dans le réacteur et conduit à une homogénéité des concentrations dans la phase gazeuse. Grâce à cette homogénéité, le réacteur peut être assimilé à un réacteur parfaitement agité fonctionnant en régime permanent en tenant compte de certains critères (Matras and Villermaux, 1973). Pour assurer l'homogénéité thermique, le réacteur isotherme est précédé d'une zone de préchauffage annulaire en quartz dans laquelle la température du gaz est augmentée jusqu'à la température du réacteur. Le gaz sortant du réacteur est ensuite transféré par une ligne chauffée métallique maintenue à 420 K à quatre chromatographes en phase gazeuse (CPG) pour analyser la vaste gamme de produits formés par les réactions.

L'étude sur le *n*-butanol et le *n*-pentanol a été la première réalisée dans le cadre de ce travail. Ces travaux ont montré que le *n*-butanol commençait à réagir vers 800 K et était entièrement consommé à 1050 K. Des températures similaires ont été observées pour la plage de température de réactivité du *n*-pentanol: 775-1050 K. Cette étude a également montré que les deux carburants ne présentaient pas de réactivité à basse température ou de zone avec un coefficient négatif de température (CNT), contrairement au *n*-butane ou au *n*-pentane. Parmi les 23 et 31 produits détectés respectivement lors de l'oxydation du *n*-butanol et du *n*-pentanol, l'aldéhyde et l'alcène associés ont été détectés pour les deux carburants. Ces résultats ont été utilisés pour développer un modèle cinétique basé sur le mécanisme CRECK (Ranzi et al., 1997; Granata et al., 2003; Ranzi et al., 2005). Le modèle était capable de reproduire la réactivité du carburant, mais a aussi prédit une petite zone de CNT pour le *n*-pentanol dans des conditions pauvre en carburant. Le modèle a également réussi à reproduire les profils de fraction molaire des principaux produits. Ce modèle a montré que la position α avait un rôle important dans la réactivité de la chaîne alkyle. En effet, la fonction alcool augmentait la réactivité à cette position, ce qui conduisait à la formation de produits spécifiques, tels que l'aldéhyde de même taille que le carburant associé.

L'oxydation du *n*-butanal et du *n*-pentanal a également été étudiée. Le *n*-butanal commençait à réagir à 600 K et était consommé aux alentours de 1075 K. Il ne montrait aucune réactivité à basse température, sauf dans des conditions faible en carburant et entre 575 et 700 K. Au contraire, le *n*-pentanal montrait une réactivité à basse-température pour toutes les conditions étudiées entre 650 et 725 K, dont l'ampleur était fonction de la richesse en oxygène. En effet, plus la teneur en oxygène était importante, plus la zone de CNT était ample. Dans l'ensemble, le *n*-Pentanal commençait à réagir à 575 K et était entièrement consommé à 1025 K. Cette différence de réactivité des deux molécules pourrait s'expliquer par la différence de longueur de leurs chaînes alkyle. 20 produits ont été détectés et quantifiés au cours des expériences d'oxydation au *n*-butanal et 29 produits pour le pentanal. Pour les deux carburants, une quantité importante de monoxyde de carbone a été observée parmi les produits d'oxydation. L'aldéhyde C_{n-1} a également été détecté parmi les produits des deux carburants. Au cours des expériences sur le *n*-pentanal, de l'acide pentanoïque a été détecté dans les produits, mais sa quantification a été limitée par sa très faible quantité dans le mélange. Un modèle cinétique a été développé pour reproduire la réactivité du carburant et mieux évaluer les voies de décomposition des aldéhydes linéaires. Ce modèle était capable de reproduire la conversion du carburant et en particulier la zone de CNT observée expérimentalement. Il en ressort que la formation importante de monoxyde de

carbone pourrait s'expliquer par une décarboxylation rapide des carburants, due à une réactivité importante de la position α. La formation d'autres produits spécifiques résultait de la réactivité de la chaîne alkyle. Le modèle a également prouvé que la longueur de la chaîne alkyle avait un impact important sur la réactivité des molécules. En effet, plus la chaîne alkyle était longue, plus l'influence de la fonction aldéhyde était faible.

Une étude a également été menée sur les acides butanoïque et pentanoïque. Cette étude était la première sur ces composés dans les conditions étudiées. Ce travail a été largement affecté par de nombreuses difficultés expérimentales. Les propriétés corrosives des acides ont décomposé certaines des gommes du système, ce qui a créé des problèmes d'obstruction dans le pilote. De plus, des problèmes d'adsorption pouvaient survenir en raison de la forte teneur en oxygène de ces molécules. Par conséquent, la quantification du carburant était complexe. Afin de réduire ce problème, un insert et une boucle d'échantillonnage avec un revêtement de surface ont été installés dans les chromatographes en phase gazeuse. La plage de température de réactivité de l'acide butanoïque se situait autour de 850-1000 K pour l'oxydation, sauf dans des conditions riches en carburant où la conversion complète n'a jamais été atteinte. En ce qui concerne l'acide pentanoïque, l'intervalle de réactivité était d'environ 850-975 K dans des conditions d'oxydation. Pour compléter cette étude, des expériences de pyrolyse ont été réalisées pour l'acide pentanoïque, mais certaines petites entrées d'oxygène inattendues ne permettent pas d'exploiter les données. L'analyse des produits de combustion des deux carburants a montré qu'une formation importante de dioxyde de carbone était observée par rapport à celle de monoxyde de carbone. Ainsi, il a été supposé que la fonction acide réagit pour donner du dioxyde de carbone. Néanmoins, le modèle cinétique développé a montré, contrairement à notre hypothèse, que la fonction acide n'était pas la principale position réactive. La réactivité était localisée sur la chaîne alkyle avec un fort effet inhibiteur de la fonction acide sur l'atome de carbone à proximité.

L'oxydation atmosphérique du furanne a également été étudiée. Le furane commençait à réagir à 800 K et était complètement consommé à 1050 K dans des conditions pauvres en carburant. Pour les conditions riches en carburant et stœchiométriques, un comportement instable a été observé pour des températures supérieures à 1000 K, mais on peut supposer que la conversion complète du carburant était atteinte dans ces conditions. Au cours de cette étude, 18 produits ont été identifiés, parmi lesquels l'acétaldéhyde et l'acroléine, deux des principaux produits. Les données expérimentales ont ensuite été comparées aux prévisions de deux modèles. Le premier modèle est celui développé par Tran et al. (2015a) et contenait un sous-mécanisme pour la description de la réactivité à basse température du furanne. L'autre modèle testé est le modèle CRECK, utilisé dans toute cette thèse pour les autres carburants. La prédiction globale de la conversion du carburant et de la formation des produits par le modèle de Tran et al. était bonne, alors que le modèle CRECK n'était pas capable de reproduire la réactivité à basse température. Mais on peut supposer que le modèle CRECK pourrait gérer la décomposition du furanne à basse température avec l'ajout du sous-mécanisme mis au point par Tran et al. (2015a) dans leur mécanisme global.

Concernant l'étude de l'oxydation des composés oxygénés aromatiques, le benzaldéhyde a été choisi comme molécule étudiée. C'est un combustible dont l'oxydation n'a été pas fréquemment étudiée et sa décomposition peut donner des indications sur la réactivité de composés aromatiques oxygénés plus grands. Le benzaldéhyde commençait à

réagir à 750 K et la conversion complète était atteinte à 1025 K. Au cours de sa décomposition, 48 produits ont été détectés. Les principaux sont le monoxyde de carbone, le phénol et l'acroléine. Le crésol et le dibenzofurane étaient également des produits importants dans des conditions riches en carburant. Un sous-mécanisme dédié à l'oxydation du benzaldéhyde a été développé pour reproduire les données expérimentales obtenues. L'hypothèse d'une décarboxylation rapide du carburant a été retenue. Le modèle était capable de reproduire la réactivité du carburant et la formation des produits principaux. Cependant, quelques différences sur les profils d'acétaldéhyde et de styrène ont été observées. L'analyse du modèle a également mis en évidence le fait qu'un cycle phénol / phénoxy régissait la réactivité du benzaldéhyde.

En parallèle du travail expérimental, des modèles cinétiques semi-détaillés ont été développés pour chaque composé. Chaque sous-mécanisme a été développé en fonction des résultats expérimentaux obtenus à Nancy et les performances du modèle y ont été comparées. Les sous-mécanismes développés pour les acides carboxyliques et le benzaldéhyde ont été les premiers développés spécifiquement pour reproduire la réactivité de ces composés.

Dans le cas des composés linéaires, grâce aux résultats du modèle, nous avons essayé de définir des règles cinétiques et des classes de réactions pour chaque famille et pour l'ensemble de ces familles chimiques. Leurs réactivités ont ainsi été comparées et il est apparu qu'aucune règle générale ne peut être établie. La meilleure hypothèse consiste à considérer chaque molécule comme composée d'un fragment spécifique oxygéné et d'un fragment alkyle. La réactivité de chaque fragment est régie par ses propres règles. Il pourrait être intéressant d'étudier l'extension de ce modèle à des molécules plus complexes, telles que des composés multi-substitués (tels que des diols ou des dials) ou à des fonctions spécifiques au cœur de la chaîne alkyle (comme par exemples des cétones ou des alcools secondaires)(voir la Figure 12).

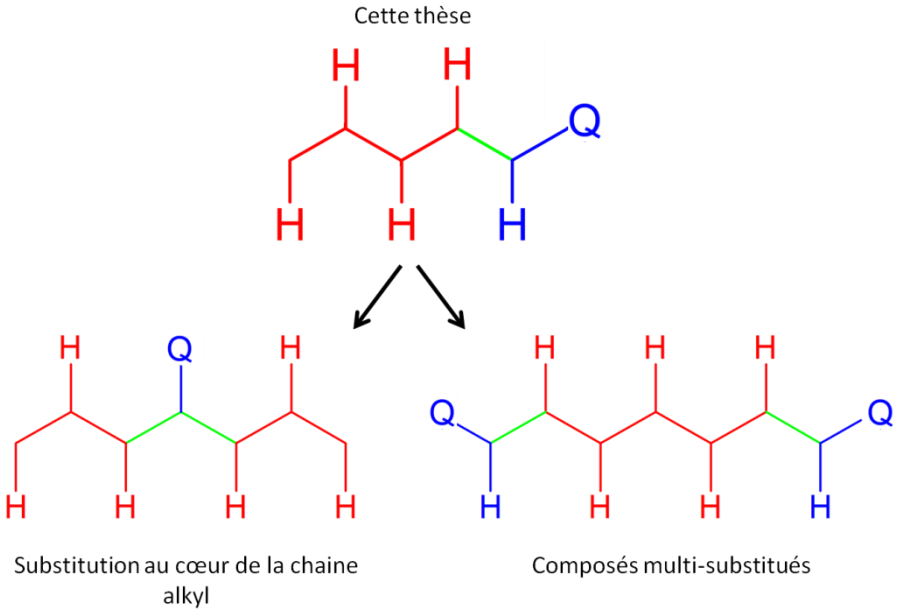

Figure : 12. Schéma du développement potentiel pour la représentation des composés substitués au cœur de la chaine ou multi-substitués.

Une perspective à plus long terme serait de créer un mélange synthétique des composés étudiés pour remplacer les bio-huiles de référence. Ces bio-huiles de référence devraient être étudiées grâce à la chromatographie bidimensionnelle pour définir leur

composition. Après cela, les résultats expérimentaux sur l'oxydation du mélange de substitution doit être comparée à ceux de la bio-huile. Il sera important de vérifier la concordance des résultats au niveau de la réactivité du mélange, mais aussi de la distribution des produits formés. Ensuite, les performances du modèle permettant de prédire la réactivité doivent être comparées aux résultats expérimentaux, afin de vérifier si une voie ou une interaction entre les composés est manquante. De plus, l'utilisation d'une CGxCG pourrait améliorer les résultats expérimentaux obtenus. On pourrait observer plus de produits et la distinction des isomères pourrait donner des informations importantes sur les voies de réaction. Malheureusement, cet appareil n'était disponible qu'à la toute fin de mon travail de thèse. La séparation du benzène et de l'un de ses isomères linéaires a montré la faisabilité de la méthode.

Dans le cadre du projet IMPROOF, ce travail avait aussi pour tâche de proposer une formulation de substituts pour les bio-huiles et une extension de la base de données expérimentale liée à ces composés. Sur la base du modèle cinétique développé au cours de cette thèse, une modélisation CFD avec une chimie assez détaillée sera réalisée et appliquée au futur brûleur des fours de craquage à la vapeur. Une évaluation de l'efficacité énergétique des bio-huiles et des émissions de polluants sera réalisée. Cependant, certaines propriétés physiques peuvent limiter l'utilisation de bio-huiles en tant que combustibles de fours de craquage à la vapeur. En effet la viscosité et l'acidité sont deux paramètres importants pouvant limiter leur utilisation à l'échelle industrielle. Le problème de la corrosion et les coûts d'investissement liés au transport des bio-huiles pourraient également constituer des obstacles trop importants à surmonter pour l'utilisation de bio-huiles comme combustibles.

Ce travail a conduit à la publication de trois articles évalués par des pairs:

- Les travaux sur l'oxydation des aldéhydes ont donné lieu à une publication dans le Proceedings of Combustion Institute: (Pelucchi et al., 2019. An experimental and kinetic modelling study of n-C_4C_6 aldehydes oxidation in a jet-stirred reactor. Proc. Combust. Inst. 37, 389–397.)
- Les travaux sur l'oxydation des acides carboxyliques ont été publiés dans le Chemical Engineering Journal: (Namysl et al., 2019. A first evaluation of butanoic and pentanoic acid oxidation kinetics. Chem. Eng. J. 373, 973–984.).
- L'étude sur l'oxydation du benzaldéhyde a été publiée dans le journal Combustion and Flame: (Namysl et al., 2019, Experimental and Modeling Study of Benzaldehyde Oxidation, accepté Septembre 2019).

TABLE OF CONTENTS

TABLE OF FIGURES

TABLE OF TABLES

I. INTRODUCTION

Energy is one of the fundamental pillars of the progress of humanity. Since the discovery of fire until the invention of nuclear power plant, the development of humanity has been led by its capacity to produce energy from different sources and mainly fossil ones. But nowadays producing energy in sufficient quantity without any environmental impact has become a prevailing question over brut energy production. Concerns are no more limited to quantity but rather to notions of quality. The programmed exhaustion of fossil stock along with the deterioration of the planetary ecosystem must lead to a new era of development and research of alternative eco-friendly and responsible solutions.

I.1. Context

In 2019 the worldwide population is estimated to be around 7.715 billion inhabitants by the United Nation, which is a 1 billion increase compared to 6.145 billion inhabitants in 2000 (United Nation et al., 2019). This important growth of the population leads to a more and more important demand in energy over the world and especially in the developing countries, such as China or India.

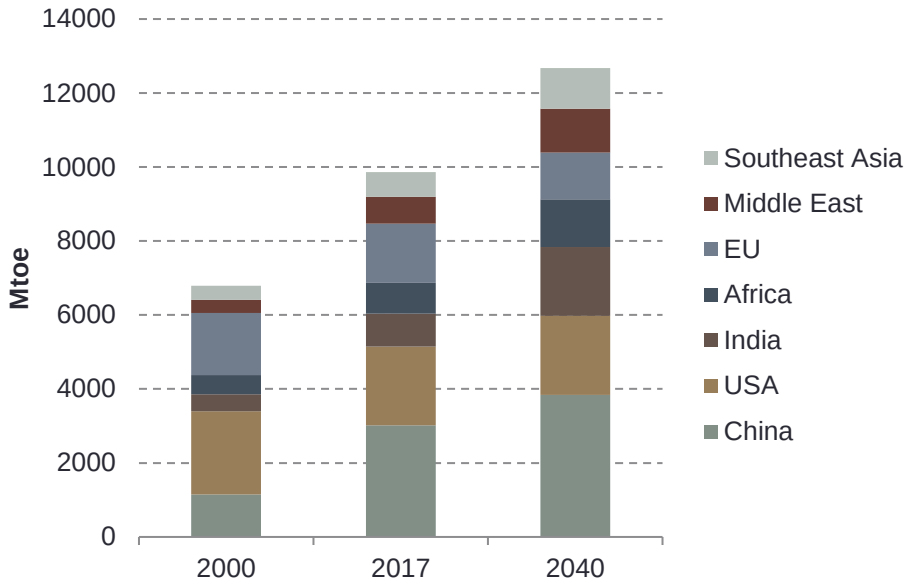

Figure 1. Energy demand over the years for different geographical area in Mtoe (Million tonnes of oil equivalent)(IEA, 2018b).

As shown in Figure 1, the International Energy Agency (IEA) estimates the world demand to grow from around 9000 Mtoe in 2017 to around 13,000 Mtoe in 2040, with an increase in almost every region of the globe (IEA, 2018b). In order to respond to the future world demand, two answers are possible: to increase the consummation of energy supply like fossil fuels or to develop new source of energy such as biofuels.

In 2016, fossil fuels represented about 80% of the world total primary energy supply, as shown in Figure 2. However, this resource is limited and has a huge impact on the environment pollution because of the production of greenhouse gases. So the development of new energy sources is essential to sustain the growth of the population and of the energy demand.

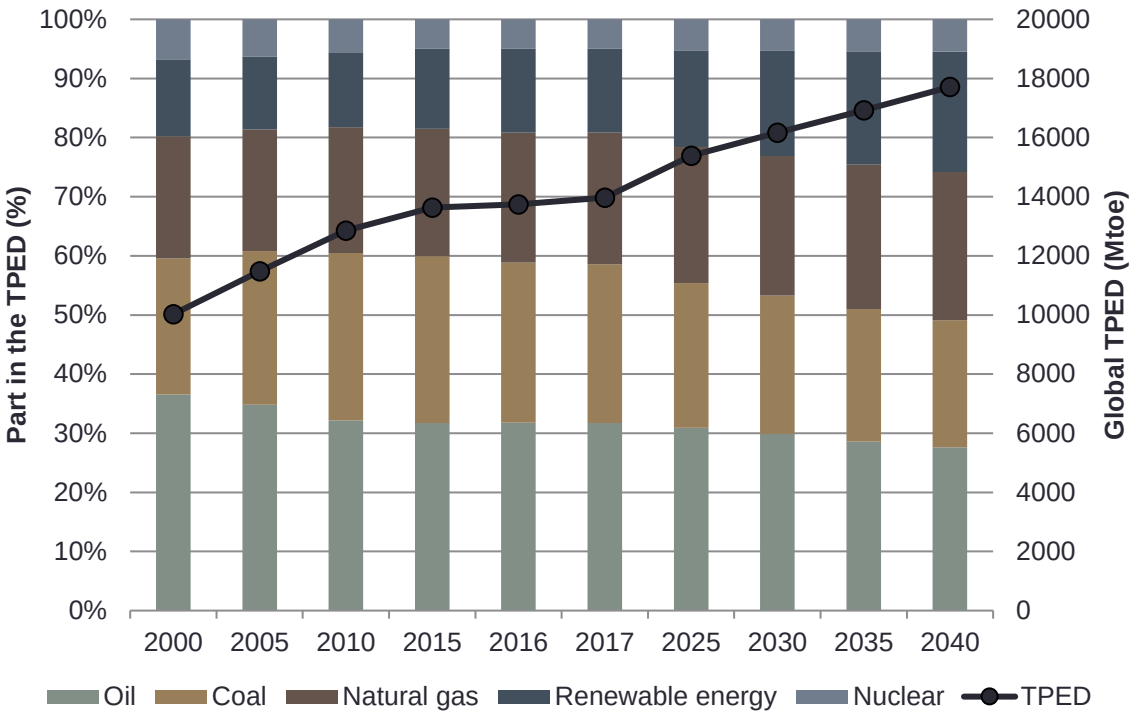

Figure 2. Total primary energy demand (TPED) by source over the years in Mtoe (Megatonnes of oil equivalents)(IEA, 2018a).

Figure 3 presents a more detailed overview of the different sources of renewable energy. The main source is bioenergy which correspond to energy generated from the conversion of solid, liquid and gaseous products derived from biomass. Its part in the energy mix is estimated to grow in the future years due to its immediate availibility and to the environmental concern. The category “Other” corresponds to the contribution of wind, solar panel, solar thermal and geothermal energy. The part of renewable energy is going to increase in the next years according to the IEA (IEA, 2019) and especially the one related to biomass. The other sources of renewable energy are also supposed to increase but in a lower extent than biomass.

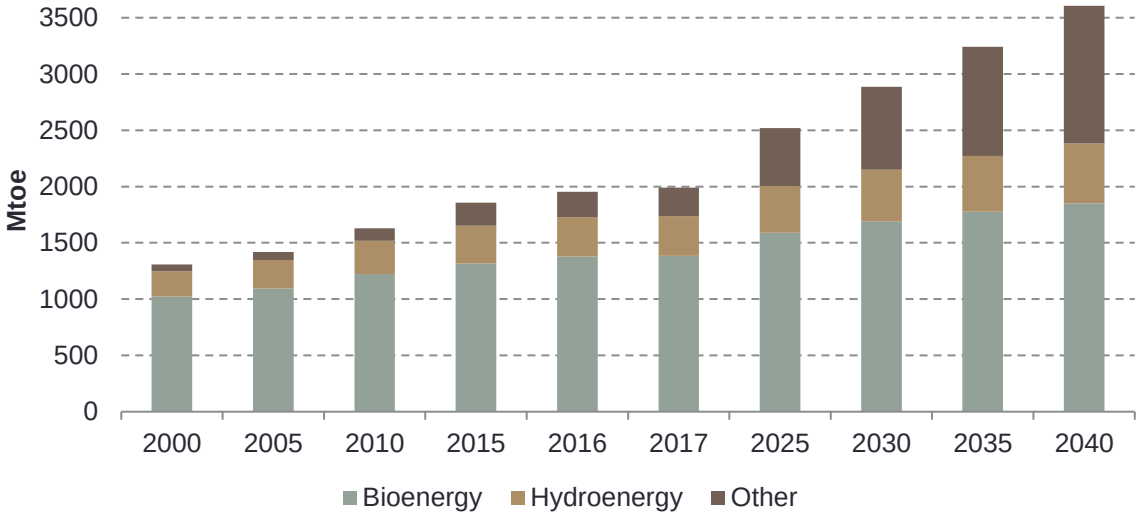

Figure 3. Source of renewable energy in Mtoe over the years (IEA, 2019).

In parallel of the problem of the energy demand, there is also that of the global warming and emissions of pollutants. The ecology and the environmental protection are more and more a concern for the future of energy. Many efforts have been recently performed to limit the emission of greenhouse gases and other pollutants. One of the main greenhouse gases is carbon dioxide, CO_2, which is mainly produced by one sector of activity: the industrial sector (see Figure 4) (IEA, 2018c).

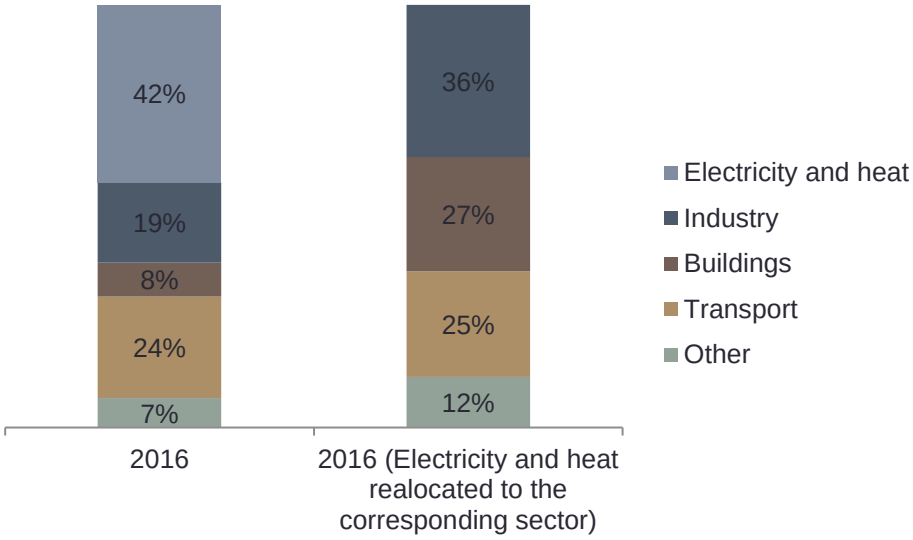

Figure 4. Global CO_2 emissions by sector in 2016 (IEA, 2018c).

The other sector that produced around 25% of the CO_2 emission is transportation. These both activities are also responsible for other pollutants emissions like nitrogen oxides (NO_x), sulfur dioxide (SO_2), particulate matter (PM) and especially fine particles, as shown in Figure 5 (IEA, 2018d).

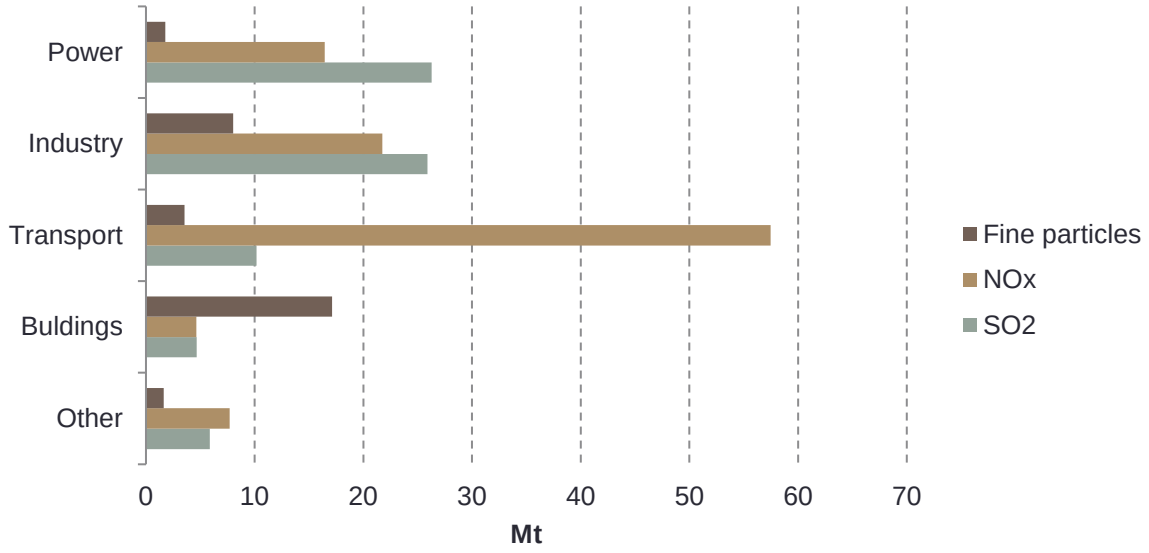

Figure 5. Emission of different pollutants in Millions tons (Mt) for different sectors in 2015(IEA, 2018d).

Thus, it is important and critical to reduce the impact of these two sectors by proposing alternatives to their actual operation. That is why a focus on biofuels is made in the industrial world and for transportation in order to drastically reduce CO_2 emissions. However, our knowledge about their impact on the emission of other pollutants, like NO_X, remains limited and need to be studied to validate biofuels as a sustainable replacement to actual energy suppliers.

I.2. Biomass: origin, production and composition.

Biomass can be defined as any organic matter, i.e. biological material, available on a renewable basis. It includes feedstock derived from animals or plants, such as wood and agricultural crops, and organic waste from municipal and industrial sources (IEA and FAO, 2017). Biomass sources can be sorted in three main categories depending on the original source: biomass from residues and waste, from forestry and from agriculture. Figure 6 presents the different sources described before and the types of biomass that can be produced from them.

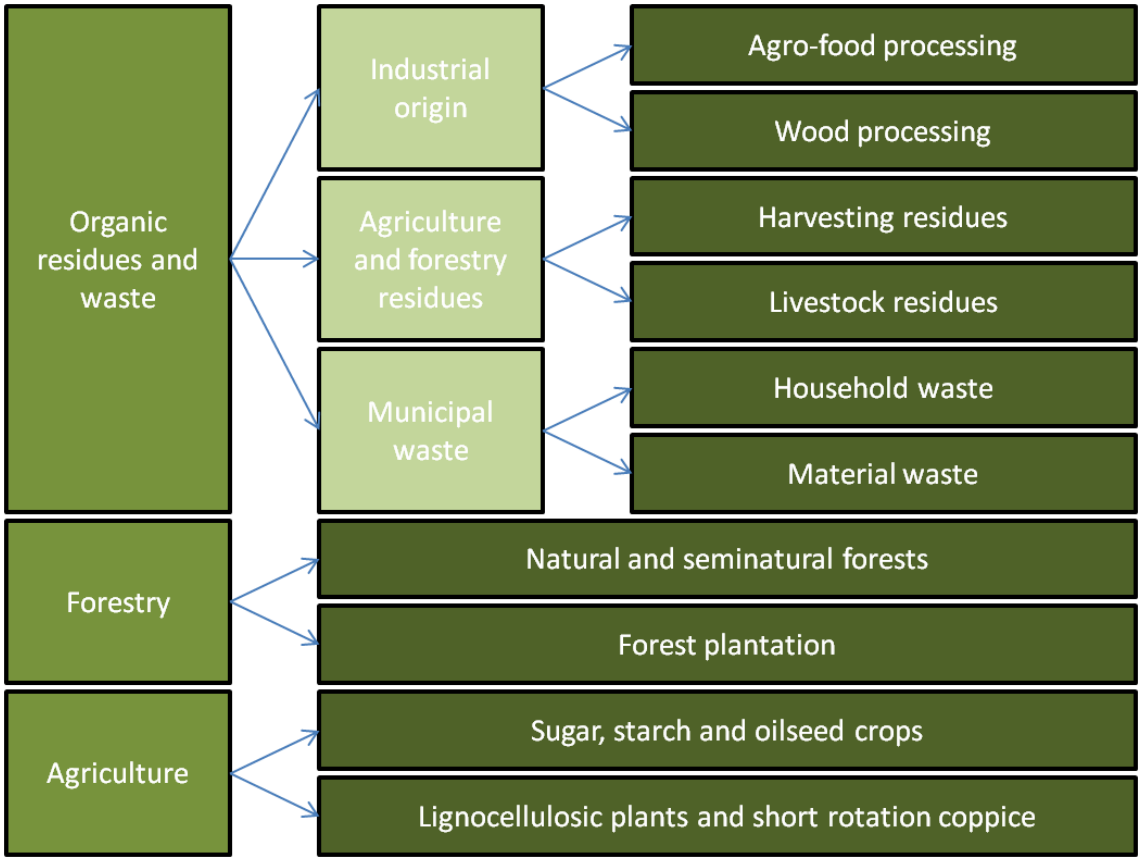

Figure 6. Biomass types according to origin (IEA and FAO, 2017).

Most of the final types of biomass among the 10 presented in Figure 6 come from vegetal sources, mainly composed of lignocellulosic matter (Chirat, 2017). This kind of biomass is composed of three polymers:

- Cellulose (around 50%)
- Hemicelluloses (30-20%)
- Lignin (20-30%)

Cellulose is composed of a linear polymer of glucose, as shown in Figure 7. It is the most abundant polysaccharide on earth with a global stock of 100 billion tons available. It is used in the paper industry and also in the pharmaceutical field for additive synthesis.

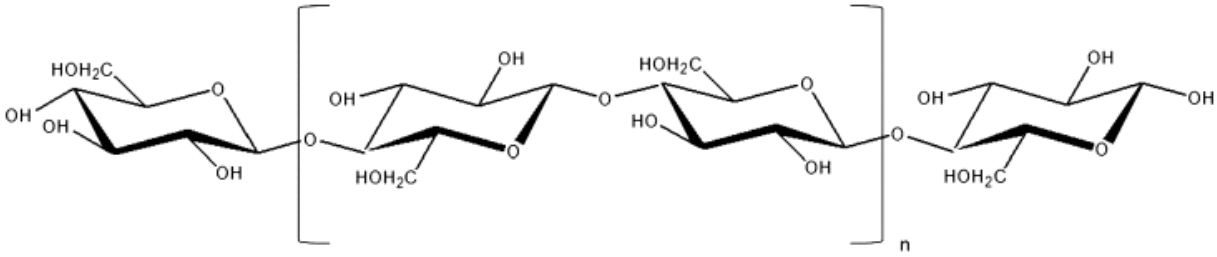

Figure 7. Structure of cellulose polymer (Chirat, 2017).

Contrary to cellulose, hemicelluloses are composed of different monosaccharides: hexoses and pentoses. The composition in hemicelluloses is very variable depending on the sources. The main sugars present in wood and forming hemicelluloses are represented in Figure 8.

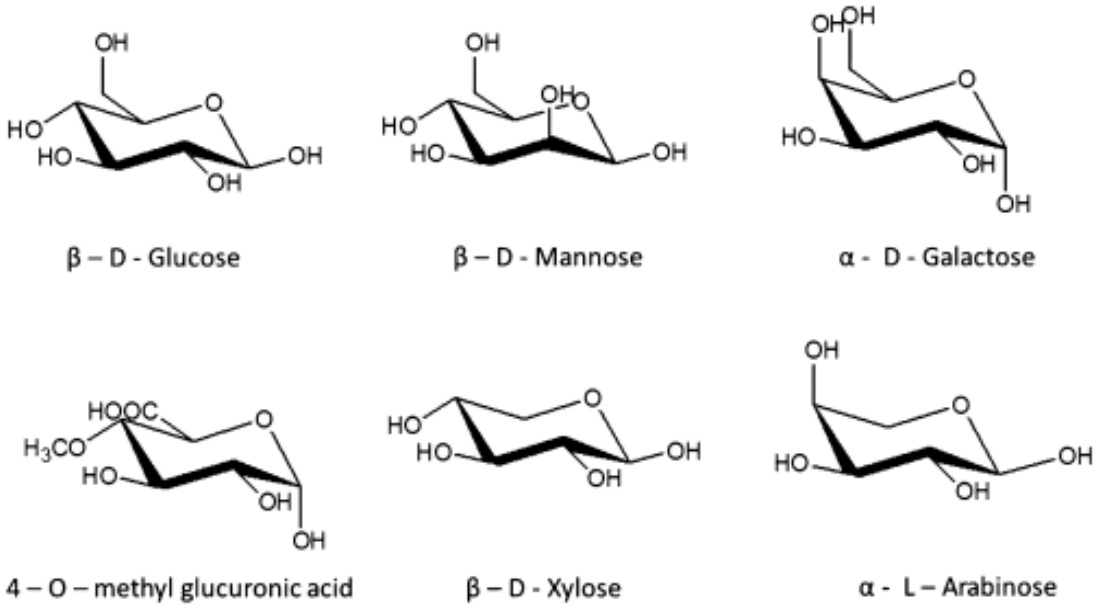

Figure 8. Monosaccharide molecules composing hemicelluloses (Chirat, 2017).

The last element composing vegetal biomass is lignin. Lignin is the second main compounds in wood and ensures the stiffness of any vegetal species structure. Lignin is composed of phenyl propane units linked together by ether bridges to form a complex polymer. It is the only component that can produce aromatic compounds similar to those produced by petrochemistry. Figure 9 presents an example of lignin structure, showing the presence of phenyl units.

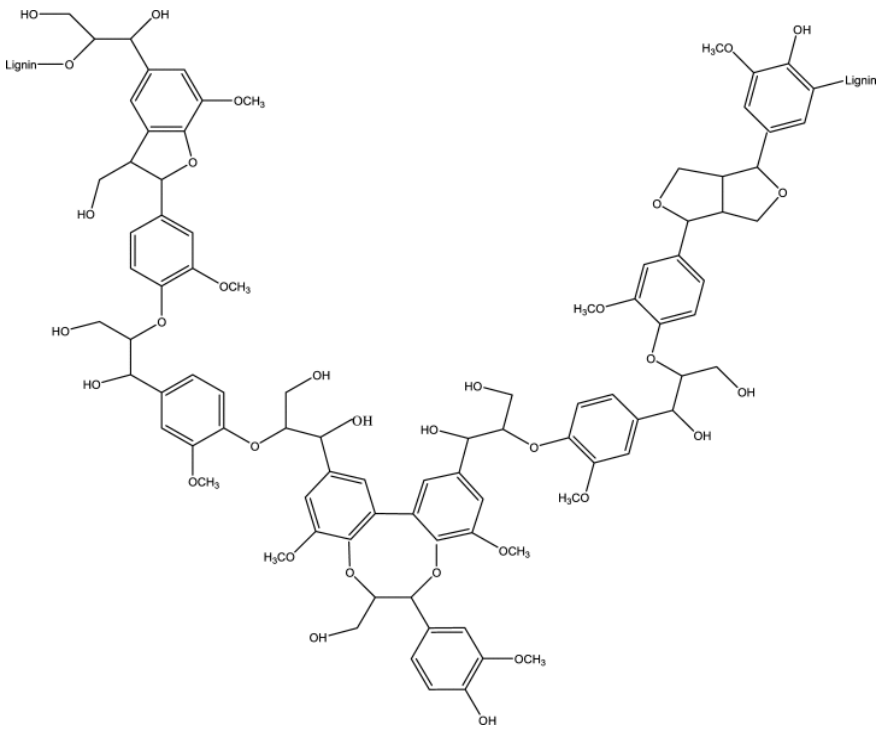

Figure 9. Example of structure representing lignin polymer (Chirat, 2017).

I.3. Biomass transformation

There are multiple ways to use biomass to produce energy (IEA and FAO, 2017). Some lead to the production of biofuels for transportation and other lead to the direct production of electricity or heat by combustion as shown in Figure 10. This figure also presents examples of process and products for different biomass feedstock.

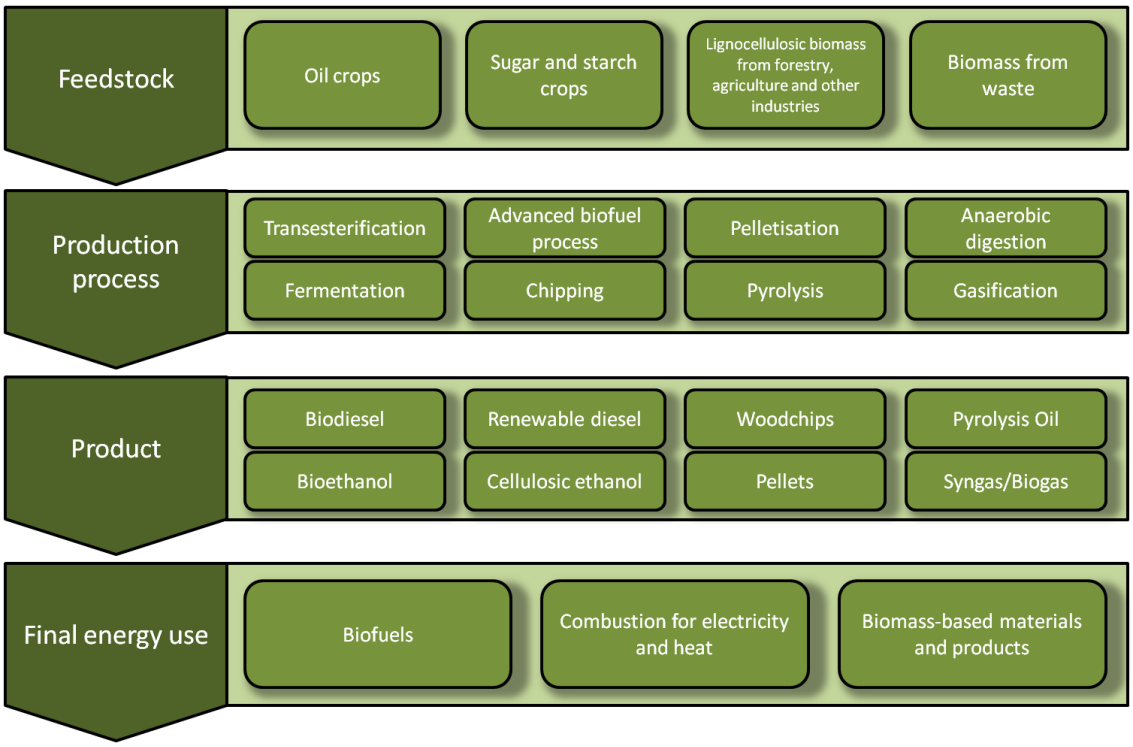

Figure 10. From biomass to energy : bioenergy pathways (IEA and FAO, 2017).

A part of biomass is also used to produce materials and products for industry or other fields.

Biomass can be directly used to produce heat by combustion, but it is often more interesting to use biomass as a source for other intermediates, that will be more energetically efficient. Bio-oil and biogas are two of these products, which can be used as fuels in the industrial world. It will help to decrease the consumption of fossil fuels and will also help to reduce drastically the CO_2 production of some facilities.

I.3.1. Biogas

Biogas is mainly produced by the anaerobic digestion process of biomass (Appels et al., 2008). The composition of biogas depends on the biomass source (see Table 1). It is primarily composed of methane and carbon dioxide. However it also contains smaller amounts of hydrogen sulfide and ammonia and is normally saturated with water vapor. Small amounts of aromatics and organo-chlorinated and –fluorated compounds can be found in biogas from household waste.

Biogas must be desulfurizated and dried before utilization to prevent corrosive damage. Since the sources of biogas anaerobic digestion are different, the methane composition derived from the biogas varies from 30-70% with content in hydrogen sulfide of 100-1000 ppm, and in ammonia of 5-100 ppm.

Table 1. Biogas and natural gas composition according to the source (Persson et al., 2006).

Components	Landfill gas	Digestion biogas	North Sea natural gas	Dutch natural gas
CH_4 % vol	45 (30-65)	63 (53-70)	87 (-)	81 (-)
Higher hydrocarbons % vol	0	0	12	3.5
CO_2 % vol	40 (15-50)	47 (30-50)	1.2 (-)	1 (-)
N_2 % vol	15 (5-40)	0.2 (-)	0.3 (-)	14 (-)
O_2 % vol	1 (0-5)	0 (-)	0 (-)	0 (-)
H_2 % vol	0-3	0	0	-
H_2S ppm vol	<100 (0-500)	<1000 (0-10^4)	1.5 (1-2)	- (-)
NH_3 ppm vol	5	<100	0	-
Total chlorine (as Cl^-) mg/m^3	20-200	0-5	0	-

The composition of biogas has a strong influence on its physical properties. The main difference by the comparison with natural gas is the lower heating value (high content of CO_2) and the larger density for biogas.

I.3.2. Bio-oil

There are mainly two ways to produce bio-oil from biomass. The first one is the liquefaction of biomass under pressure in order to obtain oil. This oil needs some additional purification steps to isolate a fraction which can be used as a fuel. The other way is the pyrolysis of biomass. With this second process, three main products are obtained as presented in Figure 11:

- Coke or char, which is the solid residue.
- Gases mainly composed of CO, CO_2, CH_4 …
- Liquids corresponding to the bio-oil.

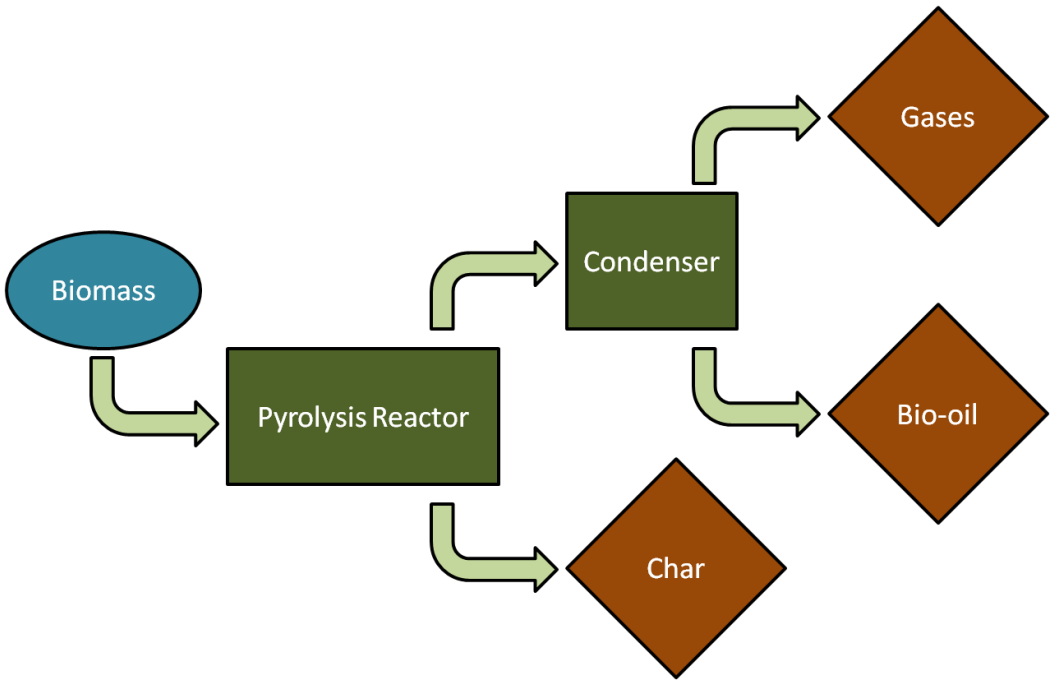

Figure 11. Schematic diagram for pyrolysis process (Guedes et al., 2018).

In order to maximize the production of oil, some parameters of the pyrolysis process have to be controlled. The first one is the pyrolysis final temperature. To maximize the production of oil, this temperature has to be set around 500°C (Onay and Kockar, 2003; Uzun et al., 2007). The second one is the heating rate (Onay and Kockar, 2003; Pütün et al., 2007). A heating rate of 300°C min^{-1} increases the production of oil compared to a rate of 30°C min^{-1}. Pyrolysis with this first value of heating rate is called “fast” pyrolysis. Temperature and heating rate are the two most significant parameters to maximize the production of bio-oil, but there are also other minor parameters to consider (origin of the biomass, particle size, flow rate and composition of sweeping gas, residence time…). Many processes already exist to produce bio-oil like Haloclean® or Fortum Otso®.

Some bio-oil compositions found in literature are compared below in Table 2. This Table presents several bio-oils: their biomass of origin and their production process, mainly fast pyrolysis. For some clarity, each bio-oil is described by a number. This number will be used in the next section. Bio-oil 10 was not produced by fast-pyrolysis, but it is still considered here due to the high number of compounds identified in this study.

Table 2. Summary of main bio-oil studies from the literature.

Reference	Type of biomass	Type of pyrolysis	Reaction Temp. (°C)	N°
(Oasmaa and Czernik, 1999)	Various[1]	Various	-	1
(Azargohar et al., 2013)	Saw dust	Fast pyrolysis	400-475-550	2
(Azargohar et al., 2013)	Flax straw	Fast pyrolysis	400-475-550	2
(Azargohar et al., 2013)	Poultry Litter	Fast pyrolysis	400-475-550	5
(Azargohar et al., 2013)	Wheat Straw	Fast pyrolysis	400-475-550	6
(Pütün et al., 2007)	Tobacco residue	Fast pyrolysis	550	3
(Abedi et al., 2015)	Unknown[2]	Unknown conditions		4
(Negahdar et al., 2016)	Wheat Straw	Fast pyrolysis	480	7
(Negahdar et al., 2016)	Pinewood	Fast pyrolysis	500	8
(Djokic et al., 2012)	Pinewood[3]	Fast pyrolysis	Unknown	9
(Bertero et al., 2012)	Pinewood	Conventional pyrolysis	550	10

I.4. Bio-oil description

This section is dedicated to the description of bio-oils by considering their properties and their compositions.

I.4.1. Bio-oil properties

A bio-oil is not only described by its chemical composition but also by its physical properties. The aim is to obtain bio-oils with the same properties as a petroleum fuel or even better. The physical properties of oils are described in several publications (Oasmaa and Czernik, 1999; Zhang et al., 2007; Bertero et al., 2012; Azargohar et al., 2013; Abedi et al., 2015). Basic data about bio-oils and petroleum fuels were extracted from these later publications and are presented in Table 3.

The data given in Table 3 are presented in the form of a range of values because these properties are actually significantly dependent on the type of biomass and pyrolysis process used. The composition in cellulose, hemicelluloses and lignin for vegetal biomass or the protein fraction in animal biomass is directly responsible for some oil characteristics, such as viscosity or heating value. Biomass with a high content of lignin or protein has a higher viscosity. Furthermore, for a same amount of lignin in the biomass, the viscosity of the oil increases with the pyrolysis temperature (Azargohar et al., 2013). For this reason, it is hard to characterize precisely a bio-oil. However, a general trend can be observed: the bio-oils have a larger content of water, which lowers their High Heating Value (HHV), compared to petroleum fuels. So, this high amount of water reduces their thermal efficiency, but it also

[1] About 150 Samples of oil were used
[2] Provided by Biomass Technology Group (BTG-BTL), The Netherlands
[3] Data presented in this work are extracted from the crude bio-oil results

reduces the viscosity of bio-oil. The difference in viscosity and in pH can also lead to problems in combustion devices, such as corrosion or tube-obstruction. The Department of Energy of the USA published some recommendations for materials that are corrosion resistant (DOE, 2019). These problems involve that a crude bio-oil is never a good fuel, but many solutions exist (Bertero et al., 2012; Zhang et al., 2007) to improve the bio-oils as fuels, like thermal treatment or hydrodeoxygenation.

Table 3. Typical properties of pyrolysis bio-oil and petroleum fuels.

Physical property	Bio-oil 1 (Oasmaa and Czernik, 1999)	Bio-oil 2 (Azargohar et al., 2013)	Gasoline (Guibet, 1997)	Diesel (Guibet, 1997)
Water (wt %)	15-30	13-38	-	-
Density at 25°C(kg/L)	1.1-1.3	0.9-1.2	0.74	0.84
Viscosity (40-50°C) (cP)	40-100	24-418	0.7	7.6
pH[4]	2-3.7	-	-	-
High Heating Value (MJ/kg)	16-19	20-34	≈40	≈40
Total acid number (mg KOH/ g)	50-100	40-150	-	-

I.4.2. Bio-oil composition (elemental and chemical)

The first point in the chemical comparison between different fuels is the elemental composition. There are indeed official regulations on them: for example, the sulfur content is limited in the fuels used in engines. The elemental composition can give some clues about the pollutants that the fuel can produce during combustion processes. Table 4 presents some elemental composition from literature for bio-oils and petroleum-based fuels.

Table 4. Elemental composition of some bio-oils (see Table 2 for original biomass and production process) and petroleum-based fuels.

Element	Bio-oil 1 (Oasmaa and Czernik, 1999)	Bio-oil 2 (Azargohar et al., 2013)	Bio-oil 3 (Pütün et al., 2007)	Bio-oil 4 (Abedi et al., 2015)	Gasoline (Guibet, 1997)	Diesel (Guibet, 1997)
C (wt %)	32-49	60-76	66.02	45.83	83	85
H (wt %)	6.9-8.6	6-13	8.5	7.15	16	14
O (wt %)	44-66	10-30	27.76	46.15	<1	<1
N (wt %)	<0.2	0.4-10	3.02	0.87	<1	<1
S (wt %)	<0.05	<0.3	-	-	<0.03	0.05

Bio-oils show many differences with petroleum fuels. The carbon content in bio-oils is indeed lower than that in petroleum fuels, but the oxygen content is higher for bio-oils. Some bio-oils have also particularly higher nitrogen content than petroleum fuels, which can lead in the case of combustion to a higher production of NO_x. However, the amount of sulfur is very low for oils, which is an advantage compared to petroleum-based fuels for combustion.

For the different bio-oils, the elemental composition changes with the type of biomass of origin. The carbon content in bio-oils is not constant: for example it is around 40% for bio-oil 1 and 66% for bio-oil 3 of Table 4. The same observation can be made with the

[4] pH does not apply to fuel free of water, such as gasoline and diesel

proportion of oxygen and nitrogen. The amount of hydrogen is however almost constant around 7% in weight and the proportion of sulfur can often be considered as negligible. These differences in the elemental composition can also be seen in the chemical composition of the biomass of origin. Woody biomass presents a higher lignin content than that from wheat shell for example (Bertero et al., 2012). This initial composition impacts directly the final composition of the bio-oil due to the chemical differences between cellulose, hemicellulose and lignin. Furthermore, in the case of oils from animal biomass, the composition is totally different from a vegetal one, because they also contain proteins.

Many authors tried to characterize bio-oils, but none succeeded in identifying their entire composition. Bio-oils can present a very large spectrum of components; thus, with the goal of comparing bio-oils, every component is classified among chemical families. However, there is no unified classification, so one needs to be chosen. The classification used in this work is the same as the one used by Negahdar (2016). It contains three basic families of compounds: non-aromatic compounds, heterocyclic compounds and aromatic compounds. Each one can be divided in chemical subfamilies. This method allows to compare different bio-oils. Table 5 presents a comparison of the composition of three bio-oils.

Table 5. Comparison of the composition of three bio-oils in weight % (see Table 2 for original biomass and production process).

Type of bio-oil	**Bio-oil 5** (Azargohar et al., 2013)	**Bio-oil 6** (Azargohar et al., 2013)	**Bio-oil 7** (Negahdar et al., 2016)
Non-aromatic compounds			
Alcohols	4.5	-	0.32
Carboxylic Acids	3.7	2.8	4.85
Aldehydes	-	5.5	1.48
Ketones	-	1.2	4.94
Ethers	-	-	-
Hydrocarbons	-	-	-
Nitrogen-containing compounds	-	-	-
Esters	-		0.06
Heterocyclic compounds			
Furans	-	-	0.72
Pyrans	-	-	0.07
Carbohydrates	-	-	0.04
Other	-	-	1.27
Non-aromatic Hydrocarbons	-	-	0.05
Non-aromatic Nitrogen-containing compounds	13.6	-	-
Aromatic compounds			
Hydrocarbons	-	-	-
Oxygenated Compounds	-	-	0.86
Aldehydes	-	-	0.07
Phenols	14.7	13	1.11
Benzenediols	-	-	0.54
Phenol Derivatives	-	-	0.88
Nitrogen-containing compounds	-	-	-
Mass of bio-oil identified in weight %	36.5	22.5	17.3

Figure 12 graphically summarizes the information presented in Table 5. The percentage of bio-oil not identified is always more than the half of the global mass and the

"known" part is divided in many chemical subfamilies. Bio-oil 7 has a lower content in aromatic compounds compared to the other oils and especially for the phenols. Only bio-oil 5 includes non-aromatic heterocyclic nitrogen-containing compounds. It is the only one produced from an animal biomass. The nitrogen atoms come mainly from the proteins present in the original biomass. This shows how the chemical composition of oil strongly depends on the biomass origin. This also well shows the complexity of a bio-oil in terms of composition.

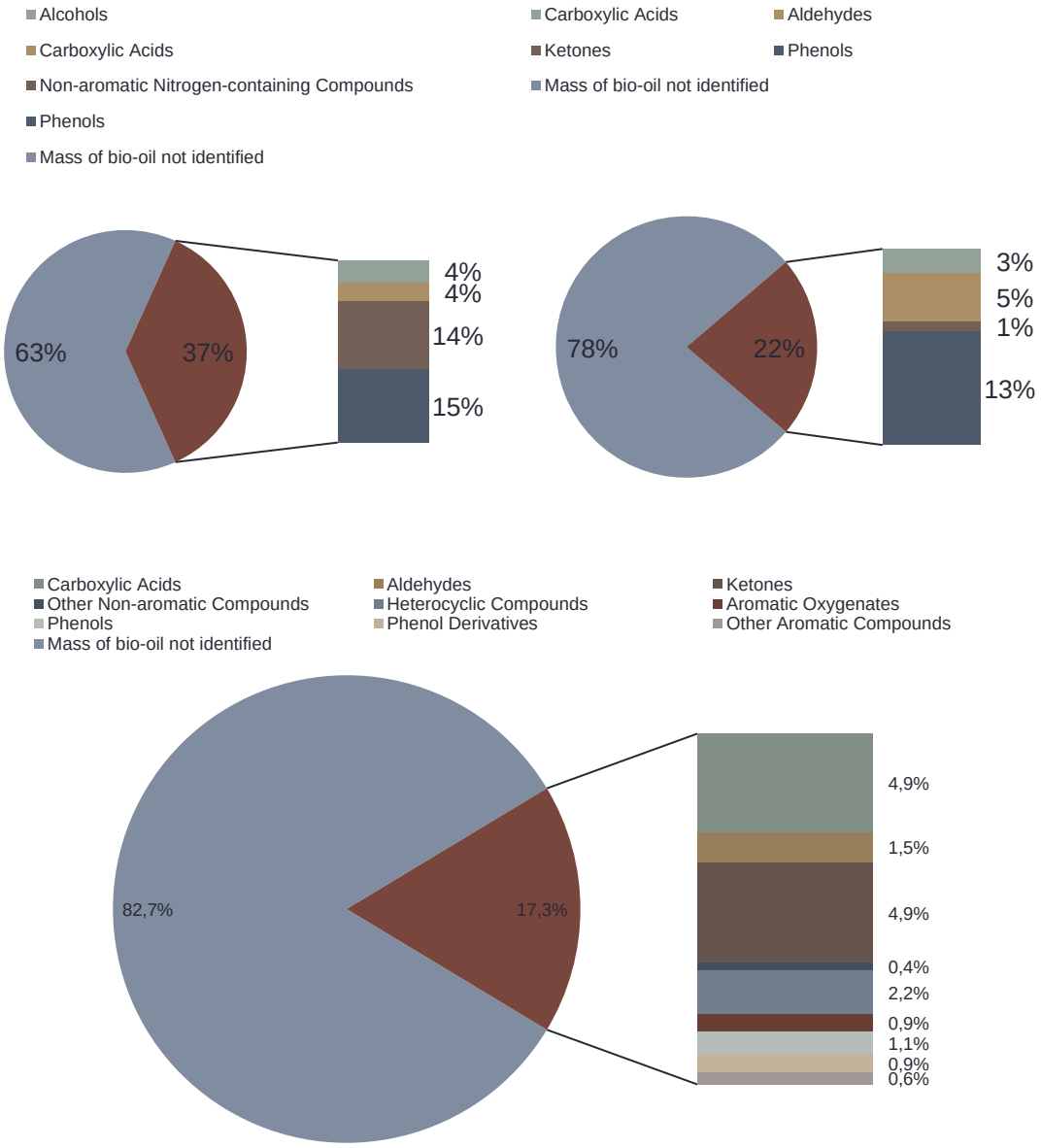

Figure 12. Graphical summary of the data shown in Table 5. Comparison of the composition of three bio-oils in weight % (top left: Bio-oil 5, top right: Bio-oil 6 and bottom: Bio-oil 7).

Even with the same type of biomass of origin, the composition of the oil can change a lot. The process parameters, such as the temperature of pyrolysis, have indeed some impact on the decomposition chemistry of the biomass. Table 6 presents a comparison between three different oils coming from the same type of biomass (pinewood) but produced by three different installations of pyrolysis. Two installations are fast pyrolysis pilots and the third one is a conventional pyrolysis set-up (more process condition data are given in Table 2). These oils were investigated in three different studies.

Table 6. Comparison of the composition of three bio-oils derived from the same type of biomass (in weight %).

Type of bio-oil	**Pinewood**		
	Bio-oil 8 (Negahdar et al., 2016)	**Bio-oil 9** (Djokic et al., 2012)	**Bio-oil 10** (Bertero et al., 2012)
Non-aromatic Compounds			
Alcohols	0.27	0.217	9.15
Carboxylic Acids	4.9	3.036	18.71
Aldehydes	2.82	5.158	4
Ketones	2.39	1.482	19.63
Ethers	-	-	0.31
Hydrocarbons	-	-	0.8
Nitrogen-containing Compounds	-	-	0.86
Esters	0.21	-	8.29
Heterocyclic Compounds			
Furans	1.62	0.676	5.95
Pyrans	0.24	-	1.49
Carbohydrates	0.08	3.075	1.01
Other	7.05	-	1.42
Non-aromatic Hydrocarbons	-	-	-
Non-aromatic Nitrogen-containing Compounds	-	-	0.31
Aromatic Compounds			
Hydrocarbons	-	-	-
Oxygenated Compounds	0.27	-	-
Aldehydes	0.08	-	-
Phenols	0.3	-	5.41
Benzenediols	0.9	1.111	-
Phenol Derivatives	1.47	-	10.33
Nitrogen-containing Compounds	-	-	0.35
Mass of bio-oil identified in weight %	22.6	14.8	88.0

The three bio-oils have different composition specificities and it can be observed that more components have been identified for bio-oil 10 than for bio-oil 8 and 9. Also each study did not reach the same percentage of identified mass, which can explain some differences between the results. The compositions diverged on the amount of some components: the content of carboxylic acids, ketones and phenol derivatives is much higher in the bio-oil 10. The results can be summarized in terms of large chemical families: non-aromatic, heterocyclic and aromatic compounds, as presented in Figure 13.

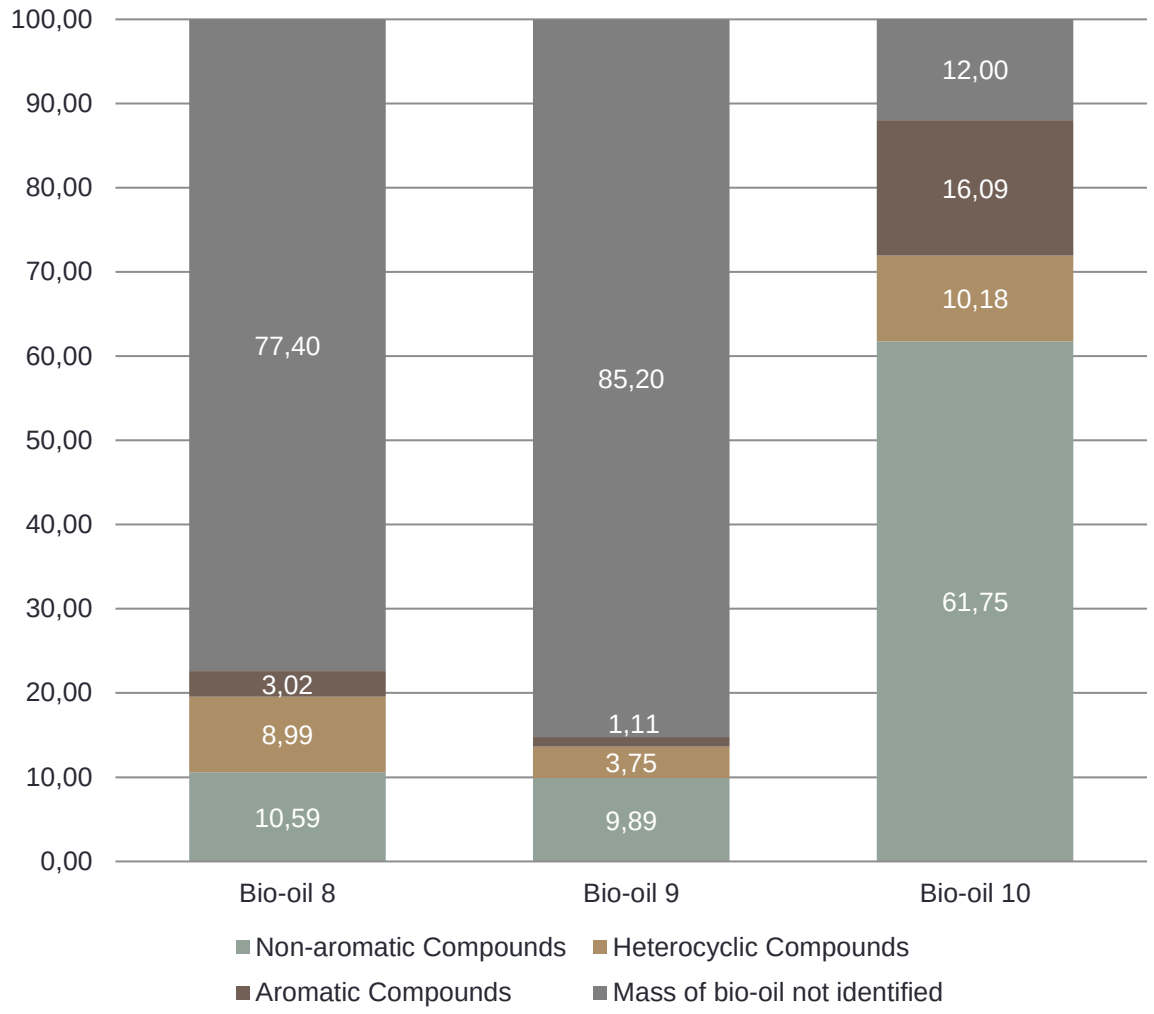

Figure 13. Summary of the data presented in Table 6. Comparison of the composition of three bio-oils derived from the same type of biomass (in weight %).

For each study, the bio-oil is mainly composed of non-aromatic compounds (as far as the identified part is concerned). For the bio-oils 8 and 9, the amount of aromatic compounds is the lowest fraction, whereas bio-oil 10 presents almost as much aromatic species as heterocyclic compounds.

In summary, the composition of a bio-oil is a very complex mixture of chemical species. The composition is influenced by many parameters like the type of biomass used or the pyrolysis conditions. Some studies have detected and identified around 200 compounds in bio-oils, but this represents only 17% to 22% of the global mass (Negahdar et al., 2016). So a large part of the bio-oil composition is not known yet. However, considering the identified fraction of the bio-oils, the chemical composition can be known and described using chemical families. This is why many proposed surrogates of bio-oils are mainly based on this composition in terms of chemical families rather than on the chemical distribution directly. It is assumed that the global composition in terms of families of the identified part is representative of the whole bio-oil.

I.5. Objectives of the PhD

The IMPROOF project is funded by the European Union under the Spire framework (Djokic et al., 2017). Its objective is to improve the energy efficiency in the case of steam cracking furnaces by 20% and in parallel to decrease by 25% per ton of ethylene the emission of pollutants like NOx or greenhouse gases. The consortium gathers 11 entities from 6 different countries, including 7 industrial partners which give this project a specific industrial orientation.

To reach the objectives the project has been focused on three improvements:

- The development of a new design and materials for the coils used in the furnace: The use of new 3D design for the coils with new materials will prevent the formation of coke at the surface of the reactor. The minimization of this layer will help to reduce the formation of CO_2 during the cracking. The new design will also help to optimize the heat transfer at the wall.
- The implementation of high emissivity coating on the wall of the furnace: In order to reduce the consumption of fuel in the furnace, new coatings with high emissivity have been studied. They will help to recover a part of the heat and so lower fuel consumption to reach the same temperature.
- The use of alternative and renewable fuels like biogas and bio-oil: to decrease the CO_2 impact of the steam cracking furnaces, the use of renewable fuel produced from biomass has been considered. These fuels can be biogas or bio-oil and will decrease the net CO_2 production of the plant.

Combinations of laboratory studies, simulations and industrial pilots have been set in place to test and validate the results of each improvement proposition. This PhD is focused on the part concerning alternative fuels and especially bio-oils. The first task was to define a surrogate for bio-oils using the data presented in this chapter. Using the classification proposed by Negahdar (2016), six chemical families were selected. Then an experimental database of the surrogate combustion products obtained in a jet-stirred reactor has been established. This database was then used for the development and validation of detailed kinetic models in order to reproduce the fuel combustion. Simulations of the obtained results were performed in collaboration with the team of Prof. Faravelli at Politechnico di Milano.

This manuscript will be divided in different parts:

- The first chapter presenting a state of the art of molecules selected as surrogate or from the same chemical family.
- The second chapter is a description of the experimental set-up and of the analytical tools used in the present work to obtain experimental data.
- The third chapter will be dedicated to the presentation of the experimental results obtained for the linear oxygenated molecules and of the models developed.
- The fourth chapter will present the study of the cyclic oxygenated fuels and of their kinetic models.
- A conclusion summarizing the achievements and limitations of the present work as well as perspectives and recommendations for future studies in this field.

Figure 14 presents a scheme of the IMPROOF project and the place of this work within its framework.

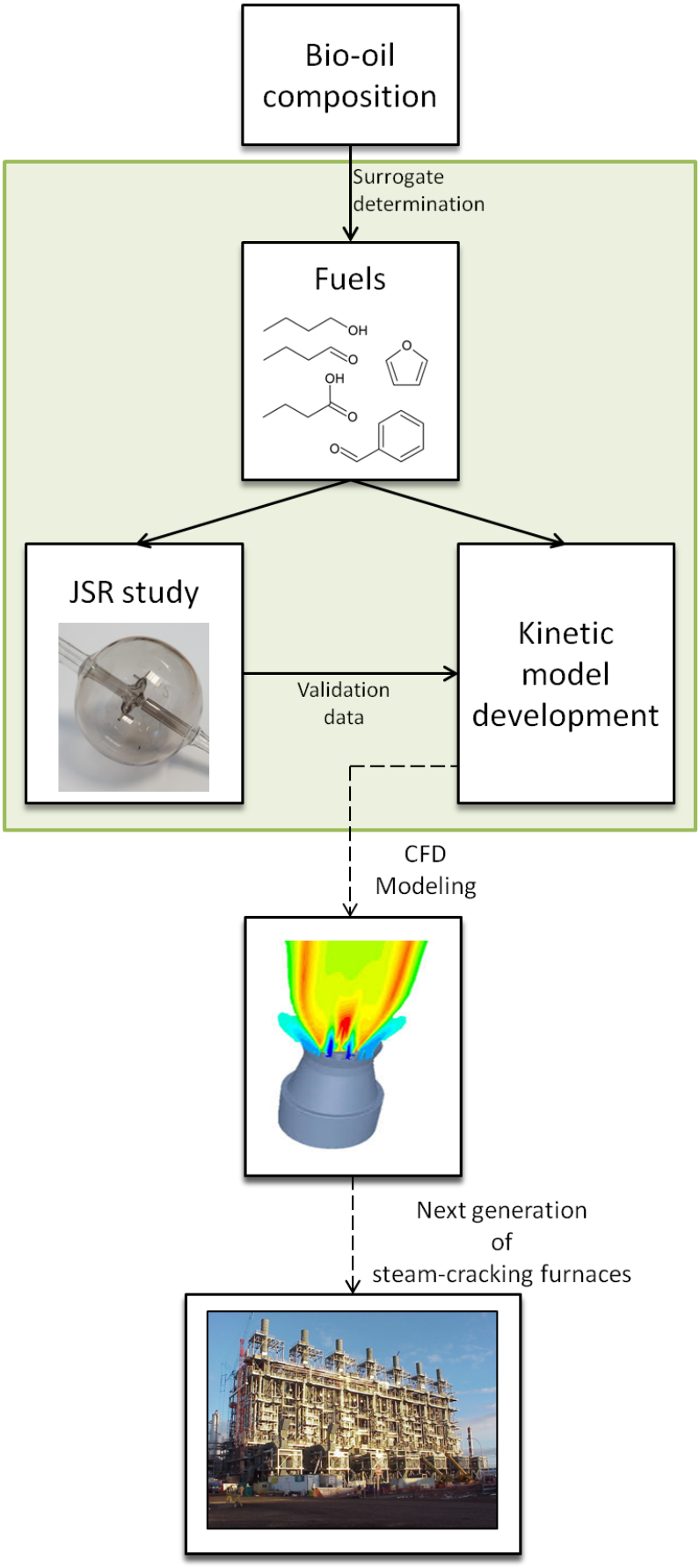

Figure 14. Scheme presenting the IMPROOF project and the place of this PhD in this framework.

II. BIBLIOGRAPHICAL REVIEW ON THE LINEAR AND CYCLIC MOLECULES CONTAINING OXYGEN OR NITROGEN PRESENT IN BIO-OILS

As it was seen in the previous part, bio-oils are complex mixtures of organic compounds. There are almost as many chemical compositions as studies on the subject. However, some trends can be observed. Indeed, to better assess the reactivity of bio-oils and to understand the formation pathways of the products, which can also be pollutants, it is necessary to surrogate the composition of these bio-oils.
Using the classification of Negahdar (2016) and the compositions of some reference bio-oils, which are both presented in part 1.4.2, a composition of a surrogate mixture for bio-oil can be formulated. This surrogate is not composed of chemical species but includes chemical families, like alcohols or acids. This approach allows a better flexibility and makes possible to surrogate every kind of existing bio-oil. To have the best prediction of the bio-oil reactivity, our surrogate is composed of 6 different chemical families:

- Alcohols and diols
- Aldehydes and ketones
- Carboxylic acids
- Furan and derivatives
- Oxygenated aromatics
- Nitrogen–containing compounds

By understanding the behavior and the combustion products formation of each family, we would be able to have a better assessment of the reactivity of bio-oils. Our surrogate composition is graphically summarized in Figure 15.

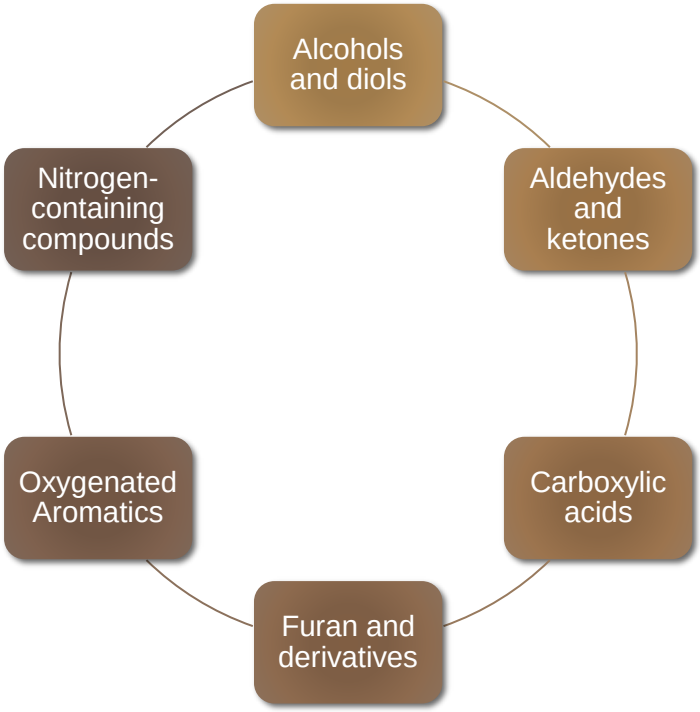

Figure 15. Composition of the surrogate for bio-oils.

For each family, a literature review has been carried out. The aim is to identify the experimental results and kinetic model already published and to detect what can be missing for a complete assessment of the reactivity of those compounds. This state of the art will help us to select relevant compounds to be studied next. In the following part, this state of the art about the experimental oxidation, combustion and pyrolysis studies concerning these chemical families is presented in details.

II.1. Alcohols and diols (non-aromatic)

Alcohols are already used in biofuels and this is especially the case for ethanol. They represent a large part of the non-aromatic fraction of bio-oils (see part 1.4.2). The amount of alcoholic species can even be increased by the hydrotreatment of crude bio-oils (Djokic et al., 2012). That is why the alcoholic fraction is significant. In this section, a review of the work previously made about alcohols is given. Publications about ethanol are first presented, then publications about propanol, to finish with publications on heavier alcohols (C_4-C_8).

II.1.1. Ethanol

Ethanol can be used as a pure fuel or as an additive in fuels due to his high octane number (Research Octane Number or RON=120 and Motor Octane Number or MON=99) (Ballerini, 2006). It is also one of the products formed during bio-fuel oxidation. An extensive review about alcohol combustion and pyrolysis studies has been made a few years ago by Sarathy et al. (2014). It presents experimental and modeling works published before 2014 on the combustion of alcohols, including ethanol, and indicates that alcohols are suitable fuels for combustion engines, with especially the advantages of using high molecular weight alcohols in term of energy densities. In their work, Sarathy et al. decomposed alcohol oxidation mechanism in 30 reaction classes, separated in high-temperature reaction classes and low-temperature reaction classes. This work highlighted specific reaction pathways, such as the unimolecular reactions at high-temperatures (dehydration and dehydrogenation).
Our report presents here only the publications on ethanol reactions available only after this review (those published from 2013) as summarized in Table 7.

Table 7. Main experimental studies on ethanol from 2013.

Experimental Conditions	Reference
Ethanol	
Premixed flame	
T=300-2100 K; P=0.06 atm; Φ=0.7-1.3	(Tran et al., 2013a)
Rapid compression machine	
T=825-985 K; P=10-50 atm; Φ=0.3-1	(Mittal et al., 2014)
Tubular flow reactor	
T=400-1200 K; P=1 atm; Φ=0.8-1.2	(Herrmann et al., 2014)
Shock tube	
T=1047-2518 K; P=1-2 atm; Φ=∞-1	(Aghsaee et al., 2015)
Combustion bomb	
T=318-473 K[5]; P= 1-5 atm; Φ=0.7-1.5	(Aghsaee et al., 2015)

Five studies on ethanol were performed after 2013. The first one was carried out in a low-pressure laminar premixed flame (0.06 atm) (Tran et al., 2013a). The setup was coupled with gas chromatographs to performed online gas analyses. The mole fractions of 20 products were measured during the combustion of methane/ethanol mixture and used to develop a kinetic model for ethanol oxidation involving 87 species in 760 reactions. Figure 16

[5] initial temperature

shows the experimental results and the performance of the model developed for the ethanol flame for three different equivalence ratios. The mechanism was also compared to data from the literature and a satisfactory agreement was obtained between experimental and computed results. During the experiments, the dilution was kept at 78% with a mole fraction of oxygen around 0.2. So the fuel inlet mole fraction varies as shown in Figure 16.

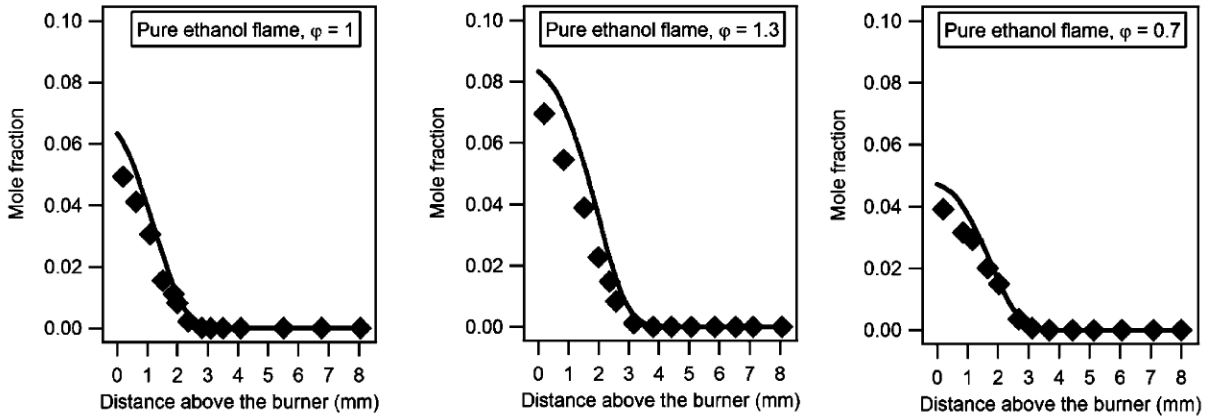

Figure 16. Mole fraction profiles of ethanol in laminar premixed flames (Points are experiments and lines are simulations). Figure extracted from (Tran et al., 2013a).

After that, a study in a rapid compression machine was performed to measure ignition delay times (Mittal et al., 2014). This study was carried out under high pressure (10-50 atm) and for lean to stoichiometric conditions ($0.3 \leq \varphi \leq 1$). The data obtained were used to develop a kinetic model to improve the prediction of ignition delay times. During this study, the effect of pressure on autoignition delay times was measured and the importance of hydroperoxyl radicals was reported. The quantification of species during low temperature oxidation of ethanol and dimethylether was performed using a laminar flow reactor at atmospheric pressure (Herrmann et al., 2014). The composition of the gas was determined by time-of-flight mass spectrometry. Experimental data were then compared to computed data using the model of Cancino et al. (2010) for the oxidation of ethanol. Some differences were observed between experimental and computed data, suggesting further needs of improvements for this model. The laminar flame speed of ethanol has been studied in 2015 for different pressures and equivalence ratios in a combustion bomb (Aghsaee et al., 2015). The pyrolysis and oxidation of ethanol were also studied in a shock tube during this work. The mechanism developed by Ranzi and co-workers (2012) was used to model the experimental data and a good agreement was found.

II.1.2. Propanol

Propanol is the first alcohol to present two isomers. The first one is *n*-propanol, which can be used as an engine fuel with its high-octane number (RON=118 and MON=98). But its production is too expensive to be a common fuel; however, it is often used as a solvent. The second one is *iso*-propanol, which is used as an intermediate of reaction in chemistry and in medical field. It is also used as fuel additive in “gas dryer”. Sarathy et al. have also made a review concerning the studies about propanol until 2014 (Sarathy et al., 2014). Table 8 presents the main experimental studies published more recently.

Table 8. Main experimental studies on propanol after 2013.

Experimental Conditions	Reference
Propanol	
Combustion bomb (*n*-propanol)	
T=343-393 K[6]; P=3.5-11 atm; Φ=0.7-1.6	(Gong et al., 2015)
Shock tube (*n*- and *iso*-propanol)	
T=1150-1550 K; P=1 atm; Φ=∞-0.5-1-2	(Jouzdani et al., 2017)
Counterflow diffusion flame (*n*- and *iso*-propanol)	
T=400 K[6]; P=1 atm	(Alfazazi et al., 2016)

Only three publications were published after 2013. The first one (Gong et al., 2015) deals with a comparative study of *n*-propanol, propanal, acetone and propane laminar flame speeds. The study was carried out in a combustion bomb under high pressure (3.5 to 11 atm) and for a range of equivalence ratios from lean to rich conditions (0.7 ≤ φ ≤ 1.6). The main result is that propanal presents the highest flame speed in contrary to acetone. They explained this difference by the stability of the radical formed during the combustion. The results of this study will be further detailed in the section dedicated to aldehydes and ketones. Another study has been performed by Alfazazi et al. on *n*- and *iso*- propanol oxidation in a counterflow diffusion flame. They measured autoignition temperature by varying the air temperature, as well as extinction times for both propanol isomers and also for two butanol isomers (1- and *iso*-butanol). This study shows that *n*-propanol and 1-butanol have similar ignition temperatures and extinction limits. This also shows that the substituted alcohols produce more propene and propargyl radical than normal alcohols. The last study was performed by Jouzdani et al. (2017). The two propanol isomer pyrolysis was studied in a shock tube at average pressures of 3.5, 5.0, and 11 atm and over a temperature range of 1150–1550 K. The oxidation of those compounds was also investigated in the same apparatus for three equivalence ratios (0.5-1-2). Ignition delay times were measured indicating a higher reactivity for *n*-propanol under oxidizing conditions, as shown in Figure 17.

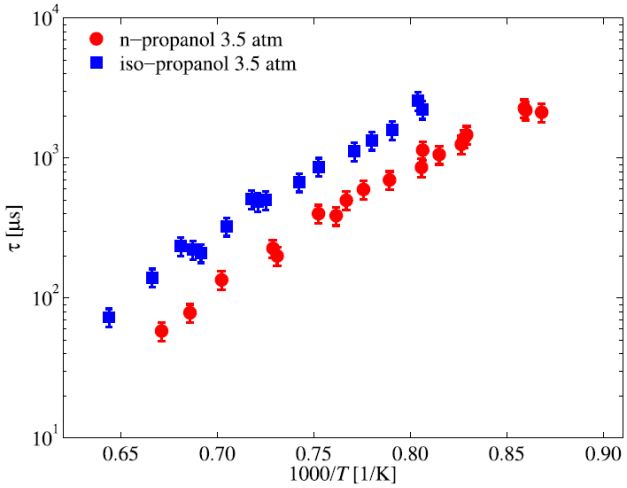

Figure 17. Isomer effect on propanol ignition (3.5 atm) in argon under stoichiometric conditions. Figure extracted from (Jouzdani et al., 2017).

[6] initial temperature

II.1.3. Heavier alcohol

In comparison to ethanol, heavier alcohols (from C_4) exhibit a higher heating value, as presented by Sarathy et al. (2014), making them preferable bio-fuels or fuel additives in term of energy density. In the present review, we consider the publications published after 2009 to have an overview on the recent data published during the last ten years. However, due to the over abundance of these studies, especially for C_4 alcohols, we consider only the experimental studies on C_4 to C_8 alcohols providing a detailed species dataset, which are more relevant to the work planned in the IMPROOF project frame (Djokic et al., 2017). Concerning experiments on laminar flame speeds and ignition delay time measurements, one can refer to the review made by Sarathy et al. (2014).

Table 9 presents the experimental studies carried out for linear butanol isomers combustion, oxidation and pyrolysis. Experiments about the two branched butanol isomers are presented in Table 10. Table 11 summarizes the oxidation, combustion and pyrolysis studies about C_5-C_8 alcohols.

Experiments dealing with species measurements are available for all the isomers of butanol over a large range of temperatures and pressures; from 300 to 2000 K and from 0.007 to 12.5 atm. In addition, the studies cover a large range of equivalence ratios from fuel lean conditions (e.g. 0.28) to pyrolysis. Experiments were carried out in different types of reactors: jet-stirred reactors, counterflow diffusion flames, tubular flow reactors and premixed flames. The publications show that the oxidation of the butanol isomers produced high concentrations of carbonyl compounds and some enolic compounds. Due to the high number of studies, only the experiments performed in jet-stirred reactors, the reactor used in the present work, will be described.

Dagaut et al. studied *n*-butanol oxidation at 10 atm under fuel-lean and fuel-rich conditions. The experiments were carried out between 750 and 1100 K (Dagaut et al., 2009). The profiles for CO, CO_2, H_2O, H_2, C_1–C_4 hydrocarbons, and C_1–C_4 oxygenated compounds were measured by Fourier-transform infrared (FTIR) spectroscopy and off-line gas chromatography (GC) analyses. CO, CO_2, H_2O, H_2, CH_4, formaldehyde, ethylene and propene are the main products identified. The oxidation of *n*-butanol was also studied by Sarathy et al. but at atmospheric pressure and for a larger temperature range (750-1300 K) (Sarathy et al., 2009). They also performed gas chromatography analyses and detected the same products as Dagaut et al. (2009). They also performed experiments in a counterflow diffusion flame. Togbé et al. studied also two other isomers of butanol (*2*- and *iso*-butanol) in a jet-stirred reactor at 10 atm and for temperatures from 770 to 1250 K. They investigated conditions from fuel-lean (Φ=0.28) to fuel-rich (Φ=4). GC and infrared (IR) spectroscopy were used for the analyses and the results were consistent with the previous studies. It could also be noticed that no oxidation study was performed in tubular flow reactors, but only pyrolysis ones.

Table 9. Main experimental studies dealing with species concentration measurements during *n*-butanol and 2-butanol combustion, oxidation and pyrolysis.

Experimental Conditions	Reference
<u>*n*-Butanol</u>	
Jet-stirred reactor	
T=750-1100 K; P=10 atm; Φ= 0.5-2	(Dagaut et al., 2009)
T=750-1300 K; P=1 atm; Φ= 0.5-2	(Sarathy et al., 2009)
Counterflow diffusion flame	
T=300-2000 K; P=1 atm;	(Sarathy et al., 2009)
T=400-1800 K; P=1 atm;	(Grana et al., 2010)
Tubular flow reactor	
T=880-1010 K; P=1.5-1.7 atm; Φ= ∞	(Van Geem et al., 2010)
T=600-807 K; P=1.7 atm; Φ= ∞	(Harper et al., 2011)
T=800-1500 K; P=0.007-1 atm; Φ= ∞	(Cai et al., 2012b)
T=880-1010 K; P=1.5-1.7 atm; Φ= ∞	(Van Geem et al., 2012)
Premixed flame	
T=500-1900 K; P=0.02-0.033 atm; Φ= 1-1.4	(Hansen et al., 2011)
T=500-2000 K; P=0.04 atm; Φ= 1.7	(Oßwald et al., 2011)
P=0.04 atm; Φ= 0.7-1.8	(Cai et al., 2012b)
Combustion bomb	
T=350 K[7]; P=0.89 atm; Φ= 0.8-1.4	(Sarathy et al., 2009)
<u>2-Butanol</u>	
Jet-stirred reactor	
T=770-1250 K; P=10 atm; Φ=0.28-4	(Togbé et al., 2010b)
Counterflow diffusion flame	
T=400-1800 K; P=1 atm;	(Grana et al., 2010)
Tubular flow reactor	
T=880-1010 K; P=1.5-1.7 atm; Φ= ∞	(Van Geem et al., 2010)
T=880-1500 K; P=0.007-1 atm; Φ= ∞	(Cai et al., 2013)
Premixed flame	
T=500-2000 K; P=0.04 atm; Φ= 1.7	(Oßwald et al., 2011)
P=0.04 atm; Φ= 0.7-1.8	(Cai et al., 2013)

Some studies have investigated the impact of the carbon skeleton on the final product composition. McEnally and Pfefferle carried out experiments on methane nonpremixed flame at atmospheric pressure with the addition of the four butanol isomers and the two butane isomers (McEnally and Pfefferle, 2005). They show that depending of the additive the distribution of the products between aldehydes, ketones and hydrocarbons varies. The formation of aldehydes and ketones is favored in the case of alcoholic fuels but the formation

[7] initial temperature

of benzene is not affected by the presence of the hydroxyl group. It is more affected by the presence of a branch in the structure of the molecule. The structure of butanol isomers has then a strong influence on the related-combustion products.

Table 10. Main experimental studies dealing with species concentration measurements during *iso*-butanol and *tert*-butanol combustion, oxidation and pyrolysis.

Experimental Conditions	Reference
<u>*iso*-Butanol</u>	
Jet-stirred reactor	
T=770-1250 K; P=10 atm; Φ=0.28-4	(Togbé et al., 2010b)
Counterflow diffusion flame	
T=400-1800 K; P=1 atm	(Grana et al., 2010)
Tubular flow reactor	
T=550-1100 K; P=1.7 atm; Φ= ∞	(Merchant et al., 2013)
T=950-1850 K; P=0.04-1 atm; Φ= ∞	(Cai et al., 2014)
Premixed flame	
T=500-2000 K; P=0.04 atm; Φ= 1.7	(Oßwald et al., 2011)
T=500-1900 K; P=0.015-0.03 atm; Φ= 1-1.5	(Hansen et al., 2013)
<u>*tert*-Butanol</u>	
Counterflow diffusion flame	
T=400-1800 K; P=1 atm	(Grana et al., 2010)
T=365-400 K[8]; P=1 atm	(Lefkowitz et al., 2012)
Tubular flow reactor	
T=880-1010 K; P=1.5-1.7 atm; Φ= ∞	(Van Geem et al., 2010)
T=950-1850 K; P=0.004-0.016 atm; Φ= ∞	(Cai et al., 2012a)
T=675-950 K; P=12.5 atm; Φ= 1	(Lefkowitz et al., 2012)
Premixed flame	
T=500-2000 K; P=0.04 atm; Φ= 1.7	(Oßwald et al., 2011)

As shown in Table 11, experimental data on C_5-C_8 alcohols are more scarce when dealing with species measurements. The combustion of pentanol isomers with species detection was mainly studied in jet-stirred reactors (Togbé et al., 2011; Dayma et al., 2011; Sarathy et al., 2013; Serinyel et al., 2014). Studies in jet-stirred reactors were carried out under a pressure of 10 atm, over a range of temperatures from 500 K to 1200 K, and for lean to rich conditions (Φ = 0.35-4). The species concentrations were determined by gas chromatography and FTIR spectroscopy. The authors pointed out that, during pentanol isomers oxidation, aldehydes and unsaturated hydrocarbons are the main products. Indeed the associated aldehydes, with the same carbon skeleton as the fuel, are always one of the main oxidation products. The transmission of the carbon skeleton can also be observed on the hydrocarbon products. For example, pentene is observed as products of pentanol through reactions of dehydration, as shown in Figure 18 (Sarathy et al., 2014).

[8] initial temperature

Table 11. Main experimental studies dealing with species concentration measurements during the combustion of C_5-C_8 alcohols.

Experimental Conditions	Reference
***n*-Pentanol**	
Jet-stirred reactor	
T=750-1220 K; P=10 atm; Φ= 0.35-4	(Togbé et al., 2011)
***iso*-Pentanol**	
Jet-stirred reactor	
T=530-1220 K; P=10 atm; Φ= 0.35-4	(Dayma et al., 2011)
T=750-1200 K; P=5 atm; Φ= 0.35-4	(Sarathy et al., 2013)
2-Methylbutan-1-ol	
Jet-stirred Reactor	
T=700-1200 K; P=10 atm; Φ= 0.5-4	(Serinyel et al., 2014)
***n*-Hexanol**	
Jet-stirred reactor	
T=600-1100 K; P=10 atm; Φ= 0.5-3.5	(Togbé et al., 2010a)
T=500-1100 K;P=1 atm; Φ=0.5-1-2	(Rodriguez, 2016)
Counterflow diffusion flame	
T=400-1800 K; P=1 atm	(Yeung and Thomson, 2013)
***n*-Octanol**	
Jet-stirred reactor	
T=500-1200 K; P=10 atm; Φ=0.5-2	(Cai et al., 2015)
Shock tube	
T=800-1400 K; P=20-40 atm; Φ=1	(Cai et al., 2015)

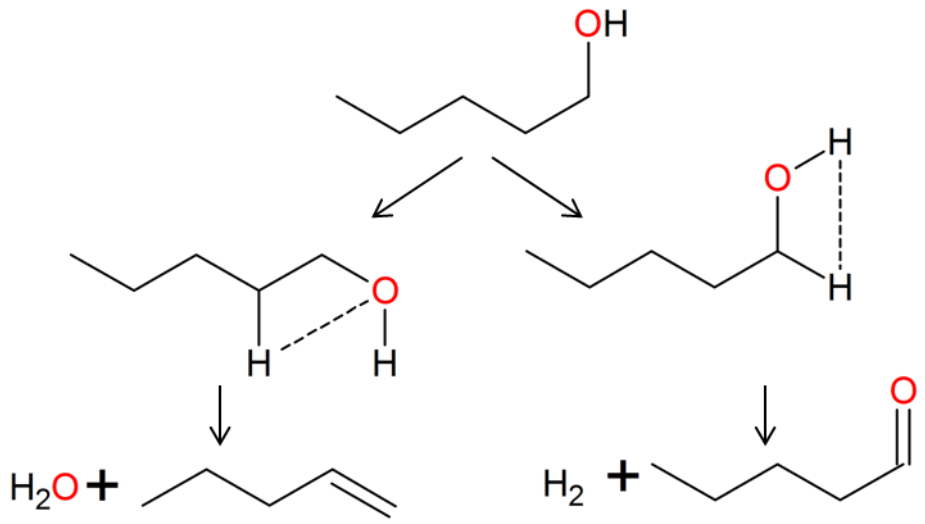

Figure 18. Unimolecular reaction of *n*-pentanol leading to the formation of water and 1-pentene (dehydration) or to *n*-pentanal and hydrogen (dehydrogenation).

The oxidation of all hexanol isomers has not been yet studied during a joint study but three publications on the combustion of *n*-hexanol were released. Experiments were carried out in a jet-stirred reactor (Togbé et al., 2010a) and in a counterflow diffusion flame (Yeung and Thomson, 2013) for a large range of temperature (500-1400 K) and under atmospheric and high (10 atm) pressures. Togbé et al. used gas chromatography and FTIR spectroscopy to detect the oxidation products. They obtained very similar results to the previous study about lighter alcohol oxidation (Togbé et al., 2011; Dayma et al., 2011; Sarathy et al., 2013; Serinyel et al., 2014). Rodriguez et al. studied *n*-hexanol oxidation in a jet-stirred reactor at atmospheric pressure (Rodriguez, 2016). They obtained similar results to the previous alcohol studies made in Orleans in terms of products formation but no negative temperature coefficient (NTC) area was observed compared to the other studies.

Finally, *n*-octanol oxidation was also studied because of its potential as engine fuel. Cai et al. (2015) investigated for the first time *n*-octanol oxidation in a jet-stirred reactor and a shock tube at high pressure (10 to 40 atm) over a range of temperatures from 500 to 1200 K and from 800 to 1400 K, respectively. Ignition delay times and species concentration profiles were measured. The species concentrations were measured with an FTIR (online) spectroscopy and gas chromatography (off-line) during the JSR experiments. With the support of these data, a detailed kinetic mechanism has been developed. It consists of 1280 species and 5537 reactions and was written on the base of reaction classes and their corresponding rate rules.

II.1.4. Conclusion

A large number of publications on alcohol oxidation were published during the last years; however only a few studies concerned C_5-C_8 alcohol combustion. Studies about diols combustion were also searched, but no relevant publication was published on this topic. While some results were published for several pentanol isomers, only the linear isomers of hexanol and octanol were recently studied. Complementary data about the species concentration profiles could be useful to improve kinetic models for the combustion of alcohols. Furthermore, it could be possible to detect some general trends about alcohol combustion as a function of their carbon chain length or substitution. That is why more experiments on heavy alcohols need to be carried out.

II.2. Aldehydes and ketones

Aldehydes and ketones are, like alcohols, an important characteristic fraction of the non-aromatic part of bio-oils. They are, furthermore, important intermediates of reaction during the combustion of alcohols, which is why their behavior during oxidation has always been an interesting subject of studies. Those compounds are also intermediates during alkanes oxidation (Herbinet et al., 2011; Bahrini et al., 2013; Bugler et al., 2017).

Table 12 presents the main experimental studies about the combustion, oxidation and pyrolysis of formaldehyde and acetaldehyde. Many computational studies were also published about the combustion of formaldehyde (Shvartsberg et al., 2015; Christensen et al., 2016; Luo and Liu, 2017) (not shown in Table 12).The main experimental studies about propanal and butanal are presented in Table 13. Finally, Table 14 presents the main experimental studies about pentanal and hexanal.

II.2.1. C_1-C_2 Aldehydes

The combustion of formaldehyde has been studied since 1986 (Vandooren et al., 1986). A flat flame under lean conditions (Φ=0.22) was used at low pressure (P=0.03 atm) to measure species concentrations with a molecular beam mass spectrometer. The same laboratory performed another study at low pressure in a premixed flame in 2012 for temperatures from 400 to 1800 K and for lean and stoichiometric conditions (Φ=0.2-1) (Dias et al., 2012). Gases were analyzed with mass-spectrometry and those results were used to improve a kinetic mechanism (Dias and Vandooren, 2011). The final mechanism contains 568 reactions for 107 chemical species. The model was able to reproduce the experimental results obtained.

Hidaka et al. (1993a, 1993b) also studied formaldehyde pyrolysis and combustion using shock tubes at various pressures (P=0.06-3 atm) over a range of temperatures of T=1200-2000 K. They followed the decay of formaldehyde with time-resolved IR-laser absorption and IR-emission in both studies. The oxidation of formaldehyde was studied over a large range of equivalence ratios (Φ= 0.25-4). In 1998, another study used a shock tube to determine rate coefficients for unimolecular decomposition of formaldehyde and H-abstractions by H and HO_2 on formaldehyde (Eiteneer et al., 1998). The experiments were carried out over a range of pressures between 0.7 and 2.5 atm and over a range of equivalence ratios going from pyrolysis to lean conditions (Φ= ∞-0.17).

The oxidation of formaldehyde was also studied in a tubular flow reactor (Glarborg et al., 2003) at atmospheric pressure, over a lower range of temperatures (T=800-1400 K) for equivalence ratios from 0.004 to 1.5. The influence of nitric oxide was also investigated. The gases were analyzed by ultraviolet (UV) and IR analyzers for NO, CO and CO_2. They showed that nitric oxide has an effect on the reactivity depending on the equivalence ratio: inhibiting under fuel-rich conditions and promoting under fuel-lean ones.

The studies on acetaldehyde pyrolysis began in the 60s. In 1967, Laidler and Liu studied its thermal decomposition in a static vessel at 800 K and for low pressures (P=0.01-0.7 atm) with the help of gas chromatography (Laidler and Liu, 1967). The high-temperature pyrolysis of acetaldehyde was investigated in 1975 by Colket et al. (1975) in a turbulent flow reactor using also chromatography for the gas analysis. They showed that the main products were CO, CH_4, H_2, C_2H_6 and C_2H_4. These experiments allowed determining rate constants for key reactions in pyrolysis, such as the unimolecular decomposition of acetaldehyde in CH_3 and HCO or the H-abstraction by CH_3. The pyrolysis had also been studied in a shock tube by Kern et al. (1990) but the analysis were performed this time with a time-of-flight mass spectrometer. They measured species concentration over the temperature range 1200-1800 K for low pressures (P=0.2-0.4 atm) and they identified the same main products as the previous described study (Colket et al., 1975).

Latter, experiments in a shock tube were performed by Gupte et al. (2007) for higher temperatures (T=1550-2400 K) and over a larger range of pressures (P=0.05-0.7 atm). Bentz et al. (2008) also performed pyrolysis experiments in a shock tube with H-atom resonance absorption spectrometry as detection technique. They also studied the reaction between acetaldehyde and H-atoms. Rate coefficients were determined for the pyrolysis and for the reaction with H-atoms over a temperature range from 1040 to 1650 K.

Table 12. Main experimental studies about formaldehyde and acetaldehyde combustion, oxidation and pyrolysis.

Experimental Conditions	Reference
Formaldehyde	
Premixed flame	
T=600-1800 K; P=0.03 atm; Φ=0.22	(Vandooren et al., 1986)
T=400-1800 K; P=0.03 atm; Φ=0.2-1	(Dias et al., 2012)
Shock tube	
T=1200-2000 K; P=1.3-3 atm; Φ= ∞	(Hidaka et al., 1993a)
T=1400-1900 K; P=0.06 atm; Φ= ∞-4	(Hidaka et al., 1993b)
T=1300-2270 K; P=0.7-2.5 atm; Φ= ∞-0.17	(Eiteneer et al., 1998)
Tubular flow reactor	
T=800-1400 K; P=1 atm; Φ=0.004-1.5	(Glarborg et al., 2003)
Acetaldehyde	
Batch reactor	
T=800 K; P=0.01-0.7 atm; Φ=∞	(Laidler and Liu, 1967)
T=320-540 K; P=0.08 atm; Φ=0.17	(Baldwin et al., 1970)
T=553-713 K; Φ=0.14-1.7	(Kaiser et al., 1986)
Tubular flow reactor	
T=1000-1240 K; P=1 atm; Φ=∞	(Colket et al., 1975)
Microtubular reactor	
T=1400-1675 K; P=0.1-0.2 atm; Φ=∞	(Vasiliou et al., 2011)
T=1000-1900 K; P=0.07-0.3atm; Φ=∞	(Vasiliou et al., 2012)
Jet-stirred reactor	
T=900-1300 K; P=1-10 atm; Φ=0.1-2	(Dagaut et al., 1995)
Shock tube	
T=1200-1800 K; P=0.2-0.4 atm; Φ=∞	(Kern et al., 1990)
T=1230-2530 K; P=2-5 atm; Φ=0.5-2	(Dagaut et al., 1995)
T=1320-1897 K; P=0.13 atm; Φ=0.8-1.7	(Won et al., 2000)
T=1550-2400 K; P=0.05-0.7 atm; Φ=∞	(Gupte et al., 2007)
T=1000-1700 K; P=1.2-2.8 atm; Φ=∞-3	(Yasunaga et al., 2008)
T=1040-1650 K; P=1-5 atm; Φ=∞	(Bentz et al., 2008)
T=1273-1620 K; P=0.34-1.6 atm; Φ=∞	(Wang et al., 2016a)
Rapid compression machine	
T=580 K; P=3-15 atm; Φ=0.2-0.5	(Griffiths and Hasko, 1984)
Premixed flame	
T=500-2000 K; P=0.05 atm; Φ=0.75-1.25	(Leplat and Vandooren, 2010)
T=298-358 K[9]; P=1atm; Φ=0.3-1.8	(Christensen et al., 2015)
T=438-2064 K; P=0.02-0.04atm; Φ=1-1.7	(Tao et al., 2017)

[9] initial temperature

The pyrolysis was studied in a microtubular reactor by Vasiliou et al. (2011, 2012). Using vacuum ultraviolet photoionization mass spectroscopy and infrared absorption spectroscopy, they identified the early decomposition products (i.e. CH_3, CH_2=C=O, CH_2=CHOH, HC≡CH…) and thermal decomposition pathways. More recently in 2016, Wang et al. (2016a) performed experiments in a shock tube at temperatures of 1273-1618 K and for pressures going from 0.34 to 1.6 atm.

The first recorded study on acetaldehyde oxidation was performed by Baldwin et al. (1970) in a static vessel. They studied its oxidation over the temperature range 600-800 K to better assess the negative temperature coefficient area reactivity. They showed that this behavior was due to the competition between the branching reaction: CH_3+O_2=>HCHO+OH and the reversible formation of CH_3O_2: $CH_3+O_2=CH_3O_2$. Latter the oxidation of acetaldehyde was studied in a rapid compression machine to investigate the two-stage ignition of an acetaldehyde/air mixture (Griffiths and Hasko, 1984). In 1986, Kaiser et al. (1986) carried out experiments in a batch reactor at temperatures of 553 and 713 K for fuel-rich to fuel-lean conditions. The results were used to develop a detailed kinetic mechanism and to study the negative temperature coefficient zone between 550 and 900 K.

Dagaut et al. (1995) used a jet-stirred reactor at high temperatures (T=900-1300 K) over a pressure range 1-10 atm to perform species concentration measurements with gas chromatography. They also measured ignition delay times in a shock tube for lean to rich conditions (Φ=0.5-2). More recently, Won et al. (2000) performed ignition delay time measurements in a shock tube by following the OH radical emission and the pressure profile. They developed a mechanism consisting of 110 reactions and 34 species.

Yasunaga et al. (2008) performed experiments on acetaldehyde for both pyrolysis and oxidation. They measured species profiles thanks to time-resolved UV and IR-laser absorptions. They also used time-resolved IR emission and single pulse technique in complement of the previous techniques. A shock tube was used under pressures between 1.2 and 2.8 atm and over a temperature range of 1000-1700 K. The pyrolysis and oxidation data obtained allowed the development of a mechanism of 178 reaction steps and 50 species. The submechanisms of methane, ethylene, ethane, formaldehyde, and ketene were found to play an important role in the acetaldehyde oxidation mechanism.

An experimental and numerical study of acetaldehyde combustion was carried out by Leplat et al. in 2010 (2010). They studied the structure of several flames and they measured species mole fraction profiles at low pressure (P=0.05 atm) and over a large range of equivalence ratios (Φ=0.75-1.25) with a molecular beam mass spectrometer system with electron impact ionization. Christensen et al. (2015) measured laminar burning velocities of acetaldehyde/air mixture. Experiments were carried out at 298, 318, 338, 348 and 358 K. A comparison with several models and the experimental data was performed and the model developed by Leplat et al. gave the best predictions (Leplat and Vandooren, 2010). The chemical structure of laminar premixed flames was studied by Tao et al. (2017) at low-pressure over an equivalence ratio range from 1 to 1.7. With molecular beam synchrotron photo-ionization mass spectrometry, they identified and quantified about 40 species. They observed for the first time the formation of ethanol and butanal.

II.2.2. C_{3+} Aldehydes

The oxidation of propanal has only been studied since the last 6 years. Veloo et al. studied the oxidation of propanal in a jet-stirred reactor and in a flame. Species concentration profiles and laminar flame speeds were measured with a FTIR spectrometer and gas chromatography (off-line) coupled with a thermal conductivity detector (TCD), a flame ionization detector (FID) or a mass spectrometer (Veloo et al., 2013a). A detailed kinetic model, consisting of 327 species and 1618 reactions, was tested against these experimental data.

As presented in the previous section, a study was also performed about laminar flame speed measurements of C_3 oxygenated fuels (Gong et al., 2015), including propanol, propanal and acetone, to study the effects of different functional groups. It showed that propanal has the highest flame speed in contrary to acetone. These differences came from the concentrations of intermediate species generated. In the case of propanal, the hydrogen radical concentration was higher than for the other fuels. This leads to an acceleration of the reaction, which increases the reactivity. Figure 19 presents the results obtained during this study at 393 K and atmospheric pressure. It can be observed that propanal has indeed a higher reactivity than the other compounds, especially in rich mixtures.

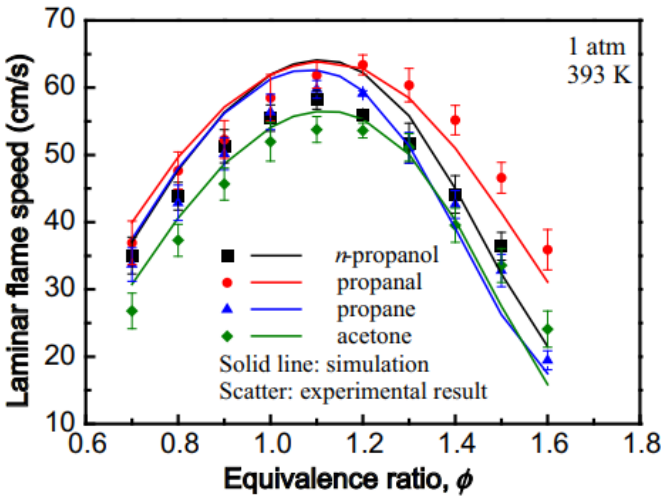

Figure 19. Laminar flame speeds of *n*-propanol, propanal, propane, and acetone/air premixed flames as a function of the equivalence ratio at 393 K and 1 atm. Figure extracted from (Gong et al., 2015).

Yang et al. (2016) studied propanal ignition in a shock tube to compare it to propane, *n*-propanol and *iso*-propanol ignitions. The temperatures were ranging from 1050 to 1800 K, pressures from 1.2 to 16.0 atm and equivalence ratios of 0.5, 1.0, and 2.0. It was found that ignition delays are in the order of:

propane > *iso*-propanol > *n*-propanol > propanal.

This result is similar to the one obtained by Gong et al (2015). The differences in reactivity came from the stability of the intermediates produced; the intermediates of propanal and *n*-propanol are indeed less stable than those of propane and iso-propanol.

Table 13. Main experimental studies about propanal and butanal combustion and oxidation.

Experimental Conditions	Reference
Propanal	
Jet-stirred reactor	
T=500-1100 K; P=10 atm; Φ=0.3-2	(Veloo et al., 2013b)
Counterflow diffusion flame	
T=343 K[10]; P=1 atm; Φ=0.75-1.6	(Veloo et al., 2013b)
Combustion bomb	
T=343-393 K[10]; P=1 atm; Φ=0.7-1.6	(Gong et al., 2015)
Premixed flame	
T=500-1600 K; P=0.03 atm; Φ=1-1.7	(Dias et al., 2016)
Shock tube	
T=1100-1900 K; P=1-3 atm; Φ=0.5-2	(Pelucchi et al., 2015)
T=1050-1800 K; P=1.2-16 atm; Φ=0.5-1-2	(Yang et al., 2016)
***n*-Butanal**	
Jet-stirred reactor	
T=500-1200 K; P=10 atm; Φ=0.3-2	(Veloo et al., 2013b)
Counterflow diffusion flame	
T=343 K[10]; P=1 atm; Φ=0.75-1.6	(Veloo et al., 2013b)
Shock tube	
T=1100-1650 K; P=1.3-10 atm; Φ=0.5-2	(Zhang et al., 2013)
T=1100-1900 K; P=1-3 atm; Φ=0.5-2	(Pelucchi et al., 2015)

The last experimental study on propanal pyrolysis and oxidation with product detection is the work of Pelucchi et al. (2015). It also concerned butanal and pentanal pyrolysis and oxidation and took place in shock tubes at pressures between 1 and 3 atm over a temperature range of 1100 to 1900 K for different equivalence ratios. Measurements of species concentration profiles under pyrolysis conditions and of ignition delay time for oxidation were performed. Propanal showed the highest reactivity, whereas butanal was the least reactive. Figure 20 shows the results obtained for *n*-pentanal oxidation during the shock tube experiments. It also compares the results with modeling using the POLIMI mechanism and NUIG mechanism. The POLIMI mechanism gives overall a better agreement.

Zhang et al. (2013) also measured ignition delay times for butanal using a shock tube in a temperature range of 1100-1650 K at pressures of 1.3, 5 and 10 atm and equivalence ratios of 0.5, 1 and 2. With these data, a kinetic model was developed on the basis of a literature review. The obtained agreement between experimental and computed data was satisfactory.

[10] initial temperature

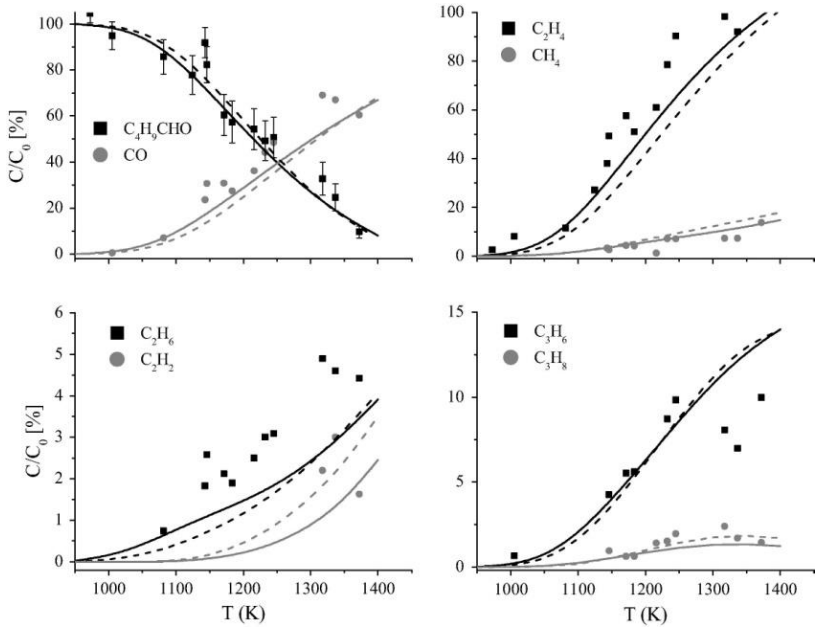

Figure 20. Predicted and experimental concentration profiles from shock tube pyrolysis of 3% *n*-pentanal in argon (*τ* = 2.3 ms). Experiments (symbols), POLIMI mechanism (solid lines) and NUIG mechanism (dashed lines). Figure extracted from (Pelucchi et al., 2015).

In the last years, experiments in premixed flames were carried out at low pressure (P=0.03 atm) for stoichiometric to rich conditions (Φ=1-1.7) by Dias et al. (2016). Species mole fraction profiles were measured by molecular beam mass spectrometry. This work leads to an extension of the mechanism of Dias and Vandooren (2011) to propanal and its simulations compared well with the experimental data.

Table 14. Main experimental studies about *n*-pentanal and *n*-hexanal combustion.

Experimental Conditions	Reference
***n*-Pentanal**	
Shock tube	
T=1100-1900 K; P=1-3 atm; Φ=0.5-2	(Pelucchi et al., 2015)
***n*-Hexanal**	
Jet-stirred reactor	
T=475-1100 K; P=1 atm; Φ=0.5-2	(Rodriguez et al., 2017)

Regarding *n*-hexanal, its oxidation in a jet-stirred reactor was carried out by Rodriguez et al. (2017) following the mole fractions of some usual stable combustion species and also that of important minor products using IR continuous wave-cavity ring-down spectroscopy (cw-CRDS), such as H_2O_2, water or formaldehyde. The experiments were carried out under atmospheric pressure and over a range of temperatures from 475 to 1100 K. The influence of the equivalence ratio was studied for three conditions (0.5-1-2). This study succeeded in detecting and quantifying some specific products like hexanoic acid and lactones. This work demonstrated the difference of reactivity between long chain aldehydes and long chain alkanes: aldehydes had a significantly higher reactivity.

II.2.3. Ketones

Concerning ketones, the oxidation of acetone, butanone, pentanone and cyclohexanone were studied over the last years. Table 15 presents a review of publications about the combustion of acetone and butanone, whereas Table 16 presents the results obtained for 3-pentanone and cyclohexanone.

Table 15. Main experimental studies about acetone and butanone combustion and oxidation.

Experimental Conditions	Reference
Acetone	
Combustion bomb	
T=298 K[11]; P=1 atm; Φ=0.8-1.6	(Pichon et al., 2009)
T=343-393 K[11]; P=1 atm; Φ=0.7-1.6	(Gong et al., 2015)
Premixed flame	
T=300-2000 K; P=1 atm; Φ=0.6-1.5	(Chong and Hochgreb, 2011)
T=298-358 K[11]; P=1 atm; Φ=0.6-1.6	(Nilsson et al., 2013)
T=600-1400 K; P=0.027 atm; Φ=1.1-1.72	(Dias et al., 2015)
Shock tube	
T=1050-1650 K; P=1.2-3.2 atm; Φ=1	(Sato and Hidaka, 2000)
T=1340-1930 K; P=1 atm; Φ=0.5-2	(Pichon et al., 2009)
T=1150-1550 K; P=1-4 atm; Φ=0.5-2	(Davidson et al., 2010)
T=550-900 K; P=1-12.5 atm; Φ=0.5-2	(Akih-Kumgeh and Bergthorson, 2011)
T=700-1000 K; P=20-40 atm; Φ=1	(Minwegen et al., 2017)
Tubular flow reactor	
T=700-1500 K; P=1 atm; Φ=0.14-2.7	(Alzueta et al., 2010)
Butanone	
Shock tube	
T=1250-1850 K; P=1 atm; Φ=0.5-2	(Serinyel et al., 2010a)
T=1100-1400 K; P=3-6.5 atm; Φ=0.5-1	(Badra et al., 2014)
T=850-1280 K; P=20-40 atm; Φ=1	(Burke et al., 2016)
Jet-stirred reactor	
T=700-1300 K; P=1-10 atm; Φ=0.5-2	(Thion et al., 2017)
Premixed flame	
T=500-2000 K; P=0.05 atm	(Decottignies et al., 2002)
Rapid compression machine	
P=1-5 atm; Φ=0.7-1.3	(Burke et al., 2016)

Acetone oxidation experiments were carried out over a temperature range of 298-2000 K, at pressures from 0.027 to 40 atm and for equivalence ratios from 0.5 to 2 (Akih-Kumgeh and Bergthorson, 2011; Alzueta et al., 2010; Chong and Hochgreb, 2011; Davidson et al., 2010; Dias et al., 2015; Gong et al., 2015; Minwegen et al., 2017; Nilsson et al., 2013;

[11] initial temperature

Pichon et al., 2009; Sato and Hidaka, 2000). Combustion chambers, premixed flames, shock tubes and a flow reactor were used to perform measurements of ignition delay times, flame speeds, species concentration profiles, respectively. The effect of nitric oxide on acetone oxidation in a tubular flow reactor was also studied (Alzueta et al., 2010). It has been shown that the addition of NO does not have a significant effect on acetone oxidation.

Shock tubes and a rapid compression machine were used to perform the measurements of butanone ignition delay times. These were studied over a temperature range of 500-1850 K, at pressures from 0.05 to 40 atm and for equivalence ratios from 0.5 to 2 (Badra et al., 2014; Burke et al., 2016; Decottignies et al., 2002; Serinyel et al., 2010a). A study in a jet-stirred reactor was also performed to measure species concentration profiles (Thion et al., 2017) thanks to FTIR spectroscopy and gas chromatography. The experiments were made at pressures of 1 and 10 atm, over a temperature range of 700-1300 K, for lean to rich conditions Φ=0.5-2. Ethylene, hydrogen and methane were identified as the main hydrocarbons products, whereas formaldehyde, acetaldehyde and methyl vinyl ketone were the main oxygenated products detected. A model was developed and compared with these data, but the author came to the conclusion that more data were needed especially to predict the formation of methyl ketene and methyl vinyl ketone.

Table 16. Main experimental studies about pentanone and cyclohexanone combustion and oxidation.

Experimental Conditions	Ref
3-Pentanone	
Shock tube	
T=1250-1850 K; P=1 atm; Φ=0.5-2	(Serinyel et al., 2010b)
T=1150-1550 K; P=1-4 atm; Φ=0.5-2	(Davidson et al., 2010)
T=1350-1530 K; P=2.5 atm; Φ=1.5	(Lam et al., 2012)
T=690-1270 K; P=10-40 atm; Φ=0.5-1	(Fikri et al., 2013)
Combustion bomb	
T=305 K[12]; P=10 atm; Φ=0.75-1.4	(Serinyel et al., 2010b)
Cyclohexanone	
Jet-stirred reactor	
T=530-1220 K; P=10 atm; Φ=0.5-4	(Serinyel et al., 2015)

Regarding the combustion of 3-pentanone, its combustion was studied in shock tubes mainly, as well as in a combustion chamber. The shock tube experiments were carried out at pressures between 1 and 40 atm over a temperature range of 690-1850 K and for equivalence ratios from 0.5 to 2 (Davidson et al., 2010; Serinyel et al., 2010b; Lam et al., 2012; Fikri et al., 2013). The experiments in combustion chamber were at 305 K, 10 atm and for equivalence ratios from 0.75 to 1.4. Ignition delay times and laminar flame speeds were measured (Serinyel et al., 2010b).

The kinetics of cyclohexanone oxidation was studied in a jet-stirred reactor at high pressure (10 atm) for lean, stoichiometric and rich conditions over a temperature range of 530-1220 K by Serinyel et al. (2015). This study provides species concentration data

[12] Initial temperature

measured by FTIR spectroscopy and gas-chromatography, which were used to test a model developed by the authors. The products detected were hydrogen, H_2O, CO, CO_2, methane, formaldehyde, ethane, ethylene, acetylene, acetaldehyde, propene, acrolein, 1-butene, 1,3-butadiene, methyl vinyl ketone, 1,3-cyclopentadiene, cyclopentene, 2-cyclohexen-1-one, and also 1,5-hexadiene, benzene, styrene (less than 10 ppm). Cyclopentene and 1,3-cyclopentadiene were identified as important intermediates. The computed and the experimental data were in a relative good agreement.

II.2.4. Conclusion

Even if several studies were performed for the combustion of aldehydes and ketones, studies recording species formation during the oxidation remain scarce. More research has to be carried out on aldehyde oxidation to quantify species formation as these are an important part of bio-oils as well as important intermediates in bio-fuel combustion.

II.3. Carboxylic acids

Carboxylic acids, called acids further in the text, like alcohols represent a large part of the non-aromatic compounds present in bio-oils. Table 6 (see I.4.2) shows that they can be even present in larger amount than alcohols. Despite this abundance, only limited studies on the oxidation of acids were reported and none laminar flame speed measurements or JSR experiments. Table 17 presents main studies about organic acid pyrolysis, oxidation and combustion carried out under gas phase conditions.

Four studies were carried out on formic acid reactions, with three of them made before 2000. The first one is a study in a batch reactor of the decomposition of formic acid (Blake and Hinshelwood, 1960) with measurements of the production of CO and CO_2. Later, these experiments were repeated over a larger range of temperatures in batch and flow reactors. From these experiments, Arrhenius kinetic values for the thermal decomposition of formic acid were determined. Shock tube experiments were also presented for formic acid decomposition in two papers (Saito et al., 1984, 2005). Experiments were carried out over a temperature range of 1300-2000 K and rate constants were determined from these results. Furthermore, some ab initio calculations were made to calculate transition states for two decomposition pathways:

(1) $HCOOH+Ar \rightarrow CO+H_2O+Ar$
(2) $HCOOH+Ar \rightarrow CO2+H_2+Ar$

It was found experimentally that pathway (1) is the main decomposition channel, as it is explained by ab initio calculations. Pathway (1) is indeed that with the lowest potential energy.

Acetic acid pyrolysis was more studied than its oxidation. Two studies have been performed in batch reactor, one at atmospheric pressure (Blake and Jackson, 1968) and one under low-pressure (Bamford and Dewar, 1949).

Acetic acid pyrolysis was also studied in tubular flow reactor by Blake and Jackson at 800-1035 K and under low-pressure (0.01-0.21 atm) (Blake and Jackson, 1969). They detected ketene, water, methane and carbon dioxide as the main reaction products. Then another study at higher temperatures (1300-1950 K) and atmospheric pressure was

performed in a tubular flow reactor by Mackie and Doolan (1984). They identified the same products than in the previous study.

Table 17. Main experimental studies about the combustion and pyrolysis of carboxylic acids.

Experimental Conditions	Reference
Formic Acid	
Batch reactor	
T=700-800 K; P=0.06-0.26 atm; Φ=∞	(Blake and Hinshelwood, 1960)
T=730-1053 K; P=1 atm; Φ=∞	(Blake et al., 1971)
Tubular flow reactor	
T=1250-1850 K; P=1 atm; Φ=∞	(Blake et al., 1971)
Shock tube	
T=1300-2000 K; P=1 atm; Φ=∞	(Saito et al., 1984)
T=1300-2000 K; P=1 atm; Φ=∞	(Saito et al., 2005)
T=1230-1820 K; P=1-6.5 atm; Φ=∞	(Elwardany et al., 2015)
Acetic Acid	
Batch reactor	
T=730-870 K; P=1 atm; Φ=∞	(Blake and Jackson, 1968)
T=780-1200 K; P=0.04 atm; Φ=∞	(Bamford and Dewar, 1949)
Tubular flow reactor	
T=330 K[13]; P=0.001 atm; Φ=∞	(Butkovskaya et al., 1995)
T=800-1035 K; P=0.01-0.21 atm; Φ=∞	(Blake and Jackson, 1969)
T=1300-1950 K; P=1 atm; Φ=∞	(Mackie and Doolan, 1984)
Shock tube	
T=1230-1820 K; P=1-6.5 atm; Φ=∞	(Elwardany et al., 2015)
Laminar premixed flame	
T=400-1800 K; P=0.05 atm; Φ=0.77-1.05	(Leplat and Vandooren, 2012)

The last study in a tubular flow reactor was carried out at 330 K and very low-pressure (0.001 atm) by Butkovskaya et al. (1995). They used IR chemiluminescence technique to measure CO_2 and HO_2 emissions. More recently two studies were performed in a laminar premixed flame (Leplat and Vandooren, 2012) and in a shock tube (Elwardany et al., 2015). Leplat and Vandooren studied the oxidation of acetic acid under fuel-lean and stoichiometric conditions at 0.05 atm and for temperatures between 400 K and 1800 K. They detected large amount of CH_2CO in the front flame with molecular beam mass spectrometry with electron ionization. Elwardany studied also the pyrolysis but at higher pressure than before (1.6-5 atm) and for higher temperatures (1230-1820 K). They used laser-absorption measurements to quantify CO, CO_2 and water emissions. Based on this, they then proposed rate constants values for the decarboxylation (1) and dehydration (2) reactions of formic and acetic acid:

(1) $HCOOH \Rightarrow H_2+CO_2$ and (2) $HCOOH \Rightarrow CO+H_2O$

(1) $CH_3COOH \Rightarrow CH_4+CO_2$ and (2) $CH_3COOH \Rightarrow CH_2CO+H_2$

[13] initial temperature

Cavallotti et al. recently performed a theoretical study about acetic acid decomposition. Rate constants for its unimolecular decomposition were determined integrating the 1D master equation over a Potential Energy Surface (PES) investigated at the M06-2X/aug-cc-pVTZ level. Energies were computed at the CCSD(T)/aug-cc-pVTZ level using a basis set size correction factor determined at the DF-MP2/aug-cc-pVQZ level. Three decomposition channels were considered: CO_2 + CH_4, CH_2CO + H_2O, and CH_3 + COOH. Rate constants were computed in the 700–2100 K and 0.1–100 atm temperature and pressure ranges. H-abstractions reactions rate constants calculations with different radicals (H, OH, OOH, O_2 and CH_3) were performed at the same level of theory.

Concerning the H-atom abstractions, the primary position in acetic acid was investigated and compared to alkane primary position. Cavallotti et al. showed that acetic acid primary position is less reactive than the alkane equivalent but also than an alkane secondary position as showed in Figure 21. For the alkane position, the rate constants are those proposed by Ranzi et al (1993).

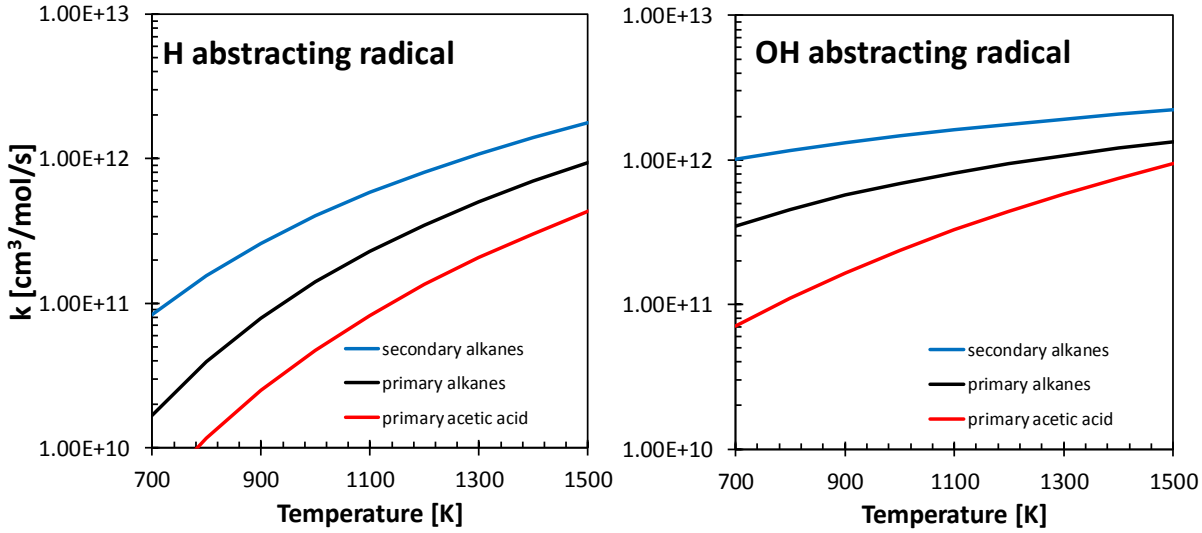

Figure 21. Comparison between H-abstraction rate constants for primary position in acetic acid (Cavallotti et al., 2018) and primary and secondary positions in alkanes (Ranzi et al., 2014). Left panel: R=H, right panel: R=OH.

The interactions with the carboxylic function inhibit the H-abstraction making it a factor of ~3-4 lower than an alkane primary position over the temperature range of interest. This study also showed the importance of the stabilized radical (*CH_2(C=O)-OH) in the kinetic model and in particular for the prediction of flame speed.

These rates were integrated in the POLIMI kinetic model and simulations for the pyrolysis and oxidation were performed. Simulations were validated over the data of Mackie and Doolan, as shown in Figure 22 (Mackie and Doolan, 1984). Simulation of acetic acid pyrolysis and combustion showed that the adopted kinetic model is able to predict well acetic acid decomposition and the formation of its main primary products in all the investigated systems. The only exception is ketene, whose formation is well predicted at low temperatures, but underpredicted in combustion and slightly overpredicted in pyrolysis. In addition, the formation of secondary species, in particular C_2 species, CO and H_2 in pyrolysis, is underpredicted.

They showed that acetic acid decomposition mainly starts through molecular reactions (E_a ~71-74 kcal/mol), due to the high activation energy of the unimolecular initiation reactions (E_a ~93-110 kcal/mol). The two main molecular reactions are decarboxylation and dehydration.

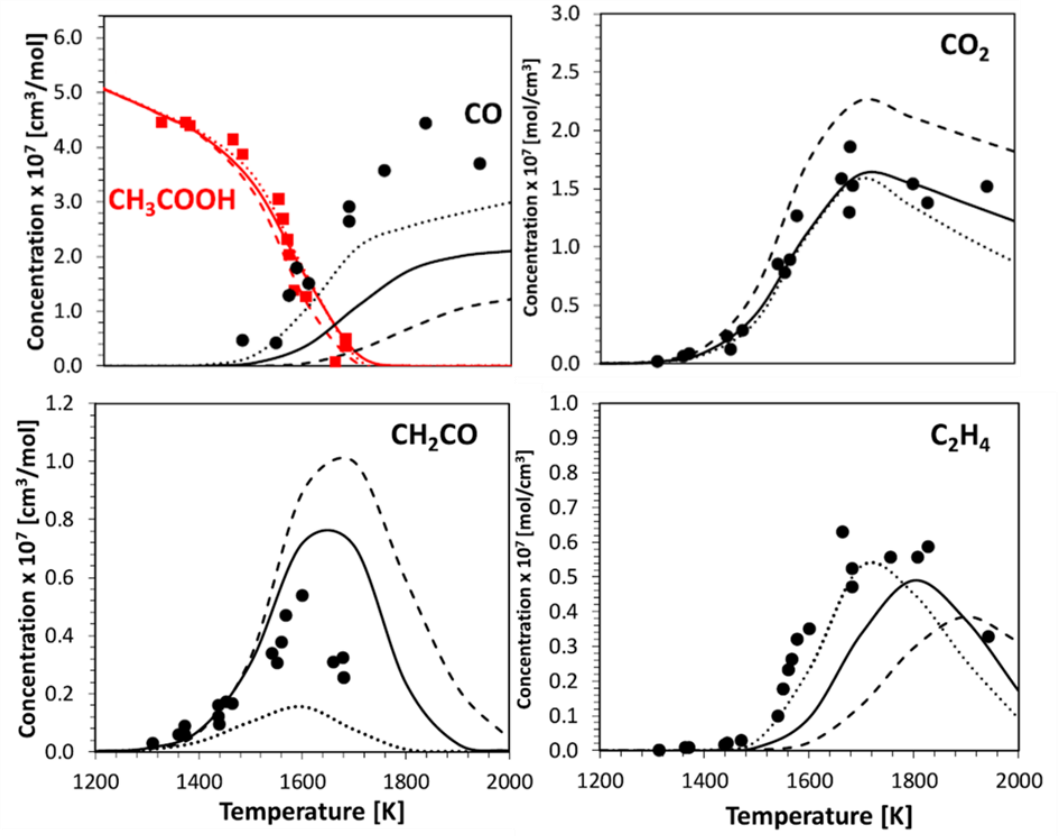

Figure 22. Comparison between the model computed results (lines) using three model (plain line: (Cavallotti et al., 2018), bline:line :(Christensen and Konnov, 2016) and dotted line : Aramco (Metcalfe et al., 2013)) and the experimental data (dots) (Mackie and Doolan, 1984) (shock tube, 5% acetic acid in Ar at 1 atm and 0.1ms.). Extracted from (Cavallotti et al., 2018).

II.3.1. Conclusion

While some studies were carried out on the oxidation of formic and acetic acids, none was made for butanoic and pentanoic acids. No species concentration profiles obtained during the oxidation or pyrolysis of acids were reported recently: the only study that measured species distribution is the one of Blake and Hinshelwood (1960). That is why to better understand acid reaction mechanism, experimental data are highly needed, especially for acid containing from 4 and 5 carbon atoms.

II.4. Furanic compounds

Furanic compounds, here defined as derivatives of tetrahydrofuran (THF) and furan, are potential biofuels, which are present in large fractions in bio-oils obtained from biomass fast-pyrolysis. These biofuels with favorable octane number (ex. RON = 131 for 2-methylfuran) can be used as blending agents with petroleum-based fuels or as complete replacement. Figure 23 shows the structures of THF and one of its derivatives, 2-methyltetrahydrofuran (MTHF), and Table 18 presents publications dealing with the combustion, oxidation and pyrolysis of these two species.

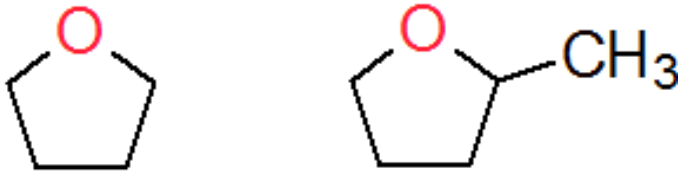

Figure 23. Structure of tetrahydrofuran (on the left) and 2-methyltetrahydrofuran (on the right).

II.4.1. Saturated furans

The pyrolysis of tetrahydrofuran was first studied by Klute and Walters in a batch reactor (1946) and then by McDonald et al. under similar experimental conditions (T=800-840 K and P=0.26 atm) (1951). Acetaldehyde and formaldehyde have been identified as intermediate products. The products found in gas analysis are ethylene, carbon monoxide and methane together with smaller percentages of higher unsaturated compounds, hydrogen and ethane. Lifshitz et al. also studied tetrahydrofuran pyrolysis, but experiments were performed in a shock tube under a pressure above 1 atm and over a range of temperatures of T=900-1600 K (Lifshitz et al., 1986a). They identified a large range of products with gas chromatography (H_2, CH_4, C_2H_4, C_2H_2, C_3H_4, C_3H_4, 1-C_4H_8, C_4H_6, C_4H_4, and C_4H_2). The oxidation of tetrahydrofuran was studied in a batch reactor by Molera et al. at low temperatures (T=480-540 K) and under low pressure (P=0.2 atm) for an equivalence ratio of 2.75 (Molera et al., 1988). They identified primary reaction products by gas chromatography: succinic acid, formaldehyde, water, acrolein, furan, acetaldehyde, hydroperoxides (HPO), carbon monoxide, carbon dioxide, and ethylene. High-pressure (20-40 atm) ignition delay times were studied by Uygun et al. (2014) in a shock tube at temperatures from 690 K to 1100 K.

Dagaut et al. studied the oxidation of tetrahydrofuran in a shock tube and in a jet-stirred reactor (Dagaut et al., 1998). They respectively measured ignition delay times and species concentration profiles for temperatures from 800 to 1800K, pressures from 2 to 10 atm and for lean to rich conditions (Φ=0.5-2). Species mole fraction profiles were measured using offline gas chromatography. The main products of the oxidation of THF were H_2, CO, CO_2, CH_4, C_2H_4, CH_2O and C_3H_6. C_2H_6, C_3H_4, 1-C_4H_8, C_2H_2, CH_3CHO and C_2H_5CHO were also formed in the reaction at lower concentration levels.

Table 18. Main experimental studies about tetrahydrofuran and 2-methyltetrahydrofuran oxidation, combustion and pyrolysis.

Experimental Conditions	Reference
Tetrahydrofuran	
Batch reactor	
T=800-840 K; P=0.26 atm; Φ=∞	(Klute and Walters, 1946)
T=820 K; P=0.26 atm; Φ=∞	(McDonald et al., 1951)
T=480-540 K; P=0.20 atm; Φ=2.75	(Molera et al., 1988)
Shock tube	
T=900-1600 K; P > 1 atm; Φ=∞	(Lifshitz et al., 1986a)
T=1000-1800 K; P=2-5 atm; Φ=0.5-2	(Dagaut et al., 1998)
T=690-1100 K; P=20-40 atm; Φ=1	(Uygun et al., 2014)
T=600-750 K; P=20-40 atm; Φ=0.5-2	(Tran et al., 2015b)
Jet-stirred reactor	
T=800-1100 K; P=1-10 atm; Φ=0.5-2	(Dagaut et al., 1998)
T=800-1100 K; P=1 atm; Φ=0.5-2	(Vanhove et al., 2015)
Rapid compression machine	
T=640-900 K; P=5-10 atm; Φ=1	(Vanhove et al., 2015)
Premixed flame	
T=500-2000 K; P=0.02-0.03 atm; Φ=1-1.75	(Kasper et al., 2011)
T=900-2200 K; P=0.06 atm; Φ=0.7-1.3	(Tran et al., 2013b)
Tubular flow reactor	
T=400-700 K; P=0.01-2.6 atm	(Antonov et al., 2016)
2-Methyltetrahydrofuran	
Premixed flame	
T=400-2100 K; P=0.04 atm; Φ=1.7	(Moshammer et al., 2013)
T=298-398 K[14]; P=1 atm; Φ=0.6-1.6	(De Bruycker et al., 2017)
T=500-2000 K; P=0.06 atm; Φ=0.7-1.3	(De Bruycker et al., 2017)
Tubular flow reactor	
T=900-1100 K; P=1.7 atm; Φ=∞	(De Bruycker et al., 2017)

The combustion of tetrahydrofuran was studied in premixed flames at low pressures (P=0.02-0.03 atm) for fuel-rich and stoichiometric conditions by Kasper et al. (2011). 60 species were detected and quantified in each flame using mass spectroscopy. They identified water, carbon monoxide, carbon dioxide and hydrogen as main products. Recently, Tran et al. (2013b) studied the combustion of tetrahydrofuran in a premixed flame at low pressure (P=0.06 atm) using a different analytical technique, *i.e.* gas chromatography, to measure stable species profiles for fuel-lean to fuel-rich conditions. As example, the profiles of flame temperature and major species are presented in Figure 24. They identified the same

[14] initial temperature

major products than the previous study. The latter study also provided the data of laminar burning velocities and ignition delay times of THF.

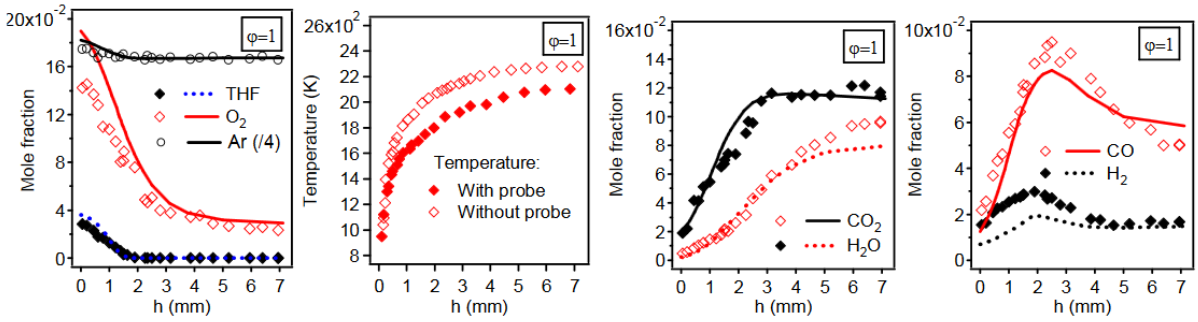

Figure 24. Major species and temperature profiles measured in THF premixed flame experiments (symbols: experiments; lines: simulation) Figure extracted from (Tran et al., 2013b).

A study investigating the low-temperature oxidation of THF was also performed in a jet-stirred reactor and a rapid compression machine by Vanhove et al. (2015). Jet-stirred reactor experiments were performed at atmospheric pressure for lean to rich conditions in order to measure species profiles over a range of temperatures from 800 to 1100 K with gas chromatography. In the same time, ignition delay times were measured in a rapid compression machine under high pressures (P=5-10 atm). Those data have been used for the validation of a recent kinetic model (Fenard et al., 2018). This model is able to well reproduce the experimental data obtained by Vanhove et al. (2015).

Antonov et al. (2016) examined the competition among reaction pathways from O_2 additions in the low-temperature oxidation of THF. The experiments were performed in a tubular flow reactor coupled with synchrotron photoionization mass spectrometric technique over a large range of pressures (P=0.01-2.6) and a temperature range of 400-700 K. The aim of this study was to quantify the competition between reaction pathways concerning O_2 additions at low temperatures, so the conditions were very lean (Φ=0.0001-0.02). According to their results, they proposed a sub-mechanism for low-temperature THF oxidation.

Regarding MTHF, its pyrolysis was recently studied in a tubular flow reactor at 1.7 atm and over a range of temperatures of 900-1100K by De Bruycker et al. (2017). Species detection and measurement were performed with the help of gas chromatography and of two-dimensional gas chromatography (GCxGC) coupled with a time-of-flight mass spectrometer. Besides hydrocarbons, several oxygenated products were detected in the reactor effluent, including CO, H_2O, formaldehyde, acetaldehyde and ketene. Species measurements were also performed by gas chromatography in a low-pressure premixed flat flame under different conditions (φ=0.7, 1 and 1.3). During this study, a premixed flame was also used to measure laminar burning velocities for the combustion of the fuel at atmospheric pressure. These measurements were made under lean to rich fuel conditions (Φ=0.6-1.6). They detected more oxygenated compounds under those conditions. Another study was performed on 2-methyltetrahydrofuran in premixed flames at low pressure (P=0.04 atm) and for an equivalence ratio equal to 1.7 (Moshammer et al., 2013). The aim was to measure species concentration profiles using a time-of-flight molecular-beam mass spectroscopy.

II.4.2. Unsaturated furans

Even if furans and tetrahydrofurans are classified in the same furan family, because of the presence of double bonds, furans exhibit a very different oxidation behavior than tetrahydrofurans. Due to their complexity, studies on furans are still needed to understand fully their combustion. Figure 25 displays the structure of furan and some its alkyl-derivative (2-methylfuran and 2,5-dimethylfuran), and Table 19 presents a review of publications about the combustion and pyrolysis of furan. The experiments dealing with furan akylderivates are listed in Table 20.

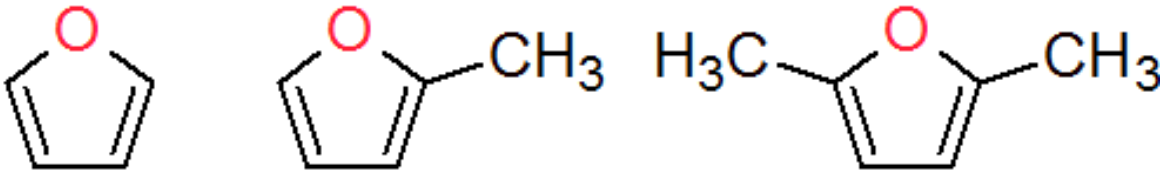

Figure 25. Structures of furan (on the left), 2-methylfuran (in the middle) and 2,5-dimethylfuran (on the right).

Furan and methyl furan

Studies of the reactions of furan started in the 80s, however only its thermal decomposition was then studied (Grela et al., 1985; Lifshitz et al., 1986b). The experiments were carried out in a shock tube (Lifshitz et al., 1986b) and in a tubular flow reactor (Grela et al., 1985) over a temperature range of 1050-1460K at low and high pressures (0.001 and 2 atm). Later, Organ and Mackie (1991) investigated the pyrolysis of furan in a shock tube at higher pressures (15-22 atm).

Table 19. Main experimental studies about furan combustion, oxidation and pyrolysis.

Experimental Conditions	Reference
Furan	
Shock tube	
T=1050-1460 K; P=2 atm; Φ=∞	(Lifshitz et al., 1986b)
T=1100-1700 K; P=15-22 atm; Φ=∞	(Organ and Mackie, 1991)
T=1300-1900 K; P=1-10 atm; Φ=0.5-2	(L. Wei et al., 2012)
T=950-1600 K; P=2-12 atm; Φ=0.5-2	(Eldeeb and Akih-Kumgeh, 2014)
Premixed flame	
T=600-1900 K; P=0.05 atm; Φ=1.4-2.2	(Tian et al., 2011)
T=500-2500 K; P=0.02-0.04 atm; Φ=1-1.7	(Liu et al., 2014)
Tubular flow reactor	
T=1050-1270 K; P=0.001 atm; Φ=∞	(Grela et al., 1985)
T=700-1200 K; P=1 atm; Φ=0.5-2	(Tran et al., 2017)

During the 2010s, the oxidation of furan was extensively studied. In 2011, a study was carried out in premixed furan flames coupled with molecular-beam mass spectroscopy with synchrotron-based tunable VUV photoionization (Tian et al., 2011). The experiments were performed over a temperature range of 600-1900 K, at low pressure (0.05 atm) and under rich conditions (Φ=1.4-2.2). Another study was carried out in a shock tube by Eldeeb et al. (2014) over the same equivalence ratio range, but for higher pressures (2-12 atm). Ignition delay time measurements were also performed during this study. In 2014, a new study in premixed flames was carried out for furan combustion under low pressures (0.02-0.04 atm) and under stoichiometric and rich conditions (Φ=1-1.7) (Liu et al., 2014). In this study, more than 50 species (CO_2, H_2O, H_2, CH_3…) were detected and identified using mass spectrometry and gas-chromatography.

The reactivity of 2-methylfuran was studied in shock tubes, in premixed flames and in a tubular flow reactor. Only two studies were on the pyrolysis of 2-methylfuran, one in a shock tube at a pressure of 2 atm (Lifshitz et al., 1997) and the other one in a tubular flow reactor at 0.001 atm (Grela et al., 1985). Three studies on the oxidation of this fuel were carried out in shock tubes (Somers et al., 2013a; Wei et al., 2013; Eldeeb and Akih-Kumgeh, 2014) over a range of temperatures of 950-1800 K, for pressures from 1 to 12 atm and over a large range of equivalence ratios (Φ=0.25-2). A combustion bomb was used to measure laminar burning velocities (Ma et al., 2014) at atmospheric pressure for 2-methylfuran blended with *iso*-octane (percentage of *iso*-octane in the mixture: 0, 20, 50, 100 %). Related-combustion species of 2-methylfuran were also studied in premixed flames (Tran et al., 2015a, 2014; Wei et al., 2012) under low pressures (0.02-0.04 atm). The experiments were carried out over a temperature range of 400-2500 K and under lean to rich conditions (Φ=0.8-1.7).

Dimethylfuran

Another alkyl derivative of furan is 2,5-dimethylfuran (DMF). This compound is also known to be a potential biofuel; thus its reactivity has been largely studied since the first oxidation work 10 years ago (Wu et al., 2009).

DMF oxidation and pyrolysis were studied in shock tubes, in a jet-stirred reactor, in a combustion bomb, in tubular flow reactors and in premixed flames. The first study of DMF was about its thermal decomposition in a tubular flow reactor at low pressure and over the temperature range 1050-1270 K (Grela et al., 1985). Then Lifshitz et al. (1998) studied DMF thermal decomposition in a shock tube at 2 atm and over a temperature range of 1050-1400 K. Djokic et al. (2013) studied the thermal decomposition of DMF at 1,7 atm and over a range of temperatures from 873 to 1100 K. Using gas chromatography, species detection showed the formation of mono- and polyaromatics at high conversions. A study in shock tubes was performed to study the reaction of DMF in presence of hydrogen atoms at pressures from 1.6 to 4.8 atm (Friese et al., 2013). The pyrolysis of DMF was also studied in tubular flow reactors (Cheng et al., 2014) under low pressures (P=0.004-1 atm) and under higher pressures (P=1-40 atm) by Alexandrino et al. (2015). In the latter work, the oxidation of DMF was also investigated under a large range of equivalence ratios (φ=∞-0.03).

Table 20. Main experimental studies about furan derivatives combustion, oxidation and pyrolysis.

Experimental Conditions	Reference
2-Methylfuran	
Shock tube	
T=1100-1400 K; P=2 atm, Φ=∞	(Lifshitz et al., 1997)
T=1100-1700 K; P=1-10 atm; Φ=0.25-2	(Wei et al., 2013)
T=1200-1800 K; P=1 atm; Φ=0.5-2	(Somers et al., 2013a)
T=950-1600 K; P=2-12 atm; Φ=0.5-2	(Eldeeb and Akih-Kumgeh, 2014)
Premixed flame	
P=0.04 atm; Φ=0.8-1.5	(Wei et al., 2012)
T=500-2500 K; P=0.02-0.04 atm; Φ=1-1.7	(Tran et al., 2014)
T=400-2500 K; P=0.04 atm; Φ=1.7	(Tran et al., 2015a)
Combustion bomb	
T=333-393 K[15]; P=1 atm; Φ=0.8-0.9	(Ma et al., 2014)
Tubular flow reactor	
T=1050-1270 K; P=0.001 atm; Φ=∞	(Grela et al., 1985)
T=700-1200 K; P=1 atm; Φ=0.5-2	(Tran et al., 2017)
2,5-Dimethylfuran	
Shock tube	
T=1050-1400 K; P=2 atm; Φ=∞	(Lifshitz et al., 1998)
T=970-1240 K; P=1.6-4.8 atm; Φ=∞	(Friese et al., 2013)
T=1300-1831 K; P=1-4 atm; Φ=0.5-1.5	(Sirjean et al., 2013)
T=1200-1350 K, P=2-2.5 atm, φ=∞	(Somers et al., 2013b)
T=950-1600 K; P=2-12 atm; Φ=0.5-2	(Eldeeb and Akih-Kumgeh, 2014)
T=1000-1400 K; P=5-12 atm; Φ=0.5-2	(Eldeeb and Akih-Kumgeh, 2015)
Jet-stirred reactor	
T=770-1220 K, P=10 atm, φ=0.5-2	(Somers et al., 2013b)
Combustion bomb	
T=393-2000 K; P=1-7.5 atm; Φ=0.8-1.5	(Wu et al., 2010)
T=393-2500 K; P=1 atm; Φ=0.8-1.5	(Wu et al., 2011)
T=393-2000 K; P=1 atm; Φ=0.9-1.5	(Li et al., 2012)
Tubular flow reactor	
T=1050-1270 K; P=0.001 atm; Φ=∞	(Grela et al., 1985)
T=873-1098 K; P=1.7 atm; Φ=∞	(Djokic et al., 2013)
T=780-1500 K, P=0.004-1 atm, φ=∞	(Cheng et al., 2014)
T=500-1400 K, P=1-40 atm, φ=∞-0.03	(Alexandrino et al., 2015)
T=700-1200 K; P=1 atm; Φ=0.5-2	(Tran et al., 2017)
Premixed flame	
T=400K; P=0.04 atm; Φ=2	(Wu et al., 2009)
T=298-358 K[15]; P=1-7.5 atm; Φ=0.6-1.6	(Somers et al., 2013b)
T=500-2500K; P=0.02-0.04 atm; Φ=1-1.7	(Togbé et al., 2014)
T=400-2500 K; P=0.04 atm; Φ=1.7	(Tran et al., 2015a)

[15] initial temperature

The first study to focus on its oxidation was carried out by Wu et al. (2009) in a premixed flame for a rich condition (Φ=2). The oxidation of DMF was also studied in combustion bomb at atmospheric pressure and for lean to rich conditions (Φ=0.8-1.5) (Wu et al., 2011). In 2012, a study was carried out in a constant volume bomb in order to measure laminar burning velocities for DMF and *iso*-octane blends (Li et al., 2012). The experiments were performed at atmospheric pressure and for DMF percentage in *iso*-octane from 0% to 30%.

Sirjean et al. (2013) studied the oxidation of DMF in a shock tube by measuring ignition delay times. Experiments were carried out at pressures from 1 to 4 atm for lean to rich conditions and over a range of temperatures from 1300 to 1831 K. The first kinetic model has also been proposed. In 2013, Somers et al. (2013b) also investigated DMF oxidation in a shock tube, in a jet-stirred reactor and in premixed flames. The pyrolysis of DMF was studied in a shock tube and oxidation experiments were carried out in a JSR and premixed flames under pressure (1-10 atm). Lean to rich conditions were studied in both systems (Φ=0.6-2). Another study of DMF oxidation was carried out in a shock tube under pressures from 2 to 12 atm and over a large range of equivalence ratios (Φ=0.5-2) (Eldeeb and Akih-Kumgeh, 2014). Eldeeb and Akih-Kumgeh (2015) also performed other measurements in a shock tube; ignition delay times were determined for pressures from 5 to 12 atm and for temperatures from 1000 to 1400 K. The experiments were carried out for DMF/*iso*-octane and a 1:1 mixture by volume.

Two studies were carried out in premixed flames coupled to electron ionization molecular-beam mass spectrometer and GCs at low pressures (P=0.02-0.04 atm), one over a range of equivalence ratios of 1-1.7 (Togbé et al., 2014) and the other one only under rich conditions (Φ=1.7)(Tran et al., 2015a).

Tran et al. (2017) carried out a comparative study of the oxidation of furan and its alkyl derivatives (2-methylfuran and 2,5-dimethylfuran). The oxidation studies were performed for low- to moderate-temperatures at atmospheric pressure and for lean to rich conditions (Φ=0.5-2) in a tubular flow reactor coupled to electron ionization molecular-beam mass spectrometer and GCs. Based on these new data, a kinetic model was developed with improvements of the low-temperature chemistry of these fuels and the computed and experimental results were compared as shown in Figure 26.

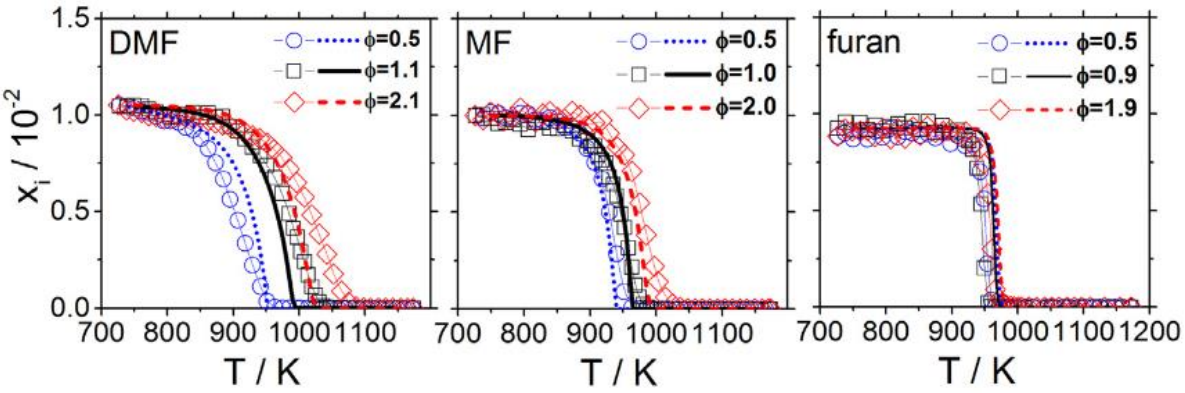

Figure 26. Fuel mole fractions as a function of reactor temperature (Symbols: experiment; lines: LMT model) (Tran et al., 2017).

The overall agreement between the model results and the experimental data is correct. However, some deviations can be observed, such as a shift of 50 K in the prediction of the reactivity for furan oxidation.

II.4.3. Conclusion

Many publications have been published on the reactivity of furan and its alkyl derivatives, especially a lot on DMF. Concerning furanic components, the understanding of their chemistry is possible thanks to the important database available even if any JSR facility has never been used. For tetrahydrofuran and its derivatives, the database is less important and especially no studies are available for dimethyl-tetrahydrofuran. Studies about the low-temperature oxidation have still to be done to understand the decomposition chemistry. Therefore, some research and experiments need to be done in this way.

II.5. Oxygenated aromatics

Oxygenated aromatic compounds (phenol, anisole, catechol, guaiacol, vanillin…) are gaining academic and industrial interest due to their presence in bio-oils produced from biomass fast pyrolysis (Nowakowska et al., 2014; Pejpichestakul et al., 2018; Pelucchi et al., 2019). Therefore, the influence of different functional groups on their combustion properties should be systematically addressed. Moreover, the impact of oxygenated aromatics on polycyclic aromatic hydrocarbons formation and soot growth should be better analyzed, as the high aromatic content of bio-oils could lead to undesired increased formation of particulate matter (Wang, 2011). In order to represent this fraction of the bio-oil, phenol, catechol, anisole, benzaldehyde and guaiacol can be good surrogates. Cresols are also good surrogates for the aromatics present in bio-oil and very few relevant publications for this molecule were found in the literature. The structure of these species is presented in Figure 27.

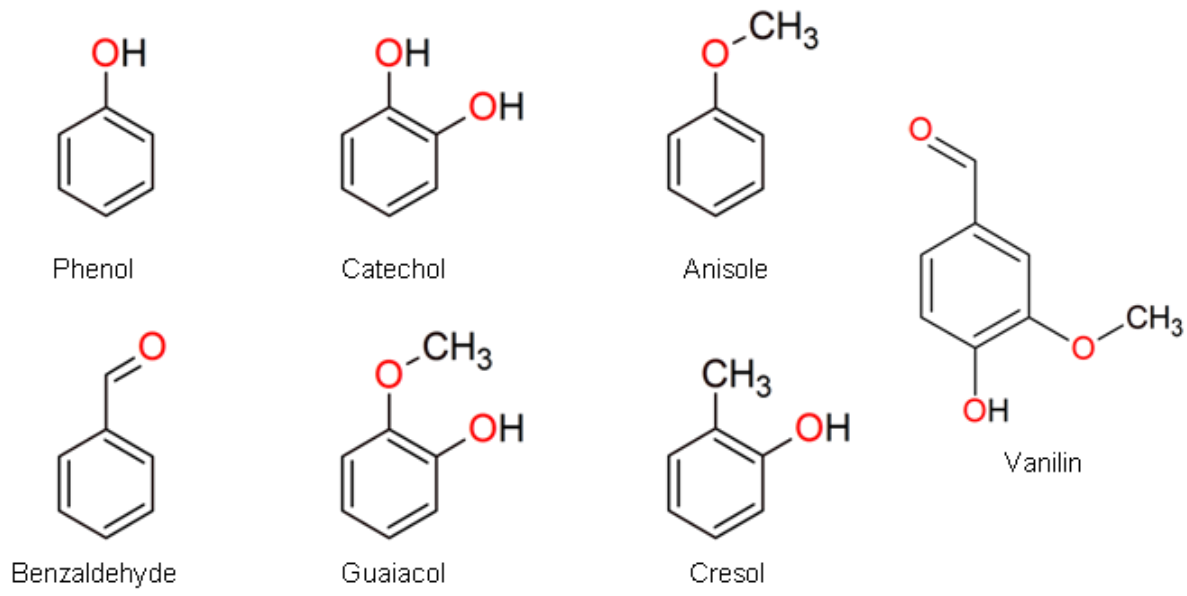

Figure 27. Structures of different oxygenated compounds present in bio-oils and possible surrogates.

For all these compounds, it can be noticed that their pyrolysis have been more studied than their oxidation and especially very few flame studies were reported as detailed further in the text.

II.5.1. Phenol and catechol

The pyrolysis of phenol was significantly more studied than its combustion. Table 21 presents the main experimental studies about phenol and catechol. The kinetics of hydrogen and hydroxyl radical attack on phenol were first studied in a shock tube (He et al., 1988). Experiments were performed over a range of temperatures from 1000 to 1150 K and over a range of pressures from 2.5 to 5 atm. Lovell et al. (1989) performed pyrolysis experiments in a tubular flow reactor at atmospheric pressure for temperatures over 1000 K. They identified the main pyrolysis products as being CO, 1,3-cyclopentadiene and benzene. Other phenol pyrolysis experiments were carried out under H_2 atmosphere in a tubular flow reactor at atmospheric pressure by Manion and Louw but over a larger range of temperatures (T=922-1175 K) (Manion and Louw, 1989). They identified the same main products as (Lovell et al., 1989). The pyrolysis of phenol was also studied in a shock tube at 2.5 atm (Horn et al., 1998). They deduced from their results that the main initiation pathway is: $C_6H_5O \Leftrightarrow C_6H_6O \Leftrightarrow C_5H_6+CO$.

Table 21. Main experimental studies about phenol and catechol combustion, oxidation and pyrolysis.

Experimental Conditions	Reference
Phenol	
Tubular flow reactor	
T=922-1175 K; P=1 atm; H2 atmosphere	(Manion and Louw, 1989)
T=1064-1162 K; P=1 atm; Φ=∞	(Lovell et al., 1989)
T=1170 K; P=1 atm; Φ=∞-0.6-1.7	(Brezinsky et al., 1998)
Shock tube	
T=1000-1150 K; P=2.5-5 atm-elementary step study	(He et al., 1988)
T=1450-1650 K; P=2.5 atm; Φ=∞	(Horn et al., 1998)
Catechol	
Tubular flow reactor	
T=1000 K; P=1 atm; Φ=∞	(Wornat et al., 2001)
T=500-1000 K; P=1 atm; Φ=∞	(Ledesma et al., 2002a)
T=700-1000 K; P=1 atm; Φ=∞	(Ledesma et al., 2002b)
T=700-1000 K; P=1 atm; Φ=∞	(Marsh et al., 2004)
T=350-650 K; P=1 atm; Φ=0.1-6	(Shin et al., 2004)
T=250-1000 K; P=1 atm; Φ=∞	(Lomnicki et al., 2008)
Batch reactor	
T=873 K; Φ=∞	(Asmadi et al., 2011a)
Cresol	
Batch reactor	
T=873 K; Φ=∞	(Asmadi et al., 2011a)

Brezinsky et al. (1998) studied the pyrolysis and the oxidation of phenol (φ=0.64 to 1.73) in a tubular flow reactor at atmospheric pressure near 1170 K. They found like the other studies that the main products formed during the pyrolysis were 1,3-cyclopentadiene, CO and benzene. In the case of the oxidation, 1,3-cyclopentadiene was still one of the main product, but other major species were also detected: CO, CO_2, acetylene, benzene, 1,3-butadiene, ethylene and methane.

Concerning catechol its pyrolysis was also more studied than its combustion. The only combustion study was carried out under heterogeneous cracking conditions at atmospheric pressure in a tubular flow reactor (Wornat et al., 2001). Nanoparticles of iron oxide were used and decreased the temperature at which catechol started to react. The equivalence ratio shown in Table 21 was determined from the value of the flows given in the study. Concerning pyrolysis, many studies were carried out in flow tubes in order to study the formation of polycyclic aromatic hydrocarbons (Wornat et al., 2001; Ledesma et al., 2002a, 2002b; Marsh et al., 2004). The pyrolysis of catechol was studied using gas-chromatography coupled with a FID and high pressure liquid chromatography (Ledesma et al., 2002a). Experiments were carried out in a tubular flow reactor over a range of temperatures of 500-1000 K and at atmospheric pressure. The pyrolysis of catechol was also studied in a tubular flow reactor at atmospheric pressure but for a wider range of products identified (Lomnicki et al., 2008). A large variety of products was identified by on-line gas-chromatography coupled with mass spectroscopy including phenol, benzene, dibenzofuran, dibenzo-p-dioxin, phenylethyne, styrene, indene, anthracene, naphthalene, and biphenylene. A study was also performed in a batch reactor for the pyrolysis of catechol and cresol under N_2 atmosphere at 873 K (Asmadi et al., 2011a). Catechol was more reactive than cresol, because of the presence of the -OH group instead of the -CH_3 group.

II.5.2. Anisole

Like phenol and catechol, the pyrolysis of anisole was more studied than its combustion, even if it is an important intermediate in kinetic mechanisms of aromatic compound oxidation. Table 22 presents main experimental studies about anisole pyrolysis and oxidation.

The pyrolysis of anisole was first studied by Schlosberg et al. (1983) in a batch reactor at a constant temperature of 723 K and at atmospheric pressure. The main products were methane and CO. Other detected products were H_2, water and phenol. The first study of the thermal decomposition of anisole at higher temperature was carried out by Lin and Lin (1986). Experiments were performed in a shock tube between 1000 and 1580 K. Following CO concentration by CO lasers, they demonstrated the decomposition of anisole into C_6H_5O and CH_3 and the importance of the two following channels:

$$C_6H_5O = CO+C_5H_5$$
$$C_6H_5O+CH_3 = \text{Cresol}$$

Pecullan et al. (1997) were the first to study both the pyrolysis and the oxidation of anisole in the same study. Experiments were made at high temperatures (T=999-1003 K) and at atmospheric pressure in a tubular flow reactor. They showed that the addition of oxygen did not have any impact on the products formed during oxidation compared to pyrolysis.

Table 22. Main experimental studies about anisole pyrolysis and oxidation.

Experimental Conditions	Reference
Anisole	
Batch reactor	
T=723 K; P=1 atm; Φ=∞	(Schlosberg et al., 1983)
Shock tube	
T=1000-1580 K; P=0.4-0.9 atm; Φ=∞	(Lin and Lin, 1986)
Perfectly stirred reactor	
T=850-1000 K; P=0.015-0.12 atm; Φ=∞	(Mackie et al., 1989)
Tubular flow reactor	
T=793-1020 K; P=1 atm; Φ=∞	(Arends et al., 1993)
T=999-1003 K; P=1 atm; Φ=∞-1.7	(Pecullan et al., 1997)
T=1023-1173 K; Φ=∞	(Platonov et al., 2001)
T=873-1373 K; P=1 atm; Φ=∞	(Friderichsen et al., 2001)
T=293-1573 K; Φ=∞	(Scheer et al., 2010)
T=573-1323 K; P=0.0005 atm; Φ=∞	(Li et al., 2014)
Jet-stirred reactor	
T=673-1173 K; P=1 atm; Φ=∞-1	(Nowakowska et al., 2014)

The pyrolysis of anisole was also studied in a tubular flow reactor but with the goal to detect products with a heavier weight than anisole (Platonov et al., 2001). They classified the products of pyrolysis in categories (light, phenolic and hydrocarbon) as a function of temperature. They showed that with an increase of the temperature less phenolic compounds were produced in favor of the two other types of products. The pyrolysis of anisole at atmospheric pressure in a tubular flow reactor was also studied by Friderichsen et al. (2001). Using a time-of-flight mass spectroscopy and FTIR spectroscopy, they identified some free radicals and other intermediates of the reaction so they were able to describe more precisely the formation of naphthalene. The same team (Scheer et al., 2010) performed another study with the same analysis techniques to validate the mechanism of decomposition of anisole proposed by the previous studies. The pyrolysis of anisole in a tubular flow reactor was also analyzed using vacuum ultraviolet single-photon ionization time-of-flight mass spectrometry (Li et al., 2014). During this latter study a comparison between the decomposition of three compounds (anisole, phenyl ethyl ether, and p-methyl anisole) was made and showed that the three compounds behave the same during the pyrolysis process.

Mackie et al. (1989) studied the pyrolysis of anisole in a perfectly stirred reactor for lower pressures (P=0.015-0.12 atm) and lower temperatures (T=850-1000 K). This reactor was similar to a jet-stirred reactor but the injection of the gas in the reactor is different. They also observed that CO and cresols were the main products and they identified phenol as one of the most important secondary products. In 1993 the pyrolysis of anisole mixed with hydrogen or fluorotoluene was investigated in a tubular flow reactor between 793 and 1020 K (Arends et al., 1993). Fluorotoluene was used to study in particular the methyl-oxygen bond homolysis. A kinetic model was developed during this study consisting of 37 reactions and 23 species. For some species (i.e. anisole, phenol, methane…), the predictions and the

experimental observations were in a good agreement; but some deviations for other species (i.e. CO, benzene…) were observed.

A study in jet-stirred reactor (Nowakowska et al., 2014) was performed to study the impact of methoxyphenol compounds on the production of polycyclic aromatic hydrocarbons under pyrolysis and stoichiometric oxidation conditions. A detailed kinetic model was developed consisting of 303 species and 1922 reactions and a good agreement was obtained with the experimental data. Figure 28 shows anisole depletion measured by gas chromatography and the prediction of the model. It can be seen that the overall agreement is good.

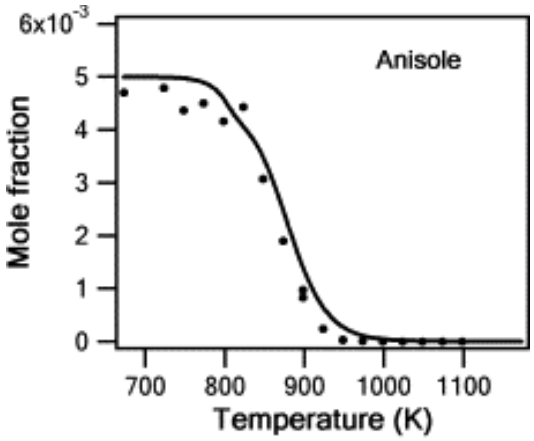

Figure 28. Mole fraction profile of anisole during oxidation experiments under stoichiometric conditions from (Nowakowska et al., 2014).

II.5.3. Benzaldehyde

Benzaldehyde is an aromatic aldehyde commonly considered in bio-oil surrogate formulation, and an important intermediate in the oxidation of other aromatic reference fuels such as toluene. Table 23 presents main experimental studies about benzaldehyde pyrolysis.

Table 23. Main experimental studies about benzaldehyde pyrolysis and oxidation.

Experimental Conditions	Reference
Benzaldehyde	
Batch reactor	
T=573-963 K; P=1 atm; Φ=∞	(Hurd and Bennett, 1929)
T=614-657 K; P < 1 atm; Φ=∞	(Solly and Benson, 1971)
Tubular flow reactor	
T=1050-1270 K; P=0.001 atm; Φ=∞	(Grela and Colussi, 1986)
T=450-1300 K; P=1 atm; Φ=∞	(Bruinsma et al., 1988b)
T=1200-1800 K; P=0.2 atm; Φ=∞	(Vasiliou et al., 2013)

Benzaldehyde oxidation has never been previously investigated experimentally and no product formation profiles were reported in the very limited pyrolysis studies available in the literature. Benzaldehyde pyrolysis has been studied in batch reactors by Hurd and Bennet (1929) and by Solly and Benson (1971) covering a temperature range from 573K to

963K at atmospheric pressure. Experiments on this reaction have also been carried out in tubular flow reactors by Grela and Colussi (1986) at high temperatures (1005-1270K) and low-pressure (P=0.001atm), by Bruinsma et al. (1988a) at atmospheric pressure and over a temperature range from 773 K to 1173 K and by Vasiliou et al. (Vasiliou et al., 2013) between 1200 K and 1800 K and between 0.1 and 0.2 kPa. These studies showed that benzaldehyde easily decomposes to phenyl radical plus H atoms and CO:

$$C_6H_5CHO\ (+M) \rightarrow C_6H_5CO + H \rightarrow C_6H_5 + CO + H$$

contrary to the typical decomposition of aliphatic aldehydes where the alkyl acyl bond is the weakest (R-CHO). However, none of these studies provided mole fraction profiles for the fuel or the decomposition products for benzaldehyde pyrolysis.

II.5.4. Guaiacol

Guaiacol is also a good candidate for a bio-oil surrogate, due to its similarity with lignin. Furthermore, it could be an important intermediate from the decomposition of polycyclic oxygenated compounds. Table 24 presents main experimental studies about guaiacol pyrolysis. Most of the experiments on guaiacol were performed in batch reactors under pyrolysis conditions.

The first published study was performed by Vuori and Bredenberg (1987). They succeeded in identifying phenol and catechol as main products at 623 K with a gas chromatograph coupled to a mass spectrometer. Suryan et al. (1989) studied the effect of substituted groups on anisole and specially hydroxyl and methoxy groups. Experiments were carried out at very low pressure (P=0.1 Pa atm). Asmadi et al. studied the pyrolysis of syringol and guaiacol (Asmadi et al., 2011b) and the pyrolysis of the mixture of both (Asmadi et al., 2011c). For syringol and guaiacol, the methoxy group was detected as the initiator of the decomposition for T > 623 K. They showed that during the early stage of pyrolysis, the tar formation was favored in the case of the mixture.

The most recent study was performed by Cheng et al. (2017). Using mass spectroscopy and FTIR spectroscopy, they showed that o-quinonemethide is a low-temperature intermediate during the pyrolysis of guaiacol and they also proved that salicyl aldehyde is a higher temperature intermediate. Custodis et al. (2014) carried out experiments in a tubular flow reactor at atmospheric pressure using mass spectroscopy and under high-vacuum pyrolysis conditions. Their objective was to study the fast pyrolysis of lignin using surrogates compounds: guaiacol and diphenylether. They studied the intermediates formed during the pyrolysis and concluded that the stabilization of the primary intermediates could lead to a better product selectivity of lignin toward desired compounds.

Nowakowska et al. (2018) studied also the pyrolysis and the oxidation under stoichiometric conditions of guaiacol in a jet-stirred reactor between 623 and 923 K. With the help of gas chromatography, 22 species were detected for pyrolysis experiments and 42 for oxidation ones. Those data were used for the development of a kinetic model, based on the one developed for anisole by the same team (Nowakowska et al., 2014). The model successfully predicts the consumption of guaiacol and the formation of the main products such as catechol or methyl catechols.

Table 24. Main experimental studies about guaiacol pyrolysis.

Experimental Conditions	Reference
Guaiacol	
Batch reactor	
T=623-673 K; P=1 atm; Φ=∞	(Vuori and Bredenberg, 1987)
T=300-1275 K; P=0.1 Pa; Φ=∞	(Suryan et al., 1989)
T=823 K; P=1 atm; Φ=∞	(Asmadi et al., 2011c)
T=623-823 K; P=1 atm; Φ=∞	(Asmadi et al., 2011b)
T=300-850 K; P=1 atm; Φ=∞	(Cheng et al., 2017)
Tubular flow reactor	
T=873-1123 K; P≤1 atm; Φ=∞	(Custodis et al., 2014)
Jet-stirred reactor	
T=623-923 K; P=1 atm; Φ=∞-1	(Nowakowska et al., 2018)

II.5.5. Conclusion

Several studies were performed on the pyrolysis of oxygenated aromatic compounds and especially for phenol, catechol, anisole and guaiacol. However, more studies have to be done under oxidation conditions and on intermediate species detection and quantification. It could be a huge help in order to develop more accurate detailed kinetic mechanisms.

II.6. Nitrogen-containing compounds

Nitrogen-containing compounds are specific species also present in bio-oils. They are mainly produced from biomass from animal origins. The nitrogen atoms come indeed from the proteins present in the biomass of origin (Azargohar et al., 2013). These compounds could lead to the emissions of nitrogen oxides, which are pollutants with a huge impact on human health and environment (World Health Organization, 2006). Nitrogen-containing compounds are mostly present under the form of cyclic molecules in bio-oils (Azargohar et al., 2013; Negahdar et al., 2016). To surrogate this fraction of bio-oils, pyrrole and pyridine can be used for unsaturated compounds and pyrrolidine for saturated ones. Figure 29 displays the structures of these three compounds.

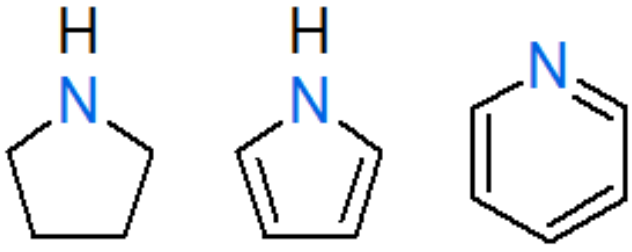

Figure 29. Structures of pyrrolidine (on the left), pyrrole (in the middle) and pyridine (in the right).

Table 25 presents studies on pyrrolidine combustion and Table 26 presents studies on pyrrole and pyridine.

Table 25. Main experimental studies about pyrrolidine.

Experimental Conditions	Reference
Pyrrolidine	
Premixed flame	
P=0.04 atm; Φ=1.4	(Wang et al., 2011)
Shock tube	
T=900-1400 K; P=1 mPa; Φ=∞	(Lifshitz et al., 1987)
Tubular flow reactor	
T=950-1450 K; P=0.04 atm; Φ=∞	(Lucassen et al., 2013)

Only three relevant studies were found about pyrrolidine combustion and pyrolysis. The first study was carried out in a shock tube at very low pressure (P=1 mPa) for the pyrolysis by Lifshitz et al. (1987). They succeeded in identifying some stable reaction products using gas chromatography and mass spectrometry. They observed that the main product among the nitrogen-containing compounds was hydrogen cyanide (HCN).

Later a study in premixed flame was carried out by Wang et al. (2011) to study the combustion of pyrrolidine at low pressure (P=0.04 atm) under rich conditions (Φ=1.4) and to propose a decomposition pathway. Using molecular-beam mass spectrometry with tunable synchrotron vacuum ultraviolet photoionization, about 50 species were identified including nitric oxide or hydrogen cyanide. The last study on pyrrolidine was performed by the same team as the previous one (Lucassen et al., 2013). They used a tubular flow reactor at low pressure (P=0.04 atm) to study the pyrolysis of this fuel using the same analytic tools. They also observed that the main product among the nitrogen-containing compounds was HCN followed by acetonitrile.

The first study about pyrrole was carried out in a shock tube under pyrolysis conditions (Lifshitz et al., 1989). This study is not so different from the previous one on pyrrolidine. However they observed more products during the pyrolysis of pyrrole. Another pyrolysis study was carried out in a shock tube (Mackie et al., 1991). The pressure was set between 7.5 and 13.5 atm and the temperature was over a range of 1200 to 1700 K. They used gas chromatography with mass spectroscopy and FTIR spectroscopy to determine species concentrations.

Concerning pyridine, its pyrolysis was first studied in 1980, then its oxidation in 1982 by Houser et al (1980, 1982). A tubular flow reactor at atmospheric pressure was used in both cases. For the pyrolysis the main volatile products were HCN and C_2H_2, whereas, for oxidation, NO and NO_2 had a bigger contribution in the gas composition. In 1990, a shock tube coupled with GCs, mass- and FTIR spectroscometers was used to quantify the products of pyridine pyrolysis (Mackie et al., 1990). These experiments were made at high pressures (P=7-11 atm) and the main volatile products at high temperature was again HCN. The thermal decomposition of pyrazine, pyrimidine and pyridine in a shock tube was studied at low pressures (P=0.2-0.5 atm) (Kiefer et al., 1997). Major products observed were HCN, acetylene, cyanoacetylene and diacetylene.

Table 26. Main experimental studies about pyrrole and pyridine.

Experimental Conditions	Reference
Pyrrole	
Tubular flow reactor	
T=700-1500 K; P=1 atm; Φ=0.9-22	(Lumbreras et al., 2001)
T=1250-1700 K; P=0.002 atm; Φ=∞	(Hong et al., 2009)
T=800-1400 K; P=1 atm; Φ=0.07-0.2	(Yamamoto et al., 2012)
T=700-1100 K; P=1 atm; oxy-fuel conditions	(Wang et al., 2016b)
Shock tube	
T=1050-1450 K; P=1 mPa; Φ=∞	(Lifshitz et al., 1989)
T=1200-1700 K; P=7.5-13.5 atm; Φ=∞	(Mackie et al., 1991)
T=1100-1800 K; P=2-5.6 atm; Φ=0.5-2	(MacNamara and Simmie, 2003)
Pyridine	
Shock tube	
T=1300-1800 K; P=7-11 atm; Φ=∞	(Mackie et al., 1990)
T=1600-2300 K; P=0.2-0.5 atm; Φ=∞	(Kiefer et al., 1997)
T=1000-2200 K; P=8-20 atm; Φ=0.6-5	(Ikeda et al., 2000)
T=1590-2340 K; P=2.2-3.4 atm; Φ=∞	(Memon et al., 2000)
T=1100-1800 K; P=2-5.6 atm; Φ=0.5-3	(MacNamara and Simmie, 2003)
Tubular flow reactor	
T=875-1050 K; P=1 atm; Φ=∞	(Houser et al., 1980)
T=675-775 K; P=1 atm; Φ=0.25-15.5	(Houser et al., 1982)
T=700-1500 K; P=1 atm; Φ=0.06-6	(Alzueta et al., 2002)
T=700-1100 K; P=1 atm; oxy-fuel conditions	(Wang et al., 2016b)
Premixed flame	
T=400-1850 K; P=0.02-0.04 atm; Φ=0.5-2	(Tian et al., 2008)

The oxidation of pyridine (Ikeda et al., 2000) was also studied in a shock tube for very rich to lean conditions (Φ=0.6-5) for temperatures from 1000 to 2200 K and for pressures from 8 to 20 atm. NO formation was only observed under lean and stoichiometric conditions. The pyrolysis in a shock tube was again investigated by Memon et al. in 2000 (Memon et al., 2000). The pressure was over a range of 2.2 to 3.4 atm and the temperatures ranged from 1600 to 2350 K. With these data a decomposition pathway was proposed: a C-H scission into a decomposition of the pyridyl radical into C_4H_3 and HCN.

An experimental study of pyridine oxidation both in the absence and in the presence of NO has been performed (Alzueta et al., 2002) in a tubular flow reactor at atmospheric pressure and over a range of temperatures from 700 to 1500 K. The main nitrogen-containing species formed were HCN, NO and N_2O. Adding NO as bath gas decreased the temperature for the observation of the fuel conversion. As presented in the previous part, ignition delay times were measured for pyrrole and pyridine in shock tubes (MacNamara and Simmie, 2003) (See Figure 30). Under the same conditions, pyridine exhibits a higher reactivity than pyrrole.

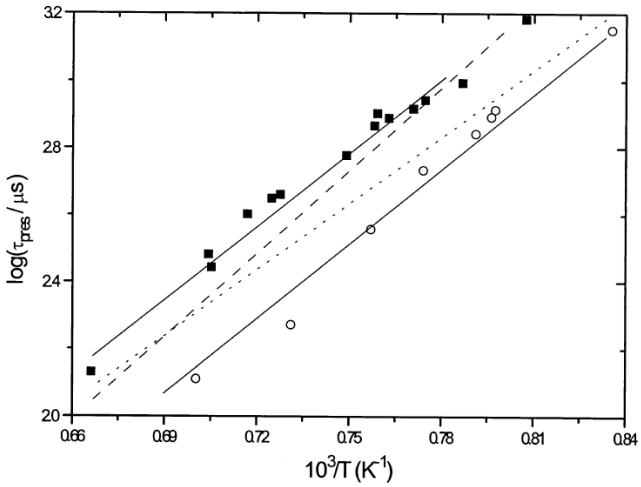

Figure 30. Ignition delay time comparisons. Dots: experiments of (MacNamara and Simmie, 2003)(■ pyrrole ○ pyridine). Lines: model of (Wu et al., 2011), dashed lines model of (Thyagarajan and Bhaskaran, 1991). (Fuel = 1.0 %, Φ=1.0 and pressure 2.2 atm).

Oxidation of pyridine was studied in a low pressure premixed flame (Tian et al., 2008) for lean to rich conditions (Φ=0.5-2) with tunable synchrotron vacuum ultraviolet (VUV) photoionization and molecular-beam mass spectrometry techniques. About 80 intermediates were identified and many new species, especially nitrogenous ones were detected in this work.

II.6.1. Conclusion

Nitrogen-containing compounds are very important species in bio-oils, especially concerning their ability to form NO_x and nitrogen containing organic molecules like HCN. The combustion and pyrolysis of pyrrolidine, pyrrole and pyridine were studied under several conditions, but no experiment was carried out in a jet-stirred reactor. The specificities of this kind of reactor could be used to obtain additional data in order to improve and develop detailed kinetic models for this category of molecules.

II.7. Conclusion of the state of the art

Concerning bio-oils, the complexity of the composition does not allow us to define a clear surrogate yet. Bio-oil composition determination is still limited by analytical tools, even if some new techniques are now available (e.g., two-dimensional gas chromatography). The composition of the biomass of origin is determinant in the final composition as much as the process conditions. However, it is possible to characterize the compounds present in the oil in term of chemical families.

This chapter shows that many studies were found in the literature for light alcohols (i.e. ethanol or propanol) or small aldehydes (mainly acetaldehyde), but the heavier compounds, such as pentanol or pentanal, were significantly less studied. Other oxygenated compounds decompositions, such as the carboxylic acids or aromatic aldehydes, were also less investigated. In addition, almost only the pyrolysis of oxygenated aromatic compounds was studied with a lack of data under oxidation conditions. Knowledge about the formed pollutants and their formation pathways are still missing.

Our approach was thus to study each of these families by carefully choosing some representative compounds and to determine their combustion behaviors. The present manuscript presents a comprehensive study in a jet-stirred reactor with gas-chromatography analysis of the oxidation of C_4-C_5 linear alcohols, aldehydes and carboxylic acids, as well as that of furan and benzaldehyde. To our best knowledge, the studies on carboxylic acids and benzaldehyde oxidation are the first ever published.

III. EXPERIMENTAL SET-UP AND METHODS

The main part of this PhD work has been dedicated to the production of experimental data. The aim was to use, as a fuel, molecules which surrogates a part of the bio-oils as described in the previous chapter. The results produced are the identification and the mole fraction profiles of the combustion products. These data will help to understand the decomposition chemistry of the fuel and will allow the identification of the kinetic pathways controlling the reactivity.

This part of the manuscript is dedicated to the presentation of the experimental apparatus and of the method used to obtain the results.
The experimental apparatus is composed of 4 areas:

I: Liquid fuel storage and flow control

II: Gas flow control and evaporation chamber

III: Pre-heating and reactor

IV: Pressure control and gas chromatographs (GC) for analysis

Figure 31 shows a schematic of the setup of the reactor, here a jet-stirred reactor (JSR), with the analytical tools used for this study, gas chromatographs.

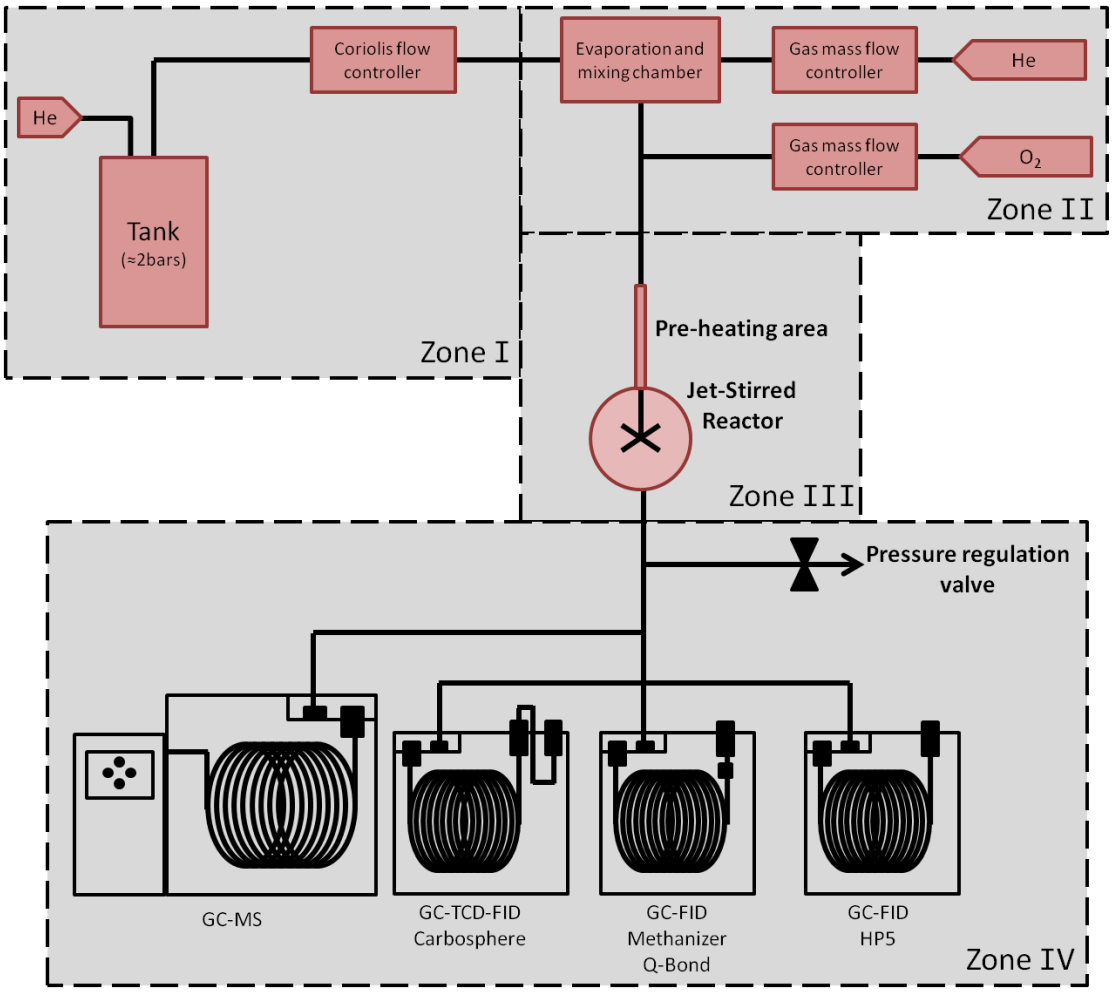

Figure 31.Schematic of the JSR facility used in this study.

Each part of the set-up will be presented and detailed in the next pages.

III.1. List of the fuel studied

During this work, eight fuels have been experimentally studied. Table 27 summarizes the list of studied fuels and some of their chemicophysical properties. All the fuels have been provided by Sigma-Aldrich. They have been sorted according to the different chemical families they surrogate:

- Alcohols
- Aldehydes
- Carboxylic acids
- Tetrahydrofuran, furan and derivatives
- Oxygenated aromatics

Table 27. Fuel information and chemical properties.

Fuel name	Structure	Chemical formula	Molar mass (g/mol)	Boiling point (°C)	Purity
n-Butanol	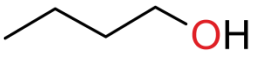	$C_4H_{10}O$	74.12	117	99%
n-Pentanol	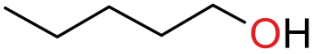	$C_5H_{12}O$	88.15	138	99%
n-Butanal	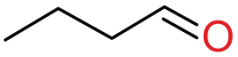	C_4H_8O	72.11	75	99%
n-Pentanal	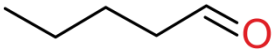	$C_5H_{10}O$	86.13	103	97%
Butanoic acid	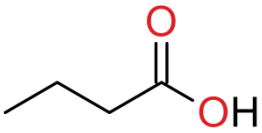	$C_4H_8O_2$	88.11	164	99%
Pentanoic acid	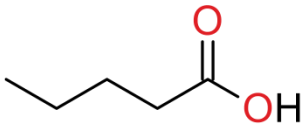	$C_5H_{10}O_2$	102.14	185	99%
Furan		C_4H_4O	68.07	32	99%[16]
Benzaldehyde	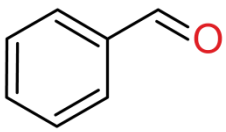	C_7H_6O	106.12	179	99%

[16] Stabilized with 250 ppmw butylated hydroxytoluene

III.2. Liquid storage and liquid flow control

In this work, only liquid fuels are studied. They are stored in a metallic tank pressurized with helium. The pressure in the tank is set in order to allow an easy flow of the liquid into the liquid flow controller to around 2 bars.
To measure the liquid flow rate exiting the tank, a Coriolis flow controller has been installed after the tank. Its role is to measure the liquid flow continuously and to send the information to a valve placed downstream. The inlet flow rate is regulated to ensure a stable flow during the experiments. Figure 32 shows a screenshot of the liquid flow regulation. It can be seen that the actual value (green line) is stabilized around the set-point value (red line). At a certain time after reaching the set-point value, the flow is disturbed but the regulation succeeds in stabilizing the flow.

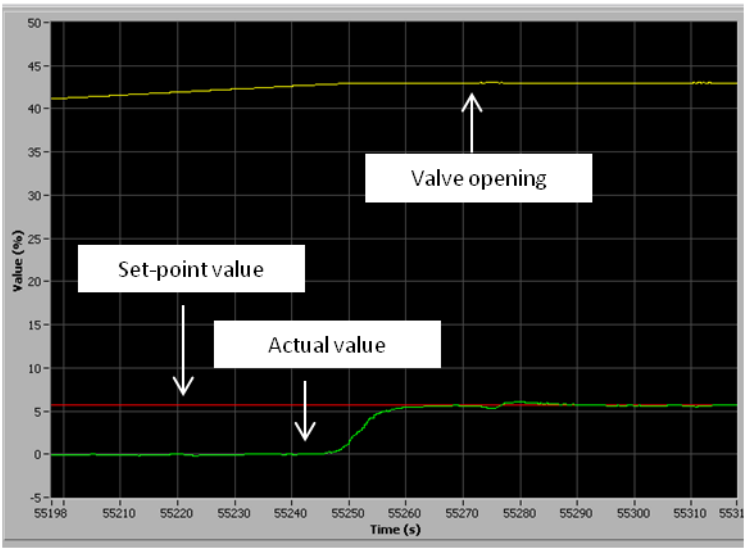

Figure 32. Screenshot of the liquid flow regulation during the start of an experiment.

The flow controller measures the mass flow rate of the liquid thanks to the Coriolis Effect. The controller gives so an absolute value of the flow rate, independent of the liquid going through the flow controller with an relative error around 1%.

III.3. Gas inlet

The experiments are performed under diluted conditions (0.5%mol of fuel). Helium is chosen as bath gas for all the experiments. The dilution helps to control the temperature homogeneity inside the reactor by limiting the exothermic reaction influence on the reactor temperature. It is also the carrier gas of the chromatographs used for the analysis in order to keep the same bath gas all along the experiments.
The flow rate of the gases is measured by thermal mass flow controllers, such as the one shown in Figure 33.

Figure 33. Picture of the three mass flow controllers installed on the set-up.

Those apparatuses have a relative error of 0.5%, which makes them very reliable to measure the flow rates of the different gases. Depending on the maximal flow rate value the corresponding flow-meter is chosen in order to have the same range of flow. The maximal range of work for each flow-meter is presented in Table 28.

Table 28. Range of flow rate for each flow meter depending on the gas used

Gas	Oxygen	Helium	Compressed air (Flush)
Maximal flow rate in nL/min	0.2	2	2

Three kinds of flow meters are selected corresponding to the three used gases: oxygen, helium and also compressed air. Compressed air is not used during the experiments but between two experiments as a flush. An important flow of air is used in order to purge the reactor and the line after each experiment. It prevents the adsorption of products at the walls of the set-up between two experiments and helps to clean the set-up of the low volatility species. This flush is used during the experiments on carboxylic acids.

III.4. Evaporation and mixing chamber

To produce vapor from the liquid fuel, a device using the controlled evaporation and mixing technology is placed before the entrance of the reactor. This device works in two main steps:

- Mixing of the liquid and the bath gas into an aerosol
- Evaporation of the aerosol at constant temperature

The main aim of this apparatus is to lower the boiling point of the liquid by diluting it in the bath gas and by creating an aerosol with the liquid. So the evaporator temperature is very close from the one of the liquid but is largely enough to have a pure gas phase. It also ensures that the fuel does not react in this part of the set-up as the temperature is too low to promote the reactivity.

III.5. Determination of the inlet composition and calculation of the flow rate required

In order to control the experimental conditions, we need to calculate the flow rate of each inlet species. We have first to determine the inlet mole fraction of each of these compounds. The fraction of fuel is fixed and then the mole fraction of oxygen will be deduced from the stoechiometric combustion equation and from the equivalence ratio imposed. The stoichiometric combustion equation for a standard hydrocarbon in presence of oxygen is:

$$C_nH_y + zO_2 \rightarrow nCO_2 + \frac{y}{2}H_2O \text{ with } z = \left(n + \frac{y}{4}\right) \quad (1)$$

In this equation, z is the stoechiometric coefficient of oxygen. This value will be used to calculate the equivalence ratio φ. This value represents the deviation of experimental conditions to the stoechiometric case. The equivalence ratio φ is calculated by:

$$\varphi = \frac{x_{fuel}/x_{o_2}}{\left(x_{fuel}/x_{o_2}\right)_{stoechio}} = \frac{x_{fuel}/x_{o_2}}{1/z} = \frac{x_{fuel} * z}{x_{o_2}} \quad (2)$$

And as we have already fixed the inlet mole fraction x_{fuel}, we can calculate the mole fraction of oxygen with the equation (3).

$$x_{o_2} = x_{fuel} * z/\varphi \quad (3)$$

The mole fraction of helium is then calculated to complete the mixture as it is the bath gas. After those calculations, the mole fractions of each inlet compounds are known for any equivalence ratios. Typically experiments will be carried out for three equivalence ratios:

- φ=1: corresponding to the stoechiometric conditions.
- φ=0.5: oxygen fraction is higher than the stoechiometric one and so it is fuel-lean conditions.
- φ=2: contrary to the previous conditions, it is fuel-rich conditions.

The mole fractions are then used in the process of the mass flow rate determination as explained below:

$$mass\ flow\ rate = total\ mole\ flow\ rate * \ mole\ fraction * molar\ mass$$

$$\text{with } total\ mole\ flow\ rate = \frac{pressure * volume\ of\ the\ reactor}{R * temperature * residence\ time}$$

where R is the ideal gas constant. Examples of calculation Excel worksheet are given in Appendix I.

III.6. Jet-stirred reactor

The JSR consists of a fused silica sphere (volume 92 cm^3) equipped with four injection nozzles positioned in a cross located at the center of the sphere. Figure 34 shows a picture of a jet-stirred reactor. The gas enters the reactor via the tube on the left and exits the reactor trough the tube on the right. In the center, the four nozzles in a cross shaped can be seen.

Figure 34. Picture of a jet-stirred reactor. The cross shaped nozzle can be seen in the center of the reactor.

The inner diameter of the nozzle is around 0.3 mm which leads to the creation of turbulent jets inside the sphere. This injection method ensures high turbulence in the reactor and leads to homogeneity in product concentration of the gas phase. Thanks to this homogeneity, the reactor can be assimilated to a perfectly stirred reactor working under steady-state conditions considering some criteria (Matras and Villermaux, 1973):

- Minimal gaseous jet speed to have a turbulent flow

$$Re > 800 \; and \; so \; \tau \leq \frac{\rho A R^3}{230 \eta d}$$

- Maximal gaseous jet speed equal to the one of sound to keep the reactor intact

$$\tau \geq \frac{4}{3} \frac{R^3}{d^2 c_{sound}(T,P)}$$

- Recycling rate of gas higher than 30 to have a mixing time inferior to the residence time

$$\frac{R}{d} > 64$$

where *Re* is the Reynolds number, R is the reactor radius, d the nozzle internal diameter, ρ the gas density, η the gas dynamic viscosity, τ the residence time and A a constant.
Once those parameters are correctly set, the reactor can be considered as perfectly stirred and the concentrations are taken as equal in each point of the reactor.

To ensure thermal homogeneity, the isothermal JSR is preceded by a quartz annular preheating zone, in which the temperature of the gas is increased up to the reactor temperature as described in Figure 35. The gas residence time inside the annular preheater is very short compared to its residence time inside the reactor (a few percent) so the reactivity in this section is negligible. So the low temperature reactions are not important in the preheating area and we can consider that reactions only occur in the spherical reactor section. The heating is ensured by resistances (Thermocoax) carefully rolled to fit the reactor and the preheating zone shapes, which allows flexibility and swiftness in the heating of each area. Temperatures are measured by several K-type thermocouples: one is located in a glass finger inside the inlet cross for the actual reaction temperature measurement, and two

are located between the resistances and the external wall of the reactor for the temperature control. The resistance allows increasing the temperature up to 1273K, above that the reactor could be damaged and the resistance will quickly deteriorate themselves. To have a better energetically efficiency, the reactor and the resistance are wrapped into insulating silica wool maintained by aluminum foils and steal wire as show in Figure 35.

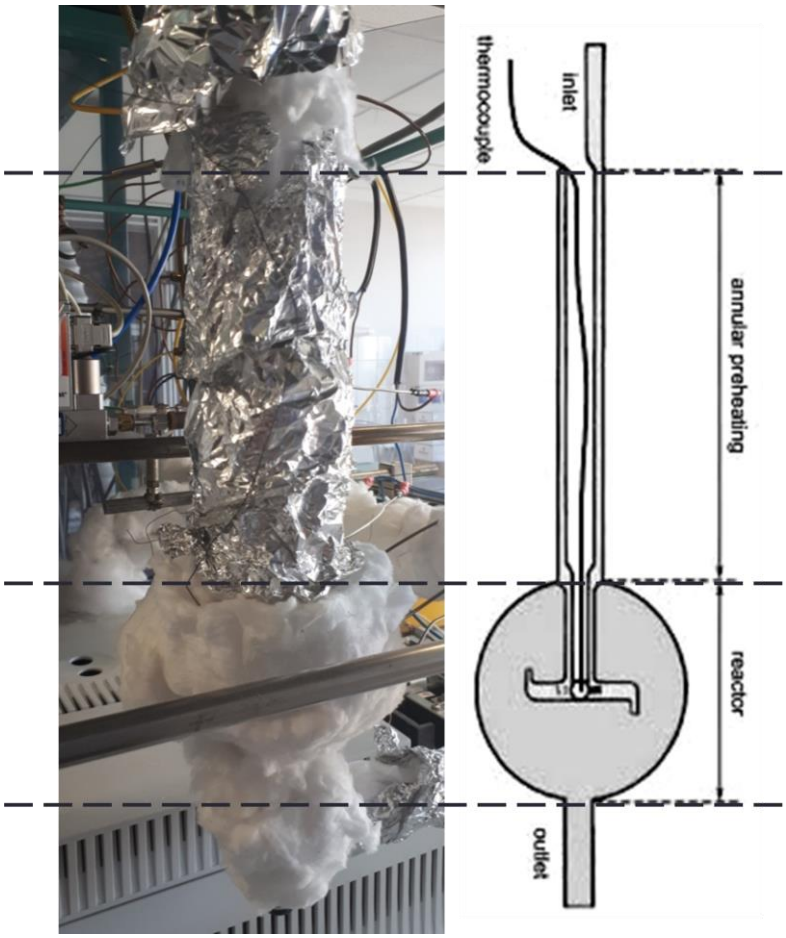

Figure 35. Picture of the reactor used for the experiments insulated and scheme of the reactor with description of each part.

III.7. Gas chromatograph analysis

The outlet gas leaving the reactor is then transferred by a metallic heated line maintained at 420 K to three gas chromatographs (GCs) to analyze the wide range of products formed by the reactions, similar to the three one presented in Figure 36.

Figure 36. Picture of the three chromatographs used for the analysis. From the left to the right: Shimadzu GC-2014, Agilent 6850 and Agilent 7890A.

The first chromatograph, equipped with a Carbosphere packed column, a thermal conductivity detector (TCD) and a flame ionization detector (FID), is used for the quantification of light-weight compounds like methane, ethylene, acetylene and ethane. The second chromatograph is fitted with a Q-Bond capillary column and a FID preceded by a methanizer and is used for the quantification of compounds containing from 2 carbon atoms, like acetylene or ethylene, up to species containing up to 5 carbon atoms. The methanizer (nickel catalyst for hydrogenation) allows the detection of species like CO, CO_2 and CH_2O with a good sensitivity and increases the sensitivity for species containing oxygenated functional groups in a general manner. A third gas chromatograph equipped with a HP-5 capillary column is used for the detection of the heaviest compounds (C_{5+}). The identification of reaction products is performed using another gas chromatograph equipped with both type of capillary columns and coupled to a mass spectrometer (quadrupole).

Figures 37, 38 and 39 present three examples of chromatographs obtained for three different oxidation experiments. Figure 37 shows 5 peaks corresponding to different products obtained during butanol oxidation. The peaks are well separated and are in a Gaussian shape. However, the fourth peak corresponds to the co-elution of acetylene and ethylene and thus it is impossible to quantify each product separately. In this case another gas chromatograph with another column has been used for the quantification of each product.

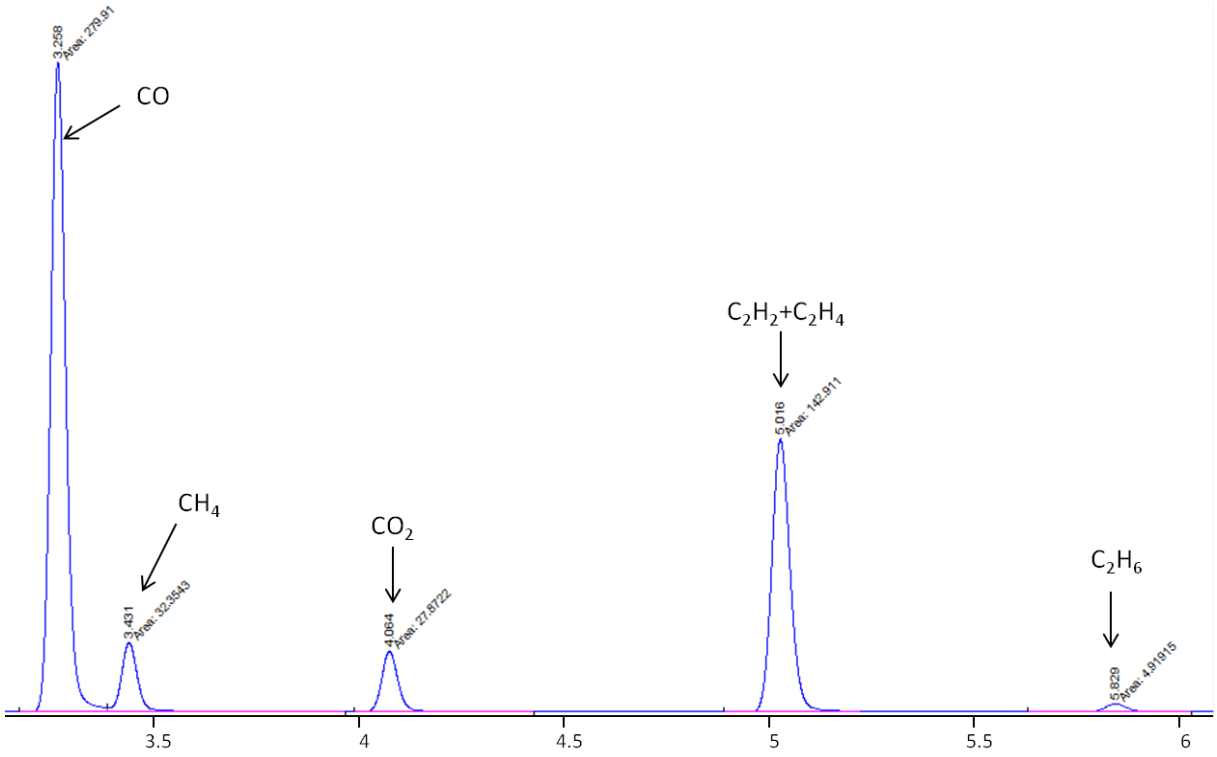

Figure 37. Products peaks during butanol oxidation at 900 K under stoichiometric conditions (Plot-Q column).

Figure 38 presents the peak of butanoic acid obtained for an oxidation experiment at 975 K. The peak in this case does not have a Gaussian shape and thus its quantification is more complex than usual. Furthermore the long retention time (2 mins) may lead to co-elution with other compounds.

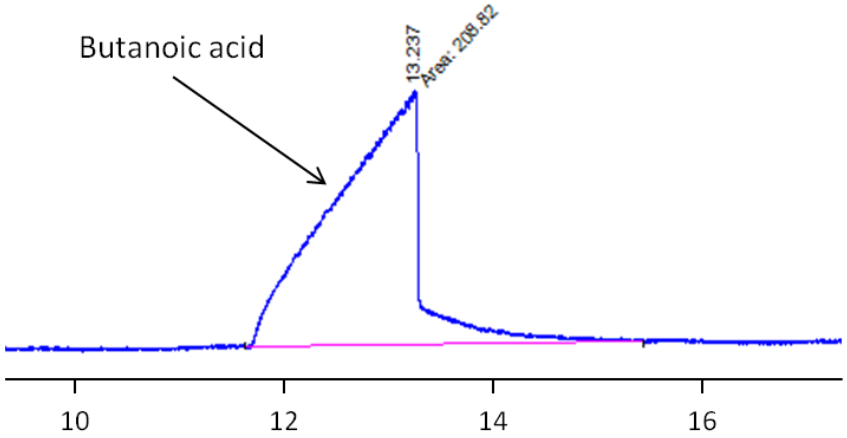

Figure 38. Butanoic acid peak during oxidation experiments at 975 K under stoichiometric conditions (HP-5 column).

Figure 39 presents a chromatogram obtained during the oxidation of benzaldehyde. In this case, we can observe that the number of peak is important and that several peaks are under the detection limit. Also some peaks do not have a Gaussian shape, they present an important tailing, which can lead to a higher uncertainty in the mole fraction determination.

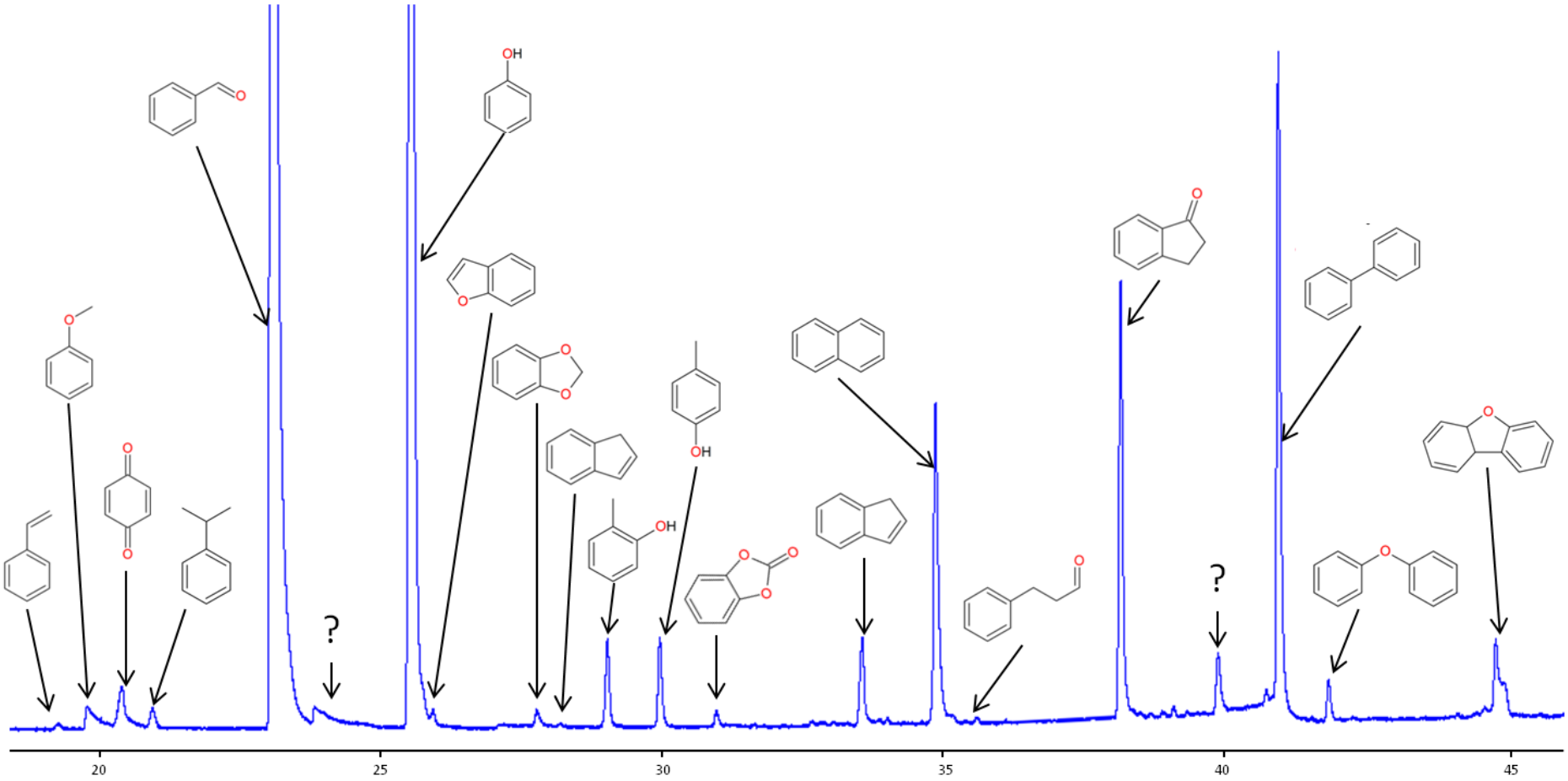

Figure 39. Products peaks during benzaldehyde oxidation at 925 K under stoichiometric conditions (HP-5 column).

Two methods could be used to sample the gas:

- Using a metallic heated line connecting the outlet of the reactor to the inlet of the gas chromatograph. In this case we talk of an online analysis. The gas is then injected in the GC thanks to a 6-way valve equipped with a sampling loop.
- With a trap at liquid nitrogen temperature located at the outlet of the reactor. It is an offline analysis. The trap condensates the outlet gases which are then dissolved in a solvent (e.g. acetone or ethanol). This liquid sample is then injected in the GCs with a syringe. The main limitation is that the “permanent gases” are not trapped. Only the heaviest fraction of the gases is sampled with this technique. Furthermore some recombination products can be formed with the solvent used for the dilution of the liquefied sample. On the contrary with an online analysis, the probability to form recombination products is lower and all the gases are analyzed even the lightest. That is why we used mainly online analysis for the identification of our reaction products.

It is possible that condensation and physical adsorption occur on some surfaces in the manifolds (cold points, valve, gums). This could affect the quality of the results and solutions have to be found to limit those phenomena as much as possible. This problem can specifically occurs with highly oxygenated molecules such as acids.One solution consists in coating the surface with the fuel before the occurrence of any reactions (Doolan et al., 1986). In our case, the surfaces are constantly heated to limit the condensation of the heaviest compounds, so the controlled coating of the surfaces is not possible. In some cases a flow of air is also set to purge the system of any product traces. Also some components in chromatographs are prone to adsorption; especially the sampling loop (mounted on a six-way valve for injection), and the inlet liner in the injector. Thus, these compponents , adapted to the study of acids, were supplied by the Restek company and used for the experiments. An inlet liner made of deactivated silica and a surface-coated sampling loop treatment were installed to minimize the occurrence of adsorption. All these equipments are also suitable for the study and analysis of other oxygenated compounds like alcohols or aldehydes.

Table 29 summarizes the uncertainty sources and their quantifications related to these experiments.

Table 29 : Uncertainty quantification of the experimental setup.

Uncertainty sources	Uncertainty bounds
Temperature in the reactor	±5K
Temperature in the transfer line	±7K
Impurity of the fuels and the gases	<1%
Fuel calibration	±5%
Products calibration by effective carbon number method	±10%
Products calibration with standards	±5%
Flow rate of liquid fuel	±1%
Flow rate of gases	±0.5%
Residence time	±2%

This table exibits that the main uncertainties come from the product calibrations and especially the one by the effective carbon number method. The next part is dedicated to a description of the calibration method.

III.8. Calibrations of the gas chromatographs

Calibrations are performed by injecting gaseous and liquid external standards when available. So we can obtain a factor k between the mole fraction of the species and the area of the corresponding peak measured as defined in equation (4).

$$x_i = k_i * A_i \quad (4)$$

In the equation (4), A is the measured area on the chromatogram and x is the corresponding mole fraction. Larger is the area; higher is the mole fraction of the associated compound. The products that have been directly calculated are: O2, CO, CO_2, CH_4, C_2H_2, C_2H_4, C_2H_6 and the fuels.

For species, which could not be directly calibrated with a standard, the effective carbon number (ECN) method, relying on the properties of the FID with respect of the structure of the molecule, was used to obtain calibration coefficients. This method requires:

- To know the effective carbon number of the species.
- To have the calibration coefficient of at least one specie, called the reference (ref).

To obtain the calibration coefficient for a species i, we use the equation (5).

$$k_i = \frac{n_{ref}}{n_i} * k_{ref} \quad (5)$$

where n is the effective carbon number and k the calibration coefficient defined by the equation (2). The number n can be calculated by adding the contribution of each carbon atom of the molecule following the Table 30 below.

Table 30. Contribution of each type of group to the ECN.

Atom/Group	Type	Contribution
C	Aliphatic	1
C	Aromatic	1
C	Olefinic	0.95
C	Acetylenic	1.3
C=O	Carbonyl	0
C-O-C	Ether	1
CH_2-OH	Primary Alcohol	0.4
CH-OH	Secondary Alcohol	0.25
C-OH	Tertiary Alcohol	0.75

Table 31 summarizes the effective carbon number for the fuels studied.

Table 31. ECN of the fuels studied in this work.

Fuel name	Structure	ECN	Fuel name	Structure	ECN
n-Butanol	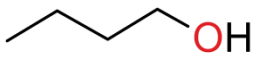	3.4	*n*-Pentanol	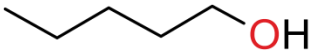	4.4
n-Butanal	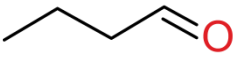	3	*n*-Pentanal	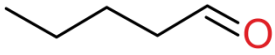	4
Butanoic acid	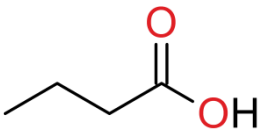	3	Pentanoic acid	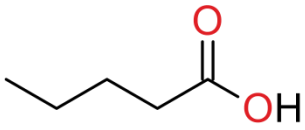	4
Benzaldehyde	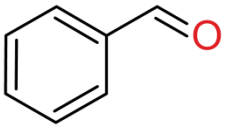	6	Furan		2.85

Those ECN are used as the references to calculate the calibration coefficients of the products obtained in the corresponding experiments. Another possible reference species is methane, which is directly calibrated with an external standard.

III.9. Two-dimensional chromatography or GCxGC

In the last years, the two-dimensional chromatography has been developed and used in laboratories as an advanced analytical method. This technique has the advantage to have a better separative power than the classical unidimensional chromatography. It was first described in the 90s by Liu and Phillips (Liu and Phillips, 1991). Later, in 2013, Seeley and Seeley made a review about the multidimensional gas chromatography (Seeley and Seeley, 2013).

Comprehensive two-dimensional gas chromatography or GCxGC is one kind of multidimensional gas chromatography. Contrary to the heart-cutting two-dimensional gas chromatography, the whole sample is flowing in the two dimensions in this case. It consists of a succession of two separation stages connected with a modulator as presented in Figure 40.The separation is assured by a column similar to the one already existing for classical chromatography. Each sample or product is forced to go through both columns. The role of the modulator is to connect both columns and to transfer the compounds from the first dimension to the second one continuously.

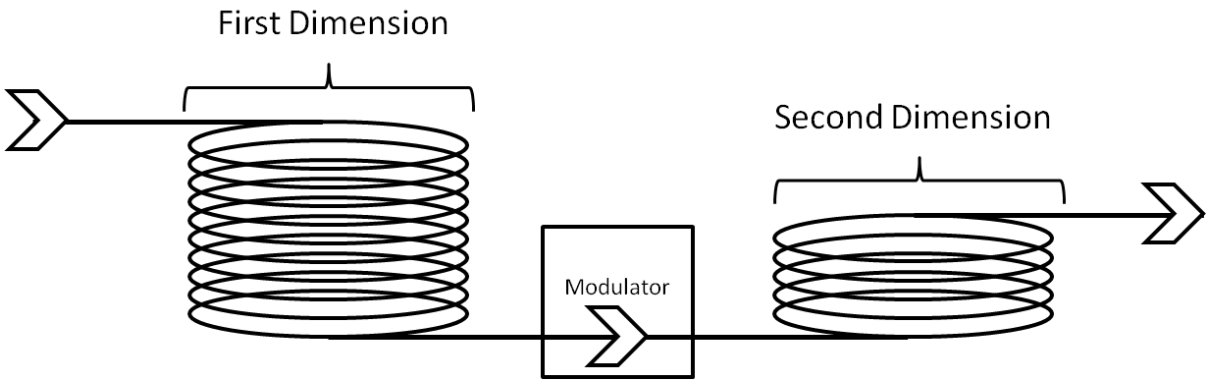

Figure 40. Scheme of a GCxGC with the two columns and the modulator between them.

The modulator is a capillary silica tube without any coating cooled down constantly by an air flow. This air flow has previously been cooled by liquid nitrogen and is at about 77K. So the species at the exit of the first column are trapped and focused in the capillary tube. Then the tube is heated by a hot air pulse and the components are injected in the second column. Figure 41 shows a scheme of a cryogenic modulator.

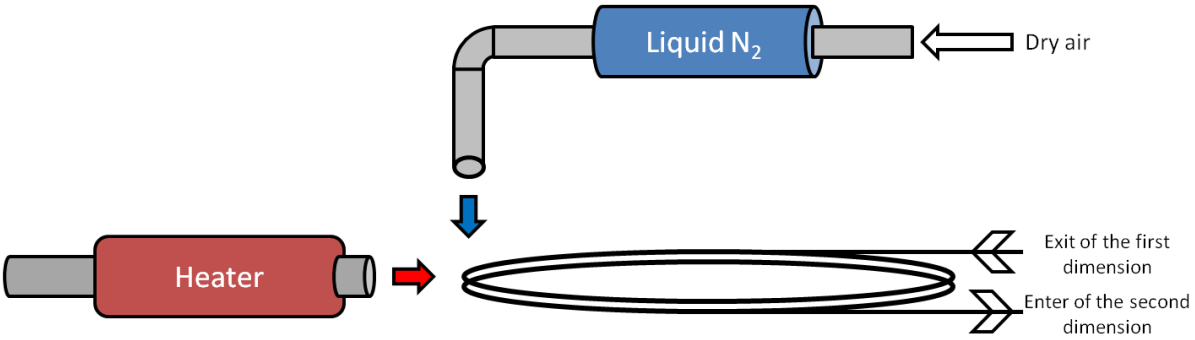

Figure 41. Scheme of a modulator for GCxGC. The flow of cool air is constantly blown on the tube. The hot jet is pulsed in order to release the compounds from the trap into the second column.

The hot jet is pulsed at a given frequency. This period of trapping is called the modulation time and is one of the important parameters of the GCxGC. The modulation time or period must be longer than the retention times of the different species in the second dimension. Thus it limits the length of the second column in order to avoid a remixing of the compounds in the second dimension. The second dimension can also be set in a secondary oven to have a temperature profile hotter in the second dimension than in the first one, which reduces the retention times in this dimension.

The two separation stages of a GCxGC have to respect the principle of orthogonality. The two stages should have two independent separative displacements, which mean that the two columns should not separate the compounds on the same properties or not in the same order of magnitude. In Nancy the separation is performed based on the polarity of the compounds. The first stage is a rxi5 capillary column of 30 meters long with an inner diameter of 0.32 mm and a film thickness of 0.5 µm. The second stage is a rxi17 capillary column of 1.4 meters long with an inner diameter of 0.25 mm and a film thickness of 0.25 µm. The two columns are connected with an open tube of 1.1 meters with an inner diameter of 0.1 mm. The GCxGC has been coupled with an FID and the same mass spectrometer previously presented.

Thanks to the two separation stages, the compounds are separated in a two-dimension space. The compounds are characterized by two retention times, one for each dimension. Figure 42 presents the results of the analysis of the same sample on a classical unidimensional GC and the GCxGC. The sample corresponds to the oxidation of benzaldehyde under stoichiometric conditions.

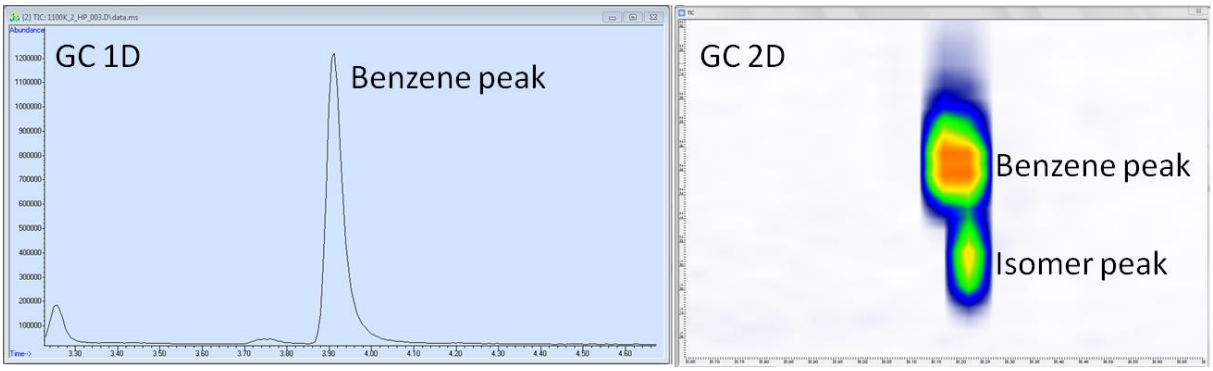

Figure 42. Analysis of the benzene peak on unidimensional GC and on GCxGC for benzaldehyde oxidation.

In the case of Figure 42, the GCxGC made it possible to detect another species which was co-eluted with the peak of benzene. This second species present in much lower amount is likely one of the linear isomers of benzene, such as hexadienyne. This linear isomer of benzene was also previously detected during the pyrolysis of cyclopentene using SVUV-PIMS (Herbinet et al., 2016). Figure 43 shows the projection of this peak in 2D on the two dimensions.

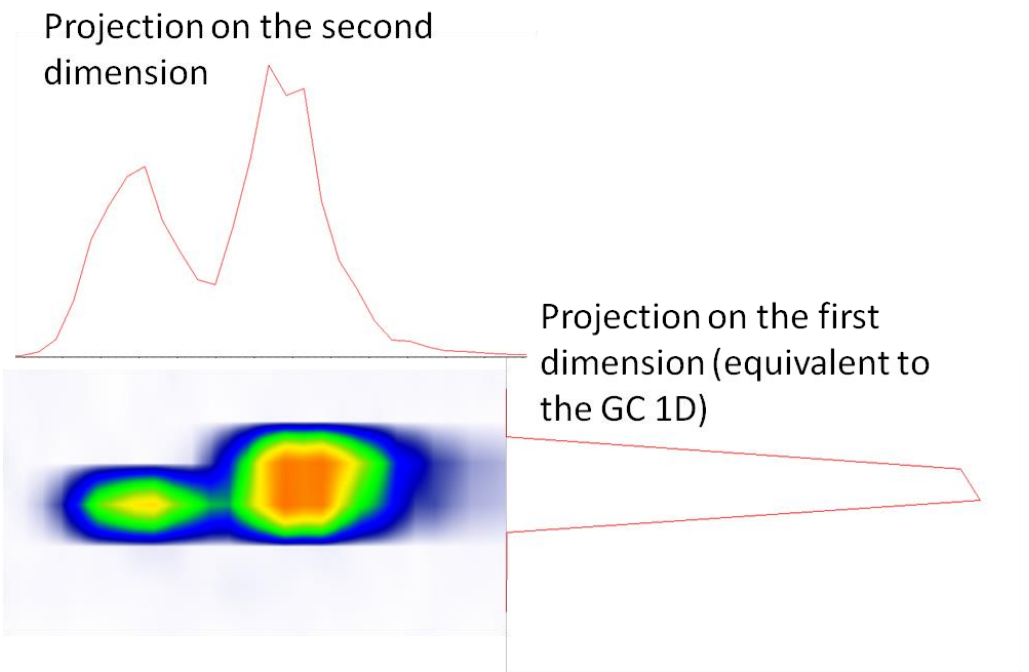

Figure 43. Projection of the peak presented in Figure 38 along the two dimensions.

The jet-stirred reactor and the analytical tools presented in this section are used for investigating the different fuel oxidations. Thanks to the gas chromatography, species detection, identification and quantification are possible. Those data are then used to develop new kinetic mechanism, which are also presented in the next chapter.

IV. OXIDATION OF LINEAR OXYGENATED COMPOUNDS

This chapter presents the results obtained for the linear oxygenated compounds studied in this work. It is divided in four parts. The first one presents the work performed on alcohol oxidation: *n*-pentanol and *n*-butanol. The second describes the results obtained for *n*-pentanal and *n*-butanal oxidation and then the study on pentanoic and butanoic acid is presented. In each part, the experimental results are described and discussed. Then a presentation of the mechanism developed in collaboration with the team of Prof. Faravelli in Politenico di Milano is proposed and results are discussed. The last part is dedicated to a comparison of the reactivity of all the compounds listed above to highlight the influence of the functional group.

This work led to the publication of two peer-reviewed papers:

- The work on aldehyde oxidation led to a publication in the Proceedings of the Combustion Institute: (Pelucchi et al., 2019. An experimental and kinetic modelling study of n-C_4C_6 aldehydes oxidation in a jet-stirred reactor. Proc. Combust. Inst. 37, 389–397.)
- The work on carboxylic acid oxidation was published in the Chemical Engineering Journal (Namysl et al., 2019. A first evaluation of butanoic and pentanoic acid oxidation kinetics. Chem. Eng. J. 373, 973–984.).

In this section, only the main results from these studies are presented. The raw experimental data are given in Appendix II, with a nomenclature of the detected species in Appendix I.

IV.1. *n*-Pentanol and *n*-butanol oxidation

This part is dedicated to the presentation of experimental and theoretical results obtained during the oxidation of *n*-pentanol and *n*-butanol, two surrogates for the alcohol fraction present in bio-oil. These data were obtained using the setup and analytical tools previously described (Chapter III).

IV.1.1. Experimental results

This first section presents the experimental results obtained. The fuel conversion is first discussed and in a second part the carbon balance and reaction product selectivity analysis are displayed with the mole fraction profiles of the main products. The experiments have been carried out in a jet-stirred reactor at 800 Torr and between 500 K and 1100 K. Three equivalence ratios have been studied (0.5-1-2) for a fuel inlet mole fraction of 0.5 %.

Fuel conversion

The oxidation of both fuels has been studied in the experimental set-up described previously. Figure 44 presents the mole fraction profiles for *n*-butanol and *n*-pentanol obtained between 500 and 1100 K for the three equivalence ratios. Error bars are about 5 % in respect with the incertitude presented in the previous chapter. This figure also presents a comparison of the reactivity of the two fuels for each equivalence ratio with the results previously obtained by Rodriguez et al. for *n*-hexanol (Rodriguez, 2016). Those results were obtained under the same conditions.

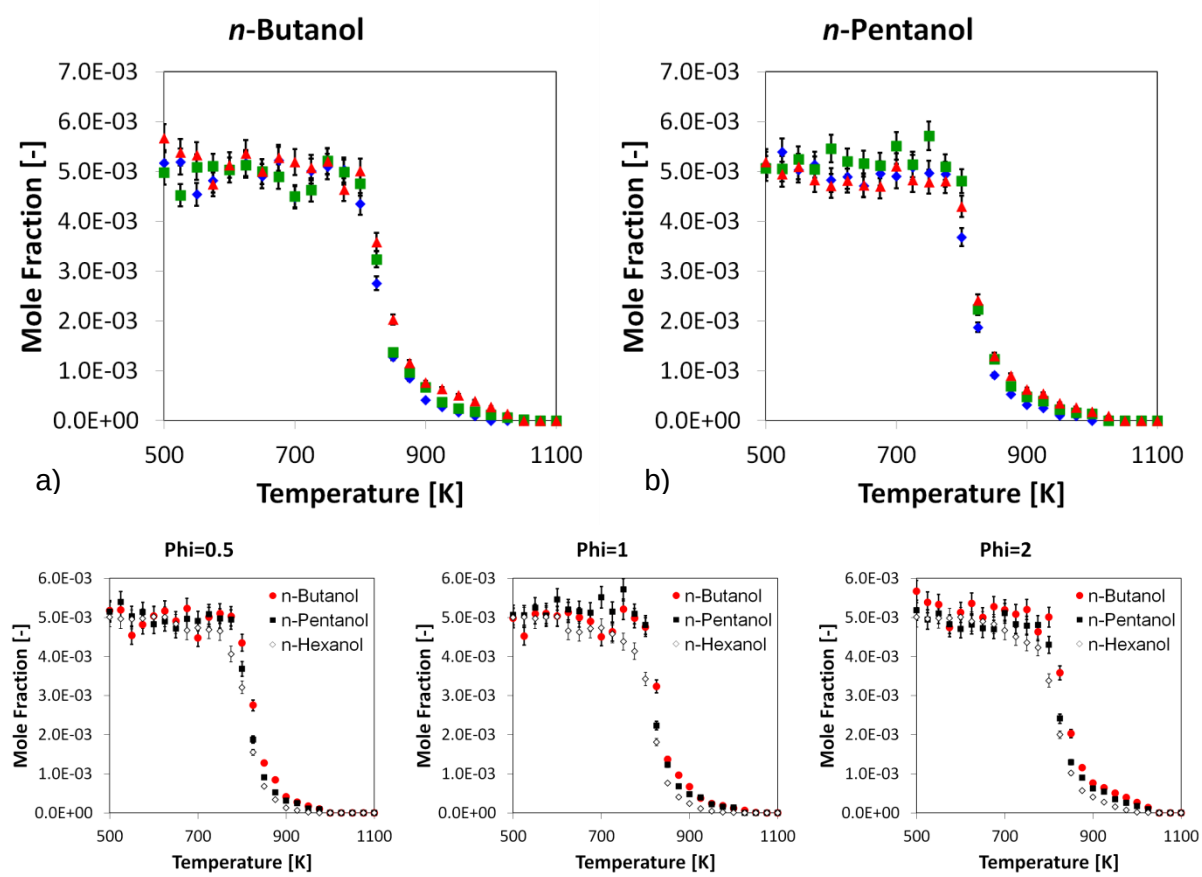

Figure 44. Fuel conversion for a) *n*-butanol and b) *n*-pentanol oxidation and reactivity comparison for each equivalence ratio (*n*-hexanol data from (Rodriguez, 2016)) (Symbols: ♦ phi=0.5, ■ phi=1, ▲ phi=2) (Error bar ±5%).

Butanol does not react between 500 K and 800 K. Its reactivity area is from 800 K to 1050 K. The equivalence ratio does not have a notable influence on the conversion. Similar trends are observed for pentanol. It starts to react at 775 K and is fully consumed at 1050 K. Such as butanol, pentanol conversion is not really influenced by the equivalence ratio.

Contrary to butane and pentane, the two alcohol fuels do not exhibit any low-temperature reactivity or negative-temperature coefficient (NTC) area (Bahrini et al., 2013; Bugler et al., 2017). *n*-Hexanol does not exhibit also any NTC area The alcohol function may have an impact on the reactivity of the alkyl chain at the lowest temperature by inhibiting the reactivity. Figure 44 also shows that *n*-butanol, *n*-pentanol and *n*-hexanol conversions are almost identical under the same conditions. It indicates that the length of the alkyl chain has only a limited impact on the reactivity. Thus we may assume that the fuel reactivity is strongly influenced by the oxygenated function.

Carbon balance and selectivity analysis

During *n*-butanol oxidation, 23 products were detected and quantified: CO, CH_4, CO_2, acetylene, ethylene, ethane, propene, propane, formaldehyde, oxirane, acetaldehyde, 1-butene, 1-3 butadiene, 2-butene, methyloxirane, acrolein, propanal, 1-pentene, 2-pentene, butanal, tetrahydrofuran, 2-3 butanediol, 2-butenal. The overall carbon balance was around 100 % (±10 %). So we can consider that all the main products were detected and quantified during these experiments. The detection of the two pentene linear isomers was unexpected due to the C_4 skeleton of the fuel. These products may come from the recombination of

smaller alkyl radicals. C_4 unsaturated hydrocarbons were also detected and may come from other recombination reactions or from the dehydration of the fuel.

Figure 45 presents two selectivity analyses performed for butanol oxidation at two different temperatures: 825 K (around 50 % of conversion) and 900 K (around 90 % of conversion). This helps to highlight the main products for each temperature. The selectivities are normalized in terms of carbon atom number and are plotted with a threshold of 1 %. So only the species containing more than 1 % of the carbon atom content are displayed.

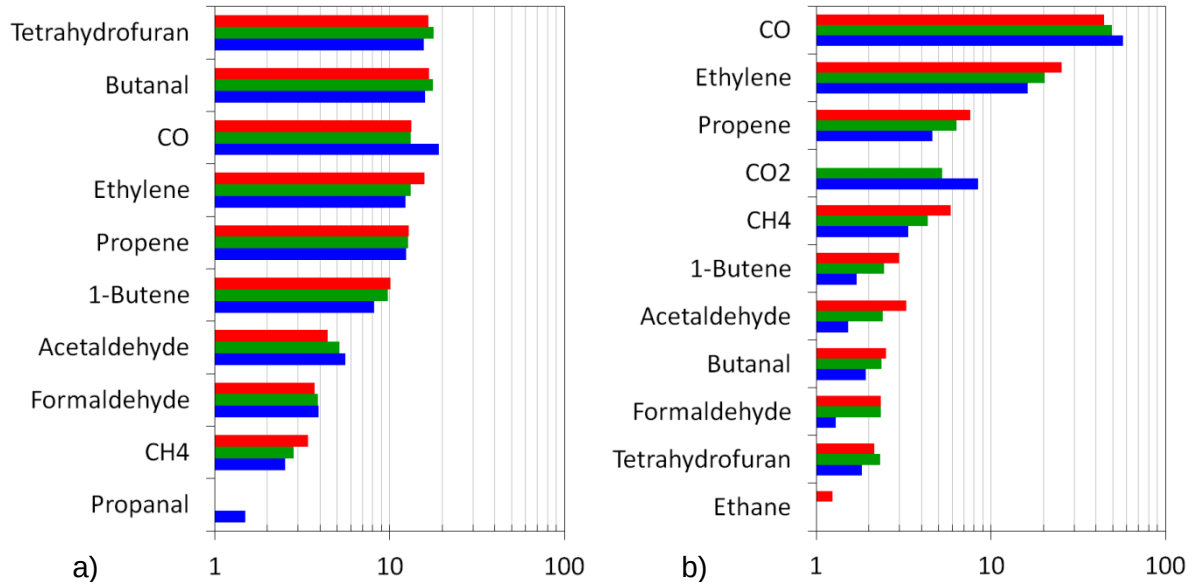

Figure 45. Reaction product selectivity analysis for *n*-butanol oxidation at a) 825 K and b) 900 K (phi=0.5, phi=1, phi=2) (Threshold: 1%) (Logarithmic scale).

At 825 K, the equivalence ratio has almost no effect on the product distribution, as showed by the selectivity analysis in Figure 45a: the distribution of the main products (tetrahydrofuran, butanal, CO, ethylene, propene) is very similar under all conditions. At higher temperature, the effect of the equivalence ratio is stronger. For example, CO_2 production is negligible under fuel-rich conditions but important under fuel-lean conditions at 900 K. The selectivity analyses also show that butanal is an important intermediate during butanol oxidation, especially at low and medium temperatures. This product may be formed by the dehydrogenation of butanol. Tetrahydrofuran is also important at low temperatures but its part is more limited at higher temperatures. At low-temperatures, aldehydes are present in an important amount (butanal, propanal, acetaldehyde and formaldehyde). At higher temperatures, ethylene and propene mole fraction are increasing and these two products become second and third main products. Over the whole butanol reactivity zone, 1-butene is produced and is one of the major products.

Figure 46 presents the mole fraction profiles of oxygen and the products presented in Figure 45 for the three studied equivalence ratios.

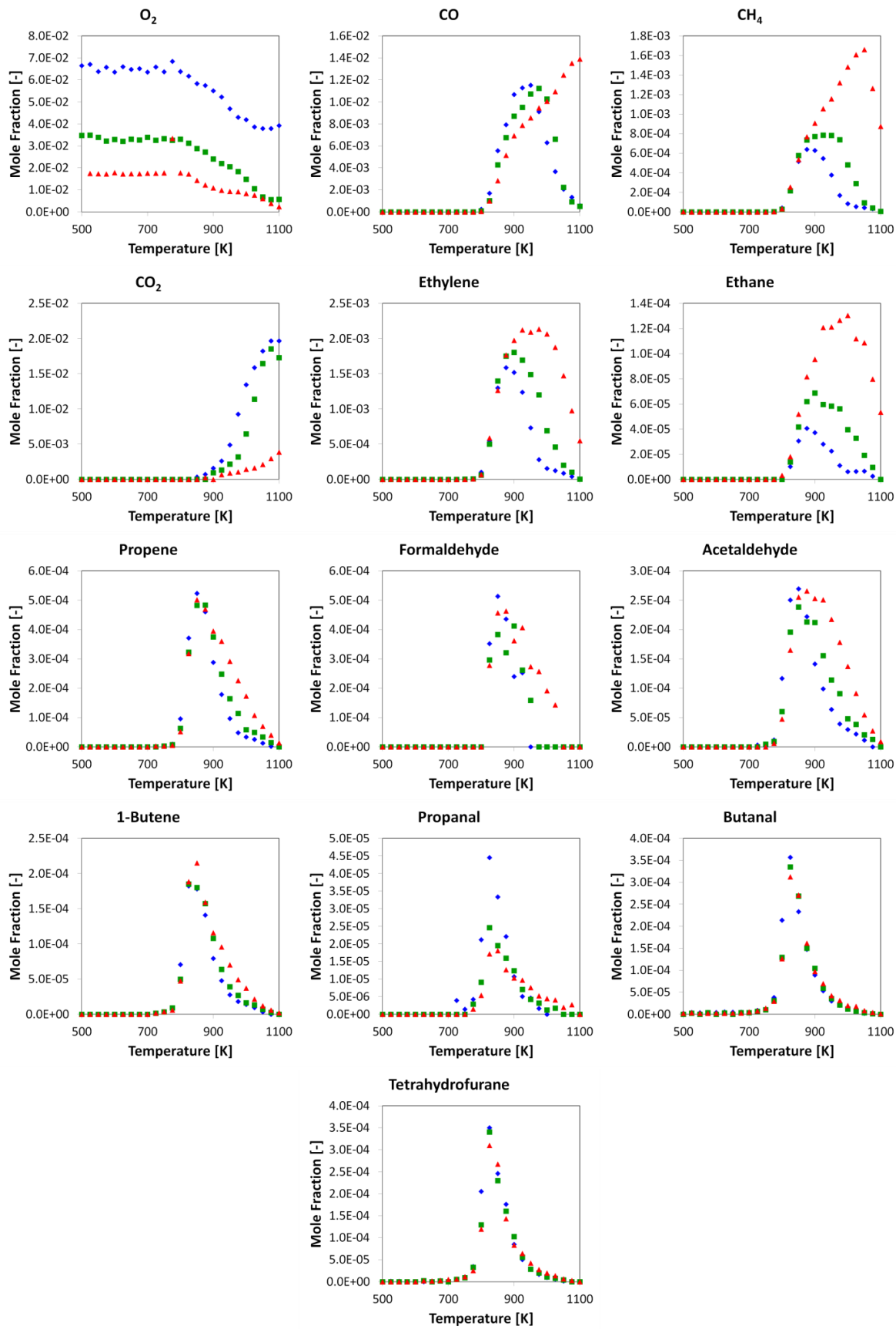

Figure 46. Mole fraction profiles of oxygen and main reaction products of *n*-butanol oxidation for the three equivalence ratios (♦ phi=0.5, ■ phi=1, ▲ phi=2).

Concerning the product mole fraction profiles, the equivalence ratio seems to have an increased impact on the product formation than for the fuel consumption, especially under fuel-rich conditions. Looking at CO_2, ethylene, acetaldehyde, methane or ethane, their formation is largely influenced by the content in oxygen in the mixture. It can also be observed that tetrahydrofuran, 1-butene and butanal have similar temperature dependence. This confirms their role as intermediates of reactions, as they are not final products of butanol oxidation. They can be the products of three different reaction pathways:

- Abstraction of the alcoholic H atom, then formation of butanal through another H-atom release or by dehydrogenation of the fuel directly.
- Dehydration of the fuel to produce 1-butene and water.
- Abstraction of the H-atom in alpha position of the alcohol function then formation of an ether ring to obtain tetrahydrofuran.

These three pathways seem to confirm the importance of the alcohol function on the reactivity of the molecule.

During pentanol experiments, 31 products were identified: *CO, CO_2, CH_4, acetylene, ethylene, ethane, propene, propane, acetaldehyde, oxirane, formaldehyde*, methanol, *1-butene, 1-3 butadiene, 2-butene, methyloxirane, acrolein, propanal*, acetone, *1-pentene, 2-pentene*, 1-4 pentadiene, 1-3 pentadiene, 2-methylfuran, pentane, methyl vinyl ketone, *butanal, tetrahydrofuran, 2-3 butanediol, 2-butenal* and pentanal. Many products had been already identified during *n*-butanol oxidation (in italic in the previous list), but other products were also quantified. Those products contain 5 carbon atoms and may come from the same types of reactions as the one presented for butanal oxidation. It could also be noticed that, in comparison with butanal oxidation, no C_{n+1} molecule (C_6 here) was detected. The overall carbon balance for pentanol oxidation experiments was around 100 % with a deviation of ±10 %.

Figure 47 presents two product selectivity analyses performed for pentanol oxidation at two different temperatures: 825 K (around 50 % of conversion) and 900 K (around 90 % of conversion). The selectivities are normalized in terms of carbon atom number and are plotted with a threshold of 1 %.

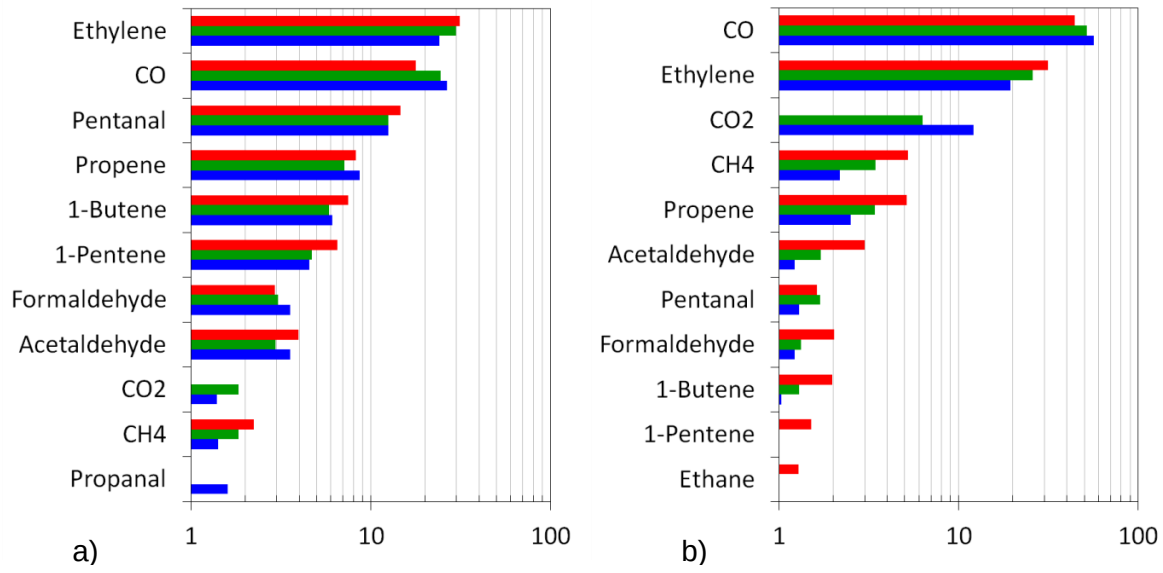

Figure 47. Reaction product selectivity analysis for *n*-pentanol oxidation at a) 825 K and b) 900 K (phi=0.5, phi=1, phi=2) (Threshold: 1%) (Logarithmic scale).

Carbon monoxide and ethylene are the two main products formed during pentanol oxidation. Similarly to butanol oxidation, aldehydes are really important in the low-temperature range. Indeed pentanal, propanal, acetaldehyde and formaldehyde are among the main products. At higher temperature, the unsaturated hydrocarbons are more dominant, with an increased formation of propene. 1-Butene and 1-pentene are also important products at the two selected temperatures, especially under fuel-rich conditions. Contrary to butanol oxidation, the effect of the equivalence ratio on the product distribution is more important in the case of pentanol oxidation. It could be also observed that tetrahydrofuran has no role in the product distribution of pentanol oxidation compared to that of butanol oxidation. In the case of pentanol oxidation, no cyclic ether was observed but unsaturated hydrocarbons containing 5 carbon atoms were produced in a more important amount.

Figure 48 presents the mole fraction profiles of oxygen and the products presented in Figure 47 for the three studied equivalence ratios.

Similarly to the results obtained for butanol oxidation, the equivalence ratio has a strong effect on the formation of some products, i.e. methane, ethane, ethylene, acetaldehyde. The profiles of pentanal and 1-pentene are really similar to the one of butanal and 1-butene observed during butanol experiments. The same pathways as those proposed for butanol oxidation could be still valid for pentanol.

Rodriguez et al detected high amount of *n*-hexanal and in smaller quantities hexenes in the products of *n*-hexanol oxidation. Thus, we could assume that the reactivity of a linear alcohol is not only ruled by the alkyl chain length. The alcohol function has a strong impact on the reactivity, leading to the formation of the associated aldehyde and alkene.

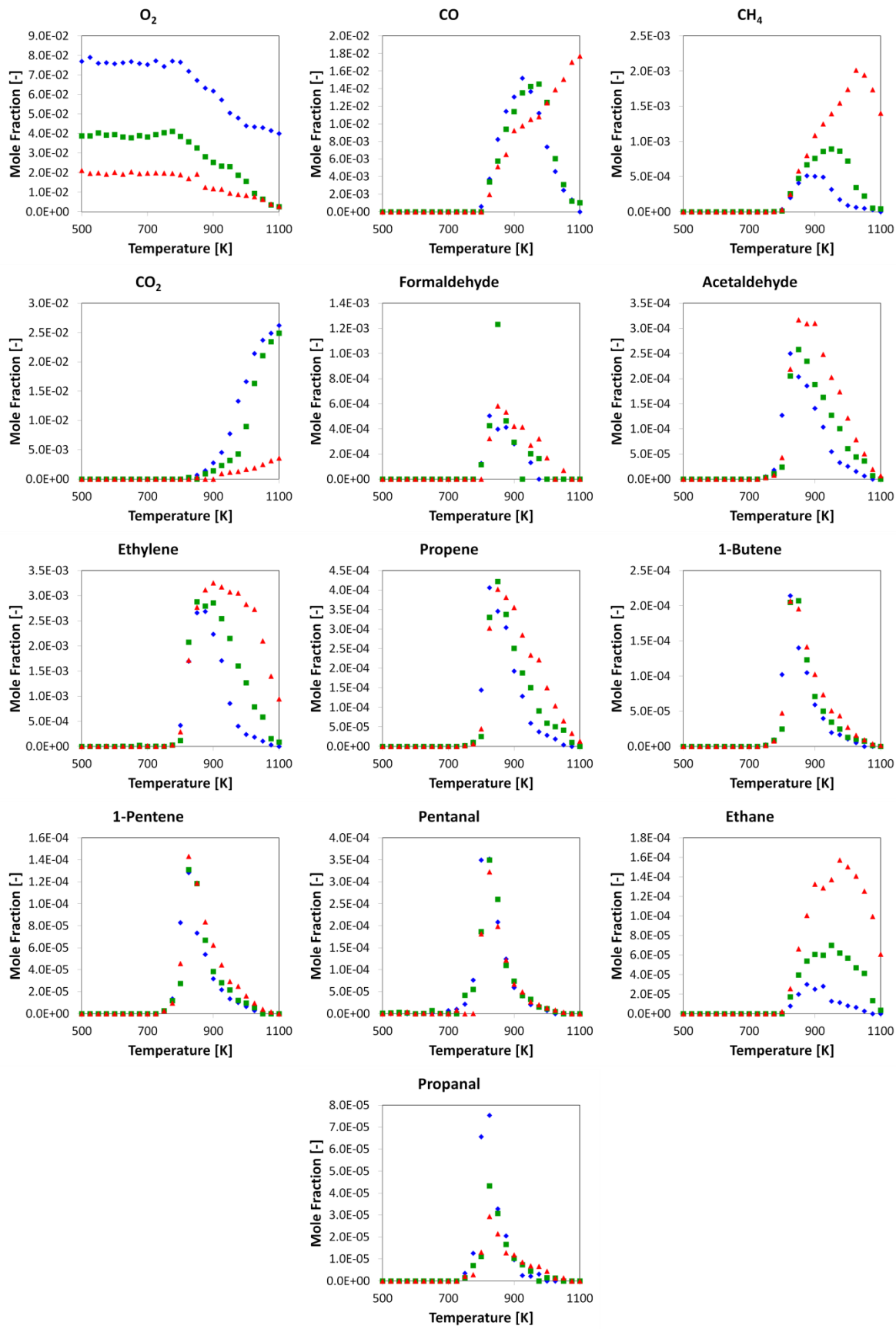

Figure 48. Mole fraction profiles of oxygen and main reaction products of *n*-pentanol oxidation for the three equivalence ratios (♦ phi=0.5, ■ phi=1, ▲ phi=2).

IV.1.2. Kinetic model

Mechanism

The OpenSMOKE++ package (Cuoci et al., 2015) has been used to perform all the kinetic simulations and analyses presented in this manuscript.

The starting point of the development of the detailed kinetic mechanism of bio-gas and bio-oil oxidation has been the state-of-the-art POLIMI framework; which is the result of 40 years of kinetic modeling activity, started with the pyrolysis of smaller hydrocarbons (Dente et al., 1979), then extended to the pyrolysis and oxidation and heavier molecules (Ranzi et al., 1997; Granata et al., 2003; Ranzi et al., 2005).

The development of such a framework has proceeded following three major targets: (i) hierarchy, (ii) modularity and (iii) generality. Such a philosophy is well suited to model both pyrolysis and oxidation paths of hydrocarbons, since combustion intrinsically proceeds as a sequential fragmentation of the fuel molecule, generating progressively smaller molecules. Then, they undergo the related oxidation paths, until the formation of final combustion products and byproducts.

This allows a significant flexibility in the management and the update of the mechanism itself, since when a mechanism is added or modified, the structure of the existing kinetic framework is the starting point of this process, and it is expected that only the modules at a lower hierarchy level will be affected by such modification.

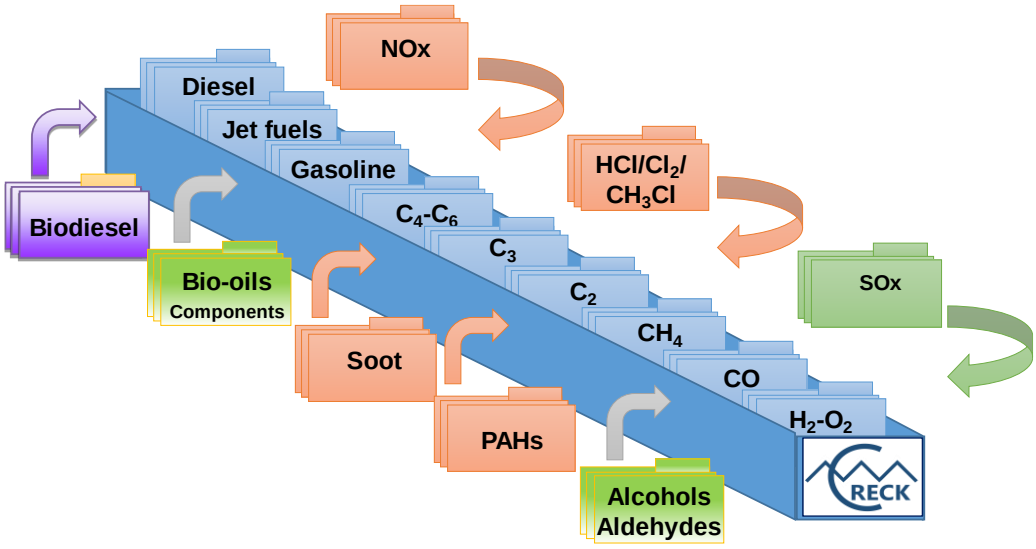

Figure 49. Structure of the POLIMI (Ranzi et al., 2012) kinetic mechanism.

Since the start of its development to model hydrocarbon pyrolysis in cracking processes (Dente et al., 1979), the CRECK model has used extensively chemical lumping methods. This lumping can be performed in two ways

- Vertical lumping: if a reaction of decomposition or isomerization is fast enough, we can replace directly a species by its products. This simplifies the mechanism by creating global reactions.
- Horizontal lumping: H-abstraction reactions can produce a lot of radicals, which are isomers and whose decompositions are similar. The related rates can be similar and the only variable is the product formed. Those radicals can be then gathered under one single species and their decomposition summarized in one lumped reaction (Zeppieri et al., 2000; Chaos et al., 2007).

An example of horizontal lumping for C_7H_{14} isomers is presented below.

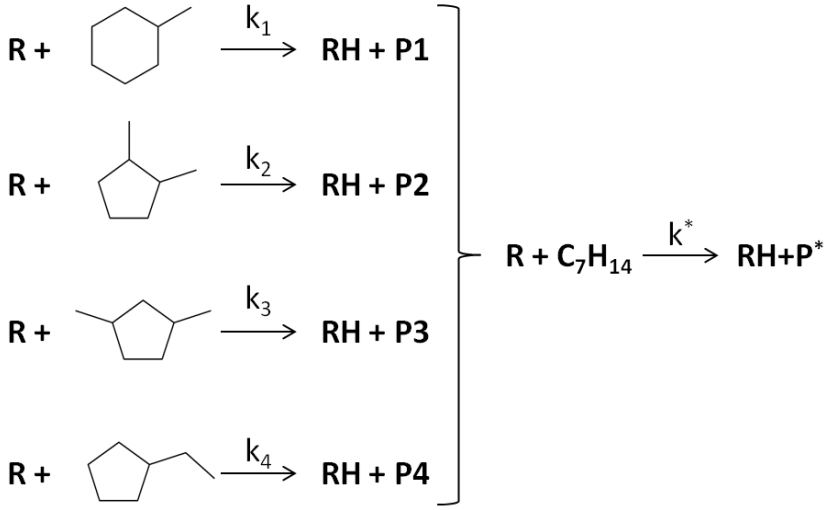

With k* and P*, the overall equivalent-component kinetic parameter and stoichiometry:

$$k^* = \sum_1^4 a_i k_i \qquad P^* = \sum_1^4 \frac{a_i k_i}{k^*} P_i$$

Where α is the weight fraction. The overall equivalent-component kinetic parameter is considered as a linear combination of the kinetic parameters involved in the lumping. Then this kinetic parameter can be developed under the form of an Arrhenius law to be incorporated in the kinetic mechanism for the lumped reaction.

In the current work, vertical and horizontal lumping have been used.

During this work, the CRECK model was updated and implements a C_0–C_3 core mechanism obtained by coupling the H_2/O_2 and C_1/C_2 from Metcalfe et al. (2013), C_3 from Burke et al. (2015), and heavier fuels from Ranzi et al. (2012, 2014).

The first step of the mechanism development was to consider the bond dissociation energies (BDEs) of our molecules of interest and to compare them with a reference, here the alkane one. Figure 50 presents the BDEs values calculated with G4 method for butane and some oxygenated equivalent molecules. These results have been presented in the work of Pelucchi et al (2016).

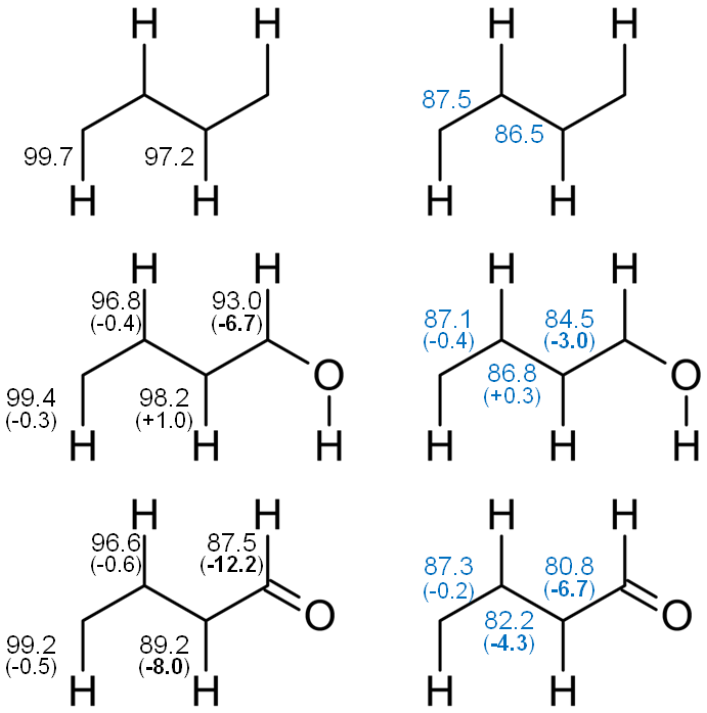

Figure 50. C-H (black) and C-C (blue) bond dissociation energies (kcal/mol) for butane, *n*-butanol and *n*-butanal from the work of Pelucchi et al (Pelucchi et al., 2016). In brackets are represented the difference in BDEs with the alkane case considered as the reference here. The most important deviations are highlighted in bold type.

This work showed that the oxygenated function has only a "limited" effect on the alkyl chain. Indeed the major deviations in terms of BDEs are observed for the carbon atom close to the oxygen. Thus a model was proposed to represent any linear alkyl molecule with an oxygenated function supported by one of its primary carbon. This model is represented in Figure 51.

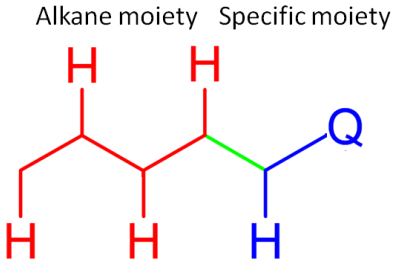

Figure 51. Model for the representation of any linear alkyl molecule with an oxygenated function supported by one of its primary carbon. "Q" represents any terminal oxygenated function (-OH, =O…).

The molecule is then divided in two parts:

- An alkyl moiety with a reactivity comparable to the one of the equivalent alkane
- A specific moiety with a reactivity influenced by the presence of the oxygenated function

The alkyl moiety reactivity is similar to the alkane one and then all the reaction classes and kinetic constants developed for the alkane can be apply to this section of the molecule. Concerning the specific moiety, the reaction classes are dependent on the type of oxygenated function. The advantage of this approach is that the length of the alkyl chain is not a limiting factor. To extend the mechanism of a C_n alcohol to the C_{n+1} alcohol, the only

additions needed are the reactions for a secondary carbon atom according to the alkane's reactivity rules and rates, which are really well known nowadays (Ranzi et al., 2015).

Tables 32, 33 and 34 present the reaction for *n*-butanol accounted in the model developed in this study. The kinetic parameters are given under the form:

$$k = A * T^n * \exp\left(\frac{-E_a}{R * T}\right)$$

With A the pre-exponential factor in $(cm^{-3}•mol^{-1})^{n-1}/s$, n the order of the reaction, T the temperature in K and Ea the activation energy in cal/mol.

BDEs of C-C, C-O, and C-H discussed above are used to estimate unimolecular decomposition reactions, responsible for radical chain initiation. Because of the microscopic reversibility principle, the rate constant of initiation reactions are derived from the rate constant of reverse barrierless radical recombination reactions. The most favored initiation reactions are those involving the lower BDEs.

H-abstraction reactions are relevant to unravel the selectivity to different products. Rate constants of the generic reaction: R•+ R'H ↔ R'•+ R H depend on the properties of the abstracting radical and the type of hydrogen to be abstracted (Ranzi et al., 1993). In other words, the BDEs of the different C-H bonds to some extent reflect the likelihood of one H-atom to be abstracted. According to the approach of Ranzi et al. (1993) rate rules for the different R• abstracting radicals in the CRECK model are expressed as:

$$k_R(T) = n_H C_{SiteH}(T) k_{ref,R}(T) = n_H C_{SiteH}(T) A_{ref,R} T^2 exp\left(-\frac{E_{ref,R}}{RT}\right)$$

where the rate rules rely on reference frequency factors and activation energies of each H-abstracting radical $(k_{ref,R}(T))$, on a per site primary alkane H-atom basis. The rates are then corrected to account for the number of H atoms and the correction term $(C_{SiteH}(T) = exp(-E_{SiteH}/RT))$ is obtained from the bond dissociation energy (or the heat of reaction), through an Evans-Polanyi relationship (Evans and Polanyi, 1936).

The problem for the mechanism development is to assess the influence of the oxygenated function on the carbons in α- and β-positions. As shown in Figure 50, alcohol and aldehyde functions do not have the same impact on the BDEs and thus it could be expected that the impact on the reactivity is also different. Then reaction classes and rate rules should be defined and detailed for each kind of chemical function. In the case of the alcohol kinetic model, the alkyl radicals formed by the H-atom abstractions were not lumped in one common species. Thus, all H-abstraction reactions for each position have been considered in the model.

During pyrolysis, the fuel radicals derived from H-abstraction reactions can either decompose through beta-scission reactions to form an unsaturated compound and a smaller radical, or isomerize to another radical. Beta-scission reactions can break a C-H bond or a C-C bond. Rate constants for these reaction classes are based on the alkane rate rules from Ranzi et al. (2001) taking into account the differences in bond dissociation energies and the formation of resonance stabilized radicals (α-radicals) from H-abstractions.

In the case of oxidation, the fuel can react in a bimolecular initiation with oxygen to form a radical and HO_2. Also the radicals formed by the fuel can add to oxygen and give an

alkyl peroxy radical. The lumped radical, named RBU1OOX for *n*-butanol mechanism, is showed in Table 32. The rates of those reactions are based on the alkane rate rules (Ranzi et al., 2001). The radical can react by isomerizations and then decompose through beta-scissions or lead to another addition to oxygen, which is the way towards branching reactions by ketohydroperoxides (presented in Table 33 for the case of *n*-butanol).

Table 32. Reactions of *n*-butanol in cal, s, mol, cc units.

Reaction	*A*	*n*	*Ea*	No.
Reactions of *n*-Butanol				
Unimolecular initiations				
$C_4H_9OH=C_2H_5+C_2H_4OH$	3.01E+25	-2.57	89900.00	(1)
$C_4H_9OH=CH_3+CH_2CH_2CH_2OH$	5.13E+26	-2.92	90470.00	(2)
$C_4H_9OH=CH_2OH+C_3H_7$	4.13E+17	-0.30	89720.00	(3)
$C_4H_9OH=OH+C_4H_9$	2.82E+29	-3.68	101930.00	(4)
$H+CH_3CH_2CH_2CH_2O=C_4H_9OH$	5.00E+13	0.00	0.00	(5)
$H+CH_3CH_2CH_2CHOH=C_4H_9OH$	5.00E+13	0.00	0.00	(6)
$H+CH_3CH_2CHCH_2OH=C_4H_9OH$	5.00E+13	0.00	0.00	(7)
$H+CH_3CHCH_2CH_2OH=C_4H_9OH$	5.00E+13	0.00	0.00	(8)
$H+CH_2CH_2CH_2CH_2OH=C_4H_9OH$	5.00E+13	0.00	0.00	(9)
Molecular reactions				
$C_4H_9OH=H_2O+C_4H_8$	1.00E+14	0.00	67600.00	(10)
$C_4H_9OH=H_2+C_3H_7CHO$	5.10E+08	1.36	69680.00	(11)
Main bimolecular initiations and H-abstractions by H-atoms				
$O_2+C_4H_9OH=>HO_2+CH_3CH_2CH_2CH_2O$	1.70E+06	2.00	48272.65	(12)
$O_2+C_4H_9OH=>HO_2+CH_3CH_2CH_2CHOH$	5.95E+06	2.00	44000.00	(13)
$O_2+C_4H_9OH=>HO_2+CH_3CH_2CHCH_2OH$	2.55E+06	2.00	44000.00	(14)
$O_2+C_4H_9OH=>HO_2+CH_3CHCH_2CH_2OH$	3.74E+06	2.00	44000.00	(15)
$O_2+C_4H_9OH=>HO_2+CH_2CH_2CH_2CH_2OH$	5.10E+06	2.00	48272.65	(16)
$H+ C_4H_9OH=>H_2+CH_3CH_2CH_2CH_2O$	3.00E+06	2.00	6349.34	(17)
$H+ C_4H_9OH=>H_2+CH_3CH_2CH_2CHOH$	1.05E+07	2.00	4000.00	(18)
$H+ C_4H_9OH=>H_2+CH_3CH_2CHCH_2OH$	4.50E+06	2.00	4000.00	(19)
$H+ C_4H_9OH=>H_2+CH_3CHCH_2CH_2OH$	6.60E+06	2.00	4000.00	(20)
$H+ C_4H_9OH=H_2+CH_2CH_2CH_2CH_2OH$	5.60E+06	2.00	6525.60	(21)

Table 33. Reactions of the radicals produced from *n*-butanol in cal, s, mol, cc units.

Reaction	*A*	*n*	*Ea*	No.
Reactions of the radicals produced from *n*-Butanol				
Isomerizations				
$CH_2CH_2CH_2CH_2OH=CH_3CH_2CH_2CH_2O$	1.60E+10	0.00	16000.00	(1)
$CH_2CH_2CH_2CH_2OH=CH_3CH_2CH_2CHOH$	2.00E+11	0.00	19600.00	(2)
$CH_3CHCH_2CH_2OH=CH_3CH_2CH_2CH_2O$	1.00E+11	0.00	23000.00	(3)
$CH_3CH_2CHCH_2OH=CH_3CH_2CH_2CH_2O$	5.00E+11	0.00	26000.00	(4)
Decompositions by beta-scissions				
$CH_3CH_2CH_2CH_2O=CH_2O+C_3H_7$	3.00E+13	0.00	15000.00	(5)
$CH_3CH_2CH_2CH_2O=H+C_3H_7CHO$	3.00E+13	0.00	26000.00	(6)
$CH_3CH_2CH_2CHOH=H+C_3H_7CHO$	3.00E+13	0.00	38000.00	(7)
$CH_3CH_2CH_2CHOH=C_2H_5+CH_3CHO$	3.00E+13	0.00	31000.00	(8)
$CH_3CH_2CHCH_2OH=H+C_3H_7CHO$	3.00E+13	0.00	38000.00	(9)
$CH_3CH_2CHCH_2OH=CH_3+C_3H_5OH$	3.00E+13	0.00	33000.00	(10)
$CH_3CH_2CHCH_2OH=OH+C_4H_8\text{-}_1$	3.00E+13	0.00	32500.00	(11)
$CH_3CHCH_2CH_2OH=H+C_4H_7OH$	3.00E+13	0.00	38000.00	(12)
$CH_3CHCH_2CH_2OH=CH_2OH+C_3H_6$	6.00E+13	0.00	31000.00	(13)
$CH_2CH_2CH_2CH_2OH=C_2H_4+C_2H_4OH$	3.00E+13	0.00	30000.00	(14)
Addition to O_2, isomerization of RBU1OOX and decomposition of QBU1OOX				
$O_2+CH_3CH_2CHCH_2OH=>RBU1OOX$	1.00E+12	0.00	0.00	(15)
$O_2+CH_3CHCH_2CH_2OH=>RBU1OOX$	1.00E+12	0.00	0.00	(16)
$O_2+CH_2CH_2CH_2CH_2OH=>RBU1OOX$	2.00E+12	0.00	0.00	(17)
RBU1OOX=>QBU1OOX	4.18E+09	0.39	19621.30	(18)
QBU1OOX=>RBU1OOX	1.76E+05	1.59	11124.06	(19)
$QBU1OOX=>HO_2+0.5C_3H_7CHO+0.5C_4H_7OH$	5.05E+07	1.82	23182.10	(20)
$QBU1OOX=>OH+0.2CH_2O+0.15C_2H_4$ $+1.3CH_3CHO+0.2C_3H_5OH+0.15CH_3CO_2H$	1.02E+16	-1.01	23327.45	(21)
$QBU1OOX=>0.5O_2+OH+C_4H_8O$	2.78E+10	0.37	17120.70	(22)
$QBU1OOX=>H_2O+HCO+C_2H_5CHO$	4.00E+10	0.00	13000.00	(23)

Table 34. End of the Table 33. Reactions of the radicals produced from *n*-butanol in cal, s, mol, cc units.

Reaction	*A*	*n*	*Ea*	No.
Reactions of the radicals produced from *n*-Butanol via O_2 addition				
Addition to O_2 of QBU1OOX and decompositions of ZBU1OOX and KEHYBU1				
O_2+QBU1OOX=>ZBU1OOX	2.50E+12	0.00	0.00	(1)
ZBU1OOX=>O_2+QBU1OOX	3.00E+13	0.00	30000.00	(2)
ZBU1OOX=>OH+KEHYBU1	4.18E+09	0.39	19621.30	(3)
KEHYBU1=>OH+0.6CH_2OH+0.6CH_2O+ 0.4CH_3CHO+0.6CH_2CO+0.4CH_3OCO	2.50E+15	0.00	40000.00	(4)
KEHYBU1=>OH+0.5CO+0.5CH_2O+ 0.5PC_2H_4OH+0.5CH_3CO+0.5CH_3CO_2H	5.00E+15	0.00	40000.00	(5)
KEHYBU1=>OH+0.4PC_2H_4OH+0.6CH_2CHO+ 0.4CHOCHO+0.6CH_3CO_2H	1.50E+15	0.00	40000.00	(6)

The development of a detailed kinetic mechanism of higher-chain alcohols started from the consolidated studies on lighter compounds, i.e. propanol (Frassoldati et al., 2010), butanol (Grana et al., 2010) and pentanol (Nativel et al., 2016) isomers. Thus, the rules applied to *n*-butanol were extended to *n*-pentanol in terms of low temperature reaction pathways (Pelucchi et al., 2017a). To do so, the assumption that the effect of the OH group has a “chemical” effect only up to the β position was made (Figure 52), and could be then extended to heavier alcohols, too.

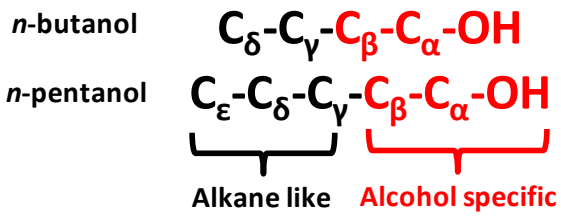

Figure 52. Effect of OH functional group on different alcohols.

Analysis of the results

This section is dedicated to the analysis of the results obtained with the model presented previously and its comparison with the experimental data. Then an overview of the decomposition pathways for the two fuels is given.

Figure 53 presents the performance of the model compared to the experimental data presented earlier.

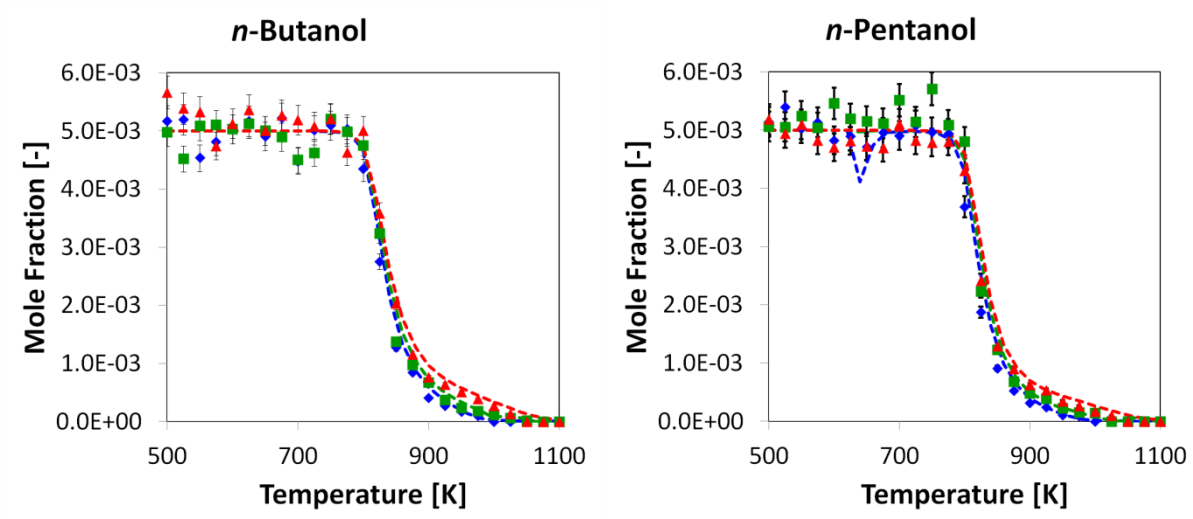

Figure 53. Fuel conversion for *n*-butanol and *n*-pentanol oxidation compared to the model results (Symbols: ♦ phi=0.5, ■ phi=1, ▲ phi=2) (Error bar ±5%).

The model is able to reproduce the reactivity onset for both fuels. It is also able to reproduce the equivalence ratio effect on the fuel conversion. However, the model slightly underestimates the fuel conversion under fuel-rich conditions. The model also predicts an NTC area under fuel-lean conditions for *n*-pentanol, which was not clearly observed in experiments. The assumption of an alkane moiety in the molecule may explain this result, as pentane exhibits such behavior.

Figures 54 and 55 present a comparison between the computed data and the experimental results for *n*-butanol and *n*-pentanol oxidation main products respectively.

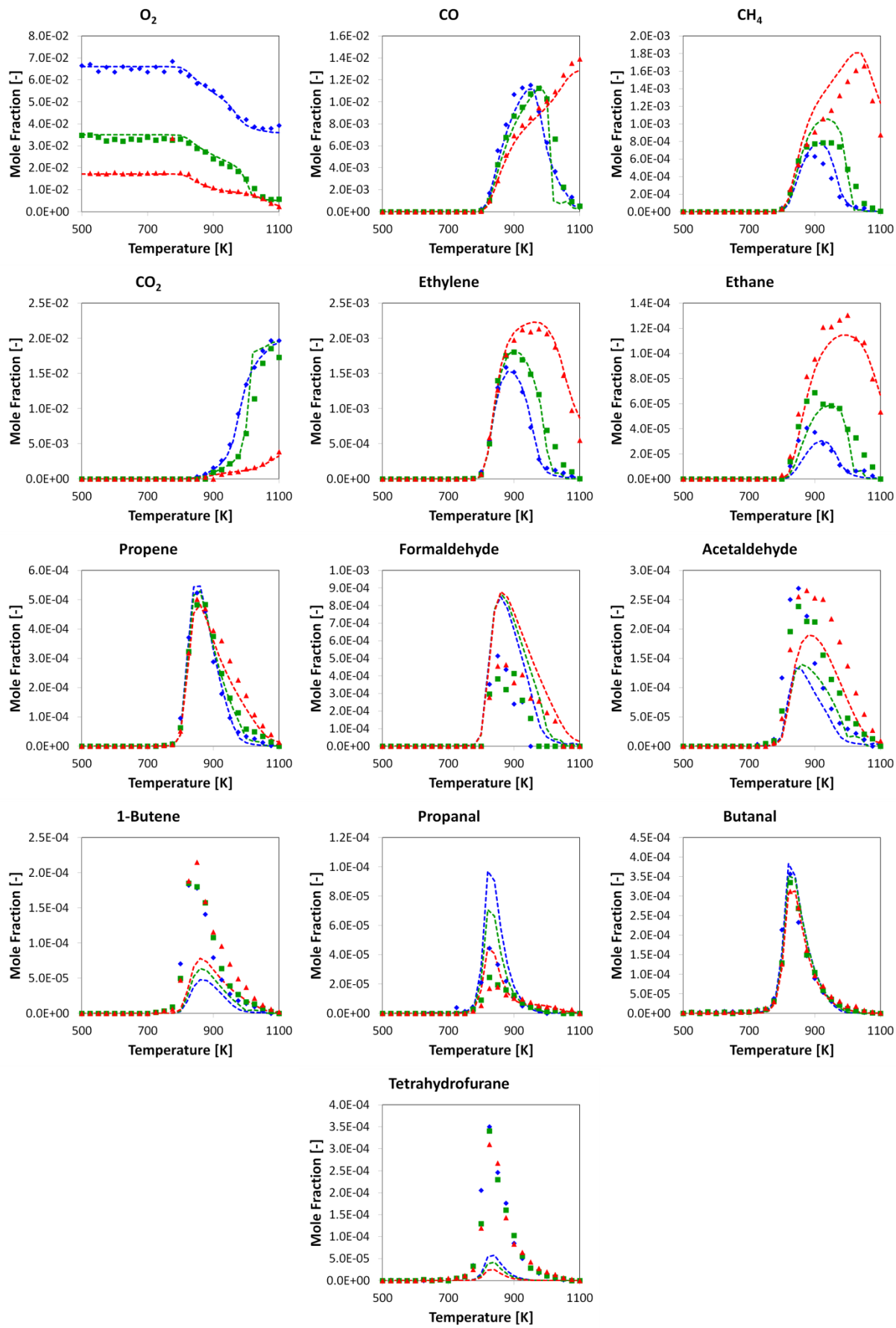

Figure 54. Mole fraction profiles of oxygen and main reaction products of *n*-butanol oxidation compared to the model computed results for the three equivalence ratios (♦ phi=0.5, ■ phi=1, ▲ phi=2).

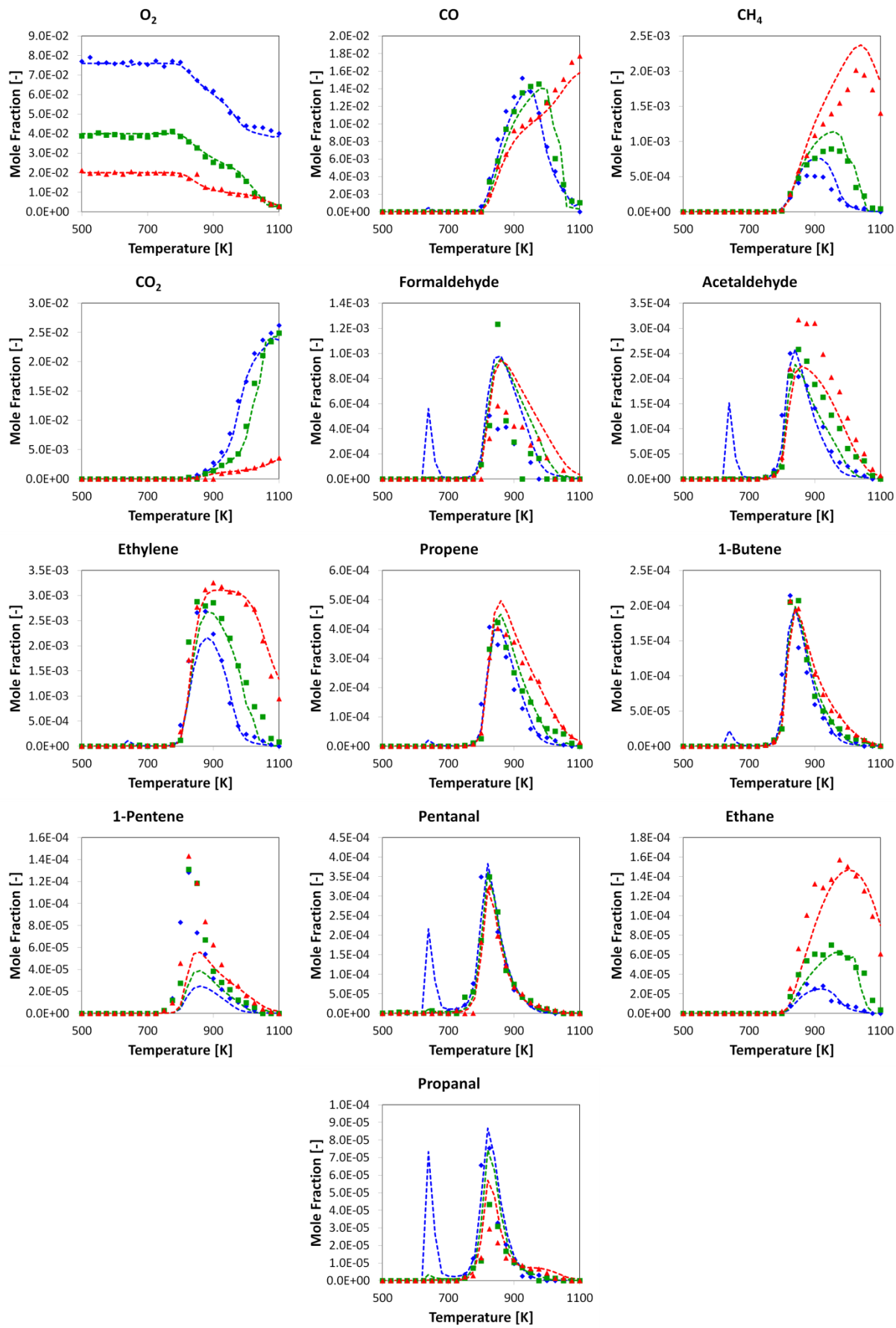

Figure 55. Mole fraction profiles of oxygen and main reaction products of *n*-pentanol oxidation compared to the model computed results for the three equivalence ratios (♦ phi=0.5, ■ phi=1, ▲ phi=2).

It can be observed that the overall agreement is better in the case of pentanol than butanol. However, some pentanol products (mainly formaldehyde, acetaldehyde, propanal and pentanal) also exhibit a NTC area which was not observed. For both fuel, the associated alkene mole fraction profiles (1-butene and 1-pentene) are under-estimated by the model. This may indicate a problem on the kinetics of the dehydration reaction of the fuel. But as the mole fraction profile of water was not measured, it is complicated to affirm that surely. It can also be observed that formaldehyde formation is over-estimated by the model for both fuels. Formaldehyde could be formed via the decomposition of the radical formed via the departure of the alcoholic H-atom. This pathway may be over-estimated. In the case of butanol, acetaldehyde mole fraction profiles are slightly under-estimated, while methane and propanal ones are over-estimated.

Figure 56 shows a rate of decomposition analysis for *n*-butanol at 825 K. The percentages represent the carbon-atom decomposition flow. This figure shows that butanol mainly decomposes through radical pathways. The molecular pathway, dehydration, is indeed negligible in the model prediction under our conditions.

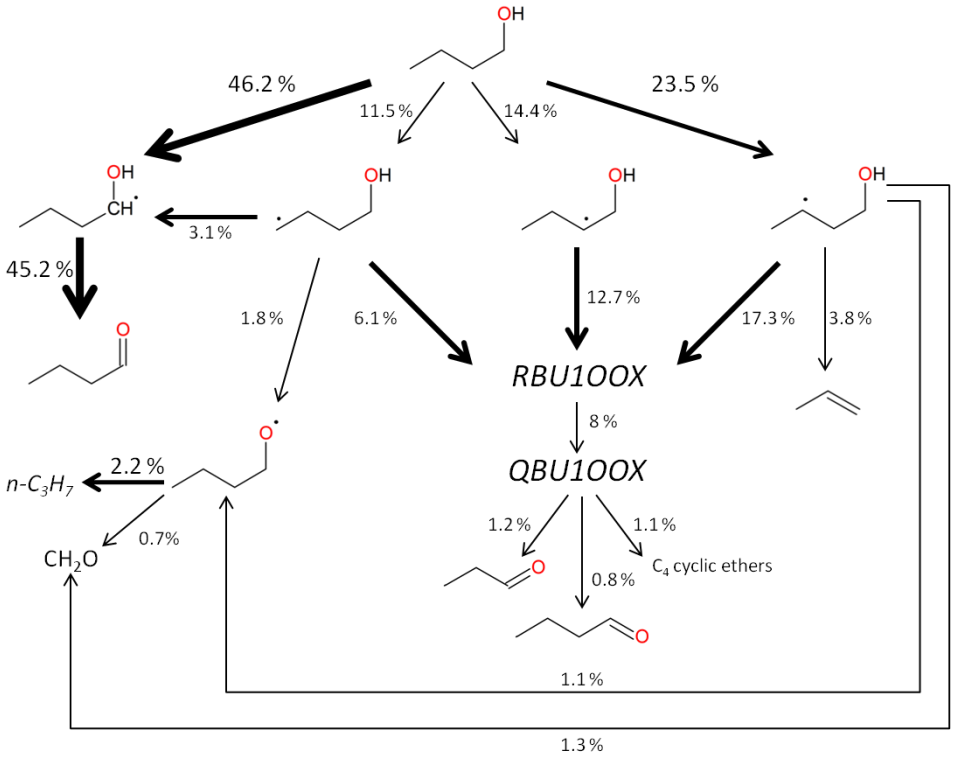

Figure 56. Rate of decomposition analysis for *n*-butanol at 825 K under stoichiometric conditions.

The radical mainly formed is the α-radical at 46%, which indicates that the reactivity of the molecule is influenced by the alcoholic function. The radical decomposes to butanal almost exclusively. The other radicals add on oxygen to give the lumped species RBU1OOX, which is more precisely described on Figure 57.

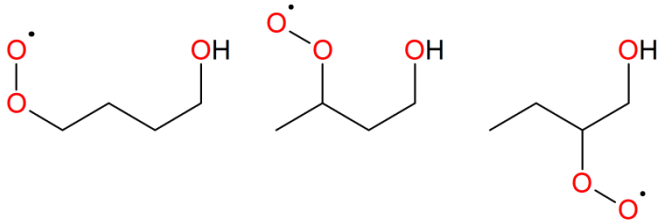

Figure 57. Radicals represented by the lumped species RBU1OOX in the model.

This radical is the initiator of the pathway leading to the formation of THF. The radicals produced from the fuel can also isomerize into the radical RO•, which give formaldehyde and an *n*-propyl radical.

Figure 58 presents a sensitivity analysis for butanol at 825 K under stoichiometric conditions. In red are highlighted the reactions increasing the reactivity and in blue the ones slowing down the reactivity.

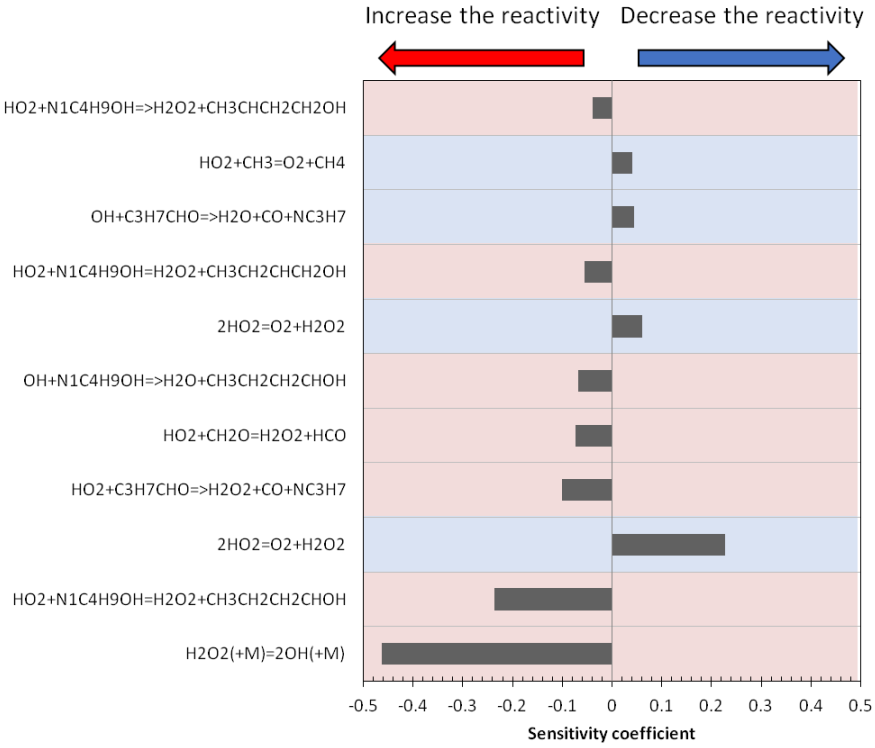

Figure 58. Sensitivity analysis of *n*-butanol oxidation to rate constants at 825 K under stoichiometric conditions.

The reactions involving the fuel are the H-abstraction reactions with HO_2 and OH. The most important are the two reactions of the two radicals on the α-position of the alcohol function, which here promote the reactivity. Thus it is logical to see that the reactions consuming the radical HO_2 are decreasing the reactivity. It also interesting to note the impact of butanal and formaldehyde on the selectivity, as they are both involved in a branching reaction through the transformation of HO_2 into H_2O_2.

IV.1.3. Conclusion

During this work, the oxidation of *n*-butanol and *n*-pentanol has been investigated. The most interesting reaction products observed were butanal, THF and 1-butene. Their production showed that the alcohol function has a large impact on the reactivity of the molecule. To confirm this hypothesis, a model has been developed on the base of the CRECK mechanism. Analogies and fragmentation of the alcohol in two moieties allowed us to establish a kinetic mechanism, which is able to reproduce both fuels reactivity. The model confirmed that the α-position in the alkyl chain was important due to the presence of the alcohol function.

IV.2. *n*-Pentanal and *n*-butanal oxidation

In this part, the experimental and theoretical results obtained during the oxidation of *n*-pentanal and *n*-butanal (two surrogates for the aldehyde fraction present in bio-oil) are presented. These data were obtained using the setup and analytical tools described in the previous chapter. This work was published in a peer-reviewed journal (Pelucchi, M., Namysl, S., Ranzi, E., Frassoldati, A., Herbinet, O., Battin-Leclerc, F., Faravelli, T., 2019. An experimental and kinetic modelling study of n-C4C6 aldehydes oxidation in a jet-stirred reactor. Proc. Combust. Inst. 37, 389–397. https://doi.org/10.1016/j.proci.2018.07.087).

IV.2.1. Experimental results

The experimental results are presented in the following order: first the fuel conversion is discussed and then in a second part the carbon balance and selectivity analysis are presented with the mole fraction profiles of the products. The experiments have been carried out in a jet-stirred reactor at 800 Torr and between 500 K and 1100 K. Three equivalence ratios have been studied (0.5-1-2) for a fuel inlet mole fraction of 0.5 %.

Fuel conversion

Figure 59 presents the mole fraction profiles for *n*-butanal and *n*-pentanal conversions between 500 and 1100 K for the three equivalence ratios. It also presents the results obtained by Rodriguez et al. on *n*-hexanal oxidation under similar conditions (Rodriguez et al., 2017).

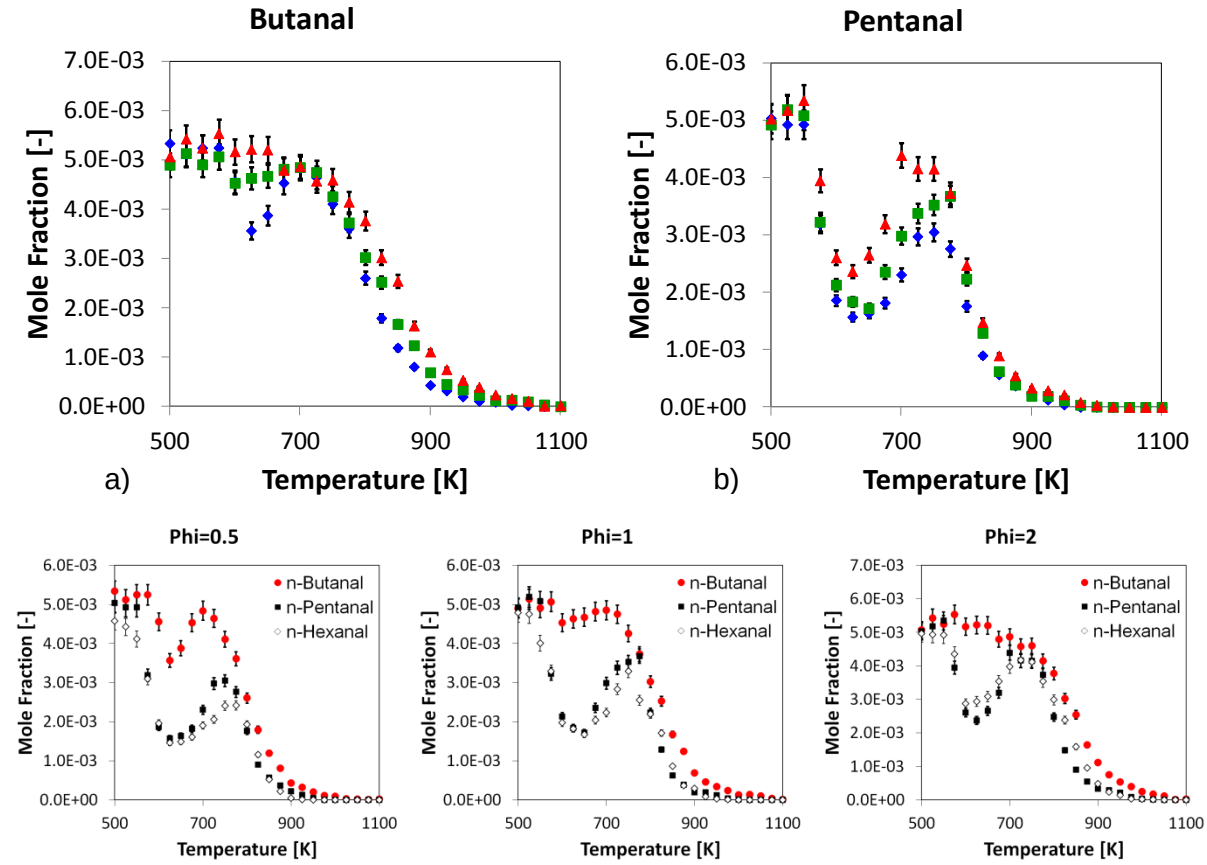

Figure 59. Fuel conversion for a) *n*-butanal and b) *n*-pentanal oxidation and reactivity comparison for each equivalence ratio (n-hexanal data from (Rodriguez et al., 2017)) (Symbols: ♦ phi=0.5, ■ phi=1, ▲ phi=2) (Error bar ±5%).

n-Butanal starts to react at 600 K and is fully consumed at 1075 K, whereas *n*-pentanal starts to react at 575 K and is fully consumed at 1025 K. *n*-Pentanal exhibits for each equivalence ratio a marked NTC (negative temperature coefficient) area between 650 and 725 K whereas *n*-butanal only presents this trend under fuel-lean conditions between 575 and 700 K. The amplitude of the NTC in the case of *n*-pentanal is related to the equivalence ratio: the more concentrated oxygen, the larger the conversion at low-temperature. The NTC of *n*-pentanal has the same order of magnitude than the one of *n*-hexanal. Under the stoichiometric conditions, *n*-butanal seems to present also an NTC area but it is less pronounced. Overall *n*-pentanal is much more reactive than *n*-butanal as shown in Figure 59. This higher reactivity may be due to the longer alkyl chain in the case of pentanal and hexanal. It could also be noticed that the C_5 and C_6 fuel reactivity are very similar.

Pentanal contained impurities in non-negligeable amounts and has only a purity of 98.8% after analysis (97% minimal purity according to Sigma-Aldrich). The impurities are mainly 2-methylbutanal (0.14%$_{mol}$ in the inlet) and *n*-butanal (0.8%$_{mol}$ in the inlet), which decomposition profiles are presented in Figure 60. Those impurities did not seem to have any impact on the results given their low concentration and structure similarities compared to the fuel of interest.

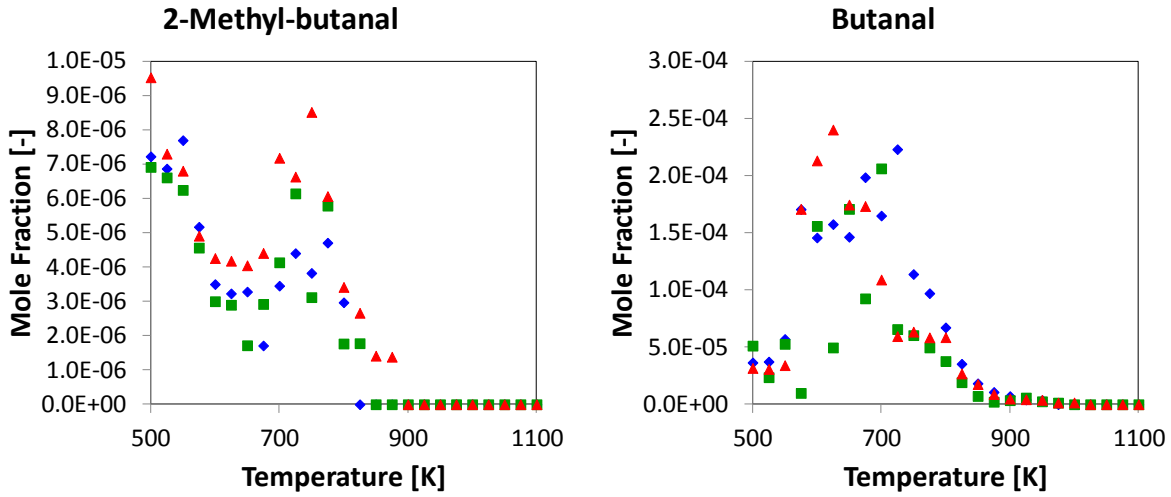

Figure 60. Mole fraction profiles of the impurities present in *n*-pentanal fuel inlet.

Carbon balance and selectivity analysis

During the oxidation of *n*-butanal, 20 products have been identified: CO, CO_2, CH_4, acetylene, ethylene, ethane, propene, propane, formaldehyde, oxirane, acetaldehyde, methanol, methyloxirane, propanal, 1-butene, 2-butene, 1.3-butadiene, 2-butenal, acrolein and 1-pentene. The carbon balance stays within the range of 100±10% for *n*-butanal and *n*-pentanal oxidation under every condition, indicating that all main reaction products were detected during the study.

Figure 61 presents two selectivity analyses performed for *n*-butanal oxidation at two different temperatures: 625 and 825 K. The first temperature (625 K) corresponds to the beginning of the NTC area for the fuel-lean condition and 825 K to a conversion of 25 % in the high-temperature region for the stoichiometric condition. The selectivities are normalized over the number of carbon into the molecules. So here we have directly the selectivity in terms of carbon atom distribution. Also the plots only present the main products, as a

threshold of 1 % has been set. That is why carbon dioxide is not present on the selectivity plot at 875 K.

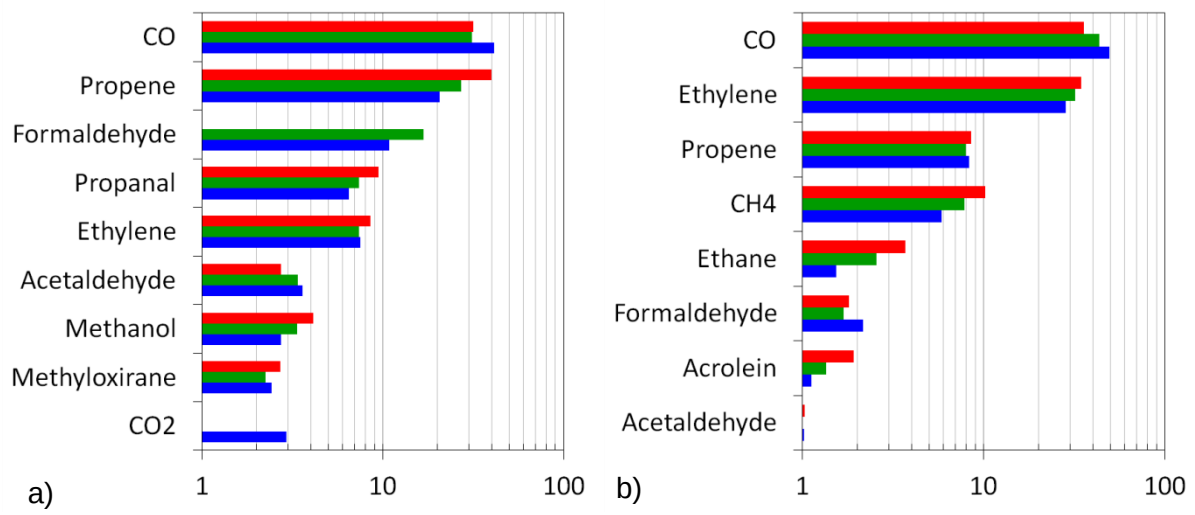

Figure 61. Reaction product selectivity analysis for *n*-butanal oxidation at a) 625 K and b) 875 K (phi=0.5, phi=1, phi=2) (Threshold: 1%) (Logarithmic scale).

It must be noticed that the no-detection of formaldehyde at 625 K for fuel-rich condition may have a non-negligible effect on the selectivity by increasing the value of the other selectivities. This is due to the shape of the peak of formaldehyde, which increases the detection limit for this compound on our GCs.

The main product formed is carbon monoxide under every condition. It is formed directly from *n*-butanal and the departure of the aldehydic function from the alkyl chain. The main products at 625 K are oxygenated products, contrary to 875 K main products, which are two hydrocarbons. At both temperatures we observed propene and ethylene produced by the decomposition of the alkyl chain of *n*-butanal. At the lowest temperatures, propene is the most important hydrocarbon, but at higher temperatures (after the NTC region) the decomposition into methane and ethylene dominates.

Figure 62 presents the mole fraction profiles of oxygen and the products displayed in Figure 63 for the three studied equivalence ratios.

From Figure 62, it can be observed that the reaction products can be classified in two categories: those starting to be produced at low temperatures (before the NTC area) and those starting to be produced only at high temperatures (after the NTC area), as summarized in Table 35. This trend confirms the low temperature reactivity and the NTC area observed for fuel conversion. Indeed some products are produced in the first reactivity area (before the NTC area), such as propene or methyloxirane as shown in Figure 62.

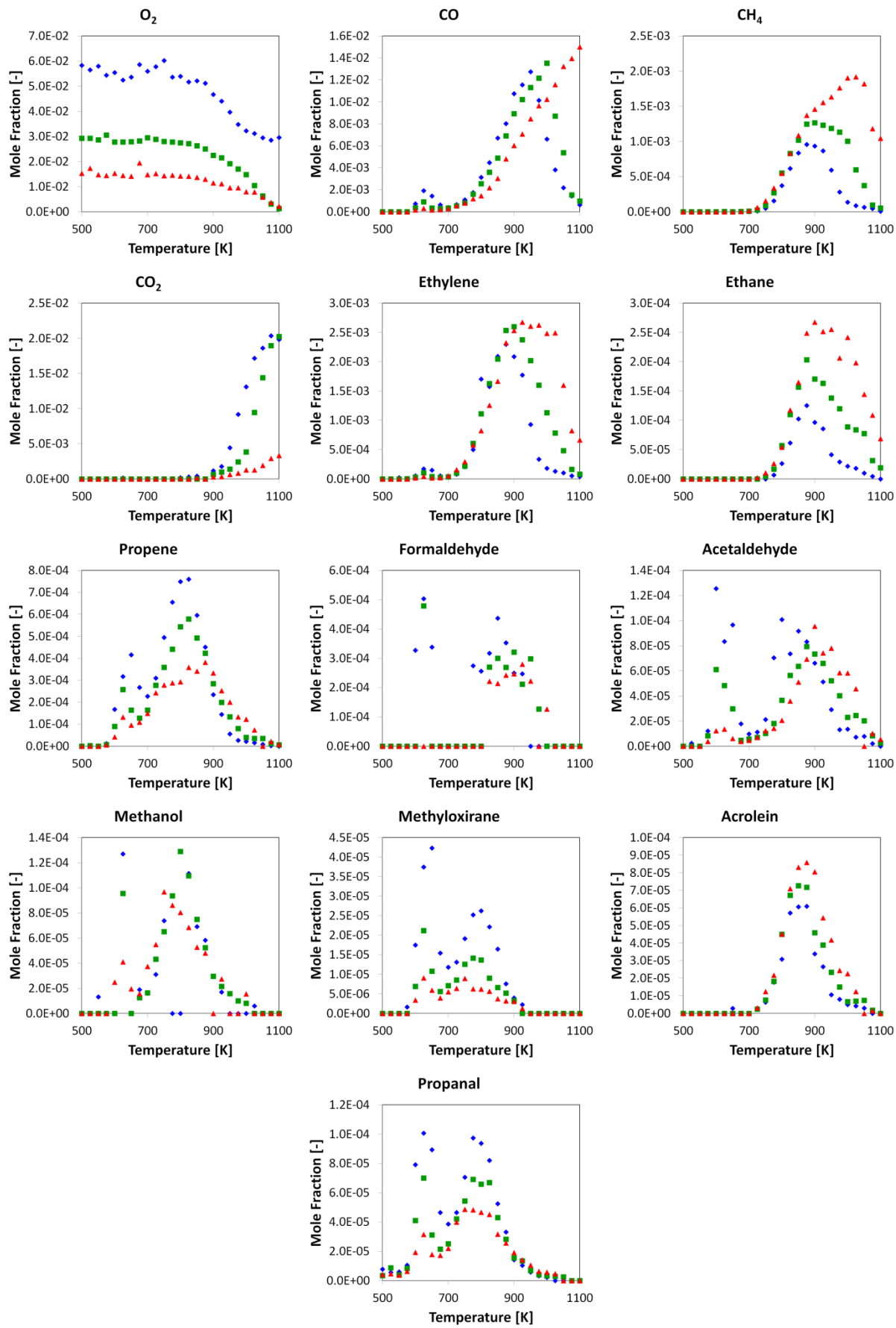

Figure 62. Mole fraction profiles of oxygen and main reaction products of *n*-butanal oxidation for the three equivalence ratios (♦ phi=0.5, ■ phi=1, ▲ phi=2).

Table 35. Products of *n*-butanal oxidation sorted depending of their temperature zone of production (in red and italic: oxygenated compounds and in black and bold: hydrocarbons).

Products present before the NTC area	Products present only after the NTC area
CO	**CH_4**
Ethylene	*CO_2*
Propene	**Acetylene**
Propane	**Ethane**
Formaldehyde	**1-Butene**
Oxirane	**1-3 Butadiene**
Acetaldehyde	**2-Butene**
Methanol	*Acrolein*
Methyloxirane	
Propanal	
1-Pentene	
2-Butenal	

The products of Table 35 can also be classified depending if they are oxygenated or not. We can observe that the oxygenated molecules are mainly produced in the first reactivity area whereas the hydrocarbons are mainly formed in the third reactivity area (after the NTC zone). The detection of 1-pentene was not expected as it contains more carbon atoms than the fuel itself. Its formation is due to recombination reactions of smaller alkyl radicals.

In the case of *n*-pentanal oxidation, 29 species have been detected. The products identified and quantified are: *CO, CH_4, CO_2, acetylene, ethylene, ethane, propene, propane, formaldehyde, oxirane, acetaldehyde, 1-butene, 1,3-butadiene, 2-butene E, 2-butene Z*, furan, *2-propenal, propanal*, acetone, 2,3-dihydrofuran, 2,3-dimethyloxirane, ethyloxirane, pentane, methyl vinyl ketone, *n*-butanal, 2-butanone, *2-butenal*, 2-methyl-butanal and pentanoic acid (*italic*: products also identified during *n*-butanal oxidation).

Figure 63 presents two selectivity analyses for *n*-pentanal oxidation. The first one is at 625 K, which corresponds to the end of the low temperature reactivity area, and the second one is at 800 K, so around 50 % conversion under the stoichiometric condition. The plots are also normalized in terms of carbon atom number and with a threshold of 2%.

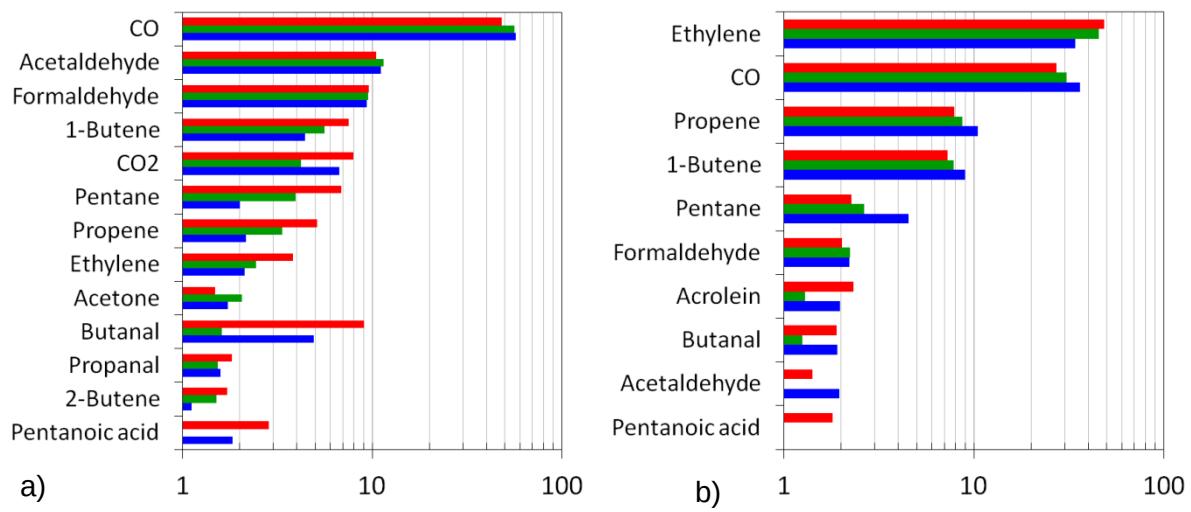

Figure 63. Reaction product selectivity analysis for *n*-pentanal oxidation at a) 625 K and b) 800 K (**phi=0.5**, **phi=1**, **phi=2**) (Threshold: 2%).

Pentanal product distribution for the two temperatures seems to present less difference than *n*-butanal product distribution. Except methane, carbon dioxide and acetone which are only produced at either low or high temperature, all the other products are observed in both temperature zones. CO is the major product for both temperatures. However at 800 K, hydrocarbons such as ethylene or propene are dominant, whereas formaldehyde and acetaldehyde are the most significant at 625 K. So the same trend as for *n*-butanal oxidation is observed.

During the experiments, pentanoic acid formation has been detected, as shown in Figure 64. Rodriguez et al. also suspected the formation of hexanoic acid during the oxidation of *n*-hexanal (Rodriguez et al., 2017). Butanoic acid was not experimentally observed during *n*-butanal oxidation, but its lower reactivity may explain concentrations below the detection limits of our analytical tools. Carboxylic acids seem to be typical oxidation products of aldehyde oxidation. However their accurate quantification is still really tricky and the profiles proposed here are only indicative.

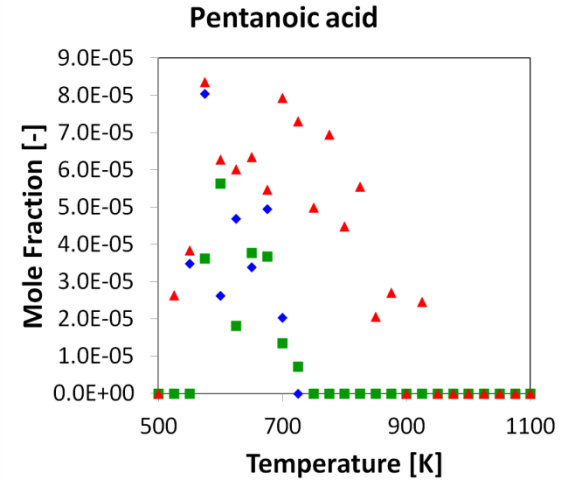

Figure 64. Pentanoic acid mole fraction profiles for the three equivalence ratios during pentanal oxidation experiments (♦ phi=0.5, ■ phi=1, ▲ phi=2).

Figure 65 presents the mole fraction profiles of oxygen and the main products for the three equivalence ratios.

Similarly to *n*-butanal oxidation, the products of *n*-pentanal oxidation can be sorted among different classes. Some product yields are more important at low temperature, such as formaldehyde, acetaldehyde, propanal, acetone and *n*-butanal. On the other side, ethylene, acrolein, carbon monoxide, methane and carbon dioxide yields are more important in the high temperature region (after the NTC zone). The product distribution is very similar to the one obtained for the oxidation of *n*-butanal, with the addition of some new compounds specific to *n*-pentanal oxidation. Those compounds are mainly products with 4 or 5 carbon atoms, such as *n*-pentane, *n*-butanal or pentanoic acid. Pentane formation could be explained by the recombination of smaller alkyl radical and is not directly linked to the fuel decomposition.

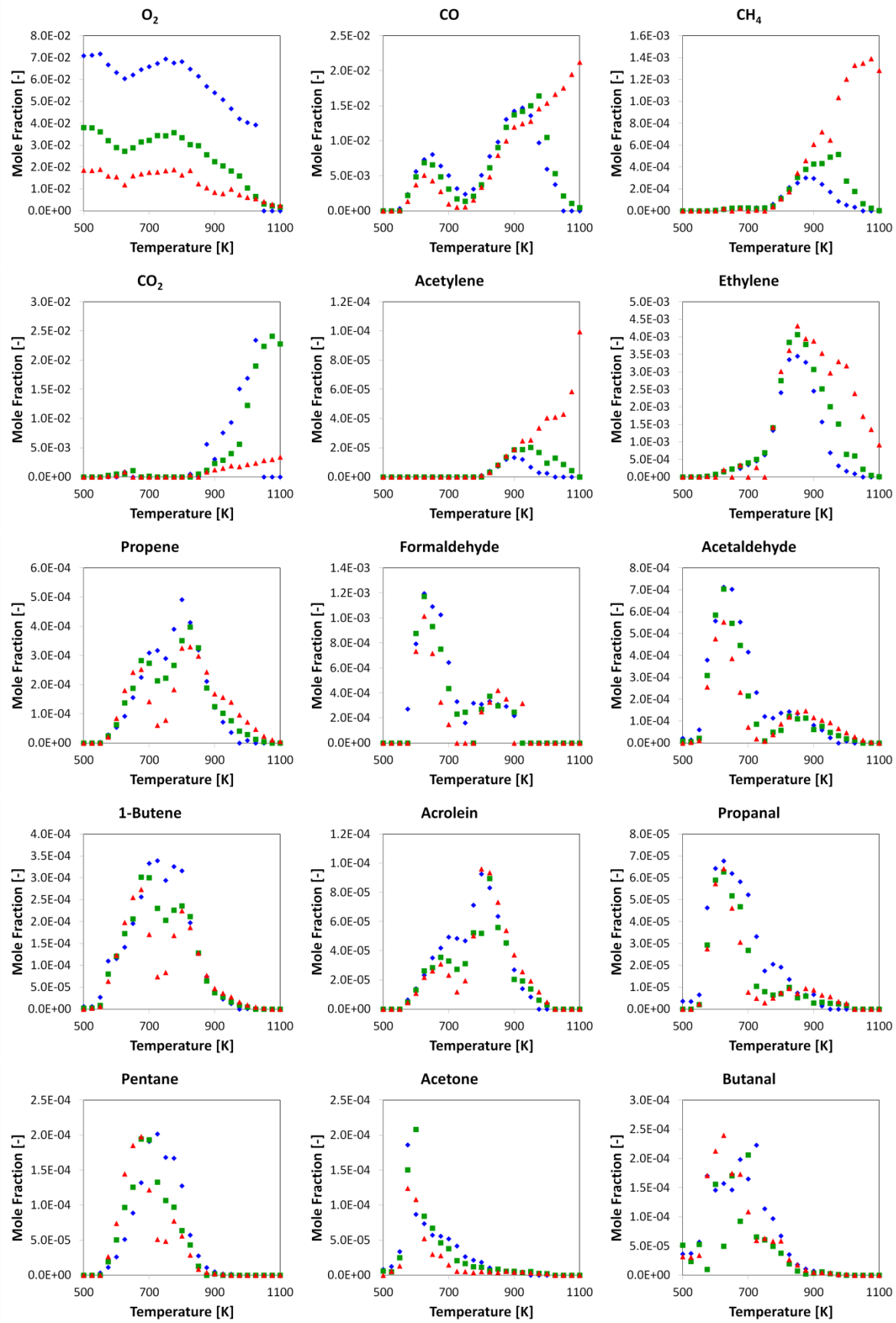

Figure 65. Mole fraction profiles of oxygen and main reaction products of *n*-pentanal oxidation for the three equivalence ratios (♦ phi=0.5, ■ phi=1, ▲ phi=2).

For both fuels, the formation of the C_{n-1} aldehydes was observed. Propanal and *n*-butanal are important products of the low-temperature oxidation of *n*-butanal and *n*-pentanal respectively as shown in Figure 62 and 65. Their importance then seems to decrease with the increase of the temperature. The main problem during *n*-pentanal oxidation was that *n*-butanal was also an impurity of the inlet, so its quantification is not reliable.

IV.2.2. Kinetic modeling

This section is dedicated to the presentation of the model developed for aldehyde oxidation. In order to have a larger view, the work of Rodriguez et al. (Rodriguez et al., 2017) about *n*-hexanal oxidation has also been taken in account for the mechanism development.

Mechanism

The model was developed on the base of the CRECK mechanism already presented in Section IV.1.2, which has been extended in order to reproduce the low-temperature oxidation of linear aldehydes. The CRECK kinetic model, obtained by extending the lumped version of C_3–C_4 aldehydes oxidation (Pelucchi et al., 2015, 2017b) to *n*-pentanal and *n*-hexanal, consists of 416 species and 11,500 reactions. The thermodynamic properties of C_4-C_6 aldehyde specific species were taken from different previous studies (Veloo et al., 2013a, 2013b; Rodriguez et al., 2017).

Table 36 presents the main reaction involved in the decomposition of *n*-butanal. RALD4X refers to the lumped species corresponding to the three alkyl radicals produced by the fuel and showed in Figure 66.

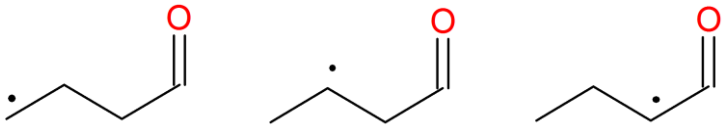

Figure 66. Radicals represented by the lumped species RALD4X in the model.

The mechanism for pentanal and hexanal is similar and is an extension of this mechanism. Table 37 presents the reaction of the radicals produced from *n*-butanal.

The detailed mechanism was lumped in order to reduce the number of species involved and the overall number of reactions according to procedures already discussed and adopted for many fuels (Ranzi et al., 2001, 2014). . The aim was to remove from the mechanism the intermediates that decompose quickly, by their products. So, the mechanism contains less products and reactions, without degrading the reproduction of the reactivity. For example, the assumption of the fast decarbonylation of carbonyl radicals (Pelucchi et al., 2017b) already allowed a first reduction. Another possibility was to gather all the radical isomer under one species in the mechanism.
The derived model was systematically extended to describe *n*-pentanal and *n*-hexanal oxidation.

Table 36. Reactions of *n*-butanal in cal, s, mol, cc units.

Reaction	*A*	*n*	*Ea*	No.
Reactions of *n*-Butanal				
Unimolecular initiations				
$C_3H_7CHO=>CH_3+HCO+C_2H_4$	1.09E+24	-2.25	90369.30	(1)
$C_3H_7CHO=C_2H_5+CH_2CHO$	5.04E+27	-3.49	84479.10	(2)
$C_3H_7CHO=HCO+nC_3H_7$	7.49E+27	-3.51	86757.50	(3)
$C_3H_7CHO=>H+CO+nC_3H_7$	2.72E+17	-0.58	88995.00	(4)
Molecular reactions				
$C_3H_7CHO=CO+C_3H_8$	1.00E+14	0.00	75000.00	(5)
$C_3H_7CHO=C_2H_6+CH_2CO$	1.00E+14	0.00	75000.00	(6)
Main bimolecular initiations and H-abstractions				
$O_2+C_3H_7CHO=>HO_2+CO+nC_3H_7$	1.19E+07	2.00	38109.91	(7)
$O_2+C_3H_7CHO=>HO_2+$RALD4X	9.37E+06	2.00	40722.49	(8)
$OH+C_3H_7CHO=>H_2O+CO+nC_3H_7$	2.00E+13	0.00	630.00	(9)
$OH+C_3H_7CHO=>H_2O+$RALD4X	2.00E+13	0.00	1700.00	(10)
$H+C_3H_7CHO=>H_2+CO+nC_3H_7$	1.60E+14	0.00	6360.00	(11)
$H+C_3H_7CHO=>H_2+$RALD4X	1.32E+07	2.00	3950.57	(12)
$HO_2+C_3H_7CHO=>H_2O_2+CO+nC_3H_7$	5.00E+12	0.00	12460.00	(13)
$HO_2+C_3H_7CHO=>H_2O_2+$RALD4X	7.60E+12	0.00	15860.00	(14)
$CH_3+C_3H_7CHO=>CO+CH_4+nC_3H_7$	1.00E+12	0.00	7234.20	(15)
$CH_3+C_3H_7CHO=>CH_4+$RALD4X	2.15E+05	2.00	4871.29	(16)
Alkyl radical decompositions				
RALD4X=>$CH_3+C_2H_3CHO$	1.00E+14	0.00	30000.00	(17)
RALD4X=>$HCO+C_3H_6$	3.00E+13	0.00	30000.00	(18)
RALD4X=>$C_2H_4+CH_2CHO$	2.00E+13	0.00	30000.00	(19)
RALD4X=>$CO+nC_3H_7$	6.00E+10	0.00	17500.00	(20)

Table 37.Reactions of the radicals produced from *n*-butanal in cal, s, mol, cc units.

Reaction	*A*	*n*	*Ea*	No.
Reactions of the radicals produced from *n*-Butanal				
Addition of RALD4X to O_2 and reactions of RALD4OOX				
O_2+RALD4X=>RALD4OOX	4.00E+12	0.00	0.00	(1)
RALD4OOX=>O_2+RALD4X	1.00E+13	0.00	31500.00	(2)
RALD4OOX=>OH+CO+C_2H_5CHO	6.00E+11	0.00	23500.00	(3)
RALD4OOX=>CO+0.5NC_3-QOOH+ 0.5IC_3-QOOH	3.00E+10	0.00	19000.00	(4)
RALD4OOX=>QA4X	1.50E+12	0.00	25000.00	(5)
QA4X=>RALD4OOX	3.00E+10	0.00	15000.00	(6)
QA4X=>OH+ETALD4X	1.00E+12	0.00	18000.00	(7)
QA4X=>HO_2+C_3H_5CHO	4.00E+13	0.00	23500.00	(8)
QA4X=>OH+C_2H4+CHOCHO	2.40E+13	0.00	23000.00	(9)
QA4X=>OH+CH_2O+C_2H_3CHO	2.40E+13	0.00	23000.00	(10)
Addition of QA4X to O_2 and reactions of ZA4X				
O_2+QA4X=>ZA4X	4.00E+12	0.00	0.00	(11)
ZA4X=>O_2+QA4X	1.00E+13	0.00	31500.00	(12)
ZA4X=>OH+CO+C_3-OQOOH	1.00E+11	0.00	18000.00	(13)
ZA4X=>OH+KEA4X	1.00E+11	0.00	18000.00	(14)
KEA4X=>OH+CH_2CHO+CHOCHO	3.00E+14	0.00	41000.00	(15)
KEA4X=>OH+HCO+$CHOCH_2CHO$	3.00E+14	0.00	41000.00	(16)
KEA4X=>OH+CO+CH_2O+CH_2CHO	6.00E+14	0.00	41000.00	(17)
KEA4X=>OH+CH_3CO+CHOCHO	3.00E+14	0.00	41000.00	(18)
KEA4X=>OH+HCO+CH_3COCHO	3.00E+14	0.00	41000.00	(19)
KEA4X=>OH+CH_2O+HCO+CH_2CO	1.00E+15	0.00	41000.00	(20)
KEA4X=>OH+CO+HCO+CH_3CHO	1.00E+15	0.00	41000.00	(21)

Analysis of the results

Figure 65 presents a comparison between the computed data and the experimental results for the two aldehyde fuels

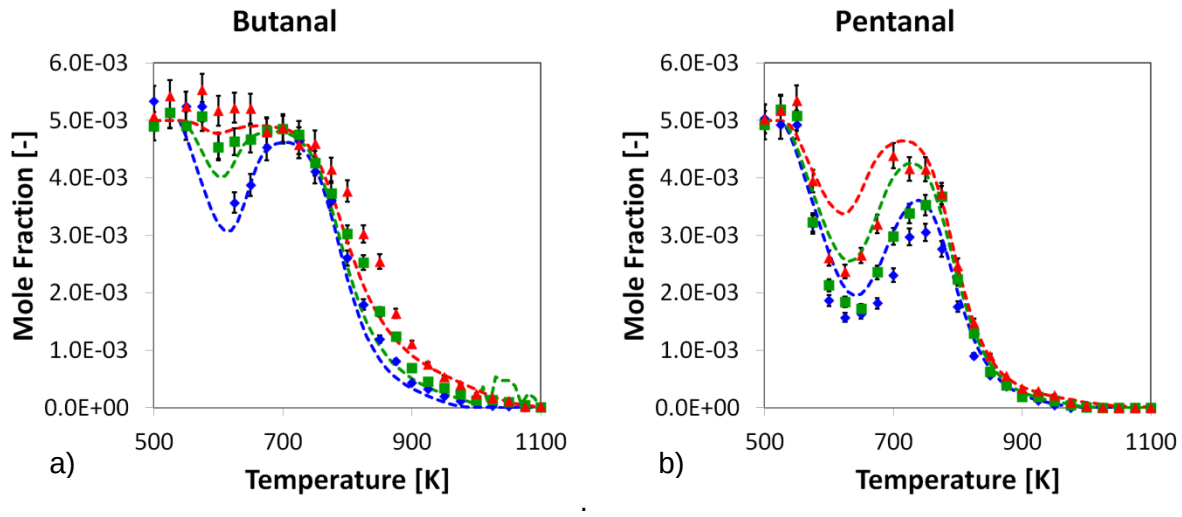

Figure 67. Fuel conversion for a) *n*-butanal and b) *n*-pentanal oxidation compared to the model results (Symbols: ♦ phi=0.5, ■ phi=1, ▲ phi=2) (Error bar ±5%).

The computed data are overall in a good agreement with the experimental results. The model is able to reproduce the fuel reactivity and catches the NTC behavior in a reasonable way. For *n*-pentanal, experiments show similar reactivities under stoichiometric and lean conditions, whereas the model predicts a larger difference. The model reproduces well the fact that *n*-butanal is less reactive than *n*-pentanal.
The model predicts an oscillatory behavior for the oxidation of *n*-butanal under stoichiometric condition. However this trend was not observed experimentally. Thus the predictions of the model for these conditions over 1000 K are not fully reliable.

Figure 68 presents a comparison between the computed data and the experimental results for *n*-butanal oxidation main products.

The product profiles also show the oscillatory behavior for *n*-butanal under stoichiometric condition at temperatures above 1000 K. Figure 69 shows the simulation results using a transient solver for oxygen and carbon monoxide mole fraction determination at 1010 K over an integration period of 30 s.

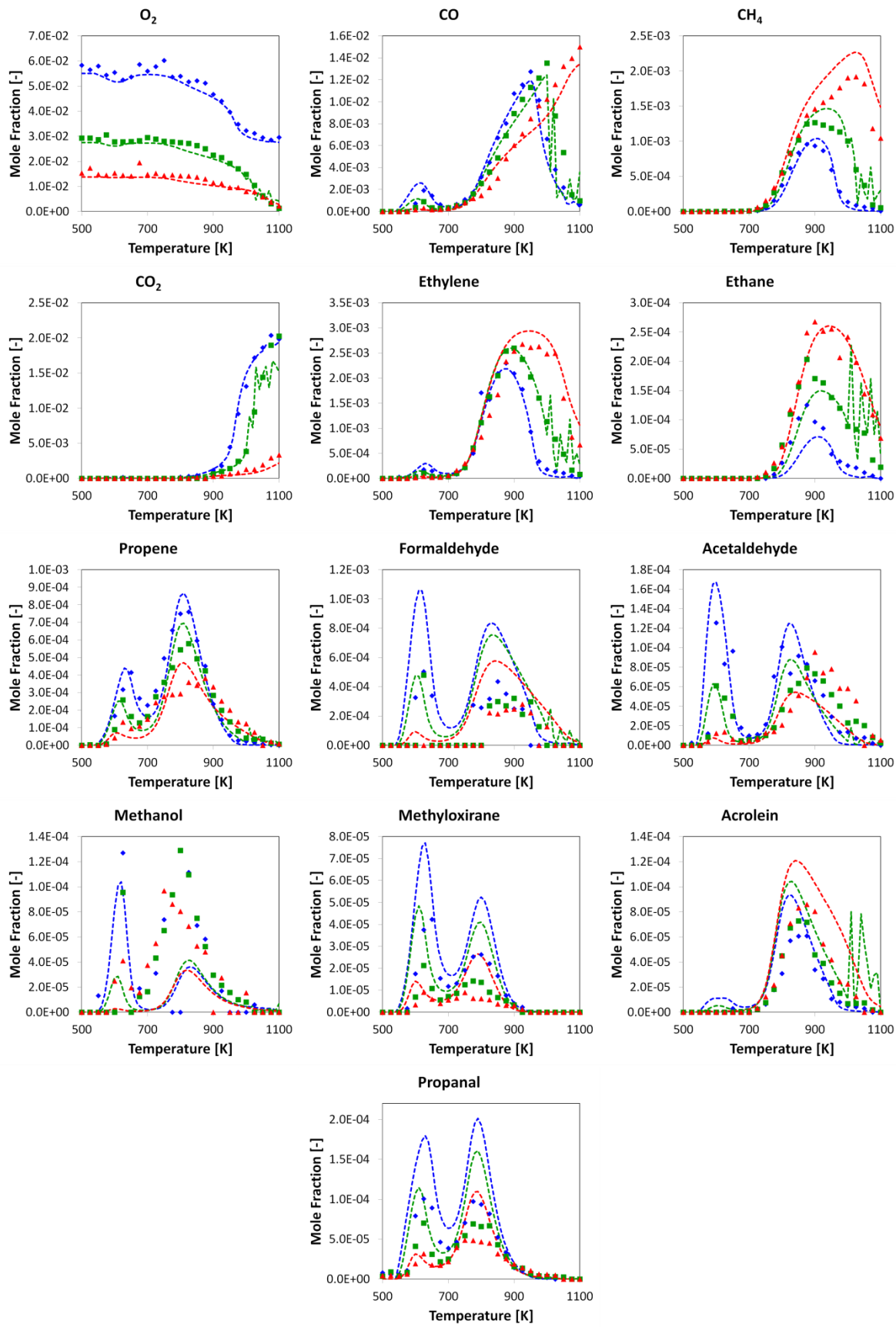

Figure 68. Mole fraction profiles of oxygen and main reaction products of *n*-butanal oxidation compared to the model computed results for the three equivalence ratios (♦ phi=0.5, ■ phi=1, ▲ phi=2).

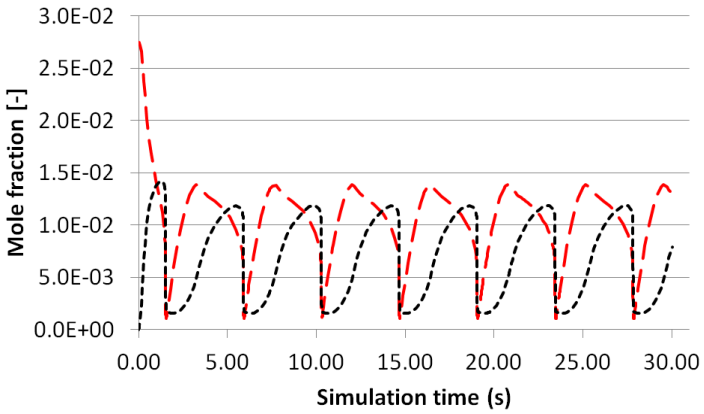

Figure 69. Computed data for oxygen (red long dashed line) and carbon monoxide (black short dashed line) under stoichiometric condition at 1010 K for 30 s of simulation time.

The mole fraction simulations are oscillating between two extreme values. The values plotted on the chart in Figure 69 are the value estimated after a simulation time of 60 s. This value has been chosen arbitrarily and is only here to stop the calculation. Thus depending on this arbitrary integration time, the mole fraction calculated is actually comprised between two extreme values and does not reflect the data recorded during the experiment. Note that oscillation behaviors have already been observed during the oxidation of methane in a jet-stirred reactor (Lubrano Lavadera et al., 2018) and that they could also occur with larger fuels (Marrodán et al., 2019). In this case, given the injection mode, the mole fraction deduced from the chromatography analysis would be a kind of average, depending on the shape of oscillations. Species mole fraction oscillations have already been detected during the oxidation of methane thank to the use of mass spectrometry with direct sampling using a capillary tube (Stagni et al., 2019).

The model is able the experimental profiles of many compounds (i.e.O_2, CO, CO_2, ethylene and propene) during butanal oxidation as shown in Figure 68. It can also be seen that some products also display an oscillatory behavior. Acrolein or ethane are very sensitive to oscillations, whereas methanol or propene are not sensitive. Formaldehyde is over-estimated with a factor of 2 for temperatures above 800 K. Methyloxirane or propanal profiles are also over-estimated by a factor 2. In the case of methanol, the low-temperature reactivity is better described by the model than the high temperature reactivity. At higher temperatures, the model under-predicts by a factor 2 methanol mole fraction profiles. Methoxy radicals are the main source of formation of methanol through H-abstraction reactions.

Figure 70 presents the results of the simulation for *n*-pentanal oxidation and the experimental profiles on the same chart. Only the species presented in the selectivity analysis are displayed here.

The overall performance of the model is very good for the other compounds. The C_1, C_2 and C_3 products formation are well described under all conditions and minor deviations are observed for the other products.

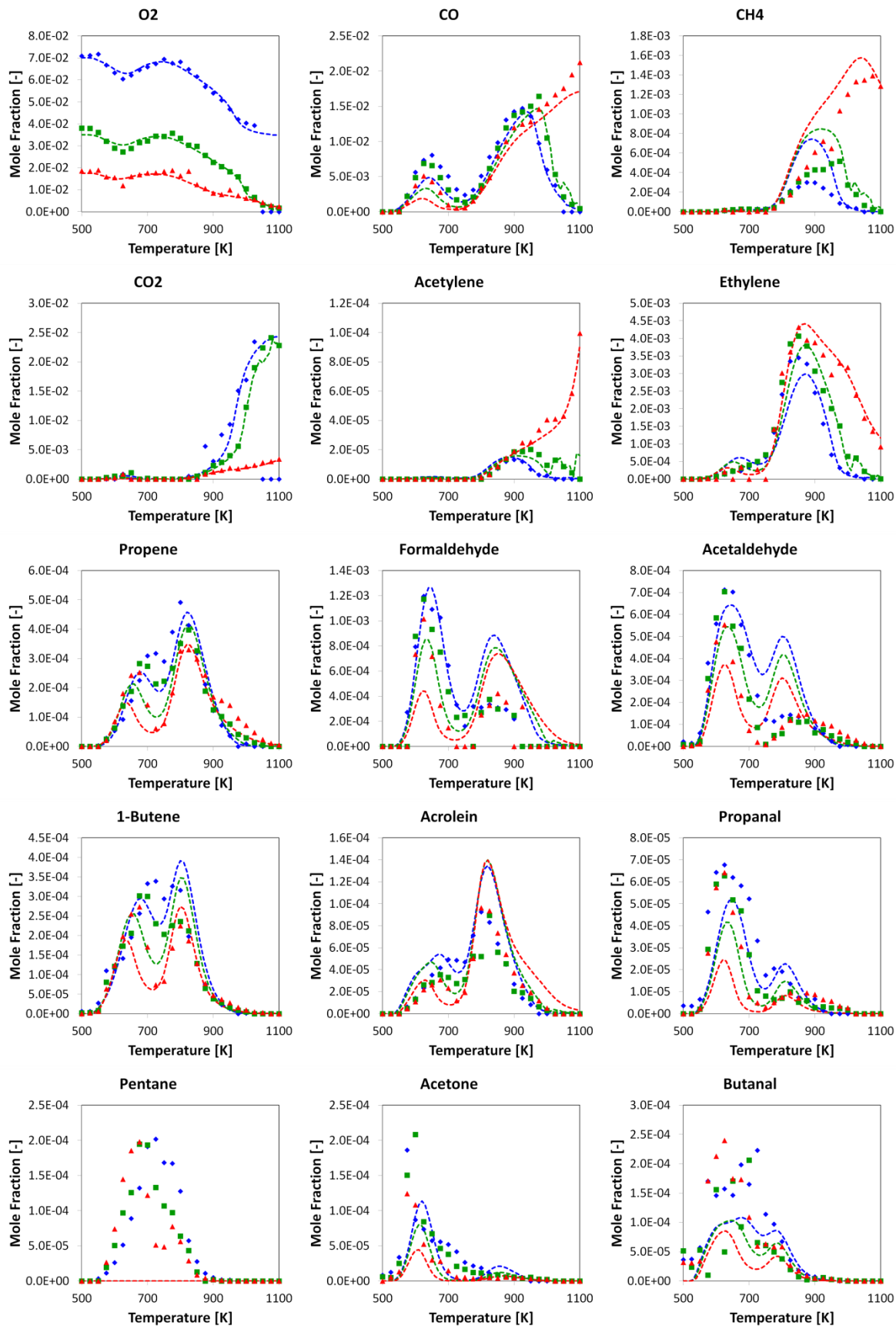

Figure 70. Mole fraction profiles of oxygen and main reaction products of *n*-pentanal oxidation compared to the model computed results for the three equivalence ratios (♦ phi=0.5, ■ phi=1, ▲ phi=2).

However, the profile of acetone is not well reproduced by the simulations. Mole fractions are under-estimated at the lowest temperatures and a second reactivity range is predicted, which was not observed experimentally. In addition the formation of *n*-butanal is underestimated over all the range of temperatures, but this may be due to the fact that butanal was an impurity in the fuel inlet. Thus its experimental profile is overestimated.

The simulation does not predict any formation of pentane (only a maximum of 0.1 ppm is predicted). Two reasons can lead to this error:

- A missing reaction pathway to produce pentane from the fuel,
- An error in the identification of this product mass spectrum with a spectrum wrongly attributed to pentane.

Due to the C_5 carbon skeleton of pentanal, the formation of pentane directly from the fuel can be considered as really limited. Many reactions are in fact predominant such as the decomposition of the carbon chain after an H atom abstraction. Thus the identification of this compound could be wrong. However the analysis performed did not allowed us to confirm or not the presence of pentane in the mixture. For this, it would have been very interesting to use the GCxGC to investigate if there is some co-elution of products under our analytical conditions.

Pentanoic acid was not present in the mechanism. The addition of pentanoic acid in the mechanism was not performed at the same time as the experimental profile was not reliable enough. Decision was made to perform a dedicated experimental study for the oxidation of carboxylic acids (see next Section).

Figure 71 presents the performance of the model for hexanal conversion and the C_{n-1} aldehyde formation, pentanal. It also shows the profiles of methane and acetaldehyde.

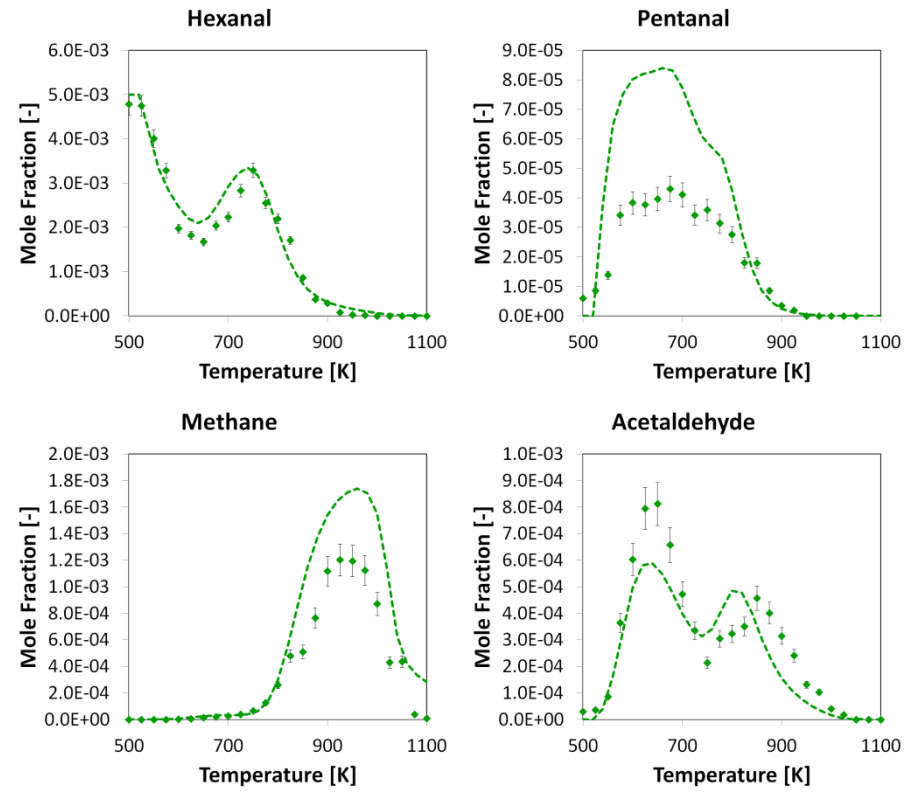

Figure 71. Hexanal (Rodriguez, 2016)and pentanal mole fractions profiles (dots) and model predictions (lines) (Error bars: 5% hexanal and 10% for the others).

The experimental values are those published by Rodriguez et al. The model succeeds in prediction hexanal conversion with a good description of the NTC area but it overestimates the production of pentanal by a factor 2, which is reasonable according to the quantity observed experimentally. The profiles of methane and acetaldehyde are well reproduced by the model.

Figure 72 presents a rate of production analysis for *n*-butanal oxidation. The nomenclature used here is then based on the one used in the developed mechanism (see Tables 36 and 37). It also contains a rate of production analysis for *n*-hexanal oxidation, as the study performed by Rodriguez et al. was also considered in the modeling (Rodriguez et al., 2017). *n*-Pentanal oxidation flux analysis is not displayed as it decomposes through an identical mechanism.

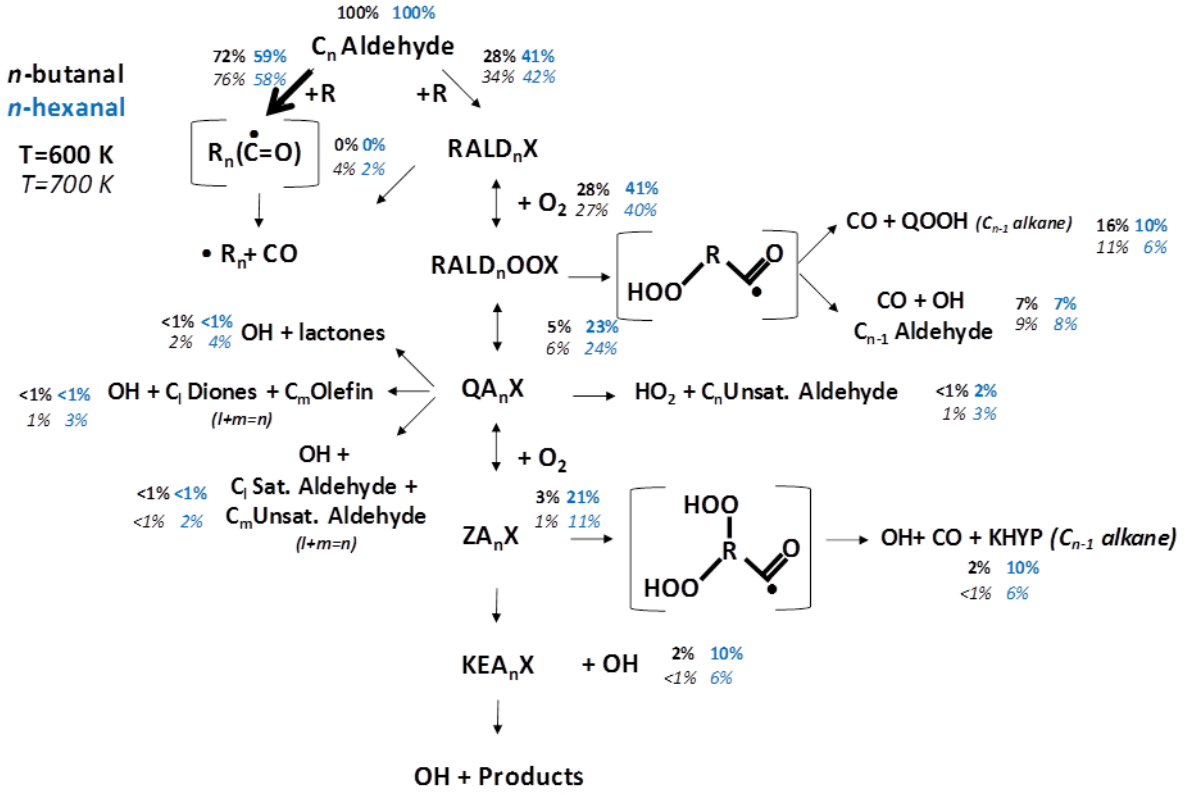

Figure 72. Rate of production analysis of the lumped low-temperature mechanism of *n*-butanal (black) and hexanal (blue) at T=600 K (bold) and T=700 K (italics). Species in brackets are not explicitly accounted for in the kinetic model.

This analysis shows that the shorter the alkyl chain in the fuel, the more important the H-abstractions on the carbonyl moiety. Indeed *n*-butanal reacts mainly through H-abstractions leading to the formation of $R_n(^{\bullet}C=O)$ radical, whereas the alkyl chain reactivity is more important for hexanal. This shows the importance of the alkyl chain weight in the aldehyde reactivity. Figure 72 also explains the formation pathway of the C_{n-1} aldehyde from the fuels. Those aldehydes are produced through the addition of the radical $RALD_nX$ (aldehyde with a radical on the alkyl chain) to oxygen. The formed radical ($RALD_nOOX$) can then decompose itself in different products or isomerize to form QA_nX. But the reactions pathway issued from this radical is of minor importance in the case of *n*-butanal (<6 %).

Figure 73, 74 and 75 present three sensitivity analyses performed at 600 K and under stoichiometric conditions for butanal, pentanal and hexanal oxidation. In red are highlighted

the reactions increasing the reactivity and in blue the ones slowing down the reactivity. The temperature (600 K) has been chosen in order to give a good overview of the low-temperature reactivity.

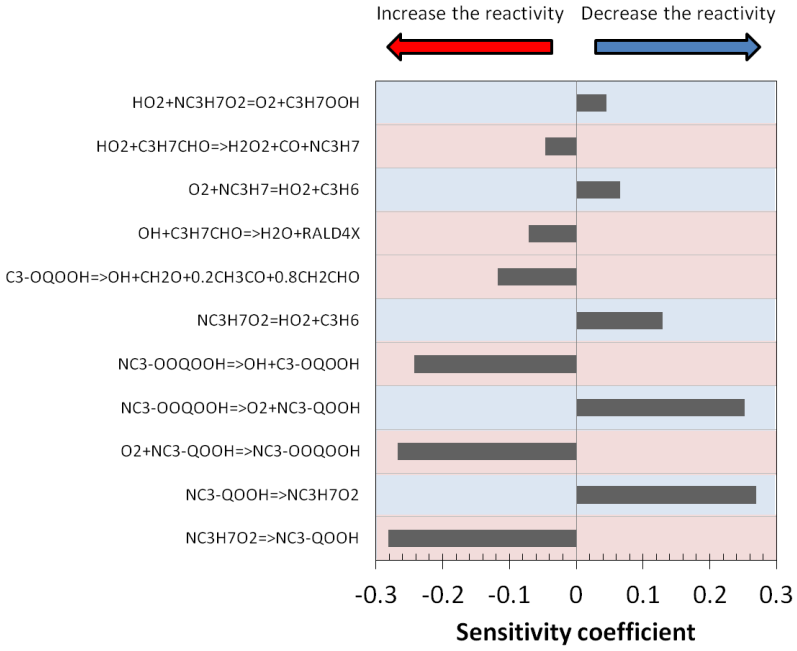

Figure 73. Sensitivity analysis of butanal oxidation to rate constants at 600 K under stoichiometric conditions.

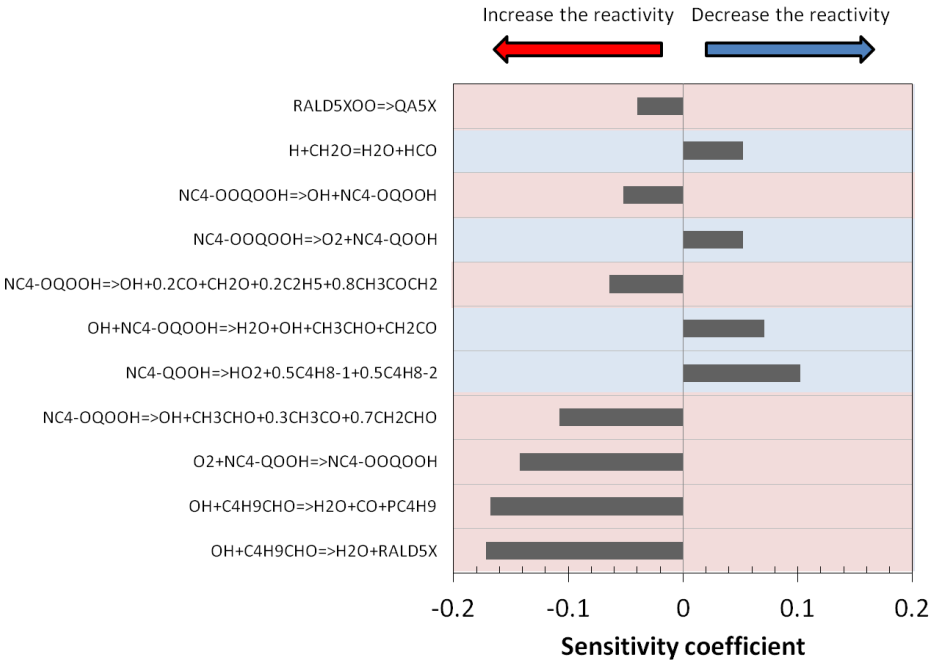

Figure 74. Sensitivity analysis of pentanal oxidation to rate constants at 600 K under stoichiometric conditions.

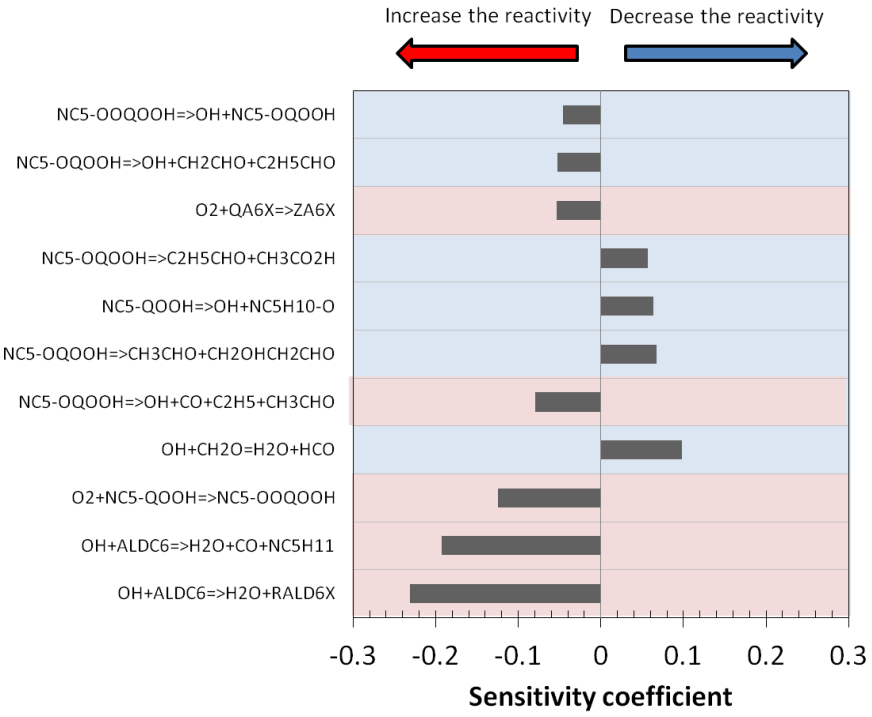

Figure 75. Sensitivity analysis of hexanal oxidation to rate constants at 600 K under stoichiometric conditions.

The sensitivity analyses show that the alkyl radical derivatives (NC3H7O2, NC3-QOOH for example) reactions are controlling the low-temperature reactivity. It can also be observed that the H-abstractions reactions by OH and HO_2 radical increase the reactivity. In the case of butanal, the low-temperature reactivity leads to a predominance of the HO_2 radical H-abstractions. The importance of the aldehyde specific reactions increases with the increase of the alkyl chain length as the H-abstraction reaction of the aldehydic H atom become less important in the low-temperature reactivity. The rest of the reactions are mainly the same as the C_{n-1} associated alkanes, propane and butane for butanal and pentanal respectively.

IV.2.3. Conclusion

This work showed that aldehyde oxidation is ruled by specific pathways influenced by the length of the alkyl chain. Many compounds were observed for *n*-butanal and *n*-pentanal oxidation and some specific products were identified. C_{n-1} aldehydes are typical products of C_n aldehyde oxidation and pentanoic acid was detected during *n*-pentanal experiments. The formation of smaller aldehydes has been explained by the reactivity of the alkyl moiety with oxygen, whereas the carbonyl moiety is responsible of the main reactivity through H-abstractions. However, this work did not succeed in explaining the formation of carboxylic acid observed experimentally.

IV.3. Pentanoic and butanoic acid oxidation

The next section is dedicated to the experiments and modeling carried out on butanoic and pentanoic acid oxidation. To our knowledge, the data presented here are the first to be published for both carboxylic acid oxidations. This work was published in Chemical Engineering Journal (Namysl, S., Pelucchi, M., Herbinet, O., Frassoldati, A., Faravelli, T., Battin-Leclerc, F., 2019. A first evaluation of butanoic and pentanoic acid oxidation kinetics. Chem. Eng. J. 373, 973–984. https://doi.org/10.1016/j.cej.2019.05.090).

IV.3.1. Experimental results

The literature scarcity is likely due to difficulties encountered during experiments. Some cares were necessary to deal with the corrosive properties of these molecules and to minimize adsorption phenomena and to obtain data as reliable as possible.

The fuel conversion and the products distribution are presented and then carbon balances and selectivity analyses are discussed. The experiments have been carried out in a jet-stirred reactor at 800 Torr and between 800 K and 1100 K. Three equivalence ratios have been studied (0.5-1-2) for a fuel inlet mole fraction of 0.5 %.

Fuel conversion

The experiments on carboxylic acids have been complicated by the corrosive properties of these compounds. Indeed some parts of the set-up were deteriorated by the acids and specially the seals and some cold points. The acids also tend to have a strong adsorption at the walls in the different parts of the set-up, preventing to keep them in the gas phase. To fight against this phenomenon, an air flush was used between two experiments and some parts of the chromatographs were replaced by new coated ones. This process is described in Part III. Despite this, the experimental error on fuel quantification is still larger than usual (±10 % instead of ±5 %). Moreover the experiments were only carried out from 800 K to 1100 K. Below 800 K, experiments were performed but the results were not reliable enough due to a large incertitude on the measurements. The pentanoic acid is likely the largest carboxylic acids which can be studied in the experimental set-up under its present configuration.

Figure 76 presents the mole fraction profiles for butanoic and pentanoic acids between 800 and 1100 K for the three equivalence ratios. It also presents a comparison of the fuel reactivity for each equivalence ratio.

Due to the longer alkyl chain of pentanoic acid, its reactivity is higher than the one of butanoic acid for the same equivalence ratio. The reactivity is shifted by 50 K between both fuels. At 1000 K, the two acids are fully decomposed except for butanoic acid under fuel-rich conditions.

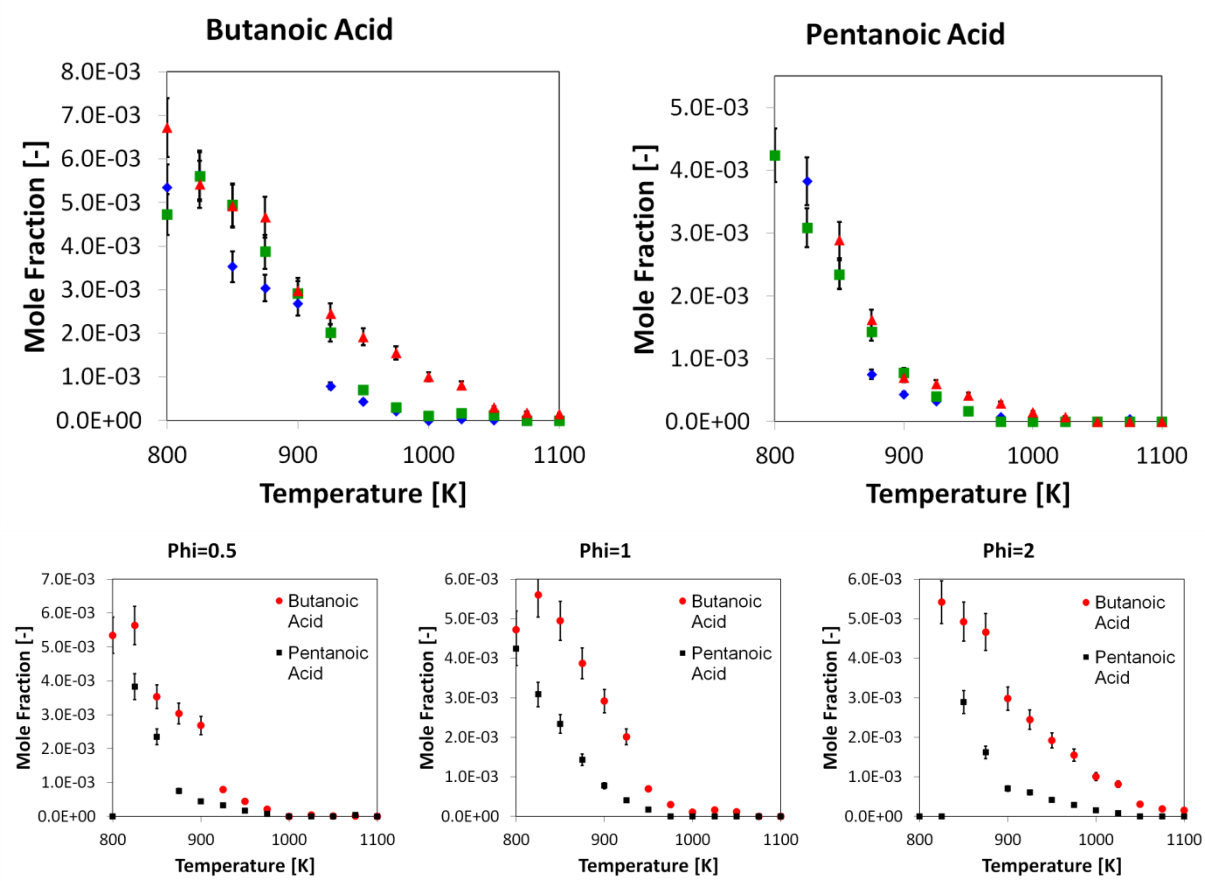

Figure 76. Fuel conversion for butanoic and pentanoic oxidation and comparison for each equivalence ratio of the reactivity (Symbols: ♦ phi=0.5, ■ phi=1, ▲ phi=2) (Error bar ±10%).

At the lowest temperatures, we can see that the measures vary a lot around the theoretical inlet set-point. The reproducibility of each measure was also really complex to obtain. This is due to the points discussed before. To determine the start and the end of the reactivity, we can also use the product profiles in complement to the results showed in Figure 76. However, we can see that, for temperatures above 850 K, the fuel profiles are nicer and for these temperatures, the reproducibility of the measurements was better. Note that the variability observed for the fuel mole fraction is likely due to problems of adsorption occurring between the reactor outlet and the gas chromatographs (and not in the reactor feed) as no variability is observed for reaction products. Thus the reaction in the jet-stirred reactor occurred under satisfactory conditions, problems for the fuel occurring only downstream.

An additional set of experiments was performed to better understand the specific chemistry of organic acids in the gas phase. The pyrolysis of pentanoic acid was carried out in the same JSR as the oxidation experiments. The inlet mole fraction has been decreased from 0.5 % to 0.2 % to reduce the potential soot formation, which may cause some severe plugging problem in addition of the problems already encountered with acids. The fuel conversion is presented in Figure 77.

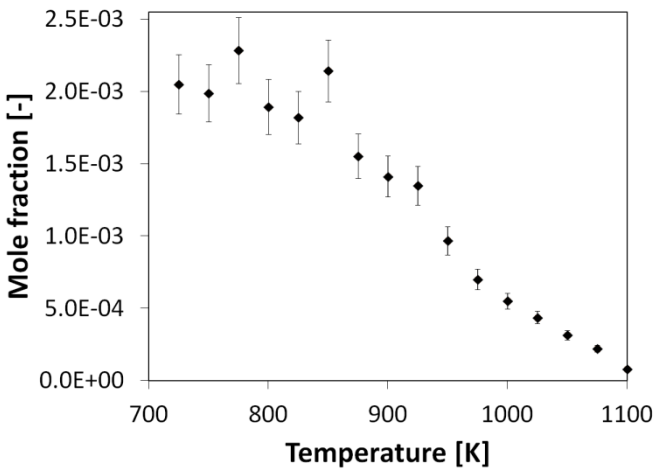

Figure 77. Fuel conversion for pentanoic acid pyrolysis (inlet fuel fraction 0.2%) (Error bar ±10 %).

The start of reactivity for pyrolysis is at 875 K (looking at the product profiles and taking into account uncertainties on the fuel measurements) and the fuel is almost fully consumed at 1100 K. This range of temperature is shifted to higher temperature by around 50 K compared to the fuel-rich oxidation of pentanoic acid, which is consistent with the expectations. The JSR maximal temperature of operation is 1200 K but it has been chosen to limit the maximal temperature of the experiments to 1100 K as the formation of soot may cause problems above this temperature.
These experiments have been performed in order to complete the potential database for the next model development. Indeed pyrolysis experiments may help the identification of some unimolecular reactivity or molecular pathways that are relevant for those compounds.

Carbon balance and selectivity analysis

The carbon balance obtained for temperatures between 800 and 900 K is flawed by the huge incertitude on fuel measurements. Thus the carbon balance is not around 10 % of deviation as usual. It is about ±30 % for pentanoic acid experiments for temperatures between 800 and 950 K and below ±10 % above 950 K. In the case of butanoic acid, the carbon balance remains around ±15 % over the whole range of temperatures. For pyrolysis experiments, the carbon balance is in average around ±9 %.

18 products have been identified during butanoic acid oxidation. The detected products are: carbon monoxide, carbon dioxide, methane, acetylene, ethylene, ethane, propene, propane, formaldehyde, methanol, oxirane, acetaldehyde, ethanol, acrolein, propanal, acetone, 1-butene and 1.3-butadiene. The products carbon atom number varies from 1 (carbon monoxide, methane…) to 4 atoms (1-butene, 1.3-butadiene). For the molecule containing 4 carbon atoms, as the fuel has a C_4 skeleton, they surely are produced via recombination reaction of smaller alkyl radicals.

During pentanoic acid oxidation, 34 products have been identified. All the products detected during butanoic acid oxidation have also been detected during pentanoic acid oxidation. The products detected in addition are: 1-butyne, 2-butene (both isomers), methyl-oxirane, furan, 2.3-dimethylcyclopropane, ethyloxirane, 2-pentene (both isomers), 2-propen-2-ol, 2.3-dihydrofuran, methyl vinyl ketone, butanal, 2-butanone, 1.2-dihydrofuran, benzene and pentanal. Some products like the C_4 unsaturated observed are typically produced from the C_5 alkyl chain decomposition and thus were not detected during butanoic acid oxidation.

Figure 78 shows the carbon sensitivity analyses performed for butanoic and pentanoic acid oxidation. The analyses have been carried out for all the equivalence ratios. The temperatures are selected so that the carbon balance is in the range ±10 % and for the same conversion for each fuel (85 % here).

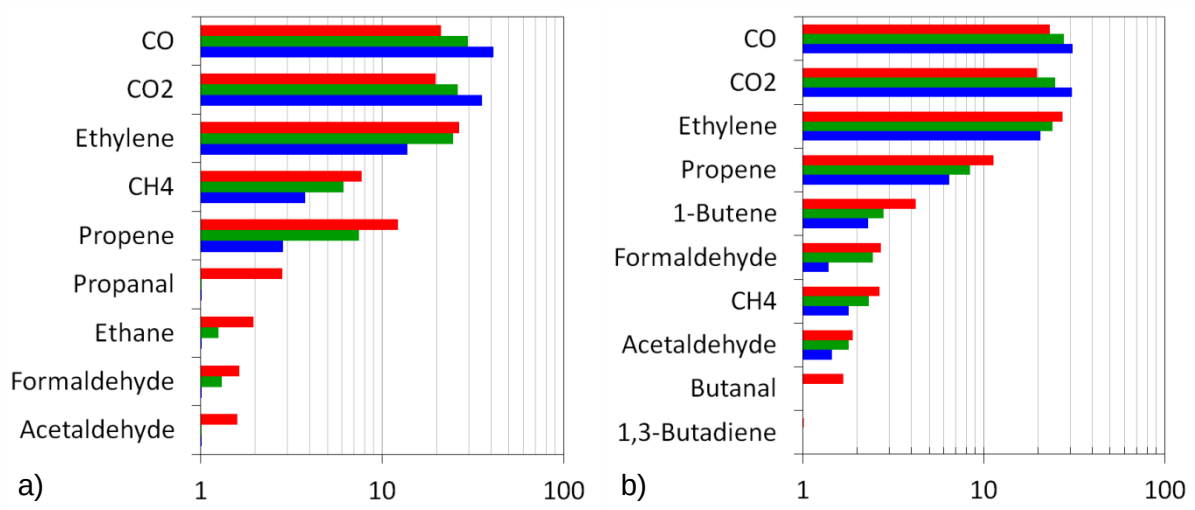

Figure 78. Reaction product selectivity analysis for a) butanoic and b) pentanoic oxidation at 950 K and 900 K respectively (85 % conversion) (phi=0.5, phi=1, phi=2) (Threshold: 1%).

Figure 79 presents the mole fraction profiles for oxygen and the main products obtained during butanoic acid oxidation experiments (products displayed in Figure 78).

Carbon monoxide, carbon dioxide and ethylene are the major products for both fuels. Large amounts of methane and propene are also observed for both fuels. Methane formation is mainly due to H-abstraction reactions by CH_3 radicals, but those radicals are also responsible of the formation of ethane by recombination reactions between themselves. So the high amount of CH_3 radical in the mixture may explain the large amounts of methane and ethane observed. Ethylene and acetylene are produced from ethane through successive dehydrogenation reactions.

Figure 80 presents the mole fraction profiles for oxygen and the main products obtained during pentanoic acid oxidation experiments, which were displayed in Figure 78.

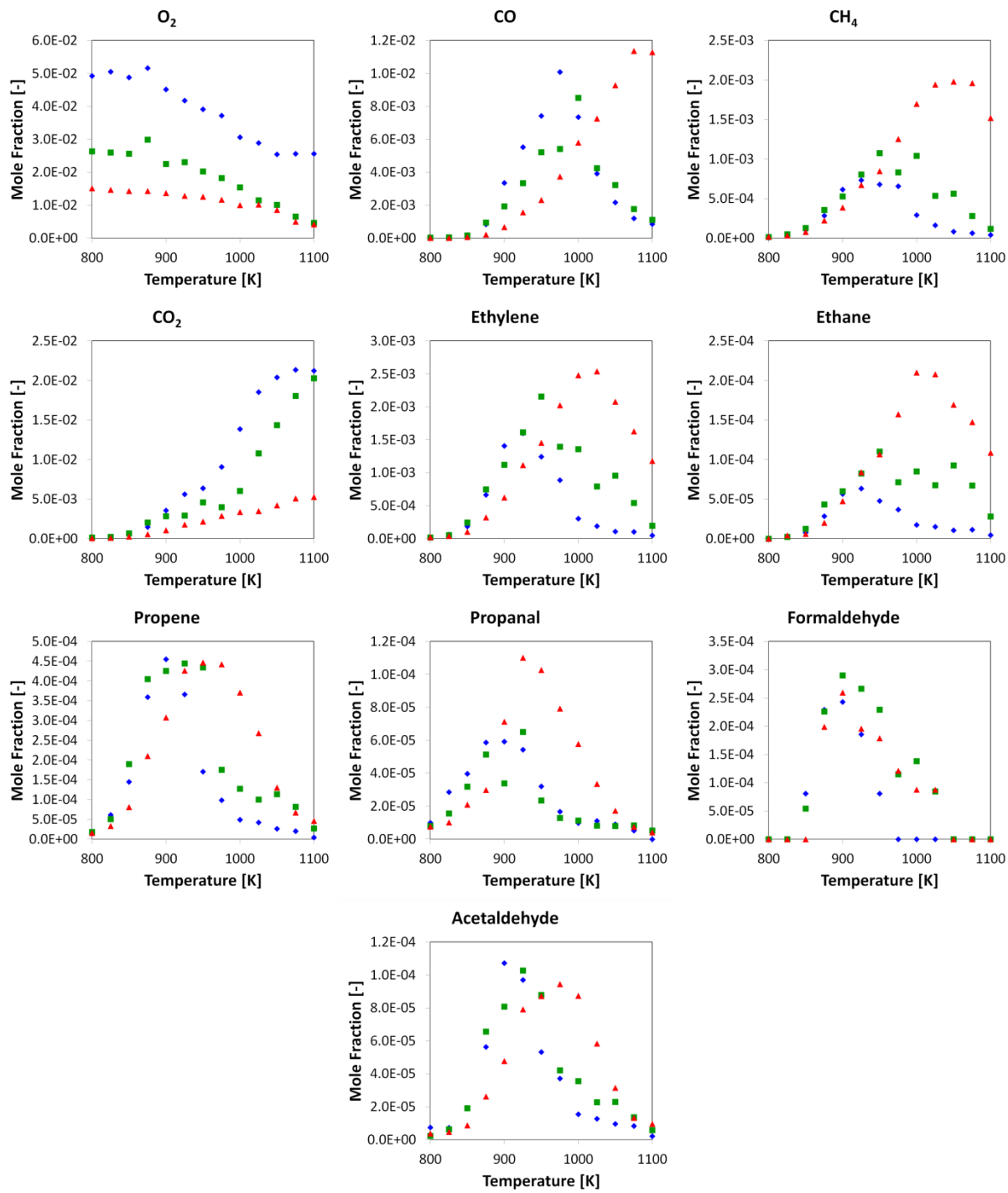

Figure 79. Mole fraction profiles of oxygen and main reaction products of butanoic acid oxidation for the three equivalence ratios (♦ phi=0.5, ■ phi=1, ▲ phi=2).

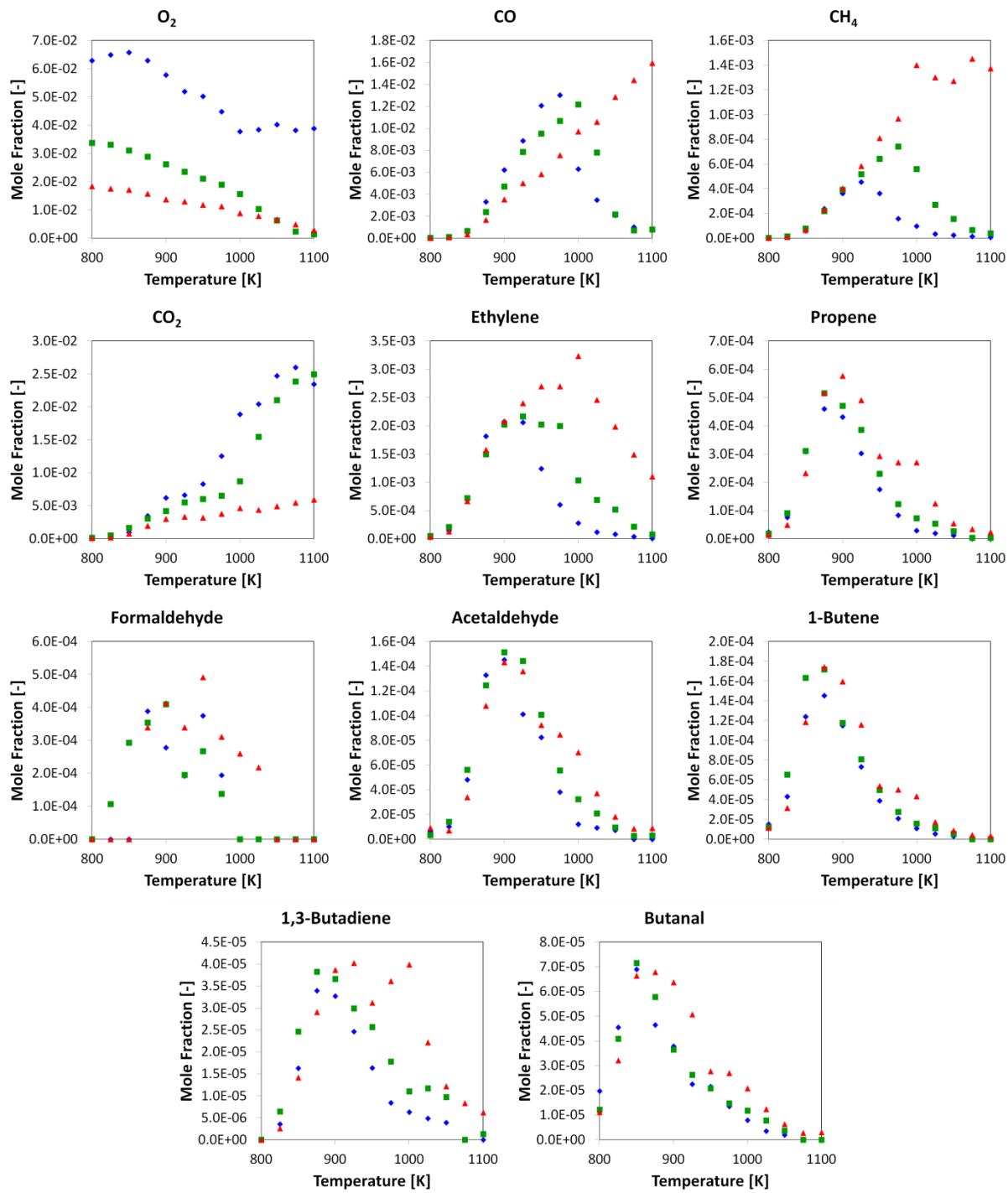

Figure 80. Mole fraction profiles of oxygen and main reaction products of pentanoic acid oxidation for the three equivalence ratios (♦ phi=0.5, ■ phi=1, ▲ phi=2).

Concerning the oxygenated compounds, many aldehydes are observed during the decomposition of the two fuels. Formaldehyde, acetaldehyde, propanal and *n*-butanal are indeed present in the mixture. *n*-Butanal and propanal seem to be specific products of pentanoic and butanoic acids, respectively.

Below 850 K for butanoic acid oxidation, the mole fraction ratio between carbon monoxide and dioxide indicates that the formation of carbon dioxide is dominant, as shown in Figure 81.

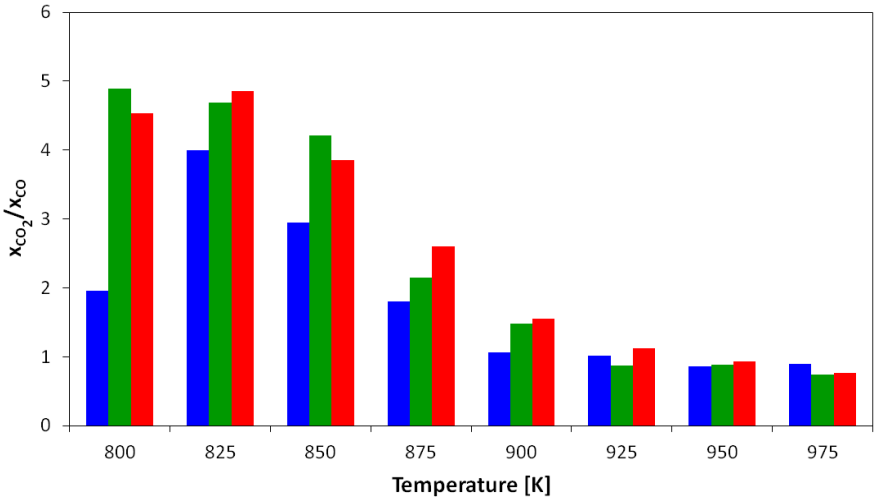

Figure 81. Mole fraction ratio between carbon dioxide and carbon monoxide for the three equivalence ratios during butanoic acid experiments (■ phi=0.5, ■ phi=1, ■ phi=2).

Above 1000 K, carbon monoxide is oxidized into carbon dioxide, but between 800 and 900 K, carbon dioxide is produced in larger quantity without any obvious consumption of carbon monoxide into carbon dioxide. Its formation may be explained by a reaction of the fuel producing carbon dioxide and especially from the carboxylic acid function.

Concerning pyrolysis experiments on pentanoic acid, 32 products have been detected: carbon monoxide and dioxide, methane, acetylene, ethylene, ethane, propene, propane, formaldehyde, oxirane, acetaldehyde, ethanol, 1-butene, 2-butene (both isomers), 1.3-butadiene, acrolein, dimethylcyclopropane, ethyloxirane, 2-propen-1-ol, 2-pentene (both isomers), 2.3- dihydrofuran, cyclopentene, methyl vinyl ketone, butanal, 2-butanone, benzene, cyclohexadiene, cyclopentanone and pentanal. Figure 82 shows a selectivity analysis performed at 950 K and thus for a conversion of 50 %. Figure 83 presents the mole fraction of the products presented in the selectivity analysis (see Figure 82).

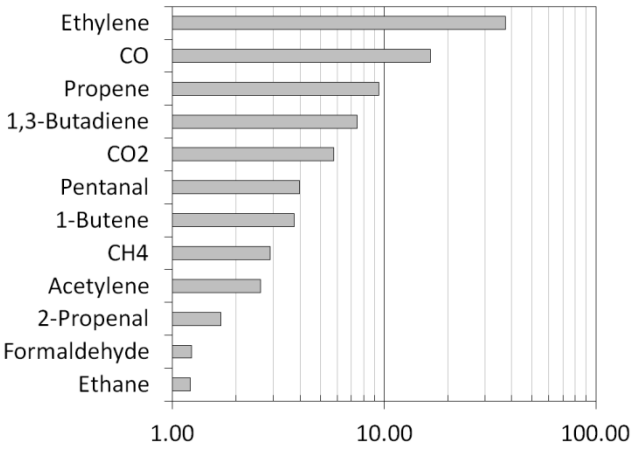

Figure 82. Reaction product selectivity analysis for pentanoic acid pyrolysis at 950 K (50% conversion) (Threshold: 1%).

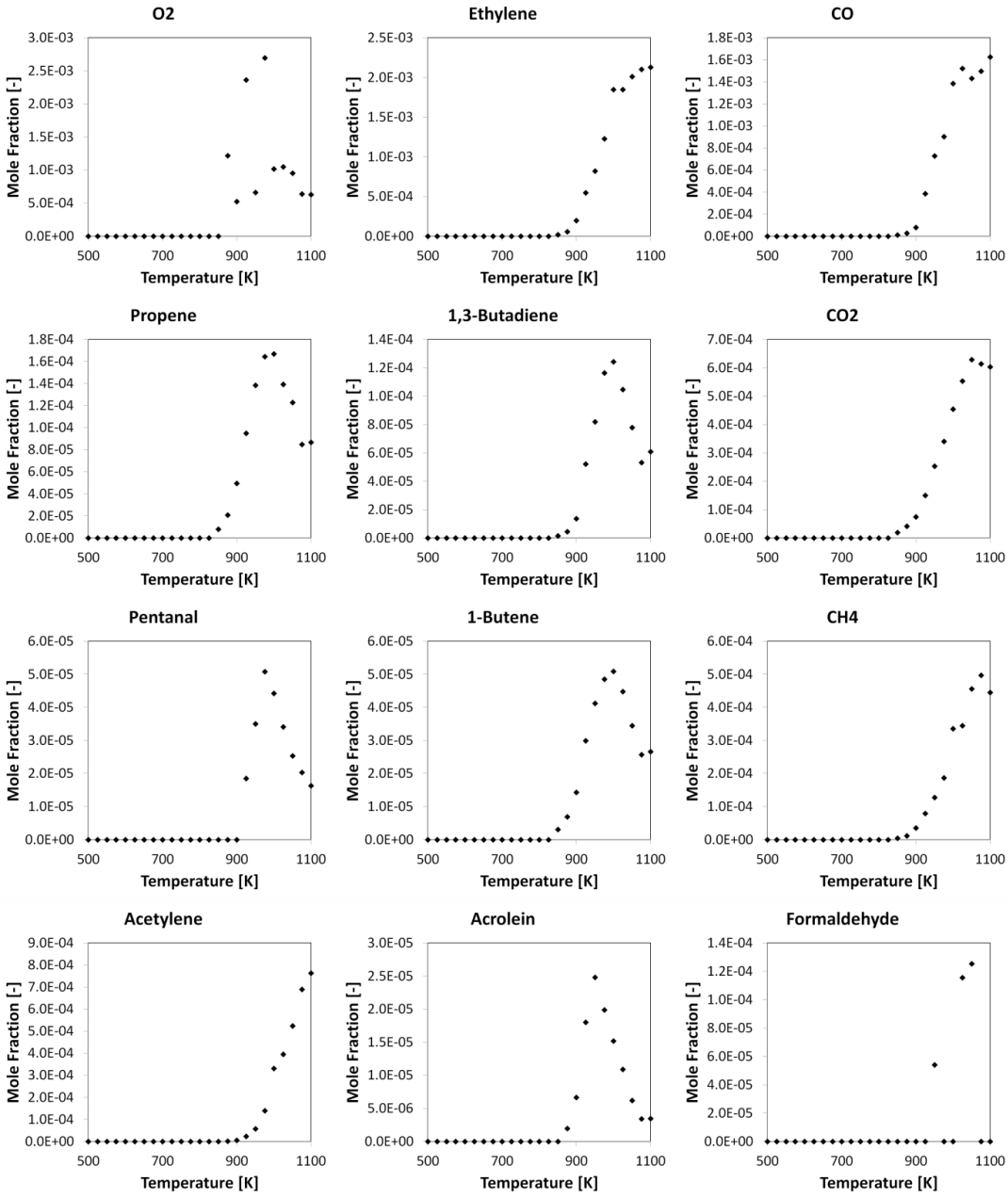

Figure 83. Mole fraction profiles of oxygen and main reaction products of pentanoic acid.

The selectivity analysis shows that ethylene and carbon monoxide are the main products of our experiments. Carbon dioxide may be produce by some reactions involving the acid function or by oxidation of carbon monoxide. The relative large amount of oxygenated compounds (pentanal, carbon dioxide, acrolein and formaldehyde) may indicate that the conditions were not fully controlled. Indeed a leak of air may be responsible of an unintentional inlet of oxygen. This hypothesis is also supported by the detection of oxygen (around 1000 ppm) thanks to the gas chromatographs. Thus it has been chosen to develop the kinetic model only on the oxidation results and not on the pyrolysis results, as they are not reliable enough.

IV.3.2. Kinetic model

In the next section, the kinetic model developed is presented. The predictions given by the model are then compared to the experimental results.

Mechanism

In the coming part, the mechanism developed in the frame of this study is presented. The model has been developed during a short-term mission of one month in Milano funded by the SMARTCATS COST action. The same approach than the one presented in IV.1.2 has been used. The mechanism developed by Cavallotti et al (Cavallotti et al., 2018) for acetic acid has been extended in order to reproduce the reactivity of pentanoic and butanoic acids.

Thermodynamic properties for butanoic acid, pentanoic acid and their radicals were estimated using software THERGAS (Muller et al., 1995) that implements Benson's group additivity rules (Benson et al., 1969).

Rate constants for the different reaction classes can be treated according to the recent work of Cavallotti et al. (Cavallotti et al., 2018) for acetic acid when referring to the acid specific moiety. Concerning the remaining part of the molecule, established rate rules for alkanes (Ranzi et al., 2014, 2015) are adopted in this work.

Acetic acid mostly decomposes through molecular decomposition pathways (E_a~71-74 kcal/mol) due to the much larger activation energies of unimolecular initiation reactions (E_a~93-110 kcal/mol) (Cavallotti et al., 2018). However, conventional radical initiation pathways are more important for acids with a longer carbon chain, as the effect of the carboxylic substitution vanishes. In particular, while a limited contribution is expected from the strong C-O and O-H bonds, the weak C_α-C_β can overcome or compete with decarboxylation and dehydration reactions. Despite the hierarchical development of kinetic subsets for higher C_4 and C_5 acids requires the inclusion of molecular and unimolecular initiation reactions, it has to be noted that under the experimental conditions presented in this work these reactions do not play a dominant role. Better insights on their importance can be obtained from an experimental investigation of butanoic and pentanoic acids in pyrolytic conditions.

Table 38 presents the reaction implemented in the CRECK mechanism for the reaction of butanoic acid during pyrolysis and combustion.

Table 38. Reactions of butanoic acid in cal, s, mol, cc units.

Reaction	*A*	*n*	*Ea*	No.
Reactions of Butanoic acid				
Unimolecular initiations				
$C_3H_7COOH = H_2O + C_2H_5CHCO$	9.44E+12	0.25	73083.23	(1)
$C_3H_7COOH => OH + CO + n\text{-}C_3H_7$	1.00E+16	0.00	105500.00	(2)
$C_3H_7COOH = HOCO + n\text{-}C_3H_7$	7.06E+36	-5.89	103725.77	(3)
$C_3H_7COOH = C_2H_5 + CH_2COOH$	1.00E+17	0.00	80500.00	(4)
$C_3H_7COOH = CH_3 + CH_2CH_2COOH$	1.00E+17	0.00	88000.00	(5)
$C_3H_7COOH => H + CO_2 + NC_3H_7$	1.00E+16	0.00	106400.00	(6)
$C_3H_7COOH = H + RBUTANOICA$	1.00E+16	0.00	94300.00	(7)
$H + RBUTANOICC = C_3H_7COOH$	5.00E+13	0.00	0.00	(8)
$H + RBUTANOICB = C_3H_7COOH$	5.00E+13	0.00	0.00	(9)
Main bimolecular initiations and H-abstractions				
$O_2 + C_3H_7COOH => HO_2 + CO_2 + n\text{-}C_3H_7$	1.02E+06	2.00	48272.65	(7)
$O_2 + C_3H_7COOH = HO_2 + RBUTANOICA$	4.47E+05	2.26	48338.87	(8)
$O_2 + C_3H_7COOH = HO_2 + RBUTANOICB$	3.40E+06	2.00	44000.00	(9)
$O_2 + C_3H_7COOH = HO_2 + RBUTANOICC$	5.10E+06	2.00	48272.65	(10)
$OH + C_3H_7COOH => H_2O + CO_2 + n\text{-}C_3H_7$	5.37E+00	3.44	-761.33	(11)
$OH + C_3H_7COOH = H_2O + RBUTANOICA$	1.26E+01	3.51	-2496.29	(12)
$OH + C_3H_7COOH = H_2O + RBUTANOICB$	3.00E+09	1.00	50.00	(13)
$OH + C_3H_7COOH = H_2O + RBUTANOICC$	4.50E+09	1.00	1540.75	(14)
$H + C_3H_7COOH => H_2 + CO_2 + n\text{-}C_3H_7$	2.14E+09	1.30	16754.75	(15)
$H + C_3H_7COOH = H_2 + RBUTANOICA$	1.33E+03	3.04	3494.45	(16)
$H + C_3H_7COOH = H_2 + RBUTANOICB$	6.00E+06	2.00	4000.00	(17)
$H + C_3H_7COOH = H_2 + RBUTANOICC$	1.12E+07	2.00	6525.60	(18)
$CH_3 + C_3H_7COOH > CO_2 + CH_4 + n\text{-}C_3H_7$	2.94E+04	2.33	13465.19	(19)
$CH_3 + C_3H_7COOH = CH_4 + RBUTANOICA$	5.80E+01	3.16	5875.07	(20)
$CH_3 + C_3H_7COOH = CH_4 + RBUTANOICB$	6.00E+04	2.00	5000.00	(21)
$CH_3 + C_3H_7COOH = CH_4 + RBUTANOICC$	9.00E+04	2.00	7443.70	(22)
$HO_2 + C_3H_7COOH => H_2O_2 + CO_2 + n\text{-}C_3H_7$	8.90E+03	2.33	23111.92	(23)
$HO_2 + C_3H_7COOH = H_2O_2 + RBUTANOICA$	1.52E-01	3.83	15250.00	(24)
$HO_2 + C_3H_7COOH = H_2O_2 + RBUTANOICB$	1.60E+06	2.00	16000.00	(25)
$HO_2 + C_3H_7COOH = H_2O_2 + RBUTANOICC$	1.04E+06	2.00	15025.60	(26)
$O + C_3H_7COOH => OH + CO_2 + n\text{-}C_3H_7$	1.41E+06	2.00	4691.70	(27)
$O + C_3H_7COOH = OH + RBUTANOICA$	2.36E+06	2.00	2500.00	(28)
$O + C_3H_7COOH = OH + RBUTANOICB$	4.70E+06	2.00	2500.00	(29)
$O + C_3H_7COOH = OH + RBUTANOICC$	7.05E+06	2.00	4691.70	(30)

Table 38 presents the unimolecular initiations and the main bimolecular or H-abstractions reactions. The only lumping in these reactions is the assumption of the fast decarboxylation of the radical formed via the departure of the acid H atom. The other radicals formed by H-abstractions are:

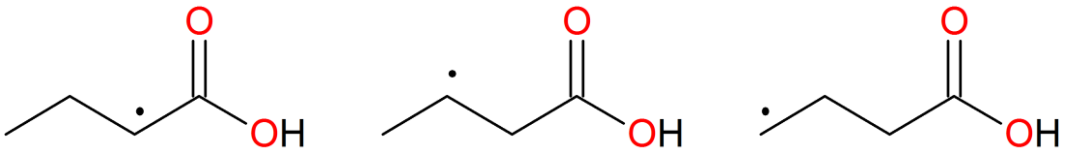

RBUTANOICA RBUTANOICB RBUTANOICC

These radicals can then isomerize or decompose through reactions similar to those of alkyl radicals. The models for pentanoic and hexanoic acids are extended from this model considering addition of the sub-mechanism linked to the addition of a secondary carbon atom in the alkyl chain.

According to the approach of Ranzi et al. (1993) presented in IV.1.2 for H-abstractions with different radicals, the rate constants from Cavallotti et al. (2018) shown in Figure 21 can be corrected to obtain an estimate of the rate parameters for H-abstractions from secondary β sites in higher molecular weights acids (propanoic, butanoic and pentanoic). The rate is modified reducing the activation energy by 2300 cal/mol (E_{SiteH}=-2300 cal/mol from primary to secondary) and accounting for the different numbers of H-atoms available on the site. The rate constants for H-abstractions from the hydroxyl function (O-H) of butanoic and pentanoic acids are adopted directly from the work on acetic acid (Cavallotti et al., 2018).

Figure 84 shows the relative selectivities to the different sites for H-abstraction reactions by OH on butanoic acid, as computed from the values adopted in this work on a per H-atom basis. As expected from the strong bond energy, the selectivity of H-abstraction from the hydroxyl group of the carboxylic function only accounts for a few percents at very high temperatures for the case R=OH (>10% at 1100 K). 30-35% selectivities are observed for H-abstractions from the secondary position in β. H-abstractions from the secondary alkane-like position (γ) shows the higher yields at low temperatures (500 K) (45%) decreasing to 28% at 1100 K. Concerning the primary position δ, 20-30% yields is observed over all the temperature range.

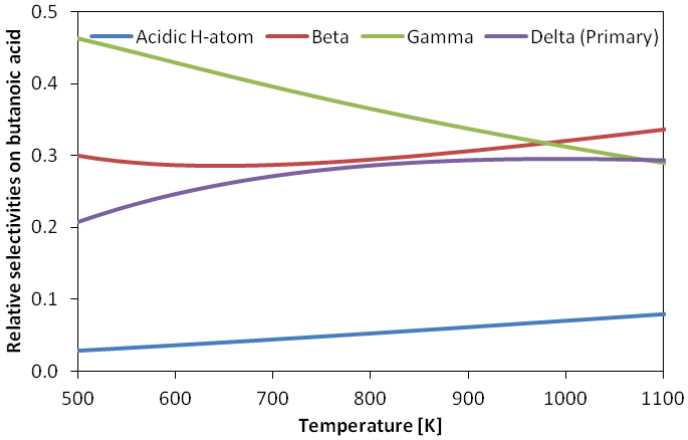

Figure 84. Relative selectivities to the different H-abstraction sites on butanoic acid on a per H-atom basis. (OH abstractor).

The previous study from Cavallotti and co-workers (Cavallotti et al., 2018) highlighted the importance of secondary chemistry of the resonance stabilized β radical (*CH_2(C=O)-OH) in acetic acid for the predictions of the laminar flame speeds measured by Christensen and Konnov (Christensen and Konnov, 2016). Preliminary evaluations by Cavallotti et al. (Cavallotti et al., 2018) have been considered in this study to describe the decomposition reactions of these radicals and their interactions with H atoms.

Concerning β-decomposition reactions of β-radicals, rate constants are obtained by increasing the reference activation energy for beta-scission reactions (~30 kcal/mol (Ranzi et al., 2001)) by 2 kcal/mol in the case of butanoic acid producing methyl radical and acrylic acid (C_2H_3(C=O)-OH), as shown in Table 39 and 40, and by 1 kcal/mol in the case of pentanoic acid where ethyl radical is produced instead. The decomposition reactions of the remaining fuel radicals (Table 40) to form unsaturated species and an alkyl radical, or to form unsaturated acids (butenoic and pentenoic acids) and H, are based on analogy with alkane rate rules (Ranzi et al., 2014).

Table 39. Decomposition reactions of the radicals formed from butanoic acid in cal, s, mol, cc units.

Reaction	*A*	*n*	*Ea*	No.
Reactions of butanoic acid radicals				
RBUTANOICA				
RBUTANOICA=OH+C_2H_5CHCO	1.74E+29	-4.37	63089.60	(1)
H+C3H5COOH-1=RBUTANOICA	1.50E+13	0.00	3500.00	(2)
RBUTANOICA=CH_3+C_2H_3COOH	3.00E+13	0.00	32000.00	(3)
RBUTANOICA=CO_2+*n*C_3H_7	5.62E+20	-2.36	49013.60	(4)
H+RBUTANOICA=H_2O+C_2H_5CHCO	1.62E+18	-1.44	11056.50	(5)
H+RBUTANOICA=CO_2+C_3H_8	5.25E+18	-1.69	10183.10	(6)
H+RBUTANOICA=HOCO+*n*C_3H_7	2.24E+22	-2.26	16097.74	(7)
O_2+RBUTANOICA=HO_2+C_3H_5COOH-1	1.00E+12	0.00	5000.00	(8)
O_2+RBUTANOICA=>RO_2BUTANOIC	1.00E+12	0.00	0.00	(9)
RBUTANOICB				
RBUTANOICB=CO_2+*n*C_3H_7	1.60E+10	0.00	25500.00	(7)
RBUTANOICB=HOCO+C_3H_6	3.00E+13	0.00	30000.00	(8)
H+C_3H_5COOH-1=RBUTANOICB	1.50E+13	0.00	3500.00	(9)
O_2+RBUTANOICB=HO_2+C_3H_5COOH-1	1.00E+12	0.00	5000.00	(10)
O_2+RBUTANOICB=>RO_2BUTANOIC	1.00E+12	0.00	0.00	(11)
RBUTANOICC				
RBUTANOICC=CO_2+*n*C_3H_7	1.00E+11	0.00	30600.00	(12)
RBUTANOICC=>C_2H_4+CH_2COOH	3.00E+13	0.00	28500.00	(13)
C_2H_4+CH_2COOH=>RBUTANOICC	1.00E+11	0.00	15000.00	(14)
H+C_3H_5COOH-1=RBUTANOICC	1.50E+13	0.00	3500.00	(15)
O_2+RBUTANOICC=HO_2+C_3H_5COOH-1	1.00E+12	0.00	5000.00	(16)
O_2+RBUTANOICC=>RO_2BUTANOIC	1.00E+12	0.00	0.00	(17)

Table 40. Decomposition reactions of the radicals formed from butanoic acid in cal, s, mol, cc units.

Reaction	*A*	*n*	*Ea*	No.
Reactions of butanoic acid radicals				
RO2BUTANOIC				
RO2BUTANOIC=>OH+CO_2+C_2H_5CHO	2.00E+11	0.00	23500.00	(1)
RO2BUTANOIC=>O_2+0.6RBUTANOICA+ 0.25RBUTANOICB+0.15RBUTANOICC	3.00E+13	0.00	29000.00	(2)
QBUTANOIC				
RO2BUTANOIC=>QBUTANOIC	3.00E+11	0.00	22400.00	(3)
QBUTANOIC=>RO_2BUTANOIC	5.00E+10	0.00	12000.00	(4)
QBUTANOIC=>OH+CO_2+C_3H_6O	1.60E+11	0.00	18000.00	(5)
QBUTANOIC=>OH+CH_2O+C_2H_3COOH	1.00E+12	0.00	22000.00	(6)
QBUTANOIC=>HO_2+C_3H_5COOH-1	3.00E+13	0.00	18000.00	(7)
O_2+QBUTANOIC=>ZBUTANOIC	3.00E+12	0.00	0.00	(8)
ZBUTANOIC=>O_2+QBUTANOIC	3.00E+13	0.00	29000.00	(9)
ZBUTANOIC & KBUTANOIC				
ZBUTANOIC=>OH+KBUTANOIC	1.00E+11	0.00	24500.00	(10)
KBUTANOIC=>OH+HOCO+CH_2O+CH_2CO	1.65E+15	0.00	41500.00	(11)
KBUTANOIC=>OH+HOCO+$CHOCH_2CHO$	1.65E+15	0.00	41500.00	(12)
KBUTANOIC=>OH+CO+CH_2O+CH_2COOH	1.65E+15	0.00	41500.00	(13)
KBUTANOIC=>OH+CO+HOCO+CH_3CHO	1.65E+15	0.00	41500.00	(14)

Specific subsets to describe the pyrolysis and oxidation of butenoic and pentenoic acids have also been included. According to a similar approach, the carboxylic function is treated in analogy with saturated acids, while the unsaturated carbon skeleton is treated according to alkene kinetics already implemented in the CRECK model (i.e. propene and butenes). To constrain the number of species in the kinetic model, only one butenoic acid and one pentenoic acid are accounted for to represent all the isomers.

Lumped low temperature pathways have been also included in the kinetic subsets here developed. The contribution to the low temperature branching pathways of the carboxylic function can be neglected due to the strong BDE of the O-H bond and due to the lack of H-atoms on the central carbon (R-(C=O)-OH). Neither low temperature reactivity nor NTC (negative temperature coefficient) can be seen under the experimental conditions investigated in this study. For these reasons, aiming at a first simplified description of acid low/intermediate temperature kinetics, the low temperature pathways and their rate constants are considered to be analogous to those in propane for butanoic acid and to those of *n*-butane for pentanoic acid.

Overall, the CRECK model adopted in this work contains 503 species and 17025 reactions. The thermochemical properties for species not specifically belonging to the acid subset were adopted, when available, from the ATcT database of Ruscic (Ruscic, 2014) or from Burcat's database (Burcat et al., 2005).

Analysis of the results

Figure 85 shows a comparison between the experimental data and the computed results for both fuels under all conditions.

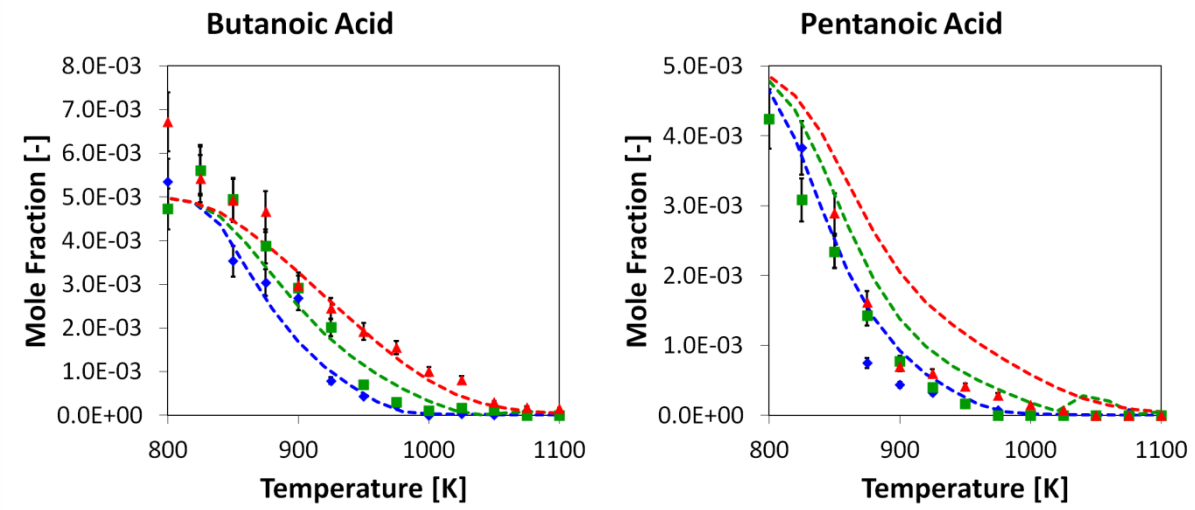

Figure 85. Fuel conversion for butanoic acid and pentanoic acid oxidation compared to the model results (Symbols: ♦ phi=0.5, ■ phi=1, ▲ phi=2) (Error bar ±10%).

The model is able to reproduce the reactivity of the fuel under all the conditions. However the model has a better description of the equivalence ratio influence for butanoic acid than for pentanoic acid. It also underestimates the onset temperature for pentanoic acid with a larger deviation for fuel-rich conditions.

Figures 88 and 89 present the results of the simulation for butanoic and pentanoic acids oxidation and the experimental profiles on the same chart. Only the species presented in the selectivity analysis are displayed here. The model has the same unstable behavior for stoichiometric conditions at the highest temperatures than the aldehyde model. This phenomenon was explained in the previous part.

For both fuels, the model is able to well reproduce the effect of the equivalence ratio. The model can also overall reproduce well the mole fraction profiles of the products. However, intermediate species are largely underestimated at the highest temperatures (T>1000 K) for the rich case although CO and CO_2, covering the most of the carbon balance, are correctly reproduced. The largest deviations are observed for acetaldehyde (CH_3CHO), where predicted yields are around 4 times lower than the experimental measurements. Acetaldehyde is mostly produced by interactions of $O/OH/O_2$ with propene and propenyl radicals (e.g. *CH=CH-CH_3), whose kinetics are outside the scope of this study. It can also be observed that the formation of propanal is shifted toward lower-temperature by 50 K. The effect of the equivalence ratio is also not reproduced: the results are in the opposite way. Propanal is largely produced by a Waddington-type mechanism (Ray and Waddington, 1973; Welz et al., 2013) summarized in Figure 86 (Reaction 1 in Table 40). The same rate constant as that adopted for the Waddington mechanism in alcohols (Pelucchi et al., 2017a) is here assumed.

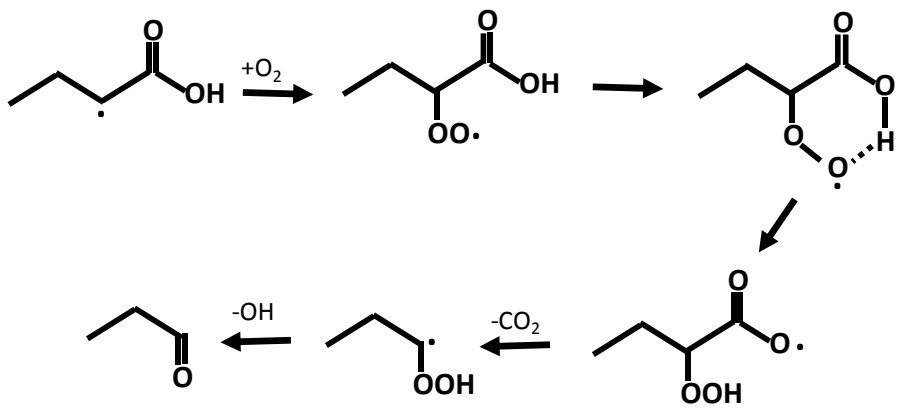

Figure 86. Waddington-type mechanism explaining the formation of C_{n-1} aldehydes from the oxidation of C_n carboxylic acids at low/intermediate temperatures.

In Figure 89, we can see that the reactivity seems to be correctly predicted when referring to O_2, CO and CO_2 profiles for pentanoic acid. More deviation are observed in the case of methane and ethane yields with the model predicting an earlier formation (i.e. ~40 K earlier). Methyl radical controls both methane and ethane formation via H-abstractions from the fuel (CH_3+Fuel=CH_4+Fuel-radical), and methyl radicals recombination (CH_3+CH_3+M=C_2H_6+M). Provided that the same rate constants for H-abstraction by CH_3 are implemented for butanoic and pentanoic acids, this disagreement was unexpected. The Waddington-type mechanism allows a correct quantitative prediction of *n*-butanal yields; despite the predicted peaks occur around 20-30 K before those experimentally observed.

In Figure 87, we can see that the model is also able to predict the early formation of carbon dioxide compared to carbon monoxide formation. In the worst case, at 825 K for pentanoic acid, the model is deviating with a factor 2 from the experimental value. The average deviation is about 25%.

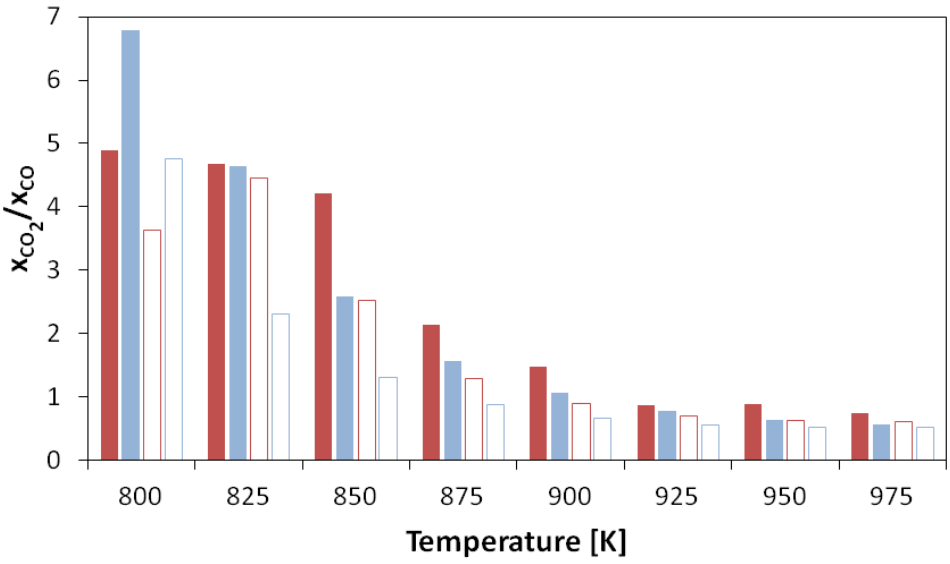

Figure 87. Mole fraction ratio between carbon dioxide and carbon monoxide for phi =1 for butanoic (full bars) and pentanoic experiments (empty bars)(in red experimental data and in blue computed results).

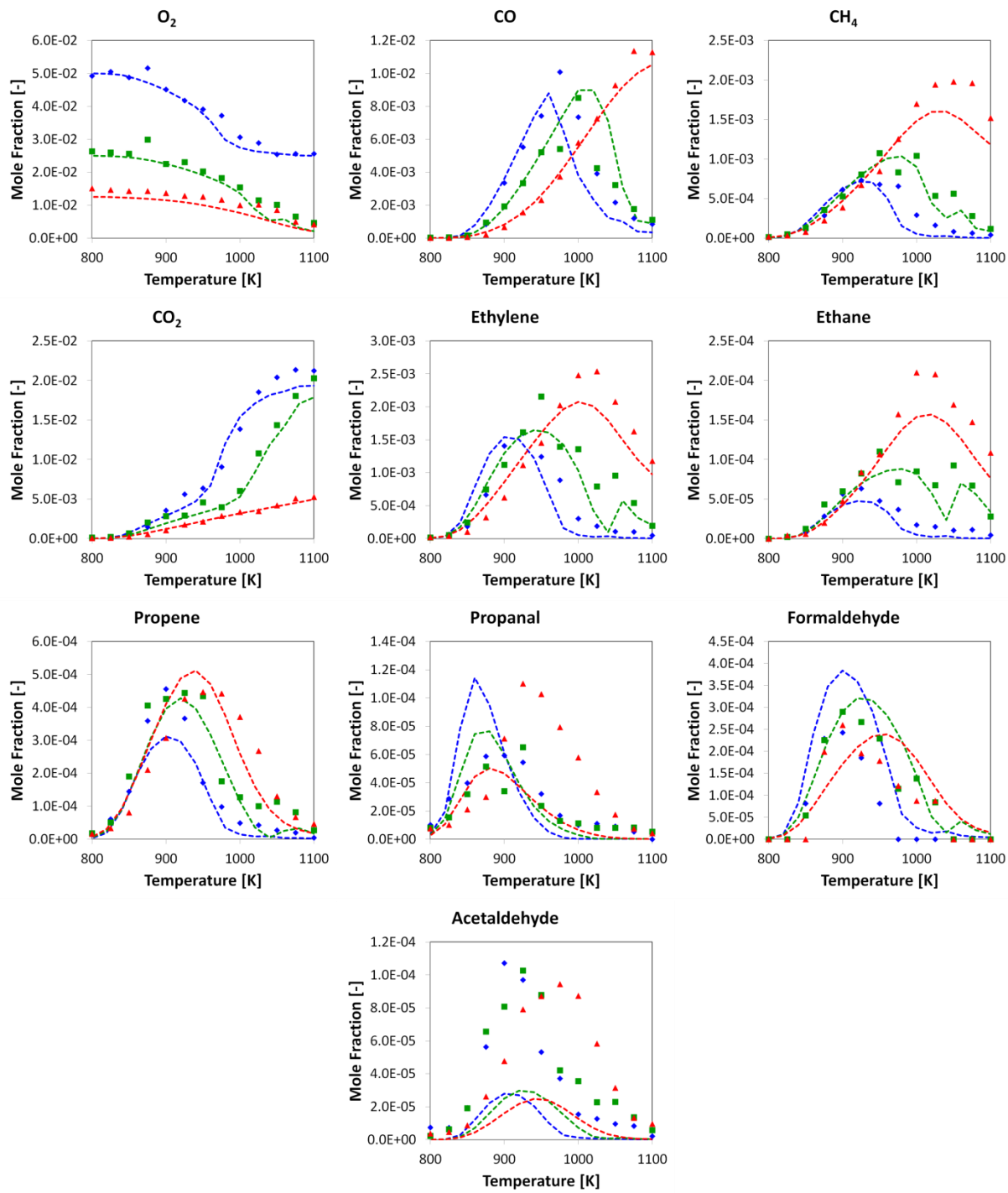

Figure 88. Mole fraction profiles of oxygen and main reaction products of butanoic acid oxidation compared to the model computed results for the three equivalence ratios (Symbols: ♦ phi=0.5, ■ phi=1, ▲ phi=2).

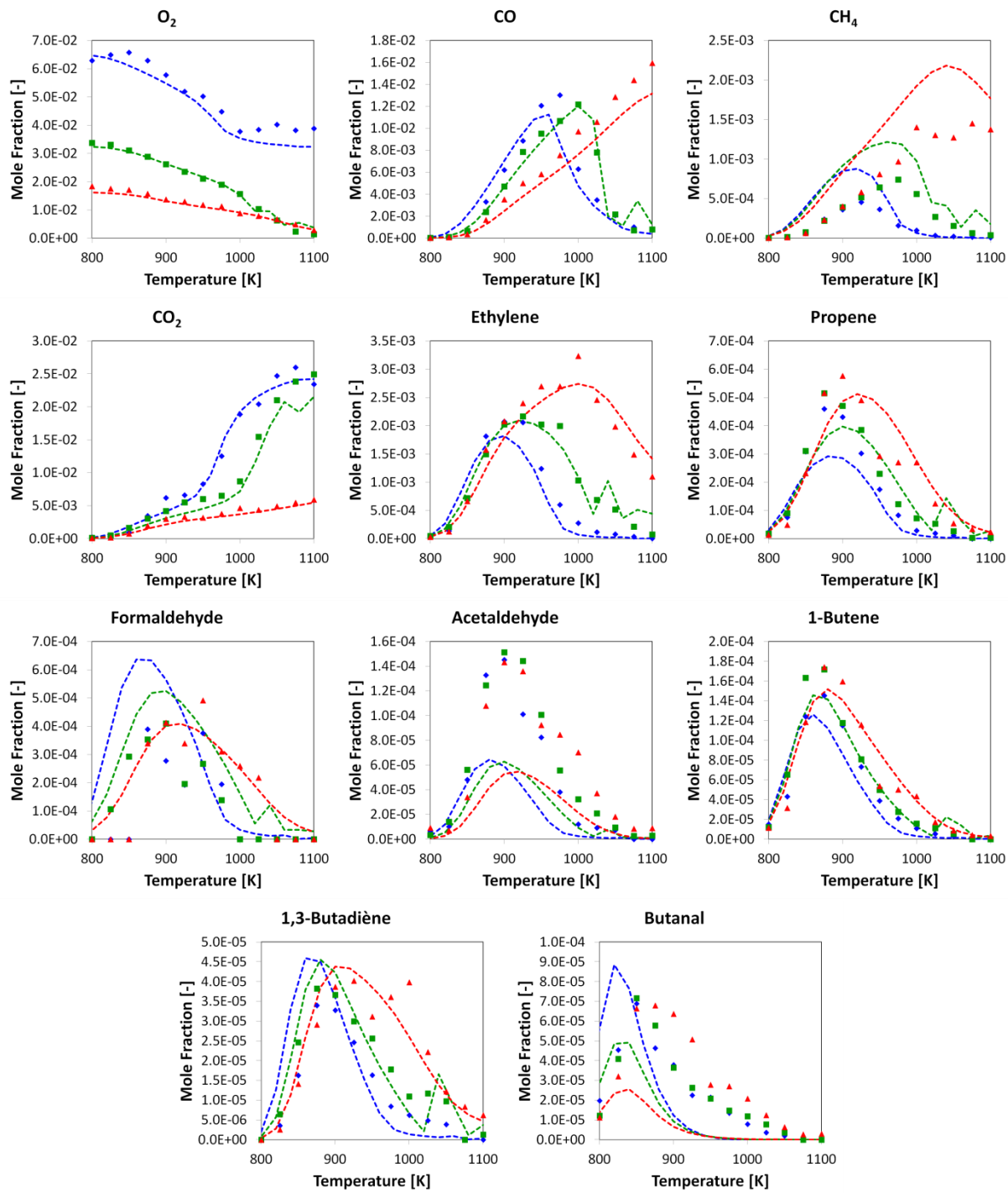

Figure 89. Mole fraction profiles of oxygen and main reaction products of pentanoic acid oxidation compared to the model computed results for the three equivalence ratios (Symbols: ♦ phi=0.5, ■ phi=1, ▲ phi=2).

Figure 90 shows a flux analysis performed at 900 K for butanoic acid oxidation. At T=900 K, ϕ=1.0, corresponding to 45 % fuel conversion, butanoic acid is almost entirely consumed by H-abstraction reactions. The main abstracting radical is OH, but also methyl radical, which contributes to a lower extent to the fuel consumption. 33% of the fuel produces the primary δ radical that is largely decomposed through β scission to form ethylene and the resonance stabilized *CH_2(C=O)-OH radical. A limited flux (2 %) corresponds to the radical addition to O_2, forming a lumped peroxy radical (RO_2). 25 % of the fuel forms the secondary γ radical, that decomposes (20.3%) to propene and HOCO, or adds to oxygen to a lower extent forming RO_2. A larger amount of peroxy radicals is produced by the radical carrying the unpaired electron in β, as its β decomposition forming propenoic acids (C_2H_3COOH) is energetically slightly less favored due to methyl elimination. Of the overall flux leading to RO_2, only a minor extent isomerizes to QOOH that is mostly decomposed to butenoic acid, not propagating the low-temperature branching pathway by means of a second addition to O_2. The Waddington-type mechanism proposed above only accounts for 0.8% of the overall flux, corresponding to 20% of the fate of RO_2 radicals.

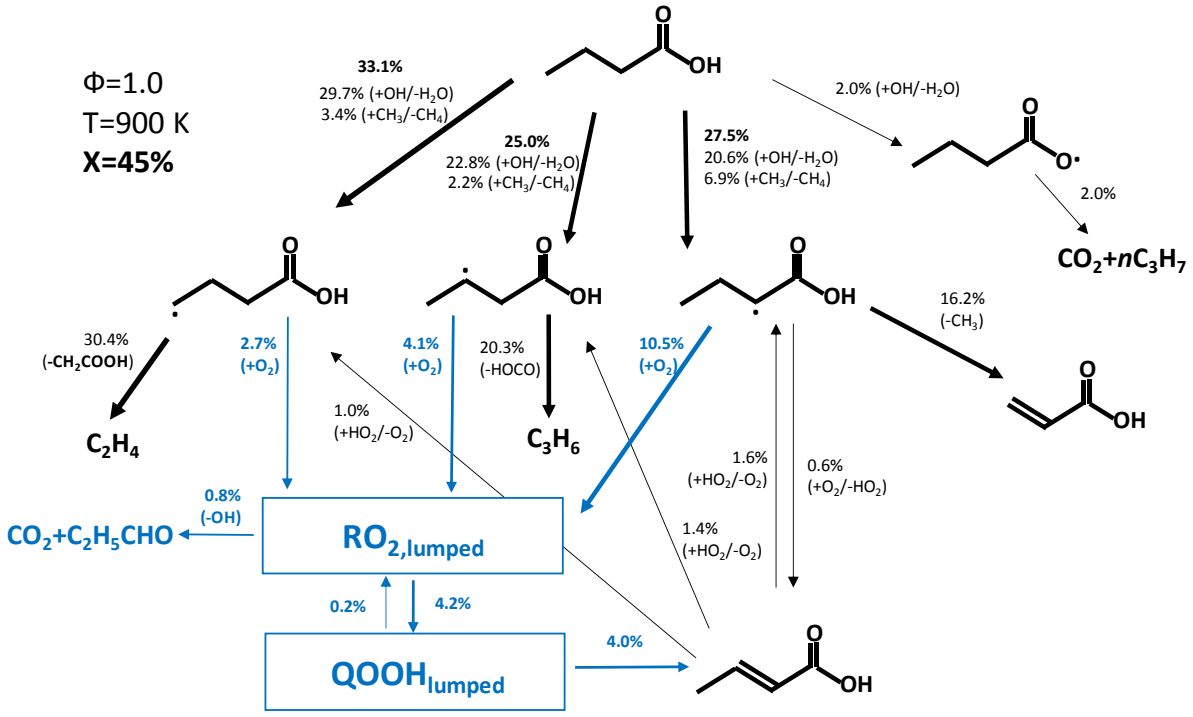

Figure 90. Rate of production analysis for butanoic acid oxidation at 900 K under stoichiometric conditions.

The model shows that the alkyl chain is responsible of the acid reactivity. The work of Cavallotti et al. (2018) showed that molecular reactions are important for acetic acid:

$$CH_3COOH \rightarrow CH_4 + CO_2$$
$$CH_3COOH \rightarrow CH_2CO + H_2O$$

Concerning carboxylic acid with a longer alkyl chain, the activation energies of the alkyl chain are less important as the effect of the oxygenated function vanished along the alkyl chain. Thus the radical decomposition pathways are dominant for butanoic and pentanoic acid (more than 80%). The reactivity is also focused on the alkyl chain, as only, 2% of the reactivity is located on the acid function. The radicals formed then can decompose themselves or add on oxygen which will produced carbon dioxide and the C_{n-1} aldehyde.

The rate flow analysis for pentanoic acid is very similar to that presented on Figure 90 for butanoic acid and leads to the same conclusion.

Figure 91 shows results from the sensitivity analysis of fuel consumption to rate constants for butanoic and pentanoic acids, at two different temperatures T=850 K and T=1050K. For both acids, at the lowest temperature, the reactivity is controlled by H_2O_2 decomposition to form two OH radicals. H_2O_2 is produced by HO_2 radicals termination and by H-abstraction on the fuel by HO_2, also highlighted as sensitive reactions. The main source of HO_2 is for both fuels the decomposition of QOOH radicals to form unsaturated acids. H-abstractions by methyl on the β-site are also found to be important for butanoic acid. Methyl radical is mostly produced by the decomposition of $*CH_2$-(C=O)-OH forming CO_2 (Cavallotti et al., 2018) and by the decomposition of β-radical forming propenoic acid. Interestingly, the Waddington-type mechanism producing propanal (C_2H_5CHO) in butanoic acid is also found to promote reactivity in pentanoic acid. The formation of butanoic radicals in pentanoic acid oxidation is related to the interactions of HO_2 with butenoic acid (HO_2+C_3H_5COOH=O_2+$R_{\beta,butanoic}$). Concerning pentanoic acid oxidation at 850 K, it is interesting to note that the decomposition of $R_{\delta,pentanoic}$ producing propene and $*CH_2$-(C=O)-OH radical decreases the reactivity since it forms one stable radical and propylene, that is mostly oxidized forming resonance stabilized allyl radical. At higher temperatures (T=1050 K) butanoic acidoxidation is dominated by reactions belonging to the core kinetic model (C_0-C_2) while H-abstractions by OH dominate pentanoic acid reactivity.

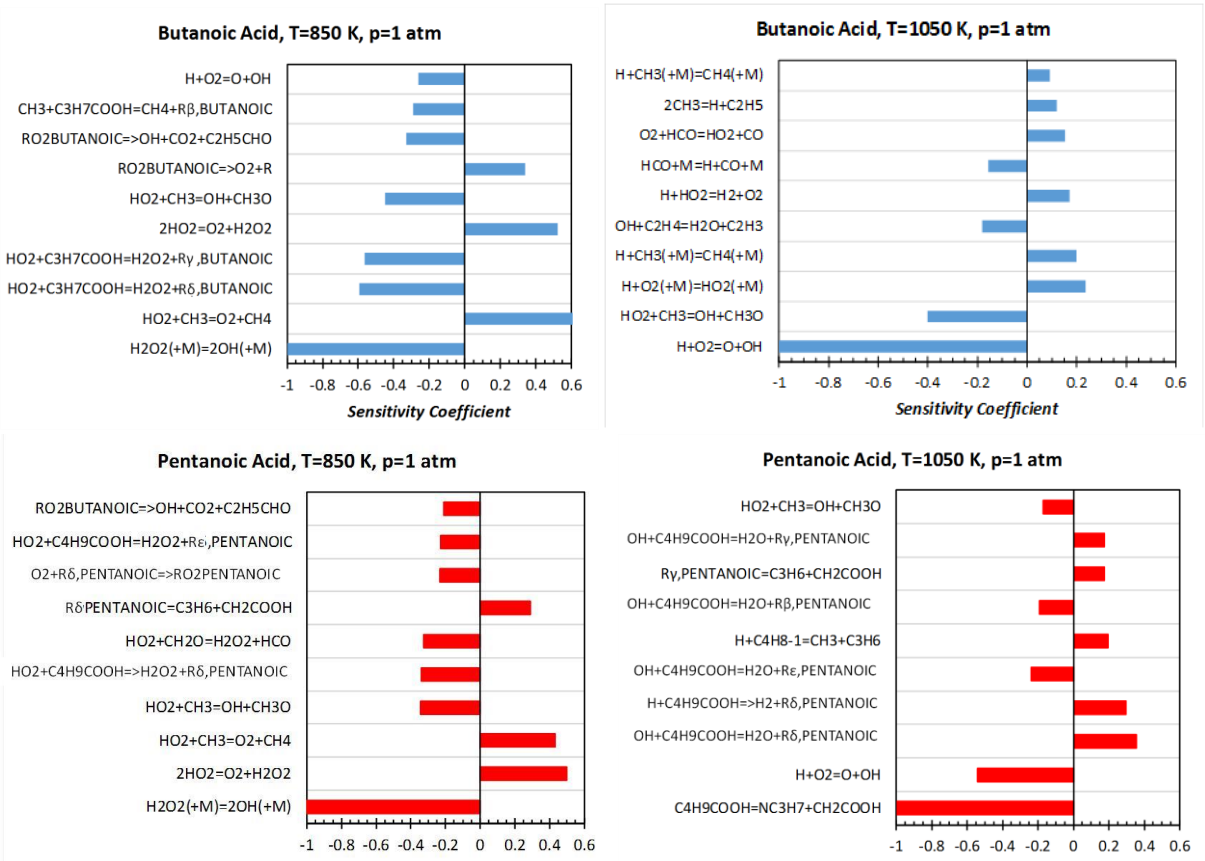

Figure 91. Normalized sensitivity coefficients of fuel consumption to rate constants at T=850 K (left) and 1050 K (right). Top panels (blue bars): butanoic acid, bottom panels (red bars): pentanoic acid.

IV.3.3. Conclusion

This work is the first kinetic study of the oxidation of two large carboxylic acids, butanoic and pentanoic acids to our knowledge. Carboxylic acids were really complex to experimentally handle in the set-up due to their corrosive properties and their high boiling points. Despite all the experimental difficulties, we were able to identify the main products of the oxidation of those compounds and these results were used to develop a kinetic mechanism. This mechanism showed that the carboxylic acid mainly reacts via H atom abstractions on the alkyl chain. The carboxylic acid function is not reactive (around 2% of the global reactivity). The mechanism was also able to predict the early production of carbon dioxide and the formation of the C_{n-1} aldehydes.

IV.4. Conclusion: reactivity comparison of C_4-C_5 linear fuels according to the initial oxidation of the terminal carbon atom

This section is dedicated to the comparison of the molecule reactivity according to the type of oxygenated function they have.

The oxidation of the molecules can be defined here as the number of C-O bonds in the molecules, as presented in Figure 92 (a C=O bond accounting for two C-O one).

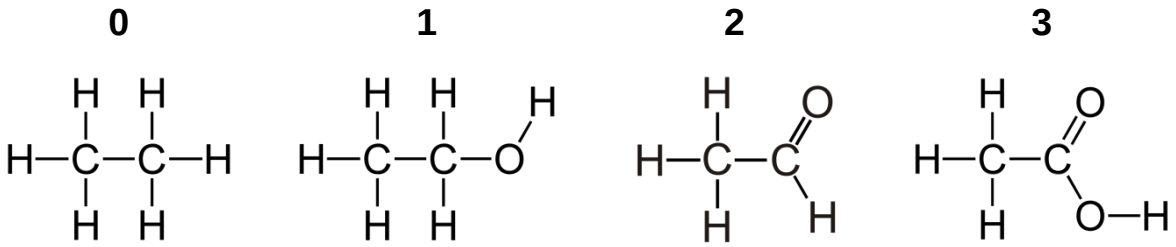

Figure 92. Evolution of the number of C-O bond in fuels containing 2 carbons.

In the case of alkanes, the carbon atoms can be defined by their position in the alkyl chain and so the number of C-H bonds they have. Depending on this value, we talk about primary, secondary and tertiary carbon atoms. The rate rules for the alkanes can be defined depending on these parameters. The idea is to verify if it could be possible to define equivalent rate rules depending of the number of C-O bonds on the carbon atom.

The first step is to check if there is any trend in the bond dissociation energies (BDE) of the molecules. Indeed, as discussed by Pelucchi et al (2016), the BDEs value can give a first guess about the reactivity of the molecules. The weakest bond could be the place of the first initiation reactions. Figure 93 presents the BDEs for *n*-butane, the reference here, and the difference in BDEs compared to it for *n*-butanol, *n*-butanal and butanoic acid (only the differences higher than 1 kcal/mol are shown for clarity).

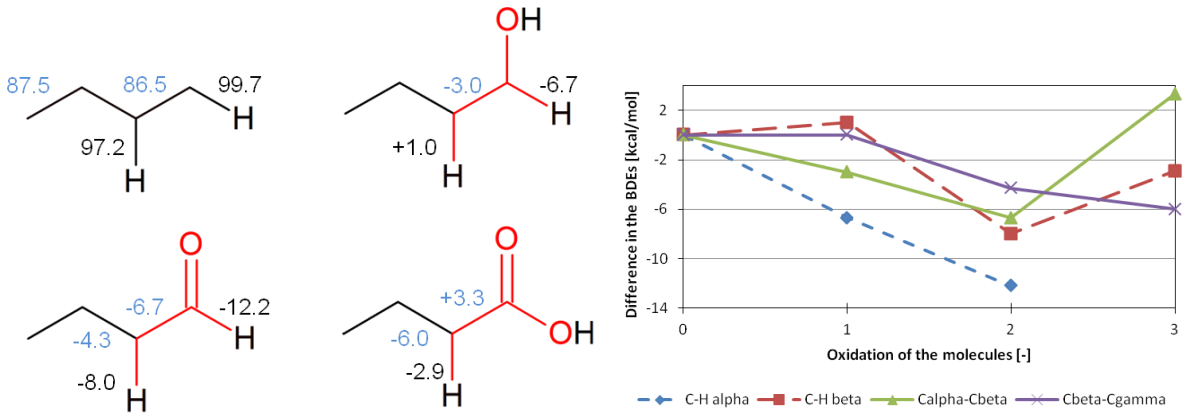

Figure 93. Comparison of the BDEs (in black the C-H bond and in blue the C-C bond) of *n*-butanol, *n*-butanal and butanoic acid compared to that of *n*-butane. In black is represented the alkane-like moiety and in red the specific one. The graph displays the evolution of the difference in BDEs compared to *n*-butane along the oxidation of the molecule.

The analysis of the BDEs reveals that there are no obvious trends concerning the evolution of the BDEs along the number of C-O bonds. Some similar behavior can be observed between the alcohol and the aldehyde, but the carboxylic acid is off any trends.

However from Figure 93, we can try to figure out which molecules are the most reactive. Due to the strong inductive effect of the aldehyde function on the alkyl chain, it seems that this class of molecules is the most reactive. Figure 94 presents two charts comparing the experimental and predicted reactivities for the C_4 and C_5 fuels presented before.

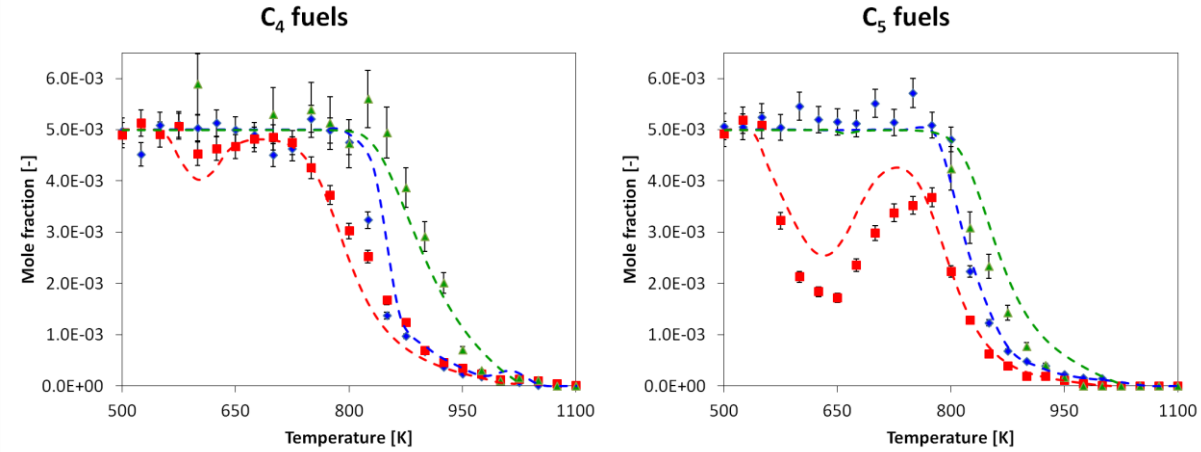

Figure 94. Comparison of the experimental (dots) and the predicted (dashed lines) reactivities of the C_4-C_5 fuels previously presented (red: aldehydes, blue: alcohols and green carboxylic acids)(Error bars: same values as reported before).

The experiments and the models are in a good agreement concerning the relative reactivity of the different fuels. It appears that aldehydes are the most reactive, with a pronounced NTC area, and that the acids are the least reactive. This observation is consistent with the conclusion that we draw from the BDE comparison. Aldehydes are also the only compounds to present a clear NTC area compared to the other molecules. However, the behavior at high temperature is similar between the three types of fuels.

Figure 95 presents the relative selectivities of the hydrogen atom position for the H-abstraction by OH radical on *n*-butane, *n*-butanol, *n*-butanal and butanoic acid over the

temperature range 500-1100 K, which is typically that used for our experiments. The kinetic data were extracted from the CRECK mechanism and are accounting for the number of carbon atoms at the associated position on the alkyl chain.

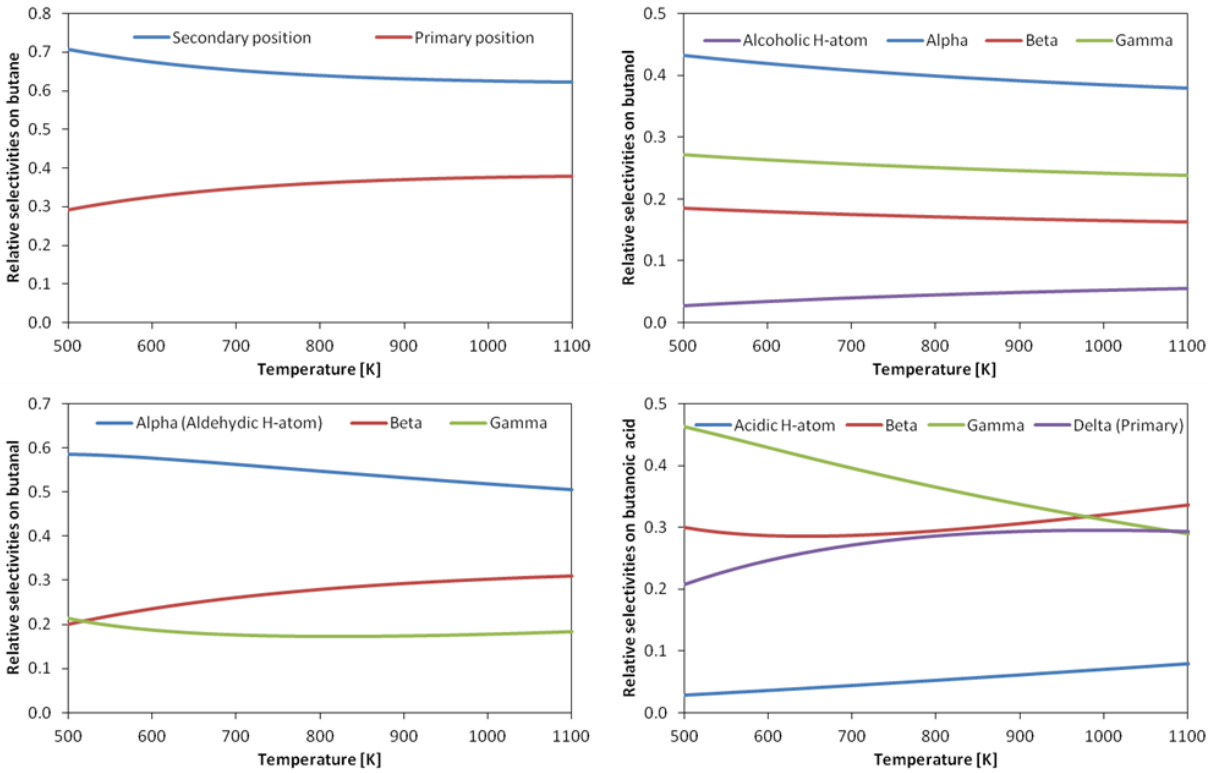

Figure 95. Relative selectivities of the different position in *n*-butane, *n*-butanol, *n*-butanal and butanoic acid toward H-abstractions by OH radicals.

The results show that the oxygenated function has an obvious effect on the favored position for the H-abstractions by OH. We can easily estimate that this conclusion is also true for any kind of radicals (as for alkanes, the distribution may be even more sensitive for H-atom abstractions involving radicals less reactive than OH). However, the influence of each function is different. In the case of the alcohol, the alpha position is favored, which is similar in the case of aldehydes. But the impact on the beta-position compared to the gamma-position is reversed. For acids, the gamma position is favored at low-temperature but acids do not react at this temperature. Around 700 K, no favored position can be determined. But the acid function is totally unreactive and forces the reactivity on the alkyl chain, contrary to the other cases where it focuses the reactivity in alpha position. This may explain why the acids are less reactive than the alcohols or aldehydes. Also this observation forced to consider each alkyl radical in the kinetic model, instead of considering a lumped one as in the alcohol or the aldehyde mechanism.

The oxygenated function has clearly an impact on the reactivity of the alkyl chain. It modifies the BDEs, favors positions for the H-abstractions and thus modifies the reactivity of the alkyl chain. However, there is no correlation between the number of C-O bonds in the molecule and its reactivity. Each type of chemical functions has a specific impact on the molecule reactivity and if any rate rules could be defined, it is sure that those rules would be specific to the kind of oxygenated function.

V. OXIDATION OF CYCLIC OXYGENATED COMPOUNDS

This chapter is dedicated to the presentation of two experimental studies performed on two cyclic oxygenated compounds. These kinds of compounds are really important in the composition of a bio-oil. Thus it is essential to study their reactivity directly and to fully assess with care their decomposition mechanism under oxidative conditions. First the study on furan oxidation will be presented. Those results will be compared with a model from the literature and the CRECK model already presented in the previous part. Then the study about benzaldehyde oxidation will be presented. The experimental data and the model developed at this occasion will be confronted in order to validate the proposed mechanism.

The raw experimental data are given in Appendix II, with a nomenclature of the analyzed species in Appendix I

The work on benzaldehyde oxidation has led to the submission of a paper in Combustion & Flame (Accepted September 2019)

V.1. Furan oxidation

During the second years of this PhD, Fanny Castéran was hired as an intern for two months to work with me on the oxidation of this fuel. This part is dedicated to the presentation of the experimental results that were obtained and to their modeling using two models.

V.1.1. Experimental results

This first section presents the experimental results obtained. The fuel conversion is first presented and, in a second part, the carbon balance and selectivity analysis are displayed with the mole fraction profiles of the main products. The experiments have been carried out in a jet-stirred reactor at 800 Torr and between 700 K and 1100 K. Three equivalence ratios have been studied (0.5-1-2) for a fuel inlet mole fraction of 0.5 %.

Fuel conversion

Figure 96 presents the conversion of furan under the three equivalence ratios tested.

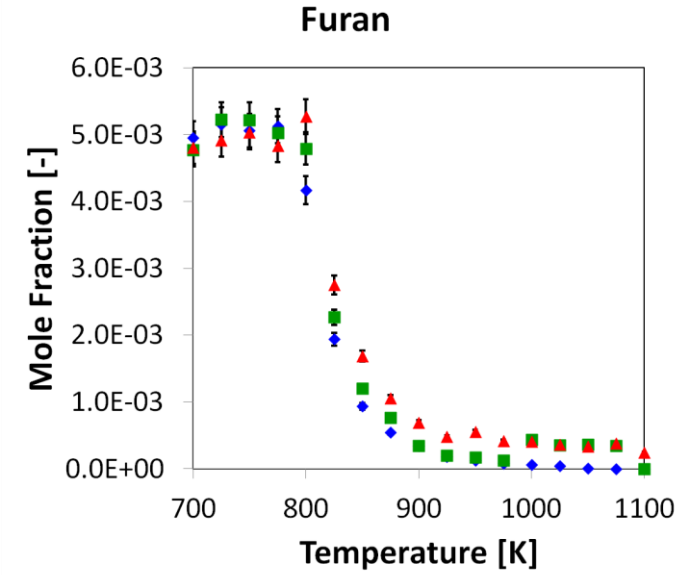

Figure 96. Furan conversion during oxidation for different equivalence ratios (Symbols: ♦ phi=0.5, ■ phi=1, ▲ phi=2) (Error bars ±5 %).

Furan starts to react around 800 K and is almost fully consumed at 900 K. So its full conversion is achieved over a very short range of temperatures. Furan oxidation does not exhibit huge differences depending on the equivalence ratio, but it can be still observed that the fuel-lean conditions are the most reactive. In the contrary it seems that the fuel-rich conditions are the least reactive, which is also strengthen by the fact that the conversion never achieves 100 % under these conditions. It can be observed that at higher temperatures (above 950 K), under stoichiometric conditions, the measurements indicated a slowdown in the conversion of furan, as shown by Figure 97. This behavior could be typically due to some oscillations in the reactor. This phenomenon has already been described in Chapter 4 2.2. Under the other conditions, those oscillations were not clearly detected. The mole fraction profiles of the products will help us to determine if there are oscillations or not.

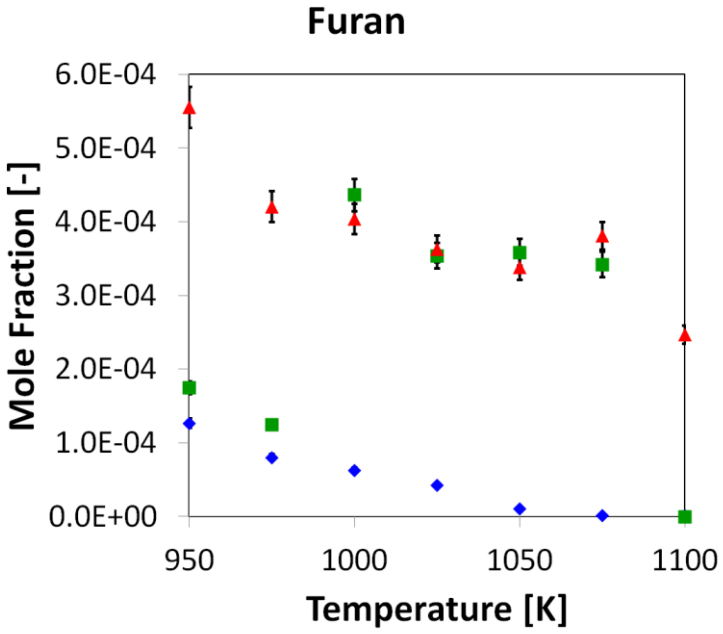

Figure 97. Furan conversion during oxidation experiments. Zoom of Figure 96 between 950 K and 1100 K (Symbols: ♦ phi=0.5, ■ phi=1, ▲ phi=2)(error bars ± 5 %).

Carbon balance and selectivity analysis

During furan oxidation 18 products were detected and identified. They can be classed among 6 different classes:

- C_1: CO, CO_2 and CH_4
- C_2: acetylene, ethylene and ethane
- C_3: allene, propyne, propene and propane
- C_4: 2-butyne
- Aldehydes: formaldehyde, acetaldehyde, acrolein and propanal
- Others: oxirane, acetone and benzene

With the GC-column used during this study, the detection of acetylene and ethylene separately was not possible. Thus, their mole fraction quantification was coupled. The overall carbon balance remained around 100 % with a deviation of ±10 %, but a more important deviation of 33 % was observed at 925 K under fuel-rich conditions. The quantification of carbon monoxide is indeed much lower than what we could expect.

Figure 98 shows selectivity analyses for furan oxidation at 825 K for the three equivalence ratios. Selectivities have been normalized according to the number of carbon atoms in the molecules and a threshold of 1 % has been used.

Main furan oxidation products at 825 K are carbon monoxide and acrolein. Carbon monoxide accounts for more than 50 % of the carbon content. Depending on the equivalence ratio, it can be seen that the importance of acrolein varies. It is also the case for acetylene and ethylene, which are more important under fuel-rich conditions. Important quantities of formaldehyde and acetaldehyde are also reported.

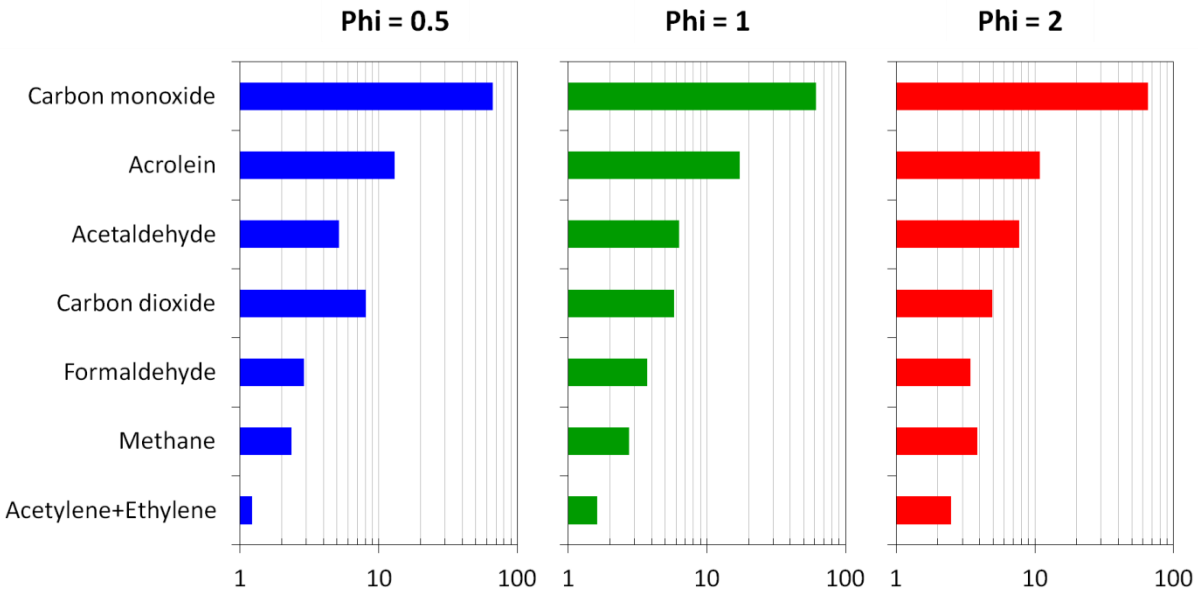

Figure 98. Reaction product selectivity analyses for furan oxidation at 825 K for the three equivalence ratios: a) fuel-lean conditions, b) stoichiometric conditions and c) fuel-rich conditions.

Figure 99 presents the mole fraction profiles of oxygen and of the products presented in Figure 98.

It can be observed that formaldehyde, acetaldehyde and acrolein have similar mole fraction profiles. At 800 K they start to be produced in a relative large amount, afterward those compounds react and their mole fractions decrease. In the other side, carbon monoxide, methane and C_2 hydrocarbons are produced in a lower amount around 850 K and their maximum of formation occurs at higher temperatures. It can also be seen that the equivalence ratio has a huge impact for those compounds and especially under fuel-rich conditions. They are indeed produced in a higher amount at those temperatures compared to the other equivalence ratios.

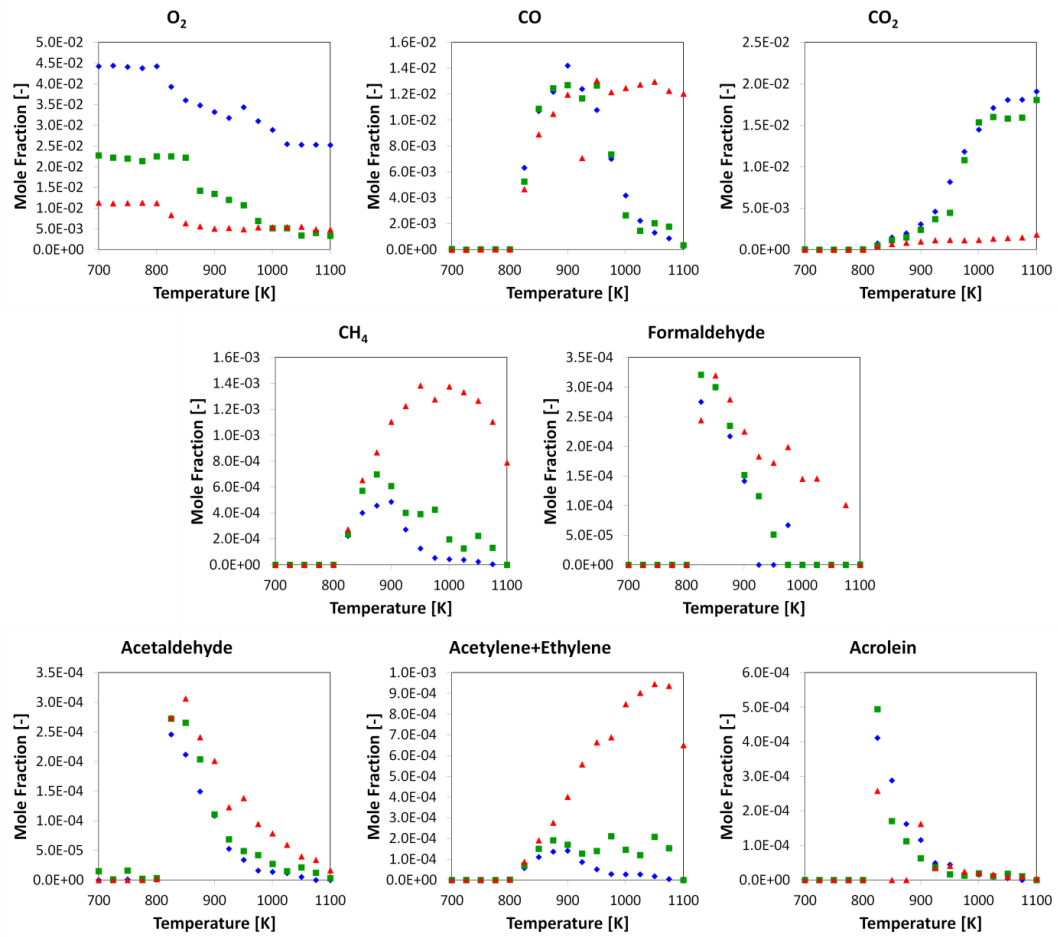

Figure 99. Mole fraction profiles of oxygen and main reaction products of furan oxidation for the three equivalence ratios (♦ phi=0.5, ■ phi=1, ▲ phi=2).

V.1.2. Kinetic model

The experimental results previously described are compared to the predictions of two models from the literature. The first one is the kinetic model developed by Tran et al. to predict the reactivity of furan, 2-methyl-furan and 2,5-dimethyl-furan from low to high temperatures (Tran et al., 2017). The second model is the CRECK mechanism previously presented in the part dedicated to the alcohol study (part IV.1). This model has only be validated for high temperatures (T>1000 K) in the case of furan oxidation, but this is the model that we used for all the other validations during this PhD thesis. Thus a comparison is interesting.

Mechanism

The model developed by Tran et al. for the oxidation of furan, methylfuran and dimethylfuran accounting for the low-temperature chemistry is an extension of a previous model developed for flame conditions (Tran et al., 2015a). According to the experimental results they obtained in a tubular flow reactor at atmospheric pressure, they determined the key-species and the relevant decomposition pathways at low-temperatures to implement them in the mechanism. The kinetic constant for the reactions were calculated thanks to theoretical computation methods. The final mechanism contains 3145 elementary reactions for 524 species. This model includes a reaction subset for HO_2-combination and O_2-addition to 2-furylmethyl and 5-methyl-2-furanylmethyl, two important stabilized radicals formed

during methylfuran and dimethylfuran oxidation. This was the first model to present this reaction subset for the oxidation of those compounds. New high-level theoretical calculations were also performed for the H-abstractions from methylfuran and dimethylfuran by O_2. Indeed those reactions were considered as really sensitive for the fuel oxidation at low- and medium temperatures. Those reaction classes were also updated for furan oxidation. However the author also recognized that some other studies should be carried out to fully assess the three compounds reactivity. The model would benefit of experimental studies about 5-methylfurural or 2-ethylfuran for example. They also recommended performing some high-level theoretical calculations concerning the addition of OH radical to the ring and its pressure dependence for the three fuels. Different reactions classes were also investigated to improve the performance of the model in predicting furan conversion (i.e. Diels-Alder reactions). But none were successful in improving the model results.

The experimental data will also be confronted to the CRECK model. The version developed during the benzaldehyde oxidation study will be used, as it already contained the furan sub-mechanism. This sub-mechanism has only been validated against data at high temperature in the case of furan. Thus some deviations with our data can occur. The description of the model has been performed previously (part IV.1.2)

Analysis of the results

Figure 100 presents the results obtained with the two models presented previously against the experimental data.

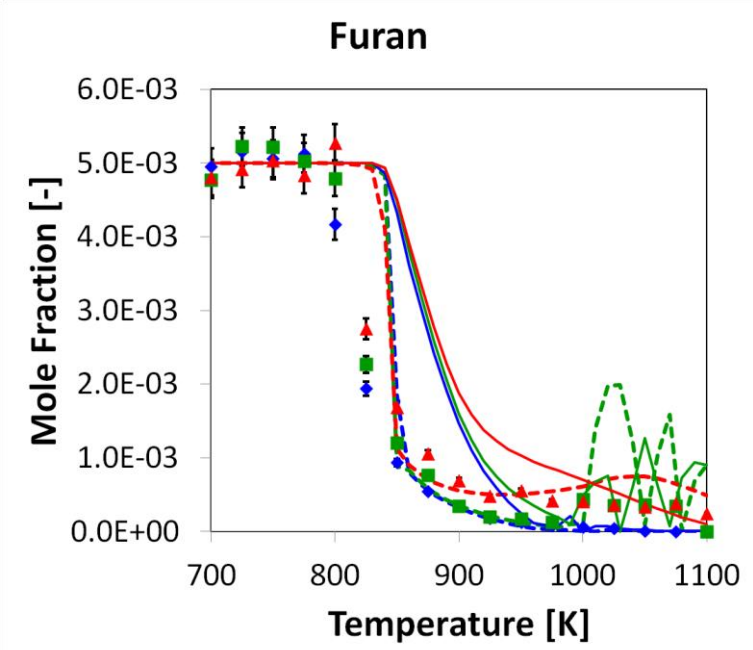

Figure 100. Fuel conversion for furan oxidation compared to the model of Tran et al. (dashed lines) and to the CRECK model (continuous lines) for the three studied equivalence ratios (Symbols: ♦ phi=0.5, ■ phi=1, ▲ phi=2) (Error bars ±5 %).

It could be noticed that the two models are not able to detect the onset of reactivity. They give similar results (around 850 K) but with a shift of +50 K compared to the experiments measurements. The same deviation was observed with the experimental results obtained by Tran et al. (2015a).

The model of Tran et al reproduces very well the fuel conversion over the temperature range 850-1100 K under fuel-lean and stoichiometric conditions. The model is

able to correctly predict the fuel consumption under fuel-rich conditions between 850 K and 950 K, but for higher temperatures deviations appear. The model is also able to detect the experimentally observed oscillatory behavior under stoichiometric conditions between 1000 K and 1100 K. The equivalence ratio dependence is also well caught by the models.
The CRECK model is less accurate at the lowest temperature. However the results are better for the highest temperatures. This was expected as the model was mainly developed to model high temperatures data. It is even performing well for temperatures higher than 1050 K under fuel-rich conditions. It also succeeds to detect the oscillatory behavior under stoichiometric conditions between 1000 K and 1100 K (Figure 100).

Figure 101 presents the performance of the model for oxygen and the main products presented in Figure 98.

The overall performance of the Tran et al. model is relatively correct. Similar to the fuel conversion predictions, the results for some products are off under fuel-rich conditions at the highest temperatures (i.e. methane or acetylene+ethylene). The model also over predicts by a factor of 2 the formation of formaldehyde and acetylene+ethylene.

Concerning products mole fraction prediction, the CRECK kinetic mechanism performances are worse than those of the model of Tran et al. mainly due to its inability to correctly predict the fuel conversion. However it well predicts the CO_2 formation and catches the shape of the mole fraction profiles of methane and of the sum acetylene+ethylene under fuel-rich conditions. The CRECK model may have some missing decomposition pathways for furan oxidation as it is unable to predict the formation of acrolein. To better reproduce furan oxidation, the reactions presented in the previous section and added in the mechanism of Tran et al. should be added in the CRECK mechanism

V.1.1. Conclusion

New experimental data have been produced for furan oxidation at atmospheric pressure in a jet-stirred reactor. During this study, 18 products were detected and quantified. Those results showed that acrolein and acetaldehyde are two of the main products formed during furan oxidation under the three studied equivalence ratios. Those experimental data were then used to compare the performance of two models. The first model tested was the one of Tran et al., which contains a submechanism dedicated for the low-temperature oxidation of furan (Tran et al., 2015a). The second model is the CRECK model, which is used systematically in this work. This model was not developed to reproduce the low-temperature reactivity of furan but mainly the high-temperature one. The comparison of the two models showed that both models have some difficulties to reproduce furan conversion at low-temperatures. But both models are able to predict the transient behavior at the highest temperatures. The discrepancies are worse for the CRECK model, but it is able to catch some products formation profiles while the model of Tran et al. is not. It could be useful to add the reactions implemented in the model of Tran et al. for the low-temperature reactivity of furan into the CRECK mechanism. With this addition, the CRECK model should be able to better reproduce furan low-temperature reactivity.

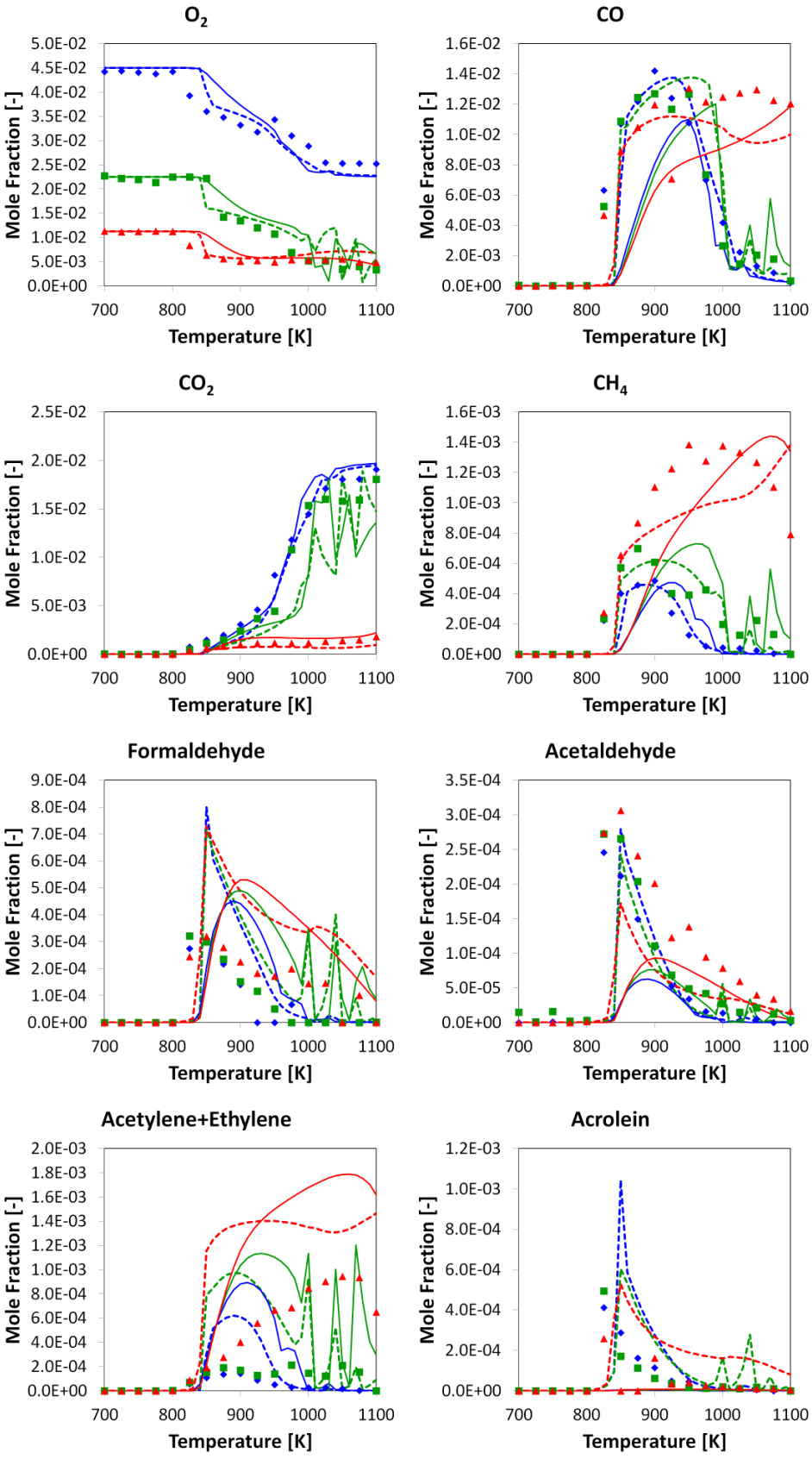

Figure 101. Mole fraction profiles of oxygen and main reaction products of furan oxidation compared to the model computed results for the three equivalence ratios (♦ phi=0.5, ■ phi=1, ▲ phi=2) (model of Tran et al. (2015a): dashed lines and CRECK model: continuous lines).

V.2. Benzaldehyde oxidation

Benzaldehyde is an aromatic aldehyde commonly considered in bio-oils surrogate formulation, and an important intermediate in the oxidation of other aromatic reference fuels such as toluene. However, its oxidation has never been previously investigated experimentally, and no product formation profiles were reported in the few studies performed under pyrolysis conditions available in the literature. In this section, the experimental results obtained for its oxidation in a jet-stirred reactor at atmospheric pressure will be presented. Those data will then be used for the validation of a model developed to predict benzaldehyde oxidation.

V.2.1. Experimental results

This first section presents the experimental results obtained. The fuel conversion is first shown and then in a second part the carbon balance and selectivity analysis are displayed with the mole fraction profiles of the main products. The experiments have been carried out in a jet-stirred reactor at 800 Torr and between 700 K and 1100 K. Three equivalence ratios have been studied (0.5-1-2) for a fuel inlet mole fraction of 0.005.

Fuel conversion

Figure 102 presents the experimental and simulated mole fraction profiles of benzaldehyde. Reported experimental error is ±5%. Benzaldehyde starts to react at 750 K and is completely consumed at 1025 K, except under fuel rich conditions. It can be observed that the equivalence ratio has only a minor impact on the conversion of the fuel.

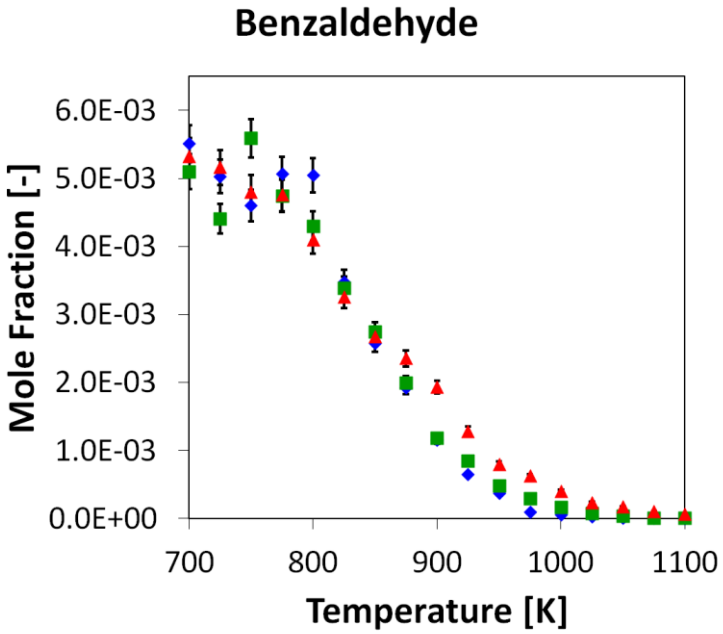

Figure 102. Experimental mole fraction profiles of benzaldehyde. (Symbols: ♦ phi=0.5, ■ phi=1, ▲ phi=2) (Error bars ±5 %).

Carbon balance and selectivity analysis

48 products have been identified during this study; they can be divided in three main categories (species in *italic* are only present under the form of traces):

- Acyclic compounds: carbon monoxide, carbon dioxide, methane, acetylene, ethylene, ethane, propene, propyne, allene, acetaldehyde, acrolein, *acetone*, butenyne, 1,3-butadiene.
- Cyclic oxygenated compounds: *cyclopentenone*, anisole, benzoquinone, phenol, benzofuran, *benzodioxol*, *hydroxybenzaldehyde*, cresol, *acetophenone*, *benzodioxol-2-one*, *methylbenzofuran*, *ethylphenol*, *cinnamaldehyde*, *diphenylether*, dibenzofuran, *indanone*.
- Cyclic hydrocarbons: 1,3-cyclopentadiene, benzene, toluene, *ethylbenzene*, *xylene*, *phenylacetylene*, styrene, *cumene*, *methylstyrene*, *indene*, *methylindene*, *dihydronaphthalene*, naphthalene, biphenyl, *acenaphthylene*.

For each experiment, the carbon mass balance was calculated and was estimated to be around 90 % of the global inlet of carbon atoms. Due to the characteristics of our analytical set-up, the quantification of hydrogen and water was not possible. It can also be noticed that neither formaldehyde nor catechol were detected during the experiments. Co-elution problem for catechol and detection limits for formaldehyde could explain their absence amongst the detected products. Those products could have been expected due to the presence of methane and phenol in the gas phase with oxygen.

Figure 103 presents the product selectivity at 850 K for the three studied equivalence ratios. All the selectivities have been calculated by taking in account the number of carbon atoms in the molecules. A threshold of 1 % has also been used, so only the main products are displayed. *p*-Cresol and *o*-cresol mole fractions were added and their participation is summarized under the name of cresol.

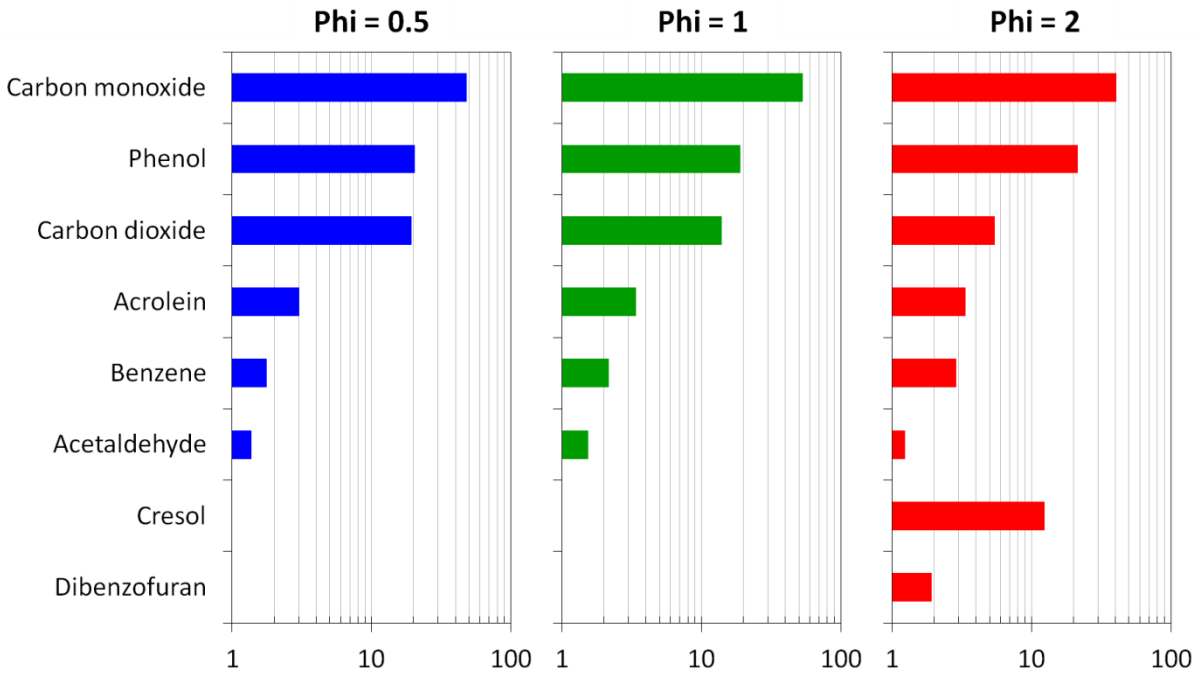

Figure 103. Reaction product selectivity analyses at 850 K for the three equivalence ratios.

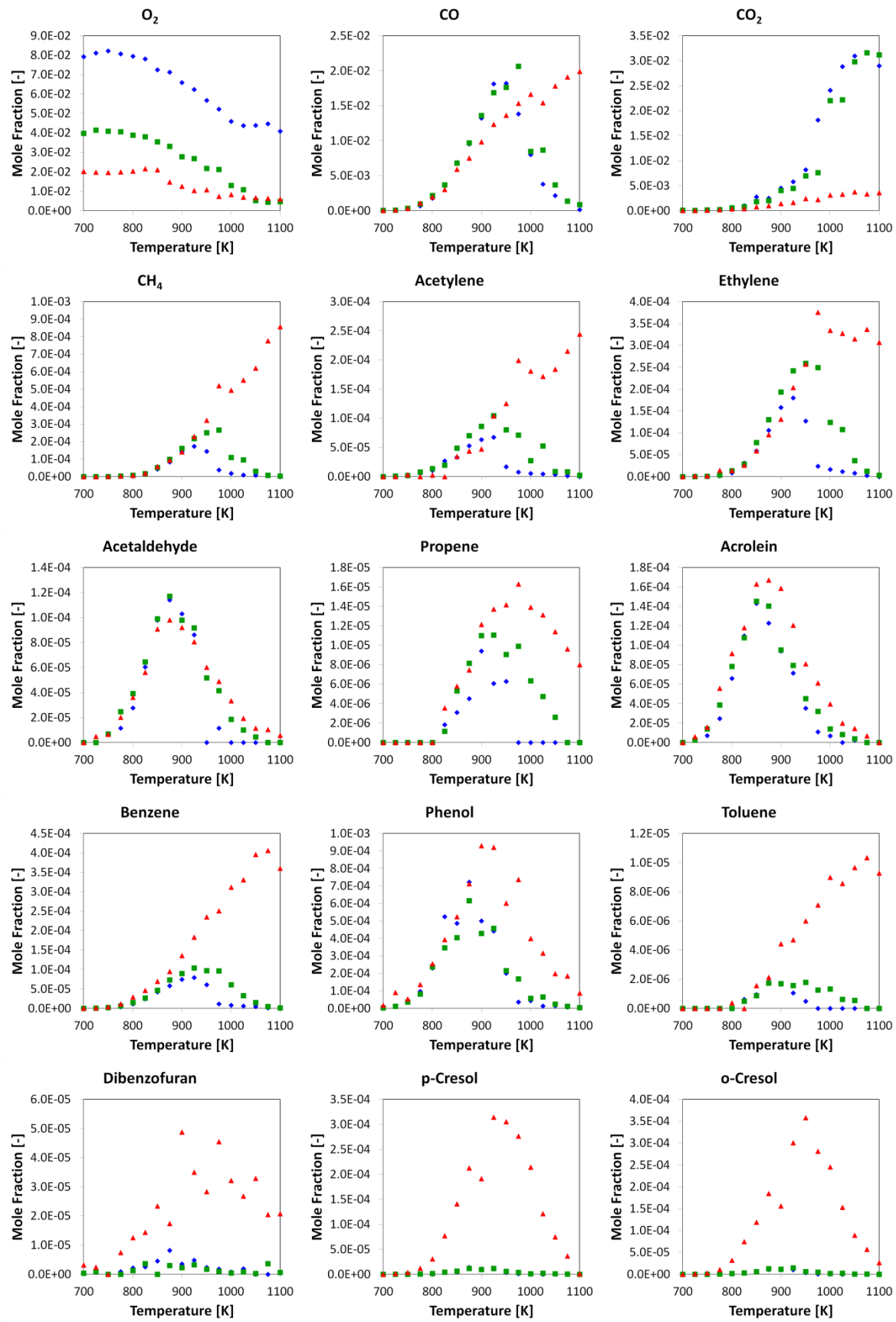

Figure 104. Mole fraction profiles of oxygen and main reaction products of benzaldehyde oxidation for the three equivalence ratios (Symbols: ♦ phi=0.5, ■ phi=1, ▲ phi=2).

Carbon monoxide and phenol are the two main products at 850 K. Carbon monoxide is mainly formed by the decomposition of the radical obtained after the abstraction of the aldehydic H-atom of benzaldehyde. This reaction also forms phenyl radical, which could explain phenol formation. Acrolein, benzene and acetaldehyde are also produced in large amounts. It can be observed that under fuel-rich conditions cresol and dibenzofuran are also formed in large quantities. Figure 104 presents the experimental mole fraction profiles of the species presented in Figure 103 and the one of oxygen and C_2-C_3 hydrocarbons.

Acetaldehyde and acrolein mole fraction profiles are not very sensitive to the equivalence ratio, whereas the importance of dibenzofuran and cresols under fuel-rich conditions can be directly seen. The cyclic aromatic compounds are more produced under fuel-rich conditions as it can be seen for benzene or phenol for example. Fuel-lean and stoichiometric conditions are very close in terms of product distribution and the mole fraction profiles of the products are very close under those two conditions

V.2.2. Kinetic modeling

Mechanism

The CRECK mechanism was used to model our experimental data. It was previously described in part IV.1.2.

Table 41 shows the primary pyrolysis and oxidation reactions of benzaldehyde, highlighting modifications and new reaction pathways implemented in this study (reactions whose parameters were estimated or taken from literature). It is composed of 18 reactions classed into different reaction types.

Benzaldehyde can react through unimolecular initiations (reactions 1-2 in Table 41). The hypothesis has been made that only the aldehydic function is reactive and that the aromatic ring cannot react by its own. Due to the lack of specific kinetic information, kinetic parameters of initiation reactions have been determined based on bond dissociation energies (BDEs) as reported in Pelucchi et al. (2019). The enthalpies of formation of the radical involved in the BDEs estimation are presented in Figure 105.

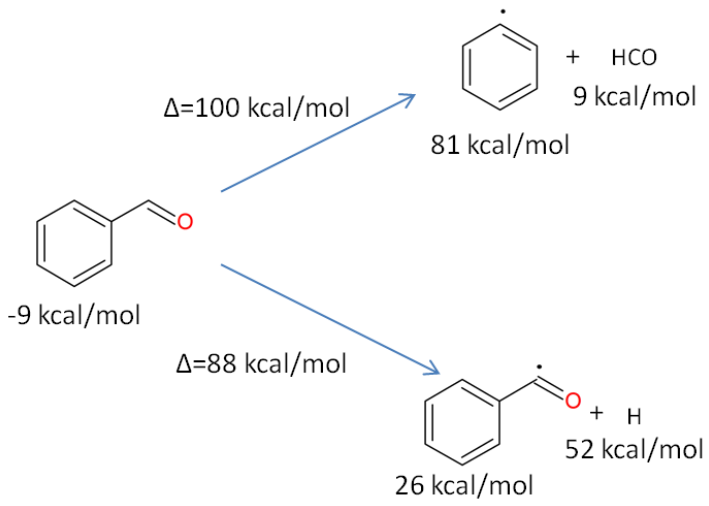

Figure 105. Unimolecular decomposition pathways of benzaldehyde, considered in the model. The values correspond to the enthalpies of formation (uncertainties ±1 kcal/mol).

Table 41. Reactions of benzaldehyde in cal, s, mol, cc units.

Reaction	*A*	*n*	*Ea*	References	No.
Reactions of Benzaldehyde					
Unimolecular initiations					
$C_6H_5CHO=HCO+C_6H_5$	*5.0E+15*	*0.0*	*98900.0*	(Pelucchi et al., 2019)	(1)
$C_6H_5CHO=C_6H_5CO+H$	*3.0E+15*	*0.0*	*89300.0*	(Pelucchi et al., 2019)	(2)
Bimolecular initiations and H-abstractions					
$O_2+C_6H_5CHO=HO_2+C_6H_5CO$	*1.4E+07*	*2.0*	*41405.9*	(Pelucchi et al., 2019) Work on RCHO (IV.2)	(3)
$OH+C_6H_5CHO=H_2O+C_6H_5CO$	*1.2E+10*	*1.0*	*-855.1*	(Pelucchi et al., 2019) Work on RCHO (IV.2)	(4)
$HO_2+C_6H_5CHO=H_2O_2+C_6H_5CO$	*3.2E+06*	*2.0*	*14062.9*	Estimated Work on RCHO (IV.2)	(5)
$CH_3+C_6H_5CHO=CH_4+C_6H_5CO$	*2.4E+05*	*2.0*	*3516.3*	(Pelucchi et al., 2019) Work on RCHO (IV.2)	(6)
$H+C_6H_5CHO =H_2+C_6H_5CO$	*1.2E+07*	*2.0*	*2573.6*	Estimated Work on RCHO (IV.2)	(7)
$C_6H_5CHO+C_7H_7=C_7H_8+C_6H_5CO$	*1.1E+05*	*2.0*	*14062.9*	(Pelucchi et al., 2019) Work on RCHO (IV.2)	(8)
$C_2H_5+C_6H_5CHO =C_2H_6+C_6H_5CO$	*1.6E+05*	*2.0*	*5128.0*	(Pelucchi et al., 2019) Work on RCHO (IV.2)	(9)
$C_6H_5+C_6H_5CHO =C_6H_6+C_6H_5CO$	*2.9E+08*	*1.0*	*867.9*	(Pelucchi et al., 2019) Work on RCHO (IV.2)	(10)
$C_5H_5+C_6H_5CHO =C_5H_6+C_6H_5CO$	*2.7E+05*	*2.0*	*12129.8*	(Pelucchi et al., 2019) Work on RCHO (IV.2)	(11)
$C_6H_5CHO+C_6H_5O=C_6H_5OH+C_6H_5CO$	*1.4E+05*	*2.0*	*10683.4*	(Pelucchi et al., 2019) Work on RCHO (IV.2)	(12)
Ipso-additions					
$C_6H_5CHO+O=C_6H_5O+HCO$	*4.0E+12*	*0.0*	*5000.0*	(Saggese et al., 2013)	(13)
$C_6H_5CHO+CH_3=C_7H_8+HCO$	*1.5E+12*	*0.0*	*4000.0*	(Pelucchi et al., 2019)	(14)
$C_6H_5CHO+C_2H_3=C_6H_5C_2H_3+HCO$	*1.2E+12*	*0.0*	*15200.0*	(Pelucchi et al., 2019)	(15)
$C_6H_5CHO+OH=C_6H_5OH+HCO$	*9.6E+13*	*0.0*	*19228.0*	(Pelucchi et al., 2019)	(16)
$C_6H_5CHO+H=C_6H_6+HCO$	*4.7E+12*	*0.0*	*8600.0*	(Pelucchi et al., 2019)	(17)
Alpha-scission decomposition					
$C_6H_5CO=C_6H_5+CO$	*5.8E+14*	*0.0*	*23000.0*	(Solly and Benson, 1971)	(18)

Reactions 3 to 12 correspond to bimolecular initiations and H-abstraction reactions. Only the bimolecular reaction with oxygen has been taken into account. The kinetic parameters of the H-abstractions from the aldehydic position have been determined based on our previous studies on linear aldehydes (IV.2).

Ipso-addition reactions on the fuel are modeled by the reactions 13 to 17 and correspond to the additions of the main radicals onto the ring at the aldehydic position. The kinetic parameters of ipso-addition reactions have been determined based on the rate rules reported in the work of Pelucchi et al. (2019). Reactions with the aromatic hydrogen atoms were considered as negligible compared to those involving the aldehydic one.

Reaction 18 is the reaction of alpha-scission of the radical C_6H_5CO formed after the abstraction of the aldehydic hydrogen atom. The rate constant of reaction 18 has been adopted from Solly and Benson (1971), as already proposed in the toluene model by Bounaceur et al. (2005). It should be noted that the value from Solly and Benson is the only high pressure limit determination available in the literature and most probably carries large uncertainties (i.e. one order of magnitude) mostly due to the very limited temperature range considered in the analysis (614-647 K). However, from a broader kinetic model perspective, the C_6H_5CO radical is very rapidly decomposed to phenyl radical and CO, without significant further interactions with the mixture. The addition of O_2 to C_6H_5CO has also been investigated, based on acetaldehyde similar reactions. However, it was shown that these reactions were negligible and a decision was made to remove them from the mechanism.

The kinetic values of reactions 5 and 7 were already present in the mechanism, but their estimation needed a reevaluation due to deviations between the model computed results and the experimental data. Thus, their kinetic constants were decreased (within the estimated uncertainty) in order to better reproduce the fuel reactivity. The pre-exponential factors of reactions 5 and 7 have so been multiplied by factors of 0.5 and 0.3, respectively, with respect to the reference values for H-abstractions from the aldehydic moiety of linear aldehydes presented in the part dedicated to linear aldehydes (IV.2). The adopted rate constant modifications are well within the uncertainty range of those parameters (a factor of 3). This uncertainty is established based on other parameters adopted in literature models (Zhang et al., 2017). In fact, Mendes et al. (Mendes et al., 2014) declared an uncertainty of 2.5-3 based on the uncertainties of the single point energies. We considered here a factor of 3 as an upper limit as uncertainties related to the treatment of anharmonicities and to the frequencies may also be present.

Analysis of the results

Figure 106 presents a comparison between the experimental fuel conversion and the results of the model for the three equivalence ratios.

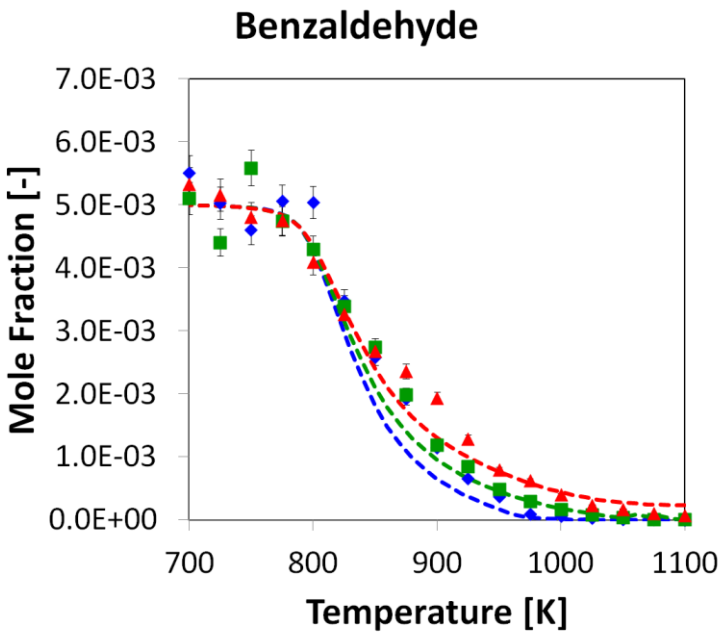

Figure 106. Fuel conversion for benzaldehyde oxidation compared to the model computed results (Symbols: ♦ phi=0.5, ■ phi=1, ▲ phi=2) (Error bars ±5 %).

The model is able to correctly predict the start of the reactivity at 750 K with a very small variation in the conversion. Then there is an acceleration of the conversion until 1000 K. The model over-predicts the fuel conversion between 825 K and 900 K but its performances above this temperature are better. Under fuel-rich conditions, the model results indicate that the full conversion is never reached and stays at a constant value, which was not observed experimentally. The model also predicts a higher difference in reactivity between fuel-lean and stoichiometric conditions, whereas the experiments do not show any significant shift between the two conditions.

Figure 107 presents the mole fraction profiles predicted by the model of the reaction products presented in Figure 103.

The agreement between the experimental results and the model predictions is good for some products such as carbon monoxide, acrolein or phenol. At the highest temperatures (T>1000 K) under fuel rich conditions, model predictions are less accurate. The model predicts mole fractions of benzene and toluene lower than what is experimentally observed, which could lead to an overprediction of ethane and methane. The model also does not predict as much acetaldehyde as experimentally measured under the three equivalence ratios. The model has also huge difficulties to match the experimental results for dibenzofuran and cresol under fuel-rich conditions. But due to the high number of aromatic compounds formed under those conditions, it is possible that the detection with the GCs was distorted by some other co-eluted products. Thus the related experimental profiles could be over-estimated. Oscillations (transient regime) were detected by the model under stoichiometric conditions above 1050 K. However, this trend was not significantly observed experimentally.

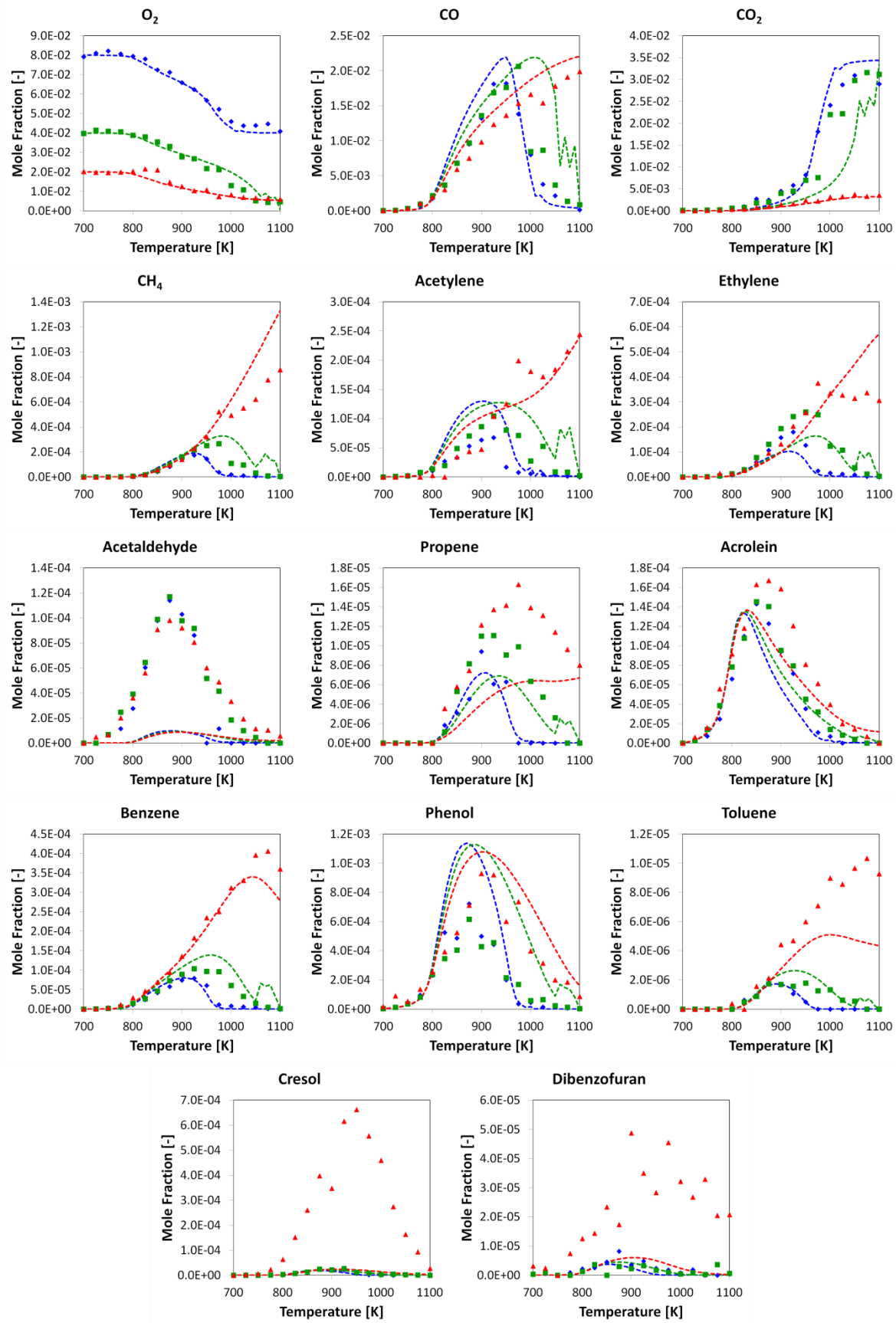

Figure 107. Mole fraction profiles of oxygen, C_2 and C_3 hydrocarbons and main products of benzaldehyde oxidation compared to the model results for the three equivalence ratios (Symbols: ♦ phi=0.5, ■ phi=1, ▲ phi=2).

Figure 108 shows a rate flux analysis of benzaldehyde oxidation at 850 K for stoichiometric conditions for a conversion of 50 %. This conversion rate has been chosen in order to investigate the primary product decomposition pathways. For clarity, some species like CO and CO_2 are not shown. Under these conditions, benzaldehyde mainly reacts by the abstractions of the aldehydic hydrogen atom as suggested by Vasiliou et al. (2013) for pyrolysis (89% at 850 K). This H-abstractions on the fuel leads to the formation of the C_6H_5CO radical, which quickly decomposes by alpha-scission in phenyl radical and carbon monoxide. The phenyl radical then leads to the phenoxy radical (C_6H_5O in Fig. 6). This radical is the precursor of almost all the products experimentally observed (e.g. acrolein, acetaldehyde, cresol…).

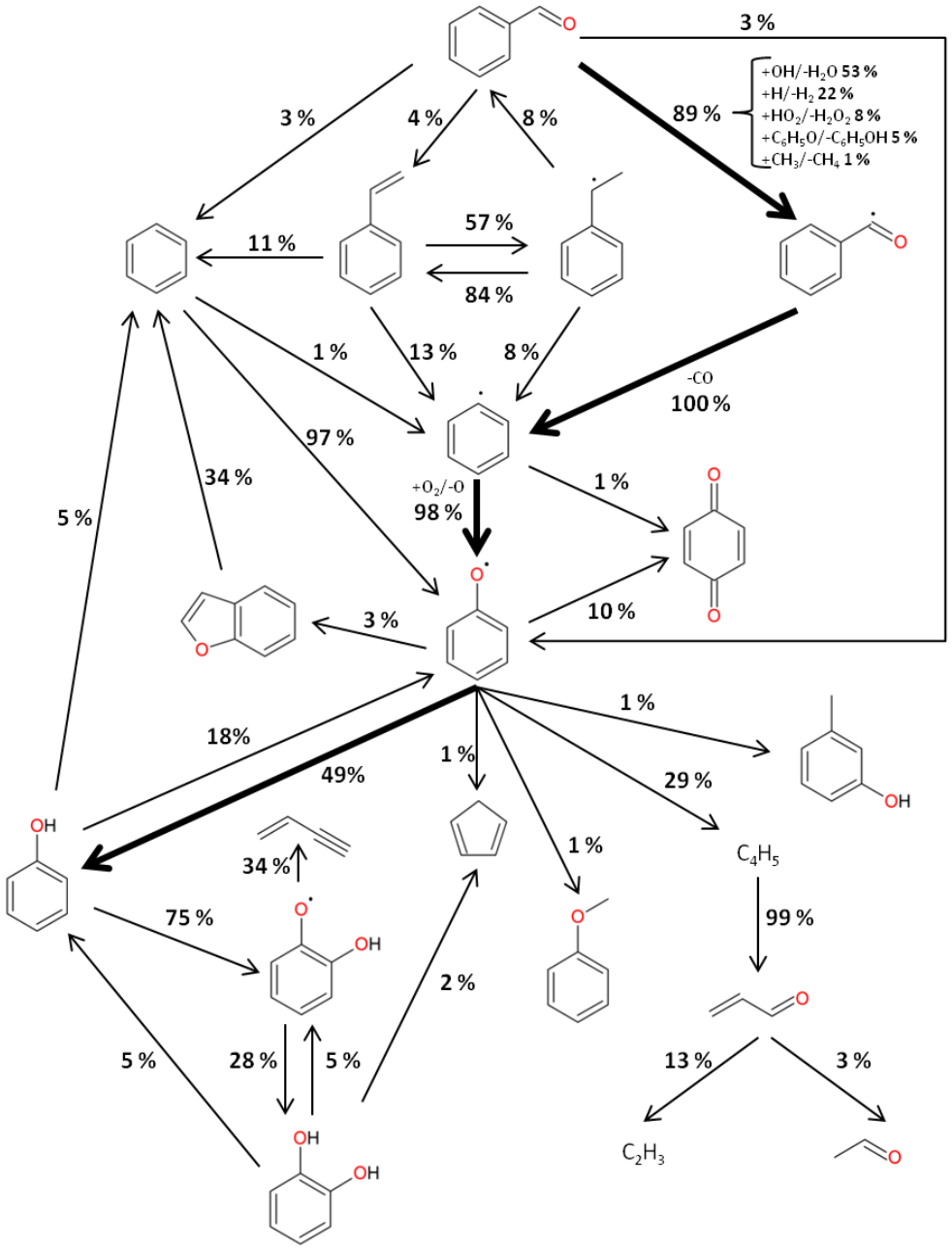

Figure 108. Rate of production analysis at 850 K and 107 kPa of benzaldehyde oxidation under stoichiometric conditions.
Percentages represent the fraction of the molar flux of consumption of the associated species.

Benzaldehyde also reacts by ipso-addition reactions of hydrogen atom and C_2H_3 radical producing benzene and styrene. Styrene can then react through different H additions on different sites. An addition on the substituted unsaturation can lead to the formation of the radical $C_6H_5CHCH_3$ or to the formation of a radical C_6H_5 and ethylene. The radical $C_6H_5CHCH_3$ can also decompose into C_6H_5 radical and ethylene or can form the fuel back with the intervention of the radical HO_2. Styrene can also react by ipso-addition reactions to form benzene.

Benzene is formed by ipso-addition of H atom on benzaldehyde, styrene and phenol. Benzene is almost exclusively transformed into C_6H_5O via two pathways:

- $O+C_6H_6=H+C_6H_5O$ (97 %)
- $R+C_6H_6=RH+C_6H_5$; $C_6H_5+O_2=C_6H_5O+O$ (1.4 %)

Thus the formation and consumption of benzene is totally ruled by ipso-addition reactions on the other aromatic compounds present in the gas phase. As discussed in Saggese et al. (2013), the resonance stabilized phenoxy radical largely contributes to phenol formation by means of H-abstraction ($C_6H_5O+RH=C_6H_5OH+R$) on C_6H_5CHO and catechol and recombination with H atoms. Indeed 49 % of the consumption flux of the radical C_6H_5 leads to to the formation of phenol. Phenol is then consumed in a significant fraction by H-abstraction reactions by O, OH, and HO_2 to give C_6H_5O radicals (18 %). Therefore, a cycle phenol/phenoxy is exhibited by the mechanism and could be important in the overall reactivity of the system.

This observation is also supported by the sensitivity analysis on benzaldehyde performed at 770 K for stoichiometric conditions and presented in Figure 109.

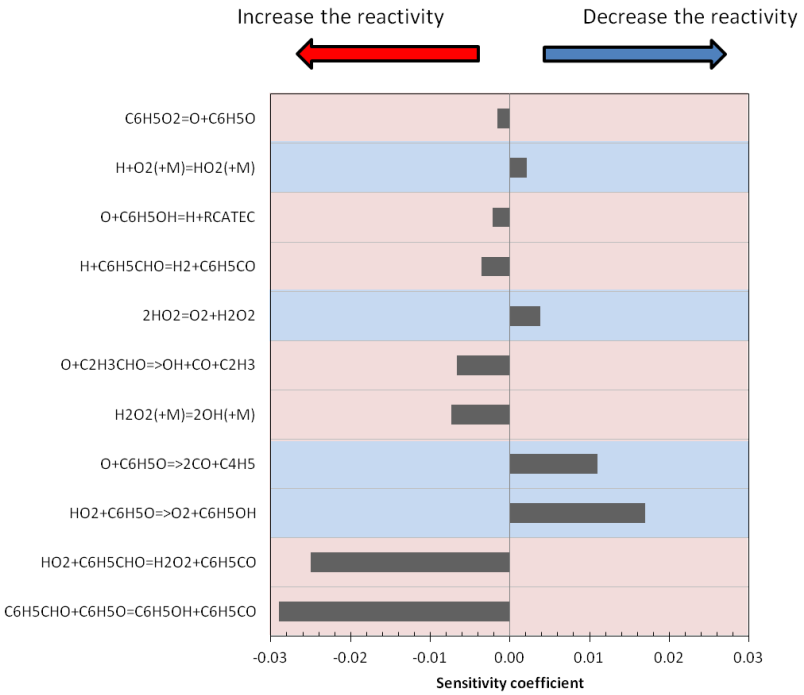

Figure 109. Sensitivity (of fuel mole fraction to reactions) analysis of benzaldehyde oxidation to rate constants at T=770 K and under stoichiometric conditions.

The most important reactions, promoting the reactivity, are the H-abstractions on the fuel by HO_2 and C_6H_5O to form the radical C_6H_5CO. This radical subsequently decomposes into C_6H_5 and C_6H_5O, contributing to the phenol/phenoxy cycle.

Phenoxy radical (C_6H_5O) and the phenol/phenoxy cycle are controlling the reactivity at low temperatures. HO_2 radical has also an important impact as it is involved in the phenol/phenoxy cycle via the reaction: $HO_2+C_6H_5O=O_2+C_6H_5OH$. This analysis confirms that the C_6H_5O radical is the key intermediate in the reactivity of benzaldehyde at low-temperature. Thus its consumption, through the reactions $HO_2+C_6H_5O=>O_2+C_6H_5OH$ and $O+C_6H_5O=>2CO+C_4H_5$, inhibits the reactivity. Furthermore, these reactions are consuming radicals by forming stable species (CO, O_2...) or by reducing the number of radical sites in the system via termination reactions. Figure 110 presents a scheme of this analysis.

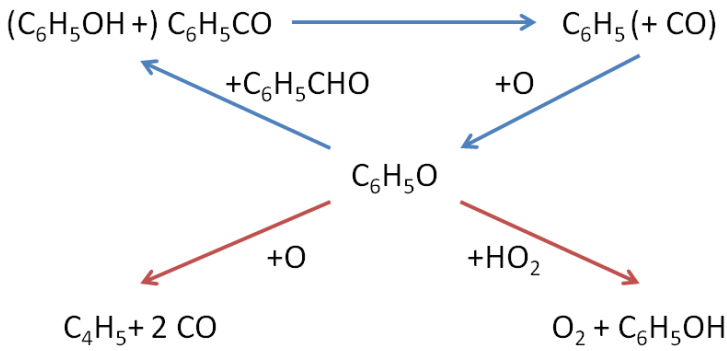

Figure 110. Scheme of the phenoxy radical reactions implied in the control of the overall reactivity of the system (in blue the accelerating propagating chain loops and in red the inhibiting reactions).

HO_2 also reacts with the fuel to give H_2O_2, which gives two OH radicals and therefore accelerates the reactivity through a multiplication of the number of radicals. The chemistry of other intermediates like acrolein (C_2H_3CHO) and catechol phenoxy-like radical (RCATEC) have also a promoting effect on the reactivity, but less dominant. Concerning the other equivalence ratios, the same analysis has been performed and the results are very similar. This observation seems to confirm the fact that the equivalence ratio has a minor impact on the overall reactivity.

Acetaldehyde and acrolein are produced by the decomposition of C_6H_5O to C_4H_5 and CO through the reaction: $O+C_6H_5O=>2CO+C_4H_5$. Subsequently the C_4H_5 radical reacts with oxygen to form HCO and acrolein: $O_2+C_4H_5=>HCO+C_2H_3CHO$. Acrolein leads mainly to the formation of C_2H_3 radical (12.5 %) via H-abstraction by OH, O, and H to give C_2H_3 and CO according to the lumped step $R+C_2H_3CHO=>RH+CO+C_2H_3$. This lumped step corresponds to the abstraction of the aldehydic H-atom followed by a decarbonylation of the radical (R-C*=O) as discussed in the case of linear aldehydes (IV.2). C_2H_3 then decomposes into formaldehyde in a large amount (30%) via the addition of oxygen. Acetaldehyde is formed by the addition-elimination reaction of OH radical from acrolein: $OH+C_2H_3CHO=>HCO+CH_3CHO$ accounting for 3 % of the consumption flux of acrolein. However the model is not able to predict the correct amount of formed acetaldehyde. This could also explain the overprediction of styrene mole fraction, due to an overproduction of C_2H_3 radicals produced from acrolein. Furthermore, the model considers the formation of formaldehyde through the reaction: $C_2H_3+O_2=H+CO+CH_2O$. The non-detection of

formaldehyde during the experiment may indicate that the transformation of acrolein into C_2H_3 and acetaldehyde needs a better assessment.

Concerning the simulated profiles of catechol, its formation is due to the ipso-addition reaction of an oxygen atom to phenol. This leads to the formation of the resonance stabilized phenoxy-like catechol radical which can then react with other species in the system abstracting an H atom and forming catechol as shown in Figure 111a.

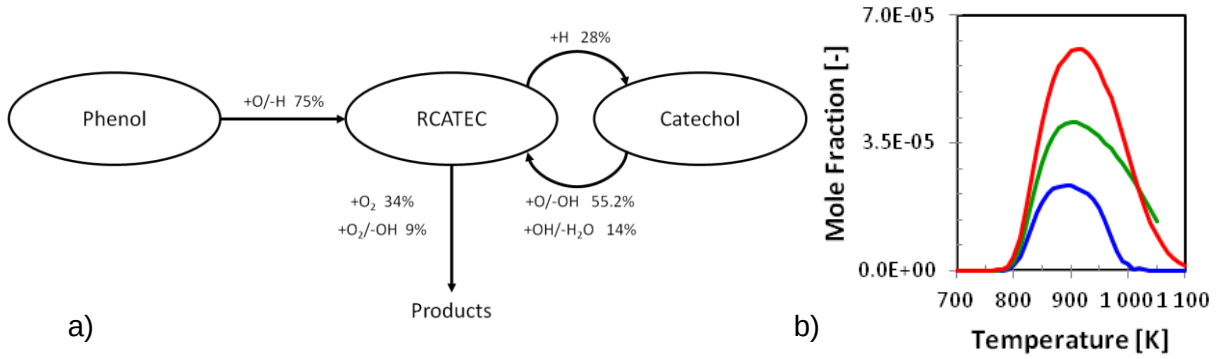

Figure 111. a) Flux rate between phenol and catechol at 850 K and b) simulation data for catechol obtained with the kinetic model.

The importance of such pathways in oxygenated aromatics has been recently pointed out by Pelucchi et al. (2019). The model predicts a mole fraction of catechol between 60 ppm under fuel-rich conditions and 25 ppm under fuel-lean conditions. A chart in Figure 111b presents the simulations results for catechol.

Despite this consideration the relative small amount of catechol predicted could lead to a more limited detection capability. Further analysis with gas chromatography and *ad hoc* analytical methods could help to detect catechol in the outlet mixture.

V.2.3. Conclusion

Benzaldehyde oxidation has been studied in a jet-stirred reactor at atmospheric pressure and thanks to gas chromatography 48 products have been identified. The results showed that carbon monoxide and phenol are the two main products. Acrolein, benzene and acetaldehyde are secondary products, whereas cresol and dibenzofuran are produced in important quantity only under fuel-rich conditions.

Based on our experimental results, a sub-mechanism dedicated to benzaldehyde oxidation has been developed and inserted in the CRECK mechanism. This sub-mechanism contains 18 reactions and has been developed on the hypothesis that the aromatic cycle is more stable than the aldehydic function. Thus the rapid release of carbon monoxide and the formation of the associated phenyl radical have been considered as preponderant. The results of the model have been confronted to the experimental results and the model is able to reproduce the fuel reactivity and the formation of the most important products. However, some discrepancies have been observed for some products. The major one is about the prediction of acetaldehyde, cresol and dibenzofuran.

VI. CONCLUSION AND PERSPECTIVES

Biofuels are promising fuels with a huge potential to replace the conventional fossil fuels. They have the advantage to have a small carbon impact and they are already used in several applications. For example, ethanol is already mixed with car gasoline to reduce the ecological impact of the private transportation. Among the biofuels, bio-oils are still under-exploited. Indeed their compositions can vary a lot and their physico-chemical properties (viscosity and acidity mainly) are constraining. This limits the use of bio-oils at a large scale.

To better assess **bio-oil oxidation or pyrolysis**, a bibliographical review about the publications dealing with the composition of bio-oils was performed. From this review, it came out that bio-oils could be described as a mixture composed of 6 types of chemical compounds:

- Alcohols
- Aldehydes and ketones
- Carboxylic acids
- Furans and derivatives
- Oxygenated aromatic compounds
- Nitrogenated compounds

The oxidation and pyrolysis of alcohols have been extensively studied during the last years, mainly due to the recent interest in biofuels. However, the long chain alcohol oxidation or pyrolysis has been less studied than the shorter ones. The same conclusion could be drawn from the review about aldehydes and ketones. Indeed the aldehydes with more than four carbon atoms have rarely been the topic of publications in this field. Concerning carboxylic acid, it could be interesting to note that mainly pyrolysis studies have been published, but only for the smallest ones: formic and acetic acids. It was mentioned explicitly that there is a need of reliable experimental data to validate the proposed kinetic mechanism and to improve the understanding of carboxylic acid chemistry during oxidation and pyrolysis. Furan family has to the contrary been the topic of many combustion related publications. However, there have been fewer studies about unsaturated furan than for saturated furan such amounts of related work has been noticed. Phenol has been extensively studied but other compounds, such as cresol or benzaldehyde, have been less studied. A lack of publications has also been observed for the nitrogen–containing compounds, as the reactions of only a few nitrogenated molecules were studied such as pyrrole or pyridine.

In the frame of this thesis and to complete some detected lack in the literature, it has been decided to produce a new dataset for some molecules owning to the chemical families previously presented. Chemical surrogates and an experimental set-up have been selected. A heated **jet-stirred reactor** operated under atmospheric pressure has been chosen to perform the experiments, due to its homogeneity in concentration and temperature. This kind of “ideal” reactor is indeed convenient for obtaining reliable data for the development and validation of kinetic models. During this work, **eight fuels have been selected and studied**. They are presented in Table 42, with their associated experimental conditions.

Table 42. List of the studied fuels and of their related experimental conditions.

Fuel name	Structure	Chemical formula	Experimental conditions
n-Butanol	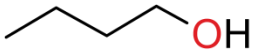	$C_4H_{10}O$	T=500-1100K, P=1 atm, φ=0.5-1-2
n-Pentanol	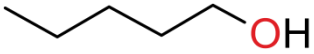	$C_5H_{12}O$	T=500-1100K, P=1 atm, φ=0.5-1-2
n-Butanal	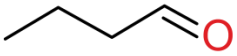	C_4H_8O	T=500-1100K, P=1 atm, φ=0.5-1-2
n-Pentanal	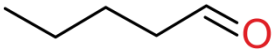	$C_5H_{10}O$	T=500-1100K, P=1 atm, φ=0.5-1-2
Butanoic acid	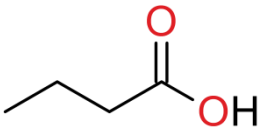	$C_4H_8O_2$	T=800-1100K, P=1 atm, φ=0.5-1-2
Pentanoic acid	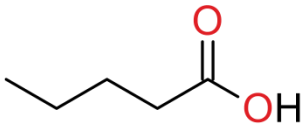	$C_5H_{10}O_2$	T=800-1100K, P=1 atm, φ=∞-0.5-1-2
Furan	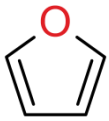	C_4H_4O	T=700-1100K, P=1 atm, φ=0.5-1-2
Benzaldehyde	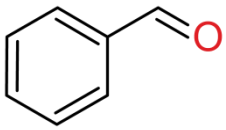	C_7H_6O	T=700-1100K, P=1 atm, φ=0.5-1-2

In parallel of the experimental work, **semi-detailed kinetic models** have been developed for each compound in collaboration with the team Prof. Faravelli of Politecnico di Milano. Each sub-mechanism has been developed in order to reproduce the experimental results obtained in Nancy and the performance of the model has been compared to them. The sub-mechanisms developed for the carboxylic acids and benzaldehyde were the first ones to be developed specifically to reproduce the reactivity of these compounds. Thanks to the model results, we tried to define rate rules and reactions classes for each family and across the chemical family. The reactivities exhibited by the different fuels have also been compared and it came out that no general rules can be drawn. The best assumption consisted in considering each molecule as composed of a specific oxygenated moiety and an alkilic one. Each moiety reactivity was ruled by its own rules.

I started by investigating the oxidation of **linear oxygenated molecules**. A study on, two **alcohols, n-butanol and n-pentanol**, was the first performed in the frame of this work. It showed that *n*-butanol started to react around 800 K and was fully consumed at 1050 K. Similar temperatures were observed for *n*-pentanol reactivity temperature range: 775-1050 K. This study also showed that both fuels did not exhibit any low-temperature reactivity or NTC area, contrary to *n*-butane or *n*-pentane. Among the 23 and 31 products detected

during, respectively, *n*-butanol and *n*-pentanol oxidation, the linear C_n aldehyde and alkene were detected for both fuels. Those results were used to develop a kinetic mechanism based on the CRECK model developed in Milano. The model was able to reproduce the fuel reactivity, but detected a small NTC area for *n*-pentanol under fuel-lean conditions. It also succeeded in predicting the mole fraction profiles of the main products. This model showed that the α-position had a huge role in the reactivity of the alkyl chain. Indeed, the alcohol function increased the reactivity at this position and this led to the formation of the specific products, such as the associated aldehydes.

To surrogate **aldehydes, n-Butanal and n-pentanal** were also studied. *n*-Butanal started to react at 600 K and was consumed around 1075 K. It did not exhibit any low-temperature reactivity except under fuel-lean conditions between 575 and 700 K. In the contrary, *n*-pentanal showed an important NTC area under all studied conditions between 650 and 725 K, which depth was dependant of the equivalence ratio. Indeed the larger the oxygen content, the stronger the NTC behavior. *n*-Pentanal started to react at 575 K and was fully consumed at 1025 K. This difference in the reactivity of the two molecules could be explained by the difference in the alkyl chain length. 20 products was detected and quantified during *n*-butanal oxidation experiments and 29 products during pentanal ones. For both fuels, an important amount of carbon monoxide was observed among the oxidation products. The Cn-1 aldehyde was also detected among the products for both fuels. During *n*-pentanal experiments, pentanoic acid was detected in the products but its quantification was limited by its very low amount in the mixture. A kinetic model was developed to reproduce the fuel reactivity and to better assess the decomposition pathways of the linear aldehydes. This model was able to reproduce the fuel reactivities and especially the NTC area experimentally observed. It showed that the important formation of carbon monoxide could be explained by a fast decarboxylation of the fuels, due to an important reactivity at the α-position. The other specific products formation was due to the alkyl chain reactivity. The model also proved that the alkyl chain length had an important impact on the molecule reactivity. Indeed, the longer the alkyl chain, the smaller the influence of the aldehydic function.

To finish with linear oxygenated compounds, **carboxylic acids** were considered. A study was performed to investigate the oxidation of **butanoic and pentanoic acids**. To our best knowledge, **this study was the first the first concerning the gas-phase reactions of these compounds**. These measurements were largely affected by many experimental difficulties. Acid corrosive properties decomposed some of the gums of the system, creating some plugging problems in the experimental set-up. Furthermore, adsorption problems could occur due to the high oxygen content in those molecules. Therefore, the fuel quantification was complex. In order to reduce this problem, a surface-coated insert and a sampling loop were installed in the gas chromatographs. Butanoic acid reactivity temperature range was around 850-1000 K for oxidation, except under fuel-rich conditions where the full conversion was never achieved. Concerning pentanoic acid, the reactivity range was around 850-975 K under oxidation conditions. To complete the study, pyrolysis experiments were carried out for pentanoic acid, but some small unexpected and non-quantified inlets of oxygen did not allow exploiting the data. The products analysis with both fuels showed that an important formation of carbon dioxide was observed compared to that of carbon monoxide. Thus, it was first assumed that the acid function is reacting to give carbon dioxide. The kinetic model developed showed, in contrary to this hypothesis, that the acid function was not the main

reactive position. The reactivity was located on the alkyl chain with a strong inhibiting effect of the acid function of the nearby carbon atom.

In a second step, I was interested by **cyclic oxygenated compounds**. The oxidation of **furan** was first carried out in the jet-stirred reactor. Furan started to react at 800 K and was fully consumed at 1050 K under fuel-lean conditions. For fuel-rich and stoichiometric conditions, unsteady behavior (oscillations) was observed for temperatures above 1000 K, but it can be assumed that the full-conversion of the fuel was then almost achieved. During this study 18 product were identified amongst them acetaldehyde and acrolein were two of the main products. The experimental data had then been compared with the predictions of two models. The first model was developed by Tran et al. (2015a) and contained a sub-mechanism for the description of the low-temperature reactivity of furan. The other tested model was the CRECK semi-detailed kinetic model, used in the study of the other fuels considered in this PhD work. The overall prediction of the fuel conversion and the products formation by the model of Tran et al. (2015a) was good, while the CRECK model was not able to well reproduce the low-temperature reactivity. But, we can assume that the CRECK model could better handle the low-temperature decomposition of furan with the addition of the sub-mechanism developed by Tran et al. in this semi-detailed mechanism.

Finally an **oxygenated aromatic compounds, benzaldehyde**, was considered. This was not a fuel, whose oxidation was frequently investigated, while its decomposition could give some clues about the reactivity of larger oxygenated aromatic compounds that can be found in large amounts in bio-oils. Benzaldehyde started to react at 750 K and its complete depletion was achieved at 1025 K. During its oxidation, 48 products were detected. The major ones are carbon monoxide, phenol and acrolein. Cresol and dibenzofuran were also important products under fuel-rich conditions. A sub-mechanism dedicated to benzaldehyde was developed to reproduce the experimental data obtained and added to the CRECK model. The assumption of a fast decarboxylation of the fuel was made. The model was able to reproduce the fuel reactivity and the main product formation. However, some discrepancies on the profiles of acetaldehyde or styrene were observed. The model analysis also highlighted the fact that a phenol/phenoxy cycle ruled the reactivity of benzaldehyde.

****

As far as perspectives are concerned, the oxidation and pyrolysis of surrogates for the molecules included in bio-oils have to be pursued. As already mentioned, the literature is very scarce for molecules containing nitrogen-atoms, such as pyrrole (C_4H_5N) for example. There are more data about phenolic compounds, but usually uncertainties in the measured product mole fractions can be large due to experimental difficulties. It would be interesting to deepen the studies about phenolic compounds with a special care taken to the sampling from the reactor and the product quantification. Amongst oxygenated molecules, there are also simple sugars for which the literature is scarce. The main difficulty with sugars is that they are solid at ambient temperature and it is not easy to have them in the gas phase, especially in a controlled way. Therefore, a system for the sublimation of the solid has to be installed on the experimental set-up instead of the evaporator used during my work.

It could also be interesting to investigate the extension of the representation of the molecules in moieties to more complex molecules, such as multi-substituted compounds

(such as diols or dials) or to specific function in the core of the alkyl chain (such as ketones or secondary alcohols) (see Figure 112).

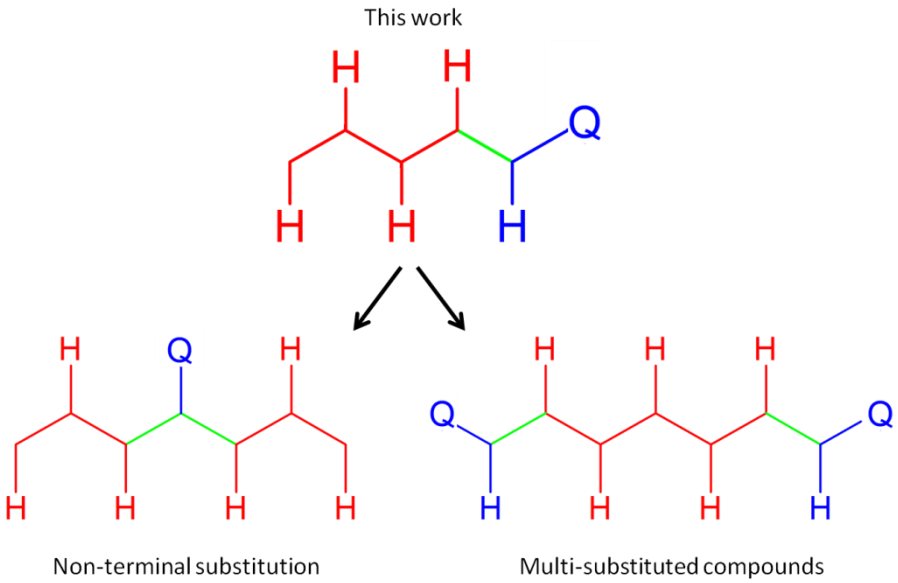

Figure 112. Scheme of the potential development for the representation of substituted compounds.

If this representation of the molecules can be extended to other types of molecules, it could be then used in the automatic generation of kinetic model. A database of kinetic rates and reaction classes could be created, allowing the construction of kinetic model for a large diversity of molecules.

Longer-term perspectives would be to create a synthetic mixture of the studied compounds to surrogate reference bio-oils. Those reference bio-oils should be studied thanks to the GCxGC to define their composition. After that, a surrogate mixture should be defined for the study of bio-oil oxidation. The product distribution and reactivity are good similarity points to verify. In addition, the performance of the model to predict the reactivity of the surrogate and the actual bio-oil should be tested in order to see if any pathway or product interaction is missing. Furthermore, the use of GCxGC could improve the experimental results obtained. More products could be separated and the distinction of the isomers could give important information concerning the reaction pathways. Unfortunately, this type of apparatus was only available at the very end of my work. The separation of benzene and one of its linear isomers showed the feasibility of the method and is very promising.

In the frame of the IMPROOF project, this work had the task to propose a surrogate formulation for bio-oils and an extension of the experimental database linked to those compounds. Based on the kinetic model developed during this PhD, computational fluid dynamics modeling with detailed chemistry are in progress and to be applied to design the future burners in the steam cracking furnaces. An evaluation of the energy efficiency of bio-oils and of the pollutants emission will be carried out. However, some physical properties can limit the use of bio-oils as fuels for steam cracking furnaces. Indeed the viscosity and the acidity are two important parameters, which can limit their utilization at an industrial scale. The corrosion problem and the investments costs to transport the bio-oils could also be obstacles too huge to overcome for the use of bio-oils as fuels.

This work can also be considered as a building block toward a better understanding of the decomposition of other intermediates formed during biomass reactions, such as tars that are the mixtures of poly-oxygenated hydrocarbons in the liquid vapors produced during biomass devolatilisation. Since biomass devolatilisation is a first step towards the gas-phase reactions induced by biomass degradation, the results on the reactions of the compounds studied in this work can indeed be relevant in the frame of a project based on the study of biomass pyrolysis or combustion. In addition, the results obtained during acid or benzaldehyde oxidation can give some first experimental clues of help for future investigations of the oxidation or the pyrolysis heavier fuels included in tars, for which the experimental difficulties encountered during this PhD could be worsened.

VII. COMMUNICATIONS AND PUBLICATIONS DURING THE THESIS

VII.1. Publications in peer reviewed journals

M. Pelucchi, S. Namysl, E. Ranzi, A. Frassoldati, O. Herbinet, F. Battin-Leclerc, T. Faravelli, An experimental and kinetic modelling study of *n*-C4C6 aldehydes oxidation in a jet-stirred reactor, Proceedings of the Combustion Institute. 37 (2019) 389–397.

S. Namysl, M. Pelucchi, O. Herbinet, A. Frassoldati, T. Faravelli, F. Battin-Leclerc, A first evaluation of butanoic and pentanoic acid oxidation kinetics, Chemical Engineering Journal. 373 (2019) 973–984.

S. Namysl, M. Pelucchi, L. Pratali Maffei, O. Herbinet, A. Stagni, T. Faravelli, F. Battin-Leclerc, Experimental and Modeling Study of Benzaldehyde Oxidation. Combustion and Flame (2019) accepted.

VII.2. Oral communications

Experimental investigation of butanoic and pentanoic acids oxidation, S. Namysl, M. Pelucchi, O. Herbinet, T. Faravelli, F. Battin-Leclerc.
Workshop: "Gas-phase Reaction Kinetics of Biofuels Oxygenated Molecules", Milano (Italy), April 2018

The oxidation of linear C4-C6 aldehydes: an experimental and kinetic modeling study, S. Namysl, M. Pelucchi, O. Herbinet, E. Ranzi, A. Frassoldati, T. Faravelli. F. Battin-Leclerc.
23th International Conference on Chemical Reactors, Ghent (Belgium), November 2018.

Experimental and modeling study of benzaldehyde oxidation, S. Namysl, M. Pelucchi, L. Pratali Maffei, O. Herbinet, A. Stagni, T. Faravelli, F. Battin-Leclerc.
2nd Quadmarts Network Workshop, Nancy (France), May 2019

Reactivity Comparison of Linear C4-C6 Alcohol, Aldehyde and Carboxylic Acid Oxidation, S. Namysl, M. Pelucchi, O. Herbinet, T. Faravelli, F. Battin-Leclerc.
11th International Conference on Chemical Kinetics, Orleans (France), June 2019.

VII.3. Poster communications

Etude de l'oxydation de molécules représentatives d'une bio-huile en réacteur parfaitement agité par jets, S. Namysl, O. Herbinet, F. Battin-Leclerc.
16ème Congrès de la Société Française de génie des Procédés, Nancy (France), July 2017.

Experimental investigation of butanoic and pentanoic acid oxidation, S. Namysl, M. Pelucchi, O. Herbinet, T. Faravelli, F. Battin-Leclerc.
25th International Symposium on Gas Kinetics, Lille (France), July 2018 and 37th International Symposium on Combustion, Dublin (Ireland), August 2018.

Experimental and modeling study of the oxidation of benzaldehyde, S. Namysl, L. Pratali Maffei , M. Pelucchi, O. Herbinet, A. Stagni, T. Faravelli, F. Battin-Leclerc.
9th European Combustion Meeting, Lisbon (Portugal), April 2019.

VIII. BIBLIOGRAPHY

Abedi, J., Nourozieh, H., Kariznovi, M., Seyedeyn-Azad, F., **2015**. Thermo-physical properties of bio-oil and its fractions: Measurement and analysis. Can. J. Chem. Eng. 93, 500–509. https://doi.org/10.1002/cjce.22140

Aghsaee, M., Nativel, D., Bozkurt, M., Fikri, M., Chaumeix, N., Schulz, C., **2015**. Experimental study of the kinetics of ethanol pyrolysis and oxidation behind reflected shock waves and in laminar flames. Proc. Combust. Inst. 35, 393–400. https://doi.org/10.1016/j.proci.2014.05.063

Akih-Kumgeh, B., Bergthorson, J.M., **2011**. Ignition of C3 oxygenated hydrocarbons and chemical kinetic modeling of propanal oxidation. Combust. Flame 158, 1877–1889. https://doi.org/10.1016/j.combustflame.2011.02.015

Alexandrino, K., Millera, Á., Bilbao, R., Alzueta, M.U., **2015**. Novel aspects in the pyrolysis and oxidation of 2,5-dimethylfuran. Proc. Combust. Inst. 35, 1717–1725. https://doi.org/10.1016/j.proci.2014.06.002

Alfazazi, A., Niemann, U., Selim, H., Cattolica, R.J., Sarathy, S.M., **2016**. Effects of Substitution on Counterflow Ignition and Extinction of C3 and C4 Alcohols. Energy Fuels 30, 6091–6097. https://doi.org/10.1021/acs.energyfuels.6b00518

Alzueta, M.U., Tena, A., Bilbao, R., **2002**. Pyridine conversion in a flow reactor and its interaction with nitric oxide. Combust. Sci. Technol. 174, 151–169. https://doi.org/10.1080/00102200290021470

Alzueta, M.U., Serinyel, Z., Simmie, J.M., Curran, H.J., **2010**. Oxidation of Acetone and Its Interaction with Nitric Oxide. Energy Fuels 24, 1511–1520. https://doi.org/10.1021/ef9015284

Antonov, I.O., Zádor, J., Rotavera, B., Papajak, E., Osborn, D.L., Taatjes, C.A., Sheps, L., **2016**. Pressure-Dependent Competition among Reaction Pathways from First- and Second-O2 Additions in the Low-Temperature Oxidation of Tetrahydrofuran. J. Phys. Chem. A 120, 6582–6595. https://doi.org/10.1021/acs.jpca.6b05411

Appels, L., Baeyens, J., Degrève, J., Dewil, R., **2008**. Principles and potential of the anaerobic digestion of waste-activated sludge. Prog. Energy Combust. Sci. 34, 755–781. https://doi.org/10.1016/j.pecs.2008.06.002

Arends, I.W.C.E., Louw, R., Mulder, P., **1993**. Kinetic study of the thermolysis of anisole in a hydrogen atmosphere. J. Phys. Chem. 97, 7914–7925. https://doi.org/10.1021/j100132a020

Asmadi, M., Kawamoto, H., Saka, S., **2011a**. Thermal reactivities of catechols/pyrogallols and cresols/xylenols as lignin pyrolysis intermediates. J. Anal. Appl. Pyrolysis 92, 76–87. https://doi.org/10.1016/j.jaap.2011.04.012

Asmadi, M., Kawamoto, H., Saka, S., **2011b**. Thermal reactions of guaiacol and syringol as lignin model aromatic nuclei. J. Anal. Appl. Pyrolysis 92, 88–98. https://doi.org/10.1016/j.jaap.2011.04.011

Asmadi, M., Kawamoto, H., Saka, S., **2011c**. The effects of combining guaiacol and syringol on their pyrolysis. Holzforschung 66, 323–330. https://doi.org/10.1515/hf.2011.165

Azargohar, R., Jacobson, K.L., Powell, E.E., Dalai, A.K., **2013**. Evaluation of properties of fast pyrolysis products obtained, from Canadian waste biomass. J. Anal. Appl. Pyrolysis 104, 330–340. https://doi.org/10.1016/j.jaap.2013.06.016

Badra, J., Elwardany, A.E., Khaled, F., Vasu, S.S., Farooq, A., **2014**. A shock tube and laser absorption study of ignition delay times and OH reaction rates of ketones: 2-Butanone and 3-buten-2-one. Combust. Flame, Special Issue on Alternative Fuels 161, 725–734. https://doi.org/10.1016/j.combustflame.2013.10.001

Bahrini, C., Morajkar, P., Schoemaecker, C., Frottier, O., Herbinet, O., Glaude, P.-A., Battin-Leclerc, F., Fittschen, C., **2013**. Experimental and modeling study of the oxidation of n-butane in a jet stirred reactor using cw-CRDS measurements. Phys. Chem. Chem. Phys. 15, 19686. https://doi.org/10.1039/c3cp53335b

Baldwin, R.R., Matchan, M.J., Walker, R.W., **1970**. The high-temperature oxidation of acetaldehyde. Combust. Flame 15, 109–123. https://doi.org/10.1016/0010-2180(70)90022-2

Ballerini, D., **2006**. Les biocarburants: état des lieux, perspectives et enjeux du développement. Technip, Paris.

Bamford, C.H., Dewar, M.J.S., **1949**. 608. The thermal decomposition of acetic acid. J. Chem. Soc. Resumed 0, 2877–2882. https://doi.org/10.1039/JR9490002877

Benson, S.W., Cruickshank, F.R., Golden, D.M., Haugen, G.R., O'Neal, H.E., Rodgers, A.S., Shaw, R., Walsh, R., **1969**. Additivity rules for the estimation of thermochemical properties. Chem. Rev. 69, 279–324. https://doi.org/10.1021/cr60259a002

Bentz, T., Striebel, F., Olzmann, M., **2008**. Shock-Tube Study of the Thermal Decomposition of CH_3CHO and CH_3CHO + H Reaction. J. Phys. Chem. A 112, 6120–6124. https://doi.org/10.1021/jp802030z

Bertero, M., de la Puente, G., Sedran, U., **2012**. Fuels from bio-oils: Bio-oil production from different residual sources, characterization and thermal conditioning. Fuel 95, 263–271. https://doi.org/10.1016/j.fuel.2011.08.041

Blake, P.G., Hinshelwood, C., **1960**. The Homogeneous Decomposition Reactions of Gaseous Formic Acid. Proc. R. Soc. Lond. Math. Phys. Eng. Sci. 255, 444–455. https://doi.org/10.1098/rspa.1960.0079

Blake, P.G., Jackson, G.E., **1968**. The thermal decomposition of acetic acid. J. Chem. Soc. B Phys. Org. 0, 1153–1155. https://doi.org/10.1039/J29680001153

Blake, P.G., Jackson, G.E., **1969**. High- and low-temperature mechanisms in the thermal decomposition of acetic acid. J. Chem. Soc. B Phys. Org. 0, 94–96. https://doi.org/10.1039/J29690000094

Blake, P.G., Davies, H.H., Jackson, G.E., **197**1. Dehydration mechanisms in the thermal decomposition of gaseous formic acid. J. Chem. Soc. B Phys. Org. 0, 1923–1925. https://doi.org/10.1039/J29710001923

Bounaceur, R., Da Costa, I., Fournet, R., Billaud, F., Battin-Leclerc, F., **2005**. Experimental and modeling study of the oxidation of toluene. Int. J. Chem. Kinet. 37, 25–49. https://doi.org/10.1002/kin.20047

Brezinsky, K., Pecullan, M., Glassman, I., **1998**. Pyrolysis and Oxidation of Phenol. J. Phys. Chem. A 102, 8614–8619. https://doi.org/10.1021/jp982177+

Bruinsma, O.S.L., Geertsma, R.S., Bank, P., Moulijn, J.A., **1988a**. Gas phase pyrolysis of coal-related aromatic compounds in a coiled tube flow reactor: 1. Benzene and derivatives. Fuel 67, 327–333. https://doi.org/10.1016/0016-2361(88)90314-6

Bruinsma, O.S.L., Tromp, P.J.J., de Sauvage Nolting, H.J.J., Moulijn, J.A., **1988b**. Gas phase pyrolysis of coal-related aromatic compounds in a coiled tube flow reactor: 2. Heterocyclic compounds, their benzo and dibenzo derivatives. Fuel 67, 334–340. https://doi.org/10.1016/0016-2361(88)90315-8

Bugler, J., Rodriguez, A., Herbinet, O., Battin-Leclerc, F., Togbé, C., Dayma, G., Dagaut, P., Curran, H.J., **2017**. An experimental and modelling study of n -pentane oxidation in two jet-stirred reactors: The importance of pressure-dependent kinetics and new reaction pathways. Proc. Combust. Inst. 36, 441–448. https://doi.org/10.1016/j.proci.2016.05.048

Burcat, A., Ruscic, B., Chemistry, Tech, T.-I.I. of, **2005**. Third millenium ideal gas and condensed phase thermochemical database for combustion (with update from active thermochemical tables). (No. ANL-05/20). Argonne National Lab. (ANL), Argonne, IL (United States). https://doi.org/10.2172/925269

Burke, S.M., Burke, U., Mc Donagh, R., Mathieu, O., Osorio, I., Keesee, C., Morones, A., Petersen, E.L., Wang, W., DeVerter, T.A., Oehlschlaeger, M.A., Rhodes, B., Hanson, R.K., Davidson, D.F., Weber, B.W., Sung, C.-J., Santner, J., Ju, Y., Haas, F.M., Dryer, F.L., Volkov, E.N., Nilsson, E.J.K., Konnov, A.A., Alrefae, M., Khaled, F., Farooq, A., Dirrenberger, P., Glaude, P.-A., Battin-Leclerc, F., Curran, H.J., **2015**. An experimental and modeling study of propene oxidation. Part 2: Ignition delay time and flame speed measurements. Combust. Flame 162, 296–314. https://doi.org/10.1016/j.combustflame.2014.07.032

Burke, U., Beeckmann, J., Kopp, W.A., Uygun, Y., Olivier, H., Leonhard, K., Pitsch, H., Heufer, K.A., **2016**. A comprehensive experimental and kinetic modeling study of butanone. Combust. Flame 168, 296–309.

Butkovskaya, N.I., Manke, G., Setser, D.W., **1995**. Observation of the Unimolecular Decomposition Pathways of Chemically Activated Acetic Acid by Fourier Transform Infrared Emission Spectrometry. J. Phys. Chem. 99, 11115–11121. https://doi.org/10.1021/j100028a011

Cai, J., Zhang, L., Yang, J., Li, Y., Zhao, L., Qi, F., **2012a**. Experimental and kinetic modeling study of tert-butanol combustion at low pressure. Energy, 2nd International Meeting on Cleaner Combustion (CM0901-Detailed Chemical Models for Cleaner Combustion) 43, 94–102. https://doi.org/10.1016/j.energy.2011.12.024

Cai, J., Zhang, L., Zhang, F., Wang, Z., Cheng, Z., Yuan, W., Qi, F., **2012b**. Experimental and Kinetic Modeling Study of n-Butanol Pyrolysis and Combustion. Energy Fuels 26, 5550–5568. https://doi.org/10.1021/ef3011965

Cai, J., Yuan, W., Ye, L., Cheng, Z., Wang, Y., Zhang, L., Zhang, F., Li, Y., Qi, F., **2013**. Experimental and kinetic modeling study of 2-butanol pyrolysis and combustion. Combust. Flame 160, 1939–1957.

Cai, J., Yuan, W., Ye, L., Cheng, Z., Wang, Y., Dong, W., Zhang, L., Li, Y., Zhang, F., Qi, F., **2014**. Experimental and kinetic modeling study of i-butanol pyrolysis and combustion. Combust. Flame 161, 1955–1971.

Cai, L., Uygun, Y., Togbé, C., Pitsch, H., Olivier, H., Dagaut, P., Sarathy, S.M., **2015**. An experimental and modeling study of n-octanol combustion. Proc. Combust. Inst. 35, 419–427. https://doi.org/10.1016/j.proci.2014.05.088

Cancino, L.R., Fikri, M., Oliveira, A.A.M., Schulz, C., **2010**. Measurement and Chemical Kinetics Modeling of Shock-Induced Ignition of Ethanol−Air Mixtures. Energy Fuels 24, 2830–2840. https://doi.org/10.1021/ef100076w

Cavallotti, C., Pelucchi, M., Frassoldati, A., **2018**. Analysis of acetic acid gas phase reactivity: Rate constant estimation and kinetic simulations. Proc. Combust. Inst. https://doi.org/10.1016/j.proci.2018.06.137

Chaos, M., Kazakov, A., Zhao, Z., Dryer, F.L., **2007**. A high-temperature chemical kinetic model for primary reference fuels. Int. J. Chem. Kinet. 39, 399–414. https://doi.org/10.1002/kin.20253

Cheng, H., Wu, S., Huang, J., Zhang, X., **2017**. Direct evidence from in situ FTIR spectroscopy that o-quinonemethide is a key intermediate during the pyrolysis of guaiacol. Anal. Bioanal. Chem. 409, 2531–2537. https://doi.org/10.1007/s00216-017-0194-0

Cheng, Z., Xing, L., Zeng, M., Dong, W., Zhang, F., Qi, F., Li, Y., **2014**. Experimental and kinetic modeling study of 2,5-dimethylfuran pyrolysis at various pressures. Combust. Flame 161, 2496–2511. https://doi.org/10.1016/j.combustflame.2014.03.022

Chirat, C., 2017. Use of vegetal biomass for biofuels and bioenergy. Competition with the production of bioproducts and materials? Comptes Rendus Phys., Demain l'énergie 18, 462–468. https://doi.org/10.1016/j.crhy.2017.10.002

Chong, C.T., Hochgreb, S., **2011**. Measurements of laminar flame speeds of acetone/methane/air mixtures. Combust. Flame 158, 490–500. https://doi.org/10.1016/j.combustflame.2010.09.019

Christensen, M., Abebe, M.T., Nilsson, E.J.K., Konnov, A.A., **2015**. Kinetics of premixed acetaldehyde + air flames. Proc. Combust. Inst. 35, 499–506. https://doi.org/10.1016/j.proci.2014.06.136

Christensen, M., Konnov, A.A., **2016**. Laminar burning velocity of acetic acid + air flames. Combust. Flame 170, 12–29. https://doi.org/10.1016/j.combustflame.2016.05.007

Christensen, M., Nilsson, E.J.K., Konnov, A.A., **2016**. A Systematically Updated Detailed Kinetic Model for CH_2O and CH_3OH Combustion. Energy Fuels 30, 6709–6726. https://doi.org/10.1021/acs.energyfuels.6b00049

Colket, M.B., Naegeli, D.W., Glassman, I., **1975**. High-temperature pyrolysis of acetaldehyde. Int. J. Chem. Kinet. 7, 223–247. https://doi.org/10.1002/kin.550070207

Cuoci, A., Frassoldati, A., Faravelli, T., Ranzi, E., **2015**. OpenSMOKE++: An object-oriented framework for the numerical modeling of reactive systems with detailed kinetic mechanisms. Comput. Phys. Commun. 192, 237–264. https://doi.org/10.1016/j.cpc.2015.02.014

Custodis, V.B.F., Hemberger, P., Ma, Z., van Bokhoven, J.A., **2014**. Mechanism of Fast Pyrolysis of Lignin: Studying Model Compounds. J. Phys. Chem. B 118, 8524–8531. https://doi.org/10.1021/jp5036579

Dagaut, P., Reuillon, M., Voisin, D., Cathonnet, M., McGuinness, M., Simmie, J.M., **1995**. Acetaldehyde Oxidation in a JSR and Ignition in Shock Waves: Experimental and Comprehensive Kinetic Modeling. Combust. Sci. Technol. 107, 301–316. https://doi.org/10.1080/00102209508907809

Dagaut, P., Mcguinness, M., Simmie, J.M., Cathonnet, M., **1998**. The Ignition and Oxidation of Tetrahydrofuran: Experiments and Kinetic Modeling. Combust. Sci. Technol. 135, 3–29. https://doi.org/10.1080/00102209808924147

Dagaut, P., Sarathy, S.M., Thomson, M.J., **2009**. A chemical kinetic study of n-butanol oxidation at elevated pressure in a jet stirred reactor. Proc. Combust. Inst. 32, 229–237. https://doi.org/10.1016/j.proci.2008.05.005

Davidson, D.F., Ranganath, S.C., Lam, K.-Y., Liaw, M., Hong, Z., H, R.K., **2010**. Ignition Delay Time Measurements of Normal Alkanes and Simple Oxygenates. J. Propuls. Power 26, 280–287. https://doi.org/10.2514/1.44034

Dayma, G., Togbé, C., Dagaut, P., **2011**. Experimental and Detailed Kinetic Modeling Study of Isoamyl Alcohol (Isopentanol) Oxidation in a Jet-Stirred Reactor at Elevated Pressure. Energy Fuels 25, 4986–4998. https://doi.org/10.1021/ef2012112

De Bruycker, R., Tran, L.-S., Carstensen, H.-H., Glaude, P.-A., Monge, F., Alzueta, M.U., Battin-Leclerc, F., Van Geem, K.M., **2017**. Experimental and modeling study of the pyrolysis and combustion of 2-methyl-tetrahydrofuran. Combust. Flame 176, 409–428. https://doi.org/10.1016/j.combustflame.2016.11.017

Decottignies, V., Gasnot, L., Pauwels, J.F., **2002**. A comprehensive chemical mechanism for the oxidation of methylethylketone in flame conditions. Combust. Flame 130, 225–240. https://doi.org/10.1016/S0010-2180(02)00377-2

Dente, M., Ranzi, E., Goossens, A.G., **1979**. Detailed prediction of olefin yields from hydrocarbon pyrolysis through a fundamental simulation model (SPYRO). Comput. Chem. Eng. 3, 61–75. https://doi.org/10.1016/0098-1354(79)80013-7

Dias, V., Vandooren, J., **2011**. Experimental and modeling studies of C_2H_4/O_2/Ar, C_2H_4/methylal/O_2/Ar and C2H4/ethylal/O2/Ar rich flames and the effect of oxygenated additives. Combust. Flame 158, 848–859. https://doi.org/10.1016/j.combustflame.2011.01.015

Dias, V., Duynslaegher, C., Contino, F., Vandooren, J., Jeanmart, H., **2012**. Experimental and modeling study of formaldehyde combustion in flames. Combust. Flame 159, 1814–1820. https://doi.org/10.1016/j.combustflame.2012.01.006

Dias, V., Vandooren, J., Jeanmart, H., **2015**. An experimental and modeling study of the addition of acetone to H2/O2/Ar flames at low pressure. Proc. Combust. Inst. 35, 647–653. https://doi.org/10.1016/j.proci.2014.05.055

Dias, V., Vandooren, J., Jeanmart, H., **2016**. Experimental and Modeling Study of Propanal/H2/O2/Ar Flames at Low Pressure. Combust. Sci. Technol. 188, 556–570. https://doi.org/10.1080/00102202.2016.1145017

Djokic, M.R., Dijkmans, T., Yildiz, G., Prins, W., Van Geem, K.M., **2012**. Quantitative analysis of crude and stabilized bio-oils by comprehensive two-dimensional gas-chromatography. J. Chromatogr. A 1257, 131–140. https://doi.org/10.1016/j.chroma.2012.07.035

Djokic, M.R., Carstensen, H.-H., Van Geem, K.M., Marin, G.B., **2013**. The thermal decomposition of 2,5-dimethylfuran. Proc. Combust. Inst. 34, 251–258. https://doi.org/10.1016/j.proci.2012.05.066

Djokic, M.R., Van Geem, K.M., Heynderickx, G.J., Dekeukeleire, S., Vangaever, S., Battin-Leclerc, F., Bellos, G., Buysschaert, W., Cuenot, B., Faravelli, T., Henneke, M., Jakobi, D., Lenain, P., Munoz, A., Olver, J., Van Goethem, M., Oud, P., 2017. IMPROOF: Integrated Model Guided Process Optimization of Steam Cracking Furnaces, in: Campana, G., Howlett, R.J., Setchi, R., Cimatti, B. (Eds.), Sustainable Design and Manufacturing **2017**. Springer International Publishing, pp. 589–600.

DOE, 2019. Materials Degradation In Biomass-Derived Oils https://www.energy.gov/sites/prod/files/2019/04/f61/Materials%20Degradation%20In%20Biomass-Derived%20Oils_NL0019454.pdf.

Doolan, K.R., Mackie, J.C., Reid, C.R., **1986**. High temperature kinetics of the thermal decomposition of the lower alkanoic acids. Int. J. Chem. Kinet. 18, 575–596. https://doi.org/10.1002/kin.550180508

Eiteneer, B., Yu, C.-L., Goldenberg, M., Frenklach, M., **1998**. Determination of Rate Coefficients for Reactions of Formaldehyde Pyrolysis and Oxidation in the Gas Phase. J. Phys. Chem. A 102, 5196–5205. https://doi.org/10.1021/jp981184v

Eldeeb, M.A., Akih-Kumgeh, B., **2014**. Reactivity Trends in Furan and Alkyl Furan Combustion. Energy Fuels 28, 6618–6626. https://doi.org/10.1021/ef501181z

Eldeeb, M.A., Akih-Kumgeh, B., **2015**. Investigation of 2,5-dimethyl furan and iso-octane ignition. Combust. Flame 162, 2454–2465. https://doi.org/10.1016/j.combustflame.2015.02.013

Elwardany, A., Nasir, E.F., Es-sebbar, Et., Farooq, A., **2015**. Unimolecular decomposition of formic and acetic acids: A shock tube/laser absorption study. Proc. Combust. Inst. 35, 429–436. https://doi.org/10.1016/j.proci.2014.06.141

Evans, M.G., Polanyi, M., **1936**. Further considerations on the thermodynamics of chemical equilibria and reaction rates. Trans. Faraday Soc. 32, 1333–1360. https://doi.org/10.1039/TF9363201333

Fenard, Y., Gil, A., Vanhove, G., Carstensen, H.-H., Van Geem, K.M., Westmoreland, P.R., Herbinet, O., Battin-Leclerc, F., **2018**. A model of tetrahydrofuran low-temperature oxidation based on theoretically calculated rate constants. Combust. Flame 191, 252–269. https://doi.org/10.1016/j.combustflame.2018.01.006

Fikri, M., Cancino, L.R., Hartmann, M., Schulz, C., **2013**. High-pressure shock-tube investigation of the impact of 3-pentanone on the ignition properties of primary reference fuels. Proc. Combust. Inst. 34, 393–400. https://doi.org/10.1016/j.proci.2012.05.101

Frassoldati, A., Cuoci, A., Faravelli, T., Niemann, U., Ranzi, E., Seiser, R., Seshadri, K., **2010.** An experimental and kinetic modeling study of n-propanol and iso-propanol combustion. Combust. Flame 157, 2–16. https://doi.org/10.1016/j.combustflame.2009.09.002

Friderichsen, A.V., Shin, E.-J., Evans, R.J., Nimlos, M.R., Dayton, D.C., Ellison, G.B., **2001**. The pyrolysis of anisole ($C_6H_5OCH_3$) using a hyperthermal nozzle. Fuel 80, 1747–1755. https://doi.org/10.1016/S0016-2361(01)00059-X

Friese, P., Simmie, J.M., Olzmann, M., **2013**. The reaction of 2,5-dimethylfuran with hydrogen atoms – An experimental and theoretical study. Proc. Combust. Inst. 34, 233–239. https://doi.org/10.1016/j.proci.2012.05.075

Glarborg, P., Alzueta, M.U., Kjærgaard, K., Dam-Johansen, K., **2003**. Oxidation of formaldehyde and its interaction with nitric oxide in a flow reactor. Combust. Flame 132, 629–638. https://doi.org/10.1016/S0010-2180(02)00535-7

Gong, J., Zhang, S., Cheng, Y., Huang, Z., Tang, C., Zhang, J., **2015**. A comparative study of n-propanol, propanal, acetone, and propane combustion in laminar flames. Proc. Combust. Inst. 35, 795–801. https://doi.org/10.1016/j.proci.2014.05.066

Grana, R., Frassoldati, A., Faravelli, T., Niemann, U., Ranzi, E., Seiser, R., Cattolica, R., Seshadri, K., **2010**. An experimental and kinetic modeling study of combustion of isomers of butanol. Combust. Flame 157, 2137–2154. https://doi.org/10.1016/j.combustflame.2010.05.009

Granata, S., Faravelli, T., Ranzi, E., **2003**. A wide range kinetic modeling study of the pyrolysis and combustion of naphthenes. Combust. Flame 132, 533–544. https://doi.org/10.1016/S0010-2180(02)00465-0

Grela, M.A., Amorebieta, V.T., Colussi, A.J., **1985**. Very low pressure pyrolysis of furan, 2-methylfuran and 2,5-dimethylfuran. The stability of the furan ring. J. Phys. Chem. 89, 38–41. https://doi.org/10.1021/j100247a011

Grela, M., Colussi, A., **1986**. Kinetics and Mechanism of the Thermal-Decomposition of Unsaturated Aldehydes - Benzaldehyde, 2-Butenal, and 2-Furaldehyde. J. Phys. Chem. 90, 434–437. https://doi.org/10.1021/j100275a016

Griffiths, J.F., Hasko, S.M., **1984**. Two-Stage Ignitions During Rapid Compression: Spontaneous Combustion in Lean Fuel-Air Mixtures. Proc. R. Soc. Lond. Math. Phys. Eng. Sci. 393, 371–395. https://doi.org/10.1098/rspa.1984.0063

Guedes, R.E., Luna, A.S., Torres, A.R., **2018**. Operating parameters for bio-oil production in biomass pyrolysis: A review. J. Anal. Appl. Pyrolysis 129, 134–149. https://doi.org/10.1016/j.jaap.2017.11.019

Guibet, J.-C., 1997. Fuels and Engines. Tome 1. Editions TECHNIP.

Gupte, K.S., Kiefer, J.H., Tranter, R.S., Klippenstein, S.J., Harding, L.B., **2007**. Decomposition of acetaldehyde: Experiment and detailed theory. Proc. Combust. Inst. 31, 167–174. https://doi.org/10.1016/j.proci.2006.08.048

Hansen, N., Harper, M.R., Green, W.H., **2011**. High-temperature oxidation chemistry of n-butanol – experiments in low-pressure premixed flames and detailed kinetic modeling. Phys. Chem. Chem. Phys. 13, 20262–20274. https://doi.org/10.1039/C1CP21663E

Hansen, N., Merchant, S.S., Harper, M.R., Green, W.H., **2013**. The predictive capability of an automatically generated combustion chemistry mechanism: Chemical structures of premixed iso-butanol flames. Combust. Flame 160, 2343–2351. https://doi.org/10.1016/j.combustflame.2013.05.013

Harper, M.R., Van Geem, K.M., Pyl, S.P., Marin, G.B., Green, W.H., **2011**. Comprehensive reaction mechanism for n-butanol pyrolysis and combustion. Combust. Flame 158, 16–41. https://doi.org/10.1016/j.combustflame.2010.06.002

He, Y.Z., Mallard, W.G., Tsang, W., **1988**. Kinetics of hydrogen and hydroxyl radical attack on phenol at high temperatures. J. Phys. Chem. 92, 2196–2201. https://doi.org/10.1021/j100319a023

Herbinet, O., Battin-Leclerc, F., Bax, S., Le Gall, H., Glaude, P.-A., Fournet, R., Zhou, Z., Deng, L., Guo, H., Xie, M., Qi, F., **2011**. Detailed product analysis during the low temperature oxidation of n-butane. Phys. Chem. Chem. Phys. PCCP 13, 296–308. https://doi.org/10.1039/c0cp00539h

Herbinet, O., Rodriguez, A., Husson, B., Battin-Leclerc, F., Wang, Z., Cheng, Z., Qi, F., **2016**. Study of the Formation of the First Aromatic Rings in the Pyrolysis of Cyclopentene. J. Phys. Chem. A 120, 668–682. https://doi.org/10.1021/acs.jpca.5b09203

Herrmann, F., Jochim, B., Oßwald, P., Cai, L., Pitsch, H., Kohse-Höinghaus, K., **2014**. Experimental and numerical low-temperature oxidation study of ethanol and dimethyl ether. Combust. Flame 161, 384–397. https://doi.org/10.1016/j.combustflame.2013.09.014

Hidaka, Y., Taniguchi, T., Kamesawa, T., Masaoka, H., Inami, K., Kawano, H., **1993a**. High temperature pyrolysis of formaldehyde in shock waves. Int. J. Chem. Kinet. 25, 305–322. https://doi.org/10.1002/kin.550250409

Hidaka, Y., Taniguchi, T., Tanaka, H., Kamesawa, T., Inami, K., Kawano, H., **1993b**. Shock-tube study of CH2O pyrolysis and oxidation. Combust. Flame 92, 365–376. https://doi.org/10.1016/0010-2180(93)90149-W

Hong, X., Zhang, L., Zhang, T., Qi, F., **2009**. An Experimental and Theoretical Study of Pyrrole Pyrolysis with Tunable Synchrotron VUV Photoionization and Molecular-Beam Mass Spectrometry. J. Phys. Chem. A 113, 5397–5405. https://doi.org/10.1021/jp9002966

Horn, C., Roy, K., Frank, P., Just, T., **1998**. Shock-tube study on the high-temperature pyrolysis of phenol. Symp. Int. Combust., Twenty-Seventh Sysposium (International) on Combustion Volume One 27, 321–328. https://doi.org/10.1016/S0082-0784(98)80419-0

Houser, T.J., McCarville, M.E., Biftu, T., **1980**. Kinetics of the thermal decomposition of pyridine in a flow system. Int. J. Chem. Kinet. 12, 555–568. https://doi.org/10.1002/kin.550120806

Houser, T.J., McCarville, M.E., Houser, B.D., **1982**. Kinetics of Oxidation of Pyridine in a Flow System. Combust. Sci. Technol. 27, 183–191. https://doi.org/10.1080/00102208208946987

Hurd, C.D., Bennett, C.W., **1929.** The pyrolysis of benzaldehyde and of benzyl benzoate. J. Am. Chem. Soc. 51, 1197–1201. https://doi.org/10.1021/ja01379a030

IEA, 2018a. TPED in the world, WEO 2018 https://www.iea.org/weo/weo2018/secure/.

IEA, 2018b. WEO2018-Presentation https://www.iea.org/media/presentations/WEO2018-Presentation.pdf.

IEA, 2018c. CO2 Emissions from Fuel Combustion 2018 Highlights.

IEA, 2018d. Air pollution emissions by sector and scenario, 2015 and 2040 https://www.iea.org/weo2018/themes/.

IEA, 2019. Statistics | World - Total Primary Energy Supply (TPES) by source (chart) https://www.iea.org//statistics/?country=WORLD & year=2016 & category=Energy%20supply & indicator=TPESbySource & mode=chart & dataTable=BALANCES.

IEA, FAO, 2017. How2Guide for Bioenergy.

Ikeda, E., Nicholls, P., Mackie, J.C., **2000**. A kinetic study of the oxidation of pyridine. Proc. Combust. Inst. 28, 1709–1716. https://doi.org/10.1016/S0082-0784(00)80571-8

Jouzdani, S., Zhou, A., Akih-Kumgeh, B., **2017**. Propanol isomers: Investigation of ignition and pyrolysis time scales. Combust. Flame 176, 229–244. https://doi.org/10.1016/j.combustflame.2016.09.022

Kaiser, E.W., Westbrook, C.K., Pitz, W.J., **1986**. Acetaldehyde oxidation in the negative temperature coefficient regime: Experimental and modeling results. Int. J. Chem. Kinet. 18, 655–688. https://doi.org/10.1002/kin.550180606

Kasper, T., Lucassen, A., Jasper, A.W., Li, W., Westmoreland, P.R., Kohse-Höinghaus, K., Yang, B., Wang, J., Cool, T.A., Hansen, N., **2011**. Identification of Tetrahydrofuran Reaction Pathways in Premixed Flames. Z. Für Phys. Chem. 225, 1237–1270. https://doi.org/10.1524/zpch.2011.0163

Kern, R.D., Singh, H.J., Xie, K., **1990**. A shock tube study of the thermal decompositions of acetaldehyde and ethylene oxide. AIP Conf. Proc. 208, 487–492. https://doi.org/10.1063/1.39379

Kiefer, J.H., Zhang, Q., Kern, R.D., Yao, J., Jursic, B., **1997**. Pyrolyses of Aromatic Azines: Pyrazine, Pyrimidine, and Pyridine. J. Phys. Chem. A 101, 7061–7073. https://doi.org/10.1021/jp970211z

Klute, C.H., Walters, W.D., **1946**. The Thermal Decomposition of Tetrahydrofuran. J. Am. Chem. Soc. 68, 506–511. https://doi.org/10.1021/ja01207a045

Laidler, K.J., Liu, M.T.H., **1967**. The Mechanism of the Acetaldehyde Pyrolysis. Proc. R. Soc. Lond. Math. Phys. Eng. Sci. 297, 365–375. https://doi.org/10.1098/rspa.1967.0073

Lam, K.-Y., Ren, W., Hong, Z., Davidson, D.F., Hanson, R.K., **2012**. Shock tube measurements of 3-pentanone pyrolysis and oxidation. Combust. Flame 159, 3251–3263. https://doi.org/10.1016/j.combustflame.2012.06.012

Ledesma, E.B., Marsh, N.D., Sandrowitz, A.K., Wornat, M.J., **2002a**. Global Kinetic Rate Parameters for the Formation of Polycyclic Aromatic Hydrocarbons from the Pyrolyis of Catechol, A Model Compound Representative of Solid Fuel Moieties. Energy Fuels 16, 1331–1336. https://doi.org/10.1021/ef010261+

Ledesma, E.B., Marsh, N.D., Sandrowitz, A.K., Wornat, M.J., **2002b**. An experimental study on the thermal decomposition of catechol. Proc. Combust. Inst. 29, 2299–2306. https://doi.org/10.1016/S1540-7489(02)80280-2

Lefkowitz, J.K., Heyne, J.S., Won, S.H., Dooley, S., Kim, H.H., Haas, F.M., Jahangirian, S., Dryer, F.L., Ju, Y., **2012**. A chemical kinetic study of tertiary-butanol in a flow reactor and a counterflow diffusion flame. Combust. Flame 159, 968–978. https://doi.org/10.1016/j.combustflame.2011.10.004

Leplat, N., Vandooren, J., **2010**. Experimental Investigation and Numerical Simulation of the Structure of CH3CHO/O2/Ar Flames at Different Equivalence Ratios. Combust. Sci. Technol. 182, 436–448. https://doi.org/10.1080/00102200903462813

Leplat, N., Vandooren, J., **2012**. Numerical and experimental study of the combustion of acetic acid in laminar premixed flames. Combust. Flame 159, 493–499. https://doi.org/10.1016/j.combustflame.2011.08.007

Li, G., Li, L., Shi, L., Jin, L., Tang, Z., Fan, H., Hu, H., **2014**. Experimental and Theoretical Study on the Pyrolysis Mechanism of Three Coal-Based Model Compounds. Energy Fuels 28, 980–986. https://doi.org/10.1021/ef402273t

Li, Q., Fu, J., Wu, X., Tang, C., Huang, Z., **2012**. Laminar Flame Speeds of DMF/Iso-octane-Air-N2/CO2 Mixtures. Energy Fuels 26, 917–925. https://doi.org/10.1021/ef201638w

Lifshitz, A., Bidani, M., Bidani, S., **1986a**. Thermal reactions of cyclic ethers at high temperatures. Part 3. Pyrolysis of tetrahydrofuran behind reflected shocks. J. Phys. Chem. 90, 3422–3429. https://doi.org/10.1021/j100406a024

Lifshitz, A., Bidani, M., Bidani, S., **1986b**. Thermal reactions of cyclic ethers at high temperatures. III. Pyrolysis of furan behind reflected shocks. J. Phys. Chem. 90, 5373–5377. https://doi.org/10.1021/j100412a096

Lifshitz, A., Bidani, M., Agranat, A., Suslensky, A., **1987**. Thermal reactions of pyrrolidine at elevated temperatures: studies with a single-pulse shock tube. J. Phys. Chem. 91, 6043–6048. https://doi.org/10.1021/j100307a045

Lifshitz, A., Tamburu, C., Suslensky, A., **1989**. Isomerization and decomposition of pyrrole at elevated temperatures: studies with a single-pulse shock tube. J. Phys. Chem. 93, 5802–5808. https://doi.org/10.1021/j100352a030

Lifshitz, A., Tamburu, C., Shashua, R., **1997**. Decomposition of 2-Methylfuran. Experimental and Modeling Study. J. Phys. Chem. A 101, 1018–1029. https://doi.org/10.1021/jp962646c

Lifshitz, A., Tamburu, C., Shashua, R., **1998**. Thermal Decomposition of 2,5-Dimethylfuran. Experimental Results and Computer Modeling. J. Phys. Chem. A 102, 10655–10670. https://doi.org/10.1021/jp982772b

Lin, C.-Y., Lin, M.C., **1986**. Thermal decomposition of methyl phenyl ether in shock waves: the kinetics of phenoxy radical reactions. J. Phys. Chem. 90, 425–431. https://doi.org/10.1021/j100275a014

Liu, D., Togbé, C., Tran, L.-S., Felsmann, D., Oßwald, P., Nau, P., Koppmann, J., Lackner, A., Glaude, P.-A., Sirjean, B., Fournet, R., Battin-Leclerc, F., Kohse-Höinghaus, K., **2014**. Combustion chemistry and flame structure of furan group biofuels using molecular-beam mass spectrometry and gas chromatography – Part I: Furan. Combust. Flame, Special Issue on Alternative Fuels 161, 748–765. https://doi.org/10.1016/j.combustflame.2013.05.028

Liu, Z., Phillips, J.B., **1991**. Comprehensive Two-Dimensional Gas Chromatography using an On-Column Thermal Modulator Interface. J. Chromatogr. Sci. 29, 227–231. https://doi.org/10.1093/chromsci/29.6.227

Lomnicki, S., Truong, H., Dellinger, B., **2008**. Mechanisms of product formation from the pyrolytic thermal degradation of catechol. Chemosphere 73, 629–633. https://doi.org/10.1016/j.chemosphere.2008.03.064

Lovell, A.B., Brezinsky, K., Glassman, I., **1989**. The gas phase pyrolysis of phenol. Int. J. Chem. Kinet. 21, 547–560. https://doi.org/10.1002/kin.550210706

Lubrano Lavadera, M., Song, Y., Sabia, P., Herbinet, O., Pelucchi, M., Stagni, A., Faravelli, T., Battin-Leclerc, F., de Joannon, M., **2018**. Oscillatory Behavior in Methane

Combustion: Influence of the Operating Parameters. Energy Fuels 32, 10088–10099. https://doi.org/10.1021/acs.energyfuels.8b00967

Lucassen, A., Wang, Z., Zhang, L., Zhang, F., Yuan, W., Wang, Y., Qi, F., Kohse-Höinghaus, K., **2013**. An experimental and theoretical study of pyrrolidine pyrolysis at low pressure. Proc. Combust. Inst. 34, 641–648. https://doi.org/10.1016/j.proci.2012.05.001

Lumbreras, M., Alzueta, M.U., Millera, A., Bilbao, R., **2001**. A Study of Pyrrole Oxidation Under Flow Reactor Conditions. Combust. Sci. Technol. 172, 123–139. https://doi.org/10.1080/00102200108945397

Luo, M., Liu, D., **2017**. On the effects of hydrogen addition in premixed formaldehyde flames. Int. J. Hydrog. Energy, The 7th International Conference on Hydrogen Production (ICH2P-2016), 8-11 May 2016, Hangzhou, China 42, 3824–3832. https://doi.org/10.1016/j.ijhydene.2016.07.046

Ma, X., Jiang, C., Xu, H., Ding, H., Shuai, S., **2014**. Laminar burning characteristics of 2-methylfuran and isooctane blend fuels. Fuel 116, 281–291. https://doi.org/10.1016/j.fuel.2013.08.018

Mackie, J.C., Doolan, K.R., **1984**. High-temperature kinetics of thermal decomposition of acetic acid and its products. Int. J. Chem. Kinet. 16, 525–541. https://doi.org/10.1002/kin.550160504

Mackie, J.C., Doolan, K.R., Nelson, P.F., **1989**. Kinetics of the thermal decomposition of methoxybenzene (anisole). J. Phys. Chem. 93, 664–670. https://doi.org/10.1021/j100339a033

Mackie, J.C., Colket, M.B., Nelson, P.F., **1990**. Shock tube pyrolysis of pyridine. J. Phys. Chem. 94, 4099–4106. https://doi.org/10.1021/j100373a040

Mackie, J.C., Colket, M., Nelson, P., Esler, M., **1991**. Shock-Tube Pyrolysis of Pyrrole and Kinetic Modeling. Int. J. Chem. Kinet. 23, 733–760. https://doi.org/10.1002/kin.550230807

MacNamara, J.P., Simmie, J.M., **2003**. The high temperature oxidation of pyrrole and pyridine; ignition delay times measured behind reflected shock waves. Combust. Flame 133, 231–239. https://doi.org/10.1016/S0010-2180(03)00002-6

Manion, J.A., Louw, R., **1989**. Rates, products, and mechanisms in the gas-phase hydrogenolysis of phenol between 922 and 1175 K. J. Phys. Chem. 93, 3563–3574. https://doi.org/10.1021/j100346a040

Marrodán, L., Song, Y., Lubrano Lavadera, M., Herbinet, O., de Joannon, M., Ju, Y., Alzueta, M.U., Battin-Leclerc, F., **2019**. Effects of Bath Gas and NOx Addition on n-Pentane Low-Temperature Oxidation in a Jet-Stirred Reactor. Energy Fuels 33, 5655–5663. https://doi.org/10.1021/acs.energyfuels.9b00536

Marsh, N.D., Ledesma, E.B., Sandrowitz, A.K., Wornat, M.J., **2004**. Yields of Polycyclic Aromatic Hydrocarbons from the Pyrolysis of Catechol [ortho-Dihydroxybenzene]: Temperature and Residence Time Effects. Energy Fuels 18, 209–217. https://doi.org/10.1021/ef010263u

Matras, D., Villermaux, J., 1973. Un réacteur continu parfaitement agité par jets gazeux pour l'étude cinétique de réactions chimiques rapides. Chem. Eng. Sci. 28, 129–137. https://doi.org/10.1016/0009-2509(73)85093-6

McDonald, G., Lodge, N.M., Walters, W.D., **1951**. The Effect of Added Gases upon the Thermal Decomposition of Tetrahydrofuran1. J. Am. Chem. Soc. 73, 1757–1760. https://doi.org/10.1021/ja01148a094

McEnally, C.S., Pfefferle, L.D., **2005**. Fuel decomposition and hydrocarbon growth processes for oxygenated hydrocarbons: butyl alcohols. Proc. Combust. Inst. 30, 1363–1370. https://doi.org/10.1016/j.proci.2004.07.033

Memon, H.U.R., Bartle, K.D., Taylor, J.M., Williams, A., **2000**. The shock tube pyrolysis of pyridine. Int. J. Energy Res. 24, 1141–1159. https://doi.org/10.1002/1099-114X(20001025)24:13<1141::AID-ER653>3.0.CO;2-S

Mendes, J., Zhou, C.-W., Curran, H.J., **2014**. Theoretical Chemical Kinetic Study of the H-Atom Abstraction Reactions from Aldehydes and Acids by Ḣ Atoms and ȮH, HȮ2,

and ĊH3 Radicals. J. Phys. Chem. A 118, 12089–12104. https://doi.org/10.1021/jp5072814

Merchant, S.S., Zanoelo, E.F., Speth, R.L., Harper, M.R., Van Geem, K.M., Green, W.H., **2013**. Combustion and pyrolysis of iso-butanol: Experimental and chemical kinetic modeling study. Combust. Flame 160, 1907–1929. https://doi.org/10.1016/j.combustflame.2013.04.023

Metcalfe, W.K., Burke, S.M., Ahmed, S.S., Curran, H.J., **2013**. A hierarchical and comparative kinetic modeling study of C1− C2 hydrocarbon and oxygenated fuels. Int. J. Chem. Kinet. 45, 638–675.

Minwegen, H., Burke, U., Heufer, K.A., **2017**. An experimental and theoretical comparison of C3–C5 linear ketones. Proc. Combust. Inst. 36, 561–568. https://doi.org/10.1016/j.proci.2016.05.050

Mittal, G., Burke, S.M., Davies, V.A., Parajuli, B., Metcalfe, W.K., Curran, H.J., **2014**. Autoignition of ethanol in a rapid compression machine. Combust. Flame 161, 1164–1171. https://doi.org/10.1016/j.combustflame.2013.11.005

Molera, M.J., Couto, A., Garcia-Dominguez, J.A., **1988**. Gas phase oxidation of tetrahydrofuran. Int. J. Chem. Kinet. 20, 673–685. https://doi.org/10.1002/kin.550200902

Moshammer, K., Vranckx, S., Chakravarty, H.K., Parab, P., Fernandes, R.X., Kohse-Höinghaus, K., **2013**. An experimental and kinetic modeling study of 2-methyltetrahydrofuran flames. Combust. Flame 160, 2729–2743. https://doi.org/10.1016/j.combustflame.2013.07.006

Muller, C., Michel, V., Scacchi, G., Côme, G.M., **1995**. THERGAS: a computer program for the evaluation of thermochemical data of molecules and free radicals in the gas phase. J. Chim. Phys. Phys.-Chim. Biol. 92, 1154–1178.

Nativel, D., Pelucchi, M., Frassoldati, A., Comandini, A., Cuoci, A., Ranzi, E., Chaumeix, N., Faravelli, T., **2016**. Laminar flame speeds of pentanol isomers: An experimental and modeling study. Combust. Flame 166, 1–18. https://doi.org/10.1016/j.combustflame.2015.11.012

Negahdar, L., Gonzalez-Quiroga, A., Otyuskaya, D., Toraman, H.E., Liu, L., Jastrzebski, J.T.B.H., Van Geem, Kevin.M., Marin, G.B., Thybaut, J.W., Weckhuysen, B.M., **2016**. Characterization and Comparison of Fast Pyrolysis Bio-oils from Pinewood, Rapeseed Cake, and Wheat Straw Using 13C NMR and Comprehensive GC × GC. ACS Sustain. Chem. Eng. 4, 4974–4985. https://doi.org/10.1021/acssuschemeng.6b01329

Nilsson, E.J.K., de Goey, L.P.H., Konnov, A.A., **2013**. Laminar burning velocities of acetone in air at room and elevated temperatures. Fuel 105, 496–502. https://doi.org/10.1016/j.fuel.2012.07.047

Nowakowska, M., Herbinet, O., Dufour, A., Glaude, P.-A., **2014**. Detailed kinetic study of anisole pyrolysis and oxidation to understand tar formation during biomass combustion and gasification. Combust. Flame 161, 1474–1488. https://doi.org/10.1016/j.combustflame.2013.11.024

Nowakowska, M., Herbinet, O., Dufour, A., Glaude, P.A., **2018**. Kinetic Study of the Pyrolysis and Oxidation of Guaiacol. J. Phys. Chem. A 122, 7894–7909. https://doi.org/10.1021/acs.jpca.8b06301

Oasmaa, A., Czernik, S., **1999**. Fuel Oil Quality of Biomass Pyrolysis OilsState of the Art for the End Users. Energy Fuels 13, 914–921. https://doi.org/10.1021/ef980272b

Onay, O., Kockar, O.M., **2003**. Slow, fast and flash pyrolysis of rapeseed. Renew. Energy 28, 2417–2433. https://doi.org/10.1016/S0960-1481(03)00137-X

Organ, P.P., Mackie, J.C., **1991**. Kinetics of pyrolysis of furan. J. Chem. Soc. Faraday Trans. 87, 815–823. https://doi.org/10.1039/FT9918700815

Oßwald, P., Güldenberg, H., Kohse-Höinghaus, K., Yang, B., Yuan, T., Qi, F., **2011**. Combustion of butanol isomers – A detailed molecular beam mass spectrometry investigation of their flame chemistry. Combust. Flame 158, 2–15. https://doi.org/10.1016/j.combustflame.2010.06.003

Pecullan, M., Brezinsky, K., Glassman, I., **1997**. Pyrolysis and Oxidation of Anisole near 1000 K. J. Phys. Chem. A 101, 3305–3316. https://doi.org/10.1021/jp963203b

Pejpichestakul, W., Ranzi, E., Pelucchi, M., Frassoldati, A., Cuoci, A., Parente, A., Faravelli, T., **2018**. Examination of a soot model in premixed laminar flames at fuel-rich conditions. Proc. Combust. Inst. https://doi.org/10.1016/j.proci.2018.06.104

Pelucchi, M., Somers, K.P., Yasunaga, K., Burke, U., Frassoldati, A., Ranzi, E., Curran, H.J., Faravelli, T., **2015**. An experimental and kinetic modeling study of the pyrolysis and oxidation of n-C3C5 aldehydes in shock tubes. Combust. Flame 162, 265–286. https://doi.org/10.1016/j.combustflame.2014.07.027

Pelucchi, M., Cavallotti, C., Ranzi, E., Frassoldati, A., Faravelli, T., **2016**. Relative Reactivity of Oxygenated Fuels: Alcohols, Aldehydes, Ketones, and Methyl Esters. Energy Fuels 30, 8665–8679. https://doi.org/10.1021/acs.energyfuels.6b01171

Pelucchi, M., Bissoli, M., Rizzo, C., Zhang, Y., Somers, K., Frassoldati, A., Curran, H.J., Faravelli, T., **2017a**. A Kinetic Modelling Study of Alcohols Operating Regimes in a HCCI Engine. SAE Int. J. Engines 10. https://doi.org/10.4271/2017-24-0077

Pelucchi, M., Ranzi, E., Frassoldati, A., Faravelli, T., **2017b**. Alkyl radicals rule the low temperature oxidation of long chain aldehydes. Proc. Combust. Inst. 36, 393–401. https://doi.org/10.1016/j.proci.2016.05.051

Pelucchi, M., Cavallotti, C., Cuoci, A., Faravelli, T., Frassoldati, A., Ranzi, E., **2019**. Detailed kinetics of substituted phenolic species in pyrolysis bio-oils. React. Chem. Eng. 4, 490–506. https://doi.org/10.1039/C8RE00198G

Persson, M., Jönsson, O., Wellinger, A., **2006**. Biogas Upgrading to Vehicle Fuel Standards and Grid Injection IEA Bionenergy.

Pichon, S., Black, G., Chaumeix, N., Yahyaoui, M., Simmie, J.M., Curran, H.J., Donohue, R., **2009**. The combustion chemistry of a fuel tracer: Measured flame speeds and ignition delays and a detailed chemical kinetic model for the oxidation of acetone. Combust. Flame 156, 494–504. https://doi.org/10.1016/j.combustflame.2008.10.001

Platonov, V.V., Proskuryakov, V.A., Ryl'tsova, S.V., Popova, Y.N., **2001**. Homogeneous Pyrolysis of Anisole. Russ. J. Appl. Chem. 74, 1047–1052. https://doi.org/10.1023/A:1013076330586

Pütün, A.E., Önal, E., Uzun, B.B., Özbay, N., **2007**. Comparison between the "slow" and "fast" pyrolysis of tobacco residue. Ind. Crops Prod. 26, 307–314. https://doi.org/10.1016/j.indcrop.2007.03.011

Ranzi, E., Dente, M., Faravelli, T., Pennati, G., **1993**. Prediction of Kinetic Parameters for Hydrogen Abstraction Reactions. Combust. Sci. Technol. 95, 1–50. https://doi.org/10.1080/00102209408935325

Ranzi, E., Faravelli, T., Gaffuri, P., Garavaglia, E., Goldaniga, A., **1997**. Primary Pyrolysis and Oxidation Reactions of Linear and Branched Alkanes. Ind. Eng. Chem. Res. 36, 3336–3344. https://doi.org/10.1021/ie960603c

Ranzi, E., Dente, M., Goldaniga, A., Bozzano, G., Faravelli, T., **2001**. Lumping procedures in detailed kinetic modeling of gasification, pyrolysis, partial oxidation and combustion of hydrocarbon mixtures. Prog. Energy Combust. Sci. 27, 99–139. https://doi.org/10.1016/S0360-1285(00)00013-7

Ranzi, E., Frassoldati, A., Granata, S., Faravelli, T., **2005**. Wide-Range Kinetic Modeling Study of the Pyrolysis, Partial Oxidation, and Combustion of Heavy n-Alkanes. Ind. Eng. Chem. Res. 44, 5170–5183. https://doi.org/10.1021/ie049318g

Ranzi, E., Frassoldati, A., Grana, R., Cuoci, A., Faravelli, T., Kelley, A.P., Law, C.K., **2012**. Hierarchical and comparative kinetic modeling of laminar flame speeds of hydrocarbon and oxygenated fuels. Prog. Energy Combust. Sci. 38, 468–501. https://doi.org/10.1016/j.pecs.2012.03.004

Ranzi, E., Frassoldati, A., Stagni, A., Pelucchi, M., Cuoci, A., Faravelli, T., **2014**. Reduced Kinetic Schemes of Complex Reaction Systems: Fossil and Biomass-Derived Transportation Fuels. Int. J. Chem. Kinet. 46, 512–542. https://doi.org/10.1002/kin.20867

Ranzi, E., Cavallotti, C., Cuoci, A., Frassoldati, A., Pelucchi, M., Faravelli, T., **2015**. New reaction classes in the kinetic modeling of low temperature oxidation of n-alkanes. Combust. Flame 162, 1679–1691. https://doi.org/10.1016/j.combustflame.2014.11.030

Ray, D.J.M., Waddington, D.J., **1973**. Gas phase oxidation of alkenes—Part II. The oxidation of 2-methylbutene-2 and 2,3-dimethylbutene-2. Combust. Flame 20, 327–334. https://doi.org/10.1016/0010-2180(73)90024-2

Rodriguez, A., 2016. Étude de la combustion de composés organiques grâce au couplage d'un réacteur parfaitement agité avec des méthodes analytiques spectroscopiques et spectrométriques : application à la détection des hydroperoxydes (PhD). Université de Lorraine.

Rodriguez, A., Herbinet, O., Battin-Leclerc, F., **2017**. A study of the low-temperature oxidation of a long chain aldehyde: n-hexanal. Proc. Combust. Inst. 36, 365–372. https://doi.org/10.1016/j.proci.2016.05.047

Ruscic, B., 2014. Uncertainty quantification in thermochemistry, benchmarking electronic structure computations, and Active Thermochemical Tables. Int. J. Quantum Chem. 114, 1097–1101. https://doi.org/10.1002/qua.24605

Saggese, C., Frassoldati, A., Cuoci, A., Faravelli, T., Ranzi, E., **2013**. A wide range kinetic modeling study of pyrolysis and oxidation of benzene. Combust. Flame 160, 1168–1190. https://doi.org/10.1016/j.combustflame.2013.02.013

Saito, K., Kakumoto, T., Kuroda, H., Torii, S., Imamura, A., **1984**. Thermal unimolecular decomposition of formic acid. J. Chem. Phys. 80, 4989–4996. https://doi.org/10.1063/1.446521

Saito, K., Shiose, T., Takahashi, O., Hidaka, Y., Aiba, F., Tabayashi, K., **2005**. Unimolecular Decomposition of Formic Acid in the Gas PhaseOn the Ratio of the Competing Reaction Channels. J. Phys. Chem. A 109, 5352–5357. https://doi.org/10.1021/jp045072h

Sarathy, S.M., Thomson, M.J., Togbé, C., Dagaut, P., Halter, F., Mounaim-Rousselle, C., **2009**. An experimental and kinetic modeling study of n-butanol combustion. Combust. Flame 156, 852–864. https://doi.org/10.1016/j.combustflame.2008.11.019

Sarathy, S.M., Park, S., Weber, B.W., Wang, W., Veloo, P.S., Davis, A.C., Togbe, C., Westbrook, C.K., Park, O., Dayma, G., Luo, Z., Oehlschlaeger, M.A., Egolfopoulos, F.N., Lu, T., Pitz, W.J., Sung, C.-J., Dagaut, P., **2013**. A comprehensive experimental and modeling study of iso-pentanol combustion. Combust. Flame 160, 2712–2728. https://doi.org/10.1016/j.combustflame.2013.06.022

Sarathy, S.M., Oßwald, P., Hansen, N., Kohse-Höinghaus, K., **2014**. Alcohol combustion chemistry. Prog. Energy Combust. Sci. 44, 40–102. https://doi.org/10.1016/j.pecs.2014.04.003

Sato, K., Hidaka, Y., **2000**. Shock-tube and modeling study of acetone pyrolysis and oxidation. Combust. Flame 122, 291–311. https://doi.org/10.1016/S0010-2180(00)00121-8

Scheer, A.M., Mukarakate, C., Robichaud, D.J., Ellison, G.B., Nimlos, M.R., **2010**. Radical Chemistry in the Thermal Decomposition of Anisole and Deuterated Anisoles: An Investigation of Aromatic Growth. J. Phys. Chem. A 114, 9043–9056. https://doi.org/10.1021/jp102046p

Schlosberg, R.H., Szajowski, P.F., Dupre, G.D., Danik, J.A., Kurs, A., Ashe, T.R., Olmstead, W.Im., **1983**. Pyrolysis studies of organic oxygenates. Fuel 62, 690–694. https://doi.org/10.1016/0016-2361(83)90308-3

Seeley, J.V., Seeley, S.K., **2013**. Multidimensional Gas Chromatography: Fundamental Advances and New Applications. Anal. Chem. 85, 557–578. https://doi.org/10.1021/ac303195u

Serinyel, Z., Black, G., Curran, H.J., Simmie, J.M., **2010a**. A Shock Tube and Chemical Kinetic Modeling Study of Methy Ethyl Ketone Oxidation. Combust. Sci. Technol. 182, 574–587. https://doi.org/10.1080/00102200903466129

Serinyel, Z., Chaumeix, N., Black, G., Simmie, J.M., Curran, H.J., **2010b**. Experimental and Chemical Kinetic Modeling Study of 3-Pentanone Oxidation. J. Phys. Chem. A 114, 12176–12186. https://doi.org/10.1021/jp107167f

Serinyel, Z., Togbé, C., Dayma, G., Dagaut, P., **2014**. An experimental and modeling study of 2-methyl-1-butanol oxidation in a jet-stirred reactor. Combust. Flame 161, 3003–3013. https://doi.org/10.1016/j.combustflame.2014.06.004

Serinyel, Z., Togbé, C., Zaras, A., Dayma, G., Dagaut, P., **2015**. Kinetics of oxidation of cyclohexanone in a jet-stirred reactor: Experimental and modeling. Proc. Combust. Inst. 35, 507–514. https://doi.org/10.1016/j.proci.2014.06.150

Shin, E.-J., R. Hajaligol, M., Rasouli, F., **2004**. Heterogeneous cracking of catechol under partially oxidative conditions. Fuel, Fundamental Mechanisms of Biomass, Pyrolysis and Oxidation 83, 1445–1453. https://doi.org/10.1016/j.fuel.2003.11.016

Shvartsberg, V.M., Bunev, V.A., Babkin, V.S., **2015**. Numerical study of the combustion chemistry of fuel-rich mixtures of formaldehyde and air. Combust. Explos. Shock Waves 51, 623–630. https://doi.org/10.1134/S0010508215060015

Sirjean, B., Fournet, R., Glaude, P.-A., Battin-Leclerc, F., Wang, W., Oehlschlaeger, M.A., **2013**. Shock Tube and Chemical Kinetic Modeling Study of the Oxidation of 2,5-Dimethylfuran. J. Phys. Chem. A 117, 1371–1392. https://doi.org/10.1021/jp308901q

Solly, R., Benson, S., 1971. Kinetics of Gas-Phase Unimolecular Decomposition of Benzoyl Radical. J. Am. Chem. Soc. 93, 2127-. https://doi.org/10.1021/ja00738a006

Somers K.P., Simmie, J.M., Gillespie, F., Burke, U., Connolly, J., Metcalfe, W.K., Battin-Leclerc, F., Dirrenberger, P., Herbinet, O., Glaude, P.-A., Curran, H.J., **2013a**. A high temperature and atmospheric pressure experimental and detailed chemical kinetic modelling study of 2-methyl furan oxidation. Proc. Combust. Inst. 34, 225–232. https://doi.org/10.1016/j.proci.2012.06.113

Somers K.P., Simmie, J.M., Gillespie, F., Conroy, C., Black, G., Metcalfe, W.K., Battin-Leclerc, F., Dirrenberger, P., Herbinet, O., Glaude, P.-A., Dagaut, P., Togbé, C., Yasunaga, K., Fernandes, R.X., Lee, C., Tripathi, R., Curran, H.J., **2013b**. A comprehensive experimental and detailed chemical kinetic modelling study of 2,5-dimethylfuran pyrolysis and oxidation. Combust. Flame 160, 2291–2318. https://doi.org/10.1016/j.combustflame.2013.06.007

Stagni, A., Song, Y., Vandewallec, L.A., Van Geem, K.M., Marin, G.B., Herbinet, O., Battin-Leclerc, F., Faravelli, T., **2019**. The role of chemistry in the oscillating combustion of hydrocarbons: an experimental and theoretical study. Chem. Eng. J. Submitted.

Suryan, M.M., Kafafi, S.A., Stein, S.E., **1989**. The thermal decomposition of hydroxy- and methoxy-substituted anisoles. J. Am. Chem. Soc. 111, 1423–1429. https://doi.org/10.1021/ja00186a042

Tao, T., Sun, W., Yang, B., Hansen, N., Moshammer, K., Law, C.K., **2017**. Investigation of the chemical structures of laminar premixed flames fueled by acetaldehyde. Proc. Combust. Inst. 36, 1287–1294. https://doi.org/10.1016/j.proci.2016.05.030

Thion, S., Diévart, P., Van Cauwenberghe, P., Dayma, G., Serinyel, Z., Dagaut, P., **2017**. An experimental study in a jet-stirred reactor and a comprehensive kinetic mechanism for the oxidation of methyl ethyl ketone. Proc. Combust. Inst. 36, 459–467. https://doi.org/10.1016/j.proci.2016.05.022

Tian, Z., Li, Y., Zhang, T., Zhu, A., Qi, F., **2008**. Identification of Combustion Intermediates in Low-Pressure Premixed Pyridine/Oxygen/Argon Flames. J. Phys. Chem. A 112, 13549–13555. https://doi.org/10.1021/jp8066537

Tian, Z., Yuan, T., Fournet, R., Glaude, P.-A., Sirjean, B., Battin-Leclerc, F., Zhang, K., Qi, F., **2011**. An experimental and kinetic investigation of premixed furan/oxygen/argon flames. Combust. Flame 158, 756–773. https://doi.org/10.1016/j.combustflame.2010.12.022

Togbé, C., Dagaut, P., Mzé-Ahmed, A., Diévart, P., Halter, F., Foucher, F., **2010a**. Experimental and Detailed Kinetic Modeling Study of 1-Hexanol Oxidation in a Pressurized Jet-Stirred Reactor and a Combustion Bomb. Energy Fuels 24, 5859–5875. https://doi.org/10.1021/ef101255w

Togbé, C., Mzé-Ahmed, A., Dagaut, P., **2010b**. Kinetics of Oxidation of 2-Butanol and Isobutanol in a Jet-Stirred Reactor: Experimental Study and Modeling Investigation. Energy Fuels 24, 5244–5256. https://doi.org/10.1021/ef1008488

Togbé, C., Halter, F., Foucher, F., Mounaim-Rousselle, C., Dagaut, P., **2011**. Experimental and detailed kinetic modeling study of 1-pentanol oxidation in a JSR and combustion in a bomb. Proc. Combust. Inst. 33, 367–374. https://doi.org/10.1016/j.proci.2010.05.003

Togbé, C., Tran, L.-S., Liu, D., Felsmann, D., Oßwald, P., Glaude, P.-A., Sirjean, B., Fournet, R., Battin-Leclerc, F., Kohse-Höinghaus, K., **2014**. Combustion chemistry and flame structure of furan group biofuels using molecular-beam mass spectrometry and gas chromatography – Part III: 2,5-Dimethylfuran. Combust. Flame, Special Issue on Alternative Fuels 161, 780–797. https://doi.org/10.1016/j.combustflame.2013.05.026

Tran, L.S., Glaude, P.-A., Fournet, R., Battin-Leclerc, F., **2013a**. Experimental and Modeling Study of Premixed Laminar Flames of Ethanol and Methane. Energy Fuels 27, 2226–2245. https://doi.org/10.1021/ef301628x

Tran, L.S., Verdicchio, M., Sirjean, B., Glaude, P.A., Battin-Leclerc, F., **2013b**. Experimental and modeling study of the structure of laminar premixed flames of Tetrahydrofuran/Oxygen/Argon.

Tran, L.-S., Togbé, C., Liu, D., Felsmann, D., Oßwald, P., Glaude, P.-A., Fournet, R., Sirjean, B., Battin-Leclerc, F., Kohse-Höinghaus, K., **2014**. Combustion chemistry and flame structure of furan group biofuels using molecular-beam mass spectrometry and gas chromatography – Part II: 2-Methylfuran. Combust. Flame, Special Issue on Alternative Fuels 161, 766–779. https://doi.org/10.1016/j.combustflame.2013.05.027

Tran, L.-S., Sirjean, B., Glaude, P.-A., Kohse-Höinghaus, K., Battin-Leclerc, F., **2015a**. Influence of substituted furans on the formation of Polycyclic Aromatic Hydrocarbons in flames. Proc. Combust. Inst. 35, 1735–1743. https://doi.org/10.1016/j.proci.2014.06.137

Tran, L.-S., Verdicchio, M., Monge, F., Martin, R.C., Bounaceeur, R., Sirjean, B., Glaude, P.-A., Alzueta, M.U., Battin-Leclerc, F., **2015b**. An experimental and modeling study of the combustion of tetrahydrofuran. Combust. Flame 162, 1899–1918. https://doi.org/10.1016/j.combustflame.2014.12.010

Tran, L.-S., Wang, Z., Carstensen, H.-H., Hemken, C., Battin-Leclerc, F., Kohse-Höinghaus, K., **2017**. Comparative experimental and modeling study of the low- to moderate-temperature oxidation chemistry of 2,5-dimethylfuran, 2-methylfuran, and furan. Combust. Flame 181, 251–269. https://doi.org/10.1016/j.combustflame.2017.03.030

United Nation, Department of Economic and Social Affairs, Population Division, 2019. World Population Prospects 2019: Highlights.

Uygun, Y., Ishihara, S., Olivier, H., **2014**. A high pressure ignition delay time study of 2-methylfuran and tetrahydrofuran in shock tubes. Combust. Flame 161, 2519–2530. https://doi.org/10.1016/j.combustflame.2014.04.004

Uzun, B.B., Pütün, A.E., Pütün, E., **2007**. Composition of products obtained via fast pyrolysis of olive-oil residue: Effect of pyrolysis temperature. J. Anal. Appl. Pyrolysis 79, 147–153. https://doi.org/10.1016/j.jaap.2006.12.005

Van Geem, K.M., Pyl, S.P., Marin, G.B., Harper, M.R., Green, W.H., **2010**. Accurate High-Temperature Reaction Networks for Alternative Fuels: Butanol Isomers. Ind. Eng. Chem. Res. 49, 10399–10420. https://doi.org/10.1021/ie1005349

Van Geem, K.M., Cuoci, A., Frassoldati, A., Pyl, S.P., Marin, G.B., Ranzi, E., **2012**. An Experimental and Kinetic Modeling Study of Pyrolysis and Combustion of Acetone–Butanol–Ethanol (ABE) Mixtures. Combust. Sci. Technol. 184, 942–955. https://doi.org/10.1080/00102202.2012.663987

Vandooren, J., de Guertechin, L.O., Van Tiggelen, P.J., **1986**. Kinetics in a lean formaldehyde flame. Combust. Flame 64, 127–139. https://doi.org/10.1016/0010-2180(86)90050-7

Vanhove, G., Yu, Y., Boumehdi, M.A., Frottier, O., Herbinet, O., Glaude, P.-A., Battin-Leclerc, F., **2015**. Experimental Study of Tetrahydrofuran Oxidation and Ignition in Low-Temperature Conditions. Energy Fuels 29, 6118–6125. https://doi.org/10.1021/acs.energyfuels.5b01057

Vasiliou, A.K., Piech, K.M., Zhang, X., Nimlos, M.R., Ahmed, M., Golan, A., Kostko, O., Osborn, D.L., Daily, J.W., Stanton, J.F., Barney Ellison, G., **2011**. The products of the thermal decomposition of CH3CHO. J. Chem. Phys. 135, 014306. https://doi.org/10.1063/1.3604005

Vasiliou, A.K., Piech, K.M., Reed, B., Zhang, X., Nimlos, M.R., Ahmed, M., Golan, A., Kostko, O., Osborn, D.L., David, D.E., Urness, K.N., Daily, J.W., Stanton, J.F., Ellison, G.B., **2012**. Thermal decomposition of CH3CHO studied by matrix infrared spectroscopy and photoionization mass spectroscopy. J. Chem. Phys. 137, 164308. https://doi.org/10.1063/1.4759050

Vasiliou, A.K., Kim, J.H., Ormond, T.K., Piech, K.M., Urness, K.N., Scheer, A.M., Robichaud, D.J., Mukarakate, C., Nimlos, M.R., Daily, J.W., Guan, Q., Carstensen, H.-H., Ellison, G.B., **2013**. Biomass pyrolysis: Thermal decomposition mechanisms of furfural and benzaldehyde. J. Chem. Phys. 139, 104310. https://doi.org/10.1063/1.4819788

Veloo P., Dagaut, P., Togbe, C., Dayma, G., Sarathy, S.M., Westbrook, C.K., Egolfopoulos, F.N., **2013a**. Jet-stirred reactor and flame studies of propanal oxidation. Proc. Combust. Inst. 34, 599–606. https://doi.org/10.1016/j.proci.2012.06.138

Veloo P., Dagaut, P., Togbé, C., Dayma, G., Sarathy, S.M., Westbrook, C.K., Egolfopoulos, F.N., **2013b**. Experimental and modeling study of the oxidation of n- and iso-butanal. Combust. Flame 160, 1609–1626. https://doi.org/10.1016/j.combustflame.2013.03.018

Vuori, A.I., Bredenberg, J.B., **1987**. Thermal chemistry pathways of substituted anisoles. Ind. Eng. Chem. Res. 26, 359–365. https://doi.org/10.1021/ie00062a031

Wang, C., Du, Y., Jin, X., Che, D., **2016b**. Pyridine and pyrrole oxidation under oxy-fuel conditions. Energy Sources Part Recovery Util. Environ. Eff. 38, 975–981. https://doi.org/10.1080/15567036.2013.824521

Wang, H., 2011. Formation of nascent soot and other condensed-phase materials in flames. Proc. Combust. Inst. 33, 41–67. https://doi.org/10.1016/j.proci.2010.09.009

Wang, S., Davidson, D.F., Hanson, R.K., **2016a**. Shock Tube Measurement for the Dissociation Rate Constant of Acetaldehyde Using Sensitive CO Diagnostics. J. Phys. Chem. A 120, 6895–6901. https://doi.org/10.1021/acs.jpca.6b03647

Wang, Z., Lucassen, A., Zhang, L., Yang, J., Kohse-Höinghaus, K., Qi, F., **2011**. Experimental and theoretical studies on decomposition of pyrrolidine. Proc. Combust. Inst. 33, 415–423. https://doi.org/10.1016/j.proci.2010.06.034

Wei, L., Tang, C., Man, X., Jiang, X., Huang, Z., **2012**. High-Temperature Ignition Delay Times and Kinetic Study of Furan. Energy Fuels 26, 2075–2081. https://doi.org/10.1021/ef300336y

Wei, L., Li, Z., Tong, L., Wang, Z., Jin, H., Yao, M., Zheng, Z., Wang, C., Xu, H., **2012**. Primary Combustion Intermediates in Lean and Rich Low-Pressure Premixed Laminar 2-Methylfuran/Oxygen/Argon Flames. Energy Fuels 26, 6651–6660. https://doi.org/10.1021/ef301173z

Wei, L., Tang, C., Man, X., Huang, Z., **2013**. Shock-Tube Experiments and Kinetic Modeling of 2-Methylfuran Ignition at Elevated Pressure. Energy Fuels 27, 7809–7816. https://doi.org/10.1021/ef401809y

Welz, O., Savee, J.D., Eskola, A.J., Sheps, L., Osborn, D.L., Taatjes, C.A., **2013**. Low-temperature combustion chemistry of biofuels: Pathways in the low-temperature (550–700K) oxidation chemistry of isobutanol and tert-butanol. Proc. Combust. Inst. 34, 493–500. https://doi.org/10.1016/j.proci.2012.05.058

Won, S.J., Ryu, J.C., Bae, J.H., Kim, Y.D., Gang, J.G., **2000**. Shock-Tube Study of the Oxidation of Acetaldehyde at High Temperature. Bull. Korean Chem. Soc. 21, 487–492.

World Health Organization (Ed.), 2006. Air quality guidelines: global update 2005: particulate matter, ozone, nitrogen dioxide, and sulfur dioxide. World Health Organization, Copenhagen, Denmark.

Wornat, M.J., Ledesma, E.B., Marsh, N.D., **2001**. Polycyclic aromatic hydrocarbons from the pyrolysis of catechol (ortho-dihydroxybenzene), a model fuel representative of entities in tobacco, coal, and lignin. Fuel 80, 1711–1726. https://doi.org/10.1016/S0016-2361(01)00057-6

Wu, X., Huang, Z., Yuan, T., Zhang, K., Wei, L., **2009**. Identification of combustion intermediates in a low-pressure premixed laminar 2,5-dimethylfuran/oxygen/argon flame with tunable synchrotron photoionization. Combust. Flame 156, 1365–1376. https://doi.org/10.1016/j.combustflame.2009.04.002

Wu, X., Huang, Z., Jin, C., Wang, X., Wei, L., **2010**. Laminar Burning Velocities and Markstein Lengths of 2,5-Dimethylfuran-Air Premixed Flames at Elevated Temperatures. Combust. Sci. Technol. 183, 220–237. https://doi.org/10.1080/00102202.2010.516037

Wu, X., Huang, Z., Wang, X., Jin, C., Tang, C., Wei, L., Law, C.K., **2011**. Laminar burning velocities and flame instabilities of 2,5-dimethylfuran–air mixtures at elevated pressures. Combust. Flame 158, 539–546. https://doi.org/10.1016/j.combustflame.2010.10.006

Yamamoto, Tsuyoshi, Kuwahara, T., Nakaso, K., Yamamoto, Takahisa, **2012**. Kinetic study of fuel NO formation from pyrrole type nitrogen. Fuel 93, 213–220. https://doi.org/10.1016/j.fuel.2011.09.032

Yang, K., Zhan, C., Man, X., Guan, L., Huang, Z., Tang, C., **2016**. Shock Tube Study on Propanal Ignition and the Comparison to Propane, *n* -Propanol, and *i* -Propanol. Energy Fuels 30, 717–724. https://doi.org/10.1021/acs.energyfuels.5b02739

Yasunaga, K., Kubo, S., Hoshikawa, H., Kamesawa, T., Hidaka, Y., **2008**. Shock-tube and modeling study of acetaldehyde pyrolysis and oxidation. Int. J. Chem. Kinet. 40, 73–102. https://doi.org/10.1002/kin.20294

Yeung, C., Thomson, M.J., **2013**. Experimental and kinetic modeling study of 1-hexanol combustion in an opposed-flow diffusion flame. Proc. Combust. Inst. 34, 795–802. https://doi.org/10.1016/j.proci.2012.06.163

Zeppieri, S.P., Klotz, S.D., Dryer, F.L., **2000**. Modeling concepts for larger carbon number alkanes: A partially reduced skeletal mechanism for n-decane oxidation and pyrolysis. Proc. Combust. Inst. 28, 1587–1595. https://doi.org/10.1016/S0082-0784(00)80556-1

Zhang, J., Pan, L., Mo, J., Gong, J., Huang, Z., Law, C.K., **2013**. A shock tube and kinetic modeling study of n-butanal oxidation. Combust. Flame 160, 1541–1549. https://doi.org/10.1016/j.combustflame.2013.04.002

Zhang, Q., Chang, J., Wang, T., Xu, Y., **2007**. Review of biomass pyrolysis oil properties and upgrading research. Energy Convers. Manag. 48, 87–92. https://doi.org/10.1016/j.enconman.2006.05.010

Zhang, Y., Somers, K.P., Mehl, M., Pitz, W.J., Cracknell, R.F., Curran, H.J., **2017**. Probing the antagonistic effect of toluene as a component in surrogate fuel models at low temperatures and high pressures. A case study of toluene/dimethyl ether mixtures. Proc. Combust. Inst. 36, 413–421. https://doi.org/10.1016/j.proci.2016.06.190

APPENDICES

I. NOMENCLATURE OF THE EXPERIMENTALLY ANALYZED SPECIES

Name	Formula	Structure	Name	Formula	Structure	Name	Formula	Structure
Propyne	C_3H_4	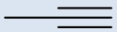	2-Propen-2-ol	C_3H_6O	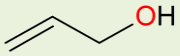	2-Butenal	C_4H_6O	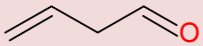
Allene	C_3H_4	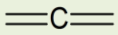	Propane	C_3H_8		Methylvinylketone	C_4H_6O	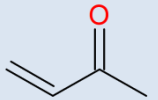
Acrolein	C_3H_4O	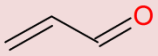	Butenyne	C_4H_4	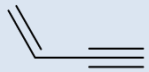	2,3-Dihydrofuran	C_4H_6O	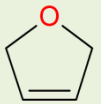
Propene	C_3H_6	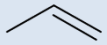	Furan	C_4H_4O	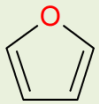	1.2-Dihydrofuran	C_4H_6O	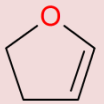
Methyloxirane	C_3H_6O	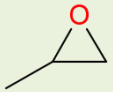	1-Butyne	C_4H_6	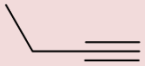	1-Butene	C_4H_8	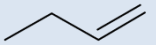
Propanal	C_3H_6O		2-Butyne	C_4H_6	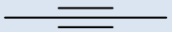	2-Butene	C_4H_8	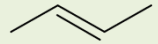
Acetone	C_3H_6O	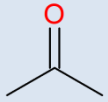	1-3 Butadiene	C_4H_6	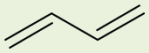	n-Butanal	C_4H_8O	

Name	Formula	Structure	Name	Formula	Structure	Name	Formula	Structure
Tetrahydrofuran	C_4H_8O		2-3 Butanediol	$C_4H_{10}O_2$	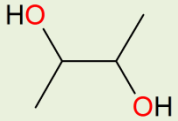	2.3-Dimethylcyclopropane	C_5H_{10}	
Ethyloxirane	C_4H_8O	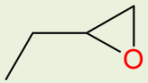	Cyclopentadiene	C_5H_6		n-Pentanal	$C_5H_{10}O$	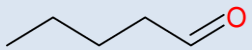
Butanone	C_4H_8O	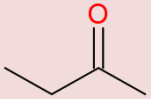	1-4 Pentadiene	C_5H_8		2-Methyl-butanal	$C_5H_{10}O$	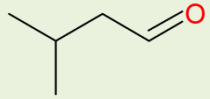
Butanoic acid	$C_4H_8O_2$	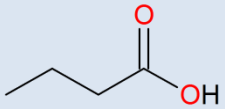	1-3 Pentadiene	C_5H_8	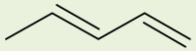	Pentanoic acid	$C_5H_{10}O_2$	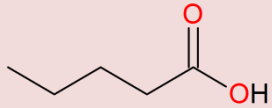
Dimethyloxirane	$C_4H_8O_2$		Cyclopentenone	C_5H_8O	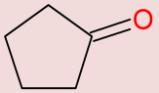	Pentane	C_5H_{12}	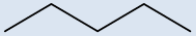
n-Butanol	$C_4H_{10}O$		1-Pentene	C_5H_{10}		n-Pentanol	$C_5H_{12}O$	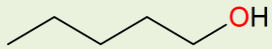
2-Methylfuran	$C_4H_{10}O$	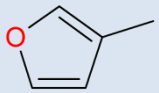	2-Pentene	C_5H_{10}	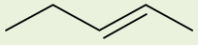	Benzoquinone	$C_6H_4O_2$	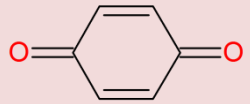

Name	Formula	Structure	Name	Formula	Structure	Name	Formula	Structure
Benzene	C_6H_6	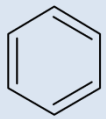	Anisole	C_7H_8O	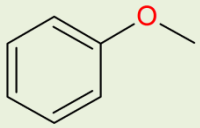	Ethylphenol	$C_8H_{11}O$	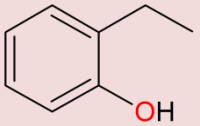
Phenol	C_6H_6O	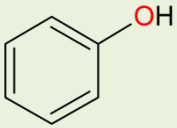	Cresol	C_7H_8O	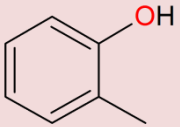	Indene	C_9H_8	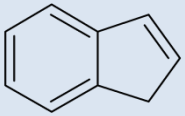
Benzodioxol-2-one	$C_7H_4O_3$	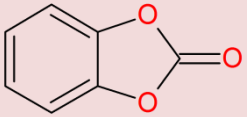	Phenylacetylene	C_8H_6	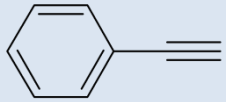	Methylbenzofuran	C_9H_8O	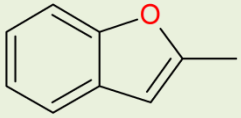
Benzaldehyde	C_7H_6O	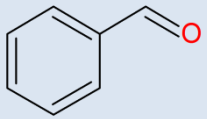	Benzofuran	C_8H_6O	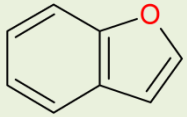	Cinnamaldehyde	C_9H_8O	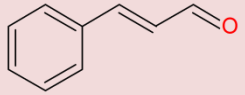
Benzodioxol	$C_7H_6O_2$	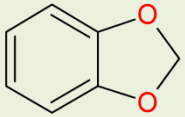	Styrene	C_8H_8	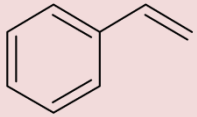	Indanone	C_9H_8O	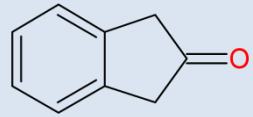
Hydroxybenzaldehyde	$C_7H_6O_2$	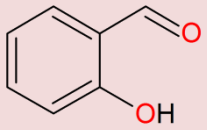	Ethylbenzene	C_8H_{10}	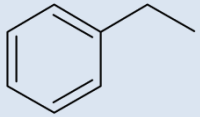	Methylstyrene	C_9H_{10}	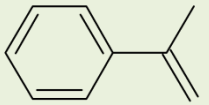
Toluene	C_7H_8	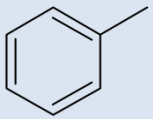	Xylene	C_8H_{10}	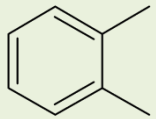	Cumene	C_9H_{12}	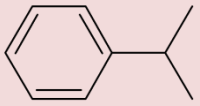

Name	Formula	Structure
Naphtalene	$C_{10}H_8$	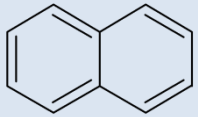
Methylindene	$C_{10}H_{10}$	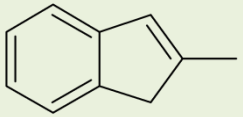
Dihydronaphthalene	$C_{10}H_{10}$	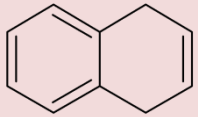
Acenaphthylene	$C_{12}H_8$	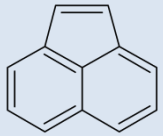
Dibenzofuran	$C_{12}H_8O$	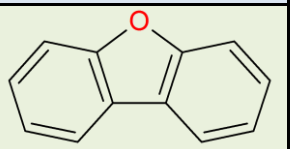
Biphenyl	$C_{12}H_{10}$	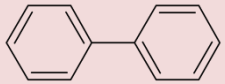
Diphenylether	$C_{12}H_{10}O$	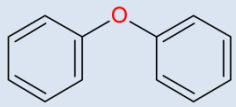

II. EXPERIMENTAL RAW DATA

II.1. Example of a calculation sheet for the determination of the initial conditions

Oxidation of *n* -butanol

$C_4H_{10}O$ 74 g/mol

Vr (cm3) 92 Coeff stoech O_2 6.5

	T (K)	T (°C)	P (Pa)	tau (s)	phi	Q (m3/s)	F (mol/s)	xfuel	xO2	xHe	F(fuel)	F(O2)	F(He)	m(fuel) (g/hr)	Q(O2) (mL/min)	Q(He) (L/min)
1	500	227	106657.9	2	1	4.60E-05	1.18E-03	0.005	0.0325	0.9625	5.90E-06	3.84E-05	1.14E-03	1.57	52.27	1.55
2	525	252	106657.9	2	1	4.60E-05	1.12E-03	0.005	0.0325	0.9625	5.62E-06	3.65E-05	1.08E-03	1.50	49.78	1.47
3	550	277	106657.9	2	1	4.60E-05	1.07E-03	0.005	0.0325	0.9625	5.36E-06	3.49E-05	1.03E-03	1.43	47.51	1.41
4	575	302	106657.9	2	1	4.60E-05	1.03E-03	0.005	0.0325	0.9625	5.13E-06	3.34E-05	9.88E-04	1.37	45.45	1.35
5	600	327	106657.9	2	1	4.60E-05	9.83E-04	0.005	0.0325	0.9625	4.92E-06	3.20E-05	9.47E-04	1.31	43.55	1.29
6	625	352	106657.9	2	1	4.60E-05	9.44E-04	0.005	0.0325	0.9625	4.72E-06	3.07E-05	9.09E-04	1.26	41.81	1.24
7	650	377	106657.9	2	1	4.60E-05	9.08E-04	0.005	0.0325	0.9625	4.54E-06	2.95E-05	8.74E-04	1.21	40.20	1.19
8	675	402	106657.9	2	1	4.60E-05	8.74E-04	0.005	0.0325	0.9625	4.37E-06	2.84E-05	8.41E-04	1.16	38.72	1.15
9	700	427	106657.9	2	1	4.60E-05	8.43E-04	0.005	0.0325	0.9625	4.21E-06	2.74E-05	8.11E-04	1.12	37.33	1.11
10	725	452	106657.9	2	1	4.60E-05	8.14E-04	0.005	0.0325	0.9625	4.07E-06	2.65E-05	7.83E-04	1.08	36.05	1.07
11	750	477	106657.9	2	1	4.60E-05	7.87E-04	0.005	0.0325	0.9625	3.93E-06	2.56E-05	7.57E-04	1.05	34.84	1.03
12	775	502	106657.9	2	1	4.60E-05	7.61E-04	0.005	0.0325	0.9625	3.81E-06	2.47E-05	7.33E-04	1.01	33.72	1.00
13	800	527	106657.9	2	1	4.60E-05	7.38E-04	0.005	0.0325	0.9625	3.69E-06	2.40E-05	7.10E-04	0.98	32.67	0.97
14	825	552	106657.9	2	1	4.60E-05	7.15E-04	0.005	0.0325	0.9625	3.58E-06	2.32E-05	6.88E-04	0.95	31.68	0.94
15	850	577	106657.9	2	1	4.60E-05	6.94E-04	0.005	0.0325	0.9625	3.47E-06	2.26E-05	6.68E-04	0.92	30.74	0.91
16	875	602	106657.9	2	1	4.60E-05	6.74E-04	0.005	0.0325	0.9625	3.37E-06	2.19E-05	6.49E-04	0.90	29.87	0.88
17	900	627	106657.9	2	1	4.60E-05	6.56E-04	0.005	0.0325	0.9625	3.28E-06	2.13E-05	6.31E-04	0.87	29.04	0.86
18	925	652	106657.9	2	1	4.60E-05	6.38E-04	0.005	0.0325	0.9625	3.19E-06	2.07E-05	6.14E-04	0.85	28.25	0.84
19	950	677	106657.9	2	1	4.60E-05	6.21E-04	0.005	0.0325	0.9625	3.11E-06	2.02E-05	5.98E-04	0.83	27.51	0.81
20	975	702	106657.9	2	1	4.60E-05	6.05E-04	0.005	0.0325	0.9625	3.03E-06	1.97E-05	5.83E-04	0.81	26.80	0.79
21	1000	727	106657.9	2	1	4.60E-05	5.90E-04	0.005	0.0325	0.9625	2.95E-06	1.92E-05	5.68E-04	0.79	26.13	0.77
22	1025	752	106657.9	2	1	4.60E-05	5.76E-04	0.005	0.0325	0.9625	2.88E-06	1.87E-05	5.54E-04	0.77	25.50	0.76
23	1050	777	106657.9	2	1	4.60E-05	5.62E-04	0.005	0.0325	0.9625	2.81E-06	1.83E-05	5.41E-04	0.75	24.89	0.74
24	1075	802	106657.9	2	1	4.60E-05	5.49E-04	0.005	0.0325	0.9625	2.74E-06	1.78E-05	5.28E-04	0.73	24.31	0.72
25	1100	827	106657.9	2	1	4.60E-05	5.36E-04	0.005	0.0325	0.9625	2.68E-06	1.74E-05	5.16E-04	0.71	23.76	0.70

Figure 113. Example of an Excel worksheet for the calculation of the initial conditions. Here for *n*-butanol oxidation under stoichiometric conditions.

II.2. Combustion of *n*-butanol

Equivalence ratio	0,5 ; 1 ; 2
$x_{1\text{-butanol}}$	0.005
Temperature (K)	500 - 1100
P (Torr)	800

Units	Mole fraction
Bath gas	Helium
Residence time (s)	2

T (K)	O_2			CO			CH_4		
	Phi=0.5	Phi=1	Phi=2	Phi=0.5	Phi=1	Phi=2	Phi=0.5	Phi=1	Phi=2
500	6.65E-02	3.48E-02	0.00E+00	0.00E+00	0.00E+00	0.00E+00	3.68E-07	0.00E+00	1.85E-06
525	6.71E-02	3.49E-02	1.74E-02	0.00E+00	0.00E+00	0.00E+00	0.00E+00	0.00E+00	2.08E-07
550	6.38E-02	3.38E-02	1.74E-02	0.00E+00	0.00E+00	0.00E+00	2.03E-07	0.00E+00	0.00E+00
575	6.58E-02	3.21E-02	1.73E-02	0.00E+00	0.00E+00	0.00E+00	0.00E+00	0.00E+00	0.00E+00
600	6.35E-02	3.29E-02	1.79E-02	0.00E+00	0.00E+00	0.00E+00	0.00E+00	0.00E+00	0.00E+00
625	6.60E-02	3.21E-02	1.73E-02	0.00E+00	0.00E+00	0.00E+00	0.00E+00	0.00E+00	0.00E+00
650	6.48E-02	3.30E-02	1.74E-02	0.00E+00	0.00E+00	0.00E+00	0.00E+00	0.00E+00	0.00E+00
675	6.52E-02	3.27E-02	1.74E-02	0.00E+00	0.00E+00	0.00E+00	0.00E+00	0.00E+00	0.00E+00
700	6.36E-02	3.39E-02	1.76E-02	0.00E+00	0.00E+00	0.00E+00	0.00E+00	0.00E+00	0.00E+00
725	6.59E-02	3.26E-02	1.76E-02	0.00E+00	0.00E+00	0.00E+00	0.00E+00	0.00E+00	0.00E+00
750	6.37E-02	3.33E-02	1.77E-02	0.00E+00	0.00E+00	0.00E+00	2.26E-07	5.28E-07	5.00E-07
775	6.84E-02	3.26E-02	3.35E-02	0.00E+00	0.00E+00	0.00E+00	1.36E-06	2.49E-06	2.02E-06
800	6.38E-02	3.30E-02	1.77E-02	2.37E-04	1.02E-04	5.36E-05	4.05E-05	2.65E-05	3.21E-05
825	6.17E-02	3.13E-02	1.73E-02	1.70E-03	1.01E-03	9.88E-04	2.26E-04	2.15E-04	2.55E-04
850	5.84E-02	2.88E-02	1.43E-02	5.57E-03	4.27E-03	2.84E-03	5.18E-04	5.76E-04	5.35E-04
875	5.76E-02	2.73E-02	1.22E-02	7.93E-03	6.76E-03	5.15E-03	6.39E-04	7.37E-04	7.69E-04
900	5.51E-02	2.40E-02	1.10E-02	1.07E-02	8.70E-03	6.92E-03	6.28E-04	7.71E-04	9.09E-04
925	5.23E-02	2.20E-02	9.87E-03	1.13E-02	9.49E-03	7.88E-03	5.47E-04	7.84E-04	1.06E-03
950	4.70E-02	2.05E-02	9.33E-03	1.15E-02	1.07E-02	8.55E-03	3.78E-04	7.82E-04	1.16E-03
975	4.30E-02	1.83E-02	9.17E-03	9.12E-03	1.12E-02	9.46E-03	1.69E-04	7.37E-04	1.32E-03
1000	4.19E-02	1.48E-02	8.33E-03	6.30E-03	1.03E-02	1.01E-02	8.28E-05	4.81E-04	1.48E-03
1025	3.87E-02	1.06E-02	7.67E-03	3.67E-03	6.61E-03	1.09E-02	5.50E-05	2.89E-04	1.61E-03
1050	3.79E-02	6.81E-03	6.01E-03	2.06E-03	2.22E-03	1.25E-02	4.30E-05	9.20E-05	1.66E-03
1075	3.79E-02	5.57E-03	3.92E-03	1.34E-03	9.22E-04	1.35E-02	3.17E-05	4.13E-05	1.26E-03
1100	3.92E-02	5.72E-03	2.37E-03	5.69E-04	5.16E-04	1.39E-02	4.78E-06	5.19E-06	8.75E-04

T (K)	CO_2			Acetylene			Ethylene		
	Phi=0.5	Phi=1	Phi=2	Phi=0.5	Phi=1	Phi=2	Phi=0.5	Phi=1	Phi=2
500	0.00E+00	0.00E+00	0.00E+00	0.00E+00	0.00E+00	0.00E+00	2.28E-06	0.00E+00	4.39E-07
525	0.00E+00	0.00E+00	0.00E+00	0.00E+00	0.00E+00	0.00E+00	0.00E+00	0.00E+00	1.80E-06
550	0.00E+00	0.00E+00	0.00E+00	0.00E+00	0.00E+00	0.00E+00	9.15E-07	0.00E+00	0.00E+00
575	0.00E+00	0.00E+00	0.00E+00	0.00E+00	0.00E+00	0.00E+00	0.00E+00	0.00E+00	3.14E-07
600	0.00E+00	0.00E+00	0.00E+00	0.00E+00	0.00E+00	0.00E+00	2.18E-07	0.00E+00	0.00E+00
625	0.00E+00	0.00E+00	0.00E+00	0.00E+00	0.00E+00	0.00E+00	0.00E+00	0.00E+00	8.44E-08
650	0.00E+00	0.00E+00	0.00E+00	0.00E+00	0.00E+00	0.00E+00	4.73E-07	0.00E+00	0.00E+00
675	0.00E+00	0.00E+00	0.00E+00	0.00E+00	0.00E+00	0.00E+00	0.00E+00	0.00E+00	2.00E-07
700	0.00E+00	0.00E+00	0.00E+00	0.00E+00	0.00E+00	0.00E+00	0.00E+00	0.00E+00	0.00E+00
725	0.00E+00	0.00E+00	0.00E+00	0.00E+00	0.00E+00	0.00E+00	0.00E+00	0.00E+00	3.36E-07
750	0.00E+00	0.00E+00	0.00E+00	0.00E+00	0.00E+00	0.00E+00	5.79E-07	1.05E-06	8.21E-07
775	0.00E+00	0.00E+00	0.00E+00	0.00E+00	0.00E+00	0.00E+00	3.65E-06	5.52E-06	4.87E-06
800	0.00E+00	0.00E+00	0.00E+00	0.00E+00	0.00E+00	0.00E+00	1.01E-04	5.94E-05	6.72E-05
825	0.00E+00	0.00E+00	0.00E+00	3.76E-07	2.82E-07	0.00E+00	5.49E-04	5.02E-04	5.87E-04
850	3.44E-04	0.00E+00	0.00E+00	4.76E-06	3.16E-06	2.39E-06	1.30E-03	1.40E-03	1.26E-03
875	7.25E-04	0.00E+00	2.56E-04	5.00E-06	7.34E-06	7.69E-06	1.59E-03	1.75E-03	1.77E-03
900	1.57E-03	9.30E-04	0.00E+00	1.03E-05	1.43E-05	1.45E-05	1.52E-03	1.80E-03	1.97E-03
925	2.61E-03	1.30E-03	6.84E-04	1.24E-05	1.49E-05	2.07E-05	1.24E-03	1.69E-03	2.12E-03
950	4.91E-03	2.14E-03	8.99E-04	1.05E-05	1.97E-05	2.81E-05	7.32E-04	1.49E-03	2.09E-03
975	9.25E-03	3.18E-03	1.05E-03	5.18E-06	1.90E-05	3.03E-05	2.79E-04	1.20E-03	2.13E-03
1000	1.35E-02	6.45E-03	1.42E-03	3.13E-06	1.43E-05	3.64E-05	1.54E-04	6.91E-04	2.07E-03
1025	1.59E-02	1.14E-02	1.62E-03	2.87E-06	1.24E-05	3.60E-05	1.23E-04	4.58E-04	1.88E-03
1050	1.82E-02	1.64E-02	2.13E-03	3.34E-06	8.33E-06	3.82E-05	8.80E-05	2.02E-04	1.47E-03
1075	1.97E-02	1.85E-02	2.95E-03	2.52E-06	7.45E-06	3.58E-05	4.05E-05	1.03E-04	9.74E-04
1100	1.97E-02	1.73E-02	3.85E-03	2.03E-07	9.39E-07	4.94E-05	2.21E-06	3.67E-06	5.49E-04

T (K)	Ethane			Propene			Propane		
	Phi=0.5	Phi=1	Phi=2	Phi=0.5	Phi=1	Phi=2	Phi=0.5	Phi=1	Phi=2
500	0.00E+00	0.00E+00	0.00E+00	0.00E+00	0.00E+00	0.00E+00	0.00E+00	0.00E+00	0.00E+00
525	0.00E+00	0.00E+00	0.00E+00	0.00E+00	0.00E+00	0.00E+00	0.00E+00	0.00E+00	0.00E+00
550	0.00E+00	0.00E+00	0.00E+00	0.00E+00	0.00E+00	0.00E+00	0.00E+00	0.00E+00	0.00E+00
575	0.00E+00	0.00E+00	0.00E+00	0.00E+00	0.00E+00	0.00E+00	0.00E+00	0.00E+00	0.00E+00
600	0.00E+00	0.00E+00	0.00E+00	0.00E+00	0.00E+00	0.00E+00	0.00E+00	0.00E+00	0.00E+00
625	0.00E+00	0.00E+00	0.00E+00	0.00E+00	0.00E+00	0.00E+00	0.00E+00	0.00E+00	0.00E+00
650	0.00E+00	0.00E+00	0.00E+00	0.00E+00	0.00E+00	0.00E+00	0.00E+00	0.00E+00	0.00E+00
675	0.00E+00	0.00E+00	0.00E+00	0.00E+00	0.00E+00	0.00E+00	0.00E+00	0.00E+00	0.00E+00
700	0.00E+00	0.00E+00	0.00E+00	0.00E+00	0.00E+00	0.00E+00	8.50E-06	0.00E+00	0.00E+00
725	0.00E+00	0.00E+00	0.00E+00	0.00E+00	0.00E+00	2.38E-06	0.00E+00	0.00E+00	0.00E+00
750	0.00E+00	0.00E+00	0.00E+00	2.76E-06	2.41E-06	2.57E-06	0.00E+00	0.00E+00	0.00E+00
775	0.00E+00	0.00E+00	0.00E+00	8.79E-06	7.50E-06	5.27E-06	0.00E+00	0.00E+00	0.00E+00
800	0.00E+00	0.00E+00	3.16E-06	9.58E-05	6.29E-05	5.15E-05	0.00E+00	0.00E+00	0.00E+00
825	1.02E-05	1.38E-05	1.81E-05	3.71E-04	3.23E-04	3.18E-04	1.01E-06	2.45E-06	2.52E-06
850	3.06E-05	4.18E-05	5.18E-05	5.23E-04	4.82E-04	5.02E-04	3.30E-06	3.44E-06	4.91E-06
875	4.07E-05	6.20E-05	8.17E-05	4.61E-04	4.84E-04	4.70E-04	3.18E-06	3.89E-06	9.29E-06
900	3.72E-05	6.86E-05	9.56E-05	2.88E-04	3.74E-04	3.95E-04	1.93E-06	5.23E-06	1.05E-05
925	2.81E-05	5.94E-05	1.21E-04	1.78E-04	2.48E-04	3.60E-04	3.04E-06	4.94E-06	1.36E-05
950	2.25E-05	5.83E-05	1.21E-04	9.66E-05	1.64E-04	2.91E-04	0.00E+00	4.12E-06	1.35E-05
975	1.10E-05	5.61E-05	1.26E-04	4.82E-05	1.14E-04	2.26E-04	0.00E+00	3.44E-06	1.24E-05
1000	6.09E-06	3.96E-05	1.30E-04	3.39E-05	5.82E-05	1.74E-04	0.00E+00	4.03E-06	1.12E-05
1025	6.25E-06	3.28E-05	1.12E-04	2.53E-05	4.88E-05	1.07E-04	0.00E+00	2.05E-06	9.98E-06
1050	6.55E-06	1.90E-05	1.09E-04	1.21E-05	3.35E-05	7.04E-05	0.00E+00	0.00E+00	1.16E-05
1075	2.59E-06	9.55E-06	7.98E-05	1.93E-06	1.45E-05	4.02E-05	0.00E+00	0.00E+00	6.11E-06
1100	0.00E+00	0.00E+00	5.34E-05	0.00E+00	0.00E+00	1.38E-05	0.00E+00	0.00E+00	2.50E-06

T (K)	Formaldehyde			Oxirane			Acetaldehyde		
	Phi=0.5	Phi=1	Phi=2	Phi=0.5	Phi=1	Phi=2	Phi=0.5	Phi=1	Phi=2
500	0.00E+00	0.00E+00	0.00E+00	0.00E+00	0.00E+00	0.00E+00	0.00E+00	0.00E+00	0.00E+00
525	0.00E+00	0.00E+00	0.00E+00	0.00E+00	0.00E+00	0.00E+00	0.00E+00	0.00E+00	0.00E+00
550	0.00E+00	0.00E+00	0.00E+00	0.00E+00	0.00E+00	0.00E+00	0.00E+00	0.00E+00	0.00E+00
575	0.00E+00	0.00E+00	0.00E+00	0.00E+00	0.00E+00	0.00E+00	0.00E+00	0.00E+00	0.00E+00
600	0.00E+00	0.00E+00	0.00E+00	0.00E+00	0.00E+00	0.00E+00	0.00E+00	0.00E+00	0.00E+00
625	0.00E+00	0.00E+00	0.00E+00	0.00E+00	0.00E+00	0.00E+00	0.00E+00	0.00E+00	0.00E+00
650	0.00E+00	0.00E+00	0.00E+00	0.00E+00	0.00E+00	0.00E+00	0.00E+00	0.00E+00	0.00E+00
675	0.00E+00	0.00E+00	0.00E+00	0.00E+00	0.00E+00	0.00E+00	0.00E+00	0.00E+00	0.00E+00
700	0.00E+00	0.00E+00	0.00E+00	0.00E+00	0.00E+00	0.00E+00	0.00E+00	0.00E+00	0.00E+00
725	0.00E+00	0.00E+00	0.00E+00	0.00E+00	0.00E+00	0.00E+00	3.30E-06	0.00E+00	0.00E+00
750	0.00E+00	0.00E+00	0.00E+00	0.00E+00	0.00E+00	0.00E+00	0.00E+00	4.53E-06	0.00E+00
775	0.00E+00	0.00E+00	0.00E+00	0.00E+00	0.00E+00	0.00E+00	1.17E-05	8.81E-06	5.79E-06
800	0.00E+00	0.00E+00	0.00E+00	0.00E+00	0.00E+00	0.00E+00	1.17E-04	6.00E-05	4.71E-05
825	3.52E-04	2.96E-04	2.78E-04	3.38E-06	2.39E-06	1.69E-06	2.50E-04	1.96E-04	1.65E-04
850	5.13E-04	3.83E-04	4.56E-04	1.54E-05	0.00E+00	9.27E-06	2.70E-04	2.39E-04	2.55E-04
875	4.36E-04	3.21E-04	4.63E-04	1.73E-05	1.78E-05	1.21E-05	2.22E-04	2.13E-04	2.66E-04
900	2.40E-04	4.13E-04	3.62E-04	1.25E-05	1.53E-05	1.21E-05	1.41E-04	2.12E-04	2.53E-04
925	2.52E-04	2.62E-04	4.07E-04	8.78E-06	8.33E-06	1.05E-05	9.89E-05	1.55E-04	2.51E-04
950	0.00E+00	1.58E-04	2.73E-04	3.69E-06	5.15E-06	6.23E-06	6.36E-05	1.14E-04	2.17E-04
975	0.00E+00	0.00E+00	2.57E-04	1.96E-06	2.42E-06	3.50E-06	3.89E-05	9.07E-05	1.78E-04
1000	0.00E+00	0.00E+00	1.92E-04	0.00E+00	2.70E-06	1.55E-06	2.95E-05	4.80E-05	1.37E-04
1025	0.00E+00	0.00E+00	1.43E-04	0.00E+00	0.00E+00	1.40E-06	2.17E-05	3.83E-05	9.11E-05
1050	0.00E+00	0.00E+00	0.00E+00	0.00E+00	0.00E+00	0.00E+00	1.15E-05	2.05E-05	5.46E-05
1075	0.00E+00	0.00E+00	0.00E+00	0.00E+00	0.00E+00	0.00E+00	0.00E+00	1.25E-05	2.72E-05
1100	0.00E+00	0.00E+00	0.00E+00	0.00E+00	0.00E+00	0.00E+00	0.00E+00	0.00E+00	8.87E-06

T (K)	1-Butene			1,3-Butadiene			2-Butene		
	Phi=0.5	Phi=1	Phi=2	Phi=0.5	Phi=1	Phi=2	Phi=0.5	Phi=1	Phi=2
500	0.00E+00	0.00E+00	0.00E+00	0.00E+00	0.00E+00	0.00E+00	0.00E+00	0.00E+00	0.00E+00
525	0.00E+00	0.00E+00	0.00E+00	0.00E+00	0.00E+00	0.00E+00	0.00E+00	0.00E+00	0.00E+00
550	0.00E+00	0.00E+00	0.00E+00	0.00E+00	0.00E+00	0.00E+00	0.00E+00	0.00E+00	0.00E+00
575	0.00E+00	0.00E+00	0.00E+00	0.00E+00	0.00E+00	0.00E+00	0.00E+00	0.00E+00	0.00E+00
600	0.00E+00	0.00E+00	0.00E+00	0.00E+00	0.00E+00	0.00E+00	0.00E+00	0.00E+00	0.00E+00
625	0.00E+00	0.00E+00	0.00E+00	0.00E+00	0.00E+00	0.00E+00	0.00E+00	0.00E+00	0.00E+00
650	0.00E+00	0.00E+00	0.00E+00	0.00E+00	0.00E+00	0.00E+00	0.00E+00	0.00E+00	0.00E+00
675	0.00E+00	0.00E+00	0.00E+00	0.00E+00	0.00E+00	0.00E+00	0.00E+00	0.00E+00	0.00E+00
700	0.00E+00	0.00E+00	0.00E+00	0.00E+00	0.00E+00	0.00E+00	0.00E+00	0.00E+00	0.00E+00
725	1.54E-06	1.35E-06	1.62E-06	0.00E+00	0.00E+00	0.00E+00	0.00E+00	0.00E+00	0.00E+00
750	3.43E-06	3.24E-06	3.63E-06	0.00E+00	0.00E+00	0.00E+00	0.00E+00	0.00E+00	1.68E-06
775	8.67E-06	9.13E-06	5.91E-06	0.00E+00	0.00E+00	0.00E+00	2.87E-06	2.78E-06	3.76E-06
800	7.06E-05	4.97E-05	4.74E-05	3.02E-06	1.55E-06	1.76E-06	3.00E-06	3.32E-06	4.32E-06
825	1.82E-04	1.85E-04	1.88E-04	1.47E-05	1.11E-05	8.30E-06	7.58E-06	6.62E-06	5.72E-06
850	1.78E-04	1.80E-04	2.15E-04	2.05E-05	1.67E-05	1.45E-05	5.34E-06	7.15E-06	6.57E-06
875	1.41E-04	1.57E-04	1.59E-04	1.90E-05	1.75E-05	1.49E-05	5.38E-06	6.27E-06	6.67E-06
900	7.95E-05	1.08E-04	1.16E-04	1.26E-05	1.41E-05	1.31E-05	3.89E-06	5.22E-06	6.27E-06
925	4.77E-05	6.39E-05	9.56E-05	8.26E-06	1.00E-05	1.36E-05	2.38E-06	3.54E-06	6.52E-06
950	2.75E-05	3.89E-05	7.00E-05	4.93E-06	8.09E-06	1.24E-05	2.40E-06	2.57E-06	4.49E-06
975	1.82E-05	2.70E-05	4.95E-05	4.29E-06	5.57E-06	1.11E-05	7.32E-07	1.94E-06	5.00E-06
1000	1.41E-05	1.62E-05	3.70E-05	3.28E-06	5.12E-06	1.05E-05	0.00E+00	3.75E-06	3.99E-06
1025	9.29E-06	1.33E-05	2.16E-05	4.14E-06	4.51E-06	7.76E-06	0.00E+00	1.85E-06	2.40E-06
1050	3.18E-06	7.07E-06	1.20E-05	2.81E-06	3.95E-06	6.48E-06	0.00E+00	0.00E+00	3.27E-06
1075	0.00E+00	2.41E-06	6.01E-06	0.00E+00	3.56E-06	4.60E-06	0.00E+00	0.00E+00	0.00E+00
1100	0.00E+00	0.00E+00	2.13E-06	0.00E+00	0.00E+00	3.14E-06	0.00E+00	0.00E+00	0.00E+00

T (K)	Methyloxirane			Acrolein			Propanal		
	Phi=0.5	Phi=1	Phi=2	Phi=0.5	Phi=1	Phi=2	Phi=0.5	Phi=1	Phi=2
500	0.00E+00	0.00E+00	0.00E+00	0.00E+00	0.00E+00	0.00E+00	0.00E+00	0.00E+00	0.00E+00
525	0.00E+00	0.00E+00	0.00E+00	0.00E+00	0.00E+00	0.00E+00	0.00E+00	0.00E+00	0.00E+00
550	0.00E+00	0.00E+00	0.00E+00	0.00E+00	0.00E+00	0.00E+00	0.00E+00	0.00E+00	0.00E+00
575	0.00E+00	0.00E+00	0.00E+00	0.00E+00	0.00E+00	0.00E+00	0.00E+00	0.00E+00	0.00E+00
600	0.00E+00	0.00E+00	0.00E+00	0.00E+00	0.00E+00	0.00E+00	0.00E+00	0.00E+00	0.00E+00
625	0.00E+00	0.00E+00	0.00E+00	0.00E+00	0.00E+00	0.00E+00	0.00E+00	0.00E+00	0.00E+00
650	0.00E+00	0.00E+00	0.00E+00	0.00E+00	0.00E+00	0.00E+00	0.00E+00	0.00E+00	0.00E+00
675	0.00E+00	0.00E+00	0.00E+00	0.00E+00	0.00E+00	0.00E+00	0.00E+00	0.00E+00	0.00E+00
700	0.00E+00	0.00E+00	0.00E+00	0.00E+00	0.00E+00	0.00E+00	0.00E+00	0.00E+00	0.00E+00
725	0.00E+00	0.00E+00	0.00E+00	0.00E+00	0.00E+00	0.00E+00	3.94E-06	0.00E+00	0.00E+00
750	0.00E+00	0.00E+00	0.00E+00	0.00E+00	0.00E+00	0.00E+00	1.44E-06	0.00E+00	0.00E+00
775	0.00E+00	0.00E+00	0.00E+00	0.00E+00	0.00E+00	0.00E+00	4.24E-06	2.90E-06	1.54E-06
800	2.12E-06	0.00E+00	0.00E+00	2.24E-06	0.00E+00	0.00E+00	2.12E-05	9.08E-06	5.35E-06
825	9.98E-06	3.16E-06	2.49E-06	1.86E-05	1.39E-05	1.39E-05	4.45E-05	2.46E-05	1.72E-05
850	8.96E-06	6.80E-06	4.25E-06	3.41E-05	2.94E-05	2.78E-05	3.34E-05	1.95E-05	1.81E-05
875	5.86E-06	4.33E-06	4.39E-06	3.21E-05	3.41E-05	2.57E-05	2.21E-05	1.59E-05	1.27E-05
900	3.12E-06	2.84E-06	2.93E-06	2.17E-05	2.65E-05	2.16E-05	1.07E-05	1.24E-05	1.03E-05
925	3.12E-06	1.87E-06	3.04E-06	1.10E-05	1.58E-05	1.82E-05	5.04E-06	7.01E-06	9.72E-06
950	0.00E+00	0.00E+00	0.00E+00	7.89E-06	9.05E-06	1.16E-05	4.61E-06	4.21E-06	7.59E-06
975	0.00E+00	0.00E+00	0.00E+00	3.25E-06	4.16E-06	8.41E-06	1.67E-06	3.20E-06	5.21E-06
1000	0.00E+00	0.00E+00	0.00E+00	3.04E-06	2.82E-06	5.18E-06	0.00E+00	1.19E-06	4.43E-06
1025	0.00E+00	0.00E+00	0.00E+00	2.76E-06	1.71E-06	2.67E-06	1.76E-06	1.75E-06	4.11E-06
1050	0.00E+00	0.00E+00	0.00E+00	1.72E-06	0.00E+00	1.42E-06	0.00E+00	0.00E+00	1.97E-06
1075	0.00E+00	0.00E+00	0.00E+00	0.00E+00	0.00E+00	0.00E+00	0.00E+00	0.00E+00	2.69E-06
1100	0.00E+00	0.00E+00	0.00E+00	0.00E+00	0.00E+00	0.00E+00	0.00E+00	0.00E+00	0.00E+00

T (K)	1-Pentene			2-Pentene			Not-Identified		
	Phi=0.5	Phi=1	Phi=2	Phi=0.5	Phi=1	Phi=2	Phi=0.5	Phi=1	Phi=2
500	0.00E+00	0.00E+00	0.00E+00	0.00E+00	0.00E+00	0.00E+00	0.00E+00	0.00E+00	0.00E+00
525	0.00E+00	0.00E+00	0.00E+00	0.00E+00	0.00E+00	0.00E+00	0.00E+00	0.00E+00	0.00E+00
550	0.00E+00	0.00E+00	0.00E+00	0.00E+00	0.00E+00	0.00E+00	0.00E+00	0.00E+00	0.00E+00
575	0.00E+00	0.00E+00	0.00E+00	0.00E+00	0.00E+00	0.00E+00	0.00E+00	0.00E+00	0.00E+00
600	0.00E+00	0.00E+00	0.00E+00	0.00E+00	0.00E+00	0.00E+00	0.00E+00	0.00E+00	0.00E+00
625	0.00E+00	0.00E+00	0.00E+00	3.19E-06	0.00E+00	0.00E+00	0.00E+00	0.00E+00	0.00E+00
650	0.00E+00	0.00E+00	0.00E+00	0.00E+00	0.00E+00	0.00E+00	0.00E+00	0.00E+00	0.00E+00
675	0.00E+00	0.00E+00	0.00E+00	0.00E+00	0.00E+00	0.00E+00	0.00E+00	0.00E+00	0.00E+00
700	0.00E+00	0.00E+00	0.00E+00	0.00E+00	0.00E+00	0.00E+00	0.00E+00	0.00E+00	0.00E+00
725	0.00E+00	0.00E+00	0.00E+00	0.00E+00	0.00E+00	0.00E+00	0.00E+00	0.00E+00	0.00E+00
750	0.00E+00	0.00E+00	0.00E+00	0.00E+00	0.00E+00	0.00E+00	0.00E+00	0.00E+00	0.00E+00
775	0.00E+00	0.00E+00	0.00E+00	0.00E+00	0.00E+00	0.00E+00	0.00E+00	0.00E+00	0.00E+00
800	1.38E-06	0.00E+00	0.00E+00	0.00E+00	0.00E+00	0.00E+00	2.39E-06	1.28E-06	2.13E-06
825	4.05E-06	1.99E-06	1.08E-06	1.06E-06	1.06E-06	8.02E-07	8.45E-06	5.89E-06	5.92E-06
850	2.25E-06	2.42E-06	1.84E-06	1.11E-06	1.47E-06	1.90E-06	1.07E-05	9.62E-06	8.97E-06
875	1.68E-06	1.83E-06	1.47E-06	1.76E-06	2.25E-06	2.16E-06	6.91E-06	7.07E-06	6.14E-06
900	6.43E-07	0.00E+00	1.36E-06	7.89E-07	1.46E-06	2.10E-06	4.32E-06	5.08E-06	5.58E-06
925	0.00E+00	7.66E-07	1.30E-06	0.00E+00	0.00E+00	1.68E-06	2.38E-06	3.42E-06	3.77E-06
950	0.00E+00	0.00E+00	9.29E-07	0.00E+00	0.00E+00	1.48E-06	1.34E-06	0.00E+00	3.04E-06
975	0.00E+00	0.00E+00	6.50E-07	0.00E+00	0.00E+00	1.33E-06	2.24E-05	3.02E-06	2.04E-06
1000	0.00E+00	0.00E+00	7.05E-07	0.00E+00	7.74E-07	1.44E-06	1.67E-06	0.00E+00	1.85E-06
1025	0.00E+00	0.00E+00	0.00E+00	0.00E+00	0.00E+00	1.05E-06	1.02E-06	0.00E+00	1.33E-06
1050	0.00E+00	0.00E+00	0.00E+00	3.80E-06	0.00E+00	1.19E-06	0.00E+00	0.00E+00	0.00E+00
1075	0.00E+00	0.00E+00	0.00E+00	0.00E+00	0.00E+00	0.00E+00	0.00E+00	0.00E+00	0.00E+00
1100	0.00E+00	0.00E+00	0.00E+00	0.00E+00	0.00E+00	0.00E+00	0.00E+00	0.00E+00	0.00E+00

T (K)	Butanal			Tetrahydrofurane			2-3-Butanediol		
	Phi=0.5	Phi=1	Phi=2	Phi=0.5	Phi=1	Phi=2	Phi=0.5	Phi=1	Phi=2
500	2.07E-06	0.00E+00	2.20E-06	0.00E+00	0.00E+00	0.00E+00	0.00E+00	0.00E+00	0.00E+00
525	3.89E-06	2.36E-06	3.19E-06	1.33E-06	0.00E+00	0.00E+00	0.00E+00	0.00E+00	0.00E+00
550	3.53E-06	0.00E+00	2.41E-06	1.31E-06	0.00E+00	0.00E+00	0.00E+00	0.00E+00	0.00E+00
575	4.25E-06	3.77E-06	2.38E-06	0.00E+00	0.00E+00	0.00E+00	0.00E+00	0.00E+00	0.00E+00
600	3.86E-06	0.00E+00	3.11E-06	0.00E+00	0.00E+00	0.00E+00	0.00E+00	0.00E+00	0.00E+00
625	5.05E-06	2.96E-06	2.41E-06	0.00E+00	2.05E-06	2.53E-06	0.00E+00	0.00E+00	0.00E+00
650	4.75E-06	0.00E+00	2.92E-06	9.93E-07	0.00E+00	1.93E-06	0.00E+00	0.00E+00	0.00E+00
675	4.55E-06	3.42E-06	2.90E-06	2.83E-06	1.85E-06	2.63E-06	0.00E+00	0.00E+00	0.00E+00
700	3.46E-06	3.21E-06	5.33E-06	1.79E-06	0.00E+00	5.15E-06	0.00E+00	0.00E+00	0.00E+00
725	9.10E-06	6.34E-06	7.51E-06	5.42E-06	5.02E-06	5.66E-06	0.00E+00	0.00E+00	0.00E+00
750	1.21E-05	1.03E-05	1.37E-05	1.07E-05	8.95E-06	1.14E-05	0.00E+00	0.00E+00	0.00E+00
775	3.82E-05	3.11E-05	2.97E-05	3.44E-05	3.24E-05	2.52E-05	0.00E+00	0.00E+00	0.00E+00
800	2.14E-04	1.29E-04	1.26E-04	2.05E-04	1.29E-04	1.20E-04	0.00E+00	0.00E+00	0.00E+00
825	3.57E-04	3.35E-04	3.12E-04	3.50E-04	3.40E-04	3.10E-04	8.94E-07	0.00E+00	0.00E+00
850	2.33E-04	2.69E-04	2.71E-04	2.46E-04	2.29E-04	2.67E-04	1.39E-06	0.00E+00	8.98E-07
875	1.47E-04	1.50E-04	1.62E-04	1.76E-04	1.60E-04	1.43E-04	1.41E-06	1.63E-06	2.59E-06
900	8.91E-05	1.04E-04	9.72E-05	8.48E-05	1.03E-04	8.32E-05	1.49E-06	0.00E+00	1.70E-06
925	5.36E-05	5.97E-05	7.01E-05	5.02E-05	5.59E-05	6.42E-05	9.33E-07	1.28E-06	1.78E-06
950	3.04E-05	3.57E-05	4.26E-05	2.86E-05	2.83E-05	4.21E-05	0.00E+00	0.00E+00	1.26E-06
975	2.03E-05	2.13E-05	3.13E-05	1.68E-05	2.00E-05	2.81E-05	0.00E+00	0.00E+00	1.36E-06
1000	1.21E-05	1.18E-05	2.00E-05	9.68E-06	1.05E-05	2.00E-05	0.00E+00	0.00E+00	1.06E-06
1025	8.01E-06	7.05E-06	1.80E-05	5.89E-06	7.72E-06	1.41E-05	0.00E+00	0.00E+00	0.00E+00
1050	2.23E-06	3.79E-06	8.25E-06	1.54E-06	4.09E-06	6.73E-06	0.00E+00	0.00E+00	0.00E+00
1075	8.65E-07	8.66E-07	3.89E-06	0.00E+00	0.00E+00	2.59E-06	0.00E+00	0.00E+00	0.00E+00
1100	0.00E+00	0.00E+00	8.65E-07	0.00E+00	0.00E+00	0.00E+00	0.00E+00	0.00E+00	0.00E+00

Experimental raw data: *n*-butanol oxidation

T (K)	2-Butenal			1-Butanol		
	Phi=0.5	Phi=1	Phi=2	Phi=0.5	Phi=1	Phi=2
500	0.00E+00	0.00E+00	0.00E+00	5.17E-03	4.98E-03	5.66E-03
525	0.00E+00	0.00E+00	0.00E+00	5.19E-03	4.52E-03	5.39E-03
550	0.00E+00	0.00E+00	0.00E+00	4.54E-03	5.09E-03	5.33E-03
575	0.00E+00	0.00E+00	0.00E+00	4.82E-03	5.10E-03	4.74E-03
600	0.00E+00	0.00E+00	0.00E+00	5.03E-03	5.03E-03	5.13E-03
625	0.00E+00	0.00E+00	0.00E+00	5.17E-03	5.13E-03	5.36E-03
650	0.00E+00	0.00E+00	0.00E+00	4.91E-03	5.00E-03	5.00E-03
675	0.00E+00	0.00E+00	0.00E+00	5.22E-03	4.89E-03	5.27E-03
700	0.00E+00	0.00E+00	4.93E-06	4.48E-03	4.50E-03	5.19E-03
725	5.44E-06	0.00E+00	0.00E+00	5.01E-03	4.63E-03	5.08E-03
750	0.00E+00	0.00E+00	0.00E+00	5.09E-03	5.21E-03	5.20E-03
775	0.00E+00	0.00E+00	0.00E+00	5.03E-03	4.98E-03	4.63E-03
800	0.00E+00	0.00E+00	0.00E+00	4.35E-03	4.75E-03	5.01E-03
825	6.44E-06	6.08E-06	2.80E-06	2.75E-03	3.24E-03	3.59E-03
850	8.39E-06	6.35E-06	5.66E-06	1.27E-03	1.37E-03	2.03E-03
875	6.30E-06	5.42E-06	5.12E-06	8.44E-04	9.69E-04	1.16E-03
900	2.76E-06	3.65E-06	4.07E-06	4.09E-04	6.72E-04	7.64E-04
925	2.39E-06	2.25E-06	3.23E-06	2.72E-04	3.74E-04	6.41E-04
950	0.00E+00	0.00E+00	2.22E-06	1.72E-04	2.39E-04	5.04E-04
975	2.03E-05	0.00E+00	0.00E+00	9.77E-05	1.81E-04	3.93E-04
1000	0.00E+00	0.00E+00	1.63E-06	0.00E+00	1.16E-04	2.70E-04
1025	0.00E+00	0.00E+00	0.00E+00	0.00E+00	6.37E-05	1.38E-04
1050	0.00E+00	0.00E+00	0.00E+00	0.00E+00	1.35E-05	0.00E+00
1075	0.00E+00	0.00E+00	0.00E+00	0.00E+00	0.00E+00	0.00E+00
1100	0.00E+00	0.00E+00	0.00E+00	0.00E+00	0.00E+00	0.00E+00

II.3. Combustion of *n*-pentanol

Equivalence ratio	0,5 ; 1 ; 2
$x_{1\text{-pentanol}}$	0.005
Temperature (K)	500 - 1100
P (Torr)	800

Units	Mole fraction
Bath gas	Helium
Residence time (s)	2

T (K)	O_2			CO			CH_4		
	Phi=0.5	Phi=1	Phi=2	Phi=0.5	Phi=1	Phi=2	Phi=0.5	Phi=1	Phi=2
500	7.70E-02	3.89E-02	2.12E-02	0.00E+00	0.00E+00	0.00E+00	0.00E+00	0.00E+00	0.00E+00
525	7.90E-02	3.88E-02	1.97E-02	0.00E+00	0.00E+00	0.00E+00	0.00E+00	0.00E+00	3.18E-06
550	7.60E-02	4.04E-02	1.99E-02	0.00E+00	0.00E+00	0.00E+00	0.00E+00	0.00E+00	0.00E+00
575	7.64E-02	3.92E-02	1.93E-02	0.00E+00	0.00E+00	0.00E+00	0.00E+00	0.00E+00	1.34E-06
600	7.57E-02	3.95E-02	2.02E-02	0.00E+00	0.00E+00	0.00E+00	0.00E+00	0.00E+00	0.00E+00
625	7.63E-02	3.82E-02	1.93E-02	0.00E+00	0.00E+00	0.00E+00	0.00E+00	0.00E+00	7.21E-07
650	7.69E-02	3.78E-02	2.06E-02	0.00E+00	0.00E+00	0.00E+00	0.00E+00	0.00E+00	0.00E+00
675	7.59E-02	3.89E-02	1.95E-02	0.00E+00	0.00E+00	0.00E+00	0.00E+00	1.17E-06	0.00E+00
700	7.53E-02	3.83E-02	1.98E-02	0.00E+00	0.00E+00	0.00E+00	0.00E+00	0.00E+00	1.29E-06
725	7.72E-02	3.96E-02	1.99E-02	0.00E+00	0.00E+00	0.00E+00	0.00E+00	0.00E+00	0.00E+00
750	7.43E-02	4.05E-02	1.98E-02	0.00E+00	0.00E+00	0.00E+00	0.00E+00	0.00E+00	0.00E+00
775	7.72E-02	4.12E-02	1.97E-02	0.00E+00	0.00E+00	0.00E+00	1.63E-06	1.88E-06	2.27E-06
800	7.65E-02	3.86E-02	1.90E-02	6.13E-04	0.00E+00	0.00E+00	3.24E-05	8.94E-06	2.85E-05
825	7.20E-02	3.58E-02	1.70E-02	3.72E-03	3.40E-03	1.95E-03	1.99E-04	2.56E-04	2.47E-04
850	6.73E-02	3.27E-02	1.93E-02	8.23E-03	5.77E-03	5.14E-03	4.10E-04	4.73E-04	5.80E-04
875	6.33E-02	2.82E-02	1.25E-02	1.14E-02	9.37E-03	6.53E-03	5.11E-04	6.69E-04	8.03E-04
900	6.18E-02	2.52E-02	1.19E-02	1.31E-02	1.14E-02	9.23E-03	5.03E-04	7.60E-04	1.09E-03
925	5.73E-02	2.34E-02	1.16E-02	1.52E-02	1.35E-02	9.78E-03	4.91E-04	8.57E-04	1.25E-03
950	5.05E-02	2.31E-02	9.58E-03	1.37E-02	1.43E-02	1.05E-02	3.18E-04	8.92E-04	1.39E-03
975	4.79E-02	1.87E-02	8.90E-03	1.12E-02	1.45E-02	1.08E-02	1.75E-04	8.61E-04	1.55E-03
1000	4.41E-02	1.55E-02	8.43E-03	7.38E-03	1.24E-02	1.24E-02	9.08E-05	7.22E-04	1.74E-03
1025	4.35E-02	9.34E-03	7.71E-03	4.59E-03	6.05E-03	1.39E-02	6.34E-05	3.45E-04	2.01E-03
1050	4.31E-02	6.35E-03	6.42E-03	2.45E-03	3.09E-03	1.51E-02	4.76E-05	2.25E-04	1.94E-03
1075	4.15E-02	3.56E-03	3.89E-03	1.35E-03	1.19E-03	1.70E-02	2.87E-05	5.38E-05	1.74E-03
1100	4.00E-02	2.50E-03	2.79E-03	0.00E+00	1.03E-03	1.77E-02	0.00E+00	4.15E-05	1.40E-03

T (K)	CO_2			Acetylene			Ethylene		
	Phi=0.5	Phi=1	Phi=2	Phi=0.5	Phi=1	Phi=2	Phi=0.5	Phi=1	Phi=2
500	0.00E+00	0.00E+00	0.00E+00	0.00E+00	0.00E+00	0.00E+00	0.00E+00	0.00E+00	0.00E+00
525	0.00E+00	0.00E+00	0.00E+00	0.00E+00	0.00E+00	1.01E-06	0.00E+00	0.00E+00	1.01E-05
550	0.00E+00	0.00E+00	0.00E+00	0.00E+00	0.00E+00	0.00E+00	0.00E+00	0.00E+00	0.00E+00
575	0.00E+00	0.00E+00	0.00E+00	0.00E+00	0.00E+00	3.21E-07	0.00E+00	0.00E+00	6.87E-06
600	0.00E+00	0.00E+00	0.00E+00	0.00E+00	0.00E+00	0.00E+00	0.00E+00	0.00E+00	0.00E+00
625	0.00E+00	0.00E+00	0.00E+00	0.00E+00	0.00E+00	1.34E-07	0.00E+00	2.22E-06	4.04E-06
650	0.00E+00	0.00E+00	0.00E+00	0.00E+00	0.00E+00	0.00E+00	0.00E+00	0.00E+00	0.00E+00
675	0.00E+00	0.00E+00	0.00E+00	0.00E+00	0.00E+00	0.00E+00	0.00E+00	1.80E-05	8.02E-07
700	0.00E+00	0.00E+00	0.00E+00	0.00E+00	0.00E+00	0.00E+00	0.00E+00	0.00E+00	1.25E-05
725	0.00E+00	0.00E+00	0.00E+00	0.00E+00	0.00E+00	0.00E+00	9.21E-07	1.64E-06	0.00E+00
750	0.00E+00	0.00E+00	0.00E+00	0.00E+00	0.00E+00	0.00E+00	3.98E-06	0.00E+00	6.94E-06
775	0.00E+00	0.00E+00	0.00E+00	0.00E+00	0.00E+00	0.00E+00	2.63E-05	2.48E-05	2.96E-05
800	0.00E+00	0.00E+00	0.00E+00	0.00E+00	0.00E+00	0.00E+00	4.17E-04	1.14E-04	2.92E-04
825	1.95E-04	2.57E-04	0.00E+00	1.51E-06	0.00E+00	2.48E-06	1.69E-03	2.07E-03	1.72E-03
850	6.90E-04	0.00E+00	2.42E-04	6.57E-06	0.00E+00	5.80E-06	2.66E-03	2.88E-03	2.77E-03
875	1.46E-03	8.82E-04	0.00E+00	1.09E-05	8.63E-06	1.19E-05	2.69E-03	2.79E-03	3.11E-03
900	2.78E-03	1.38E-03	0.00E+00	1.48E-05	1.71E-05	2.06E-05	2.23E-03	2.86E-03	3.26E-03
925	4.57E-03	2.31E-03	9.33E-04	1.49E-05	2.01E-05	1.15E-04	1.71E-03	2.54E-03	3.18E-03
950	7.76E-03	3.19E-03	1.15E-03	1.85E-05	2.44E-05	3.05E-05	8.55E-04	2.15E-03	3.07E-03
975	1.33E-02	4.29E-03	1.31E-03	1.27E-05	2.10E-05	3.93E-05	4.03E-04	1.60E-03	3.05E-03
1000	1.66E-02	8.98E-03	1.66E-03	8.29E-06	1.83E-05	4.74E-05	2.36E-04	1.27E-03	2.83E-03
1025	2.14E-02	1.63E-02	1.90E-03	7.64E-06	1.73E-05	4.97E-05	1.87E-04	7.85E-04	2.73E-03
1050	2.37E-02	2.11E-02	2.52E-03	5.97E-06	1.57E-05	5.14E-05	1.05E-04	5.83E-04	2.10E-03
1075	2.49E-02	2.34E-02	3.13E-03	4.81E-06	8.10E-06	7.52E-05	3.22E-05	1.50E-04	1.40E-03
1100	2.62E-02	2.49E-02	3.59E-03	0.00E+00	0.00E+00	7.46E-05	6.45E-07	8.37E-05	9.44E-04

Experimental raw data: *n*-pentanol oxidation

T (K)	Ethane			Propene			Propane		
	Phi=0.5	Phi=1	Phi=2	Phi=0.5	Phi=1	Phi=2	Phi=0.5	Phi=1	Phi=2
500	0.00E+00	0.00E+00	0.00E+00	0.00E+00	0.00E+00	0.00E+00	0.00E+00	0.00E+00	0.00E+00
525	0.00E+00	0.00E+00	0.00E+00	0.00E+00	0.00E+00	0.00E+00	0.00E+00	0.00E+00	0.00E+00
550	0.00E+00	0.00E+00	0.00E+00	0.00E+00	0.00E+00	0.00E+00	0.00E+00	0.00E+00	0.00E+00
575	0.00E+00	0.00E+00	0.00E+00	0.00E+00	0.00E+00	0.00E+00	0.00E+00	0.00E+00	0.00E+00
600	0.00E+00	0.00E+00	0.00E+00	0.00E+00	0.00E+00	0.00E+00	0.00E+00	0.00E+00	0.00E+00
625	0.00E+00	0.00E+00	0.00E+00	0.00E+00	0.00E+00	0.00E+00	0.00E+00	0.00E+00	0.00E+00
650	0.00E+00	0.00E+00	0.00E+00	0.00E+00	0.00E+00	0.00E+00	0.00E+00	0.00E+00	0.00E+00
675	0.00E+00	0.00E+00	0.00E+00	0.00E+00	0.00E+00	0.00E+00	0.00E+00	0.00E+00	0.00E+00
700	0.00E+00	0.00E+00	0.00E+00	0.00E+00	0.00E+00	0.00E+00	0.00E+00	0.00E+00	0.00E+00
725	0.00E+00	0.00E+00	0.00E+00	0.00E+00	0.00E+00	0.00E+00	0.00E+00	0.00E+00	0.00E+00
750	0.00E+00	0.00E+00	0.00E+00	2.87E-06	2.15E-06	1.81E-06	0.00E+00	0.00E+00	0.00E+00
775	0.00E+00	0.00E+00	0.00E+00	1.12E-05	1.04E-05	6.68E-06	0.00E+00	0.00E+00	0.00E+00
800	0.00E+00	0.00E+00	2.03E-06	1.44E-04	2.51E-05	4.52E-05	0.00E+00	0.00E+00	0.00E+00
825	7.95E-06	1.72E-05	2.57E-05	4.06E-04	3.30E-04	3.03E-04	0.00E+00	1.31E-06	4.51E-06
850	2.00E-05	3.97E-05	6.64E-05	3.46E-04	4.22E-04	4.02E-04	0.00E+00	3.59E-06	8.68E-06
875	3.00E-05	5.38E-05	1.01E-04	3.04E-04	3.37E-04	3.82E-04	0.00E+00	7.32E-06	1.32E-05
900	2.52E-05	6.07E-05	1.33E-04	1.93E-04	2.51E-04	3.56E-04	0.00E+00	6.56E-06	1.76E-05
925	2.80E-05	5.98E-05	1.29E-04	1.28E-04	1.88E-04	2.85E-04	0.00E+00	8.49E-06	1.72E-05
950	1.28E-05	7.00E-05	1.37E-04	5.91E-05	1.50E-04	2.34E-04	0.00E+00	6.48E-06	1.73E-05
975	1.14E-05	6.19E-05	1.57E-04	3.71E-05	9.09E-05	2.22E-04	0.00E+00	0.00E+00	1.88E-05
1000	8.20E-06	5.69E-05	1.50E-04	2.85E-05	5.96E-05	1.50E-04	0.00E+00	4.56E-06	1.55E-05
1025	6.45E-06	4.71E-05	1.41E-04	1.90E-05	5.07E-05	1.04E-04	0.00E+00	2.64E-06	1.52E-05
1050	2.69E-06	4.14E-05	1.26E-04	4.20E-06	4.13E-05	6.57E-05	0.00E+00	0.00E+00	1.23E-05
1075	0.00E+00	1.32E-05	9.95E-05	0.00E+00	9.86E-06	3.34E-05	0.00E+00	0.00E+00	8.49E-06
1100	0.00E+00	3.35E-06	6.09E-05	0.00E+00	0.00E+00	1.36E-05	0.00E+00	0.00E+00	4.07E-06

T (K)	Acetaldehyde			Oxirane			Formaldehyde		
	Phi=0.5	Phi=1	Phi=2	Phi=0.5	Phi=1	Phi=2	Phi=0.5	Phi=1	Phi=2
500	0.00E+00	0.00E+00	0.00E+00	0.00E+00	0.00E+00	0.00E+00	0.00E+00	0.00E+00	0.00E+00
525	0.00E+00	0.00E+00	0.00E+00	0.00E+00	0.00E+00	0.00E+00	0.00E+00	0.00E+00	0.00E+00
550	0.00E+00	0.00E+00	0.00E+00	0.00E+00	0.00E+00	0.00E+00	0.00E+00	0.00E+00	0.00E+00
575	0.00E+00	0.00E+00	0.00E+00	0.00E+00	0.00E+00	0.00E+00	0.00E+00	0.00E+00	0.00E+00
600	0.00E+00	0.00E+00	0.00E+00	0.00E+00	0.00E+00	0.00E+00	0.00E+00	0.00E+00	0.00E+00
625	0.00E+00	0.00E+00	0.00E+00	0.00E+00	0.00E+00	0.00E+00	0.00E+00	0.00E+00	0.00E+00
650	0.00E+00	0.00E+00	0.00E+00	0.00E+00	0.00E+00	0.00E+00	0.00E+00	0.00E+00	0.00E+00
675	0.00E+00	0.00E+00	0.00E+00	0.00E+00	0.00E+00	0.00E+00	0.00E+00	0.00E+00	0.00E+00
700	0.00E+00	0.00E+00	0.00E+00	0.00E+00	0.00E+00	0.00E+00	0.00E+00	0.00E+00	0.00E+00
725	0.00E+00	0.00E+00	0.00E+00	0.00E+00	0.00E+00	0.00E+00	0.00E+00	0.00E+00	0.00E+00
750	4.63E-06	3.22E-06	3.03E-06	0.00E+00	0.00E+00	0.00E+00	0.00E+00	0.00E+00	0.00E+00
775	1.80E-05	1.04E-05	8.09E-06	0.00E+00	0.00E+00	0.00E+00	0.00E+00	0.00E+00	0.00E+00
800	1.27E-04	2.37E-05	4.32E-05	2.51E-06	0.00E+00	0.00E+00	1.26E-04	1.14E-04	0.00E+00
825	2.50E-04	2.05E-04	2.19E-04	2.23E-05	1.81E-05	1.47E-05	5.03E-04	4.26E-04	3.23E-04
850	2.04E-04	2.58E-04	3.17E-04	3.49E-05	3.35E-05	3.60E-05	3.98E-04	1.23E-03	5.82E-04
875	1.86E-04	2.34E-04	3.10E-04	3.35E-05	3.35E-05	2.90E-05	4.12E-04	4.64E-04	5.34E-04
900	1.41E-04	1.88E-04	3.10E-04	2.09E-05	2.23E-05	2.32E-05	2.80E-04	2.93E-04	4.20E-04
925	1.04E-04	1.63E-04	2.48E-04	1.40E-05	1.23E-05	1.23E-05	0.00E+00	0.00E+00	4.14E-04
950	5.44E-05	1.27E-04	2.03E-04	3.21E-06	7.95E-06	7.66E-06	1.31E-04	2.02E-04	2.69E-04
975	3.27E-05	1.00E-04	1.74E-04	0.00E+00	0.00E+00	4.88E-06	0.00E+00	1.63E-04	3.21E-04
1000	2.56E-05	6.07E-05	1.22E-04	0.00E+00	1.98E-06	2.39E-06	0.00E+00	0.00E+00	1.69E-04
1025	1.51E-05	4.42E-05	7.88E-05	0.00E+00	0.00E+00	2.13E-06	0.00E+00	0.00E+00	0.00E+00
1050	6.35E-06	3.59E-05	5.02E-05	0.00E+00	0.00E+00	1.62E-06	0.00E+00	0.00E+00	7.06E-05
1075	0.00E+00	6.52E-06	1.94E-05	0.00E+00	0.00E+00	0.00E+00	0.00E+00	0.00E+00	0.00E+00
1100	0.00E+00	0.00E+00	6.51E-06	0.00E+00	0.00E+00	0.00E+00	0.00E+00	0.00E+00	0.00E+00

T (K)	Methanol			1-Butene			1,3-Butadiene		
	Phi=0.5	Phi=1	Phi=2	Phi=0.5	Phi=1	Phi=2	Phi=0.5	Phi=1	Phi=2
500	0.00E+00	0.00E+00	0.00E+00	0.00E+00	0.00E+00	0.00E+00	0.00E+00	0.00E+00	0.00E+00
525	0.00E+00	0.00E+00	0.00E+00	0.00E+00	0.00E+00	0.00E+00	0.00E+00	0.00E+00	0.00E+00
550	0.00E+00	0.00E+00	0.00E+00	0.00E+00	0.00E+00	0.00E+00	0.00E+00	0.00E+00	0.00E+00
575	0.00E+00	0.00E+00	0.00E+00	0.00E+00	0.00E+00	0.00E+00	0.00E+00	0.00E+00	0.00E+00
600	0.00E+00	0.00E+00	0.00E+00	0.00E+00	0.00E+00	0.00E+00	0.00E+00	0.00E+00	0.00E+00
625	0.00E+00	0.00E+00	0.00E+00	0.00E+00	0.00E+00	0.00E+00	0.00E+00	0.00E+00	0.00E+00
650	0.00E+00	0.00E+00	0.00E+00	0.00E+00	0.00E+00	0.00E+00	0.00E+00	0.00E+00	0.00E+00
675	0.00E+00	0.00E+00	0.00E+00	0.00E+00	0.00E+00	0.00E+00	0.00E+00	0.00E+00	0.00E+00
700	0.00E+00	0.00E+00	0.00E+00	0.00E+00	0.00E+00	0.00E+00	0.00E+00	0.00E+00	0.00E+00
725	0.00E+00	0.00E+00	0.00E+00	0.00E+00	0.00E+00	0.00E+00	0.00E+00	0.00E+00	0.00E+00
750	0.00E+00	0.00E+00	0.00E+00	2.09E-06	1.35E-06	1.47E-06	0.00E+00	0.00E+00	0.00E+00
775	0.00E+00	0.00E+00	0.00E+00	9.46E-06	8.54E-06	7.71E-06	0.00E+00	0.00E+00	0.00E+00
800	0.00E+00	0.00E+00	0.00E+00	1.02E-04	2.44E-05	4.74E-05	8.74E-06	1.12E-06	3.06E-06
825	2.73E-05	3.35E-05	0.00E+00	2.14E-04	2.05E-04	2.07E-04	3.42E-05	2.82E-05	2.49E-05
850	3.35E-05	4.52E-05	0.00E+00	1.40E-04	2.07E-04	1.96E-04	3.19E-05	3.89E-05	3.55E-05
875	1.98E-05	2.34E-05	0.00E+00	1.05E-04	1.23E-04	1.42E-04	2.90E-05	2.95E-05	3.18E-05
900	1.76E-05	1.56E-05	0.00E+00	5.92E-05	7.09E-05	1.03E-04	1.87E-05	2.03E-05	2.88E-05
925	0.00E+00	0.00E+00	0.00E+00	3.98E-05	5.02E-05	7.38E-05	1.47E-05	1.59E-05	2.32E-05
950	0.00E+00	9.21E-06	0.00E+00	1.96E-05	3.43E-05	5.07E-05	6.12E-06	1.23E-05	2.01E-05
975	0.00E+00	0.00E+00	0.00E+00	1.67E-05	2.46E-05	4.35E-05	5.74E-06	1.20E-05	1.85E-05
1000	0.00E+00	0.00E+00	0.00E+00	1.05E-05	1.28E-05	2.71E-05	3.25E-06	5.44E-06	1.36E-05
1025	0.00E+00	0.00E+00	0.00E+00	5.08E-06	1.02E-05	1.57E-05	4.69E-06	7.85E-06	1.14E-05
1050	0.00E+00	0.00E+00	0.00E+00	0.00E+00	7.36E-06	9.59E-06	1.56E-06	7.67E-06	8.38E-06
1075	0.00E+00	0.00E+00	0.00E+00	0.00E+00	1.37E-06	3.78E-06	0.00E+00	2.60E-06	5.25E-06
1100	0.00E+00	0.00E+00	0.00E+00	0.00E+00	0.00E+00	1.56E-06	0.00E+00	0.00E+00	2.23E-06

T (K)	2-Butene			Methyloxirane			Acrolein		
	Phi=0.5	Phi=1	Phi=2	Phi=0.5	Phi=1	Phi=2	Phi=0.5	Phi=1	Phi=2
500	0.00E+00	0.00E+00	0.00E+00	0.00E+00	0.00E+00	0.00E+00	0.00E+00	0.00E+00	0.00E+00
525	0.00E+00	0.00E+00	0.00E+00	0.00E+00	0.00E+00	0.00E+00	0.00E+00	0.00E+00	0.00E+00
550	0.00E+00	0.00E+00	0.00E+00	0.00E+00	0.00E+00	0.00E+00	0.00E+00	0.00E+00	0.00E+00
575	0.00E+00	0.00E+00	0.00E+00	0.00E+00	0.00E+00	0.00E+00	0.00E+00	0.00E+00	0.00E+00
600	0.00E+00	0.00E+00	0.00E+00	0.00E+00	0.00E+00	0.00E+00	0.00E+00	0.00E+00	0.00E+00
625	0.00E+00	0.00E+00	0.00E+00	0.00E+00	0.00E+00	0.00E+00	0.00E+00	0.00E+00	0.00E+00
650	0.00E+00	0.00E+00	0.00E+00	0.00E+00	0.00E+00	0.00E+00	0.00E+00	0.00E+00	0.00E+00
675	0.00E+00	0.00E+00	0.00E+00	0.00E+00	0.00E+00	0.00E+00	0.00E+00	0.00E+00	0.00E+00
700	0.00E+00	0.00E+00	0.00E+00	0.00E+00	0.00E+00	0.00E+00	0.00E+00	0.00E+00	0.00E+00
725	0.00E+00	0.00E+00	0.00E+00	0.00E+00	0.00E+00	0.00E+00	0.00E+00	0.00E+00	0.00E+00
750	0.00E+00	0.00E+00	0.00E+00	0.00E+00	0.00E+00	0.00E+00	0.00E+00	0.00E+00	0.00E+00
775	0.00E+00	0.00E+00	0.00E+00	0.00E+00	0.00E+00	0.00E+00	0.00E+00	0.00E+00	0.00E+00
800	3.33E-06	0.00E+00	0.00E+00	2.20E-06	0.00E+00	0.00E+00	1.36E-05	1.67E-06	2.50E-06
825	8.51E-06	4.50E-06	5.52E-06	7.44E-06	5.72E-06	4.33E-06	4.74E-05	4.23E-05	3.15E-05
850	4.52E-06	4.21E-06	5.75E-06	6.68E-06	6.48E-06	5.79E-06	4.67E-05	4.91E-05	4.54E-05
875	4.25E-06	4.80E-06	5.15E-06	4.50E-06	4.63E-06	3.50E-06	3.98E-05	4.28E-05	3.58E-05
900	2.56E-06	2.84E-06	5.72E-06	2.40E-06	3.12E-06	2.64E-06	2.44E-05	2.15E-05	2.96E-05
925	2.84E-06	0.00E+00	4.83E-06	0.00E+00	0.00E+00	0.00E+00	1.48E-05	2.09E-05	1.85E-05
950	0.00E+00	3.07E-06	4.57E-06	0.00E+00	0.00E+00	0.00E+00	5.02E-06	9.91E-06	1.25E-05
975	0.00E+00	0.00E+00	4.22E-06	0.00E+00	0.00E+00	0.00E+00	4.21E-06	0.00E+00	9.65E-06
1000	0.00E+00	0.00E+00	3.94E-06	0.00E+00	0.00E+00	0.00E+00	2.94E-06	3.03E-06	4.24E-06
1025	0.00E+00	0.00E+00	0.00E+00	0.00E+00	0.00E+00	0.00E+00	3.10E-06	1.64E-06	3.07E-06
1050	0.00E+00	0.00E+00	0.00E+00	0.00E+00	0.00E+00	0.00E+00	0.00E+00	0.00E+00	1.78E-06
1075	0.00E+00	0.00E+00	0.00E+00	0.00E+00	0.00E+00	0.00E+00	0.00E+00	0.00E+00	0.00E+00
1100	0.00E+00	0.00E+00	0.00E+00	0.00E+00	0.00E+00	0.00E+00	0.00E+00	0.00E+00	0.00E+00

Experimental raw data: *n*-pentanol oxidation

T (K)	Propanal			Acetone			1-Pentene		
	Phi=0.5	Phi=1	Phi=2	Phi=0.5	Phi=1	Phi=2	Phi=0.5	Phi=1	Phi=2
500	0.00E+00	0.00E+00	0.00E+00	0.00E+00	0.00E+00	0.00E+00	0.00E+00	0.00E+00	0.00E+00
525	0.00E+00	0.00E+00	0.00E+00	0.00E+00	0.00E+00	0.00E+00	0.00E+00	0.00E+00	0.00E+00
550	0.00E+00	0.00E+00	0.00E+00	0.00E+00	0.00E+00	0.00E+00	0.00E+00	0.00E+00	0.00E+00
575	0.00E+00	0.00E+00	0.00E+00	0.00E+00	0.00E+00	0.00E+00	0.00E+00	0.00E+00	0.00E+00
600	0.00E+00	0.00E+00	0.00E+00	0.00E+00	0.00E+00	0.00E+00	0.00E+00	0.00E+00	0.00E+00
625	0.00E+00	0.00E+00	0.00E+00	0.00E+00	0.00E+00	0.00E+00	0.00E+00	0.00E+00	0.00E+00
650	0.00E+00	0.00E+00	0.00E+00	0.00E+00	0.00E+00	0.00E+00	0.00E+00	0.00E+00	0.00E+00
675	0.00E+00	0.00E+00	0.00E+00	0.00E+00	0.00E+00	0.00E+00	0.00E+00	0.00E+00	0.00E+00
700	0.00E+00	0.00E+00	0.00E+00	0.00E+00	0.00E+00	0.00E+00	0.00E+00	0.00E+00	0.00E+00
725	0.00E+00	0.00E+00	0.00E+00	0.00E+00	0.00E+00	0.00E+00	0.00E+00	0.00E+00	0.00E+00
750	3.51E-06	1.39E-06	2.10E-06	0.00E+00	0.00E+00	0.00E+00	2.67E-06	2.52E-06	2.58E-06
775	1.26E-05	7.06E-06	2.83E-06	1.82E-06	0.00E+00	0.00E+00	1.36E-05	1.19E-05	9.58E-06
800	6.56E-05	1.12E-05	1.31E-05	6.10E-06	0.00E+00	0.00E+00	8.29E-05	2.73E-05	4.56E-05
825	7.53E-05	4.33E-05	2.94E-05	1.58E-05	8.74E-06	4.76E-06	1.28E-04	1.31E-04	1.43E-04
850	3.28E-05	3.08E-05	2.15E-05	1.00E-05	1.01E-05	8.13E-06	7.34E-05	1.18E-04	1.19E-04
875	2.05E-05	1.67E-05	1.29E-05	8.76E-06	6.68E-06	9.13E-06	5.39E-05	6.69E-05	8.36E-05
900	9.67E-06	1.03E-05	1.19E-05	6.53E-06	6.04E-06	8.57E-06	3.19E-05	3.83E-05	6.24E-05
925	2.51E-06	7.42E-06	8.62E-06	6.00E-06	7.80E-06	7.83E-06	2.19E-05	2.82E-05	4.45E-05
950	2.15E-06	4.45E-06	6.86E-06	2.06E-06	3.71E-06	5.95E-06	1.36E-05	2.17E-05	2.94E-05
975	3.09E-06	0.00E+00	6.60E-06	0.00E+00	0.00E+00	4.99E-06	1.03E-05	1.21E-05	2.50E-05
1000	0.00E+00	1.44E-06	4.41E-06	0.00E+00	1.05E-06	4.47E-06	6.39E-06	9.55E-06	1.61E-05
1025	0.00E+00	1.27E-06	1.32E-06	0.00E+00	0.00E+00	0.00E+00	2.96E-06	5.48E-06	9.70E-06
1050	0.00E+00	0.00E+00	1.45E-06	0.00E+00	0.00E+00	2.21E-06	0.00E+00	0.00E+00	3.97E-06
1075	0.00E+00	0.00E+00	0.00E+00	0.00E+00	0.00E+00	0.00E+00	0.00E+00	0.00E+00	1.69E-06
1100	0.00E+00	0.00E+00	0.00E+00	0.00E+00	0.00E+00	0.00E+00	0.00E+00	0.00E+00	0.00E+00

T (K)	2-Pentene			1,4-Pentadiene			1,3-Pentadiene		
	Phi=0.5	Phi=1	Phi=2	Phi=0.5	Phi=1	Phi=2	Phi=0.5	Phi=1	Phi=2
500	0.00E+00	0.00E+00	0.00E+00	0.00E+00	0.00E+00	0.00E+00	0.00E+00	0.00E+00	0.00E+00
525	0.00E+00	0.00E+00	0.00E+00	0.00E+00	0.00E+00	0.00E+00	0.00E+00	0.00E+00	0.00E+00
550	0.00E+00	0.00E+00	2.16E-06	0.00E+00	0.00E+00	0.00E+00	0.00E+00	0.00E+00	0.00E+00
575	0.00E+00	0.00E+00	0.00E+00	0.00E+00	0.00E+00	0.00E+00	0.00E+00	0.00E+00	0.00E+00
600	0.00E+00	0.00E+00	0.00E+00	0.00E+00	0.00E+00	0.00E+00	0.00E+00	0.00E+00	0.00E+00
625	0.00E+00	0.00E+00	3.59E-06	0.00E+00	0.00E+00	0.00E+00	0.00E+00	0.00E+00	0.00E+00
650	0.00E+00	0.00E+00	0.00E+00	0.00E+00	0.00E+00	0.00E+00	0.00E+00	0.00E+00	0.00E+00
675	0.00E+00	0.00E+00	0.00E+00	0.00E+00	0.00E+00	0.00E+00	0.00E+00	0.00E+00	0.00E+00
700	5.25E-06	0.00E+00	0.00E+00	0.00E+00	0.00E+00	0.00E+00	0.00E+00	0.00E+00	0.00E+00
725	0.00E+00	3.91E-06	0.00E+00	0.00E+00	0.00E+00	0.00E+00	0.00E+00	0.00E+00	0.00E+00
750	5.83E-07	5.58E-06	3.60E-06	0.00E+00	0.00E+00	0.00E+00	0.00E+00	0.00E+00	0.00E+00
775	3.10E-06	7.81E-06	3.97E-06	0.00E+00	0.00E+00	0.00E+00	0.00E+00	0.00E+00	0.00E+00
800	3.15E-06	1.90E-06	4.93E-06	1.82E-06	0.00E+00	1.09E-06	1.06E-06	0.00E+00	0.00E+00
825	3.57E-06	7.81E-06	5.16E-06	4.86E-06	3.16E-06	2.42E-06	1.23E-06	1.54E-06	1.39E-06
850	4.25E-06	7.14E-06	7.36E-06	2.11E-06	2.86E-06	2.64E-06	1.12E-06	1.17E-06	1.26E-06
875	3.23E-06	8.67E-06	5.19E-06	1.77E-06	2.12E-06	2.22E-06	9.55E-07	1.64E-06	1.06E-06
900	2.61E-06	2.20E-06	6.95E-06	8.97E-07	1.97E-06	1.35E-06	0.00E+00	0.00E+00	7.16E-07
925	3.62E-06	0.00E+00	7.57E-06	1.86E-06	0.00E+00	1.29E-06	0.00E+00	0.00E+00	7.93E-07
950	0.00E+00	4.84E-06	8.10E-06	0.00E+00	0.00E+00	2.64E-06	0.00E+00	0.00E+00	0.00E+00
975	3.69E-06	0.00E+00	6.07E-06	0.00E+00	0.00E+00	0.00E+00	0.00E+00	0.00E+00	0.00E+00
1000	2.19E-06	0.00E+00	6.19E-06	0.00E+00	0.00E+00	0.00E+00	0.00E+00	0.00E+00	0.00E+00
1025	0.00E+00	2.24E-06	4.14E-06	0.00E+00	0.00E+00	0.00E+00	0.00E+00	0.00E+00	0.00E+00
1050	2.03E-06	0.00E+00	3.51E-06	0.00E+00	0.00E+00	0.00E+00	0.00E+00	0.00E+00	0.00E+00
1075	0.00E+00	3.17E-06	4.58E-06	0.00E+00	0.00E+00	0.00E+00	0.00E+00	0.00E+00	0.00E+00
1100	0.00E+00	0.00E+00	2.46E-06	0.00E+00	0.00E+00	0.00E+00	0.00E+00	0.00E+00	0.00E+00

Experimental raw data: *n*-pentanol oxidation

T (K)	Not-identified			2-Methylfuran			Pentane		
	Phi=0.5	Phi=1	Phi=2	Phi=0.5	Phi=1	Phi=2	Phi=0.5	Phi=1	Phi=2
500	0.00E+00	0.00E+00	0.00E+00	0.00E+00	0.00E+00	0.00E+00	0.00E+00	0.00E+00	0.00E+00
525	0.00E+00	0.00E+00	0.00E+00	0.00E+00	0.00E+00	0.00E+00	0.00E+00	0.00E+00	0.00E+00
550	0.00E+00	0.00E+00	0.00E+00	0.00E+00	0.00E+00	0.00E+00	0.00E+00	0.00E+00	0.00E+00
575	0.00E+00	0.00E+00	0.00E+00	0.00E+00	0.00E+00	0.00E+00	0.00E+00	0.00E+00	0.00E+00
600	0.00E+00	0.00E+00	0.00E+00	0.00E+00	0.00E+00	0.00E+00	0.00E+00	0.00E+00	0.00E+00
625	0.00E+00	0.00E+00	0.00E+00	0.00E+00	0.00E+00	0.00E+00	0.00E+00	0.00E+00	0.00E+00
650	0.00E+00	0.00E+00	0.00E+00	0.00E+00	0.00E+00	0.00E+00	0.00E+00	0.00E+00	0.00E+00
675	0.00E+00	0.00E+00	0.00E+00	0.00E+00	0.00E+00	0.00E+00	0.00E+00	0.00E+00	0.00E+00
700	0.00E+00	0.00E+00	0.00E+00	0.00E+00	0.00E+00	0.00E+00	0.00E+00	0.00E+00	0.00E+00
725	0.00E+00	0.00E+00	0.00E+00	0.00E+00	0.00E+00	0.00E+00	0.00E+00	0.00E+00	0.00E+00
750	0.00E+00	0.00E+00	0.00E+00	0.00E+00	0.00E+00	0.00E+00	0.00E+00	0.00E+00	0.00E+00
775	1.41E-06	0.00E+00	1.08E-06	0.00E+00	0.00E+00	0.00E+00	1.27E-06	2.35E-06	0.00E+00
800	1.44E-05	4.13E-06	5.45E-06	1.81E-06	0.00E+00	0.00E+00	1.57E-05	1.62E-06	0.00E+00
825	2.68E-05	2.36E-05	2.54E-05	2.40E-06	1.67E-06	1.10E-06	2.12E-05	1.47E-05	0.00E+00
850	2.06E-05	3.20E-05	2.50E-05	1.41E-06	2.30E-06	9.85E-07	1.01E-05	8.21E-06	0.00E+00
875	1.54E-05	1.69E-05	1.80E-05	0.00E+00	0.00E+00	0.00E+00	4.60E-06	3.55E-06	0.00E+00
900	8.10E-06	9.31E-06	1.27E-05	0.00E+00	0.00E+00	0.00E+00	1.94E-06	1.55E-06	0.00E+00
925	4.39E-06	8.60E-06	9.67E-06	0.00E+00	0.00E+00	0.00E+00	1.38E-06	0.00E+00	0.00E+00
950	2.98E-06	3.93E-06	6.45E-06	0.00E+00	0.00E+00	0.00E+00	0.00E+00	0.00E+00	0.00E+00
975	3.11E-06	0.00E+00	5.43E-06	0.00E+00	0.00E+00	0.00E+00	0.00E+00	0.00E+00	0.00E+00
1000	1.49E-06	0.00E+00	3.21E-06	0.00E+00	0.00E+00	0.00E+00	0.00E+00	0.00E+00	0.00E+00
1025	0.00E+00	1.58E-06	9.78E-07	0.00E+00	0.00E+00	0.00E+00	0.00E+00	0.00E+00	0.00E+00
1050	0.00E+00	0.00E+00	1.38E-06	0.00E+00	0.00E+00	0.00E+00	0.00E+00	0.00E+00	0.00E+00
1075	0.00E+00	0.00E+00	0.00E+00	0.00E+00	0.00E+00	0.00E+00	0.00E+00	0.00E+00	0.00E+00
1100	0.00E+00	0.00E+00	0.00E+00	0.00E+00	0.00E+00	0.00E+00	0.00E+00	0.00E+00	0.00E+00

T (K)	Methyl vinyl ketone			Butanal			Tetrahydrofuran		
	Phi=0.5	Phi=1	Phi=2	Phi=0.5	Phi=1	Phi=2	Phi=0.5	Phi=1	Phi=2
500	0.00E+00	0.00E+00	0.00E+00	0.00E+00	0.00E+00	0.00E+00	0.00E+00	0.00E+00	0.00E+00
525	0.00E+00	0.00E+00	0.00E+00	0.00E+00	0.00E+00	0.00E+00	0.00E+00	0.00E+00	0.00E+00
550	0.00E+00	0.00E+00	0.00E+00	0.00E+00	0.00E+00	0.00E+00	0.00E+00	0.00E+00	0.00E+00
575	0.00E+00	0.00E+00	0.00E+00	0.00E+00	0.00E+00	0.00E+00	0.00E+00	0.00E+00	0.00E+00
600	0.00E+00	0.00E+00	0.00E+00	0.00E+00	0.00E+00	0.00E+00	0.00E+00	0.00E+00	0.00E+00
625	0.00E+00	0.00E+00	0.00E+00	0.00E+00	0.00E+00	0.00E+00	0.00E+00	0.00E+00	0.00E+00
650	0.00E+00	0.00E+00	0.00E+00	0.00E+00	0.00E+00	0.00E+00	0.00E+00	0.00E+00	0.00E+00
675	0.00E+00	0.00E+00	0.00E+00	0.00E+00	0.00E+00	0.00E+00	0.00E+00	0.00E+00	0.00E+00
700	0.00E+00	0.00E+00	0.00E+00	0.00E+00	0.00E+00	0.00E+00	0.00E+00	0.00E+00	0.00E+00
725	0.00E+00	0.00E+00	0.00E+00	0.00E+00	0.00E+00	0.00E+00	0.00E+00	0.00E+00	0.00E+00
750	0.00E+00	0.00E+00	0.00E+00	0.00E+00	0.00E+00	0.00E+00	0.00E+00	0.00E+00	0.00E+00
775	0.00E+00	0.00E+00	1.89E-06	0.00E+00	0.00E+00	0.00E+00	5.59E-06	6.31E-06	2.43E-06
800	0.00E+00	0.00E+00	3.41E-06	1.07E-05	0.00E+00	0.00E+00	1.91E-05	2.09E-06	1.68E-06
825	2.65E-06	1.39E-06	8.75E-06	1.19E-05	7.45E-06	9.40E-07	2.58E-05	1.38E-05	3.19E-06
850	1.80E-06	1.61E-06	1.93E-06	4.18E-06	4.79E-06	0.00E+00	1.07E-05	7.83E-06	2.66E-06
875	1.80E-06	1.29E-06	7.05E-07	0.00E+00	0.00E+00	0.00E+00	9.04E-06	5.49E-06	3.85E-06
900	0.00E+00	1.62E-06	9.78E-07	0.00E+00	0.00E+00	9.49E-07	3.86E-06	4.52E-06	2.31E-06
925	0.00E+00	0.00E+00	0.00E+00	0.00E+00	0.00E+00	0.00E+00	1.11E-06	0.00E+00	1.12E-06
950	0.00E+00	0.00E+00	0.00E+00	0.00E+00	0.00E+00	0.00E+00	0.00E+00	0.00E+00	1.20E-06
975	0.00E+00	0.00E+00	0.00E+00	0.00E+00	0.00E+00	0.00E+00	0.00E+00	0.00E+00	0.00E+00
1000	0.00E+00	0.00E+00	0.00E+00	0.00E+00	0.00E+00	0.00E+00	0.00E+00	0.00E+00	0.00E+00
1025	0.00E+00	0.00E+00	0.00E+00	0.00E+00	0.00E+00	0.00E+00	0.00E+00	0.00E+00	0.00E+00
1050	0.00E+00	0.00E+00	0.00E+00	0.00E+00	0.00E+00	0.00E+00	0.00E+00	0.00E+00	0.00E+00
1075	0.00E+00	0.00E+00	0.00E+00	0.00E+00	0.00E+00	0.00E+00	0.00E+00	0.00E+00	0.00E+00
1100	0.00E+00	0.00E+00	0.00E+00	0.00E+00	0.00E+00	0.00E+00	0.00E+00	0.00E+00	0.00E+00

T (K)	2-3-Butanediol			2-Butenal			Pentanal		
	Phi=0.5	Phi=1	Phi=2	Phi=0.5	Phi=1	Phi=2	Phi=0.5	Phi=1	Phi=2
500	0.00E+00	0.00E+00	0.00E+00	0.00E+00	0.00E+00	0.00E+00	0.00E+00	7.68E-07	0.00E+00
525	0.00E+00	0.00E+00	0.00E+00	0.00E+00	0.00E+00	0.00E+00	0.00E+00	1.44E-06	9.67E-07
550	0.00E+00	0.00E+00	0.00E+00	0.00E+00	0.00E+00	0.00E+00	0.00E+00	2.97E-06	0.00E+00
575	0.00E+00	0.00E+00	0.00E+00	0.00E+00	0.00E+00	0.00E+00	0.00E+00	1.69E-06	4.23E-06
600	0.00E+00	0.00E+00	0.00E+00	0.00E+00	0.00E+00	0.00E+00	0.00E+00	0.00E+00	0.00E+00
625	0.00E+00	0.00E+00	0.00E+00	0.00E+00	0.00E+00	0.00E+00	0.00E+00	4.80E-07	9.88E-07
650	0.00E+00	0.00E+00	0.00E+00	0.00E+00	0.00E+00	0.00E+00	0.00E+00	6.94E-06	0.00E+00
675	0.00E+00	0.00E+00	0.00E+00	0.00E+00	0.00E+00	0.00E+00	0.00E+00	7.19E-07	9.40E-07
700	0.00E+00	0.00E+00	0.00E+00	0.00E+00	0.00E+00	0.00E+00	6.94E-06	0.00E+00	0.00E+00
725	0.00E+00	0.00E+00	0.00E+00	0.00E+00	0.00E+00	0.00E+00	1.02E-05	0.00E+00	7.55E-06
750	0.00E+00	0.00E+00	0.00E+00	0.00E+00	0.00E+00	0.00E+00	2.16E-05	4.18E-05	0.00E+00
775	0.00E+00	0.00E+00	0.00E+00	0.00E+00	0.00E+00	0.00E+00	7.63E-05	5.51E-05	4.94E-07
800	1.57E-06	0.00E+00	0.00E+00	2.00E-06	0.00E+00	0.00E+00	3.49E-04	1.87E-04	1.82E-04
825	1.81E-06	1.73E-06	1.58E-06	9.07E-06	7.16E-06	4.14E-06	3.52E-04	3.49E-04	3.23E-04
850	2.64E-06	2.09E-06	1.26E-06	8.81E-06	1.06E-05	7.34E-06	2.08E-04	2.60E-04	1.99E-04
875	2.07E-06	1.71E-06	2.22E-06	7.49E-06	5.79E-06	6.43E-06	1.25E-04	1.10E-04	1.22E-04
900	0.00E+00	0.00E+00	1.27E-06	3.89E-06	3.52E-06	4.59E-06	5.97E-05	7.42E-05	6.74E-05
925	0.00E+00	0.00E+00	1.09E-06	1.87E-06	6.11E-06	3.73E-06	4.06E-05	4.15E-05	4.97E-05
950	0.00E+00	0.00E+00	1.02E-06	0.00E+00	0.00E+00	2.47E-06	2.03E-05	3.28E-05	2.70E-05
975	0.00E+00	0.00E+00	0.00E+00	0.00E+00	0.00E+00	2.18E-06	1.51E-05	1.52E-05	2.04E-05
1000	0.00E+00	0.00E+00	0.00E+00	0.00E+00	0.00E+00	0.00E+00	7.43E-06	1.15E-05	1.34E-05
1025	0.00E+00	0.00E+00	0.00E+00	0.00E+00	0.00E+00	1.23E-05	0.00E+00	4.93E-06	8.17E-06
1050	0.00E+00	0.00E+00	0.00E+00	0.00E+00	0.00E+00	0.00E+00	0.00E+00	0.00E+00	3.72E-06
1075	0.00E+00	0.00E+00	0.00E+00	0.00E+00	0.00E+00	0.00E+00	0.00E+00	0.00E+00	0.00E+00
1100	0.00E+00	0.00E+00	0.00E+00	0.00E+00	0.00E+00	0.00E+00	0.00E+00	0.00E+00	0.00E+00

T (K)	1-Pentanol		
	Phi=0.5	Phi=1	Phi=2
500	5.14E-03	5.06E-03	5.19E-03
525	5.40E-03	5.06E-03	4.94E-03
550	5.03E-03	5.24E-03	5.10E-03
575	5.13E-03	5.05E-03	4.83E-03
600	4.83E-03	5.46E-03	4.71E-03
625	4.90E-03	5.20E-03	4.82E-03
650	4.71E-03	5.15E-03	4.72E-03
675	4.96E-03	5.12E-03	4.70E-03
700	4.91E-03	5.51E-03	5.11E-03
725	5.08E-03	5.14E-03	4.83E-03
750	4.97E-03	5.71E-03	4.79E-03
775	4.94E-03	5.09E-03	4.81E-03
800	3.68E-03	4.81E-03	4.30E-03
825	1.87E-03	2.23E-03	2.41E-03
850	9.10E-04	1.23E-03	1.30E-03
875	5.25E-04	6.85E-04	8.98E-04
900	3.15E-04	4.77E-04	6.23E-04
925	2.48E-04	3.93E-04	5.40E-04
950	1.08E-04	2.24E-04	3.47E-04
975	8.98E-05	1.52E-04	2.58E-04
1000	0.00E+00	1.40E-04	1.73E-04
1025	0.00E+00	0.00E+00	9.47E-05
1050	0.00E+00	0.00E+00	0.00E+00
1075	0.00E+00	0.00E+00	0.00E+00
1100	0.00E+00	0.00E+00	0.00E+00

II.4. Combustion of *n*-butanal

Equivalence ratio	0,5 ; 1 ; 2
$x_{1\text{-butanal}}$	0.005
Temperature (K)	500 - 1100
P (Torr)	800

Units	Mole fraction
Bath gas	Helium
Residence time (s)	2

T (K)	O_2			CO			CH_4		
	Phi=0.5	Phi=1	Phi=2	Phi=0.5	Phi=1	Phi=2	Phi=0.5	Phi=1	Phi=2
500	5.83E-02	2.93E-02	1.53E-02	0.00E+00	0.00E+00	0.00E+00	0.00E+00	0.00E+00	0.00E+00
525	5.65E-02	2.93E-02	1.74E-02	0.00E+00	0.00E+00	0.00E+00	0.00E+00	0.00E+00	0.00E+00
550	5.80E-02	2.86E-02	1.47E-02	0.00E+00	0.00E+00	0.00E+00	3.27E-06	0.00E+00	0.00E+00
575	5.44E-02	3.05E-02	1.44E-02	0.00E+00	0.00E+00	0.00E+00	0.00E+00	0.00E+00	0.00E+00
600	5.55E-02	2.78E-02	1.53E-02	7.17E-04	3.49E-04	1.60E-04	2.31E-07	0.00E+00	0.00E+00
625	5.24E-02	2.77E-02	1.45E-02	1.92E-03	8.84E-04	3.15E-04	1.43E-06	1.14E-06	5.94E-07
650	5.37E-02	2.78E-02	1.41E-02	1.43E-03	3.27E-04	1.56E-04	2.50E-06	0.00E+00	6.38E-07
675	5.86E-02	2.81E-02	1.95E-02	6.31E-04	2.94E-04	1.81E-04	9.52E-07	1.13E-06	2.91E-06
700	5.59E-02	2.95E-02	1.48E-02	3.91E-04	3.42E-04	2.83E-04	1.88E-06	5.63E-06	1.41E-05
725	5.78E-02	2.88E-02	1.52E-02	6.39E-04	5.20E-04	5.61E-04	1.15E-05	2.70E-05	6.10E-05
750	6.02E-02	2.79E-02	1.43E-02	1.09E-03	7.87E-04	7.99E-04	4.98E-05	8.66E-05	1.53E-04
775	5.36E-02	2.78E-02	1.45E-02	1.74E-03	1.59E-03	1.18E-03	1.54E-04	2.68E-04	3.38E-04
800	5.39E-02	2.74E-02	1.42E-02	3.14E-03	2.55E-03	1.46E-03	3.72E-04	5.50E-04	5.45E-04
825	5.17E-02	2.71E-02	1.41E-02	4.48E-03	3.59E-03	2.19E-03	6.16E-04	8.28E-04	8.31E-04
850	5.22E-02	2.62E-02	1.37E-02	6.71E-03	4.88E-03	3.03E-03	8.34E-04	1.02E-03	1.09E-03
875	5.11E-02	2.50E-02	1.29E-02	8.03E-03	6.91E-03	4.80E-03	9.56E-04	1.25E-03	1.37E-03
900	4.66E-02	2.25E-02	1.14E-02	1.08E-02	8.93E-03	6.03E-03	9.33E-04	1.26E-03	1.46E-03
925	4.40E-02	2.14E-02	1.11E-02	1.15E-02	1.02E-02	7.07E-03	8.66E-04	1.23E-03	1.55E-03
950	3.96E-02	1.91E-02	9.53E-03	1.27E-02	1.13E-02	8.46E-03	5.92E-04	1.19E-03	1.63E-03
975	3.48E-02	1.70E-02	9.51E-03	1.01E-02	1.22E-02	9.64E-03	2.82E-04	1.13E-03	1.76E-03
1000	3.22E-02	1.47E-02	7.99E-03	6.61E-03	1.35E-02	1.02E-02	1.37E-04	1.00E-03	1.90E-03
1025	3.11E-02	1.04E-02	7.86E-03	3.81E-03	8.71E-03	1.16E-02	8.64E-05	5.96E-04	1.92E-03
1050	2.94E-02	6.23E-03	5.79E-03	2.19E-03	5.37E-03	1.32E-02	6.53E-05	3.73E-04	1.82E-03
1075	2.85E-02	3.10E-03	3.72E-03	1.43E-03	1.52E-03	1.39E-02	4.47E-05	9.52E-05	1.18E-03
1100	2.95E-02	1.29E-03	2.26E-03	6.22E-04	9.75E-04	1.50E-02	7.48E-06	5.04E-05	1.04E-03

T (K)	CO_2			Acetylene			Ethylene		
	Phi=0.5	Phi=1	Phi=2	Phi=0.5	Phi=1	Phi=2	Phi=0.5	Phi=1	Phi=2
500	0.00E+00	0.00E+00	0.00E+00	0.00E+00	0.00E+00	0.00E+00	0.00E+00	0.00E+00	0.00E+00
525	0.00E+00	0.00E+00	0.00E+00	0.00E+00	0.00E+00	0.00E+00	0.00E+00	0.00E+00	0.00E+00
550	0.00E+00	0.00E+00	0.00E+00	0.00E+00	0.00E+00	0.00E+00	2.32E-05	0.00E+00	0.00E+00
575	0.00E+00	0.00E+00	0.00E+00	0.00E+00	0.00E+00	0.00E+00	1.75E-06	1.47E-06	1.00E-06
600	0.00E+00	0.00E+00	0.00E+00	0.00E+00	0.00E+00	0.00E+00	5.45E-05	3.23E-05	1.51E-05
625	1.36E-04	0.00E+00	0.00E+00	0.00E+00	0.00E+00	0.00E+00	1.74E-04	1.05E-04	4.27E-05
650	0.00E+00	0.00E+00	0.00E+00	0.00E+00	0.00E+00	0.00E+00	1.50E-04	3.86E-05	1.79E-05
675	0.00E+00	0.00E+00	0.00E+00	0.00E+00	0.00E+00	0.00E+00	5.13E-05	2.68E-05	2.29E-05
700	0.00E+00	0.00E+00	0.00E+00	0.00E+00	0.00E+00	0.00E+00	3.28E-05	3.74E-05	5.55E-05
725	0.00E+00	0.00E+00	0.00E+00	2.20E-05	0.00E+00	0.00E+00	8.16E-05	9.88E-05	1.57E-04
750	0.00E+00	0.00E+00	0.00E+00	0.00E+00	0.00E+00	0.00E+00	2.07E-04	2.17E-04	2.96E-04
775	0.00E+00	0.00E+00	0.00E+00	0.00E+00	0.00E+00	0.00E+00	4.99E-04	6.05E-04	5.79E-04
800	1.67E-04	0.00E+00	8.37E-05	2.59E-07	0.00E+00	0.00E+00	1.71E-03	1.11E-03	8.23E-04
825	2.99E-04	0.00E+00	0.00E+00	1.15E-06	1.04E-06	0.00E+00	1.58E-03	1.63E-03	1.26E-03
850	4.13E-04	0.00E+00	1.55E-04	3.54E-06	2.04E-06	2.14E-06	2.09E-03	2.05E-03	1.67E-03
875	0.00E+00	0.00E+00	0.00E+00	6.01E-06	6.31E-06	4.83E-06	2.30E-03	2.53E-03	2.33E-03
900	1.15E-03	6.21E-04	3.11E-04	1.01E-05	1.11E-05	1.17E-05	2.09E-03	2.60E-03	2.54E-03
925	1.78E-03	9.75E-04	3.17E-04	1.26E-05	1.60E-05	2.09E-05	1.77E-03	2.37E-03	2.68E-03
950	4.42E-03	1.40E-03	6.37E-04	9.84E-06	1.77E-05	2.62E-05	9.29E-04	2.02E-03	2.61E-03
975	9.17E-03	2.41E-03	8.10E-04	4.54E-06	1.99E-05	7.02E-05	3.38E-04	1.60E-03	2.63E-03
1000	1.31E-02	3.83E-03	1.28E-03	2.32E-06	1.58E-05	3.73E-05	1.80E-04	1.13E-03	2.48E-03
1025	1.72E-02	9.47E-03	1.30E-03	2.30E-06	1.45E-05	4.21E-05	1.32E-04	7.83E-04	2.49E-03
1050	1.86E-02	1.44E-02	1.91E-03	2.41E-06	1.51E-05	3.85E-05	1.04E-04	4.83E-04	1.60E-03
1075	2.04E-02	1.90E-02	2.90E-03	2.28E-06	8.74E-06	3.14E-05	5.38E-05	1.62E-04	8.24E-04
1100	1.98E-02	2.03E-02	3.32E-03	0.00E+00	1.01E-05	5.43E-05	4.03E-05	7.89E-05	6.67E-04

Experimental raw data: *n*-butanal oxidation

T (K)	Ethane			Propene			Propane		
	Phi=0.5	Phi=1	Phi=2	Phi=0.5	Phi=1	Phi=2	Phi=0.5	Phi=1	Phi=2
500	0.00E+00	0.00E+00	0.00E+00	0.00E+00	0.00E+00	0.00E+00	0.00E+00	0.00E+00	0.00E+00
525	0.00E+00	0.00E+00	0.00E+00	1.62E-06	2.52E-06	0.00E+00	0.00E+00	0.00E+00	0.00E+00
550	0.00E+00	0.00E+00	0.00E+00	0.00E+00	0.00E+00	0.00E+00	0.00E+00	0.00E+00	0.00E+00
575	0.00E+00	0.00E+00	0.00E+00	1.18E-05	7.31E-06	5.96E-06	0.00E+00	0.00E+00	0.00E+00
600	0.00E+00	0.00E+00	0.00E+00	1.67E-04	8.97E-05	4.24E-05	0.00E+00	0.00E+00	0.00E+00
625	0.00E+00	0.00E+00	0.00E+00	3.18E-04	2.58E-04	1.33E-04	0.00E+00	2.28E-06	2.58E-06
650	0.00E+00	0.00E+00	0.00E+00	4.15E-04	1.63E-04	9.57E-05	0.00E+00	1.68E-06	4.17E-06
675	0.00E+00	0.00E+00	0.00E+00	2.67E-04	1.27E-04	1.09E-04	0.00E+00	0.00E+00	3.17E-06
700	0.00E+00	0.00E+00	0.00E+00	2.28E-04	1.64E-04	1.49E-04	0.00E+00	2.31E-06	3.56E-06
725	0.00E+00	0.00E+00	2.28E-06	3.09E-04	2.77E-04	2.43E-04	3.14E-06	3.59E-06	3.89E-06
750	0.00E+00	4.18E-06	1.04E-05	4.95E-04	3.58E-04	2.78E-04	3.78E-06	3.19E-06	4.22E-06
775	6.59E-06	1.68E-05	2.64E-05	6.55E-04	4.42E-04	2.88E-04	4.04E-06	7.19E-06	5.71E-06
800	2.61E-05	5.70E-05	5.40E-05	7.49E-04	5.44E-04	2.93E-04	5.40E-06	6.99E-06	6.02E-06
825	6.15E-05	1.10E-04	1.18E-04	7.60E-04	5.79E-04	3.58E-04	0.00E+00	6.52E-06	7.67E-06
850	1.03E-04	1.57E-04	1.65E-04	5.96E-04	4.92E-04	3.42E-04	4.67E-06	5.92E-06	5.66E-06
875	1.25E-04	2.03E-04	2.49E-04	4.51E-04	4.23E-04	3.82E-04	6.34E-06	9.52E-06	1.03E-05
900	9.66E-05	1.71E-04	2.68E-04	2.35E-04	2.85E-04	3.32E-04	5.36E-06	7.47E-06	1.31E-05
925	8.57E-05	1.63E-04	2.52E-04	1.45E-04	1.99E-04	2.52E-04	2.95E-06	7.63E-06	1.34E-05
950	4.15E-05	1.38E-04	2.55E-04	5.54E-05	1.33E-04	2.01E-04	2.48E-06	7.00E-06	1.67E-05
975	2.89E-05	1.20E-04	2.06E-04	2.66E-05	8.02E-05	1.34E-04	0.00E+00	5.74E-06	1.34E-05
1000	2.18E-05	8.90E-05	2.42E-04	2.20E-05	4.03E-05	1.23E-04	0.00E+00	4.75E-06	1.28E-05
1025	1.82E-05	8.39E-05	1.98E-04	1.59E-05	3.51E-05	7.42E-05	0.00E+00	3.79E-06	1.07E-05
1050	9.84E-06	7.72E-05	1.44E-04	7.61E-06	3.47E-05	0.00E+00	0.00E+00	2.57E-06	0.00E+00
1075	4.44E-06	3.14E-05	1.09E-04	2.56E-06	1.20E-05	2.12E-05	0.00E+00	0.00E+00	5.92E-06
1100	0.00E+00	1.90E-05	6.86E-05	0.00E+00	5.68E-06	8.78E-06	0.00E+00	0.00E+00	4.32E-06

T (K)	Formaldehyde			Oxirane			Acetaldehyde		
	Phi=0.5	Phi=1	Phi=2	Phi=0.5	Phi=1	Phi=2	Phi=0.5	Phi=1	Phi=2
500	0.00E+00	0.00E+00	0.00E+00	0.00E+00	0.00E+00	0.00E+00	0.00E+00	0.00E+00	0.00E+00
525	0.00E+00	0.00E+00	0.00E+00	0.00E+00	0.00E+00	0.00E+00	2.35E-06	0.00E+00	0.00E+00
550	0.00E+00	0.00E+00	0.00E+00	0.00E+00	0.00E+00	0.00E+00	0.00E+00	0.00E+00	0.00E+00
575	0.00E+00	0.00E+00	0.00E+00	0.00E+00	0.00E+00	0.00E+00	1.20E-05	8.31E-06	3.74E-06
600	3.27E-04	0.00E+00	0.00E+00	5.32E-06	0.00E+00	0.00E+00	1.25E-04	6.10E-05	1.23E-05
625	5.03E-04	4.79E-04	0.00E+00	6.21E-06	2.28E-06	0.00E+00	8.34E-05	4.83E-05	1.36E-05
650	3.38E-04	0.00E+00	0.00E+00	2.99E-06	0.00E+00	0.00E+00	9.66E-05	2.98E-05	6.16E-06
675	0.00E+00	0.00E+00	0.00E+00	0.00E+00	0.00E+00	0.00E+00	1.79E-05	4.62E-06	3.71E-06
700	0.00E+00	0.00E+00	0.00E+00	0.00E+00	0.00E+00	0.00E+00	9.71E-06	5.79E-06	4.53E-06
725	0.00E+00	0.00E+00	0.00E+00	0.00E+00	0.00E+00	0.00E+00	1.12E-05	7.01E-06	6.89E-06
750	0.00E+00	0.00E+00	0.00E+00	0.00E+00	0.00E+00	0.00E+00	2.12E-05	1.02E-05	1.24E-05
775	2.74E-04	0.00E+00	0.00E+00	2.05E-06	2.31E-06	0.00E+00	7.04E-05	1.80E-05	1.41E-05
800	2.56E-04	0.00E+00	0.00E+00	3.91E-06	3.78E-06	2.37E-06	1.01E-04	3.65E-05	2.06E-05
825	3.17E-04	2.70E-04	2.21E-04	9.84E-06	5.72E-06	3.27E-06	7.36E-05	5.63E-05	3.59E-05
850	4.36E-04	3.00E-04	2.14E-04	1.75E-05	8.73E-06	3.33E-06	9.16E-05	6.35E-05	5.11E-05
875	3.52E-04	2.69E-04	2.43E-04	1.70E-05	1.06E-05	6.53E-06	8.31E-05	7.94E-05	6.93E-05
900	2.50E-04	3.21E-04	2.47E-04	1.43E-05	1.12E-05	6.83E-06	6.62E-05	7.34E-05	9.54E-05
925	2.47E-04	2.11E-04	2.80E-04	9.27E-06	8.54E-06	5.61E-06	5.11E-05	6.59E-05	7.43E-05
950	0.00E+00	2.98E-04	2.22E-04	4.41E-06	4.67E-06	4.43E-06	2.91E-05	5.20E-05	7.81E-05
975	0.00E+00	1.27E-04	0.00E+00	0.00E+00	3.13E-06	2.96E-06	1.32E-05	4.02E-05	5.85E-05
1000	0.00E+00	0.00E+00	1.27E-04	0.00E+00	1.48E-06	1.65E-06	1.36E-05	2.29E-05	5.83E-05
1025	0.00E+00	0.00E+00	0.00E+00	0.00E+00	0.00E+00	2.23E-06	7.09E-06	2.45E-05	4.58E-05
1050	0.00E+00	0.00E+00	0.00E+00	0.00E+00	0.00E+00	0.00E+00	7.88E-06	2.01E-05	0.00E+00
1075	0.00E+00	0.00E+00	0.00E+00	0.00E+00	0.00E+00	0.00E+00	1.99E-06	8.15E-06	1.01E-05
1100	0.00E+00	0.00E+00	0.00E+00	0.00E+00	0.00E+00	0.00E+00	0.00E+00	2.52E-06	5.46E-06

T (K)	Methanol			1-Butene			1,3-Butadiene		
	Phi=0.5	Phi=1	Phi=2	Phi=0.5	Phi=1	Phi=2	Phi=0.5	Phi=1	Phi=2
500	0.00E+00	0.00E+00	0.00E+00	0.00E+00	0.00E+00	0.00E+00	0.00E+00	0.00E+00	0.00E+00
525	0.00E+00	0.00E+00	0.00E+00	0.00E+00	0.00E+00	0.00E+00	0.00E+00	0.00E+00	0.00E+00
550	1.32E-05	0.00E+00	0.00E+00	0.00E+00	0.00E+00	0.00E+00	0.00E+00	0.00E+00	0.00E+00
575	0.00E+00	0.00E+00	0.00E+00	0.00E+00	0.00E+00	0.00E+00	0.00E+00	0.00E+00	0.00E+00
600	0.00E+00	0.00E+00	2.48E-05	0.00E+00	0.00E+00	0.00E+00	0.00E+00	0.00E+00	0.00E+00
625	1.27E-04	9.56E-05	4.11E-05	0.00E+00	0.00E+00	0.00E+00	0.00E+00	0.00E+00	0.00E+00
650	0.00E+00	0.00E+00	1.96E-05	0.00E+00	0.00E+00	0.00E+00	0.00E+00	0.00E+00	0.00E+00
675	1.88E-05	1.25E-05	1.56E-05	0.00E+00	0.00E+00	0.00E+00	0.00E+00	0.00E+00	0.00E+00
700	1.61E-05	1.63E-05	3.74E-05	0.00E+00	1.60E-06	0.00E+00	0.00E+00	0.00E+00	0.00E+00
725	3.11E-05	4.32E-05	5.49E-05	0.00E+00	8.09E-07	0.00E+00	0.00E+00	0.00E+00	0.00E+00
750	7.37E-05	6.51E-05	9.69E-05	1.57E-06	3.71E-06	2.61E-06	0.00E+00	0.00E+00	0.00E+00
775	0.00E+00	9.35E-05	8.61E-05	4.20E-06	4.12E-06	3.64E-06	2.23E-06	0.00E+00	0.00E+00
800	0.00E+00	1.29E-04	8.04E-05	1.15E-05	1.18E-05	5.46E-06	1.89E-06	1.87E-06	1.04E-06
825	1.11E-04	1.10E-04	6.85E-05	1.59E-05	1.66E-05	1.08E-05	2.72E-06	1.23E-06	2.70E-06
850	6.91E-05	7.49E-05	5.28E-05	1.80E-05	2.09E-05	1.41E-05	3.04E-06	2.03E-06	1.45E-06
875	5.84E-05	5.23E-05	4.80E-05	1.46E-05	1.98E-05	1.95E-05	3.23E-06	2.77E-06	3.63E-06
900	2.94E-05	2.96E-05	0.00E+00	7.81E-06	1.37E-05	1.74E-05	2.27E-06	2.98E-06	3.39E-06
925	1.70E-05	2.13E-05	2.73E-05	5.42E-06	8.40E-06	1.50E-05	1.73E-06	2.72E-06	3.54E-06
950	0.00E+00	1.56E-05	0.00E+00	2.13E-06	7.43E-06	1.13E-05	0.00E+00	2.63E-06	4.31E-06
975	0.00E+00	1.00E-05	0.00E+00	1.24E-06	3.16E-06	6.83E-06	0.00E+00	1.38E-06	3.13E-06
1000	0.00E+00	8.04E-06	1.55E-05	1.59E-06	2.88E-06	7.09E-06	0.00E+00	1.35E-06	4.41E-06
1025	5.96E-06	0.00E+00	0.00E+00	1.69E-06	2.90E-06	4.27E-06	0.00E+00	1.93E-06	3.45E-06
1050	0.00E+00	0.00E+00	0.00E+00	0.00E+00	2.19E-06	0.00E+00	0.00E+00	1.97E-06	0.00E+00
1075	0.00E+00	0.00E+00	0.00E+00	0.00E+00	1.26E-06	1.86E-06	0.00E+00	8.37E-07	2.22E-06
1100	0.00E+00	0.00E+00	0.00E+00	0.00E+00	0.00E+00	0.00E+00	0.00E+00	0.00E+00	0.00E+00

T (K)	2-Butene			Methyloxirane			Acrolein		
	Phi=0.5	Phi=1	Phi=2	Phi=0.5	Phi=1	Phi=2	Phi=0.5	Phi=1	Phi=2
500	0.00E+00	0.00E+00	0.00E+00	0.00E+00	0.00E+00	0.00E+00	0.00E+00	0.00E+00	0.00E+00
525	0.00E+00	0.00E+00	0.00E+00	0.00E+00	0.00E+00	0.00E+00	0.00E+00	0.00E+00	0.00E+00
550	0.00E+00	0.00E+00	0.00E+00	0.00E+00	0.00E+00	0.00E+00	0.00E+00	0.00E+00	0.00E+00
575	0.00E+00	0.00E+00	0.00E+00	1.65E-06	0.00E+00	0.00E+00	0.00E+00	0.00E+00	0.00E+00
600	0.00E+00	0.00E+00	0.00E+00	1.75E-05	6.89E-06	3.41E-06	0.00E+00	0.00E+00	0.00E+00
625	0.00E+00	0.00E+00	0.00E+00	3.75E-05	2.12E-05	9.06E-06	0.00E+00	0.00E+00	0.00E+00
650	0.00E+00	0.00E+00	0.00E+00	4.23E-05	1.08E-05	5.94E-06	2.87E-06	0.00E+00	0.00E+00
675	0.00E+00	0.00E+00	0.00E+00	1.55E-05	5.56E-06	3.95E-06	0.00E+00	0.00E+00	0.00E+00
700	0.00E+00	0.00E+00	0.00E+00	1.18E-05	7.13E-06	5.50E-06	0.00E+00	0.00E+00	0.00E+00
725	0.00E+00	0.00E+00	0.00E+00	1.31E-05	8.57E-06	6.41E-06	2.91E-06	2.36E-06	3.17E-06
750	0.00E+00	0.00E+00	0.00E+00	1.91E-05	1.25E-05	8.93E-06	6.37E-06	7.59E-06	1.24E-05
775	2.67E-06	3.55E-06	2.19E-06	2.52E-05	1.42E-05	6.28E-06	1.78E-05	1.82E-05	2.17E-05
800	5.60E-06	4.42E-06	3.46E-06	2.62E-05	1.36E-05	6.19E-06	3.08E-05	4.49E-05	4.52E-05
825	6.01E-06	4.77E-06	5.63E-06	2.22E-05	9.03E-06	5.65E-06	5.71E-05	6.71E-05	7.09E-05
850	4.63E-06	5.15E-06	5.54E-06	1.65E-05	6.60E-06	3.75E-06	6.07E-05	7.27E-05	8.31E-05
875	4.58E-06	4.06E-06	5.00E-06	7.60E-06	5.18E-06	3.16E-06	6.09E-05	7.18E-05	8.59E-05
900	0.00E+00	1.14E-06	4.59E-06	3.94E-06	3.30E-06	3.04E-06	3.39E-05	4.58E-05	8.05E-05
925	0.00E+00	0.00E+00	3.62E-06	2.23E-06	0.00E+00	1.29E-06	2.66E-05	3.89E-05	5.44E-05
950	0.00E+00	0.00E+00	3.71E-06	0.00E+00	0.00E+00	0.00E+00	1.06E-05	2.34E-05	4.18E-05
975	0.00E+00	0.00E+00	0.00E+00	0.00E+00	0.00E+00	0.00E+00	8.08E-06	1.50E-05	2.44E-05
1000	0.00E+00	0.00E+00	0.00E+00	0.00E+00	0.00E+00	0.00E+00	4.97E-06	6.67E-06	2.25E-05
1025	0.00E+00	0.00E+00	0.00E+00	0.00E+00	0.00E+00	0.00E+00	4.23E-06	6.90E-06	1.24E-05
1050	0.00E+00	0.00E+00	0.00E+00	0.00E+00	0.00E+00	0.00E+00	2.93E-06	7.38E-06	0.00E+00
1075	0.00E+00	0.00E+00	0.00E+00	0.00E+00	0.00E+00	0.00E+00	0.00E+00	1.84E-06	1.55E-06
1100	0.00E+00	0.00E+00	0.00E+00	0.00E+00	0.00E+00	0.00E+00	0.00E+00	0.00E+00	0.00E+00

T (K)	Propanal			1-Pentene			2-Butenal		
	Phi=0.5	Phi=1	Phi=2	Phi=0.5	Phi=1	Phi=2	Phi=0.5	Phi=1	Phi=2
500	7.78E-06	3.45E-06	4.14E-06	0.00E+00	0.00E+00	0.00E+00	0.00E+00	0.00E+00	0.00E+00
525	5.58E-06	8.79E-06	4.64E-06	0.00E+00	0.00E+00	0.00E+00	0.00E+00	0.00E+00	0.00E+00
550	5.91E-06	3.91E-06	3.79E-06	0.00E+00	0.00E+00	0.00E+00	0.00E+00	0.00E+00	0.00E+00
575	1.05E-05	8.27E-06	6.35E-06	0.00E+00	0.00E+00	0.00E+00	0.00E+00	0.00E+00	0.00E+00
600	7.92E-05	4.10E-05	1.92E-05	3.24E-06	1.36E-06	1.59E-06	0.00E+00	0.00E+00	0.00E+00
625	1.01E-04	7.01E-05	3.15E-05	3.48E-06	3.07E-06	1.74E-06	7.10E-06	1.54E-06	0.00E+00
650	8.93E-05	3.11E-05	1.78E-05	4.90E-06	2.28E-06	2.33E-06	3.15E-06	0.00E+00	1.68E-06
675	4.66E-05	2.16E-05	1.72E-05	4.92E-06	2.15E-06	1.67E-06	2.62E-06	2.87E-06	0.00E+00
700	3.87E-05	2.51E-05	2.21E-05	7.17E-06	3.65E-06	2.66E-06	1.60E-06	1.54E-06	1.66E-06
725	4.65E-05	4.21E-05	3.98E-05	6.86E-06	5.17E-06	4.31E-06	3.22E-06	2.54E-06	3.14E-06
750	7.05E-05	5.43E-05	4.87E-05	1.11E-05	6.83E-06	5.68E-06	0.00E+00	1.05E-05	9.72E-06
775	9.73E-05	6.90E-05	4.83E-05	1.30E-05	7.88E-06	5.25E-06	1.89E-05	1.10E-05	1.67E-05
800	9.37E-05	6.57E-05	4.66E-05	1.30E-05	8.57E-06	5.66E-06	1.75E-05	2.59E-05	2.04E-05
825	8.20E-05	6.70E-05	4.51E-05	1.06E-05	7.05E-06	4.03E-06	2.69E-05	2.42E-05	3.05E-05
850	5.25E-05	4.30E-05	3.17E-05	6.53E-06	3.69E-06	3.06E-06	1.98E-05	2.03E-05	2.94E-05
875	3.32E-05	2.82E-05	2.57E-05	3.47E-06	1.55E-06	8.05E-07	1.54E-05	1.55E-05	2.38E-05
900	1.42E-05	1.55E-05	1.91E-05	1.20E-06	0.00E+00	0.00E+00	6.87E-06	9.27E-06	2.17E-05
925	1.04E-05	1.35E-05	1.42E-05	0.00E+00	0.00E+00	1.39E-06	6.37E-06	8.28E-06	1.08E-05
950	5.80E-06	6.89E-06	1.05E-05	0.00E+00	0.00E+00	0.00E+00	2.60E-06	3.94E-06	9.73E-06
975	3.28E-06	4.05E-06	6.34E-06	0.00E+00	0.00E+00	0.00E+00	2.11E-06	2.83E-06	4.79E-06
1000	2.08E-06	3.32E-06	5.77E-06	0.00E+00	0.00E+00	0.00E+00	0.00E+00	1.58E-06	2.83E-06
1025	0.00E+00	2.85E-06	4.77E-06	0.00E+00	0.00E+00	0.00E+00	0.00E+00	1.53E-06	2.91E-06
1050	0.00E+00	2.44E-06	0.00E+00	0.00E+00	0.00E+00	0.00E+00	0.00E+00	2.22E-06	0.00E+00
1075	0.00E+00	0.00E+00	0.00E+00	0.00E+00	0.00E+00	0.00E+00	0.00E+00	0.00E+00	0.00E+00
1100	0.00E+00	0.00E+00	0.00E+00	0.00E+00	0.00E+00	0.00E+00	0.00E+00	0.00E+00	0.00E+00

T (K)	Butanal		
	Phi=0.5	Phi=1	Phi=2
500	5.33E-03	4.90E-03	5.07E-03
525	5.12E-03	5.13E-03	5.43E-03
550	5.24E-03	4.91E-03	5.24E-03
575	5.24E-03	5.07E-03	5.54E-03
600	4.56E-03	4.53E-03	5.17E-03
625	3.57E-03	4.63E-03	5.22E-03
650	3.88E-03	4.67E-03	5.20E-03
675	4.53E-03	4.82E-03	4.79E-03
700	4.84E-03	4.85E-03	4.87E-03
725	4.64E-03	4.75E-03	4.57E-03
750	4.11E-03	4.26E-03	4.59E-03
775	3.61E-03	3.73E-03	4.15E-03
800	2.61E-03	3.03E-03	3.77E-03
825	1.79E-03	2.53E-03	3.02E-03
850	1.19E-03	1.67E-03	2.55E-03
875	8.10E-04	1.24E-03	1.64E-03
900	4.36E-04	6.93E-04	1.11E-03
925	3.24E-04	4.56E-04	7.55E-04
950	2.03E-04	3.45E-04	5.39E-04
975	1.12E-04	2.35E-04	4.00E-04
1000	9.49E-05	1.28E-04	2.43E-04
1025	3.20E-05	1.36E-04	1.71E-04
1050	2.28E-05	1.02E-04	1.15E-04
1075	8.30E-06	4.07E-05	1.56E-05
1100	1.71E-05	5.10E-06	2.72E-05

II.5. Combustion of *n*-pentanal

Equivalence ratio	0,5 ; 1 ; 2
$x_{n\text{-pentanal}}$	0.005
Temperature (K)	500 - 1100
P (Torr)	800

Units	Mole fraction
Bath gas	Helium
Residence time (s)	2

T (K)	O_2			CO			CH_4		
	Phi=0.5	Phi=1	Phi=2	Phi=0.5	Phi=1	Phi=2	Phi=0.5	Phi=1	Phi=2
500	7.09E-02	3.80E-02	1.86E-02	7.82E-05	0.00E+00	0.00E+00	0.00E+00	0.00E+00	0.00E+00
525	7.12E-02	3.79E-02	1.84E-02	0.00E+00	0.00E+00	0.00E+00	0.00E+00	0.00E+00	0.00E+00
550	7.17E-02	3.60E-02	1.90E-02	3.36E-04	0.00E+00	6.53E-05	2.95E-07	0.00E+00	0.00E+00
575	6.67E-02	3.21E-02	1.59E-02	2.36E-03	2.21E-03	1.36E-03	5.13E-07	5.23E-07	0.00E+00
600	6.32E-02	2.89E-02	1.55E-02	5.62E-03	4.87E-03	3.71E-03	2.68E-06	3.95E-06	0.00E+00
625	6.04E-02	2.72E-02	1.18E-02	7.31E-03	6.89E-03	5.10E-03	7.92E-06	1.28E-05	2.04E-05
650	6.21E-02	2.87E-02	1.60E-02	8.04E-03	6.55E-03	4.29E-03	1.40E-05	2.25E-05	0.00E+00
675	6.46E-02	3.15E-02	1.69E-02	6.41E-03	4.86E-03	2.76E-03	2.04E-05	2.71E-05	2.14E-05
700	6.59E-02	3.22E-02	1.76E-02	5.05E-03	3.09E-03	9.61E-04	2.91E-05	2.69E-05	0.00E+00
725	6.73E-02	3.44E-02	1.77E-02	3.17E-03	1.71E-03	5.35E-04	2.94E-05	2.19E-05	7.50E-06
750	6.94E-02	3.43E-02	1.84E-02	2.39E-03	1.37E-03	5.66E-04	3.08E-05	2.49E-05	0.00E+00
775	6.76E-02	3.58E-02	1.88E-02	3.11E-03	2.08E-03	1.56E-03	5.96E-05	4.43E-05	3.67E-05
800	6.83E-02	3.35E-02	1.64E-02	5.07E-03	3.71E-03	3.37E-03	1.25E-04	1.10E-04	1.08E-04
825	6.47E-02	3.02E-02	1.85E-02	7.80E-03	6.13E-03	4.84E-03	2.14E-04	1.97E-04	1.74E-04
850	6.16E-02	2.97E-02	1.23E-02	9.85E-03	9.05E-03	7.93E-03	2.54E-04	3.06E-04	3.44E-04
875	5.69E-02	2.56E-02	1.05E-02	1.31E-02	1.19E-02	1.00E-02	3.01E-04	3.79E-04	4.58E-04
900	5.39E-02	2.24E-02	8.50E-03	1.42E-02	1.37E-02	1.19E-02	2.97E-04	4.28E-04	6.08E-04
925	5.08E-02	2.05E-02	7.87E-03	1.47E-02	1.42E-02	1.25E-02	2.43E-04	4.33E-04	7.21E-04
950	4.66E-02	1.82E-02	9.92E-03	1.36E-02	1.50E-02	1.28E-02	1.73E-04	4.91E-04	6.47E-04
975	4.21E-02	1.59E-02	7.37E-03	9.73E-03	1.64E-02	1.46E-02	8.64E-05	5.16E-04	1.03E-03
1000	4.03E-02	1.04E-02	6.12E-03	5.94E-03	1.05E-02	1.54E-02	5.17E-05	2.73E-04	1.20E-03
1025	3.92E-02	6.52E-03	5.52E-03	3.75E-03	5.32E-03	1.66E-02	3.44E-05	1.76E-04	1.33E-03
1050	0.00E+00	3.08E-03	4.21E-03	0.00E+00	2.12E-03	1.75E-02	0.00E+00	6.61E-05	1.35E-03
1075	0.00E+00	2.29E-03	3.00E-03	0.00E+00	1.04E-03	1.95E-02	0.00E+00	2.27E-05	1.39E-03
1100	0.00E+00	1.66E-03	2.44E-03	0.00E+00	4.37E-04	2.13E-02	0.00E+00	7.31E-07	1.28E-03

T (K)	CO_2			Acetylene			Ethylene		
	Phi=0.5	Phi=1	Phi=2	Phi=0.5	Phi=1	Phi=2	Phi=0.5	Phi=1	Phi=2
500	0.00E+00	0.00E+00	0.00E+00	0.00E+00	0.00E+00	0.00E+00	0.00E+00	0.00E+00	0.00E+00
525	0.00E+00	0.00E+00	0.00E+00	0.00E+00	0.00E+00	0.00E+00	0.00E+00	0.00E+00	1.30E-05
550	0.00E+00	0.00E+00	0.00E+00	0.00E+00	0.00E+00	0.00E+00	1.19E-05	0.00E+00	0.00E+00
575	0.00E+00	2.63E-04	1.35E-04	0.00E+00	0.00E+00	0.00E+00	1.96E-05	1.98E-05	1.30E-05
600	0.00E+00	4.80E-04	2.16E-04	0.00E+00	0.00E+00	0.00E+00	7.28E-05	7.13E-05	0.00E+00
625	8.54E-04	5.20E-04	8.43E-04	0.00E+00	0.00E+00	0.00E+00	1.36E-04	1.50E-04	2.02E-04
650	0.00E+00	1.07E-03	0.00E+00	0.00E+00	0.00E+00	0.00E+00	2.09E-04	2.27E-04	0.00E+00
675	0.00E+00	0.00E+00	0.00E+00	0.00E+00	0.00E+00	0.00E+00	2.42E-04	3.10E-04	3.37E-04
700	0.00E+00	1.45E-04	0.00E+00	0.00E+00	0.00E+00	0.00E+00	3.51E-04	4.02E-04	0.00E+00
725	0.00E+00	0.00E+00	0.00E+00	0.00E+00	0.00E+00	0.00E+00	4.53E-04	4.98E-04	2.74E-04
750	0.00E+00	0.00E+00	0.00E+00	0.00E+00	0.00E+00	0.00E+00	6.29E-04	6.92E-04	0.00E+00
775	0.00E+00	0.00E+00	0.00E+00	0.00E+00	0.00E+00	0.00E+00	1.32E-03	1.41E-03	1.42E-03
800	0.00E+00	0.00E+00	0.00E+00	1.01E-06	0.00E+00	9.97E-07	2.41E-03	2.75E-03	3.01E-03
825	4.76E-04	0.00E+00	3.35E-04	4.00E-06	3.27E-06	3.06E-06	3.35E-03	3.84E-03	3.61E-03
850	0.00E+00	5.05E-04	0.00E+00	7.21E-06	8.02E-06	8.59E-06	3.45E-03	4.07E-03	4.32E-03
875	5.62E-03	1.14E-03	8.47E-04	1.21E-05	1.34E-05	1.44E-05	3.27E-03	3.78E-03	3.95E-03
900	3.05E-03	2.30E-03	1.24E-03	1.33E-05	1.85E-05	1.90E-05	2.45E-03	3.07E-03	3.88E-03
925	7.57E-03	2.87E-03	1.47E-03	1.20E-05	1.87E-05	2.47E-05	1.57E-03	2.51E-03	3.53E-03
950	9.32E-03	4.02E-03	1.89E-03	6.77E-06	2.02E-05	2.53E-05	6.87E-04	2.00E-03	2.97E-03
975	1.51E-02	5.61E-03	1.76E-03	2.92E-06	1.67E-05	3.35E-05	3.13E-04	1.51E-03	3.30E-03
1000	1.69E-02	1.23E-02	2.15E-03	2.44E-06	9.40E-06	4.04E-05	1.62E-04	6.46E-04	3.18E-03
1025	2.34E-02	1.90E-02	2.38E-03	0.00E+00	1.28E-05	4.10E-05	8.62E-05	5.97E-04	2.38E-03
1050	0.00E+00	2.24E-02	2.82E-03	0.00E+00	8.56E-06	4.30E-05	0.00E+00	2.17E-04	1.73E-03
1075	0.00E+00	2.41E-02	3.01E-03	0.00E+00	4.31E-06	5.85E-05	0.00E+00	4.30E-05	1.36E-03
1100	0.00E+00	2.28E-02	3.39E-03	0.00E+00	0.00E+00	9.95E-05	0.00E+00	5.02E-06	9.20E-04

Experimental raw data: *n*-pentanal oxidation

T (K)	Ethane			Propene			Propane		
	Phi=0.5	Phi=1	Phi=2	Phi=0.5	Phi=1	Phi=2	Phi=0.5	Phi=1	Phi=2
500	0.00E+00	0.00E+00	0.00E+00	0.00E+00	0.00E+00	0.00E+00	0.00E+00	0.00E+00	0.00E+00
525	0.00E+00	0.00E+00	0.00E+00	0.00E+00	0.00E+00	0.00E+00	0.00E+00	0.00E+00	0.00E+00
550	0.00E+00	0.00E+00	0.00E+00	2.08E-06	0.00E+00	0.00E+00	0.00E+00	0.00E+00	0.00E+00
575	0.00E+00	0.00E+00	0.00E+00	2.82E-05	2.44E-05	2.09E-05	0.00E+00	0.00E+00	0.00E+00
600	0.00E+00	0.00E+00	1.97E-06	5.37E-05	6.30E-05	8.45E-05	0.00E+00	0.00E+00	0.00E+00
625	0.00E+00	2.44E-06	3.52E-06	9.23E-05	1.38E-04	1.80E-04	0.00E+00	3.08E-06	2.07E-06
650	0.00E+00	2.39E-06	2.88E-06	1.56E-04	1.88E-04	2.43E-04	0.00E+00	2.97E-06	0.00E+00
675	3.63E-06	2.13E-06	4.37E-06	2.25E-04	2.82E-04	2.52E-04	0.00E+00	2.05E-06	0.00E+00
700	2.04E-06	3.60E-06	3.87E-06	3.09E-04	2.74E-04	1.42E-04	0.00E+00	0.00E+00	0.00E+00
725	1.97E-06	2.64E-06	1.59E-06	3.17E-04	2.13E-04	6.11E-05	0.00E+00	0.00E+00	0.00E+00
750	3.41E-06	5.33E-06	4.40E-06	2.90E-04	2.22E-04	7.81E-05	0.00E+00	0.00E+00	0.00E+00
775	5.15E-06	7.01E-06	1.86E-05	3.90E-04	2.66E-04	1.83E-04	0.00E+00	0.00E+00	0.00E+00
800	1.13E-05	1.88E-05	5.45E-05	4.92E-04	3.51E-04	3.25E-04	0.00E+00	3.48E-06	4.35E-06
825	1.85E-05	3.73E-05	7.33E-05	4.13E-04	3.98E-04	3.30E-04	0.00E+00	4.09E-06	4.66E-06
850	2.05E-05	4.75E-05	1.02E-04	3.19E-04	3.26E-04	2.98E-04	3.88E-06	5.67E-06	1.12E-05
875	2.22E-05	4.73E-05	1.24E-04	2.11E-04	1.89E-04	2.44E-04	0.00E+00	4.20E-06	1.79E-05
900	1.94E-05	4.43E-05	1.08E-04	1.22E-04	1.24E-04	1.69E-04	3.33E-06	6.15E-06	1.95E-05
925	1.86E-05	5.61E-05	1.30E-04	7.14E-05	1.02E-04	1.57E-04	0.00E+00	8.76E-06	2.50E-05
950	1.01E-05	5.19E-05	1.33E-04	3.63E-05	7.63E-05	1.40E-04	0.00E+00	6.06E-06	2.47E-05
975	0.00E+00	3.73E-05	1.27E-04	0.00E+00	4.10E-05	9.67E-05	0.00E+00	4.89E-06	0.00E+00
1000	6.81E-06	3.69E-05	1.30E-04	9.08E-06	2.86E-05	7.16E-05	0.00E+00	5.02E-06	1.92E-05
1025	2.86E-06	2.03E-05	1.23E-04	0.00E+00	1.21E-05	4.71E-05	0.00E+00	0.00E+00	1.98E-05
1050	1.53E-06	1.15E-05	9.14E-05	0.00E+00	4.31E-06	2.32E-05	0.00E+00	0.00E+00	1.29E-05
1075	0.00E+00	2.50E-06	7.17E-05	0.00E+00	0.00E+00	1.11E-05	0.00E+00	0.00E+00	6.43E-06
1100	0.00E+00	0.00E+00	5.46E-05	0.00E+00	0.00E+00	5.58E-06	0.00E+00	0.00E+00	5.02E-06

T (K)	Formaldehyde			Oxirane			Acetaldehyde		
	Phi=0.5	Phi=1	Phi=2	Phi=0.5	Phi=1	Phi=2	Phi=0.5	Phi=1	Phi=2
500	0.00E+00	0.00E+00	0.00E+00	3.73E-06	0.00E+00	0.00E+00	2.18E-05	7.67E-06	0.00E+00
525	0.00E+00	0.00E+00	0.00E+00	0.00E+00	0.00E+00	0.00E+00	1.48E-05	6.13E-06	3.38E-06
550	0.00E+00	0.00E+00	0.00E+00	1.18E-05	3.79E-06	2.28E-06	6.09E-05	2.20E-05	1.15E-05
575	2.72E-04	0.00E+00	0.00E+00	3.01E-05	1.60E-05	2.06E-05	3.79E-04	3.09E-04	2.56E-04
600	7.94E-04	8.76E-04	7.34E-04	3.79E-05	2.75E-05	2.40E-05	5.58E-04	5.84E-04	4.76E-04
625	1.20E-03	1.17E-03	1.01E-03	3.19E-05	2.49E-05	2.05E-05	7.13E-04	7.04E-04	5.53E-04
650	1.09E-03	9.31E-04	7.16E-04	2.41E-05	1.44E-05	8.48E-06	7.03E-04	5.46E-04	3.86E-04
675	1.02E-03	7.51E-04	3.28E-04	1.35E-05	1.01E-05	2.98E-06	5.53E-04	4.46E-04	2.33E-04
700	6.45E-04	4.35E-04	1.48E-04	1.13E-05	4.01E-06	1.70E-06	4.15E-04	2.15E-04	7.21E-05
725	3.32E-04	2.31E-04	0.00E+00	5.51E-06	1.98E-06	0.00E+00	2.31E-04	8.62E-05	1.87E-05
750	1.62E-04	2.45E-04	0.00E+00	3.78E-06	2.47E-06	0.00E+00	1.22E-04	9.18E-06	8.38E-06
775	3.18E-04	0.00E+00	0.00E+00	9.58E-06	8.03E-06	9.87E-06	1.14E-04	4.90E-05	3.88E-05
800	3.11E-04	2.71E-04	2.51E-04	2.72E-05	1.54E-05	2.75E-05	1.37E-04	5.86E-05	8.74E-05
825	3.33E-04	3.75E-04	3.28E-04	4.85E-05	4.55E-05	4.33E-05	1.43E-04	1.23E-04	1.19E-04
850	3.09E-04	2.97E-04	4.20E-04	5.49E-05	4.68E-05	4.97E-05	1.35E-04	1.11E-04	1.42E-04
875	2.93E-04	0.00E+00	3.53E-04	5.23E-05	3.90E-05	5.19E-05	1.13E-04	1.13E-04	1.46E-04
900	2.19E-04	2.46E-04	0.00E+00	2.94E-05	2.28E-05	3.20E-05	8.16E-05	6.13E-05	1.16E-04
925	0.00E+00	0.00E+00	3.16E-04	1.80E-05	2.12E-05	2.15E-05	5.98E-05	7.69E-05	1.04E-04
950	0.00E+00	0.00E+00	0.00E+00	4.32E-06	9.92E-06	1.25E-05	2.38E-05	4.86E-05	9.35E-05
975	0.00E+00	0.00E+00	0.00E+00	0.00E+00	5.85E-06	6.83E-06	0.00E+00	3.34E-05	6.70E-05
1000	0.00E+00	0.00E+00	0.00E+00	1.48E-06	2.61E-06	3.37E-06	7.80E-06	1.97E-05	4.75E-05
1025	0.00E+00	0.00E+00	0.00E+00	0.00E+00	0.00E+00	2.98E-06	0.00E+00	1.35E-05	2.89E-05
1050	0.00E+00	0.00E+00	0.00E+00	0.00E+00	0.00E+00	0.00E+00	3.07E-06	0.00E+00	1.36E-05
1075	0.00E+00	0.00E+00	0.00E+00	0.00E+00	0.00E+00	0.00E+00	0.00E+00	0.00E+00	4.59E-06
1100	0.00E+00	0.00E+00	0.00E+00	0.00E+00	0.00E+00	0.00E+00	0.00E+00	0.00E+00	0.00E+00

Experimental raw data: *n*-pentanal oxidation

T (K)	1-Butene			1,3-Butadiene			2-Butene E		
	Phi=0.5	Phi=1	Phi=2	Phi=0.5	Phi=1	Phi=2	Phi=0.5	Phi=1	Phi=2
500	5.83E-06	2.16E-06	0.00E+00	0.00E+00	0.00E+00	0.00E+00	0.00E+00	0.00E+00	0.00E+00
525	5.92E-06	2.50E-06	2.08E-06	0.00E+00	0.00E+00	0.00E+00	0.00E+00	0.00E+00	0.00E+00
550	2.70E-05	8.36E-06	5.85E-06	0.00E+00	0.00E+00	0.00E+00	4.25E-06	1.49E-06	1.75E-06
575	1.10E-04	8.04E-05	6.37E-05	8.06E-07	0.00E+00	0.00E+00	1.05E-05	1.02E-05	1.12E-05
600	1.15E-04	1.21E-04	1.24E-04	1.20E-06	9.38E-07	0.00E+00	1.30E-05	1.95E-05	1.90E-05
625	1.42E-04	1.73E-04	1.98E-04	1.64E-06	1.34E-06	1.78E-06	2.25E-05	2.95E-05	2.76E-05
650	1.95E-04	2.06E-04	2.55E-04	2.47E-06	2.42E-06	2.43E-06	3.56E-05	3.44E-05	3.10E-05
675	2.56E-04	3.02E-04	2.73E-04	4.67E-06	3.98E-06	3.24E-06	4.32E-05	2.19E-06	2.90E-05
700	3.33E-04	3.00E-04	1.71E-04	9.51E-06	8.65E-06	3.22E-06	4.86E-05	3.61E-05	1.39E-05
725	3.39E-04	2.31E-04	7.40E-05	1.44E-05	5.23E-06	1.72E-06	4.00E-05	2.12E-05	7.17E-06
750	2.94E-04	2.03E-04	8.35E-05	1.21E-05	7.13E-06	1.83E-06	2.60E-05	1.50E-05	3.79E-06
775	3.26E-04	2.26E-04	1.68E-04	2.07E-05	8.04E-06	4.96E-06	1.98E-05	2.68E-06	4.98E-06
800	3.16E-04	2.36E-04	2.25E-04	2.92E-05	1.40E-05	1.15E-05	1.48E-05	1.43E-06	3.87E-06
825	1.98E-04	2.12E-04	1.87E-04	2.40E-05	1.76E-05	1.33E-05	7.17E-06	1.89E-06	4.09E-06
850	1.27E-04	1.28E-04	1.28E-04	1.85E-05	1.55E-05	1.26E-05	4.14E-06	1.20E-06	2.88E-06
875	7.48E-05	6.46E-05	7.71E-05	1.15E-05	8.99E-06	1.04E-05	2.00E-06	1.19E-06	2.04E-06
900	4.03E-05	3.78E-05	4.70E-05	7.15E-06	6.30E-06	7.16E-06	1.90E-06	1.55E-06	3.86E-06
925	2.29E-05	2.80E-05	3.64E-05	3.12E-06	3.85E-06	7.68E-06	0.00E+00	0.00E+00	1.23E-06
950	1.25E-05	1.62E-05	2.76E-05	2.30E-06	4.48E-06	6.39E-06	0.00E+00	0.00E+00	1.08E-06
975	0.00E+00	8.93E-06	1.64E-05	0.00E+00	2.03E-06	5.12E-06	0.00E+00	0.00E+00	1.38E-06
1000	1.04E-06	4.91E-06	9.42E-06	1.21E-06	2.42E-06	4.01E-06	0.00E+00	0.00E+00	3.24E-06
1025	0.00E+00	0.00E+00	4.51E-06	0.00E+00	0.00E+00	5.53E-06	0.00E+00	0.00E+00	0.00E+00
1050	0.00E+00	0.00E+00	2.32E-06	0.00E+00	1.04E-06	1.84E-06	0.00E+00	0.00E+00	0.00E+00
1075	0.00E+00	0.00E+00	0.00E+00	0.00E+00	0.00E+00	1.24E-06	0.00E+00	0.00E+00	0.00E+00
1100	0.00E+00	0.00E+00	0.00E+00	0.00E+00	0.00E+00	0.00E+00	0.00E+00	0.00E+00	0.00E+00

T (K)	2-Butene Z			Furan			Acrolein		
	Phi=0.5	Phi=1	Phi=2	Phi=0.5	Phi=1	Phi=2	Phi=0.5	Phi=1	Phi=2
500	0.00E+00	0.00E+00	0.00E+00	1.48E-06	0.00E+00	0.00E+00	0.00E+00	0.00E+00	0.00E+00
525	0.00E+00	0.00E+00	0.00E+00	0.00E+00	0.00E+00	0.00E+00	0.00E+00	0.00E+00	0.00E+00
550	2.80E-06	1.27E-06	1.57E-06	4.39E-06	0.00E+00	0.00E+00	0.00E+00	0.00E+00	0.00E+00
575	5.64E-06	6.14E-06	5.61E-06	2.85E-05	1.57E-05	1.43E-05	6.26E-06	4.77E-06	4.48E-06
600	7.92E-06	1.09E-05	1.14E-05	4.57E-05	3.15E-05	2.49E-05	1.40E-05	1.30E-05	1.10E-05
625	1.31E-05	1.70E-05	1.77E-05	3.53E-05	2.31E-05	1.85E-05	2.33E-05	2.63E-05	2.18E-05
650	1.96E-05	1.94E-05	1.86E-05	2.00E-05	1.46E-05	9.09E-06	3.52E-05	2.84E-05	2.62E-05
675	2.58E-05	2.58E-05	1.70E-05	1.17E-05	8.72E-06	5.30E-06	4.19E-05	3.55E-05	3.09E-05
700	2.98E-05	2.09E-05	8.21E-06	9.29E-06	5.67E-06	1.92E-06	4.93E-05	3.30E-05	2.33E-05
725	2.45E-05	1.27E-05	5.42E-06	7.09E-06	2.47E-06	0.00E+00	4.86E-05	2.74E-05	1.18E-05
750	1.56E-05	7.75E-06	2.41E-06	4.11E-06	1.65E-06	0.00E+00	4.68E-05	3.11E-05	1.95E-05
775	1.32E-05	5.65E-06	2.92E-06	4.05E-06	2.10E-06	2.41E-06	7.13E-05	5.22E-05	5.04E-05
800	1.08E-05	5.57E-06	2.57E-06	6.80E-06	3.39E-06	3.69E-06	9.27E-05	5.19E-05	9.62E-05
825	5.44E-06	4.66E-06	3.15E-06	6.81E-06	4.55E-06	3.95E-06	8.31E-05	8.96E-05	9.35E-05
850	3.45E-06	2.96E-06	1.69E-06	4.11E-06	2.96E-06	2.61E-06	6.37E-05	5.60E-05	7.33E-05
875	2.56E-06	1.21E-06	1.93E-06	2.20E-06	0.00E+00	2.94E-06	4.49E-05	4.55E-05	5.40E-05
900	1.81E-06	1.73E-06	0.00E+00	2.21E-06	1.91E-06	1.69E-06	2.70E-05	2.04E-05	3.72E-05
925	0.00E+00	0.00E+00	1.99E-06	0.00E+00	0.00E+00	0.00E+00	1.39E-05	1.93E-05	2.56E-05
950	0.00E+00	0.00E+00	0.00E+00	0.00E+00	0.00E+00	0.00E+00	8.30E-06	1.38E-05	1.93E-05
975	0.00E+00	0.00E+00	1.64E-06	0.00E+00	0.00E+00	0.00E+00	0.00E+00	6.14E-06	1.18E-05
1000	0.00E+00	0.00E+00	0.00E+00	0.00E+00	0.00E+00	0.00E+00	0.00E+00	2.95E-06	4.96E-06
1025	0.00E+00	0.00E+00	0.00E+00	0.00E+00	0.00E+00	0.00E+00	0.00E+00	0.00E+00	0.00E+00
1050	0.00E+00	0.00E+00	0.00E+00	0.00E+00	0.00E+00	0.00E+00	0.00E+00	0.00E+00	0.00E+00
1075	0.00E+00	0.00E+00	0.00E+00	0.00E+00	0.00E+00	0.00E+00	0.00E+00	0.00E+00	0.00E+00
1100	0.00E+00	0.00E+00	0.00E+00	0.00E+00	0.00E+00	0.00E+00	0.00E+00	0.00E+00	0.00E+00

Experimental raw data: *n*-pentanal oxidation

T (K)	Propanal			Acetone			2,3-Dihydrofuran		
	Phi=0.5	Phi=1	Phi=2	Phi=0.5	Phi=1	Phi=2	Phi=0.5	Phi=1	Phi=2
500	3.57E-06	0.00E+00	0.00E+00	8.25E-06	5.84E-06	0.00E+00	0.00E+00	0.00E+00	0.00E+00
525	3.47E-06	0.00E+00	0.00E+00	1.26E-05	4.89E-06	5.63E-06	0.00E+00	0.00E+00	0.00E+00
550	6.56E-06	2.05E-06	2.41E-06	3.38E-05	2.50E-05	1.32E-05	0.00E+00	0.00E+00	0.00E+00
575	4.64E-05	2.93E-05	2.76E-05	1.86E-04	1.50E-04	1.24E-04	1.88E-06	4.57E-06	4.32E-06
600	6.43E-05	5.90E-05	5.73E-05	8.70E-05	2.08E-04	1.08E-04	6.04E-06	5.05E-06	4.16E-06
625	6.77E-05	6.27E-05	6.42E-05	7.37E-05	8.43E-05	5.25E-05	7.78E-06	5.81E-06	5.37E-06
650	6.20E-05	5.17E-05	4.61E-05	5.72E-05	6.73E-05	3.00E-05	8.63E-06	7.43E-06	5.57E-06
675	5.82E-05	4.67E-05	3.06E-05	5.57E-05	4.64E-05	2.81E-05	1.14E-05	7.85E-06	4.39E-06
700	5.23E-05	2.69E-05	7.80E-06	5.19E-05	3.79E-05	1.46E-05	8.55E-06	5.08E-06	1.78E-06
725	3.31E-05	1.04E-05	4.92E-06	4.16E-05	2.08E-05	5.74E-06	6.70E-06	2.48E-06	0.00E+00
750	1.75E-05	7.99E-06	2.89E-06	2.65E-05	1.66E-05	5.17E-06	2.48E-06	1.50E-06	0.00E+00
775	2.05E-05	6.41E-06	5.08E-06	2.15E-05	1.22E-05	3.83E-06	4.71E-06	0.00E+00	0.00E+00
800	1.92E-05	6.99E-06	7.55E-06	1.84E-05	1.13E-05	5.32E-06	1.51E-06	2.45E-06	0.00E+00
825	1.36E-05	1.00E-05	9.48E-06	1.04E-05	6.31E-06	4.97E-06	4.18E-06	4.94E-06	2.49E-06
850	7.44E-06	5.20E-06	7.20E-06	7.18E-06	8.56E-06	4.25E-06	3.56E-06	0.00E+00	2.87E-06
875	6.38E-06	5.97E-06	9.51E-06	6.13E-06	5.54E-06	5.68E-06	1.89E-06	0.00E+00	2.11E-06
900	6.64E-06	2.72E-06	8.71E-06	5.45E-06	5.51E-06	4.52E-06	1.97E-06	0.00E+00	0.00E+00
925	1.47E-06	3.16E-06	6.44E-06	3.58E-06	3.78E-06	4.74E-06	0.00E+00	0.00E+00	0.00E+00
950	0.00E+00	2.58E-06	5.70E-06	0.00E+00	5.32E-06	3.33E-06	0.00E+00	0.00E+00	0.00E+00
975	0.00E+00	2.36E-06	3.45E-06	0.00E+00	2.65E-06	2.87E-06	0.00E+00	0.00E+00	0.00E+00
1000	0.00E+00	1.65E-06	2.63E-06	0.00E+00	2.07E-06	2.12E-06	0.00E+00	0.00E+00	0.00E+00
1025	0.00E+00	0.00E+00	0.00E+00	0.00E+00	0.00E+00	0.00E+00	0.00E+00	0.00E+00	0.00E+00
1050	0.00E+00	0.00E+00	0.00E+00	0.00E+00	0.00E+00	0.00E+00	0.00E+00	0.00E+00	0.00E+00
1075	0.00E+00	0.00E+00	0.00E+00	0.00E+00	0.00E+00	0.00E+00	0.00E+00	0.00E+00	0.00E+00
1100	0.00E+00	0.00E+00	0.00E+00	0.00E+00	0.00E+00	0.00E+00	0.00E+00	0.00E+00	0.00E+00

T (K)	2,3-Dimethyloxirane			Ethyloxirane			Pentane		
	Phi=0.5	Phi=1	Phi=2	Phi=0.5	Phi=1	Phi=2	Phi=0.5	Phi=1	Phi=2
500	0.00E+00	0.00E+00	0.00E+00	0.00E+00	0.00E+00	0.00E+00	0.00E+00	0.00E+00	0.00E+00
525	0.00E+00	0.00E+00	0.00E+00	0.00E+00	0.00E+00	0.00E+00	0.00E+00	0.00E+00	0.00E+00
550	0.00E+00	0.00E+00	0.00E+00	1.15E-06	0.00E+00	0.00E+00	3.20E-06	0.00E+00	0.00E+00
575	0.00E+00	0.00E+00	0.00E+00	1.04E-05	9.93E-06	7.78E-06	1.14E-05	1.95E-05	2.65E-05
600	1.14E-06	1.59E-06	1.74E-06	1.48E-05	1.70E-05	1.39E-05	2.60E-05	5.03E-05	7.40E-05
625	0.00E+00	1.48E-06	0.00E+00	1.89E-05	0.00E+00	1.69E-05	5.13E-05	9.67E-05	1.45E-04
650	2.11E-06	2.86E-06	0.00E+00	1.67E-05	1.48E-05	1.13E-05	8.87E-05	1.26E-04	1.85E-04
675	3.70E-06	2.71E-06	3.81E-06	1.67E-05	1.39E-05	9.83E-06	1.32E-04	1.94E-04	1.98E-04
700	3.18E-06	2.21E-06	0.00E+00	1.66E-05	1.01E-05	3.88E-06	1.91E-04	1.93E-04	1.22E-04
725	0.00E+00	0.00E+00	0.00E+00	1.13E-05	6.03E-06	1.74E-06	2.02E-04	1.33E-04	5.11E-05
750	0.00E+00	0.00E+00	0.00E+00	6.26E-06	2.59E-06	0.00E+00	1.68E-04	1.07E-04	4.84E-05
775	0.00E+00	0.00E+00	0.00E+00	6.71E-06	3.15E-06	2.12E-06	1.67E-04	9.71E-05	7.73E-05
800	0.00E+00	0.00E+00	0.00E+00	5.18E-06	1.56E-06	1.79E-06	1.27E-04	6.38E-05	5.60E-05
825	0.00E+00	0.00E+00	0.00E+00	3.66E-06	2.18E-06	9.85E-07	5.74E-05	4.31E-05	2.89E-05
850	0.00E+00	0.00E+00	0.00E+00	1.94E-06	0.00E+00	0.00E+00	2.76E-05	1.28E-05	8.74E-06
875	0.00E+00	0.00E+00	0.00E+00	0.00E+00	0.00E+00	0.00E+00	1.08E-05	0.00E+00	3.97E-06
900	0.00E+00	0.00E+00	0.00E+00	0.00E+00	0.00E+00	0.00E+00	4.71E-06	1.77E-06	2.37E-06
925	0.00E+00	0.00E+00	0.00E+00	0.00E+00	0.00E+00	0.00E+00	1.64E-06	0.00E+00	1.06E-06
950	0.00E+00	0.00E+00	0.00E+00	0.00E+00	0.00E+00	0.00E+00	1.51E-06	0.00E+00	0.00E+00
975	0.00E+00	0.00E+00	0.00E+00	0.00E+00	0.00E+00	0.00E+00	0.00E+00	0.00E+00	0.00E+00
1000	0.00E+00	0.00E+00	0.00E+00	0.00E+00	0.00E+00	0.00E+00	0.00E+00	0.00E+00	0.00E+00
1025	0.00E+00	0.00E+00	0.00E+00	0.00E+00	0.00E+00	0.00E+00	0.00E+00	0.00E+00	0.00E+00
1050	0.00E+00	0.00E+00	0.00E+00	0.00E+00	0.00E+00	0.00E+00	0.00E+00	0.00E+00	0.00E+00
1075	0.00E+00	0.00E+00	0.00E+00	0.00E+00	0.00E+00	0.00E+00	0.00E+00	0.00E+00	0.00E+00
1100	0.00E+00	0.00E+00	0.00E+00	0.00E+00	0.00E+00	0.00E+00	0.00E+00	0.00E+00	0.00E+00

Experimental raw data: *n*-pentanal oxidation

T (K)	Methyl vinyl ketone			Butanal			2-Butanone		
	Phi=0.5	Phi=1	Phi=2	Phi=0.5	Phi=1	Phi=2	Phi=0.5	Phi=1	Phi=2
500	0.00E+00	0.00E+00	0.00E+00	3.65E-05	5.12E-05	3.17E-05	3.91E-06	1.74E-06	0.00E+00
525	0.00E+00	0.00E+00	0.00E+00	3.73E-05	2.36E-05	3.08E-05	2.52E-06	0.00E+00	0.00E+00
550	1.18E-06	0.00E+00	0.00E+00	5.70E-05	5.28E-05	3.42E-05	6.67E-06	2.14E-06	2.56E-06
575	7.98E-06	0.00E+00	3.81E-06	1.70E-04	9.90E-06	1.71E-04	2.81E-05	2.46E-05	1.99E-05
600	9.62E-06	0.00E+00	4.40E-06	1.46E-04	1.56E-04	2.13E-04	2.18E-05	1.85E-05	1.39E-05
625	7.87E-06	5.29E-06	6.63E-06	1.57E-04	4.96E-05	2.40E-04	1.16E-05	1.30E-05	1.04E-05
650	6.97E-06	4.61E-06	4.02E-06	1.46E-04	1.71E-04	1.74E-04	7.63E-06	5.57E-06	4.81E-06
675	6.52E-06	9.53E-06	3.37E-06	1.98E-04	9.25E-05	1.73E-04	6.33E-06	4.48E-06	3.67E-06
700	7.94E-06	6.48E-06	0.00E+00	1.65E-04	2.06E-04	1.09E-04	5.45E-06	5.86E-06	1.32E-06
725	7.05E-06	9.64E-07	0.00E+00	2.23E-04	6.57E-05	5.95E-05	3.62E-06	2.23E-06	0.00E+00
750	1.50E-06	7.49E-07	0.00E+00	1.14E-04	6.04E-05	6.34E-05	2.13E-06	0.00E+00	1.76E-06
775	2.91E-06	0.00E+00	0.00E+00	9.70E-05	4.96E-05	5.84E-05	2.31E-06	3.98E-06	1.47E-06
800	2.64E-06	1.52E-06	1.34E-06	6.72E-05	3.77E-05	5.86E-05	2.30E-06	1.84E-06	2.08E-06
825	2.26E-06	1.51E-06	1.36E-06	3.54E-05	1.93E-05	2.69E-05	2.96E-06	2.34E-06	3.39E-06
850	1.61E-06	1.50E-06	8.78E-07	1.83E-05	7.27E-06	1.76E-05	2.55E-06	1.49E-06	1.16E-06
875	1.08E-06	6.27E-06	0.00E+00	1.07E-05	2.23E-06	8.95E-06	2.51E-06	1.45E-06	1.52E-06
900	0.00E+00	0.00E+00	0.00E+00	7.14E-06	3.56E-06	4.94E-06	2.47E-06	0.00E+00	0.00E+00
925	0.00E+00	1.67E-06	0.00E+00	4.09E-06	5.83E-06	4.37E-06	0.00E+00	0.00E+00	0.00E+00
950	0.00E+00	0.00E+00	0.00E+00	3.70E-06	2.56E-06	3.85E-06	0.00E+00	0.00E+00	1.29E-06
975	0.00E+00	0.00E+00	0.00E+00	0.00E+00	1.42E-06	1.43E-06	0.00E+00	0.00E+00	0.00E+00
1000	0.00E+00	0.00E+00	0.00E+00	0.00E+00	0.00E+00	1.54E-06	0.00E+00	0.00E+00	0.00E+00
1025	0.00E+00	0.00E+00	0.00E+00	0.00E+00	0.00E+00	0.00E+00	0.00E+00	0.00E+00	0.00E+00
1050	0.00E+00	0.00E+00	0.00E+00	0.00E+00	0.00E+00	0.00E+00	0.00E+00	0.00E+00	0.00E+00
1075	0.00E+00	0.00E+00	0.00E+00	0.00E+00	0.00E+00	0.00E+00	0.00E+00	0.00E+00	0.00E+00
1100	0.00E+00	0.00E+00	0.00E+00	0.00E+00	0.00E+00	0.00E+00	0.00E+00	0.00E+00	0.00E+00

T (K)	2-Butenal			2-Methyl-butanal			Pentanal		
	Phi=0.5	Phi=1	Phi=2	Phi=0.5	Phi=1	Phi=2	Phi=0.5	Phi=1	Phi=2
500	0.00E+00	0.00E+00	0.00E+00	7.22E-06	6.91E-06	9.52E-06	5.03E-03	4.92E-03	5.02E-03
525	9.55E-06	0.00E+00	0.00E+00	6.86E-06	6.61E-06	7.30E-06	4.92E-03	5.19E-03	5.17E-03
550	1.73E-06	0.00E+00	0.00E+00	7.69E-06	6.24E-06	6.80E-06	4.93E-03	5.08E-03	5.34E-03
575	8.82E-06	4.30E-06	5.83E-06	5.17E-06	4.56E-06	4.91E-06	3.19E-03	3.23E-03	3.95E-03
600	7.34E-06	7.73E-06	5.16E-06	3.50E-06	3.00E-06	4.26E-06	1.87E-03	2.13E-03	2.61E-03
625	9.36E-06	8.52E-06	9.27E-06	3.23E-06	2.90E-06	4.18E-06	1.57E-03	1.84E-03	2.37E-03
650	9.51E-06	6.31E-06	7.47E-06	3.28E-06	1.72E-06	4.05E-06	1.63E-03	1.72E-03	2.65E-03
675	1.01E-05	9.69E-06	6.71E-06	1.71E-06	2.92E-06	4.41E-06	1.82E-03	2.36E-03	3.19E-03
700	1.36E-05	8.84E-06	1.68E-06	3.45E-06	4.13E-06	7.18E-06	2.31E-03	2.98E-03	4.39E-03
725	1.08E-05	3.87E-06	0.00E+00	4.40E-06	6.14E-06	6.63E-06	2.97E-03	3.38E-03	4.16E-03
750	7.21E-06	1.54E-06	5.13E-06	3.82E-06	3.12E-06	8.51E-06	3.05E-03	3.52E-03	4.15E-03
775	9.24E-06	7.33E-06	3.15E-06	4.71E-06	5.78E-06	6.06E-06	2.76E-03	3.68E-03	3.73E-03
800	1.18E-05	2.77E-06	6.66E-06	2.97E-06	1.77E-06	3.42E-06	1.76E-03	2.23E-03	2.47E-03
825	1.12E-05	6.45E-06	7.98E-06	0.00E+00	1.78E-06	2.66E-06	9.01E-04	1.29E-03	1.48E-03
850	6.55E-06	3.85E-06	4.55E-06	0.00E+00	0.00E+00	1.41E-06	5.66E-04	6.23E-04	8.97E-04
875	5.51E-06	4.87E-06	5.45E-06	0.00E+00	0.00E+00	1.38E-06	3.72E-04	3.89E-04	5.50E-04
900	3.45E-06	0.00E+00	5.00E-06	0.00E+00	0.00E+00	0.00E+00	2.22E-04	1.94E-04	3.36E-04
925	0.00E+00	0.00E+00	0.00E+00	0.00E+00	0.00E+00	0.00E+00	1.25E-04	1.92E-04	2.91E-04
950	0.00E+00	0.00E+00	0.00E+00	0.00E+00	0.00E+00	0.00E+00	4.20E-05	1.16E-04	2.18E-04
975	0.00E+00	0.00E+00	0.00E+00	0.00E+00	0.00E+00	0.00E+00	0.00E+00	3.88E-05	8.55E-05
1000	0.00E+00	0.00E+00	0.00E+00	0.00E+00	0.00E+00	0.00E+00	0.00E+00	6.68E-06	3.66E-05
1025	0.00E+00	0.00E+00	0.00E+00	0.00E+00	0.00E+00	0.00E+00	0.00E+00	0.00E+00	8.09E-06
1050	0.00E+00	0.00E+00	0.00E+00	0.00E+00	0.00E+00	0.00E+00	0.00E+00	0.00E+00	1.68E-06
1075	0.00E+00	0.00E+00	0.00E+00	0.00E+00	0.00E+00	0.00E+00	0.00E+00	0.00E+00	0.00E+00
1100	0.00E+00	0.00E+00	0.00E+00	0.00E+00	0.00E+00	0.00E+00	0.00E+00	0.00E+00	0.00E+00

T (K)	Pentanoic acid		
	Phi=0.5	Phi=1	Phi=2
500	0.00E+00	0.00E+00	0.00E+00
525	0.00E+00	0.00E+00	2.63E-05
550	3.49E-05	0.00E+00	3.84E-05
575	8.05E-05	3.62E-05	8.35E-05
600	2.63E-05	5.63E-05	6.27E-05
625	4.69E-05	1.82E-05	6.02E-05
650	3.39E-05	3.78E-05	6.35E-05
675	4.95E-05	3.68E-05	5.47E-05
700	2.03E-05	1.36E-05	7.93E-05
725	0.00E+00	7.21E-06	7.30E-05
750	0.00E+00	0.00E+00	4.99E-05
775	0.00E+00	0.00E+00	6.95E-05
800	0.00E+00	0.00E+00	4.49E-05
825	0.00E+00	0.00E+00	5.56E-05
850	0.00E+00	0.00E+00	2.06E-05
875	0.00E+00	0.00E+00	2.71E-05
900	0.00E+00	0.00E+00	0.00E+00
925	0.00E+00	0.00E+00	2.46E-05
950	0.00E+00	0.00E+00	0.00E+00
975	0.00E+00	0.00E+00	0.00E+00
1000	0.00E+00	0.00E+00	0.00E+00
1025	0.00E+00	0.00E+00	0.00E+00
1050	0.00E+00	0.00E+00	0.00E+00
1075	0.00E+00	0.00E+00	0.00E+00
1100	0.00E+00	0.00E+00	0.00E+00

II.6. Combustion of butanoic acid

Equivalence ratio	0,5 ; 1 ; 2
$x_{butanoic\ acid}$	0.005
Temperature (K)	500 - 1100
P (Torr)	800

Units	Mole fraction
Bath gas	Helium
Residence time	2 s

T (K)	O_2			CO			CH_4		
	Phi=0.5	Phi=1	Phi=2	Phi=0.5	Phi=1	Phi=2	Phi=0.5	Phi=1	Phi=2
500	0.00E+00	0.00E+00	0.00E+00	0.00E+00	0.00E+00	0.00E+00	0.00E+00	0.00E+00	0.00E+00
525	0.00E+00	0.00E+00	0.00E+00	0.00E+00	0.00E+00	0.00E+00	0.00E+00	0.00E+00	0.00E+00
550	0.00E+00	0.00E+00	0.00E+00	0.00E+00	0.00E+00	0.00E+00	0.00E+00	0.00E+00	0.00E+00
575	0.00E+00	0.00E+00	0.00E+00	0.00E+00	0.00E+00	0.00E+00	0.00E+00	0.00E+00	0.00E+00
600	0.00E+00	2.58E-02	0.00E+00	0.00E+00	1.67E-05	0.00E+00	0.00E+00	0.00E+00	0.00E+00
625	0.00E+00	0.00E+00	0.00E+00	0.00E+00	0.00E+00	0.00E+00	0.00E+00	0.00E+00	0.00E+00
650	0.00E+00	2.67E-02	0.00E+00	0.00E+00	0.00E+00	0.00E+00	0.00E+00	0.00E+00	0.00E+00
675	0.00E+00	0.00E+00	0.00E+00	0.00E+00	0.00E+00	0.00E+00	0.00E+00	0.00E+00	0.00E+00
700	0.00E+00	2.74E-02	0.00E+00	0.00E+00	2.44E-05	0.00E+00	0.00E+00	0.00E+00	0.00E+00
725	0.00E+00	0.00E+00	0.00E+00	0.00E+00	0.00E+00	0.00E+00	0.00E+00	0.00E+00	0.00E+00
750	0.00E+00	2.65E-02	0.00E+00	0.00E+00	2.13E-05	0.00E+00	0.00E+00	0.00E+00	0.00E+00
775	5.03E-02	2.63E-02	1.45E-02	5.04E-05	3.45E-05	1.31E-05	0.00E+00	6.70E-06	4.79E-06
800	4.92E-02	2.64E-02	1.51E-02	5.14E-05	2.61E-05	1.79E-05	4.92E-06	1.59E-05	1.91E-05
825	5.05E-02	2.60E-02	1.47E-02	5.71E-05	4.79E-05	2.25E-05	3.43E-05	4.84E-05	3.33E-05
850	4.88E-02	2.56E-02	1.43E-02	1.72E-04	1.61E-04	6.16E-05	1.02E-04	1.30E-04	7.92E-05
875	5.16E-02	2.99E-02	1.43E-02	8.28E-04	9.44E-04	2.22E-04	2.86E-04	3.55E-04	2.24E-04
900	4.51E-02	2.25E-02	1.37E-02	3.36E-03	1.92E-03	6.68E-04	6.14E-04	5.26E-04	3.86E-04
925	4.17E-02	2.30E-02	1.29E-02	5.53E-03	3.34E-03	1.56E-03	7.33E-04	8.06E-04	6.71E-04
950	3.91E-02	2.03E-02	1.26E-02	7.41E-03	5.20E-03	2.31E-03	6.78E-04	1.08E-03	8.47E-04
975	3.72E-02	1.82E-02	1.17E-02	1.01E-02	5.41E-03	3.73E-03	6.55E-04	8.32E-04	1.25E-03
1000	3.07E-02	1.54E-02	1.00E-02	7.35E-03	8.51E-03	5.79E-03	2.93E-04	1.04E-03	1.70E-03
1025	2.89E-02	1.14E-02	1.02E-02	3.93E-03	4.24E-03	7.26E-03	1.61E-04	5.36E-04	1.94E-03
1050	2.54E-02	1.01E-02	8.57E-03	2.17E-03	3.22E-03	9.28E-03	8.42E-05	5.60E-04	1.98E-03
1075	2.56E-02	6.52E-03	4.96E-03	1.21E-03	1.77E-03	1.14E-02	6.43E-05	2.80E-04	1.96E-03
1100	2.56E-02	4.62E-03	4.16E-03	8.60E-04	1.11E-03	1.13E-02	4.14E-05	1.18E-04	1.52E-03

T (K)	CO_2			Acetylene			Ethylene		
	Phi=0.5	Phi=1	Phi=2	Phi=0.5	Phi=1	Phi=2	Phi=0.5	Phi=1	Phi=2
500	0.00E+00	0.00E+00	0.00E+00	0.00E+00	0.00E+00	0.00E+00	0.00E+00	0.00E+00	0.00E+00
525	0.00E+00	0.00E+00	0.00E+00	0.00E+00	0.00E+00	0.00E+00	0.00E+00	0.00E+00	0.00E+00
550	0.00E+00	0.00E+00	0.00E+00	0.00E+00	0.00E+00	0.00E+00	0.00E+00	0.00E+00	0.00E+00
575	0.00E+00	0.00E+00	0.00E+00	0.00E+00	0.00E+00	0.00E+00	0.00E+00	0.00E+00	0.00E+00
600	0.00E+00	4.94E-05	0.00E+00	0.00E+00	0.00E+00	0.00E+00	0.00E+00	0.00E+00	0.00E+00
625	0.00E+00	0.00E+00	0.00E+00	0.00E+00	0.00E+00	0.00E+00	0.00E+00	0.00E+00	0.00E+00
650	0.00E+00	0.00E+00	0.00E+00	0.00E+00	0.00E+00	0.00E+00	0.00E+00	0.00E+00	0.00E+00
675	0.00E+00	0.00E+00	0.00E+00	0.00E+00	0.00E+00	0.00E+00	0.00E+00	0.00E+00	0.00E+00
700	0.00E+00	1.09E-04	0.00E+00	0.00E+00	0.00E+00	0.00E+00	0.00E+00	0.00E+00	0.00E+00
725	0.00E+00	0.00E+00	0.00E+00	0.00E+00	0.00E+00	0.00E+00	0.00E+00	0.00E+00	0.00E+00
750	0.00E+00	8.28E-05	0.00E+00	0.00E+00	1.81E-06	0.00E+00	0.00E+00	2.23E-06	0.00E+00
775	9.38E-05	7.83E-05	6.61E-05	0.00E+00	1.17E-05	0.00E+00	5.49E-06	4.46E-06	6.06E-06
800	1.01E-04	1.28E-04	8.11E-05	0.00E+00	1.35E-05	0.00E+00	1.09E-05	1.88E-05	1.97E-05
825	2.28E-04	2.25E-04	1.09E-04	0.00E+00	5.66E-05	0.00E+00	6.41E-05	5.31E-05	3.91E-05
850	5.07E-04	6.75E-04	2.38E-04	1.65E-06	2.34E-06	3.12E-07	1.88E-04	2.46E-04	1.01E-04
875	1.49E-03	2.02E-03	5.79E-04	1.68E-05	2.64E-05	1.76E-06	6.64E-04	7.49E-04	3.22E-04
900	3.57E-03	2.85E-03	1.04E-03	3.95E-05	3.07E-05	2.55E-05	1.41E-03	1.12E-03	6.22E-04
925	5.62E-03	2.91E-03	1.76E-03	1.35E-05	4.06E-05	3.19E-05	1.60E-03	1.62E-03	1.11E-03
950	6.38E-03	4.58E-03	2.16E-03	8.96E-06	4.62E-05	5.19E-05	1.24E-03	2.16E-03	1.45E-03
975	9.08E-03	3.97E-03	2.86E-03	8.61E-06	4.60E-05	7.67E-05	8.87E-04	1.39E-03	2.02E-03
1000	1.39E-02	6.03E-03	3.39E-03	3.44E-06	3.93E-05	1.29E-04	3.06E-04	1.36E-03	2.48E-03
1025	1.85E-02	1.08E-02	3.49E-03	3.10E-06	2.55E-05	1.38E-04	1.88E-04	7.91E-04	2.54E-03
1050	2.04E-02	1.43E-02	4.20E-03	3.95E-06	4.42E-05	1.15E-04	1.10E-04	9.58E-04	2.08E-03
1075	2.13E-02	1.80E-02	5.07E-03	4.02E-06	1.45E-05	4.36E-05	1.02E-04	5.42E-04	1.62E-03
1100	2.12E-02	2.03E-02	5.27E-03	3.15E-06	2.46E-05	7.94E-05	4.70E-05	1.95E-04	1.18E-03

T (K)	Ethane			Propene			Propane		
	Phi=0.5	Phi=1	Phi=2	Phi=0.5	Phi=1	Phi=2	Phi=0.5	Phi=1	Phi=2
500	0.00E+00	0.00E+00	0.00E+00	0.00E+00	0.00E+00	0.00E+00	0.00E+00	0.00E+00	0.00E+00
525	0.00E+00	0.00E+00	0.00E+00	0.00E+00	0.00E+00	0.00E+00	0.00E+00	0.00E+00	0.00E+00
550	0.00E+00	0.00E+00	0.00E+00	0.00E+00	0.00E+00	0.00E+00	0.00E+00	0.00E+00	0.00E+00
575	0.00E+00	0.00E+00	0.00E+00	0.00E+00	0.00E+00	0.00E+00	0.00E+00	0.00E+00	0.00E+00
600	0.00E+00	0.00E+00	0.00E+00	0.00E+00	0.00E+00	0.00E+00	0.00E+00	0.00E+00	0.00E+00
625	0.00E+00	0.00E+00	0.00E+00	0.00E+00	0.00E+00	0.00E+00	0.00E+00	0.00E+00	0.00E+00
650	0.00E+00	0.00E+00	0.00E+00	0.00E+00	0.00E+00	0.00E+00	0.00E+00	0.00E+00	0.00E+00
675	0.00E+00	0.00E+00	0.00E+00	0.00E+00	0.00E+00	0.00E+00	0.00E+00	0.00E+00	0.00E+00
700	0.00E+00	0.00E+00	0.00E+00	0.00E+00	0.00E+00	0.00E+00	0.00E+00	0.00E+00	0.00E+00
725	0.00E+00	0.00E+00	0.00E+00	0.00E+00	0.00E+00	0.00E+00	0.00E+00	0.00E+00	0.00E+00
750	0.00E+00	0.00E+00	0.00E+00	0.00E+00	2.06E-06	0.00E+00	0.00E+00	0.00E+00	0.00E+00
775	0.00E+00	0.00E+00	0.00E+00	6.56E-06	5.25E-06	7.26E-06	0.00E+00	0.00E+00	0.00E+00
800	0.00E+00	0.00E+00	0.00E+00	1.46E-05	1.78E-05	1.61E-05	0.00E+00	0.00E+00	0.00E+00
825	2.46E-06	2.24E-06	4.12E-06	6.11E-05	5.10E-05	3.33E-05	0.00E+00	0.00E+00	0.00E+00
850	7.50E-06	1.25E-05	6.04E-06	1.45E-04	1.90E-04	8.13E-05	0.00E+00	3.59E-06	2.49E-06
875	2.84E-05	4.31E-05	2.02E-05	3.60E-04	4.05E-04	2.10E-04	5.14E-06	9.94E-06	3.00E-06
900	5.66E-05	6.00E-05	4.76E-05	4.55E-04	4.26E-04	3.07E-04	3.77E-06	1.38E-05	1.85E-05
925	6.34E-05	8.22E-05	8.40E-05	3.67E-04	4.44E-04	4.26E-04	7.05E-06	1.10E-05	3.29E-05
950	4.78E-05	1.10E-04	1.07E-04	1.71E-04	4.34E-04	4.47E-04	3.72E-06	2.33E-05	4.64E-05
975	3.66E-05	7.12E-05	1.57E-04	9.86E-05	1.75E-04	4.42E-04	2.52E-06	1.07E-05	4.63E-05
1000	1.73E-05	8.52E-05	2.10E-04	4.91E-05	1.28E-04	3.71E-04	0.00E+00	9.54E-06	2.75E-05
1025	1.52E-05	6.74E-05	2.08E-04	4.27E-05	1.00E-04	2.68E-04	0.00E+00	8.62E-06	2.15E-05
1050	1.06E-05	9.28E-05	1.70E-04	2.67E-05	1.14E-04	1.30E-04	0.00E+00	1.04E-05	1.10E-05
1075	1.14E-05	6.73E-05	1.47E-04	2.00E-05	8.18E-05	6.73E-05	0.00E+00	9.19E-06	1.00E-05
1100	4.32E-06	2.79E-05	1.08E-04	4.63E-06	2.68E-05	4.64E-05	0.00E+00	3.20E-06	5.50E-06

T (K)	Oxirane			Methanol			Acetaldehyde		
	Phi=0.5	Phi=1	Phi=2	Phi=0.5	Phi=1	Phi=2	Phi=0.5	Phi=1	Phi=2
500	0.00E+00	0.00E+00	0.00E+00	0.00E+00	0.00E+00	0.00E+00	0.00E+00	0.00E+00	0.00E+00
525	0.00E+00	0.00E+00	0.00E+00	0.00E+00	0.00E+00	0.00E+00	0.00E+00	0.00E+00	0.00E+00
550	0.00E+00	0.00E+00	0.00E+00	0.00E+00	0.00E+00	0.00E+00	0.00E+00	0.00E+00	0.00E+00
575	0.00E+00	0.00E+00	0.00E+00	0.00E+00	0.00E+00	0.00E+00	0.00E+00	0.00E+00	0.00E+00
600	0.00E+00	0.00E+00	0.00E+00	0.00E+00	0.00E+00	0.00E+00	0.00E+00	0.00E+00	0.00E+00
625	0.00E+00	0.00E+00	0.00E+00	0.00E+00	0.00E+00	0.00E+00	0.00E+00	0.00E+00	0.00E+00
650	0.00E+00	0.00E+00	0.00E+00	0.00E+00	0.00E+00	0.00E+00	0.00E+00	0.00E+00	0.00E+00
675	0.00E+00	0.00E+00	0.00E+00	0.00E+00	0.00E+00	0.00E+00	0.00E+00	0.00E+00	0.00E+00
700	0.00E+00	0.00E+00	0.00E+00	0.00E+00	0.00E+00	0.00E+00	0.00E+00	0.00E+00	0.00E+00
725	0.00E+00	0.00E+00	0.00E+00	0.00E+00	0.00E+00	0.00E+00	0.00E+00	0.00E+00	0.00E+00
750	0.00E+00	0.00E+00	0.00E+00	0.00E+00	0.00E+00	0.00E+00	0.00E+00	0.00E+00	0.00E+00
775	0.00E+00	0.00E+00	0.00E+00	0.00E+00	0.00E+00	0.00E+00	0.00E+00	0.00E+00	0.00E+00
800	0.00E+00	0.00E+00	0.00E+00	0.00E+00	0.00E+00	0.00E+00	7.37E-06	2.35E-06	3.78E-06
825	0.00E+00	0.00E+00	0.00E+00	0.00E+00	0.00E+00	0.00E+00	7.19E-06	6.41E-06	4.64E-06
850	0.00E+00	4.86E-06	0.00E+00	0.00E+00	0.00E+00	0.00E+00	1.92E-05	1.92E-05	8.72E-06
875	9.13E-06	3.20E-06	0.00E+00	1.18E-05	8.05E-06	0.00E+00	5.63E-05	6.55E-05	2.62E-05
900	1.78E-05	2.02E-05	8.37E-06	1.74E-05	1.30E-05	0.00E+00	1.07E-04	8.09E-05	4.78E-05
925	1.09E-05	7.03E-06	1.04E-05	2.30E-05	8.29E-06	9.65E-06	9.71E-05	1.03E-04	7.91E-05
950	4.90E-06	8.31E-06	1.30E-05	1.55E-05	1.08E-05	0.00E+00	5.32E-05	8.79E-05	8.72E-05
975	2.68E-06	4.11E-06	1.38E-05	1.36E-05	8.94E-06	1.32E-05	3.71E-05	4.21E-05	9.45E-05
1000	0.00E+00	4.62E-06	1.68E-05	0.00E+00	0.00E+00	0.00E+00	1.54E-05	3.55E-05	8.74E-05
1025	0.00E+00	4.99E-06	1.35E-05	5.56E-06	0.00E+00	4.70E-06	1.28E-05	2.27E-05	5.83E-05
1050	0.00E+00	6.89E-06	1.01E-05	0.00E+00	0.00E+00	0.00E+00	9.69E-06	2.29E-05	3.15E-05
1075	0.00E+00	7.24E-06	4.53E-06	0.00E+00	0.00E+00	0.00E+00	8.43E-06	1.36E-05	1.33E-05
1100	0.00E+00	3.11E-06	4.39E-06	0.00E+00	0.00E+00	0.00E+00	2.23E-06	5.78E-06	9.59E-06

Experimental raw data: butanoic acid oxidation

T (K)	1-Butene			1,3-Butadiene			Ethanol		
	Phi=0.5	Phi=1	Phi=2	Phi=0.5	Phi=1	Phi=2	Phi=0.5	Phi=1	Phi=2
500	0.00E+00	0.00E+00	0.00E+00	0.00E+00	0.00E+00	0.00E+00	0.00E+00	0.00E+00	0.00E+00
525	0.00E+00	0.00E+00	0.00E+00	0.00E+00	0.00E+00	0.00E+00	0.00E+00	0.00E+00	0.00E+00
550	0.00E+00	0.00E+00	0.00E+00	0.00E+00	0.00E+00	0.00E+00	0.00E+00	0.00E+00	0.00E+00
575	0.00E+00	0.00E+00	0.00E+00	0.00E+00	0.00E+00	0.00E+00	0.00E+00	0.00E+00	0.00E+00
600	0.00E+00	0.00E+00	0.00E+00	0.00E+00	0.00E+00	0.00E+00	0.00E+00	0.00E+00	0.00E+00
625	0.00E+00	0.00E+00	0.00E+00	0.00E+00	0.00E+00	0.00E+00	0.00E+00	0.00E+00	0.00E+00
650	0.00E+00	0.00E+00	0.00E+00	0.00E+00	0.00E+00	0.00E+00	0.00E+00	0.00E+00	0.00E+00
675	0.00E+00	0.00E+00	0.00E+00	0.00E+00	0.00E+00	0.00E+00	0.00E+00	0.00E+00	0.00E+00
700	0.00E+00	0.00E+00	0.00E+00	0.00E+00	0.00E+00	0.00E+00	0.00E+00	0.00E+00	0.00E+00
725	0.00E+00	0.00E+00	0.00E+00	0.00E+00	0.00E+00	0.00E+00	0.00E+00	0.00E+00	0.00E+00
750	0.00E+00	0.00E+00	0.00E+00	0.00E+00	0.00E+00	0.00E+00	0.00E+00	0.00E+00	0.00E+00
775	0.00E+00	0.00E+00	0.00E+00	0.00E+00	0.00E+00	0.00E+00	0.00E+00	0.00E+00	0.00E+00
800	0.00E+00	0.00E+00	0.00E+00	0.00E+00	0.00E+00	0.00E+00	0.00E+00	0.00E+00	0.00E+00
825	0.00E+00	0.00E+00	0.00E+00	0.00E+00	0.00E+00	0.00E+00	0.00E+00	0.00E+00	0.00E+00
850	0.00E+00	2.31E-06	1.26E-06	2.54E-06	0.00E+00	0.00E+00	0.00E+00	3.23E-06	0.00E+00
875	6.97E-06	1.08E-05	4.47E-06	1.47E-06	0.00E+00	8.57E-07	3.59E-06	4.12E-06	0.00E+00
900	1.29E-05	1.40E-05	1.10E-05	3.59E-06	3.59E-06	1.71E-06	3.24E-06	4.94E-06	3.78E-06
925	1.22E-05	1.59E-05	2.03E-05	3.16E-06	3.86E-06	4.30E-06	0.00E+00	3.68E-06	4.82E-06
950	5.71E-06	1.63E-05	2.47E-05	1.93E-06	4.78E-06	7.21E-06	0.00E+00	3.99E-06	5.31E-06
975	3.58E-06	6.43E-06	2.86E-05	1.45E-06	2.24E-06	1.21E-05	0.00E+00	0.00E+00	5.51E-06
1000	2.47E-06	5.12E-06	2.48E-05	1.23E-06	2.12E-06	1.30E-05	0.00E+00	0.00E+00	4.44E-06
1025	3.13E-06	5.66E-06	1.51E-05	0.00E+00	2.67E-06	9.97E-06	0.00E+00	0.00E+00	0.00E+00
1050	2.05E-06	6.35E-06	0.00E+00	1.46E-06	3.41E-06	8.04E-06	0.00E+00	0.00E+00	0.00E+00
1075	3.13E-06	6.28E-06	3.03E-06	2.27E-06	3.54E-06	2.00E-06	0.00E+00	0.00E+00	0.00E+00
1100	0.00E+00	2.42E-06	3.68E-06	0.00E+00	1.43E-06	2.47E-06	0.00E+00	0.00E+00	0.00E+00

T (K)	Not identified			Acrolein			Propanal		
	Phi=0.5	Phi=1	Phi=2	Phi=0.5	Phi=1	Phi=2	Phi=0.5	Phi=1	Phi=2
500	0.00E+00	0.00E+00	0.00E+00	0.00E+00	0.00E+00	0.00E+00	0.00E+00	0.00E+00	0.00E+00
525	0.00E+00	0.00E+00	0.00E+00	0.00E+00	0.00E+00	0.00E+00	0.00E+00	0.00E+00	0.00E+00
550	0.00E+00	0.00E+00	0.00E+00	0.00E+00	0.00E+00	0.00E+00	0.00E+00	0.00E+00	0.00E+00
575	0.00E+00	0.00E+00	0.00E+00	0.00E+00	0.00E+00	0.00E+00	0.00E+00	0.00E+00	0.00E+00
600	0.00E+00	0.00E+00	0.00E+00	0.00E+00	0.00E+00	0.00E+00	0.00E+00	0.00E+00	0.00E+00
625	0.00E+00	0.00E+00	0.00E+00	0.00E+00	0.00E+00	0.00E+00	0.00E+00	0.00E+00	0.00E+00
650	0.00E+00	0.00E+00	0.00E+00	0.00E+00	0.00E+00	0.00E+00	0.00E+00	0.00E+00	0.00E+00
675	0.00E+00	0.00E+00	0.00E+00	0.00E+00	0.00E+00	0.00E+00	0.00E+00	0.00E+00	0.00E+00
700	0.00E+00	0.00E+00	0.00E+00	0.00E+00	0.00E+00	0.00E+00	0.00E+00	0.00E+00	0.00E+00
725	0.00E+00	0.00E+00	0.00E+00	0.00E+00	0.00E+00	0.00E+00	0.00E+00	0.00E+00	0.00E+00
750	0.00E+00	0.00E+00	0.00E+00	0.00E+00	0.00E+00	0.00E+00	0.00E+00	2.80E-06	0.00E+00
775	0.00E+00	0.00E+00	0.00E+00	0.00E+00	0.00E+00	0.00E+00	7.41E-06	3.44E-06	4.06E-06
800	0.00E+00	0.00E+00	0.00E+00	0.00E+00	0.00E+00	0.00E+00	1.01E-05	8.04E-06	7.60E-06
825	6.80E-06	0.00E+00	0.00E+00	1.90E-06	0.00E+00	0.00E+00	2.87E-05	1.56E-05	1.02E-05
850	9.58E-06	8.27E-06	0.00E+00	3.60E-06	6.39E-06	1.91E-06	3.97E-05	3.19E-05	2.09E-05
875	1.69E-05	1.19E-05	4.19E-06	1.12E-05	1.47E-05	4.79E-06	5.86E-05	5.14E-05	2.99E-05
900	1.37E-05	1.05E-05	5.90E-06	2.40E-05	1.97E-05	1.02E-05	5.93E-05	3.39E-05	7.12E-05
925	9.99E-06	8.29E-06	0.00E+00	2.18E-05	1.98E-05	2.20E-05	5.43E-05	6.50E-05	1.10E-04
950	8.18E-06	6.09E-06	0.00E+00	1.41E-05	1.50E-05	2.46E-05	3.21E-05	2.35E-05	1.03E-04
975	0.00E+00	0.00E+00	0.00E+00	8.11E-06	6.67E-06	2.52E-05	1.67E-05	1.30E-05	7.93E-05
1000	0.00E+00	0.00E+00	0.00E+00	4.81E-06	5.36E-06	2.50E-05	9.89E-06	1.13E-05	5.77E-05
1025	0.00E+00	0.00E+00	0.00E+00	5.26E-06	4.18E-06	1.84E-05	1.11E-05	8.12E-06	3.34E-05
1050	0.00E+00	0.00E+00	0.00E+00	3.88E-06	4.41E-06	9.62E-06	9.08E-06	7.97E-06	1.73E-05
1075	0.00E+00	0.00E+00	0.00E+00	4.06E-06	4.15E-06	2.08E-06	5.32E-06	8.26E-06	7.41E-06
1100	0.00E+00	0.00E+00	0.00E+00	0.00E+00	2.61E-06	4.37E-06	0.00E+00	5.29E-06	4.10E-06

Experimental raw data: butanoic acid oxidation

T (K)	Acetone			Butanoic Acid		
	Phi=0.5	Phi=1	Phi=2	Phi=0.5	Phi=1	Phi=2
500	0.00E+00	0.00E+00	0.00E+00	0.00E+00	0.00E+00	0.00E+00
525	0.00E+00	0.00E+00	0.00E+00	0.00E+00	0.00E+00	0.00E+00
550	0.00E+00	0.00E+00	0.00E+00	0.00E+00	0.00E+00	0.00E+00
575	0.00E+00	0.00E+00	0.00E+00	0.00E+00	0.00E+00	0.00E+00
600	0.00E+00	0.00E+00	0.00E+00	0.00E+00	5.89E-03	0.00E+00
625	0.00E+00	0.00E+00	0.00E+00	0.00E+00	0.00E+00	0.00E+00
650	0.00E+00	0.00E+00	0.00E+00	0.00E+00	0.00E+00	0.00E+00
675	0.00E+00	0.00E+00	0.00E+00	0.00E+00	0.00E+00	0.00E+00
700	0.00E+00	0.00E+00	0.00E+00	0.00E+00	5.29E-03	0.00E+00
725	0.00E+00	0.00E+00	0.00E+00	0.00E+00	0.00E+00	0.00E+00
750	0.00E+00	2.53E-06	0.00E+00	0.00E+00	5.39E-03	0.00E+00
775	0.00E+00	0.00E+00	0.00E+00	3.87E-03	5.13E-03	8.54E-03
800	1.76E-06	1.63E-06	0.00E+00	5.34E-03	4.73E-03	6.72E-03
825	2.71E-06	2.76E-06	0.00E+00	5.63E-03	5.60E-03	5.42E-03
850	3.23E-06	2.23E-06	2.10E-06	3.53E-03	4.94E-03	4.92E-03
875	4.42E-06	5.01E-06	2.25E-06	3.04E-03	3.87E-03	4.66E-03
900	9.46E-06	6.00E-06	3.01E-06	2.68E-03	2.91E-03	2.98E-03
925	7.09E-06	7.34E-06	4.25E-06	7.91E-04	2.01E-03	2.45E-03
950	4.93E-06	6.56E-06	3.73E-06	4.40E-04	6.98E-04	1.92E-03
975	3.55E-06	3.29E-06	5.87E-06	2.11E-04	2.97E-04	1.55E-03
1000	1.43E-06	3.37E-06	4.42E-06	0.00E+00	1.05E-04	1.00E-03
1025	2.98E-06	0.00E+00	3.43E-06	3.55E-05	1.61E-04	8.15E-04
1050	0.00E+00	2.64E-06	3.22E-06	5.84E-06	1.15E-04	3.01E-04
1075	0.00E+00	0.00E+00	0.00E+00	4.90E-06	0.00E+00	1.83E-04
1100	0.00E+00	0.00E+00	0.00E+00	0.00E+00	0.00E+00	1.52E-04

II.7. Combustion of pentanoic acid

Equivalence ratio	0,5 ; 1 ; 2
$x_{pentanoic\ acid}$	0.005
Temperature (K)	725 - 1100
P (Torr)	800

Units	Mole fraction
Bath gas	Helium
Residence time (s)	2

T (K)	O_2			CO			CH_4		
	Phi=0.5	Phi=1	Phi=2	Phi=0.5	Phi=1	Phi=2	Phi=0.5	Phi=1	Phi=2
725	0.00E+00	3.34E-02	0.00E+00	0.00E+00	1.18E-05	0.00E+00	0.00E+00	0.00E+00	0.00E+00
750	0.00E+00	0.00E+00	0.00E+00	0.00E+00	0.00E+00	0.00E+00	0.00E+00	0.00E+00	0.00E+00
775	6.54E-02	3.37E-02	1.80E-02	4.85E-05	2.96E-05	1.67E-05	5.62E-07	6.59E-07	5.31E-07
800	6.29E-02	3.37E-02	1.84E-02	6.63E-05	3.33E-05	2.82E-05	1.66E-06	2.30E-06	1.76E-06
825	6.48E-02	3.31E-02	1.75E-02	1.09E-04	1.10E-04	6.18E-05	8.65E-06	1.46E-05	8.69E-06
850	6.58E-02	3.11E-02	1.71E-02	5.09E-04	6.52E-04	3.44E-04	5.91E-05	7.62E-05	6.45E-05
875	6.29E-02	2.88E-02	1.57E-02	3.30E-03	2.37E-03	1.65E-03	2.39E-04	2.19E-04	2.30E-04
900	5.77E-02	2.62E-02	1.37E-02	6.19E-03	4.69E-03	3.53E-03	3.61E-04	3.90E-04	4.04E-04
925	5.19E-02	2.35E-02	1.29E-02	8.85E-03	7.85E-03	5.01E-03	4.55E-04	5.17E-04	5.82E-04
950	5.02E-02	2.11E-02	1.18E-02	1.21E-02	9.51E-03	5.82E-03	3.62E-04	6.42E-04	8.10E-04
975	4.48E-02	1.89E-02	1.12E-02	1.30E-02	1.07E-02	7.55E-03	1.57E-04	7.41E-04	9.66E-04
1000	3.77E-02	1.56E-02	8.81E-03	6.29E-03	1.22E-02	9.71E-03	9.63E-05	5.58E-04	1.40E-03
1025	3.84E-02	1.03E-02	7.85E-03	3.46E-03	7.80E-03	1.06E-02	3.25E-05	2.68E-04	1.30E-03
1050	4.02E-02	6.20E-03	6.70E-03	2.08E-03	2.16E-03	1.28E-02	2.28E-05	1.54E-04	1.27E-03
1075	3.82E-02	2.28E-03	4.84E-03	1.01E-03	7.00E-04	1.44E-02	1.39E-05	6.43E-05	1.45E-03
1100	3.88E-02	1.34E-03	2.87E-03	7.43E-04	7.92E-04	1.59E-02	7.41E-06	3.72E-05	1.37E-03

T (K)	CO_2			Acetylene			Ethylene		
	Phi=0.5	Phi=1	Phi=2	Phi=0.5	Phi=1	Phi=2	Phi=0.5	Phi=1	Phi=2
725	0.00E+00	4.30E-05	0.00E+00	0.00E+00	2.01E-06	0.00E+00	0.00E+00	1.36E-06	0.00E+00
750	0.00E+00	0.00E+00	0.00E+00	0.00E+00	0.00E+00	0.00E+00	0.00E+00	0.00E+00	0.00E+00
775	1.26E-04	9.90E-05	3.84E-05	0.00E+00	0.00E+00	0.00E+00	1.09E-05	1.08E-05	9.73E-06
800	2.08E-04	1.21E-04	7.45E-05	0.00E+00	0.00E+00	0.00E+00	3.24E-05	4.90E-05	3.32E-05
825	3.02E-04	4.90E-04	1.71E-04	2.51E-07	9.84E-07	1.48E-07	1.36E-04	2.06E-04	1.25E-04
850	9.53E-04	1.64E-03	7.56E-04	4.30E-06	7.04E-06	5.74E-06	7.11E-04	7.17E-04	6.63E-04
875	3.46E-03	3.06E-03	1.96E-03	3.22E-05	2.48E-05	2.82E-05	1.81E-03	1.49E-03	1.58E-03
900	6.17E-03	4.19E-03	2.99E-03	5.85E-05	4.18E-05	3.96E-05	2.07E-03	2.02E-03	2.08E-03
925	6.61E-03	5.50E-03	3.34E-03	2.09E-05	4.27E-05	4.40E-05	2.06E-03	2.16E-03	2.40E-03
950	8.29E-03	6.02E-03	3.19E-03	8.70E-06	3.94E-05	4.34E-05	1.24E-03	2.02E-03	2.70E-03
975	1.25E-02	6.49E-03	3.76E-03	5.64E-06	3.54E-05	3.90E-05	6.02E-04	2.00E-03	2.70E-03
1000	1.89E-02	8.68E-03	4.64E-03	3.05E-06	1.56E-05	5.44E-05	2.75E-04	1.03E-03	3.23E-03
1025	2.04E-02	1.55E-02	4.37E-03	2.64E-06	1.78E-05	3.51E-05	1.18E-04	6.85E-04	2.46E-03
1050	2.47E-02	2.10E-02	4.90E-03	3.10E-06	1.93E-05	3.52E-05	7.59E-05	5.15E-04	1.98E-03
1075	2.60E-02	2.38E-02	5.44E-03	1.57E-06	9.80E-06	4.71E-05	3.41E-05	2.12E-04	1.49E-03
1100	2.35E-02	2.49E-02	5.90E-03	3.95E-07	6.79E-06	7.85E-05	6.31E-06	7.08E-05	1.10E-03

T (K)	Ethane			Propene			Propane		
	Phi=0.5	Phi=1	Phi=2	Phi=0.5	Phi=1	Phi=2	Phi=0.5	Phi=1	Phi=2
725	0.00E+00	0.00E+00	0.00E+00	0.00E+00	3.98E-06	0.00E+00	0.00E+00	0.00E+00	0.00E+00
750	0.00E+00	0.00E+00	0.00E+00	0.00E+00	0.00E+00	0.00E+00	0.00E+00	0.00E+00	0.00E+00
775	0.00E+00	0.00E+00	0.00E+00	8.64E-06	6.53E-06	5.31E-06	0.00E+00	0.00E+00	0.00E+00
800	0.00E+00	0.00E+00	0.00E+00	2.28E-05	1.78E-05	1.34E-05	0.00E+00	0.00E+00	0.00E+00
825	0.00E+00	0.00E+00	0.00E+00	7.56E-05	8.97E-05	4.83E-05	0.00E+00	0.00E+00	0.00E+00
850	6.43E-06	7.43E-06	7.31E-06	3.08E-04	3.10E-04	2.32E-04	0.00E+00	0.00E+00	0.00E+00
875	1.59E-05	1.97E-05	3.07E-05	4.60E-04	5.14E-04	5.15E-04	0.00E+00	2.55E-06	3.37E-06
900	2.66E-05	3.55E-05	6.09E-05	4.31E-04	4.70E-04	5.76E-04	0.00E+00	4.19E-06	0.00E+00
925	3.17E-05	5.75E-05	7.63E-05	3.02E-04	3.85E-04	4.90E-04	1.99E-06	5.84E-06	0.00E+00
950	3.37E-05	5.65E-05	8.60E-05	1.74E-04	2.29E-04	2.92E-04	2.55E-06	4.55E-06	0.00E+00
975	2.27E-05	5.13E-05	1.12E-04	8.22E-05	1.23E-04	2.70E-04	0.00E+00	3.25E-06	0.00E+00
1000	3.04E-06	5.04E-05	1.47E-04	2.86E-05	7.16E-05	2.70E-04	0.00E+00	4.88E-06	0.00E+00
1025	4.35E-06	4.91E-05	1.24E-04	1.91E-05	5.25E-05	1.24E-04	0.00E+00	3.18E-06	0.00E+00
1050	4.17E-06	1.76E-05	1.03E-04	1.15E-05	2.58E-05	5.42E-05	0.00E+00	0.00E+00	0.00E+00
1075	0.00E+00	4.21E-06	8.37E-05	0.00E+00	3.10E-06	3.38E-05	0.00E+00	0.00E+00	0.00E+00
1100	0.00E+00	4.90E-06	7.39E-05	0.00E+00	3.37E-06	2.31E-05	0.00E+00	0.00E+00	4.44E-06

Experimental raw data: pentanoic acid oxidation

T (K)	Formaldehyde			Oxirane			Methanol		
	Phi=0.5	Phi=1	Phi=2	Phi=0.5	Phi=1	Phi=2	Phi=0.5	Phi=1	Phi=2
725	0.00E+00	0.00E+00	0.00E+00	0.00E+00	0.00E+00	0.00E+00	0.00E+00	0.00E+00	0.00E+00
750	0.00E+00	0.00E+00	0.00E+00	0.00E+00	0.00E+00	0.00E+00	0.00E+00	0.00E+00	0.00E+00
775	0.00E+00	0.00E+00	0.00E+00	0.00E+00	0.00E+00	0.00E+00	0.00E+00	0.00E+00	0.00E+00
800	0.00E+00	0.00E+00	0.00E+00	0.00E+00	0.00E+00	0.00E+00	0.00E+00	0.00E+00	0.00E+00
825	0.00E+00	1.06E-04	0.00E+00	0.00E+00	0.00E+00	0.00E+00	0.00E+00	0.00E+00	0.00E+00
850	0.00E+00	2.92E-04	0.00E+00	0.00E+00	1.96E-06	4.45E-06	0.00E+00	0.00E+00	0.00E+00
875	3.89E-04	3.53E-04	3.39E-04	3.54E-06	3.30E-06	3.20E-06	1.31E-05	1.06E-05	1.01E-05
900	2.78E-04	4.09E-04	4.13E-04	4.30E-06	3.87E-06	1.13E-05	1.83E-05	1.44E-05	1.46E-05
925	1.92E-04	1.95E-04	3.39E-04	2.79E-06	4.13E-06	1.43E-05	1.91E-05	1.18E-05	1.29E-05
950	3.75E-04	2.67E-04	4.92E-04	0.00E+00	2.75E-06	1.06E-05	1.54E-05	1.42E-05	0.00E+00
975	1.94E-04	1.38E-04	3.11E-04	0.00E+00	2.90E-06	1.38E-05	1.05E-05	0.00E+00	1.99E-05
1000	0.00E+00	0.00E+00	2.59E-04	0.00E+00	0.00E+00	2.05E-05	0.00E+00	0.00E+00	0.00E+00
1025	0.00E+00	0.00E+00	2.17E-04	0.00E+00	0.00E+00	1.65E-05	0.00E+00	0.00E+00	0.00E+00
1050	0.00E+00	0.00E+00	0.00E+00	0.00E+00	0.00E+00	1.42E-05	0.00E+00	0.00E+00	0.00E+00
1075	0.00E+00	0.00E+00	0.00E+00	0.00E+00	0.00E+00	1.66E-05	0.00E+00	0.00E+00	0.00E+00
1100	0.00E+00	0.00E+00	0.00E+00	0.00E+00	0.00E+00	0.00E+00	0.00E+00	0.00E+00	0.00E+00

T (K)	Acetaldehyde			1-Butene			1,3-Butadiène		
	Phi=0.5	Phi=1	Phi=2	Phi=0.5	Phi=1	Phi=2	Phi=0.5	Phi=1	Phi=2
725	0.00E+00	5.43E-06	0.00E+00	0.00E+00	2.46E-06	0.00E+00	0.00E+00	0.00E+00	0.00E+00
750	0.00E+00	0.00E+00	0.00E+00	0.00E+00	0.00E+00	0.00E+00	0.00E+00	0.00E+00	0.00E+00
775	5.62E-06	4.29E-06	3.21E-06	7.27E-06	4.65E-06	4.39E-06	0.00E+00	0.00E+00	0.00E+00
800	6.59E-06	3.30E-06	9.21E-06	1.52E-05	1.21E-05	1.14E-05	0.00E+00	0.00E+00	0.00E+00
825	1.00E-05	1.41E-05	6.92E-06	4.32E-05	6.51E-05	3.15E-05	3.51E-06	6.43E-06	2.57E-06
850	4.82E-05	5.61E-05	3.40E-05	1.24E-04	1.63E-04	1.18E-04	1.62E-05	2.46E-05	1.41E-05
875	1.33E-04	1.24E-04	1.08E-04	1.45E-04	1.72E-04	1.74E-04	3.39E-05	3.82E-05	2.91E-05
900	1.45E-04	1.51E-04	1.43E-04	1.15E-04	1.17E-04	1.60E-04	3.27E-05	3.66E-05	3.87E-05
925	1.01E-04	1.44E-04	1.36E-04	7.33E-05	8.08E-05	1.16E-04	2.46E-05	2.99E-05	4.02E-05
950	8.23E-05	1.01E-04	9.24E-05	3.89E-05	4.97E-05	5.38E-05	1.63E-05	2.56E-05	3.12E-05
975	3.81E-05	5.57E-05	8.47E-05	2.10E-05	2.77E-05	5.02E-05	8.42E-06	1.78E-05	3.61E-05
1000	1.20E-05	3.22E-05	7.03E-05	1.07E-05	1.57E-05	4.33E-05	6.25E-06	1.10E-05	3.98E-05
1025	9.23E-06	2.09E-05	3.71E-05	5.40E-06	1.11E-05	1.72E-05	4.85E-06	1.17E-05	2.22E-05
1050	7.14E-06	9.38E-06	1.81E-05	2.90E-06	5.43E-06	8.61E-06	3.86E-06	9.72E-06	1.22E-05
1075	0.00E+00	2.51E-06	8.49E-06	0.00E+00	0.00E+00	4.11E-06	0.00E+00	0.00E+00	8.33E-06
1100	0.00E+00	2.79E-06	8.90E-06	0.00E+00	0.00E+00	3.27E-06	0.00E+00	1.29E-06	6.22E-06

T (K)	1-Butyne			2-Butene E			2-Butène Z		
	Phi=0.5	Phi=1	Phi=2	Phi=0.5	Phi=1	Phi=2	Phi=0.5	Phi=1	Phi=2
725	0.00E+00	0.00E+00	0.00E+00	0.00E+00	0.00E+00	0.00E+00	0.00E+00	0.00E+00	0.00E+00
750	0.00E+00	0.00E+00	0.00E+00	0.00E+00	0.00E+00	0.00E+00	0.00E+00	0.00E+00	0.00E+00
775	0.00E+00	0.00E+00	0.00E+00	0.00E+00	0.00E+00	0.00E+00	0.00E+00	0.00E+00	0.00E+00
800	0.00E+00	0.00E+00	0.00E+00	0.00E+00	0.00E+00	0.00E+00	0.00E+00	0.00E+00	0.00E+00
825	0.00E+00	0.00E+00	0.00E+00	2.40E-06	6.44E-06	3.59E-06	1.58E-06	1.97E-06	0.00E+00
850	1.36E-06	8.34E-06	0.00E+00	3.38E-06	6.11E-06	2.74E-06	2.69E-06	2.80E-06	1.75E-06
875	4.90E-06	9.59E-06	0.00E+00	4.77E-06	6.07E-06	6.95E-06	2.80E-06	3.57E-06	3.33E-06
900	3.39E-06	5.30E-06	0.00E+00	3.87E-06	4.71E-06	3.94E-06	2.79E-06	3.24E-06	4.11E-06
925	0.00E+00	3.01E-06	0.00E+00	4.53E-06	4.60E-06	1.21E-05	2.06E-06	2.89E-06	3.62E-06
950	0.00E+00	0.00E+00	0.00E+00	3.31E-06	5.92E-06	8.69E-06	1.61E-06	2.18E-06	3.40E-06
975	0.00E+00	0.00E+00	0.00E+00	1.85E-06	4.23E-06	9.28E-06	0.00E+00	9.66E-07	3.92E-06
1000	0.00E+00	0.00E+00	0.00E+00	0.00E+00	3.89E-06	8.96E-06	0.00E+00	0.00E+00	2.32E-06
1025	0.00E+00	0.00E+00	0.00E+00	0.00E+00	0.00E+00	5.54E-06	0.00E+00	0.00E+00	2.79E-06
1050	0.00E+00	0.00E+00	0.00E+00	0.00E+00	0.00E+00	2.31E-06	0.00E+00	0.00E+00	0.00E+00
1075	0.00E+00	0.00E+00	0.00E+00	0.00E+00	0.00E+00	2.10E-06	0.00E+00	0.00E+00	0.00E+00
1100	0.00E+00	0.00E+00	0.00E+00	0.00E+00	0.00E+00	0.00E+00	0.00E+00	0.00E+00	0.00E+00

Experimental raw data: pentanoic acid oxidation

T (K)	Ethanol			Methyl-oxirane			Acrolein		
	Phi=0.5	Phi=1	Phi=2	Phi=0.5	Phi=1	Phi=2	Phi=0.5	Phi=1	Phi=2
725	0.00E+00	7.74E-06	0.00E+00	0.00E+00	0.00E+00	0.00E+00	0.00E+00	0.00E+00	0.00E+00
750	0.00E+00	0.00E+00	0.00E+00	0.00E+00	0.00E+00	0.00E+00	0.00E+00	0.00E+00	0.00E+00
775	0.00E+00	4.70E-06	0.00E+00	0.00E+00	0.00E+00	0.00E+00	0.00E+00	0.00E+00	0.00E+00
800	0.00E+00	0.00E+00	0.00E+00	0.00E+00	0.00E+00	0.00E+00	3.32E-06	0.00E+00	0.00E+00
825	0.00E+00	1.20E-05	5.21E-06	0.00E+00	0.00E+00	0.00E+00	3.25E-06	5.33E-06	2.86E-06
850	0.00E+00	5.21E-06	3.90E-06	4.37E-06	3.26E-06	2.52E-06	1.29E-05	2.07E-05	1.11E-05
875	4.80E-06	5.34E-06	4.38E-06	8.63E-06	6.75E-06	5.66E-06	4.10E-05	4.29E-05	3.17E-05
900	4.69E-06	0.00E+00	5.84E-06	6.27E-06	5.42E-06	6.33E-06	4.11E-05	4.82E-05	4.09E-05
925	0.00E+00	0.00E+00	6.69E-06	3.93E-06	4.01E-06	2.89E-06	2.43E-05	3.66E-05	3.47E-05
950	0.00E+00	0.00E+00	0.00E+00	1.23E-06	0.00E+00	0.00E+00	2.11E-05	2.34E-05	2.59E-05
975	0.00E+00	0.00E+00	0.00E+00	0.00E+00	0.00E+00	0.00E+00	7.64E-06	1.40E-05	2.10E-05
1000	0.00E+00	0.00E+00	0.00E+00	0.00E+00	0.00E+00	0.00E+00	5.66E-06	7.68E-06	1.72E-05
1025	0.00E+00	0.00E+00	0.00E+00	0.00E+00	0.00E+00	0.00E+00	2.66E-06	5.51E-06	8.62E-06
1050	0.00E+00	0.00E+00	0.00E+00	0.00E+00	0.00E+00	0.00E+00	4.56E-06	3.22E-06	4.10E-06
1075	0.00E+00	0.00E+00	0.00E+00	0.00E+00	0.00E+00	0.00E+00	0.00E+00	0.00E+00	0.00E+00
1100	0.00E+00	0.00E+00	0.00E+00	0.00E+00	0.00E+00	0.00E+00	0.00E+00	0.00E+00	0.00E+00

T (K)	Furan			Propanal			Acétone		
	Phi=0.5	Phi=1	Phi=2	Phi=0.5	Phi=1	Phi=2	Phi=0.5	Phi=1	Phi=2
725	0.00E+00	0.00E+00	0.00E+00	0.00E+00	2.71E-06	0.00E+00	0.00E+00	0.00E+00	0.00E+00
750	0.00E+00	0.00E+00	0.00E+00	0.00E+00	0.00E+00	0.00E+00	0.00E+00	0.00E+00	0.00E+00
775	0.00E+00	0.00E+00	0.00E+00	3.46E-06	1.73E-06	0.00E+00	0.00E+00	0.00E+00	0.00E+00
800	0.00E+00	0.00E+00	0.00E+00	5.20E-06	2.04E-06	0.00E+00	0.00E+00	0.00E+00	0.00E+00
825	0.00E+00	0.00E+00	0.00E+00	5.36E-06	6.27E-06	2.74E-06	0.00E+00	0.00E+00	0.00E+00
850	1.27E-06	1.89E-06	0.00E+00	1.17E-05	1.23E-05	4.88E-06	2.24E-06	3.77E-06	2.21E-06
875	2.65E-06	2.33E-06	1.23E-06	2.00E-05	1.68E-05	1.11E-05	6.13E-06	6.31E-06	3.50E-06
900	1.59E-06	3.37E-06	1.05E-06	1.85E-05	1.30E-05	1.35E-05	7.78E-06	8.10E-06	8.59E-06
925	3.65E-06	1.46E-06	1.20E-06	9.17E-06	1.18E-05	1.19E-05	5.98E-06	8.32E-06	6.82E-06
950	1.28E-06	0.00E+00	0.00E+00	8.14E-06	6.76E-06	1.01E-05	6.03E-06	4.55E-06	6.58E-06
975	1.54E-06	0.00E+00	0.00E+00	4.35E-06	4.73E-06	7.01E-06	3.25E-06	4.14E-06	5.31E-06
1000	0.00E+00	0.00E+00	0.00E+00	2.05E-06	4.52E-06	5.54E-06	0.00E+00	4.12E-06	3.64E-06
1025	0.00E+00	0.00E+00	0.00E+00	2.86E-06	3.42E-06	4.76E-06	0.00E+00	0.00E+00	2.94E-06
1050	0.00E+00	0.00E+00	0.00E+00	0.00E+00	1.92E-06	5.01E-06	0.00E+00	0.00E+00	0.00E+00
1075	0.00E+00	0.00E+00	0.00E+00	0.00E+00	0.00E+00	0.00E+00	0.00E+00	0.00E+00	0.00E+00
1100	0.00E+00	0.00E+00	0.00E+00	0.00E+00	0.00E+00	0.00E+00	0.00E+00	0.00E+00	0.00E+00

T (K)	2,3-Dimethylcyclopropane			Ethyloxirane			2-Pentene E		
	Phi=0.5	Phi=1	Phi=2	Phi=0.5	Phi=1	Phi=2	Phi=0.5	Phi=1	Phi=2
725	0.00E+00	0.00E+00	0.00E+00	0.00E+00	0.00E+00	0.00E+00	0.00E+00	0.00E+00	0.00E+00
750	0.00E+00	0.00E+00	0.00E+00	0.00E+00	0.00E+00	0.00E+00	0.00E+00	0.00E+00	0.00E+00
775	0.00E+00	0.00E+00	0.00E+00	0.00E+00	0.00E+00	0.00E+00	0.00E+00	0.00E+00	0.00E+00
800	0.00E+00	0.00E+00	0.00E+00	0.00E+00	0.00E+00	0.00E+00	0.00E+00	0.00E+00	0.00E+00
825	0.00E+00	0.00E+00	0.00E+00	0.00E+00	0.00E+00	0.00E+00	0.00E+00	0.00E+00	0.00E+00
850	0.00E+00	0.00E+00	0.00E+00	0.00E+00	1.31E-06	0.00E+00	0.00E+00	0.00E+00	0.00E+00
875	0.00E+00	2.86E-06	2.96E-06	0.00E+00	1.17E-06	2.22E-06	0.00E+00	0.00E+00	0.00E+00
900	0.00E+00	2.78E-06	4.35E-06	0.00E+00	2.07E-06	3.23E-06	0.00E+00	0.00E+00	0.00E+00
925	0.00E+00	2.19E-06	3.72E-06	9.83E-05	2.12E-06	3.09E-06	0.00E+00	0.00E+00	0.00E+00
950	0.00E+00	0.00E+00	0.00E+00	0.00E+00	0.00E+00	2.55E-06	4.62E-06	0.00E+00	0.00E+00
975	0.00E+00	0.00E+00	3.47E-06	0.00E+00	0.00E+00	2.91E-06	0.00E+00	1.28E-06	3.12E-06
1000	0.00E+00	0.00E+00	2.34E-06	0.00E+00	0.00E+00	2.92E-06	0.00E+00	0.00E+00	0.00E+00
1025	0.00E+00	0.00E+00	0.00E+00	0.00E+00	0.00E+00	2.04E-06	0.00E+00	0.00E+00	0.00E+00
1050	0.00E+00	0.00E+00	0.00E+00	0.00E+00	0.00E+00	0.00E+00	0.00E+00	0.00E+00	0.00E+00
1075	0.00E+00	0.00E+00	0.00E+00	0.00E+00	0.00E+00	0.00E+00	0.00E+00	0.00E+00	0.00E+00
1100	0.00E+00	0.00E+00	0.00E+00	0.00E+00	0.00E+00	0.00E+00	0.00E+00	0.00E+00	0.00E+00

T (K)	2-Propen-1-ol			2-Pentene Z			2,3-Dihydrofurane		
	Phi=0.5	Phi=1	Phi=2	Phi=0.5	Phi=1	Phi=2	Phi=0.5	Phi=1	Phi=2
725	0.00E+00	0.00E+00	0.00E+00	0.00E+00	0.00E+00	0.00E+00	0.00E+00	0.00E+00	0.00E+00
750	0.00E+00	0.00E+00	0.00E+00	0.00E+00	0.00E+00	0.00E+00	0.00E+00	0.00E+00	0.00E+00
775	0.00E+00	0.00E+00	0.00E+00	0.00E+00	0.00E+00	0.00E+00	0.00E+00	0.00E+00	0.00E+00
800	0.00E+00	0.00E+00	0.00E+00	0.00E+00	0.00E+00	0.00E+00	0.00E+00	0.00E+00	0.00E+00
825	0.00E+00	0.00E+00	0.00E+00	0.00E+00	0.00E+00	0.00E+00	0.00E+00	0.00E+00	0.00E+00
850	0.00E+00	1.85E-06	0.00E+00	1.96E-06	1.61E-06	1.20E-06	0.00E+00	0.00E+00	0.00E+00
875	2.17E-06	1.74E-06	2.30E-06	3.88E-06	2.60E-06	3.21E-06	1.34E-06	1.18E-06	0.00E+00
900	1.87E-06	3.04E-06	3.64E-06	3.03E-06	2.91E-06	4.43E-06	0.00E+00	0.00E+00	1.31E-06
925	1.73E-06	2.14E-06	4.44E-06	2.62E-06	2.75E-06	3.79E-06	0.00E+00	7.04E-07	1.12E-06
950	1.64E-06	3.27E-06	3.85E-06	1.73E-06	2.08E-06	2.31E-06	0.00E+00	0.00E+00	0.00E+00
975	0.00E+00	0.00E+00	0.00E+00	0.00E+00	1.84E-06	3.50E-06	0.00E+00	0.00E+00	0.00E+00
1000	0.00E+00	0.00E+00	2.25E-06	0.00E+00	0.00E+00	1.82E-06	0.00E+00	0.00E+00	1.02E-06
1025	0.00E+00	0.00E+00	2.62E-06	0.00E+00	0.00E+00	1.09E-06	0.00E+00	0.00E+00	0.00E+00
1050	0.00E+00	0.00E+00	0.00E+00	0.00E+00	0.00E+00	0.00E+00	0.00E+00	0.00E+00	0.00E+00
1075	0.00E+00	0.00E+00	0.00E+00	0.00E+00	0.00E+00	0.00E+00	0.00E+00	0.00E+00	0.00E+00
1100	0.00E+00	0.00E+00	0.00E+00	0.00E+00	0.00E+00	0.00E+00	0.00E+00	0.00E+00	0.00E+00

T (K)	Cyclopentene			Methyl vinyl ketone			Butanal		
	Phi=0.5	Phi=1	Phi=2	Phi=0.5	Phi=1	Phi=2	Phi=0.5	Phi=1	Phi=2
725	0.00E+00	0.00E+00	0.00E+00	0.00E+00	0.00E+00	0.00E+00	0.00E+00	2.34E-06	0.00E+00
750	0.00E+00	0.00E+00	0.00E+00	0.00E+00	0.00E+00	0.00E+00	0.00E+00	0.00E+00	0.00E+00
775	0.00E+00	0.00E+00	0.00E+00	0.00E+00	0.00E+00	0.00E+00	1.02E-05	6.75E-06	6.67E-06
800	0.00E+00	0.00E+00	0.00E+00	0.00E+00	0.00E+00	0.00E+00	1.97E-05	1.22E-05	1.12E-05
825	0.00E+00	0.00E+00	0.00E+00	0.00E+00	0.00E+00	0.00E+00	4.55E-05	4.09E-05	3.21E-05
850	0.00E+00	0.00E+00	0.00E+00	2.00E-06	2.35E-06	8.81E-07	6.89E-05	7.15E-05	6.63E-05
875	0.00E+00	1.12E-06	0.00E+00	3.86E-06	3.54E-06	2.50E-06	4.64E-05	5.77E-05	6.79E-05
900	0.00E+00	0.00E+00	7.94E-07	3.21E-06	3.99E-06	3.28E-06	3.78E-05	3.65E-05	6.37E-05
925	0.00E+00	0.00E+00	7.15E-07	2.49E-06	3.05E-06	3.31E-06	2.24E-05	2.62E-05	5.07E-05
950	0.00E+00	0.00E+00	0.00E+00	2.20E-06	1.55E-06	1.75E-06	2.14E-05	2.08E-05	2.77E-05
975	0.00E+00	0.00E+00	0.00E+00	0.00E+00	0.00E+00	3.30E-06	1.34E-05	1.47E-05	2.70E-05
1000	0.00E+00	0.00E+00	0.00E+00	0.00E+00	0.00E+00	2.52E-06	7.90E-06	1.18E-05	2.08E-05
1025	0.00E+00	0.00E+00	0.00E+00	0.00E+00	0.00E+00	0.00E+00	3.56E-06	7.73E-06	1.24E-05
1050	0.00E+00	0.00E+00	0.00E+00	0.00E+00	0.00E+00	0.00E+00	1.97E-06	3.60E-06	6.31E-06
1075	0.00E+00	0.00E+00	0.00E+00	0.00E+00	0.00E+00	0.00E+00	0.00E+00	0.00E+00	2.72E-06
1100	0.00E+00	0.00E+00	0.00E+00	0.00E+00	0.00E+00	0.00E+00	0.00E+00	0.00E+00	3.00E-06

T (K)	2-Butanone			1,2-Dihydrofurane			Benzene		
	Phi=0.5	Phi=1	Phi=2	Phi=0.5	Phi=1	Phi=2	Phi=0.5	Phi=1	Phi=2
725	0.00E+00	0.00E+00	0.00E+00	0.00E+00	0.00E+00	0.00E+00	0.00E+00	0.00E+00	0.00E+00
750	0.00E+00	0.00E+00	0.00E+00	0.00E+00	0.00E+00	0.00E+00	0.00E+00	0.00E+00	0.00E+00
775	0.00E+00	0.00E+00	0.00E+00	0.00E+00	0.00E+00	0.00E+00	0.00E+00	0.00E+00	0.00E+00
800	0.00E+00	0.00E+00	0.00E+00	0.00E+00	0.00E+00	0.00E+00	0.00E+00	0.00E+00	0.00E+00
825	0.00E+00	0.00E+00	0.00E+00	1.91E-06	4.28E-06	0.00E+00	0.00E+00	0.00E+00	0.00E+00
850	0.00E+00	2.64E-06	0.00E+00	5.20E-06	1.07E-05	4.01E-06	0.00E+00	0.00E+00	0.00E+00
875	4.62E-06	4.39E-06	2.21E-06	1.05E-05	1.22E-05	7.20E-06	0.00E+00	0.00E+00	0.00E+00
900	5.23E-06	3.31E-06	3.33E-06	9.95E-06	1.04E-05	8.11E-06	0.00E+00	0.00E+00	0.00E+00
925	3.06E-06	1.24E-06	2.83E-06	4.91E-06	7.64E-06	7.97E-06	6.12E-06	1.37E-06	9.96E-07
950	1.57E-06	1.63E-06	2.28E-06	4.93E-06	7.06E-06	3.95E-06	0.00E+00	0.00E+00	1.12E-06
975	0.00E+00	0.00E+00	1.57E-06	3.85E-06	3.43E-06	4.32E-06	0.00E+00	0.00E+00	2.53E-06
1000	0.00E+00	0.00E+00	1.16E-06	1.99E-06	3.77E-06	3.54E-06	0.00E+00	0.00E+00	1.76E-06
1025	0.00E+00	0.00E+00	0.00E+00	0.00E+00	1.32E-06	1.53E-06	0.00E+00	0.00E+00	1.19E-06
1050	0.00E+00	0.00E+00	0.00E+00	0.00E+00	0.00E+00	0.00E+00	0.00E+00	0.00E+00	0.00E+00
1075	0.00E+00	0.00E+00	0.00E+00	0.00E+00	0.00E+00	0.00E+00	0.00E+00	0.00E+00	0.00E+00
1100	0.00E+00	0.00E+00	0.00E+00	0.00E+00	0.00E+00	0.00E+00	0.00E+00	0.00E+00	0.00E+00

Experimental raw data: pentanoic acid oxidation

T (K)	Cyclohexadiene			Cyclopentenone			Pentanal		
	Phi=0.5	Phi=1	Phi=2	Phi=0.5	Phi=1	Phi=2	Phi=0.5	Phi=1	Phi=2
725	0.00E+00	0.00E+00	0.00E+00	0.00E+00	0.00E+00	0.00E+00	0.00E+00	0.00E+00	0.00E+00
750	0.00E+00	0.00E+00	0.00E+00	0.00E+00	0.00E+00	0.00E+00	0.00E+00	0.00E+00	0.00E+00
775	0.00E+00	0.00E+00	0.00E+00	0.00E+00	0.00E+00	0.00E+00	0.00E+00	0.00E+00	0.00E+00
800	0.00E+00	0.00E+00	0.00E+00	4.47E-06	0.00E+00	0.00E+00	0.00E+00	0.00E+00	0.00E+00
825	0.00E+00	0.00E+00	0.00E+00	0.00E+00	0.00E+00	0.00E+00	0.00E+00	0.00E+00	0.00E+00
850	0.00E+00	0.00E+00	0.00E+00	0.00E+00	0.00E+00	0.00E+00	2.80E-06	0.00E+00	0.00E+00
875	0.00E+00	0.00E+00	0.00E+00	0.00E+00	0.00E+00	0.00E+00	3.61E-06	4.60E-06	4.77E-06
900	0.00E+00	0.00E+00	0.00E+00	0.00E+00	0.00E+00	0.00E+00	3.46E-06	4.25E-06	5.83E-06
925	1.72E-06	0.00E+00	0.00E+00	0.00E+00	0.00E+00	0.00E+00	6.25E-06	3.31E-06	4.03E-06
950	0.00E+00	0.00E+00	0.00E+00	0.00E+00	0.00E+00	0.00E+00	0.00E+00	3.59E-06	5.20E-06
975	0.00E+00	0.00E+00	0.00E+00	0.00E+00	0.00E+00	0.00E+00	0.00E+00	0.00E+00	4.60E-06
1000	0.00E+00	0.00E+00	0.00E+00	0.00E+00	0.00E+00	0.00E+00	0.00E+00	0.00E+00	3.97E-06
1025	0.00E+00	0.00E+00	0.00E+00	0.00E+00	0.00E+00	0.00E+00	0.00E+00	0.00E+00	3.27E-06
1050	0.00E+00	0.00E+00	0.00E+00	0.00E+00	0.00E+00	0.00E+00	0.00E+00	0.00E+00	0.00E+00
1075	0.00E+00	0.00E+00	0.00E+00	0.00E+00	0.00E+00	0.00E+00	0.00E+00	0.00E+00	0.00E+00
1100	0.00E+00	0.00E+00	0.00E+00	0.00E+00	0.00E+00	0.00E+00	0.00E+00	0.00E+00	0.00E+00

T (K)	Pentanoic Acid		
	Phi=0.5	Phi=1	Phi=2
725	0.00E+00	9.29E-03	0.00E+00
750	0.00E+00	0.00E+00	0.00E+00
775	8.47E-03	4.11E-03	3.52E-02
800	1.37E-02	4.24E-03	3.83E-02
825	3.83E-03	3.08E-03	3.42E-02
850	2.35E-03	2.34E-03	2.89E-03
875	7.49E-04	1.43E-03	1.62E-03
900	4.35E-04	7.72E-04	7.01E-04
925	3.23E-04	4.01E-04	6.01E-04
950	1.65E-04	1.65E-04	4.16E-04
975	7.19E-05	0.00E+00	2.87E-04
1000	0.00E+00	0.00E+00	1.52E-04
1025	0.00E+00	0.00E+00	7.67E-05
1050	0.00E+00	0.00E+00	0.00E+00
1075	3.78E-05	0.00E+00	0.00E+00
1100	0.00E+00	0.00E+00	0.00E+00

II.8. Pyrolysis of pentanoic acid

Equivalence ratio	inf
$x_{pentanoic\ acid}$	0.002
Temperature (K)	650 - 1100
P (Torr)	800

Residence time	2 s
Units	Mole fraction
Bath gas	Helium

T (K)	O_2	CO	CH_4	CO_2	Acetylene	Ethylene
	Phi=inf	Phi=inf	Phi=inf	Phi=inf	Phi=inf	Phi=inf
650	0.00E+00	0.00E+00	0.00E+00	0.00E+00	0.00E+00	0.00E+00
675	0.00E+00	0.00E+00	0.00E+00	0.00E+00	0.00E+00	0.00E+00
700	0.00E+00	0.00E+00	0.00E+00	0.00E+00	0.00E+00	0.00E+00
725	0.00E+00	0.00E+00	0.00E+00	0.00E+00	0.00E+00	0.00E+00
750	0.00E+00	0.00E+00	0.00E+00	0.00E+00	0.00E+00	0.00E+00
775	0.00E+00	0.00E+00	0.00E+00	0.00E+00	0.00E+00	0.00E+00
800	0.00E+00	0.00E+00	0.00E+00	0.00E+00	0.00E+00	0.00E+00
825	0.00E+00	0.00E+00	0.00E+00	0.00E+00	0.00E+00	0.00E+00
850	0.00E+00	9.82E-06	3.92E-06	1.89E-05	0.00E+00	1.75E-05
875	1.22E-03	2.62E-05	1.21E-05	4.11E-05	4.54E-07	5.73E-05
900	5.25E-04	7.88E-05	3.57E-05	7.41E-05	4.43E-06	1.98E-04
925	2.36E-03	3.84E-04	7.90E-05	1.50E-04	2.28E-05	5.46E-04
950	6.62E-04	7.26E-04	1.27E-04	2.53E-04	5.74E-05	8.19E-04
975	2.69E-03	9.03E-04	1.87E-04	3.41E-04	1.40E-04	1.22E-03
1000	1.01E-03	1.39E-03	3.35E-04	4.54E-04	3.31E-04	1.85E-03
1025	1.05E-03	1.52E-03	3.45E-04	5.54E-04	3.94E-04	1.85E-03
1050	9.54E-04	1.43E-03	4.56E-04	6.29E-04	5.24E-04	2.01E-03
1075	6.38E-04	1.50E-03	4.97E-04	6.14E-04	6.90E-04	2.10E-03
1100	6.29E-04	1.62E-03	4.45E-04	6.03E-04	7.63E-04	2.13E-03
T (K)	Ethane	Propene	Propane	Formaldehyde	Oxirane	Acetaldehyde
	Phi=inf	Phi=inf	Phi=inf	Phi=inf	Phi=inf	Phi=inf
650	0.00E+00	0.00E+00	0.00E+00	0.00E+00	0.00E+00	0.00E+00
675	0.00E+00	0.00E+00	0.00E+00	0.00E+00	0.00E+00	0.00E+00
700	0.00E+00	0.00E+00	0.00E+00	0.00E+00	0.00E+00	0.00E+00
725	0.00E+00	0.00E+00	0.00E+00	0.00E+00	0.00E+00	0.00E+00
750	0.00E+00	0.00E+00	0.00E+00	0.00E+00	0.00E+00	0.00E+00
775	0.00E+00	0.00E+00	0.00E+00	0.00E+00	0.00E+00	0.00E+00
800	0.00E+00	0.00E+00	0.00E+00	0.00E+00	0.00E+00	0.00E+00
825	0.00E+00	0.00E+00	0.00E+00	0.00E+00	0.00E+00	0.00E+00
850	0.00E+00	7.84E-06	0.00E+00	0.00E+00	0.00E+00	0.00E+00
875	3.41E-06	2.07E-05	0.00E+00	0.00E+00	0.00E+00	0.00E+00
900	4.45E-06	4.95E-05	0.00E+00	0.00E+00	0.00E+00	0.00E+00
925	1.29E-05	9.49E-05	3.30E-06	0.00E+00	0.00E+00	6.25E-06
950	2.67E-05	1.39E-04	5.24E-06	5.40E-05	3.71E-06	3.85E-06
975	4.71E-05	1.64E-04	6.52E-06	0.00E+00	5.99E-06	8.58E-06
1000	7.63E-05	1.67E-04	8.39E-06	0.00E+00	6.98E-06	5.94E-06
1025	9.08E-05	1.39E-04	8.79E-06	1.15E-04	9.80E-06	8.15E-06
1050	8.86E-05	1.23E-04	5.86E-06	1.25E-04	1.05E-05	5.87E-06
1075	8.28E-05	8.47E-05	4.46E-06	0.00E+00	1.22E-05	5.55E-06
1100	7.68E-05	8.66E-05	4.35E-06	0.00E+00	1.78E-05	3.25E-06
T (K)	1-Butene	1,3-Butadiene	2-Butene E	2-Butene Z	Ethanol	Acrolein
	Phi=inf	Phi=inf	Phi=inf	Phi=inf	Phi=inf	Phi=inf
650	0.00E+00	0.00E+00	0.00E+00	0.00E+00	0.00E+00	0.00E+00
675	0.00E+00	0.00E+00	0.00E+00	0.00E+00	0.00E+00	0.00E+00
700	0.00E+00	0.00E+00	0.00E+00	0.00E+00	0.00E+00	0.00E+00
725	0.00E+00	0.00E+00	0.00E+00	0.00E+00	0.00E+00	0.00E+00
750	0.00E+00	0.00E+00	0.00E+00	0.00E+00	0.00E+00	0.00E+00
775	0.00E+00	0.00E+00	0.00E+00	0.00E+00	0.00E+00	0.00E+00
800	0.00E+00	0.00E+00	0.00E+00	0.00E+00	0.00E+00	0.00E+00
825	0.00E+00	0.00E+00	0.00E+00	0.00E+00	0.00E+00	0.00E+00
850	3.05E-06	1.42E-06	0.00E+00	0.00E+00	0.00E+00	0.00E+00
875	6.87E-06	4.49E-06	0.00E+00	0.00E+00	0.00E+00	1.96E-06
900	1.43E-05	1.36E-05	1.04E-06	0.00E+00	0.00E+00	6.66E-06
925	2.99E-05	5.20E-05	3.12E-06	2.28E-06	0.00E+00	1.80E-05
950	4.12E-05	8.18E-05	6.55E-06	3.43E-06	0.00E+00	2.48E-05
975	4.85E-05	1.16E-04	5.95E-06	3.16E-06	4.38E-06	1.99E-05
1000	5.08E-05	1.24E-04	6.62E-06	3.11E-06	3.15E-06	1.52E-05
1025	4.47E-05	1.05E-04	5.10E-06	3.30E-06	6.28E-06	1.09E-05
1050	3.44E-05	7.78E-05	5.18E-06	3.26E-06	4.39E-06	6.18E-06
1075	2.57E-05	5.32E-05	3.33E-06	2.30E-06	3.93E-06	3.42E-06
1100	2.66E-05	6.08E-05	3.24E-06	2.35E-06	2.67E-06	3.45E-06

T (K)	2,3-DMCP*	Ethyloxirane	2-Pentene E	2-Propen-1-ol	2-Pentene Z	2,3-Dihydrofuran
	Phi=inf	Phi=inf	Phi=inf	Phi=inf	Phi=inf	Phi=inf
650	0.00E+00	0.00E+00	0.00E+00	0.00E+00	0.00E+00	0.00E+00
675	0.00E+00	0.00E+00	0.00E+00	0.00E+00	0.00E+00	0.00E+00
700	0.00E+00	0.00E+00	0.00E+00	0.00E+00	0.00E+00	0.00E+00
725	0.00E+00	0.00E+00	0.00E+00	0.00E+00	0.00E+00	0.00E+00
750	0.00E+00	0.00E+00	0.00E+00	0.00E+00	0.00E+00	0.00E+00
775	0.00E+00	0.00E+00	0.00E+00	0.00E+00	0.00E+00	0.00E+00
800	0.00E+00	0.00E+00	0.00E+00	0.00E+00	0.00E+00	0.00E+00
825	0.00E+00	0.00E+00	0.00E+00	0.00E+00	0.00E+00	0.00E+00
850	0.00E+00	0.00E+00	0.00E+00	0.00E+00	0.00E+00	0.00E+00
875	0.00E+00	0.00E+00	0.00E+00	0.00E+00	0.00E+00	0.00E+00
900	0.00E+00	0.00E+00	0.00E+00	2.29E-06	1.83E-06	0.00E+00
925	3.09E-06	2.70E-06	0.00E+00	5.15E-06	2.60E-06	1.16E-06
950	4.83E-06	5.58E-06	0.00E+00	6.71E-06	4.09E-06	1.71E-06
975	4.20E-06	9.56E-06	0.00E+00	9.81E-06	3.89E-06	1.76E-06
1000	2.91E-06	1.15E-05	8.82E-07	4.79E-06	2.68E-06	0.00E+00
1025	2.23E-06	1.22E-05	7.17E-07	2.95E-06	1.62E-06	1.45E-06
1050	0.00E+00	1.31E-05	0.00E+00	0.00E+00	0.00E+00	0.00E+00
1075	0.00E+00	9.37E-06	0.00E+00	0.00E+00	0.00E+00	0.00E+00
1100	0.00E+00	1.46E-05	0.00E+00	0.00E+00	0.00E+00	0.00E+00

T (K)	Cyclopentene	Methyl vinyl ketone	Butanal	2-Butanone	Benzene	Cyclohexadiene
	Phi=inf	Phi=inf	Phi=inf	Phi=inf	Phi=inf	Phi=inf
650	0.00E+00	0.00E+00	0.00E+00	0.00E+00	0.00E+00	0.00E+00
675	0.00E+00	0.00E+00	0.00E+00	0.00E+00	0.00E+00	0.00E+00
700	0.00E+00	0.00E+00	0.00E+00	0.00E+00	0.00E+00	0.00E+00
725	0.00E+00	0.00E+00	0.00E+00	0.00E+00	0.00E+00	0.00E+00
750	0.00E+00	0.00E+00	0.00E+00	0.00E+00	0.00E+00	0.00E+00
775	0.00E+00	0.00E+00	6.17E-07	0.00E+00	0.00E+00	0.00E+00
800	0.00E+00	0.00E+00	6.79E-07	0.00E+00	0.00E+00	0.00E+00
825	0.00E+00	0.00E+00	3.09E-07	0.00E+00	0.00E+00	0.00E+00
850	0.00E+00	0.00E+00	1.01E-06	0.00E+00	0.00E+00	0.00E+00
875	0.00E+00	0.00E+00	1.75E-06	0.00E+00	0.00E+00	0.00E+00
900	0.00E+00	2.90E-06	2.83E-06	0.00E+00	0.00E+00	0.00E+00
925	0.00E+00	3.63E-06	6.76E-06	0.00E+00	1.10E-06	0.00E+00
950	0.00E+00	4.22E-06	7.56E-06	0.00E+00	7.15E-06	0.00E+00
975	1.34E-06	3.07E-06	6.30E-06	0.00E+00	1.76E-05	2.21E-06
1000	1.45E-06	3.62E-06	5.46E-06	0.00E+00	2.65E-05	2.18E-06
1025	1.59E-06	3.04E-06	3.03E-06	2.06E-06	3.98E-05	2.02E-06
1050	0.00E+00	0.00E+00	2.14E-06	0.00E+00	3.88E-05	0.00E+00
1075	0.00E+00	0.00E+00	7.30E-07	0.00E+00	4.38E-05	0.00E+00
1100	0.00E+00	0.00E+00	1.62E-06	0.00E+00	3.52E-05	0.00E+00

T (K)	Cyclopentanone	Cyclopentenone	Pentanal	Pentanoic Acid
	Phi=inf	Phi=inf	Phi=inf	Phi=inf
650	0.00E+00	0.00E+00	0.00E+00	2.07E-03
675	0.00E+00	0.00E+00	0.00E+00	0.00E+00
700	0.00E+00	0.00E+00	0.00E+00	0.00E+00
725	0.00E+00	0.00E+00	0.00E+00	2.05E-03
750	0.00E+00	0.00E+00	0.00E+00	1.99E-03
775	0.00E+00	0.00E+00	0.00E+00	2.28E-03
800	0.00E+00	0.00E+00	0.00E+00	1.89E-03
825	0.00E+00	0.00E+00	0.00E+00	1.82E-03
850	0.00E+00	0.00E+00	0.00E+00	2.14E-03
875	0.00E+00	0.00E+00	0.00E+00	1.55E-03
900	0.00E+00	0.00E+00	0.00E+00	1.41E-03
925	0.00E+00	0.00E+00	1.85E-05	1.35E-03
950	4.30E-06	0.00E+00	3.50E-05	9.67E-04
975	5.30E-06	6.21E-06	5.08E-05	7.00E-04
1000	0.00E+00	0.00E+00	4.42E-05	5.51E-04
1025	4.17E-06	7.21E-06	3.41E-05	4.37E-04
1050	5.14E-06	9.96E-06	2.54E-05	3.15E-04
1075	0.00E+00	7.93E-06	2.03E-05	2.22E-04
1100	0.00E+00	8.30E-06	1.63E-05	7.83E-05

*DMCP : dimethylcyclopropane

II.9. Combustion of furan

Equivalence ratio	0,5 ; 1 ; 2
x_{furan}	0.005
Temperature (K)	500 - 1100
P (Torr)	800

Units	Mole fraction
Bath gas	Helium
Residence time (s)	2

T (K)	O_2			CO			CH_4		
	Phi=0.5	Phi=1	Phi=2	Phi=0.5	Phi=1	Phi=2	Phi=0.5	Phi=1	Phi=2
500	2.40E+03	1.25E+03	6.31E+02	4.91E-06	3.28E-06	0.00E+00	0.00E+00	0.00E+00	0.00E+00
525	0.00E+00	1.26E+03	0.00E+00	0.00E+00	7.79E-06	0.00E+00	0.00E+00	0.00E+00	0.00E+00
550	2.41E+03	1.22E+03	6.34E+02	0.00E+00	6.95E-06	1.79E-05	0.00E+00	0.00E+00	4.00E-06
575	0.00E+00	1.27E+03	0.00E+00	0.00E+00	6.95E-06	1.79E-05	0.00E+00	0.00E+00	4.00E-06
600	2.41E+03	1.27E+03	6.39E+02	9.63E-06	2.97E-06	4.28E-06	0.00E+00	0.00E+00	0.00E+00
625	0.00E+00	1.26E+03	0.00E+00	0.00E+00	2.47E-06	4.28E-06	0.00E+00	0.00E+00	0.00E+00
650	2.37E+03	1.24E+03	6.36E+02	9.57E-06	7.79E-06	7.64E-06	0.00E+00	0.00E+00	0.00E+00
675	2.38E+03	1.26E+03	6.41E+02	2.81E-05	5.72E-06	3.74E-06	0.00E+00	0.00E+00	0.00E+00
700	2.36E+03	1.27E+03	6.36E+02	1.62E-05	3.84E-05	4.68E-06	0.00E+00	0.00E+00	0.00E+00
725	2.37E+03	1.24E+03	6.29E+02	2.21E-05	4.29E-06	5.33E-06	0.00E+00	0.00E+00	0.00E+00
750	2.35E+03	1.22E+03	6.35E+02	2.47E-05	6.13E-06	6.90E-06	0.00E+00	0.00E+00	0.00E+00
775	2.34E+03	1.19E+03	6.37E+02	3.05E-05	2.68E-05	8.13E-06	0.00E+00	0.00E+00	0.00E+00
800	2.36E+03	1.25E+03	6.32E+02	4.88E-05	2.91E-05	2.30E-05	0.00E+00	0.00E+00	2.47E-06
825	2.10E+03	1.25E+03	4.71E+02	6.33E-03	5.25E-03	4.67E-03	2.23E-04	2.35E-04	2.74E-04
850	1.93E+03	1.24E+03	3.60E+02	1.07E-02	1.09E-02	8.91E-03	4.01E-04	5.71E-04	6.53E-04
875	1.86E+03	7.91E+02	3.14E+02	1.22E-02	1.24E-02	1.05E-02	4.57E-04	6.97E-04	8.69E-04
900	1.77E+03	7.48E+02	2.86E+02	1.42E-02	1.27E-02	1.20E-02	4.85E-04	6.07E-04	1.10E-03
925	1.70E+03	6.70E+02	2.93E+02	1.24E-02	1.17E-02	7.08E-03	2.71E-04	4.02E-04	1.22E-03
950	1.83E+03	5.96E+02	2.76E+02	1.08E-02	1.27E-02	1.30E-02	1.27E-04	3.91E-04	1.38E-03
975	1.66E+03	3.83E+02	3.02E+02	7.01E-03	7.34E-03	1.22E-02	5.24E-05	4.25E-04	1.28E-03
1000	1.54E+03	2.89E+02	3.05E+02	4.18E-03	2.65E-03	1.25E-02	4.37E-05	1.96E-04	1.38E-03
1025	1.36E+03	2.87E+02	3.08E+02	2.22E-03	1.46E-03	1.27E-02	3.90E-05	1.26E-04	1.33E-03
1050	1.35E+03	1.91E+02	3.10E+02	1.30E-03	2.04E-03	1.30E-02	2.39E-05	2.23E-04	1.27E-03
1075	1.35E+03	2.22E+02	2.76E+02	8.63E-04	1.78E-03	1.23E-02	4.32E-06	1.31E-04	1.10E-03
1100	1.35E+03	1.85E+02	2.75E+02	2.43E-04	3.31E-04	1.20E-02	0.00E+00	0.00E+00	7.89E-04

T (K)	CO_2			Acetylene+Ethylene			Ethane		
	Phi=0.5	Phi=1	Phi=2	Phi=0.5	Phi=1	Phi=2	Phi=0.5	Phi=1	Phi=2
500	4.67E-06	6.76E-07	0.00E+00	0.00E+00	0.00E+00	0.00E+00	0.00E+00	0.00E+00	0.00E+00
525	0.00E+00	2.81E-06	0.00E+00	0.00E+00	0.00E+00	0.00E+00	0.00E+00	0.00E+00	0.00E+00
550	3.43E-06	2.60E-06	4.57E-06	0.00E+00	0.00E+00	1.71E-06	0.00E+00	0.00E+00	0.00E+00
575	0.00E+00	2.60E-06	4.57E-06	0.00E+00	0.00E+00	1.71E-06	0.00E+00	0.00E+00	0.00E+00
600	2.04E-06	0.00E+00	2.47E-06	0.00E+00	0.00E+00	0.00E+00	0.00E+00	0.00E+00	0.00E+00
625	0.00E+00	5.53E-06	2.47E-06	0.00E+00	0.00E+00	0.00E+00	0.00E+00	0.00E+00	0.00E+00
650	3.27E-06	2.03E-06	2.76E-06	0.00E+00	0.00E+00	0.00E+00	0.00E+00	0.00E+00	0.00E+00
675	4.32E-06	4.19E-06	3.39E-06	0.00E+00	0.00E+00	0.00E+00	0.00E+00	0.00E+00	0.00E+00
700	6.26E-06	2.39E-05	0.00E+00	0.00E+00	0.00E+00	0.00E+00	0.00E+00	0.00E+00	0.00E+00
725	4.92E-06	4.07E-06	5.07E-06	0.00E+00	0.00E+00	0.00E+00	0.00E+00	0.00E+00	0.00E+00
750	8.86E-06	5.80E-06	4.46E-06	0.00E+00	0.00E+00	0.00E+00	0.00E+00	0.00E+00	0.00E+00
775	1.19E-05	5.31E-06	5.86E-06	0.00E+00	0.00E+00	0.00E+00	0.00E+00	0.00E+00	0.00E+00
800	1.96E-05	4.40E-05	7.71E-06	1.46E-06	1.40E-06	2.01E-06	0.00E+00	0.00E+00	0.00E+00
825	7.67E-04	4.98E-04	3.51E-04	5.79E-05	6.97E-05	8.85E-05	2.67E-06	3.54E-06	6.86E-06
850	1.47E-03	1.12E-03	6.59E-04	1.10E-04	1.51E-04	1.91E-04	5.51E-06	1.21E-05	1.99E-05
875	1.95E-03	1.46E-03	8.16E-04	1.36E-04	1.92E-04	2.76E-04	7.70E-06	1.72E-05	4.28E-05
900	3.06E-03	2.39E-03	9.81E-04	1.42E-04	1.69E-04	4.01E-04	9.07E-06	1.80E-05	8.19E-05
925	4.60E-03	3.67E-03	1.13E-03	8.65E-05	1.27E-04	5.57E-04	5.59E-06	1.43E-05	1.14E-04
950	8.18E-03	4.43E-03	1.17E-03	5.16E-05	1.40E-04	6.64E-04	3.05E-06	1.95E-05	1.44E-04
975	1.18E-02	1.08E-02	1.15E-03	2.81E-05	2.11E-04	6.88E-04	1.06E-06	2.81E-05	1.39E-04
1000	1.45E-02	1.53E-02	1.19E-03	2.72E-05	1.46E-04	8.48E-04	1.05E-06	1.83E-05	1.66E-04
1025	1.71E-02	1.60E-02	1.30E-03	2.71E-05	1.20E-04	9.03E-04	1.37E-06	1.45E-05	1.70E-04
1050	1.80E-02	1.58E-02	1.41E-03	1.79E-05	2.08E-04	9.45E-04	1.16E-06	2.95E-05	1.68E-04
1075	1.81E-02	1.59E-02	1.48E-03	3.71E-06	1.53E-04	9.36E-04	0.00E+00	2.13E-05	1.72E-04
1100	1.91E-02	1.81E-02	1.80E-03	0.00E+00	0.00E+00	6.51E-04	0.00E+00	0.00E+00	1.12E-04

T (K)	Propene			Propane			Propyne		
	Phi=0.5	Phi=1	Phi=2	Phi=0.5	Phi=1	Phi=2	Phi=0.5	Phi=1	Phi=2
500	0.00E+00	0.00E+00	0.00E+00	0.00E+00	0.00E+00	0.00E+00	0.00E+00	0.00E+00	0.00E+00
525	0.00E+00	0.00E+00	0.00E+00	0.00E+00	0.00E+00	0.00E+00	0.00E+00	0.00E+00	0.00E+00
550	0.00E+00	0.00E+00	0.00E+00	0.00E+00	0.00E+00	0.00E+00	0.00E+00	0.00E+00	0.00E+00
575	0.00E+00	0.00E+00	0.00E+00	0.00E+00	0.00E+00	0.00E+00	0.00E+00	0.00E+00	0.00E+00
600	0.00E+00	0.00E+00	0.00E+00	0.00E+00	0.00E+00	0.00E+00	0.00E+00	0.00E+00	1.73E-05
625	0.00E+00	0.00E+00	0.00E+00	0.00E+00	0.00E+00	0.00E+00	0.00E+00	0.00E+00	1.73E-05
650	0.00E+00	0.00E+00	0.00E+00	0.00E+00	0.00E+00	0.00E+00	0.00E+00	0.00E+00	0.00E+00
675	0.00E+00	0.00E+00	0.00E+00	0.00E+00	0.00E+00	0.00E+00	0.00E+00	0.00E+00	0.00E+00
700	0.00E+00	0.00E+00	0.00E+00	0.00E+00	0.00E+00	0.00E+00	0.00E+00	0.00E+00	0.00E+00
725	0.00E+00	0.00E+00	0.00E+00	0.00E+00	0.00E+00	0.00E+00	0.00E+00	0.00E+00	0.00E+00
750	0.00E+00	0.00E+00	0.00E+00	0.00E+00	0.00E+00	0.00E+00	0.00E+00	0.00E+00	0.00E+00
775	0.00E+00	0.00E+00	0.00E+00	0.00E+00	0.00E+00	0.00E+00	0.00E+00	0.00E+00	0.00E+00
800	0.00E+00	0.00E+00	0.00E+00	0.00E+00	0.00E+00	0.00E+00	0.00E+00	0.00E+00	0.00E+00
825	6.40E-06	1.05E-05	1.21E-05	0.00E+00	0.00E+00	0.00E+00	1.70E-06	1.95E-06	1.19E-06
850	7.80E-06	1.41E-05	2.04E-05	0.00E+00	0.00E+00	1.95E-06	2.10E-06	1.62E-06	1.95E-06
875	5.03E-06	1.05E-05	2.00E-05	0.00E+00	1.82E-06	2.94E-06	1.46E-06	1.58E-06	1.81E-06
900	3.53E-06	5.38E-06	2.10E-05	0.00E+00	1.73E-06	4.70E-06	1.01E-06	1.08E-06	1.67E-06
925	1.76E-06	2.74E-06	1.67E-05	0.00E+00	1.28E-06	4.63E-06	9.66E-07	9.76E-07	2.14E-06
950	1.91E-06	2.79E-06	2.11E-05	0.00E+00	1.15E-06	5.37E-06	1.96E-06	1.43E-06	2.28E-06
975	9.54E-07	3.30E-06	1.59E-05	0.00E+00	1.58E-06	4.18E-06	1.86E-06	1.10E-06	2.24E-06
1000	0.00E+00	4.06E-06	1.77E-05	0.00E+00	0.00E+00	2.75E-06	0.00E+00	2.28E-06	4.14E-06
1025	0.00E+00	3.81E-06	1.60E-05	0.00E+00	0.00E+00	2.82E-06	0.00E+00	2.81E-06	4.58E-06
1050	0.00E+00	6.10E-06	1.59E-05	0.00E+00	0.00E+00	2.21E-06	0.00E+00	5.25E-06	6.90E-06
1075	0.00E+00	3.61E-06	1.85E-05	0.00E+00	0.00E+00	1.94E-06	2.81E-06	8.03E-06	1.42E-05
1100	0.00E+00	1.10E-07	1.14E-05	0.00E+00	7.67E-08	1.29E-06	0.00E+00	2.20E-06	1.39E-05

T (K)	Allene			Formaldehyde			Oxirane		
	Phi=0.5	Phi=1	Phi=2	Phi=0.5	Phi=1	Phi=2	Phi=0.5	Phi=1	Phi=2
500	0.00E+00	0.00E+00	0.00E+00	0.00E+00	0.00E+00	0.00E+00	0.00E+00	0.00E+00	0.00E+00
525	0.00E+00	0.00E+00	0.00E+00	0.00E+00	0.00E+00	0.00E+00	0.00E+00	0.00E+00	0.00E+00
550	0.00E+00	0.00E+00	0.00E+00	0.00E+00	0.00E+00	0.00E+00	0.00E+00	0.00E+00	0.00E+00
575	0.00E+00	0.00E+00	0.00E+00	0.00E+00	0.00E+00	0.00E+00	0.00E+00	0.00E+00	0.00E+00
600	0.00E+00	0.00E+00	0.00E+00	0.00E+00	0.00E+00	0.00E+00	0.00E+00	0.00E+00	0.00E+00
625	0.00E+00	0.00E+00	0.00E+00	0.00E+00	0.00E+00	0.00E+00	0.00E+00	0.00E+00	0.00E+00
650	0.00E+00	0.00E+00	0.00E+00	0.00E+00	0.00E+00	0.00E+00	0.00E+00	0.00E+00	0.00E+00
675	0.00E+00	0.00E+00	0.00E+00	0.00E+00	0.00E+00	0.00E+00	0.00E+00	0.00E+00	0.00E+00
700	0.00E+00	0.00E+00	0.00E+00	0.00E+00	0.00E+00	0.00E+00	0.00E+00	0.00E+00	0.00E+00
725	0.00E+00	0.00E+00	0.00E+00	0.00E+00	0.00E+00	0.00E+00	0.00E+00	0.00E+00	0.00E+00
750	0.00E+00	0.00E+00	0.00E+00	0.00E+00	0.00E+00	0.00E+00	0.00E+00	0.00E+00	0.00E+00
775	0.00E+00	0.00E+00	0.00E+00	0.00E+00	0.00E+00	0.00E+00	0.00E+00	0.00E+00	0.00E+00
800	0.00E+00	0.00E+00	0.00E+00	0.00E+00	0.00E+00	0.00E+00	0.00E+00	0.00E+00	0.00E+00
825	2.52E-06	4.21E-06	3.68E-06	2.75E-04	3.21E-04	2.44E-04	1.64E-06	1.64E-06	1.75E-06
850	3.95E-06	3.77E-06	5.78E-06	2.99E-04	3.00E-04	3.20E-04	3.55E-06	4.44E-06	3.66E-06
875	3.10E-06	4.53E-06	6.25E-06	2.17E-04	2.35E-04	2.79E-04	2.57E-06	4.07E-06	3.43E-06
900	2.47E-06	2.73E-06	7.43E-06	1.41E-04	1.52E-04	2.25E-04	2.28E-06	3.83E-06	3.02E-06
925	1.39E-06	2.26E-06	1.02E-05	0.00E+00	1.16E-04	1.83E-04	1.33E-06	1.56E-06	2.80E-06
950	2.31E-06	2.20E-06	1.22E-05	0.00E+00	5.09E-05	1.72E-04	1.33E-06	1.60E-06	2.03E-06
975	1.67E-06	3.96E-06	1.24E-05	6.66E-05	0.00E+00	1.99E-04	0.00E+00	0.00E+00	1.60E-06
1000	1.13E-06	1.19E-05	1.83E-05	0.00E+00	0.00E+00	1.45E-04	0.00E+00	0.00E+00	2.67E-07
1025	2.72E-06	1.70E-05	2.31E-05	0.00E+00	0.00E+00	1.45E-04	0.00E+00	0.00E+00	4.68E-07
1050	2.50E-06	3.14E-05	3.16E-05	0.00E+00	0.00E+00	0.00E+00	0.00E+00	0.00E+00	3.10E-07
1075	0.00E+00	4.07E-05	5.75E-05	0.00E+00	0.00E+00	1.01E-04	0.00E+00	0.00E+00	0.00E+00
1100	0.00E+00	3.83E-07	5.67E-05	0.00E+00	5.41E-07	0.00E+00	0.00E+00	2.51E-07	8.23E-07

Experimental raw data: furan oxidation

T (K)	Acetaldehyde			2-Butyne			Furan		
	Phi=0.5	Phi=1	Phi=2	Phi=0.5	Phi=1	Phi=2	Phi=0.5	Phi=1	Phi=2
500	0.00E+00	0.00E+00	0.00E+00	0.00E+00	0.00E+00	0.00E+00	5.18E-03	5.22E-03	4.73E-03
525	0.00E+00	0.00E+00	0.00E+00	0.00E+00	0.00E+00	0.00E+00	5.02E-03	4.77E-03	4.73E-03
550	0.00E+00	0.00E+00	0.00E+00	0.00E+00	0.00E+00	0.00E+00	4.86E-03	4.97E-03	4.96E-03
575	0.00E+00	0.00E+00	0.00E+00	0.00E+00	0.00E+00	0.00E+00	4.85E-03	4.97E-03	4.96E-03
600	0.00E+00	0.00E+00	0.00E+00	0.00E+00	0.00E+00	0.00E+00	4.84E-03	5.17E-03	5.11E-03
625	0.00E+00	0.00E+00	0.00E+00	0.00E+00	0.00E+00	0.00E+00	4.88E-03	5.01E-03	5.11E-03
650	0.00E+00	2.18E-06	0.00E+00	0.00E+00	0.00E+00	0.00E+00	4.93E-03	4.64E-03	5.02E-03
675	0.00E+00	0.00E+00	0.00E+00	0.00E+00	0.00E+00	0.00E+00	4.83E-03	5.03E-03	4.93E-03
700	0.00E+00	1.49E-05	0.00E+00	0.00E+00	0.00E+00	0.00E+00	4.95E-03	4.77E-03	4.80E-03
725	0.00E+00	1.05E-06	0.00E+00	0.00E+00	0.00E+00	0.00E+00	5.15E-03	5.22E-03	4.92E-03
750	1.12E-06	1.58E-05	0.00E+00	0.00E+00	0.00E+00	0.00E+00	5.06E-03	5.22E-03	5.03E-03
775	2.09E-06	2.15E-06	0.00E+00	0.00E+00	0.00E+00	0.00E+00	5.13E-03	5.02E-03	4.83E-03
800	3.38E-06	2.93E-06	1.45E-06	0.00E+00	0.00E+00	0.00E+00	4.17E-03	4.79E-03	5.27E-03
825	2.46E-04	2.72E-04	2.74E-04	1.42E-06	1.84E-06	3.00E-06	1.94E-03	2.27E-03	2.75E-03
850	2.12E-04	2.66E-04	3.06E-04	1.45E-06	2.20E-06	4.38E-06	9.34E-04	1.20E-03	1.69E-03
875	1.50E-04	2.04E-04	2.41E-04	1.17E-06	1.78E-06	3.37E-06	5.41E-04	7.65E-04	1.05E-03
900	1.09E-04	1.11E-04	2.01E-04	1.36E-06	1.13E-06	4.51E-06	3.45E-04	3.41E-04	6.93E-04
925	5.24E-05	6.84E-05	1.23E-04	0.00E+00	1.10E-06	5.99E-06	1.80E-04	1.97E-04	4.78E-04
950	3.38E-05	4.90E-05	1.38E-04	0.00E+00	1.22E-06	7.35E-06	1.26E-04	1.75E-04	5.55E-04
975	1.56E-05	4.20E-05	9.44E-05	0.00E+00	2.31E-06	8.38E-06	8.05E-05	1.25E-04	4.20E-04
1000	1.39E-05	2.69E-05	7.87E-05	0.00E+00	7.60E-06	1.28E-05	6.30E-05	4.36E-04	4.04E-04
1025	1.18E-05	1.46E-05	5.94E-05	0.00E+00	7.64E-06	1.49E-05	4.31E-05	3.54E-04	3.63E-04
1050	5.12E-06	2.09E-05	3.97E-05	1.51E-06	1.62E-05	1.75E-05	1.09E-05	3.58E-04	3.38E-04
1075	0.00E+00	1.21E-05	3.39E-05	0.00E+00	1.29E-05	2.82E-05	1.44E-06	3.42E-04	3.81E-04
1100	0.00E+00	2.91E-06	1.62E-05	0.00E+00	0.00E+00	1.84E-05	1.86E-06	7.94E-08	2.47E-04

T (K)	Acrolein			Propanal			Acetone		
	Phi=0.5	Phi=1	Phi=2	Phi=0.5	Phi=1	Phi=2	Phi=0.5	Phi=1	Phi=2
500	0.00E+00	0.00E+00	0.00E+00	0.00E+00	0.00E+00	0.00E+00	0.00E+00	0.00E+00	9.85E-07
525	0.00E+00	0.00E+00	0.00E+00	0.00E+00	0.00E+00	0.00E+00	0.00E+00	0.00E+00	9.85E-07
550	0.00E+00	0.00E+00	0.00E+00	0.00E+00	0.00E+00	0.00E+00	0.00E+00	0.00E+00	0.00E+00
575	0.00E+00	0.00E+00	0.00E+00	0.00E+00	0.00E+00	0.00E+00	0.00E+00	0.00E+00	0.00E+00
600	0.00E+00	0.00E+00	0.00E+00	0.00E+00	0.00E+00	0.00E+00	0.00E+00	0.00E+00	0.00E+00
625	0.00E+00	0.00E+00	0.00E+00	0.00E+00	0.00E+00	0.00E+00	0.00E+00	0.00E+00	0.00E+00
650	0.00E+00	0.00E+00	0.00E+00	0.00E+00	0.00E+00	0.00E+00	6.05E-07	2.31E-06	0.00E+00
675	0.00E+00	0.00E+00	0.00E+00	0.00E+00	0.00E+00	0.00E+00	0.00E+00	0.00E+00	0.00E+00
700	0.00E+00	0.00E+00	0.00E+00	0.00E+00	0.00E+00	0.00E+00	0.00E+00	0.00E+00	0.00E+00
725	0.00E+00	0.00E+00	0.00E+00	0.00E+00	0.00E+00	0.00E+00	0.00E+00	4.64E-07	0.00E+00
750	0.00E+00	0.00E+00	0.00E+00	0.00E+00	0.00E+00	0.00E+00	0.00E+00	0.00E+00	1.25E-06
775	0.00E+00	0.00E+00	0.00E+00	0.00E+00	0.00E+00	0.00E+00	0.00E+00	0.00E+00	8.58E-07
800	0.00E+00	0.00E+00	0.00E+00	0.00E+00	0.00E+00	0.00E+00	0.00E+00	1.55E-06	0.00E+00
825	4.11E-04	4.94E-04	2.58E-04	4.10E-06	3.05E-06	4.11E-06	0.00E+00	8.78E-07	8.91E-07
850	2.88E-04	1.70E-04	0.00E+00	2.31E-06	3.42E-06	4.62E-06	1.13E-06	1.20E-06	1.68E-06
875	1.62E-04	1.12E-04	0.00E+00	1.30E-06	2.01E-06	4.06E-06	1.25E-06	1.18E-06	1.73E-06
900	1.15E-04	6.23E-05	1.62E-04	1.03E-06	9.98E-07	3.77E-06	1.16E-06	7.98E-07	2.17E-06
925	4.86E-05	3.68E-05	3.40E-05	6.77E-07	6.03E-07	2.27E-06	9.11E-07	7.40E-07	2.22E-06
950	4.48E-05	1.63E-05	4.08E-05	9.53E-06	1.42E-06	2.47E-06	1.91E-06	9.23E-07	2.25E-06
975	1.40E-05	1.27E-05	2.47E-05	0.00E+00	6.65E-07	1.58E-06	0.00E+00	0.00E+00	1.46E-06
1000	1.49E-05	1.88E-05	2.01E-05	0.00E+00	0.00E+00	1.08E-06	0.00E+00	0.00E+00	1.19E-06
1025	9.19E-06	1.05E-05	1.60E-05	0.00E+00	0.00E+00	1.23E-06	0.00E+00	0.00E+00	1.41E-06
1050	5.61E-06	1.77E-05	9.61E-06	0.00E+00	0.00E+00	1.15E-06	0.00E+00	0.00E+00	0.00E+00
1075	0.00E+00	1.07E-05	1.00E-05	0.00E+00	0.00E+00	6.36E-07	0.00E+00	0.00E+00	0.00E+00
1100	0.00E+00	0.00E+00	4.11E-06	0.00E+00	0.00E+00	0.00E+00	0.00E+00	2.15E-07	0.00E+00

T (K)	Benzene		
	Phi=0.5	Phi=1	Phi=2
500	0.00E+00	0.00E+00	0.00E+00
525	0.00E+00	0.00E+00	0.00E+00
550	0.00E+00	0.00E+00	0.00E+00
575	0.00E+00	0.00E+00	0.00E+00
600	0.00E+00	0.00E+00	0.00E+00
625	0.00E+00	0.00E+00	0.00E+00
650	0.00E+00	0.00E+00	0.00E+00
675	0.00E+00	0.00E+00	0.00E+00
700	0.00E+00	0.00E+00	0.00E+00
725	0.00E+00	0.00E+00	0.00E+00
750	0.00E+00	0.00E+00	0.00E+00
775	0.00E+00	0.00E+00	0.00E+00
800	0.00E+00	0.00E+00	0.00E+00
825	0.00E+00	7.53E-06	0.00E+00
850	3.84E-06	0.00E+00	0.00E+00
875	2.07E-06	2.31E-06	0.00E+00
900	0.00E+00	0.00E+00	0.00E+00
925	0.00E+00	0.00E+00	0.00E+00
950	0.00E+00	0.00E+00	7.95E-07
975	0.00E+00	0.00E+00	7.72E-07
1000	0.00E+00	0.00E+00	0.00E+00
1025	0.00E+00	0.00E+00	0.00E+00
1050	0.00E+00	0.00E+00	0.00E+00
1075	0.00E+00	0.00E+00	0.00E+00
1100	0.00E+00	0.00E+00	0.00E+00

II.10. Combustion of benzaldehyde

Equivalence ratio	0,5 ; 1 ; 2
$x_{benzaldehyde}$	0.005
Temperature (K)	500 - 1100
P (Torr)	800

Units	Mole fraction
Bath gas	Helium
Residence time (s)	2

T (K)	O_2			CO			CH_4		
	Phi=0.5	Phi=1	Phi=2	Phi=0.5	Phi=1	Phi=2	Phi=0.5	Phi=1	Phi=2
500	8.16E-02	4.16E-02	0.00E+00	3.05E-05	8.43E-06	0.00E+00	0.00E+00	0.00E+00	0.00E+00
525	0.00E+00	4.09E-02	0.00E+00	3.43E-05	9.27E-06	0.00E+00	0.00E+00	0.00E+00	0.00E+00
550	7.99E-02	4.08E-02	0.00E+00	4.55E-05	2.26E-05	0.00E+00	0.00E+00	0.00E+00	0.00E+00
575	8.14E-02	4.28E-02	0.00E+00	3.81E-05	2.24E-05	0.00E+00	0.00E+00	0.00E+00	0.00E+00
600	8.44E-02	4.08E-02	0.00E+00	3.23E-05	1.26E-05	0.00E+00	0.00E+00	0.00E+00	0.00E+00
625	8.18E-02	4.16E-02	0.00E+00	2.54E-05	1.25E-05	0.00E+00	0.00E+00	2.73E-06	0.00E+00
650	8.11E-02	4.03E-02	0.00E+00	3.63E-05	1.91E-05	0.00E+00	0.00E+00	0.00E+00	0.00E+00
675	8.13E-02	4.14E-02	2.46E-02	2.89E-05	1.35E-05	0.00E+00	0.00E+00	0.00E+00	0.00E+00
700	7.92E-02	3.98E-02	2.03E-02	5.57E-05	4.33E-05	2.69E-05	0.00E+00	0.00E+00	0.00E+00
725	8.11E-02	4.14E-02	1.97E-02	9.79E-05	8.37E-05	1.10E-04	0.00E+00	0.00E+00	0.00E+00
750	8.22E-02	4.09E-02	1.97E-02	2.43E-04	3.20E-04	3.29E-04	2.51E-07	2.95E-07	7.11E-07
775	8.08E-02	4.06E-02	2.00E-02	6.92E-04	9.37E-04	1.09E-03	9.04E-07	1.93E-06	2.37E-06
800	7.95E-02	3.88E-02	2.03E-02	1.79E-03	2.14E-03	1.96E-03	4.20E-06	6.70E-06	7.69E-06
825	7.81E-02	3.80E-02	2.15E-02	3.57E-03	3.66E-03	3.02E-03	1.77E-05	1.60E-05	1.95E-05
850	7.24E-02	3.54E-02	2.10E-02	6.89E-03	6.80E-03	5.91E-03	4.16E-05	5.14E-05	5.67E-05
875	7.12E-02	3.30E-02	1.48E-02	9.51E-03	9.67E-03	7.51E-03	8.30E-05	9.83E-05	9.44E-05
900	6.59E-02	2.77E-02	1.25E-02	1.32E-02	1.36E-02	9.83E-03	1.41E-04	1.61E-04	1.40E-04
925	6.23E-02	2.68E-02	1.03E-02	1.81E-02	1.69E-02	1.23E-02	1.74E-04	2.18E-04	2.30E-04
950	5.67E-02	2.17E-02	1.07E-02	1.82E-02	1.76E-02	1.36E-02	1.44E-04	2.50E-04	3.21E-04
975	5.23E-02	2.12E-02	7.31E-03	1.38E-02	2.06E-02	1.54E-02	3.71E-05	2.66E-04	5.20E-04
1000	4.59E-02	1.30E-02	8.35E-03	8.01E-03	8.45E-03	1.67E-02	1.86E-05	1.09E-04	4.94E-04
1025	4.38E-02	1.08E-02	6.90E-03	3.80E-03	8.67E-03	1.54E-02	9.23E-06	9.47E-05	5.52E-04
1050	4.39E-02	5.19E-03	6.68E-03	2.16E-03	3.66E-03	1.78E-02	6.70E-06	3.07E-05	6.20E-04
1075	4.47E-02	4.38E-03	6.38E-03	1.31E-03	1.35E-03	1.91E-02	3.45E-06	7.73E-06	7.77E-04
1100	4.09E-02	4.56E-03	5.92E-03	1.54E-04	8.72E-04	1.99E-02	0.00E+00	3.14E-06	8.58E-04

T (K)	CO_2			Acetylene			Ethylene		
	Phi=0.5	Phi=1	Phi=2	Phi=0.5	Phi=1	Phi=2	Phi=0.5	Phi=1	Phi=2
500	2.70E-05	7.90E-06	0.00E+00	0.00E+00	0.00E+00	0.00E+00	0.00E+00	0.00E+00	0.00E+00
525	4.25E-05	4.02E-06	0.00E+00	0.00E+00	0.00E+00	0.00E+00	0.00E+00	0.00E+00	0.00E+00
550	4.15E-05	9.58E-06	0.00E+00	0.00E+00	0.00E+00	0.00E+00	0.00E+00	0.00E+00	0.00E+00
575	2.18E-05	7.91E-06	0.00E+00	0.00E+00	0.00E+00	0.00E+00	0.00E+00	0.00E+00	0.00E+00
600	2.44E-05	4.49E-06	0.00E+00	0.00E+00	0.00E+00	0.00E+00	0.00E+00	0.00E+00	0.00E+00
625	1.52E-05	6.43E-06	0.00E+00	0.00E+00	0.00E+00	0.00E+00	0.00E+00	2.40E-06	0.00E+00
650	3.30E-05	1.10E-05	0.00E+00	0.00E+00	0.00E+00	0.00E+00	0.00E+00	0.00E+00	0.00E+00
675	2.72E-05	1.17E-05	0.00E+00	0.00E+00	0.00E+00	0.00E+00	0.00E+00	0.00E+00	0.00E+00
700	5.49E-05	7.62E-05	1.64E-05	0.00E+00	0.00E+00	0.00E+00	0.00E+00	0.00E+00	0.00E+00
725	1.16E-04	4.14E-05	2.46E-05	0.00E+00	7.29E-07	0.00E+00	0.00E+00	0.00E+00	1.82E-06
750	1.58E-04	1.59E-04	7.52E-05	1.31E-06	1.77E-06	2.90E-06	3.22E-07	5.85E-07	1.41E-06
775	2.48E-04	2.17E-04	1.85E-04	5.18E-06	7.77E-06	0.00E+00	1.81E-06	3.74E-06	1.41E-05
800	5.50E-04	5.79E-04	3.43E-04	1.05E-05	1.37E-05	2.56E-06	8.58E-06	1.29E-05	1.38E-05
825	9.74E-04	7.64E-04	4.20E-04	2.70E-05	1.95E-05	0.00E+00	3.06E-05	2.85E-05	2.60E-05
850	2.75E-03	1.79E-03	7.99E-04	3.31E-05	4.89E-05	3.45E-05	5.91E-05	7.78E-05	5.87E-05
875	2.48E-03	1.98E-03	1.02E-03	5.27E-05	7.01E-05	4.38E-05	1.06E-04	1.30E-04	9.58E-05
900	4.48E-03	4.01E-03	1.44E-03	6.33E-05	8.63E-05	4.73E-05	1.58E-04	1.93E-04	1.31E-04
925	5.79E-03	4.48E-03	1.65E-03	6.73E-05	1.04E-04	1.04E-04	1.80E-04	2.42E-04	2.03E-04
950	8.20E-03	6.95E-03	2.42E-03	1.69E-05	8.03E-05	1.25E-04	1.27E-04	2.59E-04	2.57E-04
975	1.81E-02	7.60E-03	2.25E-03	7.46E-06	7.10E-05	1.99E-04	2.37E-05	2.49E-04	3.76E-04
1000	2.41E-02	2.20E-02	3.15E-03	5.29E-06	2.73E-05	1.81E-04	1.60E-05	1.24E-04	3.35E-04
1025	2.88E-02	2.22E-02	3.30E-03	4.62E-06	5.22E-05	1.72E-04	1.12E-05	1.07E-04	3.28E-04
1050	3.10E-02	2.98E-02	3.77E-03	3.41E-06	8.74E-06	1.84E-04	7.84E-06	3.66E-05	3.15E-04
1075	3.15E-02	3.16E-02	3.35E-03	1.29E-06	7.95E-06	2.15E-04	2.35E-06	1.17E-05	3.37E-04
1100	2.90E-02	3.12E-02	3.58E-03	0.00E+00	2.13E-06	2.44E-04	0.00E+00	2.91E-06	3.07E-04

Experimental raw data: benzaldehyde oxidation

T (K)	Ethane			Propene			Propyne		
	Phi=0.5	Phi=1	Phi=2	Phi=0.5	Phi=1	Phi=2	Phi=0.5	Phi=1	Phi=2
500	0.00E+00	0.00E+00	0.00E+00	0.00E+00	0.00E+00	0.00E+00	0.00E+00	0.00E+00	0.00E+00
525	0.00E+00	0.00E+00	0.00E+00	0.00E+00	0.00E+00	0.00E+00	0.00E+00	0.00E+00	0.00E+00
550	0.00E+00	0.00E+00	0.00E+00	0.00E+00	0.00E+00	0.00E+00	0.00E+00	0.00E+00	0.00E+00
575	0.00E+00	0.00E+00	0.00E+00	0.00E+00	0.00E+00	0.00E+00	0.00E+00	0.00E+00	0.00E+00
600	0.00E+00	0.00E+00	0.00E+00	0.00E+00	0.00E+00	0.00E+00	0.00E+00	0.00E+00	0.00E+00
625	0.00E+00	1.02E-06	0.00E+00	0.00E+00	0.00E+00	0.00E+00	0.00E+00	0.00E+00	0.00E+00
650	0.00E+00	0.00E+00	0.00E+00	0.00E+00	0.00E+00	0.00E+00	0.00E+00	0.00E+00	0.00E+00
675	0.00E+00	0.00E+00	0.00E+00	0.00E+00	0.00E+00	0.00E+00	0.00E+00	0.00E+00	0.00E+00
700	0.00E+00	0.00E+00	0.00E+00	0.00E+00	0.00E+00	0.00E+00	0.00E+00	0.00E+00	0.00E+00
725	0.00E+00	0.00E+00	0.00E+00	0.00E+00	0.00E+00	0.00E+00	0.00E+00	0.00E+00	0.00E+00
750	0.00E+00	0.00E+00	0.00E+00	0.00E+00	0.00E+00	0.00E+00	0.00E+00	0.00E+00	1.50E-06
775	0.00E+00	0.00E+00	0.00E+00	0.00E+00	0.00E+00	0.00E+00	2.18E-06	1.97E-06	2.64E-06
800	0.00E+00	0.00E+00	0.00E+00	0.00E+00	0.00E+00	0.00E+00	3.98E-06	3.68E-06	4.39E-06
825	0.00E+00	0.00E+00	0.00E+00	1.82E-06	1.13E-06	3.54E-06	6.79E-06	5.88E-06	5.36E-06
850	6.56E-07	9.09E-07	9.82E-07	3.09E-06	5.31E-06	5.80E-06	9.42E-06	8.13E-06	5.59E-06
875	1.61E-06	2.37E-06	2.09E-06	4.52E-06	8.15E-06	7.46E-06	6.33E-06	8.11E-06	7.35E-06
900	3.45E-06	5.27E-06	4.20E-06	9.40E-06	1.10E-05	1.21E-05	8.86E-06	6.96E-06	8.85E-06
925	4.96E-06	8.53E-06	9.22E-06	6.08E-06	1.10E-05	1.37E-05	6.55E-06	7.32E-06	7.36E-06
950	4.03E-06	1.07E-05	1.59E-05	6.29E-06	9.05E-06	1.42E-05	0.00E+00	4.64E-06	6.99E-06
975	6.74E-07	1.18E-05	2.28E-05	0.00E+00	9.91E-06	1.63E-05	0.00E+00	3.92E-06	6.36E-06
1000	8.81E-07	7.96E-06	2.45E-05	0.00E+00	6.34E-06	1.39E-05	0.00E+00	4.43E-06	6.62E-06
1025	3.09E-07	8.32E-06	2.59E-05	0.00E+00	4.73E-06	1.31E-05	0.00E+00	2.11E-06	4.91E-06
1050	3.73E-07	3.54E-06	2.70E-05	0.00E+00	2.59E-06	1.14E-05	0.00E+00	2.22E-06	4.46E-06
1075	0.00E+00	9.30E-07	2.77E-05	0.00E+00	0.00E+00	9.64E-06	0.00E+00	0.00E+00	4.30E-06
1100	0.00E+00	0.00E+00	2.67E-05	0.00E+00	0.00E+00	8.00E-06	0.00E+00	0.00E+00	4.09E-06

T (K)	Allene			Acetaldehyde			Butenyne		
	Phi=0.5	Phi=1	Phi=2	Phi=0.5	Phi=1	Phi=2	Phi=0.5	Phi=1	Phi=2
500	0.00E+00	0.00E+00	0.00E+00	0.00E+00	0.00E+00	0.00E+00	0.00E+00	0.00E+00	0.00E+00
525	0.00E+00	0.00E+00	0.00E+00	0.00E+00	0.00E+00	0.00E+00	0.00E+00	0.00E+00	0.00E+00
550	0.00E+00	0.00E+00	0.00E+00	0.00E+00	0.00E+00	0.00E+00	0.00E+00	0.00E+00	0.00E+00
575	0.00E+00	0.00E+00	0.00E+00	0.00E+00	0.00E+00	0.00E+00	0.00E+00	0.00E+00	0.00E+00
600	0.00E+00	0.00E+00	0.00E+00	0.00E+00	0.00E+00	0.00E+00	0.00E+00	0.00E+00	0.00E+00
625	0.00E+00	0.00E+00	0.00E+00	0.00E+00	0.00E+00	0.00E+00	0.00E+00	0.00E+00	0.00E+00
650	0.00E+00	0.00E+00	0.00E+00	0.00E+00	0.00E+00	0.00E+00	0.00E+00	0.00E+00	0.00E+00
675	0.00E+00	0.00E+00	0.00E+00	0.00E+00	0.00E+00	0.00E+00	0.00E+00	0.00E+00	0.00E+00
700	0.00E+00	0.00E+00	0.00E+00	0.00E+00	0.00E+00	0.00E+00	0.00E+00	0.00E+00	0.00E+00
725	0.00E+00	0.00E+00	0.00E+00	0.00E+00	0.00E+00	4.94E-06	0.00E+00	0.00E+00	0.00E+00
750	0.00E+00	0.00E+00	2.66E-06	6.59E-06	6.69E-06	6.57E-06	0.00E+00	0.00E+00	0.00E+00
775	3.29E-06	3.88E-06	3.24E-06	1.15E-05	2.47E-05	2.01E-05	0.00E+00	0.00E+00	1.12E-06
800	3.78E-06	6.97E-06	7.80E-06	2.76E-05	3.91E-05	3.61E-05	9.88E-07	1.94E-06	1.75E-06
825	1.14E-05	1.15E-05	9.25E-06	6.03E-05	6.43E-05	5.62E-05	2.16E-06	2.47E-06	2.44E-06
850	1.76E-05	1.99E-05	1.65E-05	9.79E-05	9.90E-05	9.09E-05	3.92E-06	5.05E-06	4.70E-06
875	1.65E-05	2.07E-05	1.96E-05	1.14E-04	1.17E-04	9.80E-05	4.38E-06	5.89E-06	7.69E-06
900	1.55E-05	1.73E-05	2.04E-05	1.03E-04	9.78E-05	9.21E-05	4.27E-06	5.83E-06	8.86E-06
925	1.52E-05	1.74E-05	1.92E-05	8.62E-05	9.18E-05	8.06E-05	3.64E-06	6.61E-06	1.15E-05
950	2.36E-06	9.30E-06	1.54E-05	0.00E+00	5.17E-05	6.03E-05	2.99E-06	4.65E-06	1.35E-05
975	0.00E+00	1.01E-05	1.57E-05	1.15E-05	4.15E-05	4.90E-05	0.00E+00	4.59E-06	1.51E-05
1000	0.00E+00	4.12E-06	1.40E-05	0.00E+00	1.85E-05	3.33E-05	0.00E+00	3.57E-06	1.76E-05
1025	0.00E+00	2.99E-06	1.10E-05	0.00E+00	9.94E-06	1.93E-05	0.00E+00	3.69E-06	1.61E-05
1050	0.00E+00	2.54E-06	9.55E-06	0.00E+00	4.38E-06	1.14E-05	0.00E+00	2.44E-06	1.76E-05
1075	0.00E+00	0.00E+00	9.18E-06	0.00E+00	0.00E+00	1.03E-05	0.00E+00	2.08E-06	1.80E-05
1100	0.00E+00	0.00E+00	8.10E-06	0.00E+00	0.00E+00	5.73E-06	0.00E+00	0.00E+00	2.12E-05

Experimental raw data: benzaldehyde oxidation

T (K)	Butadiene 1.3			Butadiene 1.2			Acrolein		
	Phi=0.5	Phi=1	Phi=2	Phi=0.5	Phi=1	Phi=2	Phi=0.5	Phi=1	Phi=2
500	0.00E+00	0.00E+00	0.00E+00	0.00E+00	0.00E+00	0.00E+00	0.00E+00	0.00E+00	0.00E+00
525	0.00E+00	0.00E+00	0.00E+00	0.00E+00	0.00E+00	0.00E+00	0.00E+00	0.00E+00	0.00E+00
550	0.00E+00	0.00E+00	0.00E+00	0.00E+00	0.00E+00	0.00E+00	0.00E+00	0.00E+00	0.00E+00
575	0.00E+00	0.00E+00	0.00E+00	0.00E+00	0.00E+00	0.00E+00	0.00E+00	0.00E+00	0.00E+00
600	0.00E+00	0.00E+00	0.00E+00	0.00E+00	0.00E+00	0.00E+00	0.00E+00	0.00E+00	0.00E+00
625	0.00E+00	0.00E+00	0.00E+00	0.00E+00	0.00E+00	0.00E+00	0.00E+00	0.00E+00	0.00E+00
650	0.00E+00	0.00E+00	0.00E+00	0.00E+00	0.00E+00	0.00E+00	0.00E+00	0.00E+00	0.00E+00
675	0.00E+00	0.00E+00	0.00E+00	0.00E+00	0.00E+00	0.00E+00	0.00E+00	0.00E+00	0.00E+00
700	0.00E+00	0.00E+00	0.00E+00	0.00E+00	0.00E+00	0.00E+00	0.00E+00	0.00E+00	0.00E+00
725	0.00E+00	0.00E+00	0.00E+00	0.00E+00	0.00E+00	0.00E+00	2.44E-06	2.39E-06	5.87E-06
750	0.00E+00	0.00E+00	0.00E+00	0.00E+00	0.00E+00	0.00E+00	7.17E-06	1.40E-05	1.57E-05
775	0.00E+00	0.00E+00	1.03E-06	0.00E+00	0.00E+00	0.00E+00	2.46E-05	3.85E-05	5.57E-05
800	0.00E+00	7.52E-07	1.38E-06	0.00E+00	0.00E+00	0.00E+00	6.59E-05	7.83E-05	9.15E-05
825	1.01E-06	1.17E-06	1.29E-06	0.00E+00	0.00E+00	0.00E+00	1.10E-04	1.08E-04	1.18E-04
850	1.84E-06	2.11E-06	3.90E-06	0.00E+00	6.43E-07	6.75E-07	1.43E-04	1.45E-04	1.63E-04
875	1.83E-06	2.83E-06	5.54E-06	0.00E+00	8.82E-07	1.14E-06	1.23E-04	1.40E-04	1.67E-04
900	2.68E-06	3.96E-06	5.83E-06	1.09E-06	9.18E-07	2.87E-06	9.41E-05	9.52E-05	1.59E-04
925	2.68E-06	4.19E-06	8.16E-06	1.20E-06	1.23E-06	1.67E-06	7.15E-05	7.94E-05	1.20E-04
950	2.45E-06	3.73E-06	9.57E-06	0.00E+00	1.21E-06	2.29E-06	3.52E-05	4.51E-05	8.08E-05
975	0.00E+00	4.04E-06	1.11E-05	0.00E+00	0.00E+00	2.95E-06	1.08E-05	3.18E-05	6.12E-05
1000	0.00E+00	3.56E-06	1.44E-05	0.00E+00	0.00E+00	2.68E-06	6.80E-06	1.40E-05	3.96E-05
1025	0.00E+00	2.97E-06	1.30E-05	0.00E+00	0.00E+00	2.07E-06	0.00E+00	8.08E-06	1.98E-05
1050	0.00E+00	2.21E-06	1.41E-05	0.00E+00	0.00E+00	0.00E+00	2.49E-06	3.81E-06	1.43E-05
1075	0.00E+00	1.73E-06	1.48E-05	0.00E+00	0.00E+00	2.29E-06	0.00E+00	0.00E+00	6.67E-06
1100	0.00E+00	0.00E+00	1.35E-05	0.00E+00	0.00E+00	0.00E+00	0.00E+00	0.00E+00	0.00E+00

T (K)	Acetone			Cyclopentadiene			Benzene		
	Phi=0.5	Phi=1	Phi=2	Phi=0.5	Phi=1	Phi=2	Phi=0.5	Phi=1	Phi=2
500	9.73E-06	3.66E-05	0.00E+00	0.00E+00	0.00E+00	0.00E+00	0.00E+00	0.00E+00	0.00E+00
525	4.40E-06	1.17E-05	0.00E+00	0.00E+00	0.00E+00	0.00E+00	0.00E+00	0.00E+00	0.00E+00
550	5.41E-06	1.82E-05	0.00E+00	0.00E+00	0.00E+00	0.00E+00	0.00E+00	0.00E+00	0.00E+00
575	4.79E-06	4.73E-06	0.00E+00	0.00E+00	0.00E+00	0.00E+00	0.00E+00	0.00E+00	0.00E+00
600	4.31E-06	3.44E-05	0.00E+00	0.00E+00	0.00E+00	0.00E+00	0.00E+00	0.00E+00	0.00E+00
625	8.57E-06	1.33E-05	0.00E+00	0.00E+00	0.00E+00	0.00E+00	0.00E+00	0.00E+00	0.00E+00
650	1.21E-05	1.50E-05	0.00E+00	0.00E+00	0.00E+00	0.00E+00	0.00E+00	0.00E+00	0.00E+00
675	5.46E-06	2.03E-05	0.00E+00	0.00E+00	0.00E+00	0.00E+00	0.00E+00	0.00E+00	0.00E+00
700	7.48E-06	3.75E-05	0.00E+00	0.00E+00	0.00E+00	0.00E+00	3.96E-07	0.00E+00	5.23E-07
725	7.35E-06	9.73E-06	9.71E-06	0.00E+00	0.00E+00	0.00E+00	4.07E-07	5.76E-07	1.28E-06
750	1.48E-05	2.59E-05	1.20E-05	0.00E+00	0.00E+00	0.00E+00	1.25E-06	1.77E-06	3.83E-06
775	1.12E-05	1.82E-05	2.29E-05	0.00E+00	0.00E+00	0.00E+00	3.86E-06	6.04E-06	1.15E-05
800	2.07E-05	6.62E-05	2.11E-05	0.00E+00	0.00E+00	0.00E+00	1.12E-05	1.46E-05	2.90E-05
825	2.60E-05	2.49E-05	2.36E-05	0.00E+00	1.16E-06	0.00E+00	2.42E-05	2.62E-05	4.62E-05
850	3.47E-05	5.19E-05	1.95E-05	1.72E-06	2.15E-06	2.59E-06	4.21E-05	4.63E-05	6.99E-05
875	1.87E-05	2.82E-05	2.07E-05	1.62E-06	2.93E-06	4.16E-06	5.80E-05	7.33E-05	9.51E-05
900	1.93E-05	2.67E-05	1.12E-05	2.13E-06	3.18E-06	3.58E-06	7.43E-05	8.94E-05	1.36E-04
925	1.07E-05	1.07E-05	1.85E-05	2.05E-06	3.03E-06	6.50E-06	7.94E-05	1.04E-04	1.83E-04
950	6.88E-06	1.19E-05	6.45E-06	0.00E+00	2.50E-06	6.36E-06	6.10E-05	9.73E-05	2.35E-04
975	1.06E-06	3.56E-06	7.07E-06	0.00E+00	4.57E-06	1.00E-05	1.15E-05	9.60E-05	2.51E-04
1000	0.00E+00	2.46E-06	3.30E-06	0.00E+00	3.31E-06	1.45E-05	7.87E-06	6.07E-05	3.12E-04
1025	3.93E-06	1.78E-06	2.69E-06	0.00E+00	2.94E-06	1.60E-05	5.97E-06	3.26E-05	3.31E-04
1050	0.00E+00	0.00E+00	0.00E+00	0.00E+00	2.10E-06	2.16E-05	4.64E-06	1.48E-05	3.96E-04
1075	0.00E+00	0.00E+00	1.23E-06	0.00E+00	1.54E-06	2.45E-05	1.46E-06	4.92E-06	4.06E-04
1100	0.00E+00	0.00E+00	6.48E-06	0.00E+00	0.00E+00	3.09E-05	0.00E+00	1.44E-06	3.60E-04

Experimental raw data: benzaldehyde oxidation

T (K)	Toluene			Cyclopentenone			Ethylbenzene		
	Phi=0.5	Phi=1	Phi=2	Phi=0.5	Phi=1	Phi=2	Phi=0.5	Phi=1	Phi=2
500	0.00E+00	0.00E+00	0.00E+00	0.00E+00	0.00E+00	0.00E+00	0.00E+00	0.00E+00	0.00E+00
525	0.00E+00	0.00E+00	0.00E+00	0.00E+00	0.00E+00	0.00E+00	0.00E+00	0.00E+00	0.00E+00
550	0.00E+00	0.00E+00	0.00E+00	0.00E+00	0.00E+00	0.00E+00	0.00E+00	0.00E+00	0.00E+00
575	0.00E+00	0.00E+00	0.00E+00	0.00E+00	0.00E+00	0.00E+00	0.00E+00	0.00E+00	0.00E+00
600	0.00E+00	0.00E+00	0.00E+00	0.00E+00	0.00E+00	0.00E+00	0.00E+00	0.00E+00	0.00E+00
625	0.00E+00	0.00E+00	0.00E+00	0.00E+00	0.00E+00	0.00E+00	0.00E+00	0.00E+00	0.00E+00
650	0.00E+00	0.00E+00	0.00E+00	0.00E+00	0.00E+00	0.00E+00	0.00E+00	0.00E+00	0.00E+00
675	0.00E+00	0.00E+00	0.00E+00	0.00E+00	0.00E+00	0.00E+00	0.00E+00	0.00E+00	0.00E+00
700	0.00E+00	0.00E+00	0.00E+00	0.00E+00	0.00E+00	0.00E+00	0.00E+00	0.00E+00	0.00E+00
725	0.00E+00	0.00E+00	0.00E+00	0.00E+00	0.00E+00	0.00E+00	0.00E+00	0.00E+00	0.00E+00
750	0.00E+00	0.00E+00	0.00E+00	0.00E+00	0.00E+00	0.00E+00	0.00E+00	0.00E+00	0.00E+00
775	0.00E+00	0.00E+00	0.00E+00	0.00E+00	0.00E+00	0.00E+00	0.00E+00	0.00E+00	2.36E-06
800	0.00E+00	0.00E+00	3.78E-07	0.00E+00	0.00E+00	0.00E+00	0.00E+00	0.00E+00	0.00E+00
825	6.19E-07	4.86E-07	0.00E+00	0.00E+00	0.00E+00	0.00E+00	0.00E+00	0.00E+00	0.00E+00
850	9.49E-07	8.65E-07	1.57E-06	0.00E+00	0.00E+00	0.00E+00	0.00E+00	0.00E+00	0.00E+00
875	1.79E-06	1.74E-06	2.14E-06	0.00E+00	0.00E+00	0.00E+00	5.64E-06	0.00E+00	0.00E+00
900	1.66E-06	1.69E-06	4.42E-06	0.00E+00	0.00E+00	0.00E+00	3.56E-06	0.00E+00	0.00E+00
925	1.05E-06	1.57E-06	4.71E-06	0.00E+00	0.00E+00	1.11E-05	0.00E+00	0.00E+00	0.00E+00
950	4.93E-07	1.78E-06	6.01E-06	0.00E+00	0.00E+00	0.00E+00	0.00E+00	0.00E+00	0.00E+00
975	0.00E+00	1.26E-06	7.09E-06	0.00E+00	0.00E+00	9.83E-06	0.00E+00	0.00E+00	3.32E-06
1000	0.00E+00	1.33E-06	8.98E-06	0.00E+00	0.00E+00	0.00E+00	0.00E+00	0.00E+00	2.39E-06
1025	0.00E+00	6.22E-07	8.57E-06	0.00E+00	0.00E+00	0.00E+00	0.00E+00	0.00E+00	0.00E+00
1050	0.00E+00	5.48E-07	9.67E-06	0.00E+00	0.00E+00	0.00E+00	0.00E+00	0.00E+00	0.00E+00
1075	0.00E+00	0.00E+00	1.03E-05	0.00E+00	0.00E+00	0.00E+00	0.00E+00	0.00E+00	0.00E+00
1100	0.00E+00	0.00E+00	9.28E-06	0.00E+00	0.00E+00	0.00E+00	0.00E+00	0.00E+00	0.00E+00

T (K)	Xylene			Phenylacetylene			Styrene		
	Phi=0.5	Phi=1	Phi=2	Phi=0.5	Phi=1	Phi=2	Phi=0.5	Phi=1	Phi=2
500	0.00E+00	0.00E+00	0.00E+00	0.00E+00	0.00E+00	0.00E+00	0.00E+00	0.00E+00	0.00E+00
525	0.00E+00	0.00E+00	0.00E+00	0.00E+00	0.00E+00	0.00E+00	0.00E+00	0.00E+00	0.00E+00
550	0.00E+00	0.00E+00	0.00E+00	0.00E+00	0.00E+00	0.00E+00	0.00E+00	0.00E+00	0.00E+00
575	0.00E+00	0.00E+00	0.00E+00	0.00E+00	0.00E+00	0.00E+00	0.00E+00	0.00E+00	0.00E+00
600	0.00E+00	0.00E+00	0.00E+00	0.00E+00	0.00E+00	0.00E+00	0.00E+00	0.00E+00	0.00E+00
625	0.00E+00	0.00E+00	0.00E+00	0.00E+00	0.00E+00	0.00E+00	0.00E+00	0.00E+00	0.00E+00
650	0.00E+00	0.00E+00	0.00E+00	0.00E+00	0.00E+00	0.00E+00	0.00E+00	0.00E+00	0.00E+00
675	0.00E+00	0.00E+00	0.00E+00	0.00E+00	0.00E+00	0.00E+00	0.00E+00	0.00E+00	0.00E+00
700	0.00E+00	0.00E+00	0.00E+00	0.00E+00	0.00E+00	0.00E+00	0.00E+00	0.00E+00	0.00E+00
725	0.00E+00	0.00E+00	0.00E+00	0.00E+00	0.00E+00	0.00E+00	0.00E+00	0.00E+00	0.00E+00
750	0.00E+00	0.00E+00	0.00E+00	0.00E+00	0.00E+00	9.68E-07	0.00E+00	0.00E+00	0.00E+00
775	0.00E+00	0.00E+00	0.00E+00	0.00E+00	0.00E+00	2.38E-06	0.00E+00	0.00E+00	4.41E-07
800	0.00E+00	0.00E+00	0.00E+00	0.00E+00	0.00E+00	0.00E+00	3.72E-07	6.36E-07	1.05E-06
825	0.00E+00	1.68E-06	0.00E+00	0.00E+00	1.00E-06	0.00E+00	1.27E-06	8.48E-07	3.91E-06
850	0.00E+00	0.00E+00	0.00E+00	0.00E+00	0.00E+00	0.00E+00	1.13E-06	1.69E-06	0.00E+00
875	0.00E+00	0.00E+00	0.00E+00	2.30E-06	0.00E+00	0.00E+00	1.78E-06	1.64E-06	3.25E-06
900	0.00E+00	0.00E+00	0.00E+00	0.00E+00	0.00E+00	0.00E+00	1.65E-06	1.50E-06	5.26E-06
925	0.00E+00	0.00E+00	5.53E-07	0.00E+00	0.00E+00	0.00E+00	8.87E-07	1.45E-06	6.10E-06
950	0.00E+00	0.00E+00	1.30E-06	0.00E+00	0.00E+00	1.17E-06	2.65E-07	5.19E-07	6.73E-06
975	0.00E+00	0.00E+00	9.29E-07	0.00E+00	0.00E+00	8.85E-07	0.00E+00	5.30E-07	7.66E-06
1000	0.00E+00	0.00E+00	2.03E-06	0.00E+00	0.00E+00	8.85E-07	0.00E+00	3.99E-07	9.54E-06
1025	0.00E+00	0.00E+00	1.44E-06	0.00E+00	0.00E+00	9.20E-07	0.00E+00	5.79E-07	8.60E-06
1050	0.00E+00	0.00E+00	1.83E-06	0.00E+00	0.00E+00	1.70E-06	0.00E+00	5.83E-07	1.10E-05
1075	0.00E+00	0.00E+00	2.11E-06	0.00E+00	0.00E+00	3.29E-06	0.00E+00	0.00E+00	1.36E-05
1100	0.00E+00	0.00E+00	1.17E-06	0.00E+00	0.00E+00	3.80E-06	0.00E+00	0.00E+00	1.03E-05

Experimental raw data: benzaldehyde oxidation

T (K)	Anisole			Benzoquinone			Cumene		
	Phi=0.5	Phi=1	Phi=2	Phi=0.5	Phi=1	Phi=2	Phi=0.5	Phi=1	Phi=2
500	0.00E+00	0.00E+00	0.00E+00	1.10E-05	0.00E+00	0.00E+00	0.00E+00	0.00E+00	0.00E+00
525	0.00E+00	0.00E+00	0.00E+00	7.69E-06	0.00E+00	0.00E+00	0.00E+00	0.00E+00	0.00E+00
550	0.00E+00	0.00E+00	0.00E+00	1.57E-05	0.00E+00	0.00E+00	0.00E+00	2.07E-05	0.00E+00
575	0.00E+00	0.00E+00	0.00E+00	5.14E-06	0.00E+00	0.00E+00	0.00E+00	0.00E+00	0.00E+00
600	0.00E+00	0.00E+00	0.00E+00	1.20E-05	0.00E+00	0.00E+00	0.00E+00	2.12E-05	0.00E+00
625	0.00E+00	0.00E+00	0.00E+00	9.92E-06	0.00E+00	0.00E+00	0.00E+00	0.00E+00	0.00E+00
650	0.00E+00	0.00E+00	0.00E+00	5.37E-06	0.00E+00	0.00E+00	0.00E+00	2.33E-05	0.00E+00
675	0.00E+00	0.00E+00	0.00E+00	1.26E-05	0.00E+00	0.00E+00	0.00E+00	0.00E+00	0.00E+00
700	0.00E+00	0.00E+00	3.30E-05	1.16E-05	0.00E+00	6.28E-06	0.00E+00	0.00E+00	0.00E+00
725	0.00E+00	0.00E+00	6.21E-06	7.75E-06	0.00E+00	1.14E-05	0.00E+00	0.00E+00	0.00E+00
750	0.00E+00	0.00E+00	0.00E+00	0.00E+00	0.00E+00	8.19E-06	0.00E+00	0.00E+00	0.00E+00
775	0.00E+00	0.00E+00	0.00E+00	1.34E-05	0.00E+00	0.00E+00	0.00E+00	0.00E+00	9.08E-06
800	3.00E-06	2.93E-06	1.01E-05	8.46E-06	0.00E+00	3.76E-06	2.61E-07	4.50E-07	5.65E-07
825	8.11E-06	2.63E-07	2.40E-05	0.00E+00	0.00E+00	1.11E-05	1.02E-06	6.65E-07	2.12E-06
850	8.06E-06	4.30E-06	2.58E-05	6.26E-07	0.00E+00	1.05E-05	2.37E-06	1.73E-06	4.21E-06
875	8.39E-06	1.01E-05	2.73E-05	7.68E-06	0.00E+00	7.68E-06	3.69E-06	2.65E-06	4.42E-06
900	8.62E-06	0.00E+00	4.07E-05	1.80E-05	0.00E+00	1.58E-05	3.53E-06	2.53E-06	5.97E-06
925	6.85E-06	0.00E+00	3.03E-05	1.56E-05	0.00E+00	9.77E-06	2.09E-06	2.78E-06	4.90E-06
950	6.16E-06	0.00E+00	5.50E-05	2.37E-05	0.00E+00	3.12E-05	1.70E-06	1.27E-06	5.35E-06
975	0.00E+00	2.70E-06	2.27E-05	5.70E-06	0.00E+00	1.20E-05	7.73E-07	8.24E-07	2.10E-06
1000	3.59E-06	0.00E+00	2.06E-05	3.73E-05	0.00E+00	2.50E-05	1.02E-06	4.06E-07	1.39E-06
1025	4.74E-06	0.00E+00	1.46E-05	1.80E-05	0.00E+00	1.93E-05	0.00E+00	0.00E+00	6.36E-07
1050	1.61E-06	1.18E-06	1.36E-05	2.39E-05	0.00E+00	1.96E-05	0.00E+00	0.00E+00	5.25E-07
1075	1.03E-06	0.00E+00	9.75E-06	3.97E-05	0.00E+00	4.44E-05	0.00E+00	0.00E+00	1.37E-07
1100	0.00E+00	0.00E+00	6.62E-07	2.39E-05	0.00E+00	2.15E-05	0.00E+00	0.00E+00	0.00E+00

T (K)	Benzaldehyde			Methylstyrene			Phenol		
	Phi=0.5	Phi=1	Phi=2	Phi=0.5	Phi=1	Phi=2	Phi=0.5	Phi=1	Phi=2
500	4.78E-03	5.22E-03	5.00E-03	0.00E+00	0.00E+00	0.00E+00	4.54E-06	0.00E+00	0.00E+00
525	4.87E-03	4.95E-03	5.00E-03	0.00E+00	0.00E+00	0.00E+00	3.38E-06	8.60E-07	0.00E+00
550	5.42E-03	4.91E-03	5.00E-03	0.00E+00	0.00E+00	0.00E+00	2.89E-06	0.00E+00	0.00E+00
575	4.81E-03	4.57E-03	5.00E-03	0.00E+00	0.00E+00	0.00E+00	1.67E-06	8.45E-07	0.00E+00
600	5.40E-03	5.44E-03	5.00E-03	0.00E+00	0.00E+00	0.00E+00	1.83E-06	0.00E+00	0.00E+00
625	4.93E-03	4.97E-03	5.00E-03	0.00E+00	0.00E+00	0.00E+00	4.03E-06	1.64E-06	0.00E+00
650	4.54E-03	5.26E-03	5.00E-03	0.00E+00	0.00E+00	0.00E+00	2.04E-06	0.00E+00	0.00E+00
675	5.27E-03	5.10E-03	5.00E-03	0.00E+00	0.00E+00	0.00E+00	3.41E-06	1.25E-06	0.00E+00
700	5.51E-03	5.10E-03	5.32E-03	0.00E+00	0.00E+00	0.00E+00	5.28E-06	2.52E-06	1.82E-05
725	5.03E-03	4.41E-03	5.16E-03	0.00E+00	0.00E+00	0.00E+00	1.15E-05	1.14E-05	9.14E-05
750	4.60E-03	5.59E-03	4.80E-03	0.00E+00	0.00E+00	0.00E+00	3.42E-05	3.56E-05	5.40E-05
775	5.07E-03	4.75E-03	4.76E-03	0.00E+00	0.00E+00	0.00E+00	9.70E-05	8.16E-05	1.36E-04
800	5.04E-03	4.30E-03	4.10E-03	0.00E+00	0.00E+00	0.00E+00	2.31E-04	2.37E-04	2.55E-04
825	3.48E-03	3.39E-03	3.26E-03	0.00E+00	0.00E+00	0.00E+00	5.24E-04	3.45E-04	3.93E-04
850	2.58E-03	2.75E-03	2.67E-03	0.00E+00	0.00E+00	0.00E+00	4.86E-04	4.04E-04	5.24E-04
875	1.93E-03	1.99E-03	2.36E-03	0.00E+00	0.00E+00	0.00E+00	7.22E-04	6.16E-04	7.13E-04
900	1.15E-03	1.19E-03	1.93E-03	0.00E+00	0.00E+00	0.00E+00	4.99E-04	4.29E-04	9.30E-04
925	6.53E-04	8.51E-04	1.28E-03	0.00E+00	0.00E+00	0.00E+00	4.42E-04	4.56E-04	9.21E-04
950	3.74E-04	4.84E-04	7.97E-04	0.00E+00	0.00E+00	0.00E+00	2.00E-04	2.15E-04	6.01E-04
975	9.31E-05	2.94E-04	6.26E-04	0.00E+00	0.00E+00	0.00E+00	3.66E-05	1.69E-04	7.37E-04
1000	5.75E-05	1.70E-04	4.00E-04	0.00E+00	0.00E+00	3.03E-06	4.44E-05	5.80E-05	4.00E-04
1025	2.60E-05	7.89E-05	2.35E-04	0.00E+00	0.00E+00	1.93E-06	1.34E-05	6.47E-05	3.15E-04
1050	1.02E-05	4.04E-05	1.71E-04	0.00E+00	0.00E+00	1.24E-06	1.54E-05	2.40E-05	1.99E-04
1075	6.42E-06	7.63E-06	1.03E-04	0.00E+00	0.00E+00	0.00E+00	7.17E-06	1.22E-05	1.85E-04
1100	0.00E+00	5.02E-06	6.86E-05	0.00E+00	0.00E+00	8.32E-07	5.83E-06	4.01E-06	8.74E-05

Experimental raw data: benzaldehyde oxidation

T (K)	Benzofuran			1,3-Benzodioxol			2-Hydroxybenzaldehyde		
	Phi=0.5	Phi=1	Phi=2	Phi=0.5	Phi=1	Phi=2	Phi=0.5	Phi=1	Phi=2
500	0.00E+00	0.00E+00	0.00E+00	0.00E+00	0.00E+00	0.00E+00	0.00E+00	0.00E+00	0.00E+00
525	0.00E+00	0.00E+00	0.00E+00	0.00E+00	0.00E+00	0.00E+00	0.00E+00	0.00E+00	0.00E+00
550	0.00E+00	0.00E+00	0.00E+00	0.00E+00	0.00E+00	0.00E+00	0.00E+00	0.00E+00	0.00E+00
575	0.00E+00	0.00E+00	0.00E+00	0.00E+00	0.00E+00	0.00E+00	0.00E+00	0.00E+00	0.00E+00
600	0.00E+00	0.00E+00	0.00E+00	0.00E+00	0.00E+00	0.00E+00	0.00E+00	0.00E+00	0.00E+00
625	0.00E+00	0.00E+00	0.00E+00	0.00E+00	0.00E+00	0.00E+00	0.00E+00	0.00E+00	0.00E+00
650	0.00E+00	0.00E+00	0.00E+00	0.00E+00	0.00E+00	0.00E+00	0.00E+00	0.00E+00	0.00E+00
675	0.00E+00	0.00E+00	0.00E+00	0.00E+00	0.00E+00	0.00E+00	0.00E+00	0.00E+00	0.00E+00
700	0.00E+00	0.00E+00	0.00E+00	0.00E+00	0.00E+00	0.00E+00	0.00E+00	0.00E+00	0.00E+00
725	0.00E+00	0.00E+00	0.00E+00	0.00E+00	0.00E+00	3.82E-06	0.00E+00	0.00E+00	0.00E+00
750	0.00E+00	0.00E+00	0.00E+00	0.00E+00	1.51E-06	5.69E-06	0.00E+00	0.00E+00	4.90E-07
775	0.00E+00	0.00E+00	0.00E+00	1.18E-06	8.03E-07	1.23E-05	0.00E+00	0.00E+00	2.29E-06
800	0.00E+00	0.00E+00	0.00E+00	2.01E-06	2.03E-06	1.84E-05	0.00E+00	0.00E+00	0.00E+00
825	0.00E+00	1.28E-07	0.00E+00	3.80E-06	2.57E-06	2.81E-05	0.00E+00	0.00E+00	0.00E+00
850	6.36E-07	2.33E-06	0.00E+00	2.58E-06	5.13E-06	2.67E-05	0.00E+00	0.00E+00	0.00E+00
875	3.84E-06	7.22E-07	5.84E-07	3.84E-06	5.11E-06	2.73E-05	0.00E+00	0.00E+00	0.00E+00
900	3.31E-06	4.17E-06	0.00E+00	3.11E-06	5.08E-06	2.45E-05	0.00E+00	0.00E+00	0.00E+00
925	2.97E-06	1.94E-06	6.28E-07	3.11E-06	3.03E-06	3.24E-05	0.00E+00	0.00E+00	0.00E+00
950	1.06E-06	1.16E-06	1.78E-06	1.01E-06	1.92E-06	3.97E-05	0.00E+00	0.00E+00	0.00E+00
975	0.00E+00	4.48E-07	0.00E+00	0.00E+00	8.10E-07	2.06E-05	0.00E+00	0.00E+00	0.00E+00
1000	0.00E+00	0.00E+00	7.24E-07	6.08E-07	7.81E-07	1.37E-05	0.00E+00	0.00E+00	3.20E-06
1025	0.00E+00	0.00E+00	0.00E+00	0.00E+00	8.09E-07	5.95E-06	0.00E+00	0.00E+00	2.62E-06
1050	0.00E+00	0.00E+00	0.00E+00	0.00E+00	3.57E-07	6.52E-07	0.00E+00	0.00E+00	1.39E-06
1075	0.00E+00	0.00E+00	7.12E-07	1.15E-06	8.82E-07	4.84E-07	0.00E+00	0.00E+00	0.00E+00
1100	0.00E+00	0.00E+00	4.88E-07	0.00E+00	0.00E+00	5.20E-07	0.00E+00	4.39E-07	0.00E+00

T (K)	Indene			o-Cresol			Acetophenone		
	Phi=0.5	Phi=1	Phi=2	Phi=0.5	Phi=1	Phi=2	Phi=0.5	Phi=1	Phi=2
500	0.00E+00	0.00E+00	0.00E+00	0.00E+00	0.00E+00	0.00E+00	0.00E+00	0.00E+00	0.00E+00
525	0.00E+00	0.00E+00	0.00E+00	0.00E+00	0.00E+00	0.00E+00	0.00E+00	0.00E+00	0.00E+00
550	0.00E+00	0.00E+00	0.00E+00	0.00E+00	0.00E+00	0.00E+00	0.00E+00	0.00E+00	0.00E+00
575	0.00E+00	0.00E+00	0.00E+00	0.00E+00	0.00E+00	0.00E+00	0.00E+00	0.00E+00	0.00E+00
600	0.00E+00	0.00E+00	0.00E+00	0.00E+00	0.00E+00	0.00E+00	0.00E+00	0.00E+00	0.00E+00
625	0.00E+00	0.00E+00	0.00E+00	0.00E+00	0.00E+00	0.00E+00	0.00E+00	0.00E+00	0.00E+00
650	0.00E+00	0.00E+00	0.00E+00	0.00E+00	0.00E+00	0.00E+00	0.00E+00	0.00E+00	0.00E+00
675	0.00E+00	0.00E+00	0.00E+00	0.00E+00	0.00E+00	0.00E+00	0.00E+00	0.00E+00	0.00E+00
700	0.00E+00	0.00E+00	0.00E+00	0.00E+00	0.00E+00	0.00E+00	0.00E+00	0.00E+00	0.00E+00
725	0.00E+00	0.00E+00	0.00E+00	0.00E+00	0.00E+00	1.11E-06	0.00E+00	0.00E+00	2.00E-06
750	0.00E+00	0.00E+00	1.27E-07	0.00E+00	0.00E+00	2.74E-06	0.00E+00	0.00E+00	4.34E-06
775	0.00E+00	2.08E-07	4.48E-07	5.08E-07	2.83E-07	1.07E-05	3.67E-07	2.90E-07	5.58E-06
800	5.00E-07	5.33E-07	8.31E-07	9.03E-07	1.51E-06	3.23E-05	0.00E+00	4.44E-07	6.25E-06
825	8.07E-07	6.45E-07	2.28E-06	3.55E-06	3.16E-06	7.46E-05	0.00E+00	3.51E-07	5.25E-06
850	8.08E-07	7.11E-07	2.31E-06	5.06E-06	6.22E-06	1.19E-04	0.00E+00	0.00E+00	4.42E-06
875	5.58E-07	6.53E-07	2.67E-06	1.05E-05	1.26E-05	1.85E-04	0.00E+00	0.00E+00	1.93E-06
900	6.82E-07	3.64E-07	2.70E-06	1.03E-05	1.12E-05	1.56E-04	0.00E+00	0.00E+00	0.00E+00
925	1.49E-07	3.04E-07	3.89E-06	1.02E-05	1.41E-05	3.01E-04	0.00E+00	0.00E+00	0.00E+00
950	0.00E+00	3.39E-07	5.91E-06	3.78E-06	5.86E-06	3.58E-04	0.00E+00	0.00E+00	2.76E-06
975	0.00E+00	2.07E-07	5.14E-06	5.64E-07	4.72E-06	2.81E-04	0.00E+00	0.00E+00	3.98E-07
1000	0.00E+00	2.85E-07	8.94E-06	7.44E-07	1.73E-06	2.45E-04	0.00E+00	0.00E+00	1.80E-06
1025	0.00E+00	3.01E-07	1.06E-05	0.00E+00	2.12E-06	1.53E-04	0.00E+00	0.00E+00	1.18E-06
1050	0.00E+00	2.79E-07	1.73E-05	0.00E+00	7.37E-07	8.89E-05	0.00E+00	0.00E+00	9.26E-07
1075	0.00E+00	0.00E+00	2.71E-05	0.00E+00	4.89E-07	5.69E-05	0.00E+00	0.00E+00	1.18E-06
1100	0.00E+00	0.00E+00	2.42E-05	0.00E+00	0.00E+00	2.67E-05	0.00E+00	0.00E+00	0.00E+00

Experimental raw data: benzaldehyde oxidation

T (K)	p-Cresol			1,3-Benzodioxol-2-one			Methylbenzofuran		
	Phi=0.5	Phi=1	Phi=2	Phi=0.5	Phi=1	Phi=2	Phi=0.5	Phi=1	Phi=2
500	0.00E+00	0.00E+00	0.00E+00	0.00E+00	0.00E+00	0.00E+00	0.00E+00	0.00E+00	0.00E+00
525	0.00E+00	0.00E+00	0.00E+00	0.00E+00	0.00E+00	0.00E+00	0.00E+00	0.00E+00	0.00E+00
550	0.00E+00	0.00E+00	0.00E+00	0.00E+00	0.00E+00	0.00E+00	0.00E+00	0.00E+00	0.00E+00
575	0.00E+00	0.00E+00	0.00E+00	0.00E+00	0.00E+00	0.00E+00	0.00E+00	0.00E+00	0.00E+00
600	0.00E+00	0.00E+00	0.00E+00	0.00E+00	0.00E+00	0.00E+00	0.00E+00	0.00E+00	0.00E+00
625	0.00E+00	0.00E+00	0.00E+00	0.00E+00	0.00E+00	0.00E+00	0.00E+00	0.00E+00	0.00E+00
650	0.00E+00	0.00E+00	0.00E+00	0.00E+00	0.00E+00	0.00E+00	0.00E+00	0.00E+00	0.00E+00
675	0.00E+00	0.00E+00	0.00E+00	0.00E+00	0.00E+00	0.00E+00	0.00E+00	0.00E+00	0.00E+00
700	0.00E+00	0.00E+00	0.00E+00	0.00E+00	0.00E+00	0.00E+00	0.00E+00	0.00E+00	5.02E-07
725	0.00E+00	0.00E+00	1.29E-06	0.00E+00	0.00E+00	5.51E-06	0.00E+00	0.00E+00	0.00E+00
750	0.00E+00	0.00E+00	3.37E-06	0.00E+00	0.00E+00	7.76E-06	0.00E+00	0.00E+00	0.00E+00
775	7.06E-07	3.22E-07	1.20E-05	0.00E+00	0.00E+00	1.41E-05	7.92E-07	2.89E-07	0.00E+00
800	4.88E-07	1.68E-06	3.09E-05	0.00E+00	6.61E-07	1.80E-05	7.03E-07	0.00E+00	2.30E-05
825	4.50E-06	4.09E-06	7.68E-05	2.46E-06	2.70E-07	2.52E-05	4.29E-07	2.90E-07	0.00E+00
850	4.91E-06	5.98E-06	1.41E-04	1.52E-06	9.61E-07	2.67E-05	0.00E+00	3.73E-07	0.00E+00
875	1.38E-05	1.17E-05	2.13E-04	3.45E-06	1.77E-06	2.88E-05	0.00E+00	0.00E+00	0.00E+00
900	1.06E-05	9.59E-06	1.91E-04	4.54E-06	0.00E+00	1.55E-05	0.00E+00	1.06E-06	1.21E-06
925	1.07E-05	1.17E-05	3.14E-04	2.95E-06	1.68E-06	2.01E-05	0.00E+00	0.00E+00	4.38E-06
950	3.38E-06	5.65E-06	3.05E-04	1.18E-06	0.00E+00	2.84E-05	0.00E+00	5.19E-07	0.00E+00
975	9.89E-07	3.73E-06	2.77E-04	0.00E+00	5.37E-07	8.01E-06	0.00E+00	0.00E+00	2.14E-06
1000	9.22E-07	1.12E-06	2.14E-04	0.00E+00	0.00E+00	4.10E-06	0.00E+00	0.00E+00	3.36E-06
1025	0.00E+00	1.85E-06	1.21E-04	0.00E+00	0.00E+00	1.82E-06	0.00E+00	0.00E+00	2.21E-06
1050	8.89E-07	6.67E-07	7.50E-05	0.00E+00	0.00E+00	0.00E+00	0.00E+00	0.00E+00	1.42E-06
1075	0.00E+00	3.24E-07	3.68E-05	0.00E+00	0.00E+00	1.44E-06	0.00E+00	0.00E+00	2.02E-06
1100	0.00E+00	0.00E+00	7.15E-07	0.00E+00	0.00E+00	7.68E-07	0.00E+00	0.00E+00	1.36E-06

T (K)	Ethylphenol			Methylindene			1,2-Dihydronaphthalene		
	Phi=0.5	Phi=1	Phi=2	Phi=0.5	Phi=1	Phi=2	Phi=0.5	Phi=1	Phi=2
500	0.00E+00	0.00E+00	0.00E+00	0.00E+00	0.00E+00	0.00E+00	0.00E+00	0.00E+00	0.00E+00
525	0.00E+00	0.00E+00	0.00E+00	0.00E+00	0.00E+00	0.00E+00	0.00E+00	0.00E+00	0.00E+00
550	0.00E+00	0.00E+00	0.00E+00	0.00E+00	0.00E+00	0.00E+00	0.00E+00	0.00E+00	0.00E+00
575	0.00E+00	0.00E+00	0.00E+00	0.00E+00	0.00E+00	0.00E+00	0.00E+00	0.00E+00	0.00E+00
600	0.00E+00	0.00E+00	0.00E+00	0.00E+00	0.00E+00	0.00E+00	0.00E+00	0.00E+00	0.00E+00
625	0.00E+00	0.00E+00	0.00E+00	0.00E+00	0.00E+00	0.00E+00	0.00E+00	0.00E+00	0.00E+00
650	0.00E+00	0.00E+00	0.00E+00	0.00E+00	0.00E+00	0.00E+00	0.00E+00	0.00E+00	0.00E+00
675	5.68E-07	0.00E+00	0.00E+00	0.00E+00	0.00E+00	0.00E+00	0.00E+00	0.00E+00	0.00E+00
700	3.77E-07	2.44E-07	7.67E-07	0.00E+00	0.00E+00	0.00E+00	0.00E+00	0.00E+00	0.00E+00
725	0.00E+00	0.00E+00	7.54E-07	0.00E+00	0.00E+00	0.00E+00	0.00E+00	0.00E+00	0.00E+00
750	0.00E+00	2.12E-07	7.47E-07	0.00E+00	0.00E+00	0.00E+00	0.00E+00	0.00E+00	0.00E+00
775	0.00E+00	0.00E+00	7.04E-07	0.00E+00	0.00E+00	9.86E-07	0.00E+00	0.00E+00	8.92E-07
800	0.00E+00	0.00E+00	0.00E+00	3.12E-07	0.00E+00	2.54E-06	0.00E+00	0.00E+00	0.00E+00
825	0.00E+00	0.00E+00	1.03E-06	5.05E-07	8.43E-07	2.79E-06	0.00E+00	1.45E-07	2.13E-06
850	0.00E+00	2.15E-07	1.10E-06	0.00E+00	2.42E-07	4.84E-06	0.00E+00	2.83E-07	2.04E-06
875	0.00E+00	0.00E+00	2.18E-06	0.00E+00	0.00E+00	3.39E-06	0.00E+00	0.00E+00	1.53E-06
900	0.00E+00	0.00E+00	1.04E-06	0.00E+00	6.53E-07	3.88E-06	0.00E+00	1.56E-07	8.94E-07
925	0.00E+00	0.00E+00	8.91E-06	0.00E+00	0.00E+00	8.03E-06	0.00E+00	0.00E+00	1.36E-06
950	0.00E+00	0.00E+00	9.37E-06	0.00E+00	0.00E+00	1.01E-05	0.00E+00	0.00E+00	2.05E-06
975	0.00E+00	0.00E+00	6.75E-06	0.00E+00	0.00E+00	9.09E-06	0.00E+00	0.00E+00	1.60E-06
1000	0.00E+00	0.00E+00	6.83E-06	0.00E+00	0.00E+00	9.52E-06	0.00E+00	0.00E+00	7.71E-07
1025	0.00E+00	0.00E+00	4.97E-06	0.00E+00	0.00E+00	7.45E-06	0.00E+00	0.00E+00	7.02E-07
1050	0.00E+00	0.00E+00	5.19E-06	0.00E+00	0.00E+00	7.53E-06	0.00E+00	0.00E+00	2.84E-06
1075	0.00E+00	0.00E+00	6.00E-06	0.00E+00	0.00E+00	5.16E-06	0.00E+00	0.00E+00	4.87E-06
1100	0.00E+00	0.00E+00	4.12E-06	0.00E+00	0.00E+00	3.66E-06	0.00E+00	0.00E+00	4.24E-06

Experimental raw data: benzaldehyde oxidation

T (K)	1,3-Dihydronaphthalene			Naphtalene			Cinnamaldehyde		
	Phi=0.5	Phi=1	Phi=2	Phi=0.5	Phi=1	Phi=2	Phi=0.5	Phi=1	Phi=2
500	4.18E-05	0.00E+00	0.00E+00	0.00E+00	0.00E+00	0.00E+00	0.00E+00	0.00E+00	0.00E+00
525	5.37E-05	0.00E+00	0.00E+00	0.00E+00	0.00E+00	0.00E+00	0.00E+00	0.00E+00	0.00E+00
550	3.87E-05	0.00E+00	0.00E+00	0.00E+00	0.00E+00	0.00E+00	0.00E+00	0.00E+00	0.00E+00
575	4.96E-05	0.00E+00	0.00E+00	0.00E+00	0.00E+00	0.00E+00	0.00E+00	0.00E+00	0.00E+00
600	4.39E-05	0.00E+00	0.00E+00	0.00E+00	0.00E+00	0.00E+00	0.00E+00	0.00E+00	0.00E+00
625	0.00E+00	8.67E-07	0.00E+00	0.00E+00	0.00E+00	0.00E+00	0.00E+00	0.00E+00	0.00E+00
650	0.00E+00	0.00E+00	0.00E+00	0.00E+00	0.00E+00	0.00E+00	0.00E+00	0.00E+00	0.00E+00
675	0.00E+00	0.00E+00	0.00E+00	0.00E+00	0.00E+00	0.00E+00	0.00E+00	0.00E+00	0.00E+00
700	0.00E+00	3.21E-06	0.00E+00	0.00E+00	0.00E+00	0.00E+00	0.00E+00	0.00E+00	0.00E+00
725	0.00E+00	0.00E+00	8.73E-05	0.00E+00	0.00E+00	0.00E+00	0.00E+00	0.00E+00	0.00E+00
750	4.83E-07	3.87E-07	1.75E-04	0.00E+00	0.00E+00	0.00E+00	0.00E+00	0.00E+00	0.00E+00
775	1.67E-06	8.08E-07	6.06E-06	0.00E+00	0.00E+00	0.00E+00	0.00E+00	0.00E+00	0.00E+00
800	2.35E-06	1.31E-06	9.07E-05	0.00E+00	0.00E+00	3.15E-06	0.00E+00	0.00E+00	0.00E+00
825	1.77E-06	9.06E-07	7.45E-05	0.00E+00	3.13E-07	7.44E-06	0.00E+00	0.00E+00	1.08E-06
850	1.14E-06	4.88E-07	0.00E+00	2.23E-07	4.76E-07	8.72E-06	0.00E+00	0.00E+00	0.00E+00
875	1.08E-06	4.66E-07	1.14E-05	4.48E-07	8.33E-07	1.28E-05	0.00E+00	0.00E+00	1.45E-06
900	0.00E+00	0.00E+00	6.41E-05	0.00E+00	1.16E-06	1.28E-05	0.00E+00	0.00E+00	2.80E-06
925	0.00E+00	0.00E+00	1.06E-05	0.00E+00	6.71E-07	2.45E-05	0.00E+00	0.00E+00	1.92E-06
950	0.00E+00	0.00E+00	6.40E-06	0.00E+00	6.90E-07	4.96E-05	0.00E+00	0.00E+00	3.29E-06
975	0.00E+00	0.00E+00	8.14E-06	0.00E+00	5.70E-07	4.05E-05	0.00E+00	0.00E+00	3.38E-06
1000	0.00E+00	0.00E+00	6.74E-06	0.00E+00	4.53E-07	9.66E-05	0.00E+00	0.00E+00	4.26E-06
1025	0.00E+00	0.00E+00	4.90E-06	0.00E+00	6.02E-07	1.27E-04	0.00E+00	0.00E+00	2.98E-06
1050	0.00E+00	0.00E+00	5.33E-06	0.00E+00	3.19E-07	1.62E-04	0.00E+00	0.00E+00	3.30E-06
1075	0.00E+00	2.63E-07	4.66E-06	0.00E+00	0.00E+00	2.48E-04	0.00E+00	0.00E+00	1.98E-06
1100	0.00E+00	1.10E-07	4.55E-06	0.00E+00	0.00E+00	1.98E-04	0.00E+00	0.00E+00	0.00E+00

T (K)	Biphenyl			Diphenyl ether			Acenaphthylene		
	Phi=0.5	Phi=1	Phi=2	Phi=0.5	Phi=1	Phi=2	Phi=0.5	Phi=1	Phi=2
500	0.00E+00	0.00E+00	0.00E+00	0.00E+00	0.00E+00	0.00E+00	0.00E+00	0.00E+00	0.00E+00
525	0.00E+00	0.00E+00	0.00E+00	0.00E+00	0.00E+00	0.00E+00	0.00E+00	0.00E+00	0.00E+00
550	0.00E+00	0.00E+00	0.00E+00	0.00E+00	0.00E+00	0.00E+00	0.00E+00	0.00E+00	0.00E+00
575	0.00E+00	0.00E+00	0.00E+00	0.00E+00	0.00E+00	0.00E+00	0.00E+00	0.00E+00	0.00E+00
600	0.00E+00	0.00E+00	0.00E+00	0.00E+00	0.00E+00	0.00E+00	0.00E+00	0.00E+00	0.00E+00
625	0.00E+00	0.00E+00	0.00E+00	0.00E+00	0.00E+00	0.00E+00	0.00E+00	0.00E+00	0.00E+00
650	0.00E+00	0.00E+00	0.00E+00	0.00E+00	0.00E+00	0.00E+00	0.00E+00	0.00E+00	0.00E+00
675	0.00E+00	0.00E+00	0.00E+00	0.00E+00	0.00E+00	0.00E+00	0.00E+00	0.00E+00	0.00E+00
700	0.00E+00	0.00E+00	0.00E+00	0.00E+00	0.00E+00	0.00E+00	0.00E+00	0.00E+00	0.00E+00
725	0.00E+00	0.00E+00	3.74E-07	0.00E+00	0.00E+00	0.00E+00	0.00E+00	0.00E+00	2.34E-07
750	0.00E+00	1.56E-07	0.00E+00	0.00E+00	0.00E+00	0.00E+00	0.00E+00	0.00E+00	0.00E+00
775	3.34E-07	2.96E-07	2.48E-06	4.19E-07	4.52E-07	8.12E-07	0.00E+00	0.00E+00	0.00E+00
800	3.14E-07	5.75E-07	4.73E-06	5.13E-07	9.59E-07	9.15E-06	0.00E+00	0.00E+00	3.68E-06
825	3.90E-07	1.94E-07	6.71E-06	6.60E-07	1.76E-06	1.10E-06	0.00E+00	0.00E+00	0.00E+00
850	3.67E-07	3.37E-07	9.92E-06	6.66E-07	5.56E-07	1.02E-05	0.00E+00	0.00E+00	0.00E+00
875	0.00E+00	2.82E-07	1.18E-05	6.46E-07	2.67E-07	2.55E-06	0.00E+00	0.00E+00	0.00E+00
900	0.00E+00	2.81E-07	1.41E-05	4.53E-07	1.18E-07	3.68E-06	0.00E+00	0.00E+00	0.00E+00
925	7.28E-07	5.32E-07	1.66E-05	0.00E+00	0.00E+00	5.14E-06	0.00E+00	0.00E+00	0.00E+00
950	5.32E-07	0.00E+00	1.59E-05	0.00E+00	0.00E+00	5.77E-06	0.00E+00	0.00E+00	1.99E-07
975	6.67E-07	0.00E+00	2.16E-05	0.00E+00	9.59E-08	7.67E-06	0.00E+00	0.00E+00	4.80E-07
1000	3.97E-07	0.00E+00	2.27E-05	0.00E+00	0.00E+00	7.50E-06	0.00E+00	0.00E+00	9.35E-07
1025	0.00E+00	5.06E-07	1.86E-05	0.00E+00	0.00E+00	5.81E-06	0.00E+00	0.00E+00	1.57E-06
1050	0.00E+00	0.00E+00	2.22E-05	0.00E+00	0.00E+00	6.14E-06	0.00E+00	0.00E+00	3.82E-06
1075	0.00E+00	0.00E+00	2.01E-05	0.00E+00	0.00E+00	3.62E-06	0.00E+00	0.00E+00	4.30E-06
1100	0.00E+00	0.00E+00	1.52E-05	0.00E+00	0.00E+00	3.19E-06	0.00E+00	0.00E+00	6.24E-06

Experimental raw data: benzaldehyde oxidation

T (K)	Dibenzofuran			Indanone		
	Phi=0.5	Phi=1	Phi=2	Phi=0.5	Phi=1	Phi=2
500	0.00E+00	0.00E+00	0.00E+00	0.00E+00	0.00E+00	0.00E+00
525	0.00E+00	0.00E+00	0.00E+00	4.08E-06	0.00E+00	0.00E+00
550	3.36E-07	0.00E+00	0.00E+00	0.00E+00	0.00E+00	0.00E+00
575	7.71E-07	0.00E+00	0.00E+00	0.00E+00	0.00E+00	0.00E+00
600	0.00E+00	0.00E+00	0.00E+00	0.00E+00	0.00E+00	0.00E+00
625	0.00E+00	5.78E-07	0.00E+00	0.00E+00	0.00E+00	0.00E+00
650	1.42E-06	0.00E+00	0.00E+00	0.00E+00	0.00E+00	0.00E+00
675	0.00E+00	0.00E+00	0.00E+00	0.00E+00	0.00E+00	0.00E+00
700	3.74E-07	3.21E-07	3.17E-06	0.00E+00	0.00E+00	0.00E+00
725	6.33E-07	8.67E-07	2.48E-06	5.01E-07	0.00E+00	0.00E+00
750	0.00E+00	0.00E+00	0.00E+00	0.00E+00	0.00E+00	0.00E+00
775	8.87E-07	0.00E+00	7.46E-06	1.70E-06	4.72E-06	0.00E+00
800	2.13E-06	1.25E-06	1.25E-05	0.00E+00	2.14E-06	0.00E+00
825	2.56E-06	3.66E-06	1.44E-05	2.63E-06	3.01E-06	0.00E+00
850	4.57E-06	0.00E+00	2.34E-05	4.49E-06	0.00E+00	0.00E+00
875	8.18E-06	3.03E-06	1.74E-05	1.76E-05	2.62E-06	8.82E-07
900	3.53E-06	2.21E-06	4.88E-05	9.02E-06	0.00E+00	0.00E+00
925	4.83E-06	3.24E-06	3.50E-05	3.97E-05	2.70E-05	1.54E-06
950	2.38E-06	1.69E-06	2.83E-05	3.06E-05	8.69E-06	3.18E-06
975	1.77E-06	9.72E-07	4.54E-05	3.73E-05	1.57E-05	4.43E-06
1000	8.26E-07	4.68E-07	3.22E-05	1.90E-05	1.17E-05	5.16E-06
1025	1.88E-06	7.96E-07	2.68E-05	1.95E-05	2.52E-05	4.96E-06
1050	0.00E+00	2.53E-07	3.29E-05	2.87E-06	3.23E-06	6.66E-06
1075	0.00E+00	3.61E-06	2.05E-05	5.22E-06	1.96E-05	5.66E-06
1100	4.62E-07	6.04E-07	2.08E-05	2.39E-06	6.16E-06	7.08E-06

Experimental study of the formation of pollutants during the combustion of bio-oil surrogate molecules

Keywords: combustion, bio-oils, kinetics

In 2016, fossil fuels represented about 80% of the world total primary energy supply. However, this resource is limited and has a huge impact on the environment pollution because of the production of greenhouse gases. In order to drastically reduce greenhouse gases emissions, a focus on biofuels, and especially bio-oils, is made in the industrial world and for transportation. The IMPROOF project is funded by the European Union under the SPIRE framework. Its objective is to improve the energy efficiency in the case of steam cracking furnaces by 20% and in parallel to decrease by 25% per ton of ethylene the emission of pollutants like NOx or greenhouse gases. This PhD is focused on the part concerning the use of alternative fuels and especially bio-oils for the heating of the steam cracking furnaces.

To better assess bio-oil oxidation or pyrolysis, a bibliographical review about the publications dealing with the composition of bio-oils have been performed. From this review, it comes out that bio-oils could be described as a mixture composed of six main types of chemical compounds: alcohols, aldehydes, carboxylic acids, furans and derivatives, oxygenated aromatic compounds and nitrogen organic compounds.

In order to complete some detected lack in the literature, the aim of this thesis was to produce a new experimental dataset for molecules owning to the five first chemical families previously presented. A jet-stirred reactor was chosen to perform the experiments, due to its homogeneity in concentration and composition. This kind of “ideal” reactor is indeed convenient for the development of reliable data for the development and validation of kinetic models. During this work, eight fuels were selected and studied: *n*-butanol, *n*-pentanol, *n*-butanal, *n*-pentanal, butanoic acid, pentanoic acid, furan and benzaldehyde. For each fuel, the experimental results were used to develop and validate a kinetic model. Those models were afterward used to study the decomposition pathways of the studied species.

Etude expérimentale de la formation de polluants lors de la combustion de molécules modèles de bio-huiles

Mots-clés : combustion, bio-huile, cinétique

En 2016, les combustibles fossiles représentaient environ 80% de l'approvisionnement mondial total en énergie primaire. Cependant, cette ressource est limitée et a un impact énorme sur la pollution de l'environnement en raison de la production de gaz à effet de serre. C’est pourquoi le monde industriel et des transports s’intéressent aux biocarburants, en particulier aux bio-huiles, afin de réduire considérablement les émissions de gaz à effet de serre. Le projet IMPROOF est un projet financé par l'Union européenne dans le cadre du programme SPIRE. Son objectif est d'améliorer de 20% l'efficacité énergétique des fours de vapocraquage et, parallèlement, de réduire de 25% par tonne d'éthylène les émissions de polluants tels que les NOx ou les gaz à effet de serre. Cette thèse porte sur l'utilisation de combustibles de substitution, notamment de bio-huiles, pour le chauffage des fours de vapocraquage.

Afin de mieux évaluer l'oxydation ou la pyrolyse de la bio-huile, une revue bibliographique des publications traitant de la composition des bio-huiles a été réalisée. Il ressort de cette revue que les bio-huiles peuvent être décrites comme un mélange composé de six principaux types de composés chimiques : les alcools, les aldéhydes, les acides carboxyliques, les furannes et leurs dérivés, les composés aromatiques oxygénés et les composés azotés organiques.

Afin de compléter certaines lacunes relevées dans la littérature, le but de cette thèse était de produire un nouvel ensemble de données expérimentales pour certaines molécules appartenant aux cinq premières familles chimiques précédemment présentées. Un réacteur agité par jets a été choisi pour réaliser les expériences en raison de son homogénéité de concentration et de composition. Ce type de réacteur «idéal» convient en effet pour le développement de données fiables pour le développement et la validation de modèles cinétiques. Au cours de ce travail, huit combustibles ont été sélectionnés et étudiés : le *n*-butanol, le *n*-pentanol, le *n*-butanal, le *n*-pentanal, l’acide butanoïque, l’acide pentanoïque, le furane ainsi que le benzaldéhyde. Pour chacun de ces carburants, les résultats expérimentaux ont été utilisés pour développer et valider un modèle cinétique. Ces modèles ont ensuite été utilisés pour étudier les voies de décomposition des espèces étudiées.